Advances in
QUANTUM CHEMISTRY
UNSTABLE STATES IN THE CONTINUOUS SPECTRA, PART I: ANALYSIS, CONCEPTS, METHODS, AND RESULTS

<u>VOLUME</u> **60**

Special Editors

CLEANTHES A. NICOLAIDES
Theoretical and Physical Chemistry Institute
National Hellenic Research Foundation
Athens, Greece

ERKKI BRÄNDAS
Department of Quantum Chemistry
Uppsala University
Uppsala, Sweden

Editors

JOHN R. SABIN
Quantum Theory Project
University of Florida
Gainesville, Florida

ERKKI BRÄNDAS
Department of Quantum Chemistry
Uppsala University
Uppsala, Sweden

Working together to grow
libraries in developing countries

www.elsevier.com | www.bookaid.org | www.sabre.org

ELSEVIER   BOOK AID
           International   Sabre Foundation

There is a plethora of phenomena in chemical physics and in atomic, molecular, nuclear, and solid state physics whose dynamics is determined by the presence of *unstable states in the continuous spectra* (USCSs). In fact, the possibilities of formation and the significance of such states have increased in the last few decades because of the large variety of novel situations involving the interaction of matter with well-characterized beams of particles and, especially, with lasers.

Experimental and theoretical interest in USCSs has existed since the early days of quantum mechanics. For example, a textbook picture of such an unstable state is that of the one-dimensional potential with a local minimum and a finite barrier that is used to explain, in terms of quantum mechanical tunneling, the instability of a nucleus, the concomitant emission of an alpha particle, and its energy. Another textbook example of basic importance is the formal construction of a wave packet from a superposition of a complete set of stationary states and the determination, at least for simple one-dimensional motion, of its time evolution. Finally, another example often presented in books is the appearance of structures ("peaks") in the energy-dependent transition rates (cross sections) over the smoothly varying continuum characterizing a physico-chemical process, which are normally called *resonances* and which are associated with the transient formation of USCSs.

The experimental and theoretical study and description of USCSs (of resonance states) can be carried out either on the energy axis (which has been the most extensively used approach) or along the time axis. The Hamiltonians in terms of which they are described may be field-free or may include the interaction with external static or dynamic electromagnetic fields. In the latter case, novel situations and phenomena emerge as a function of the interplay between field parameters and the field-free spectra. In fact, with the continuing development of new probes and of sophisticated experimental techniques, the prospects of measuring properties of yet unknown such states in real systems have increased considerably.

In contradistinction to the well-established quantum mechanics of the low-lying discrete states and to the corresponding computational methods, which

are normally based on Hermitian formalisms valid in the Hilbert space of square-integrable functions, the rigorous treatment of resonance states and of the related observables gives rise to complex and intriguing physical, mathematical, and computational challenges. With regard to formalism and phenomenology, the fundamental reason for this fact is the physical and mathematical presence of the open channels of the multichannel (in general) scattering continuum. Furthermore, for polyelectronic systems that must be tackled realistically and quantitatively, the requirements are increased sharply by the omnipresence of the *many-body problem*.

The volume in hand contains articles that review as well as analyze and expand on the topics with which they deal. According to the invitation letter by the Editors (in the Summer of 2009), they were written in a style chosen by each author and without any constraint on the number of pages. Although proper referencing was considered as a critical element in the presentation and discussions, these articles were not expected to provide a catalogue of methods and of results. Instead, the Editors asked from the authors to discuss one or more themes of their choice, placing the emphasis on their own contributions, on the background that is related to them, and on possible comparisons with related work. All articles were subjected to "friendly yet critical" reviews, provided by international experts in each field who were recommended by the contributors.

<div style="text-align: right">

Cleanthes A. Nicolaides
Athens, Greece
and
Erkki J. Brändas
Uppsala, Sweden

</div>

CONTRIBUTORS

Numbers in parentheses indicate the pages where the authors' contributions can be found.

G. Alber (457)
Institut für Angewandte Physik, Technische Universität Darmstadt, Hochschulstraße 4a, 64289 Darmstadt, Germany

O. Atabek (51)
Institut des Sciences Moléculaires d'Orsay, Bâtiment 350, Université Paris-Sud 11 Campus d'Orsay, 91405 Orsay, France

Philippe Durand (1)
Laboratoire de Chimie et Physique Quantiques, IRSAMC, Université de Toulouse et CNRS, 31062 Toulouse cedex 4, France

Gastón García-Calderón (407)
Instituto de Física, Universidad Nacional Autónoma de México, Apartado Postal 20 364, 01000 México, D.F., México

Arseni Goussev (269)
School of Mathematics, University of Bristol, University Walk, Bristol BS8 1TW, UK

Yannis Komninos (333)
Theoretical and Physical Chemistry Institute, National Hellenic Research Foundation, 48 Vasileos Constantinou Avenue, Athens 11635, Greece

R. Lefebvre (51)
Institut des Sciences Moléculaires d'Orsay, Bâtiment 350, Université Paris-Sud 11 Campus d'Orsay, 91405 Orsay, France
UFR de Physique Fondamentale et Appliquée, UPMC, 75005, Paris, France

G. Leuchs (457)
Max Planck Institute for the Science of Light - Günther-Scharowsky-Str.1, Bau 24, 91058, Erlangen, Germany

J. Martorell (485)
Departament d'Estructura i Constituents de la Materia, Universitat de Barcelona, 08028 Barcelona, Spain

Theodoros Mercouris (333)
Theoretical and Physical Chemistry Institute, National Hellenic Research Foundation, 48 Vasileos Constantinou Avenue, Athens 11635, Greece

J. G. Muga (485)
Departamento de Química Física, Universidad del País Vasco – Euskal Herriko Unibertsitatea, Apdo. 644, 48080 Bilbao, Spain

T. T. Nguyen-Dang (51)
Département de Chimie, Université Laval, Québec, G1K 7P4, Canada

Cleanthes A. Nicolaides (163, 333)
Theoretical and Physical Chemistry Institute, National Hellenic Research Foundation, 48 Vasileos Constantinou Avenue, Athens 11635, Greece

Ivana Paidarová (1)
J. Heyrovský Institute of Physical Chemistry, Academy of Sciences of the Czech Republic, v.v.i 182 23 Praha 8, Czech Republic

Roman Schubert (269)
School of Mathematics, University of Bristol, University Walk, Bristol BS8 1TW, UK

Moshe Shapiro (105)
Departments of Chemistry and Physics, The University of British Columbia, Vancouver V6T1Z1, Canada
Department of Chemical Physics, The Weizmann Institute, Rehovot 76100, Israel

D. W. L. Sprung (485)
Department of Physics and Astronomy, McMaster University, Hamilton, Ontario L8S 4M1, Canada

M. Stobińska (457)
Max Planck Institute for the Science of Light - Günther-Scharowsky-Str.1, Bau 24, 91058, Erlangen, Germany

Ioannis Thanopulos (105)
Theoretical and Physical Chemistry Institute, National Hellenic Research
Foundation, Athens 11635, Greece

E. Torrontegui (485)
Departamento de Química Física, Universidad del País Vasco – Euskal
Herriko Unibertsitatea, Apdo. 644, 48080 Bilbao, Spain

Holger Waalkens (269)
School of Mathematics, University of Bristol, University Walk, Bristol BS8
1TW, UK
Johann Bernoulli Institute for Mathematics and Computer Science, Univer-
sity of Groningen, PO Box 407, 9700 AK Groningen, The Netherlands

Stephen Wiggins (269)
School of Mathematics, University of Bristol, University Walk, Bristol BS8
1TW, UK

Unstable States: From Quantum Mechanics to Statistical Physics

Ivana Paidarová[a] and **Philippe Durand**[b]

Contents

Abstract
Influenced by the ideas of Jaynes and Prigogine from the mid-1950s, we present a unified formulation of dynamics and thermodynamics of irreversible processes. Our approach originates in the quantum theory of resonances described by effective Hamiltonians. The concept of effective Hamiltonian is extended to the concept of effective Liouvillian that deals with macroscopic

[a] J. Heyrovský Institute of Physical Chemistry, Academy of Sciences of the Czech Republic, v.v.i. 182 23 Praha 8, Czech Republic

[b] Laboratoire de Chimie et Physique Quantiques, IRSAMC, Université de Toulouse et CNRS, 31062 Toulouse cedex 4, France

E-mail address: ivana.paidarova@jh-inst.cas.cz (I. Paidarová)

observables and brings insight into the dissipative nonequilibrium thermody-namics. The time-energy/frequency Fourier–Laplace transformation and the use of projectors focus on the variables of interest. The line profiles and dynamics in quantum mechanics are treated on the same footing. The long macroscopic times in statistical physics are derived from short microscopic times by means of hierarchies of effective Liouvillians and perturbation theory in the complex plane. The theory is illustrated on solvable models of quasi–continua and continua related to fluctuations and dissipation and on a model of kinetics of a chemical reaction implying a short-lived (resonance) transition state.

1. INTRODUCTION

Unstable states and resonances are ubiquitous in nature. Their timescales vary in a huge range from a few femtoseconds for molecular excited states, over seconds in our world, to millions of years for the solar system stability. The present study is devoted to resonances in molecules. Within this domain the characteristic times vary typically from femtoseconds to seconds. We focus on the dynamical and spectroscopic properties of typical quantum irreversible processes. Another aspect of this study is understanding the pathway from the microscopic to the macroscopic world, the traditional subject of statistical physics. From a mathematical viewpoint the irrelevant degrees of freedom are described in terms of discrete and continuous spectra. With the aim to provide generic results, we use a unique theoretical scheme based on the Fourier–Laplace transformation and projectors. We advocate the advantages to work with the variable energy extended in the complex plane instead of solving directly the Schrödinger equation with the vari-able time. The theory benefits in this way from the "rigidity" properties of analytic functions, in particular, from analytical continuation. In addition, the Fourier–Laplace transform in quantum mechanics establishes a direct link between the dynamics and the spectroscopies. The systematic use of projectors focuses on the observables of interest and on the derivation of their effective interactions. There is some freedom in the choice of these observables which may be, however, crucial and depends on the relevant timescales. For example, the chemical kinetics can be investigated by either considering or excluding the transition states: the choice depends on the characteristic times of the experiment.

Since the field investigated in this review is broad, it is difficult to attribute a precise definition to the resonances, quasi-bound states, unstable states, etc. We have in mind that the terms unstable states and resonances belong to the general scientific and technical vocabulary. Narrow and broad reso-nances are found in electricity, mechanics, as well as in the spectroscopies where they are associated with the narrow and broad profiles (bumps). On the other side, the terms bound states and quasi-bound states will be used in

their usual meaning in quantum mechanics. We will not discuss the mathematical properties of the wavefunctions of the quasi-bound states and of the continua. Regarding the differences between resonances, quasi-bound states and the mathematical aspects of the theory, the reader is advised to read the proceedings of the Uppsala Resonance Workshop in 1987 [1, 2]. These two references, which represent the state of the art in the 1980s, focus on the spectral theories of resonances, whereas our review is mainly centered on Green functions.

To follow the scale of complexity, the review is divided into three parts. The first two parts deal with the key concept of effective Hamiltonians which describe the dynamical and spectroscopic properties of interfering resonances (Section 2) and resonant scattering (Section 3). The third part, Section 4, is devoted to the resolution of the Liouville equation and to the introduction of the concept of effective Liouvillian which generalizes the concept of effective Hamiltonian. The link between the theory of quantum resonances and statistical physics and thermodynamics is thus established. Throughout this work we have tried to keep a balance between the theory and the examples based on simple solvable models.

2. QUANTUM RESONANCES

2.1. Theory

The dynamics of a system described by the Hamiltonian H is characterized by the evolution operator

$$U(t) = e^{-iHt/\hbar}. \tag{1}$$

Instead of considering $U(t)$ it is useful to investigate its Fourier–Laplace transform, the resolvent or Green operator

$$G[z] = \frac{1}{z - H}. \tag{2}$$

z is the energy extended in the complex plane. The operator $U(t)$ is recovered by the inverse Laplace transformation (see Appendix A). If we are interested in the dynamics of a small number of n quasi-bound states (resonances) there is too much information in $G[z]$ and we project the Green function into the *inner space* of these states. The partition technique (see appendix B and Chap. 4 of Ref. [3]) provides

$$\frac{1}{z - H}P = \Omega(z)\frac{P}{z - H^{\text{eff}}(z)}; \quad \Omega(z) = P + \frac{Q}{z - H}HP; \quad Q = 1 - P. \tag{3}$$

P projects into the inner space of n unstable quasi-bound states which are either true observable resonances or wave packets in the continuum (decay channels) taking a significant part in the dynamics. These latter may be either strongly or weakly coupled to the resonances. We shall treat in the same way the resonances and the quasi-bound states of interest and hence we call equally "resonance" or "quasi-bound state" any state belonging to the inner space. $Q = 1 - P$ projects onto the complementary *outer space*. The energy-dependent wave operator $\Omega(z)$ establishes a one-to-one correspondence between the n states belonging to the inner space and the states belonging to the outer space. $\Omega(z)$ extends the concept of wave operator previously defined for bound states [4, 5]. Let us transform the expression on the left of Eq. (3) into the basic equation

$$(z - H)\,\Omega(z) = P\,[z - H^{\text{eff}}(z)]. \tag{4}$$

This equation generalizes an inhomogeneous Schrödinger equation which was given, almost one half a century ago, by Löwdin in the framework of the partitioning technique (see Eq. (46) in Ref. [6] and Appendix B). Denoting by $\mathcal{E}(z)$, $\phi(z)$ an eigensolution of $H^{\text{eff}}(z)$ continued into the second Riemann sheet, and multiplying both sides of Eq. (4) (on the right) by $\phi(z)$ leads to

$$(z - H)\Omega(z)\phi(z) = [z - \mathcal{E}(z)]\,\phi(z). \tag{5}$$

At the poles of the resolvent, when $z = \mathcal{E}(z)$, Eq. (5) reduces to the Gamow–Siegert equation

$$H\psi(z) = z\,\psi(z); \quad \psi(z) = \Omega(z)\,\phi(z). \tag{6}$$

$\psi(z)$ describes a decreasing in time quasi-stationary state. Contrary to the Lippmann–Schwinger equation, which requires scattering boundary conditions, $\psi(z)$ does require outgoing boundary conditions commensurate with the Gammow–Siegert method. It is inherent in the complex technique and defined in a nonambiguous manner as a continued wavefunction in the second Riemann sheet.

To investigate the resonances, the useful part of the resolvent is projected into the inner space. Multiplying Eq. (3) on the left by P and using the intermediate normalization $P = P\Omega(z)$ results in

$$P\frac{1}{z - H}P = \frac{P}{z - H^{\text{eff}}(z)}. \tag{7}$$

Equation (7) shows the significance of the effective Hamiltonian which is directly related to the spectroscopic and dynamical observables, as lineshapes (see the end of this section) and transition probabilities. The effective Hamiltonian can be written as the sum of the projection of the exact Hamiltonian into the inner space and of the *energy-shift operator* [3, 7]:

$$H^{\text{eff}}(z) = PHP + R(z), \tag{8}$$

where

$$R(z) = PH\frac{Q}{z-H}HP. \tag{9}$$

Q projects into the complementary outer space, $P + Q = 1$. From Eqs. (8, 9 and 3) we get the compact expression

$$H^{\text{eff}}(z) = PH\Omega(z) \tag{10}$$

which shows that the wave operator $\Omega(z)$ allows to determine the effective Hamiltonian by a simple multiplication. The theory aims to produce effective Hamiltonians that depend as less as possible on the energy, similar to the almost frequency-independent resistances in the macroscopic world. This important statement is discussed in the last paragraph of this section. It will be shown that a one-dimensional effective Hamiltonian can describe the profile and the irreversible decay of an isolated resonance weakly coupled to a continuum (Section 2.2.1), whereas a two-dimensional effective Hamiltonian is required to understand damped Rabi oscillations [5, 7] (Section 2.2.2). We have investigated several models leading to z-independent effective Hamiltonians in Refs. [8–10]. More realistic models can be found in Refs. [11–18]. In all cases the inner space contains the states relevant to the dynamics at the various timescales of interest [7]. In the next two paragraphs, we describe two exactly solvable model Hamiltonians that are realistic enough to foresee the main dynamical and spectroscopic properties (lineshapes) of interacting resonances.

EFFECTIVE HAMILTONIANS FROM QUASI-CONTINUA TO CONTINUA

We recall a model considered in Ref. [9] that implies several resonances or quasi-bound states decaying into several channels. The model generalizes the original Fano model [19] and other models that discretize the continuum [7, 20, 21]. It is closely related to continuous models initially introduced in nuclear physics [22, 23]. The continuous models are efficient for the investigation of line profiles and irreversible evolutions; nevertheless, it is advantageous to begin from quasi-continua instead of continua. First, the mathematics is simpler, because one remains inside the Hilbert space of square-integrable functions; second, it is possible to determine exact expressions of the effective Hamiltonian; and finally, the properties of the continua are recovered when the energy spacings of the quasi-continua tend to zero [7].

The model describes n quasi-bound states interacting with m quasi-continua. The quasi-bound states $|i\rangle; (i = 1, 2, \ldots, n)$ span the inner space whose projector is P. The orthonormalized states $|ka\rangle; (a = 1, 2, \ldots, m)$ span the complementary outer space whose projector is

Resonances				Decay channel a				Decay channel b			
E_1^0	H_{12}	$\cdots$	H_{1n}	v_1^a	v_1^a	v_1^a	$\cdots$	v_1^b	v_1^b	v_1^b	$\cdots$
H_{21}	E_2^0	$\cdots$	H_{2n}	v_2^a	v_2^a	v_2^a	$\cdots$	v_2^b	v_2^b	v_2^b	$\cdots$
.	.	$\cdots$	.	.	.	.	$\cdots$	.	.	.	$\cdots$
H_{n1}	H_{n2}	$\cdots$	E_n^0	v_n^a	v_n^a	v_n^a	$\cdots$	v_n^b	v_n^b	v_n^b	$\cdots$
v_1^a	v_2^a	$\cdots$	v_n^a	0							
v_1^a	v_2^a	$\cdots$	v_n^a		$-\delta_a$						
v_1^a	v_2^a	$\cdots$	v_n^a			$+\delta_a$					
$\triangleright$	$\triangleright$	$\cdots$	$\triangleright$				$\ddots$				
v_1^b	v_2^b	$\cdots$	v_n^b					0			
v_1^b	v_2^b	$\cdots$	v_n^b						$-\delta_b$		
v_1^b	v_2^b	$\cdots$	v_n^b							$+\delta_b$	
.	.	$\cdots$	.								$\ddots$

Figure 1.1   Matrix representation of the model Hamiltonian in the basis of n quasi-bound states (inner space) and of the states belonging to the decay channels $a,b,\dots$ (outer space).

$$Q = \sum_{k,a} |ka\rangle\langle ka|; \quad \langle ka|k'b\rangle = \delta_{kk'}\delta_{ab};$$

$$k,k' = 0, \pm 1, \pm 2, \dots \quad \text{and} \quad a, b = 1, 2, \dots, m.$$

The matrix representation of H in the basis of $|i\rangle; (i = 1, 2, \dots, n)$ (inner space) and of $|ka\rangle$ (outer space) is given in Figure 1.1. Inside the inner space, the off-diagonal matrix elements are denoted $H_{ij} = \langle i|H|j\rangle$ and the diagonal terms $E_i^0 = \langle i|H|i\rangle$. The indexes $a,b,\cdots$ characterize the quasi-continua (decay channels). The matrix representation of the Hamiltonian is diagonal in the outer space. The energy of the state $|ka\rangle$ is $k\delta_a$. The energies of the quasi-continua extend from $-\infty$ to $+\infty$ $(k = 0,\pm 1,\pm 2,\dots)$; δ_a is the energy spacing between the neighboring levels in channel a. The couplings between the inner space and the quasi-continua $v_i^a = \langle ka|H|i\rangle; (i = 1, 2, \dots, n; a = 1, 2, \dots, m)$ do not depend on the index k. Because the matrix representation of the model Hamiltonian is diagonal in the outer space, the effective Hamiltonian (10) can be easily calculated. The use of

$$\sum_{k \in \mathcal{Z}} (z - k)^{-1} = \frac{\pi}{\tan \pi z}; \quad \mathcal{Z} = \{0, \pm 1, \pm 2, \dots\}$$

leads to the exact effective Hamiltonian

$$H^{\text{eff}}(z) = \hat{H} - \frac{\text{i}}{2}\,\hat{\Gamma}(z). \tag{11}$$

$\hat{H} \equiv PHP$ is the projection of H into the inner space. $\hat{\Gamma}(z)$ is expressed as a sum over the channels:

$$\hat{\Gamma}(z) = \sum_{a=1}^{m} \hat{\Gamma}_a(z); \quad \hat{\Gamma}_a(z) = 2\pi |V_a\rangle\langle V_a| \times \text{i} \cot\left(\frac{\pi z}{\delta_a}\right). \tag{12}$$

$\hat{\Gamma}_a(z)$ characterizes the dissipation in channel a and $|V_a\rangle$ couples the inner to the outer space:

$$|V_a\rangle = \sum_{i=1}^{n} V_i^a |i\rangle; \qquad V_i^a = \frac{1}{\sqrt{\delta_a}}\, v_i^a. \tag{13}$$

If all energy spacings δ_a are equal to δ, Eq. (12) becomes

$$\hat{\Gamma}(z) = \hat{\Gamma} \times \text{i} \cot\left(\frac{\pi z}{\delta}\right); \quad \hat{\Gamma} = \sum_{a=1}^{m} \hat{\Gamma}_a; \quad \hat{\Gamma}_a = 2\pi |V_a\rangle\langle V_a|. \tag{14}$$

Using only the first term of the Fourier series

$$\text{i} \cot\left(\frac{\pi z}{\delta}\right) = 1 + 2\sum_{k=1}^{\infty} \exp\left(\text{i}\,\frac{2\pi k z}{\delta}\right), \tag{15}$$

expression (11) becomes

$$H^{\text{eff}} = \hat{H} - \frac{\text{i}}{2}\,\hat{\Gamma}, \tag{16}$$

where

$$\hat{H} = PHP; \quad \hat{\Gamma} = 2\pi \sum_{a=1}^{m} |V_a\rangle\langle V_a|.$$

The effective Hamiltonian (16) is energy-independent. It provides the exact dynamics for times shorter than $\tau = 2\pi\hbar/\delta$ [5]. Since τ can be arbitrarily increased by decreasing δ, the effective Hamiltonian (16) is considered as exact for true continua.

EFFECTIVE HAMILTONIAN FROM THE METHOD OF MOMENTS
The method of moments, which is currently used in quantum mechanics for calculating densities of states (see, e.g., Refs. [3, 24]), is applied to the dynamics. We aim to investigate the exact solution $\psi(t) = \exp\left(-\text{i} H t/\hbar\right)|\phi\rangle$ that can be expanded as

$$|\psi(t)\rangle = |\phi\rangle - \text{i}\frac{t}{\hbar}H|\phi\rangle - \frac{t^2}{2\hbar^2}H^2|\phi\rangle \cdots \tag{17}$$

For short times the dynamics is supported by the states $H^k|\phi\rangle$; $(k = 0, 1, \ldots)$ which generate the basis of the method of moments [3]. The Gram–Schmidt procedure applied to $|\phi\rangle$, $H|\phi\rangle$, $H^2|\phi\rangle,\ldots$ generates the orthonormal basis $|i\rangle$; $(i = 1, 2, \cdots)$. One should note that there is a problem of defining operator ranges and domains for actual moments and that this procedure may be highly singular [25]. It is possible to remedy this problem by eliminating, at each step, the singular functions that appear in the method of moments. The first three matrix representations are

$$H^{\text{eff}}(z) = E_1 + R_1(z) \tag{18}$$

$$\mathbf{H}^{\text{eff}}(z) = \left[\begin{array}{cc} E_1 & \Delta E \\ \Delta E & E_2 + R_2(z) \end{array} \right] \tag{19}$$

$$\mathbf{H}^{\text{eff}}(z) = \left[\begin{array}{ccc} E_1 & \Delta E & 0 \\ \Delta E & E_2 & H_{23} \\ 0 & H_{23} & E_3 + R_3(z) \end{array} \right], \tag{20}$$

where $E_i = \langle i|H|i\rangle$, $R_i(z) = \langle i|R(z)|i\rangle$, and $H_{ij} = \langle i|H|j\rangle$. An advantage of using an orthonormal basis is that the matrix elements have a well-defined meaning: The diagonal elements correspond to energies and the off-diagonal elements to energy dispersions. For example, $\Delta E = [\,\langle 1|H^2|1\rangle - \langle 1|H|1\rangle^2\,]^{\frac{1}{2}}$ represents the fluctuation of the energy in the initial state. The matrix of the level-shift operator is diagonal. Although the determination of the $R_i(z)$ or similar quantities for actual systems is not trivial [26], the applications presented in Sections 2.2 and 2.3 show that simple matrix representations, such as Eqs. (19 and 20), can provide general results in many domains ranging from the line profiles (Fano profiles) to the fundamentals of fluctuation and dissipation. The various approximations of $R(z)$ lead to approximate resolvents which have the structure of Padé approximants and benefit of their analytical properties [3] as it is shown in Section 2.2.4.

LINESHAPES FROM EFFECTIVE HAMILTONIANS

The link between the effective Hamiltonians and the spectroscopies lies along the real axis in the complex plane. Using the notation $z = E + i\epsilon$ and separating the real and imaginary part of the resolvent give

$$\langle\phi|\frac{1}{E - H + i\epsilon}|\phi\rangle = \langle\phi|\mathcal{P}\frac{1}{E - H}|\phi\rangle - i\pi\,\langle\phi|\delta(E - H)|\phi\rangle, \tag{21}$$

where $\mathcal{P}$ is the Cauchy principal part and $\delta(E - H)$ is the Dirac function. The lineshape $I(E)$ is defined as the density of the quasi-bound state ϕ at the energy E

$$I(E) = \langle \phi | \delta(E - H)] \phi \rangle; \qquad \int_{-\infty}^{+\infty} I(E) \mathrm{d}E = 1. \qquad (22)$$

The lineshapes are not directly observable but they resemble the measurable line profiles (see Section 3 and Ref. [27] p. 184). In order to relate the lineshapes to the effective Hamiltonian we separate the Hermitian and non-Hermitian part of $H^{\mathrm{eff}}(z)$

$$H^{\mathrm{eff}}(E + \mathrm{i}\epsilon) = \hat{H} + \hat{\Delta}(E) - \mathrm{i}\,\frac{\hat{\Gamma}(E)}{2}. \qquad (23)$$

$\hat{\Delta}(E)$ and $\hat{\Gamma}(E)$ are Hilbert transform from one another [7]. Since the lifetime of the quasi-bound state ϕ is much longer than the lifetime of the relevant part of the continuum $QH|\phi\rangle$, the Hermitian operators $\hat{\Delta}(E)$ and $\hat{\Gamma}(E)$ are smooth functions within the energy range of interest. It results that the energy dependence of the level-shift operator can be neglected and that the effective Hamiltonian becomes energy independent

$$H^{\mathrm{eff}} = \hat{H} - \mathrm{i}\,\frac{\hat{\Gamma}}{2}. \qquad (24)$$

This energy independence appears as well in the previous model Hamiltonian when the quasi-continuum tends to a continuum (16). The Hermitian part of the level-shift operator is often negligible and was neglected in Eq. (24). Using Eq. (7) the lineshape can be expressed in terms of the poles of the Green function (see Section 2.2.2)

$$I(E) = -\frac{1}{\pi}\mathrm{Im}\langle \phi | \frac{1}{E - H^{\mathrm{eff}}} | \phi \rangle. \qquad (25)$$

$I(E)$ can be easily obtained from Eq. (25) by diagonalization of a small-dimensional non-Hermitian effective Hamiltonian. This is not true if the effective Hamiltonian has the form of a Jordan block (see p. 475 in Ref. [2]). A simple example of Jordan structure is the matrix representation (30) in Section 2.2.2 when $\Gamma_c = 4\Delta$. In this nonphysical case the two eigenvalues coalesce at the value $-2\mathrm{i}\Delta$.

In the following sections we will apply the theory to a resonance decaying into a continuum (Section 2.2) and to several resonances decaying into one or several continua (Section 2.3). The physics is described and understood by means of energy-independent effective Hamiltonians (16) and from the method of moments. In Section 2.2 the use of a unique two-dimensional matrix representation ($n = 2$) of the effective Hamiltonian will allow us to produce the most basic Breit–Wigner and Fano profiles as well as an elementary formulation of the fluctuation–dissipation theorem. In Section 2.3 more elaborate matrix representations ($n = 3$) will be used to investigate

several interfering resonances thus providing an elementary interpretation of the dips and peaks of experimental spectra. Finally, we investigate the dynamics of two vibrational resonances in I_2Ne. It will be shown on this actual system how it is possible to pass from a calculation along the real-energy axis (close-coupling method) to a two-dimensional non-Hermitian effective Hamiltonian which contains the relevant information concerning the dynamics.

## 2.2. One isolated resonance

2.2.1. Breit–Wigner profile
The infinite matrix representation of the Fano model [7, 19, 28] can be written in the form

$$
\begin{pmatrix}
0 & v & v & v & \cdots \\
v & 0 & 0 & 0 & \\
v & 0 & -\delta & 0 & \\
v & 0 & 0 & +\delta & \\
\vdots & & & & \ddots
\end{pmatrix}.
\tag{26}
$$

The energy of the discrete state ϕ coupled to the quasi-continuum is taken as the origin of the energies. δ is the constant energy difference between the levels of the quasi-continuum and v measures the interaction between the discrete state and the quasi-continuum states $|k\rangle$, $k = 0, \pm 1, \pm 2, \ldots$. The above notation as well as the exact solution of this model can be found in the complement C_I of Ref. [7].

Figure 1.2 illustrates the resonance $|\phi\rangle$ decaying into a quasi-continuum (left side) and into a true continuum (right side). The black rectangle is the useful part of the continuum implied in the dynamics. It corresponds to the wavefunction $H|\phi\rangle$ (a doorway state in spectroscopy), which is the second term in the method of moments (see Eq. (17)). The physical results are obtained at the limit $\delta \to 0$ while v^2/δ remains constant. The transition rate Γ to the continuum is equal to

$$
\Gamma = \frac{2\pi\, v^2}{\delta}.
\tag{27}
$$
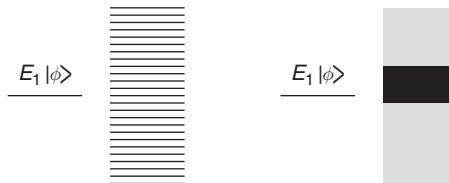
Figure 1.2   From a quasi-continuum to a continuum.
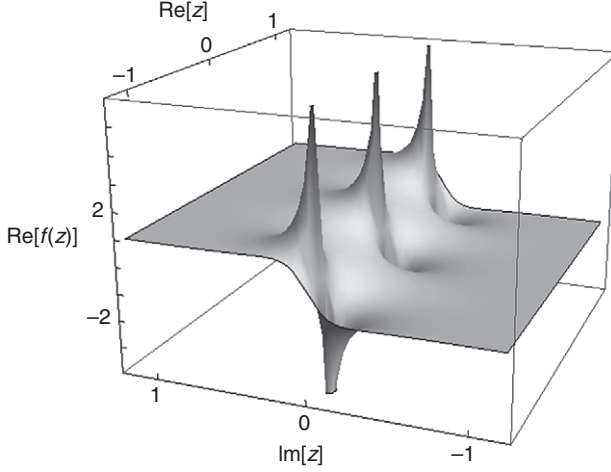
Figure 1.3   Representation of the real part of $f(z) = \mathrm{i}\cot(\pi z/\delta)$ as a function of z for $\delta = 1$. This quantity tends to 1 when z tends to $\mathrm{i}\infty$; it tends to ∞ for the real values $z = k\delta;\ (k = 0, \pm 1, \pm 2, \ldots)$.

The time evaluation depends on the strength of the coupling δ/v as discussed in Ref. [5]. We recall here the irreversible dynamics corresponding to a weak coupling ($\delta/v \ll 1$). The dynamics is projected into the one-dimensional inner space spanned by the initial state ϕ. For times $t \ll 2\pi\hbar/\delta$ the initial state decays into the quasi-continuum, whereas for larger times, recurrences may appear. $H^{\mathrm{eff}}(z)$ is represented by the unique term

$$E(z) = -\mathrm{i}\frac{\Gamma\hbar}{2}\cdot\mathrm{i}\cot\left(\frac{\pi z}{\delta}\right). \tag{28}$$

The real part of $\mathrm{i}\cot(\pi z/\delta)$ is shown in Figure 1.3.

It is quite remarkable that all information needed to compute the survival amplitude $\langle\phi|\psi(t)\rangle$ (autocorrelation function) is contained in $E(z)$ as given by Eq. (28). This information is highly singular near the real-energy axis, where distributions appear for the values $k\delta,\ (k = 0, \pm 1, \pm 2, \ldots)$. In order to obtain the first terms of the temporal evolution of the autocorrelation function from the initial time $t = 0$, $E(z)$ is expanded in Fourier series. Assuming $\hbar = 1$,

$$E(z) = -\mathrm{i}\frac{\Gamma}{2} - \mathrm{i}\Gamma\sum_{k=1}^{\infty}\exp\left(\frac{2\pi\mathrm{i}kz}{\delta}\right). \tag{29}$$

The inverse Fourier–Laplace transformation of $1/(z - E(z))$ provides the autocorrelation function (survival probability) represented in Figure 1.4. The
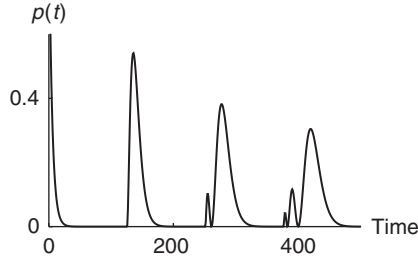
Figure 1.4   Irreversible survival probability $p(t) = |\langle\phi|\psi(t)\rangle|^2$ as a function of time. Recurrences occur at times $t_k = 2\pi k\hbar/\delta$; $k = 1,2,\ldots$ ($\delta = 1$, arbitrary units).

initial exponential decay of the resonance arising from the term $-i\Gamma\hbar/2$ in Eq. (29) is followed by recurrences at the times $t_k = 2\pi k\hbar/\delta$ for $k = 1, 2, 3,\ldots$. As expected the recurrence times tend to infinity when the spacing δ tends to zero and the quasi-continuum becomes a true continuum. The above analysis is illustrative for at least three reasons:

- It provides a simple example of nonexponential decay of a resonance a still active subject of research [29, 30].
- It opens the way to a deeper understanding of the physics of quasi-continua and continua.
- It could clarify the theoretical status of the absorbing potentials used in actual calculations to avoid spurious recurrences caused by the basis set incompleteness [11, 12, 31].

2.2.2. Fluctuation–dissipation–oscillations

In this example the method of moments is applied to a simple model of a resonance weakly or strongly coupled to the continuum [32]. We use the two-dimensional matrix representation (19). Under the assumption that there are no other resonances embedded in the continuum, it is justified to neglect the dependence of $R_2(z)$ on z because the width of the resonance, Γ, is much smaller than the width of the relevant continuum, Γ_c, within the useful range of energy (see complement $C_{III}.5$ in Ref. [7]). In more physical terms the lifetime of the resonance is much longer that the microscopic relaxation time. The examples given in the two following sections: (i) Fano profiles and (ii) hydrogen atom in an electric field, illustrate how the macroscopic times can be derived from usually nonobservable much shorter microscopic times.

Separating the real and imaginary parts of $R_2 \simeq \Delta_c - i\frac{\Gamma_c}{2}$ allows to transform Eq. (19) into

$$\mathbf{H}^{\text{eff}} = \begin{bmatrix} E_1 & \Delta E \\ \Delta E & E_c - \mathrm{i}\frac{\Gamma_c}{2} \end{bmatrix} \qquad |1\rangle \underline{\quad E_1 \quad} \cdots \cdots \quad \blacksquare \quad E_c, \Gamma_c \tag{30}$$

E_c and Γ_c are the energy and the width of the useful part of the continuum (doorway state) [22, 33]. The two-dimensional non-Hermitian effective Hamiltonian (30) is the simplest matrix representation linking the microscopic level characterized by the complex energy $E_c - \mathrm{i}\Gamma_c/2$ to the macroscopic level of interest (the resonance). In Eq. (30), the energy of the resonance E_1 is real. We will see below that if the resonance is weakly coupled to the microscopic level ($\Delta E \ll \Gamma_c$), the complex part of energy can be uncovered by perturbation in the complex plane (see Eq. (38)). In addition, the information contained in Eq. (30) is sufficient to derive the basic Breit–Wigner and Fano profiles. It means that the effective Hamiltonian (30) is representative of the power of non-Hermitian representations for computing and understanding the physics of quantum unstable states.

The spectral decomposition of the effective Hamiltonian reads

$$H^{\text{eff}} = |\phi_1\rangle\langle\tilde{\phi}_1|\,\mathcal{E}_1 + |\phi_2\rangle\langle\tilde{\phi}_2|\,\mathcal{E}_2. \tag{31}$$

The eigenenergies $\mathcal{E}_1$ and $\mathcal{E}_2$ are complex; $\langle\tilde{\phi}_1|$ and $\langle\tilde{\phi}_2|$ are the duals of $|\phi_1\rangle$ and $|\phi_2\rangle$ [8]. The inverse Fourier–Laplace transformation (Appendix A) and the Cauchy theorem lead to the time-dependent wavefunction

$$\phi(t) = \tilde{c}_1 \exp\left(-\mathrm{i}\frac{\mathcal{E}_1}{\hbar}t\right)|\phi_1\rangle + \tilde{c}_2 \exp\left(-\mathrm{i}\frac{\mathcal{E}_2}{\hbar}t\right)|\phi_2\rangle, \tag{32}$$

where

$$\tilde{c}_1 = \langle\tilde{\phi}_1|\phi\rangle; \qquad \tilde{c}_2 = \langle\tilde{\phi}_2|\phi\rangle. \tag{33}$$

From Eq. (32) the survival probability

$$P(t) = |\langle\phi|\phi(t)\rangle|^2 \tag{34}$$

and the lineshape

$$I(E) = -\frac{1}{\pi}\,\mathrm{Im}\left(\frac{f_1}{E - \mathcal{E}_1} + \frac{f_2}{E - \mathcal{E}_2}\right), \qquad f_i = \langle\phi|\phi_i\rangle\langle\tilde{\phi}_i|\phi\rangle; (i = 1, 2) \tag{35}$$
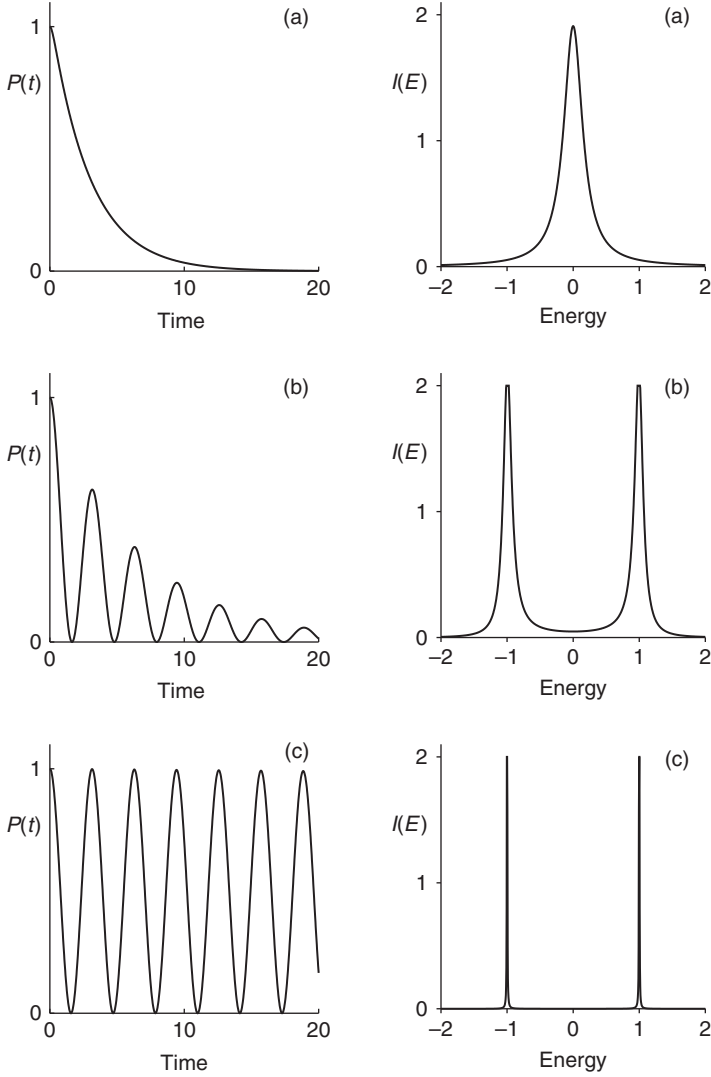
Figure 1.5 Dissipation and oscillations: From weak to strong coupling. The effective Hamiltonian is given by Eq. (30). The dynamics (34) (on the left) and the lineshapes (35) (on the right) of a system prepared in the initial state |1⟩. (a) weak coupling ($\Gamma_c = 12$), (b) intermediate coupling ($\Gamma_c = 0.3$), (c) strong coupling ($\Gamma_c = 0.001$) (arbitrary units).

can be obtained. The capability of the model was illustrated in Ref. [32]. The survival probabilities with the associated lineshapes presented in Figure 1.5 (Fig. 1. in Ref. [32]) show why the dynamics changes gradually from an irreversible exponential decay (a) to Rabi oscillations (c) with decreasing Γ_c. The

results in Figure 1.5 were obtained from the exact diagonalization of the effective Hamiltonian; however, if we proceed by perturbation in the complex plane, the relationship between fluctuation and dissipation is revealed. Assuming that the diagonal terms are dominant in Eq. (30), perturbation theory provides the complex eigenenergies

$$\mathcal{E}_1 = E_1 + \frac{(\Delta E)^2}{E_1 - E_c + i\frac{\Gamma_c}{2}} + \cdots ;$$

$$\mathcal{E}_2 = E_c - i\frac{\Gamma_c}{2} + \frac{(\Delta E)^2}{E_c - E_1 - i\frac{\Gamma_c}{2}} + \cdots \tag{36}$$

In addition, if we assume that $|E_c - E_1| \ll \Gamma_c$, Eq. (36) reduces to

$$\mathcal{E}_1 = E_1 - i\frac{\Gamma}{2} + \cdots ,$$

$$\mathcal{E}_2 = E_c - i\frac{\Gamma_c}{2} + i\frac{\Gamma}{2} + \cdots , \tag{37}$$

where

$$\Gamma = 4\frac{(\Delta E)^2}{\Gamma_c}. \tag{38}$$

Equation (38) provides a simple form of the *fluctuation–dissipation* theorem that relates the fluctuations to dissipation. Here the fluctuation in energy ΔE is related to the dissipation coefficient Γ appearing in the exponential decay of $P(t) \simeq \exp\left(-\frac{\Gamma}{\hbar}t\right)$. The same expression (38) was derived by Cohen-Tannoudji et al. from a "coarse-grained" expression of the rate of variation of the density matrix (operator) describing a statistical mixture of states (see §D in Chapter IV of Ref. [7]). Because the expression (38) was derived by perturbation, the conditions of validity of perturbation theory must be satisfied. The eigenfunctions associated with $\mathcal{E}_1$ and $\mathcal{E}_2$ are

$$|\phi_1\rangle = |1\rangle + 2i\frac{\Delta E}{\Gamma_c}|2\rangle + \cdots ,$$

$$|\phi_2\rangle = |2\rangle - 2i\frac{\Delta E}{\Gamma_c}|1\rangle + \cdots . \tag{39}$$

The validity of this expansion requires

$$\Delta E \ll \Gamma_c. \tag{40}$$

Let us define two correlation and dissipation times by

$$\tau_c = \frac{\hbar}{\Gamma_c}; \quad \tau = \frac{\hbar}{\Gamma}. \tag{41}$$

Then condition (40) can be transformed into

$$\tau_c \ll \tau, \tag{42}$$

which means that the microscopic correlation time must be much shorter than the macroscopic correlation time. Condition (42) can also be transformed into

$$\Delta E \cdot \tau \gg \frac{\hbar}{2}, \tag{43}$$

which is compatible with the energy–time uncertainty relation. To conclude this section we summarize:

- A simple expression of the fluctuation–dissipation theorem was established and its range of validity was determined within the standard perturbation theory.
- We anticipate that the results derived from wavefunctions and effective Hamiltonians will be generalized in Section 4 to density matrices and effective Liouvillians if the time evolution starts out of a mixed equilibrium state.
- We stress again the advantage to use perturbation theory in the complex plane (energy or frequency) instead of the usual time-dependent perturbation theory.

2.2.3. Fano profiles

The derivation of the fluctuation–dissipation theorem (38) was based on the simple model Hamiltonian (30). This effective Hamiltonian is employed again to investigate asymmetric profiles in spectroscopy implying quantum interferences with the continuum.

Instead of using perturbation theory we shall determine the exact Green function associated with the initial state

$$|\phi\rangle = \cos\theta \, |1\rangle + \sin\theta \, |2\rangle. \tag{44}$$

The probabilities of exciting simultaneously the resonance and the continuum at the initial time are $\cos^2\theta$ and $\sin^2\theta$, respectively.

Assuming $E_1 = E_c = 0$, the direct calculation of the Green function (22) gives

$$G(E) = \frac{E + \Delta E \sin 2\theta + i\frac{\Gamma_c}{2} \cos^2\theta}{E\left(E + i\frac{\Gamma_c}{2}\right) - (\Delta E)^2} \tag{45}$$

and the intensity (line profile)

$$I(E) = \left| \frac{E\sin\theta + \Delta E \cos\theta}{E\left(E + i\frac{\Gamma_c}{2}\right) - (\Delta E)^2} \right|^2 \frac{\Gamma_c}{2\pi}. \tag{46}$$

It allows the direct determination of the Fano q parameter (see Eq. (20) in Ref. [34]):

$$q = 2 \frac{\Delta E}{\Gamma} \cdot \cot \theta. \tag{47}$$

The expression (47) is exact for the z-independent effective Hamiltonian (30). It is the product of two factors: the ratio of the fluctuation in energy of the resonance, ΔE, to its width, Γ, and the ratio of the probability amplitudes to excite the resonance ($\cos \theta$) or the continuum ($\sin \theta$) at the initial time. The parameter q characterizes the asymmetry of the profile (see Eq. (21) in Ref. [28]). A detailed description of our approach to Fano profiles is given in Refs. [8, 34]. The formula (47) has a large range of validity whatever might be the type of spectroscopy (dipolar electric, magnetic, etc.). Figure 1.6 represents the survival probabilities and the lineshapes as a function of the degree of excitation of the continuum at the initial state. In case (a) only the resonance state $|1\rangle$ is excited which produces an almost exponential decay and a Breit–Wigner profile. Cases (b) and (c) display nonexponential decays and typical Fano profiles resulting from interferences between $|1\rangle$ and the relevant part $|2\rangle$ of the continuum (doorway state).

2.2.4. Hydrogen atom in an electric field

We have shown in the previous sections that an exactly solvable model can provide generic results concerning line profiles and dynamics. The physics was discussed in terms of resonances and effective Hamiltonians. These concepts are also of fundamental importance for real systems. Here we recall the simplest one: a hydrogen atom in its ground state exposed to a static electric field described in Refs. [10, 35].

As soon as the atom is subjected to the field, the bound state 1s becomes a resonance. There is an extended literature devoted to the determination of the energies and the widths of resonances in the hydrogen atom. Among the methods which require complex parameters and complex solutions it is worth mentioning the Weyl's theory, originating from 1910, which interprets the resonance in terms of poles in the complex plane. References to the Weyl's theory and accurate results can be found in Ref. [36]; see also the discussion in Ref. [1], page 779.

For weak fields of amplitude $\mathcal{E} \ll 0.1$ a.u., ionization is mainly due to the tunneling of the electron through the Coulomb barrier and the survival probability $P(t)$ of the ground state follows approximately an exponential law. The order of magnitude of the width Γ of the resonance is given approximately by the quasi-classic theory [37]:

$$P(t) = \exp\left(-\frac{\Gamma t}{\hbar}\right), \qquad \Gamma = \frac{4}{\mathcal{E}} \exp\left(-\frac{2}{3\mathcal{E}}\right). \tag{48}$$
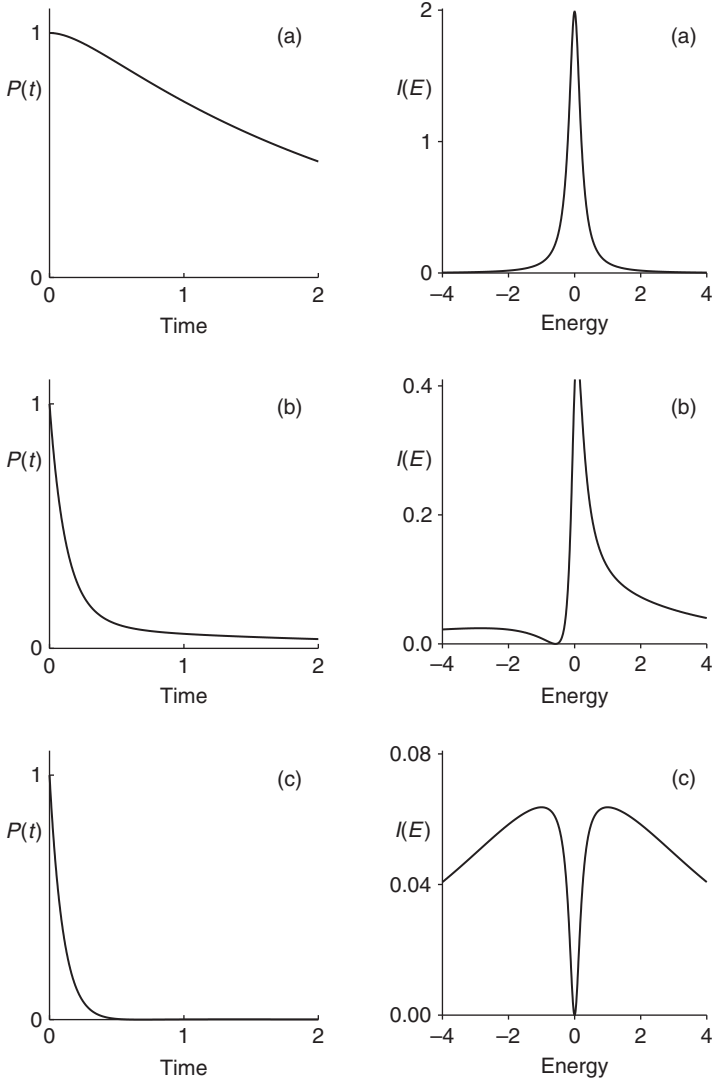
Figure 1.6 Fano profiles proceeding from the effective Hamiltonian (30). The survival probabilities $P(t)$ (34) (on the left) and the lineshapes $I(E)$ (35) (on the right) are represented for the initial state $|\phi\rangle = \cos\theta\,|1\rangle + \sin\theta\,|2\rangle$. (a) $\theta = 0$, $q = \infty$, (b) $\theta = \frac{\pi}{3}$, $q = \frac{5}{\sqrt{3}}$, (c) $\theta = \frac{\pi}{2}$, $q = 0$ (arbitrary units).

For strong field, $\mathcal{E} > 0.1$ a.u., the decay of the ground state does not follow an exponential law [38–41]. We provided in Ref. [35] an accurate description of the nonexponential decay of the H atom, initially in the 1s state, at any time t and especially at $t \gg 10$ a.u. (long-time dynamics). At short

time, $t \ll 10$ a.u., the states mainly implied in the dynamics are the ground state $|1\rangle = 1s$ and the doorway state $|2\rangle = z_\times 1s = r\cos\theta_\times 1s$ of symmetry p ($l = 1$), which provides the main contribution to the dipolar polarization of the atom ($\alpha = 4$ a.u.; the exact value is $\alpha = 4.5$ a.u.). In the basis of the two states $|1\rangle$ and $|2\rangle$, the projector onto the model space is $P = |1\rangle\langle 1| + |2\rangle\langle 2|$ and the energy-dependent effective Hamiltonian can be written in the form

$$\mathbf{H}^{\mathrm{eff}}(z) = \begin{bmatrix} -1/2 & \mathcal{E} \\ \mathcal{E} & R(z) \end{bmatrix}; \qquad R(z) = \langle 2|H\frac{Q}{z-H}H|2\rangle. \tag{49}$$

$\mathcal{E}$ is the amplitude of the electric field (in a.u.). $R(z)$ is the energy-shift (9) and $Q = 1 - P$ is the projector onto the complementary space. The inversion of $\mathbf{H}^{\mathrm{eff}}(z)$ provides the exact expression of the Green function corresponding to the initial state $1s$:

$$G(z) = \frac{1}{z - E(z)}; \qquad E(z) = -\frac{1}{2} + \frac{\mathcal{E}^2}{z - R(z)}. \tag{50}$$

The level-shift is approximated by the least-square fit

$$R(z) = \sum_{k=1}^{3} \frac{c_k}{z - e_k}, \tag{51}$$

where c_k and e_k are real and complex constants [10]. Finally, the Green function is written in the form of Padé approximant

$$G(z) = \frac{P(z)}{Q(z)}, \tag{52}$$

where $Q(z)$ and $P(z)$ are fifth- and fourth-order polynomials, respectively. The Green function along the real-energy axis can be written as

$$G(E) = \sum_{k=1}^{5} \frac{f_k}{E - \mathcal{E}_k}; \qquad \sum_{k=1}^{5} f_k = 1. \tag{53}$$

The complex energies $\mathcal{E}_k$ ($k = 1,2,\ldots,5$) are the roots of the polynomial $Q(z)$ and the f_k's are generalized oscillator strengths. The inverse Fourier–Laplace transformation provides the survival probability $P(t)$ of the initial state $1s$

$$P(t) = \left| \sum_{k=1}^{5} f_k \exp\left(-i\frac{\mathcal{E}_k}{\hbar}t\right) \right|^2 \tag{54}$$
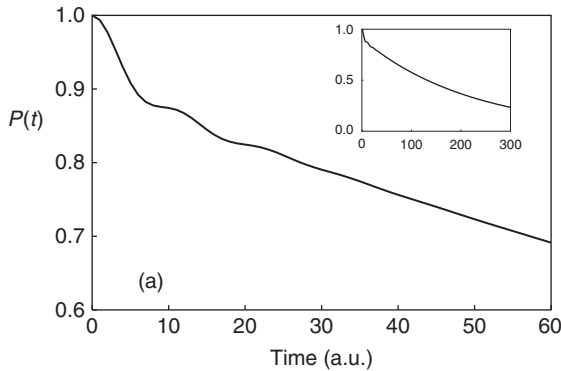
Figure 1.7   Decay of the resonance 1s of the hydrogen atom. The atom is subjected at $t = 0$ to a static electric field of amplitude $\mathcal{E} = 0.08$ a.u..

and the probability of ionization $1 - P(t)$. Equations (53 and 54) generalize Eqs. (35 and 34), which are valid for an energy-independent effective Hamiltonian, since in Eqs. (53 and 54) the summation is up to five instead of $n = 2$ the dimension of the inner space. Here the dependence on the energy is in $R(z)$. Figure 1.7 shows the survival probability of the ground state of H as a function of time. The agreement between Figure 1.7 and the full-line curve in Fig. 1 of Ref. [40] is almost perfect. This is significant since the calculations were performed by different approaches: a complex scaled Hamiltonian [2] in Ref. [35] and a two-dimensional energy-dependent effective Hamiltonian Ref. [10]. The excellent agreement was also confirmed by recently developed Coulomb wavefunction discrete variable representation of Peng and Starace [39].

2.3. Several interfering resonances

It was shown in the previous section that modeling one resonance decaying into a unique continuum and a two-dimensional effective Hamiltonian, $n = 2$, led to the Breit–Wigner and Fano profiles. The model is justified for isolated resonances. When there are two or several states close in energy, the couplings between their amplitudes produce new interference patterns which are the fingerprints of the quantum world. Two model examples illustrate how higher dimensional matrix representation of effective Hamiltonian, typically $n = 3$, can interpret a large variety of spectroscopic profiles. The study of the dynamics of two vibrational resonances of the molecule I_2Ne [11] demonstrates how to extract from real *ab initio* calculations a small two-dimensional Hamiltonian containing the main information that explains the exponential and nonexponential decay of the two resonances.

2.3.1. q-Reversal effect

An illustrative application of the effective Hamiltonian approach is the interpretation of the q-reversal effect [42] as the interference of three quasi-bound states ($n = 3$) decaying into a unique continuum [9]. The two functions are true narrow resonances of widths Γ_1 and Γ_2. The third quasi-bound state with much shorter lifetime ($\Gamma_3 \gg \Gamma_1$ and $\Gamma_3 \gg \Gamma_2$) describes the relevant part of continuum and produces the large bumps (background) under the narrow resonances.

The three-dimensional inner space is spanned by the resonances $|1\rangle$ and $|2\rangle$ and by the quasi-bound state $|3\rangle$ describing the relevant part of the continuum. The matrix representation (lower part) of the effective Hamiltonian is written in the form

$$\mathbf{H}^{\text{eff}} = \begin{bmatrix} E_1^0 & \cdot & \cdot \\ H_{21} & E_2^0 & \cdot \\ H_{31} & H_{32} & E_3^0 \end{bmatrix} - \frac{i}{2} \begin{bmatrix} \Gamma_{11} & \cdot & \cdot \\ \sqrt{\Gamma_{22}\Gamma_{11}} & \Gamma_{22} & \cdot \\ \sqrt{\Gamma_{33}\Gamma_{11}} & \sqrt{\Gamma_{33}\Gamma_{22}} & \Gamma_{33} \end{bmatrix}. \tag{55}$$

E_i^0 ($i = 1,2,3$) are the zero-order energies of the quasi-bound states $|i\rangle$ of partial widths $\Gamma_{ii} = 2\pi V_i^2$, V_i's are the components of the coupling vector $|V_a\rangle$ (13). The index a was suppressed because there is only one decay channel. The V_i's are assumed to be real and positive. To excite selectively the resonances the initial states are chosen successively as

$$\begin{aligned} \phi_{++} &= c\,(\ \ \phi_1 + \phi_2) + \phi_3 \\ \phi_{+-} &= c\,(\ \ \phi_1 - \phi_2) + \phi_3 \\ \phi_{-+} &= c\,(- \phi_1 + \phi_2) + \phi_3 \\ \phi_{--} &= c\,(- \phi_1 - \phi_2) + \phi_3. \end{aligned} \tag{56}$$

ϕ_1, ϕ_2, and ϕ_3 are the eigenstates of H^{eff} and c is a constant. Figure 1.8 indicates clearly that the q-reversal effect described in Ref. [42] can be understood in terms of constructive and destructive interferences between the resonances and the continuum. The straightforward interpretation of the q-reversal effect in terms of resonances interfering with a short-lived state generalizes the description of Fano profiles resulting from interferences between a resonance and a quasi-bound state of much larger width [8].

2.3.2. Interference dips and peaks in spectra

Another interesting application of the effective Hamiltonian explains the origin of the dips and peaks in photabsorption spectra. The model of spectrum incorporates into the inner space the relevant states of the continuum weakly interacting with the resonances [43]. This can be done by considering more than one decay channel. Such extension was discussed in detail in Ref. [8] and we sketch here only the principal idea.
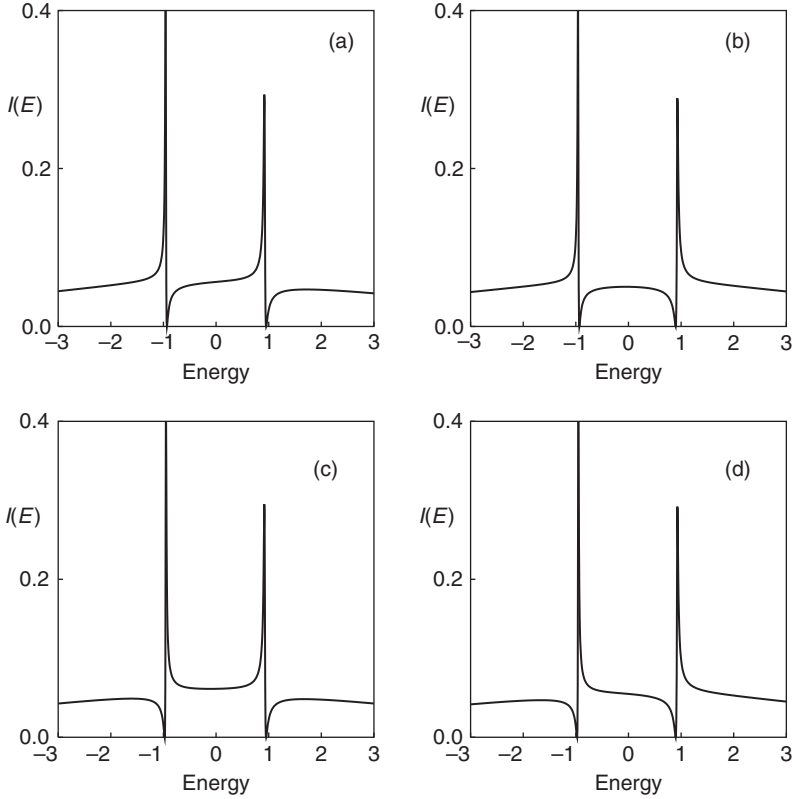
Figure 1.8 *q*-Reversal effect in lineshapes corresponding to the effective Hamiltonian (55) with the two resonances |1⟩ and |2⟩ coupled weakly to the continuum, and the short-lived quasi-bound state |3⟩ coupled strongly to the continuum. The lineshapes *I(E)* (22) represented in (a), (b), (c), and (d) correspond, respectively, to the initial states ϕ_{++}, ϕ_{+-}, ϕ_{-+}, and ϕ_{--} (56).

The model represents two resonances interfering dynamically through two continua. The inner space is spanned by the resonances |1⟩ and |2⟩ and the quasi-bound (short-lived) state |3⟩ modeling the background. The three-dimensional matrix representation of the effective Hamiltonian (lower part) is written in the form

$$\mathbf{H}^{\text{eff}} = \begin{bmatrix} E_1^0 & \cdot & \cdot \\ 0 & E_2^0 & \cdot \\ 0 & 0 & E_3^0 \end{bmatrix} - \frac{i}{2}\left(\begin{bmatrix} \Gamma_1 & \cdot & \cdot \\ \Gamma_{21} & \Gamma_2 & \cdot \\ \Gamma_{31} & \Gamma_{32} & \Gamma_3 \end{bmatrix} + \begin{bmatrix} \Gamma_1 & \cdot & \cdot \\ \pm\Gamma_{21} & \Gamma_2 & \cdot \\ \pm\Gamma_{31} & \pm\Gamma_{32} & \Gamma_3 \end{bmatrix} \right).$$

The second and third matrices correspond to the two continua. Assuming again that the width of the state describing the background is much larger
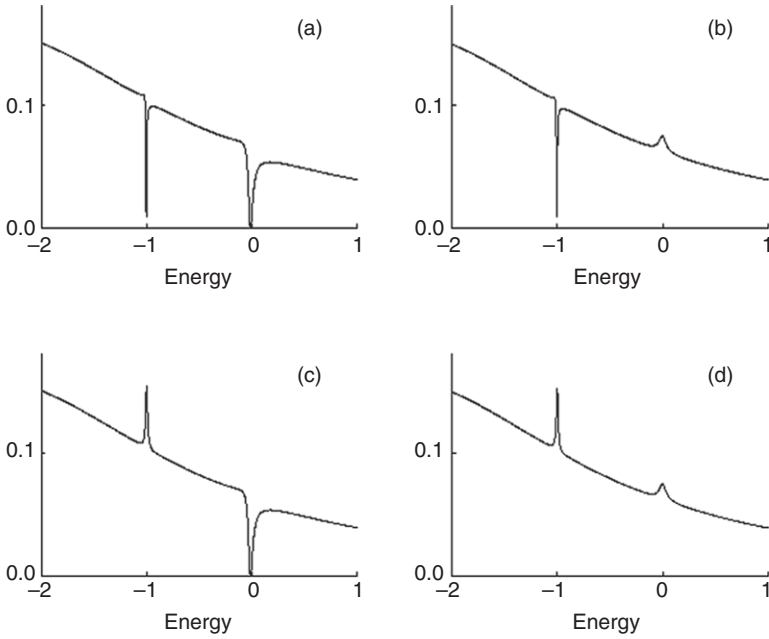
Figure 1.9 Characteristic shapes of absorption spectra corresponding to four combinations of the signs of couplings in $\mathbf{H}^{\text{eff}}$. For details see Fig. 5 in Ref. [8] and discussion therein.

than the widths of the resonances ($\Gamma_3 \gg \Gamma_1$ and $\Gamma_3 \gg \Gamma_2$), and that the three states are equally excited at the initial state, $\phi \propto (|1\rangle + |2\rangle) + |3\rangle$, various forms of the absorption spectra may be reproduced. The dips and peaks in Figure 1.9 are controlled by the signs of the couplings [8].

2.3.3. Vibrational resonances in I_2Ne

A quite generic example of two interacting resonances is found in Ref. [11] dealing with high vibrational levels of the I_2Ne system excited to the B electronic state of I_2. The resonance states are labeled $|v,n\rangle$, n being the quantum number associated with the Ne–I_2 stretching motion, v labels the vibrations related to the I–I coordinate. The two quasi-bound states $|\phi_1\rangle = |35,0\rangle$ and $|\phi_2\rangle = |34,4\rangle$ are nearly degenerate and coupled to various quasi-bound states and continua (see Figure 1.10). Such a picture is frequently found in molecular physics (diexcited Rydberg states, collision with highly charged ions, nonadiabatic transitions, etc.). The two resonances $|\phi_1\rangle$ and $|\phi_2\rangle$ span a two-dimensional inner space. The matrix representation of the effective Hamiltonian in the basis of the discrete states $|\phi_1\rangle = |35,0\rangle$ and $|\phi_2\rangle = |34,4\rangle$ is (see Table 1, case (a) in Ref. [11])
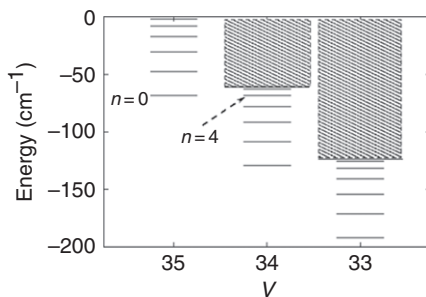
Figure 1.10   Quasi-bound states and continua in I_2–Ne (T shape). v labels the vibrational levels related to the I–I coordinate and n those of the Ne-I_2 coordinate. Figure taken from Ref. [11] with permission of EPJ.

$$H^{\text{eff}} = \begin{pmatrix} -68.20 - i\,.82 & -1.21 - i\,.07 \\ -1.21 - i\,.07 & -67.63 - i\,.02 \end{pmatrix}. \tag{57}$$

The z-dependence of the effective Hamiltonian $H^{\text{eff}}(z)$ was eliminated by choosing z equal to the mean energy of the two resonances ($z = 67$ cm^{-1}). The complex symmetric matrices are the fingerprints of the dynamics of the decaying resonances. The matrix representation (57) shows that the static interaction between the two states $\simeq 1$ cm^{-1} is much larger that the imaginary part -0.07 cm^{-1} of the coupling. Thus, the dynamics of these van der Waals states can be described in terms of two weakly-interacting resonances, the parameters of which were directly extracted from the full Hamiltonian without any empirical or semi-empirical parametrization. The density of states and the corresponding dynamics proceeding from four initial states are represented and compared with the close-coupling results in Figure 1.11 (Fig. 3 in Ref. [11]) and Figure 1.12 (Fig. 2. in Ref. [11]), respectively.

From the discussion in Ref. [11] we point out:

- The non-Lorentzian shapes are related to the nonexponential decays (a) and (b).
- The almost Breit–Wigner profiles correspond to the almost exponential decays of the two weakly interacting resonances in (c) and (d). The interference between the two resonances in (b) is similar to the interferences appearing in Fano profiles (Section 2.2.3, Figure 1.6).
- The excellent agreement between the results obtained by the method of close coupling and those derived from the effective Hamiltonian illustrates the numerical accuracy of the effective resolvent in realistic applications.
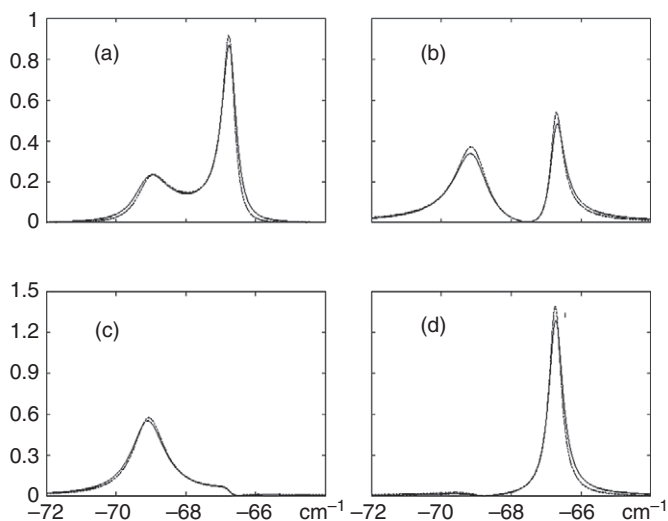
Figure 1.11   Density of states in I_2Ne for four initial states (a) $\phi = \phi_1$, (b) $\phi = \phi_2$, (c) $\phi = (\phi_1 + \phi_2)/\sqrt{2}$, (d) $\phi = (\phi_1 - \phi_2)/\sqrt{2}$. Full line: effective resolvent method; dotted line: close-coupling calculation.
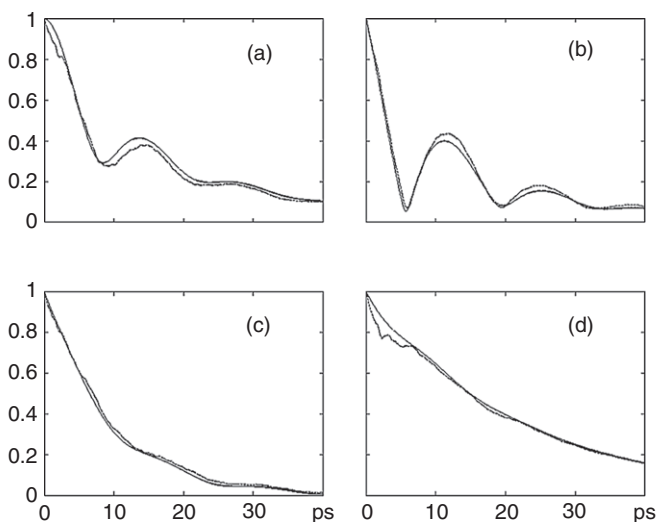
Figure 1.12   Modulus of the autocorrelation function (survival probability), $|c(t)|$, for the initial states given in the caption of Figure 1.11. Full line: effective resolvent method; dotted line: close-coupling.

3. COLLISIONS

Resonances are currently observed in collision processes. We will show in this section, how they can be studied in the framework of the partitioning technique by means of the effective Hamiltonians discussed in Section 2. The theory is described below and illustrated by model applications in Section 3.2.

3.1. Theory

We do not intend to give here a profound description of scattering theory that can be found in the textbooks, e.g., Refs. [44–46] and review articles Refs. [47–50]. We shall recall the definition of the transition operator and, in a second step, extend the model Hamiltonian of Section 2 to derive exact expressions of the on-shell transition matrix [51].

The transitions between the scattering states are governed by the transition operator $T(z)$ [52] defined by

$$Q \frac{1}{z - H} Q = \frac{Q}{z - H_0} + \frac{Q}{z - H_0} T(z) \frac{Q}{z - H_0}. \tag{58}$$

As discussed in Section 2.1, Q corresponds to the states of the continuum which contribute directly to the background of the cross section (term $T_1(z)$ in Eq. (61)). As above, the projector P is associated with unstable states implied in the collisional process. Expression (58) assumes a partition of the Hamiltonian into an unperturbed Hamiltonian H_0 and a perturbation V:

$$H = H_0 + V. \tag{59}$$

Using the partition technique (see Appendix B) the transition operator can be expressed as

$$T(z) = T_1(z) + T_2(z), \tag{60}$$

where

$$T_1(z) = QV \frac{Q}{1 - G_0 V}; \quad T_2(z) = \frac{Q}{1 - V G_0} V \frac{P}{z - H^{\text{eff}}(z)} V \frac{Q}{1 - G_0 V}. \tag{61}$$

$T_1(z)$ describes the direct transitions (the background of the cross sections); it depends smoothly on the energy. The resonant term $T_2(z)$ of the second order with respect to V depends strongly on the energy. $T_2(z)$ may be the dominant term of $T(z)$ near the poles of $P/(z - H^{\text{eff}}(z))$. For actual systems which require approximations, $T_1(z)$ is expanded in power of V

$$T_1(z) = Q[V + V G_0 V + \cdots] Q. \tag{62}$$

The convergence of this series is better than the convergence of the standard Born series because the singularities caused by the resonances have been transferred into the resonant term $T_2(z)$. To produce results of a general validity (spectroscopy and dynamics) we derive an exact expression of the transition operators that extend the model investigated in Section 2. The unperturbed part of the Hamiltonian is chosen in the form

$$H_0 = PHP + \sum_{a=1}^{m} \int |Ea\rangle E \langle Ea| \, dE. \tag{63}$$

H_0 is assumed to be diagonal in the basis of the collision states. $|Ea\rangle$ is the collision (or scattering) state of energy E belonging to the channel a. In the following the indexes a, b, $c \cdots$ will label the channels. The collision states are normalized in energy

$$\langle Ea|E'b\rangle = \delta_{ab}\, \delta(E - E'); \qquad \sum_{a=1}^{m} \int |Ea\rangle \langle Ea| \, dE = Q. \tag{64}$$

δ_{ab} is the Kronecker symbol and $\delta(E - E')$ is the Dirac function. The perturbative part of the Hamiltonian is written as [51]

$$V = \sum_{a=1}^{m} \left(|V_a\rangle \langle a| + |a\rangle \langle V_a| \right) + \sum_{a,b=1}^{m} V_{ab}\, |a\rangle \langle b|. \tag{65}$$

V_a belongs to the inner space of the resonances; $|a\rangle$ is a wave packet of the continuum a participating in the decay of the resonances into the channel a (doorway state). V_{ab} models the interactions inside and between the decay channels. The drastic limitation of the number of states characterizing V makes it possible to derive an exact expression of the effective Hamiltonian. Using Eq. (10) one finds the exact expressions of $T_1(z)$ and $T_2(z)$

$$T_1(z) = \sum_{a,b=1}^{m} (\mathbf{T}_1)_{ab}\, |a\rangle \langle b|; \qquad \mathbf{T}_1 = \mathbf{V} \frac{1}{1 - \mathbf{G}_0(z)\mathbf{V}}. \tag{66}$$

$(\mathbf{T}_1)_{ab}$ means the component ab of the matrix $\mathbf{T}_1$. Similarly, one finds for the resonant part of the transition operator (60)

$$T_2(z) = \sum_{a,b=1}^{m} (\mathbf{T}_2)_{ab}\, |a\rangle \langle b|; \qquad \mathbf{T}_2 = \frac{1}{1 - \mathbf{V}\mathbf{G}_0(z)}\, \mathbf{T}^{\text{eff}}\, \frac{1}{1 - \mathbf{G}_0(z)\mathbf{V}}. \tag{67}$$

The components of $\mathbf{T}^{\text{eff}}$ are

$$(\mathbf{T}^{\text{eff}})_{ab} = \langle V_a| \frac{P_0}{z - H^{\text{eff}}(z)} |V_b\rangle; \quad a,b = 1, 2, \ldots, m. \tag{68}$$

The two $m \times m$ matrices $\mathbf{G}_0(z)$ and $\mathbf{V}$ are defined by

$$\mathbf{G}_0(z) = \begin{bmatrix} G_a(z) & 0 & \cdots \\ 0 & G_b(z) & \cdots \\ \vdots & \vdots & \end{bmatrix} \quad \text{and} \quad \mathbf{V} = \begin{bmatrix} V_{aa} & V_{ab} & \cdots \\ V_{ba} & V_{bb} & \cdots \\ \vdots & \vdots & \end{bmatrix}, \quad (69)$$

where

$$G_a(z) = \langle a | \frac{Q_0}{z - H_0} | a \rangle.$$

The expression

$$H^{\text{eff}}(z) = PHP + \sum_{a,b=1}^{m} \left(\frac{1}{1 - \mathbf{G}_0(z)\mathbf{V}} \mathbf{G}_0(z) \right)_{ab} |V_a\rangle\langle V_b| \quad (70)$$

extends the results of Section 2. $\mathbf{G}_0(z)$ contains information concerning the energy shifts and the energy densities. When there is no interaction inside and between the continua, $H^{\text{eff}}(z)$ reduces to

$$H^{\text{eff}}(z) = PHP + \sum_{a=1}^{m} G_a(z)|V_a\rangle\langle V_a|. \quad (71)$$

Expressions (70) and (71) are especially useful when the density of states varies strongly within the energy range of interest, e.g., near the energy thresholds (see the analysis of giant resonances in Section 3.2.2). If the densities are constant the expression (71) is even simpler. In this case, $G_a(z) = -i\pi$, we recover the expression (16) [23, 53–56]:

$$H^{\text{eff}} = PHP - i\pi \sum_{a=1}^{m} |V_a\rangle\langle V_a|. \quad (72)$$

Expression (70) has no direct computational interest. Its usefulness is to provide a general framework to investigate cross sections. The physical quantity of interest is not the transition operator (60), but its matrix elements between the continua, the scattering states, whose projector is Q, that are peaked within a narrow range of energy. These matrix elements define the on-shell T matrix

$$\mathbf{T} = \mathbf{D}^{1/2}(\mathbf{T}_1 + \mathbf{T}_2)\mathbf{D}^{1/2}, \quad \text{where} \quad \mathbf{D} = -\frac{1}{\pi}\text{Im}\,\mathbf{G}_0(z) \quad (73)$$

and the unitary matrix $\mathbf{S}$

$$\mathbf{S} = \mathbf{1} - 2\pi\,i\,\mathbf{T}. \quad (74)$$

The eigenvalues $\lambda_k = \exp{(2\mathrm{i}\delta_k)}$ $(k = 1, 2, \ldots, m)$ of the matrix $\mathbf{S}$ provide the phase shifts δ_k. The lifetime $\mathbf{Q}$ matrix [57, 58] is related to $\mathbf{S}$ by

$$\mathbf{Q} = \mathbf{S}^{\dagger}\left(-\mathrm{i}\hbar\frac{\mathrm{d}}{\mathrm{d}E}\right)\mathbf{S}. \tag{75}$$

It is easy to determine $\mathbf{Q}$ from the scattering matrix $\mathbf{S}$ and of its derivative $\mathrm{d}\mathbf{S}/\mathrm{d}E$. Simple expressions in closed form can be obtained when $\mathbf{D}$ does not depend on the energy (Markovian approximation). This situation is usually encountered far from the energy thresholds. In this case, the choice $\mathbf{D} = \mathbf{1}$ leads to $\mathbf{G}_0(z) = -\mathrm{i}\pi\,\mathbf{1}$ and from Eqs. (65) and (67) one gets the exact formula

$$\frac{\mathrm{d}\mathbf{S}}{\mathrm{d}E} = -2\pi\mathrm{i}\,\frac{1}{1 + \mathrm{i}\pi\,\mathbf{V}}\,\frac{\mathrm{d}\mathbf{T}^{\mathrm{eff}}}{\mathrm{d}E}\,\frac{1}{1 + \mathrm{i}\pi\,\mathbf{V}}. \tag{76}$$

The components of $\mathrm{d}\mathbf{T}^{\mathrm{eff}}/\mathrm{d}E$ are determined from Eq. (68) as

$$\left(\frac{\mathrm{d}\mathbf{T}^{\mathrm{eff}}}{\mathrm{d}E}\right)_{ab} = -\langle V_a|\,\frac{P_0}{(E - H^{\mathrm{eff}})^2}\,|V_b\rangle; \quad a,b = 1, 2, \ldots, m. \tag{77}$$

Equation (77) underlines again the importance of the concept of effective Hamiltonian which contains also the information concerning the time delays.

3.2. Resonant scattering

The central role played by the effective Hamiltonian in the resonant part of the transition operator (60) is illustrated in two model applications.

3.2.1. A single resonance
We consider a single resonance of width Γ decaying into a unique channel. In the basis of the resonance $|1\rangle$ the effective Hamiltonian reduces to the scalar

$$H^{\mathrm{eff}} = -\frac{\mathrm{i}}{2}\,\frac{\Gamma}{1 + \mathrm{i}\pi\,V}. \tag{78}$$

The $\mathbf{T}$ and $\mathbf{S}$ matrices reduce to the scalar quantities

$$T(E) = \frac{1}{\pi}\,\frac{\pi\,V\,E + \Gamma/2}{(1 + \mathrm{i}\pi\,V)E + \mathrm{i}\Gamma/2}; \quad S(E) = \frac{(1 - \mathrm{i}\pi\,V)E - \mathrm{i}\Gamma/2}{(1 + \mathrm{i}\pi\,V)E + \mathrm{i}\Gamma/2}. \tag{79}$$

It is clear that $|S(E)|^2 = 1$. The pole of $S(E)$ provides the complex energy $\mathcal{E}_r = E_r - \mathrm{i}\Gamma_r/2$ of the resonance

$$E_r = -\pi\,\frac{\Gamma}{2}\,\frac{V}{1 + \pi^2\,V^2}; \quad \Gamma_r = \frac{\Gamma}{1 + \pi^2\,V^2}. \tag{80}$$
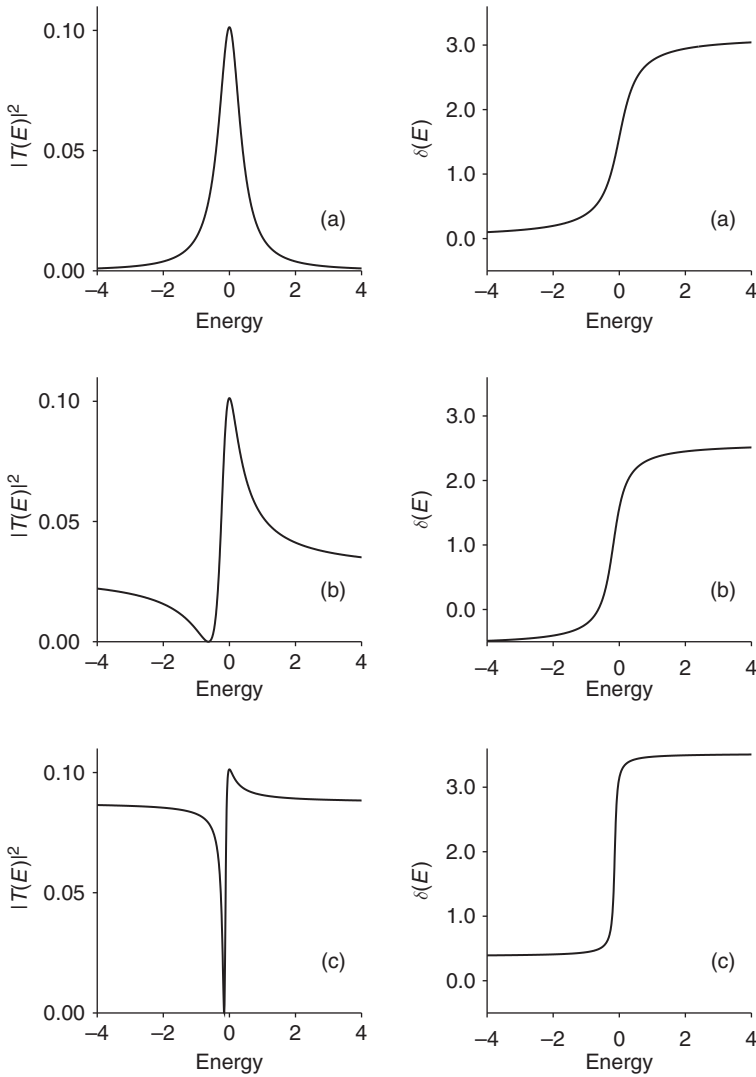
Figure 1.13 Resonant scattering (cross sections and phase shifts). Plot of $|T(E)|^2$ and of the phase shift $\delta(E)$ determined from $S(E)$ as a function of the energy (79). (a) $V = 0$, (b) $V = 0.2$, and (c) $V = 0.8$. In the three cases the width of the zero-order resonance is $\Gamma = 0.8$ (arbitrary units).

For a fixed value of Γ, Γ_r decreases from Γ to zero when V varies from zero to $\pm\infty$. The quantity $|T(E)|^2$ closely related to the cross section is plotted in Figure 1.13 as a function of the energy for three values of V.

In case (a) ($V=0$) there is no contribution of the nonresonant part of T and it results in a pure Lorentzian profile. In cases (b) and (c) ($V=0.2$ and 0.8,

respectively) asymmetric profiles appear which are similar to the Fano profiles [28]. The shape of these profiles is directly related to the pole of $S(E)$. It may be checked from Eq. (79) that the window (the zero of the cross section) is reached for the energy $E = -\Gamma/2\pi V$, i.e., $E = -0.64$ in (b) and $E = -0.16$ in (c). We have already shown that Fano profiles may be interpreted in terms of interferences between a long-lived resonance and a short-lived quasi-bound state participating to the dynamics and describing the relevant part of the continuum [8, 34]. This model could have been used here as well. Nevertheless, in order to illustrate the capabilities of the model Hamiltonians we have chosen to derive asymmetric profiles proceeding from a coupling within the collision space. A lot of physics is introduced through the definition of the inner space which may contain not only true resonances, directly observable, but also various "intermediate structures," "resonances," or "doorway states" which create bumps of intermediate character in the cross sections (see Ref. [22], Chapter 9).

3.2.2. Giant resonances

The model is based on a set of zero-order resonances decaying into a single channel near an energy threshold (see Ref. [51]). In atomic physics these resonances may be, e.g., a Rydberg series of autoionizing states. The model provides a simple explanation of the collective character of the wavefunction of a giant resonance and of its energy shift directly related to a rapid variation of the density of states near the energy threshold.

Here we consider a simple model of six noninteracting resonances of zero-order energies $E_i^0 = i - 1$, $(i = 1, 2, \ldots, 6)$ and of identical partial width Γ_0. The effective Hamiltonian is written as

$$H^{\text{eff}}(z) = \sum_{i=1}^{6} (i-1)|i\rangle\langle i| + G(z)|V\rangle\langle V|. \tag{81}$$

The matrix representation of the Hermitian part of (81) is diagonal in the basis of the discrete states $|i\rangle$, $(i = 1, 2, \ldots, 6)$. The couplings between the resonances and the continuum are assumed to be identical and characterized by

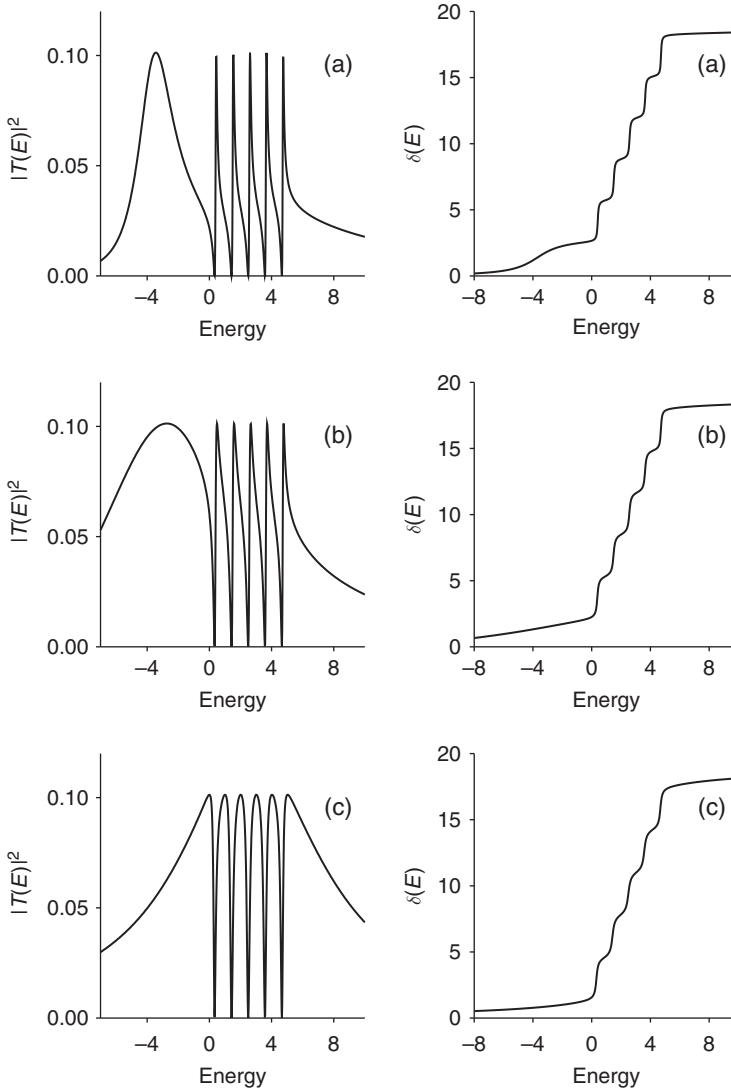$$|V\rangle = \left(\frac{\Gamma_0}{2\pi}\right)^{1/2} \sum_{i=1}^{n} |i\rangle. \tag{82}$$

The Green function $G(z)$ is chosen in the form

$$G(z) = \ln\left(\frac{\zeta+1}{\zeta-1}\right); \quad \zeta = \frac{2}{\Delta_0}(z - E_0) + i\eta, \tag{83}$$

where

$$E_0 = \frac{E_{\text{thr}} + E_{\text{end}}}{2}; \quad \Delta_0 = \frac{E_{\text{end}} - E_{\text{thr}}}{2}. \tag{84}$$

E_{thr} is the energy of the threshold. The density of states is constant from E_{thr} to E_{end}. We neglect the background ($\mathbf{V}=0$) and, since there is only one decay channel, $\mathbf{T}$ reduces to the scalar quantity

Figure 1.14 Giant resonances (cross sections and phase shifts). The parameters of the Green function (83) are (a) $E_{\text{thr}} = 0$; (b) $E_{\text{thr}} = -10$; (c) $E_{\text{thr}} = -100$ (arbitrary units).

$$T(E) = \langle V | \frac{P_0}{E - H^{\text{eff}}(E)} | V \rangle. \tag{85}$$

The notation $H^{\text{eff}}(E)$ in Eq. (85) underlines the dependence of the effective Hamiltonian on the energy. Note that the transition term $T(E)$ and the lineshape

$$I(E) = -\frac{1}{\pi} \text{Im} \langle \phi | \frac{P_0}{E - H^{\text{eff}}(E)} | \phi \rangle \tag{86}$$

investigated in Section 2 are expressed in terms of the matrix elements of $P/(E - H^{\text{eff}}(E))$. Consequently, the cross sections, proportional to $|T(E)|^2$, and $I(E)$ have similar shapes. Figure 1.14 represents $|T(E)|^2$, assimilated to the cross section as a function of the energy (on the left) and the corresponding phase shifts (on the right) for three values of the threshold energy. In case (a) the zero-order energies of the resonances (from 0 to 5) are near the energy threshold $E_{\text{thr}} = 0$ and the extended structure (on the left) at the energy $E = -3$ corresponds to the giant resonance. The case (c) corresponding to a constant density of states was recently investigated to illustrate the formation of short-lived states from broad interfering resonances in a model study of collision of an electron with an hydrogen molecule [59].

4. STATISTICAL PHYSICS

The two previous sections were devoted to modeling quantum resonances by means of effective Hamiltonians. From the mathematical point of view we have used two principal tools: projection operators that permit to focus on a few states of interest and analytic continuation that allows to uncover the complex energies. Because the time-dependent Schrödinger equation is formally equivalent to the Liouville equation, it is attractive to try to solve the Liouville equation using the same tools and thus establishing a link between the dynamics and the nonequilibrium thermodynamics. For that purpose we will briefly recall the definition of the correlation functions which are similar to the survival and transition amplitudes of quantum mechanics. Then two models of regression of a fluctuation and of a chemical kinetic equation including a transition state will be presented.

4.1. Theory

We outline briefly in this section how to link the theory of quantum resonances to statistical physics and thermodynamics by extending the concept of effective Hamiltonian as recently discussed in Ref. [60]. The quantum Liouville–von Neumann equation is written in the form

$$\frac{\text{d}\rho}{\text{d}t} = -\text{i} L \rho. \tag{87}$$

ρ is the density operator and L is the Liouville operator (Liouvillian). The formal solution of Eq. (87) is

$$\rho(t) = \mathrm{e}^{-\mathrm{i}Lt}\rho(0); \qquad t \geq 0. \tag{88}$$

$\rho(0)$ is the density at the initial time and $\mathrm{e}^{-\mathrm{i}Lt}$ is the unitary evolution operator. The theoretical developments presented below are based on the formal analogy between Eq. (87) and the expression (1) in Section 2. The time-dependent mean value of an observable A can be written in the form

$$\langle A \rangle(t) = \mathrm{Tr}\,[A\,\rho(t)] = \mathrm{Tr}\,[A\,\mathrm{e}^{-\mathrm{i}Lt}\rho(0)]. \tag{89}$$

We shall use the Schrödinger representation which among other advantages reveals the temporal evolution of the density and provides a direct connection with standard quantum mechanics. Let us begin by considering only one observable A of interest. The maximum entropy criterion (Ref. [61] and IX-21 of Ref. [21]) provides the initial nonequilibrium density ($t = 0$)

$$\rho(0) = \frac{1}{Z}\,\mathrm{e}^{-\beta(H-aA)}; \qquad \beta = \frac{1}{k_B T}. \tag{90}$$

Z is the partition function, a is the scalar quantity conjugate to A and k_B is the Boltzmann constant; a could be, e.g., an electric field and A the electric dipolar moment operator of the system. We assume that at the initial time the system is not far from equilibrium and expand the density to first order in a (see Ref. [62]). The expected value of an observable B is expressed as the Mori scalar product that refers to the equilibrium density [62, 63]

$$\langle B \rangle(t) = \beta\,a\,\langle B|\,\mathrm{e}^{-\mathrm{i}Lt}|A\rangle. \tag{91}$$

It is assumed in Eq. (91) that B is centered. Expression (91) shows that up to a multiplicative constant, the dynamics of B is contained in the time correlation function [64]

$$C_{AB}(t) = \langle B|\,\mathrm{e}^{-\mathrm{i}Lt}|A\rangle. \tag{92}$$

Hereafter we shall focus on the determination of $C_{AB}(t)$. Although the expression (92) is rather formal, it is an efficient starting point to derive general results concerning the dynamics [60] and the temporal evolution of the entropy [65]. Note that $C_{AB}(t)$ looks like a transition amplitude in quantum mechanics. The relevance of this analogy was advocated many years ago by Cohen-Tannoudji in his lectures at Collège de France [21]. In complete analogy with quantum mechanics and using our approach of the theory of resonances [9, 51], we shall transpose the concept of effective Hamiltonian into the new concept of *effective Liouvillian* which is the key to derive

macroscopic results from the underlying microscopic dynamics. With the aim to determine macroscopic characteristic times from much shorter microscopic times, it is convenient to consider the Fourier–Laplace transform of the correlation function:

$$C_{AB}[z] = \langle B| \frac{1}{z - L} |A \rangle. \tag{93}$$

The complex variable z (Im $z < 0$) is homogenetic to a frequency. The resolvent $1/(z - L)$ is the Fourier–Laplace transform of the evolution operator (see Appendix A). Expression (93) shows that the dynamics is reduced to the determination of the matrix element of the resolvent between two observables. Therefore only a reduced dynamics has to be investigated. For that purpose we shall define more precisely the observables and the operators of interest. The theory is formulated in the framework of the Liouville space of the operators and based on hierarchies of effective Liouvillians which are especially convenient to study reduced dynamics at various macroscopic and microscopic timescales (see Appendix B).

The most obvious variables of interest are the *slow macroscopic variables* represented by the operators $A, B, C, \ldots$ Because the statistical mechanics provides the macroscopic properties from the microscopic world, we also need to deal with *fast microscopic variables* most often the flux variables. Expressions (91) and (92) show that, at short time, the dynamics is dominated by the first few terms of the expansion

$$e^{-iLt} A = A - iLAt + \frac{1}{2!}(iL)^2 A t^2 + \cdots \tag{94}$$

The notation $\dot{A} = iLA$, $\ddot{A} = (iL)^2 A, \ldots$ recalls that classical and quantum Liouvillians are time derivatives. The dissipative fluxes refer to the dynamically accessible microstates. They also provide the basis of the so-called extended thermodynamics [66]. For example, in the linear response theory [67], the dynamical susceptibilities are proportional to the time derivatives of the correlation functions [63]

$$\chi_{BA}(t) = \beta \langle B| e^{-iLt} |\dot{A} \rangle. \tag{95}$$

In addition to the dissipative fluxes, other short-lived observables directly implied in the dynamics may be required. An important example is the transition state on a reaction path of a chemical reaction (see Section 4.3).

Since we are interested in a few observables and their fluxes, we shall project the Liouvillian dynamics onto the space of the relevant observables. The equations of Section 2 still hold if one replaces the H by L and H^{eff} by L^{eff} (see Appendix B). P projects the dynamics onto the space of the observables.
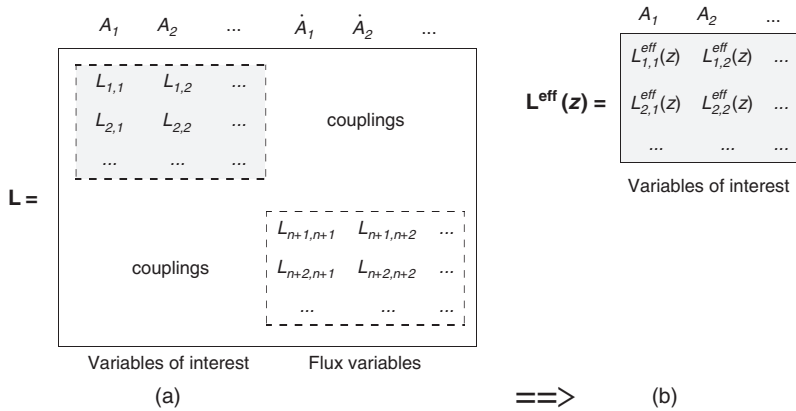
Figure 1.15   Matrix representation of the Liouvillian. (a) $2n \times 2n$ matrix representation of the Liouvillian in the basis of n observables and of their fluxes. (b) $n \times n$ matrix representation of the z-dependent effective Liouvillian derived from (a) in the basis of the n observables.

The use of projectors and of small-dimensional matrix representations of the Liouvillian makes possible to pass from the microscopic to the macroscopic world. The basic idea is that the macroscopic variables are weakly coupled to the microscopic degrees of freedom. The matrix representation of L^{eff} in the basis of n variables of interest A_i and of their fluxes $\dot{A}_i$ ($i = 1, 2, \ldots, n$) is sketched in the panel (a) of Figure 1.15. The possible pathway from a z-independent effective Liouvillian (supposed to be exact) to a smaller z-dependent effective Liouvillian (see panel (b)) of Figure 1.15) will be discussed in the following sections. It is at this stage that the long-lived macroscopic characteristic times are revealed by perturbation in the complex plane. The main advantage of working in the complex plane lies here. The same formalism is able to describe decays and oscillations characterizing the return to equilibrium.

4.2. Regression of a fluctuation

The first application of the effective Liouvillians [9, 65] models the regression of a fluctuation. We consider one observable A and its flux $\dot{A}$. It is convenient to introduce an orthonormal base in the Liouville space of the operators A and $\dot{A}$:

$$|1\rangle = \frac{1}{\Delta A}|A\rangle; \qquad |2\rangle = \frac{1}{\Delta \dot{A}}|\dot{A}\rangle, \tag{96}$$

where

$$\Delta A = \langle A|A\rangle^{1/2}; \qquad \Delta \dot{A} = \langle \dot{A}|\dot{A}\rangle^{1/2}. \tag{97}$$

ΔA and $\Delta\dot{A}$ are fluctuations because the observable A is centered. The matrix representation of the effective Liouvillian (see (B.7) in Appendix B) in the basis $|1\rangle$, $|2\rangle$ is

$$\mathbf{L}^{\text{eff}}(z) = \begin{bmatrix} 0 & i\Delta \\ -i\Delta & -iM_{22}(z) \end{bmatrix}. \tag{98}$$

$\Delta = \frac{\Delta\dot{A}}{\Delta A}$ and $M_{22}(z)$ is the matrix element $\langle 2|M(z)|2\rangle$. All the other matrix elements of the memory operator are zero [63]. The appearance of the factor i corresponds to the Hermitian definition of the Liouvillian which is not universal. Equation (98) is an exact z-dependent expression. This z-dependence can be eliminated by approximating $M_{22}(z)$ by a positive constant Γ (Markovian approximation). This approximation is justified since the microscopic correlation time is much shorter than the regression time of the fluctuation. Then Eq. (98) transforms into the z-independent effective Liouvillian

$$\mathbf{L}^{\text{eff}} = \begin{bmatrix} 0 & i\Delta \\ -i\Delta & -i\Gamma \end{bmatrix}. \tag{99}$$

The non-hermiticity of $\mathbf{L}^{\text{eff}}$ arises from the dissipative term $-i\Gamma$. If we are interested in the temporal evolution of the fluctuation, the dynamics can be projected into the one-dimensional (scalar) frequency-dependent Liouvillian

$$L^{\text{eff}}(z) = \frac{\Delta^2}{z + i\Gamma}. \tag{100}$$

The inverse Fourier–Laplace transformation of the Green function in the case of a weak coupling ($\Delta \ll \Gamma$) leads to

$$\langle A\rangle(t) = \frac{\beta a(\Delta A)^2}{2\sqrt{\frac{\Gamma^2}{4} - \Delta^2}} [\gamma_+ \, e^{-\gamma_- t} - \gamma_- \, e^{-\gamma_+ t}] \tag{101}$$

$$\gamma_\pm = \frac{\Gamma}{2} \pm \sqrt{\frac{\Gamma^2}{4} - \Delta^2}.$$

An oscillation decay is found in the case of a strong coupling ($\Delta \gg \Gamma$)

$$\langle A\rangle(t) = \beta a(\Delta A)^2 \left(\cos\omega t + \frac{\Gamma}{2} \frac{\sin\omega t}{\omega} \right) e^{-\frac{\Gamma}{2} t} \tag{102}$$

$$\omega = \sqrt{\Delta^2 - \frac{\Gamma^2}{4}}.$$

The two dynamical regimes are presented in Figure 1.16. In the case (a) the system is weakly coupled to the heat bath (reservoir) and $\langle A\rangle(t)$ decays as $e^{-\gamma t}$. The friction $\gamma \simeq \Delta^2/\Gamma$ links the fluctuation Δ to the dissipative term γ.
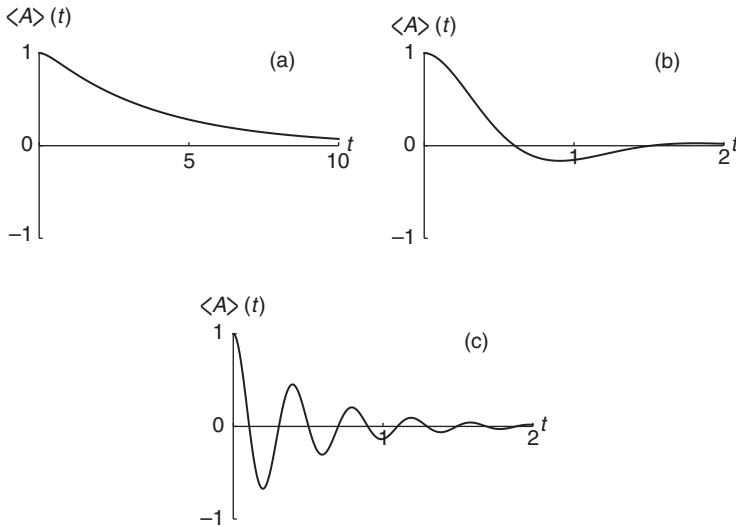
Figure 1.16 Regression of a fluctuation. Temporal evolution of $\langle A \rangle (t)$. (a) weak coupling: $\Delta = 1$ (b) intermediate coupling: $\Delta = 4$ (c) strong coupling: $\Delta = 16$ (arbitrary units).

In the case (c) (strong coupling) the oscillations are damped because the system tends irreversibly to equilibrium.

We conclude this paragraph by recalling that the analysis of the decay of a fluctuation is old and well documented since the appearance of the book of de Groot and Mazur [68] who discussed the subject in relationship with the statistical foundations of nonequilibrium thermodynamics. However, contrary to their lengthy and heuristic itinerary, the approach presented here is straightforward: the initial state refers to a density of probability and all results are derived from classical or quantum mechanics. In addition, we are able to describe oscillating regimes directly related to the intensity of the coupling between the system and the reservoir. Because we consider only one observable regressing to zero at equilibrium, the entropy production [63], expressed as

$$\frac{1}{k_B} \frac{dS}{dt} = -\frac{1}{2} \frac{d}{dt} \left[\frac{\langle A \rangle (t)}{\Delta A} \right]^2 \tag{103}$$

leads to the expression of the entropy as a function of time:

$$\frac{1}{k_B} S(t) = -\frac{1}{2} \frac{\langle A \rangle^2 (t) - \langle A \rangle^2 (0)}{(\Delta A)^2}; \qquad S(0) = 0. \tag{104}$$

To get quantitative results the fluctuation ΔA in Eqs. (103 and 104) has to be evaluated. For example, for a Brownian particle of mass m, embedded in a thermal bath at temperature T, the variation of the entropy is given by

$$S(t = \infty) - S(t = 0) = k_B \frac{\frac{1}{2} m v^2(0)}{2 \langle \frac{1}{2} m v^2 \rangle} = \frac{Q}{T}, \tag{105}$$

where $v(0)$ is the initial velocity of the particle and the fluctuation of its velocity $\langle v^2 \rangle$ is directly related to the temperature. One recovers the Clausius's formula established in the framework of a purely irreversible processes (uncompensated heat).

4.3. Chemical kinetics

The aim of this section is to derive from first principles a kinetic equation for a simple model of a chemical reaction proceeding toward equilibrium. The simplest case is when the forward and reverse reactions are of the first-order (see, e.g., Chapter 25 of Ref. [69])

$$A \rightleftharpoons B. \tag{106}$$
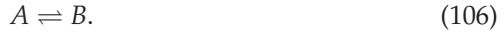
One can find in the textbooks that the concentrations of the two species, e.g., conformers, obey the phenomenological first-order differential equations

$$\frac{d[A]}{dt} = -k_A [A] + k_B [B], \tag{107}$$

$$\frac{d[B]}{dt} = k_A [A] - k_B [B],$$

where k_A and k_B are empirical rate constants. We will determine them by including in the dynamics a short-lived transition state C [69]. The reduced dynamics is projected on the basis of the operators $|A\rangle$, $|B\rangle$, and $|C\rangle$ representing the concentrations $[A]$, $[B]$, and $[C]$ of the chemical entities A, B, and C. $|C\rangle$ is analogous to the short-lived flux variable taken into account in the decay of a fluctuation. The matrix representation of the effective Liouvillian in the basis $|A\rangle$, $|B\rangle$, and $|C\rangle$, assumed to be orthogonal, can be written as

$$\mathbf{L}^{\text{eff}} = \begin{bmatrix} 0 & 0 & i\Delta_A \\ 0 & 0 & i\Delta_B \\ -i\,\Delta_A & -i\,\Delta_B & -i\Gamma \end{bmatrix}. \tag{108}$$

The roots of irreversibility come from the couplings Δ_A and Δ_B between the chemical species and the transition state characterized by its lifetime $\tau \simeq \frac{1}{\Gamma}$. The dynamics can be obtained exactly by diagonalizing the matrix (108). However, to obtain concentration, which are the observable quantities, it is useful to project the dynamics on the space of the operators representing the chemical concentrations $[A]$ and $[B]$. One finds the exact z-dependent two-dimensional effective Liouvillian

$$\mathbf{L}^{\text{eff}}(z) = \frac{1}{z + i\Gamma} \begin{bmatrix} \Delta_A^2 & \Delta_A \Delta_B \\ \Delta_A \Delta_B & \Delta_B^2 \end{bmatrix}. \tag{109}$$

Assuming a weak coupling between the chemical species and the transition state which plays the role of an effective continuum, we get the frequency-independent effective Liouvillian

$$\mathbf{L}^{\mathrm{eff}} = \begin{bmatrix} -\mathrm{i}\,\dfrac{\Delta_A^2}{\Gamma} & -\mathrm{i}\,\dfrac{\Delta_A\Delta_B}{\Gamma} \\[2ex] -\mathrm{i}\,\dfrac{\Delta_A\Delta_B}{\Gamma} & -\mathrm{i}\,\dfrac{\Delta_B^2}{\Gamma} \end{bmatrix}. \tag{110}$$

Comparing Eq. (110) with the empirical expression (107) produces the rate constants

$$k_A = \frac{\Delta_A^2}{\Gamma}; \qquad\qquad k_B = \frac{\Delta_B^2}{\Gamma}. \tag{111}$$

In the case of weak coupling ($\Delta_A^2 + \Delta_B^2 \ll \Gamma^2$), currently associated with slow reactions, the exact solution is

$$[A](t) = \frac{k_B}{k_A + k_B}\,([A]_0 + [B]_0) + \frac{k_A[A]_0 - k_B[B]_0}{k_A + k_B}\,c(t), \tag{112}$$

where

$$c(t) = \frac{1}{2\sqrt{\dfrac{\Gamma^2}{4} - (\Delta_A^2 + \Delta_B^2)}}(\gamma_+\,\mathrm{e}^{-\gamma_- t} - \gamma_-\,\mathrm{e}^{-\gamma_+ t}); \tag{113}$$

$$\gamma_\pm = \frac{\Gamma}{2} \pm \sqrt{\frac{\Gamma^2}{4} - (\Delta_A^2 + \Delta_B^2)}.$$

In Eq. (113), $c(t)$ is a normalized correlation function, ($c(t = 0) = 1$), which goes to zero when $t \to \infty$. One obtains for [B] a similar expression by exchanging A and B in Eq. (112). For strong coupling, $\Delta_A^2 + \Delta_B^2 \gg \Gamma^2$, expression (112) remains valid upon choosing

$$c(t) = [\cos(\omega t) + \frac{\Gamma}{2\omega}\sin(\omega t)]\,\mathrm{e}^{-\frac{\Gamma}{2}t}; \qquad \omega = \sqrt{\Delta_A^2 + \Delta_B^2 - \frac{\Gamma^2}{4}} \tag{114}$$

and one obtains chemical oscillations. The variations of the concentrations of the chemical species A and B which tend to constants at infinite time are represented in Figure 1.17. Similarly, as for the fluctuations, the damped oscillations appear when there is a strong coupling between the chemical species and the transition state (case (c)) which plays the role of a continuum. Steady oscillations would require an energy or a mass transfer from the surroundings which is excluded from our hypothesis of a time-independent Hamiltonian. As a whole, the regimes displayed in Figures 1.16 and 1.17 are similar. They describe irreversible processes of unstable states.
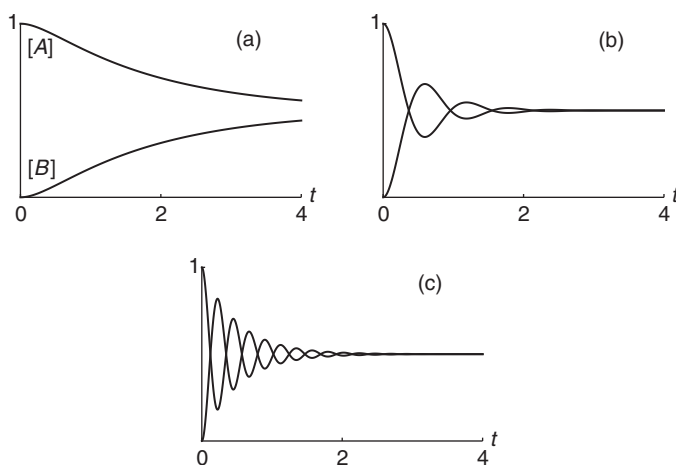
Figure 1.17   Kinetics of the reaction $A \rightleftharpoons B$. Concentrations $[A](t)$ and $[B](t)$ as a function of time. (a) $\Delta_A = 1$, (b) $\Delta_A = 4$, (c) $\Delta_A = 10$ (arbitrary units).
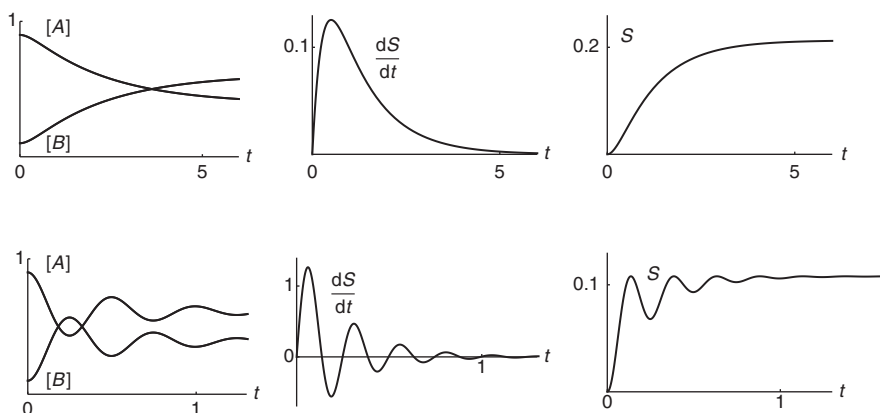
Figure 1.18   Kinetics of the reaction $A \rightleftharpoons B$. Concentrations, rates of entropy production, and variation of the entropy as a function of time. Upper row: weak coupling ($\Delta_A = 1$, $\Delta_B = -0.8$); lower row: strong coupling ($\Delta_A = 8$, $\Delta_B = -10$). The initial concentrations are $[A]_0 = 0.9$, $[B]_0 = 0.1$ (arbitrary units).

The temporal evolution of the concentrations $[A]$ and $[B]$, the entropy production $\frac{dS}{dt} = \frac{dS_A}{dt} + \frac{dS_B}{dt}$ and the entropy S are illustrated in Figure 1.18. The first row corresponds to the current situation of a chemical reaction for a system weakly interacting with the bath, whereas the damped oscillations, lower row, correspond to a strong intramolecular coupling mediated through the transition state.

5. CONCLUDING REMARKS

We have presented a unified formulation of dissipative dynamics based on the quantum theory of resonances. The reversible and dissipative contributions to the dynamics are gathered in small-dimensional non-Hermitian effective Hamiltonians and effective Liouvillians with well-defined theoretical status. The formulation tends to fill the gap between the dynamics and the thermodynamics. It has many advantages:

- The mathematical framework is simple and rigorous, based on the analytical properties of the Fourier–Laplace transformation: the energies and the lifetimes are assigned to the poles of Green functions.
- The Fourier–Laplace transformation provides a one-to-one correspondence between the dynamics and the spectroscopic properties: quantum interferences and line profiles.
- The use of projectors focuses on a few number of variables of interest in the spirit of thermodynamics.
- The irreversible transfer of energy from the relevant degrees of freedom to the irrelevant degrees of freedom (quasi-continua, continua, heat baths) is emphasized.
- The long macroscopic lifetimes can be derived from the short microscopic lifetimes by standard perturbation theory in the complex plane.
- An elementary demonstration of the fluctuation–dissipation theorem is presented.
- The approach helps to derive rigorous non-Hermitian formulations of the dynamics of unstable states.

ACKNOWLEDGMENT

APPENDICES

A. FOURIER–LAPLACE TRANSFORMATION

With a notation adapted to quantum mechanics, the Fourier–Laplace transformation of a time-dependent function $f(t)$ is defined by

$$f[z] = \frac{1}{i\hbar} \int_0^\infty dt\, f(t)\, e^{\frac{izt}{\hbar}}. \tag{A.1}$$

For $t > 0, f(t)$ is recovered by the inverse transformation

$$f(t) = \frac{1}{2\pi i} \int_C dz f[z] \, e^{-\frac{izt}{\hbar}}. \tag{A.2}$$

The variable $z = E + i\epsilon$ represents an *energy* extended in the complex plane ($\epsilon > 0$). The integration path in the complex plane is counterclockwise (see, e.g., Ref. [5]). We shall also use the notation $f(z) = if[z]$. Some useful properties adapted from Ref. [70] are

$$f(t) \longleftrightarrow f[z] \tag{A.3}$$

$$i\hbar \frac{df}{dt} \longleftrightarrow zf[z] - f(t = 0) \tag{A.4}$$

$$i\hbar \, \delta(t) \longleftrightarrow 1 \tag{A.5}$$

$$\theta(t) \longleftrightarrow \frac{1}{z} \tag{A.6}$$

$$U(t) = e^{-i\frac{H}{\hbar}t} \longleftrightarrow \frac{1}{z - H} \tag{A.7}$$

$$i\hbar \frac{dU}{dt} \longleftrightarrow \frac{H}{z - H} \tag{A.8}$$

$$f(t) \star g(t) \longleftrightarrow i\hbar f[z] \cdot g[z]. \tag{A.9}$$

The convolution product is defined by

$$f(t) \star g(t) = \int_0^t f(\tau) g(t - \tau) \, d\tau = \int_0^t f(t - \tau) g(\tau) \, d\tau. \tag{A.10}$$

$\delta(t)$ is the Dirac function, $\theta(t)$ is the Heaviside function, and H is the Hamiltonian operator. The above expressions still holds for statistical physics by setting $\hbar = 1$. Then $z = \omega + i\epsilon$ acquires the meaning of a *frequency* extended in the complex plane ($\epsilon > 0$). Expressions (A.7 and A.8) transform into

$$U(t) = e^{-iLt} \longleftrightarrow \frac{1}{z - L} \tag{A.11}$$

$$i\frac{dU}{dt} \longleftrightarrow \frac{L}{z - L} \tag{A.12}$$

where L is the Liouvillian operator.

B. PARTITIONING TECHNIQUE

B.1. Quantum mechanics

The Hilbert space of the wavefunctions is partitioned into a finite n-dimensional *inner space*, which is generated by the resonances and the unstable states of interest, and its orthogonal complements the *outer space*. The projectors onto the inner and the outer space are P and Q, respectively: $P + Q = 1$. In the basis of the quasi-bound states $|i\rangle; (i = 1, 2, \ldots, n)$, the projector into the inner space can be written as

$$P = \sum_{i=1}^{n} |i\rangle\langle i|; \quad \langle i|j\rangle = \delta_{ij}; \quad i, j = 1, 2, \ldots, n. \tag{B.1}$$

It is convenient to write the partition of the resolvent in the form [7, 10]

$$
\begin{aligned}
\frac{1}{z - H} &= \frac{P}{z - H^{\text{eff}}(z)} \\
&+ \frac{Q}{z - H} H \frac{P}{z - H^{\text{eff}}(z)} + \frac{P}{z - H^{\text{eff}}(z)} H \frac{Q}{z - H} \\
&+ \frac{Q}{z - H} + \frac{Q}{z - H} H \frac{P}{z - H^{\text{eff}}(z)} H \frac{Q}{z - H},
\end{aligned}
\tag{B.2}
$$

where

$$H^{\text{eff}}(z) = PHP + R(z); \quad R(z) = PH \frac{Q}{z - H} HP. \tag{B.3}$$

$z = E + i\epsilon$ is the energy extended in the complex plane and the resolvent $1/(z-H)$, unambiguously defined for $\text{Im}(z) < 0$, is assumed to be analytically continued in the second Riemann sheet [38].

The effective Hamiltonian $H^{\text{eff}}(z)$ is the sum of the projected Hamiltonian and of the *level-shift operator* [7]. For any initial state belonging to the inner space, the relevant information is contained in the resolvent projected, on the right, in the inner space. The dependence of $H^{\text{eff}}(z)$ on z can be reduced by time-filtering (see Section 2.2.1) or by extending the dimension of the inner space. $P/(z-H^{\text{eff}}z)$ and $Q/(z-H)$ are short-hand notations for the inversion of $P(z-H^{\text{eff}}(z))P$ in the inner space and $Q(z-H)Q$ in the outer space, respectively. If the initial state belongs to the inner space, the dynamics is obtained from the *reduced resolvent*

$$\frac{1}{z - H} P = \frac{P}{z - H^{\text{eff}}(z)} + \frac{Q}{z - H} H \frac{P}{z - H^{\text{eff}}(z)}. \tag{B.4}$$

If we are only interested in the dynamics projected in the inner space, the relevant information is contained in the *projected resolvent*

$$P\frac{1}{z-H}P = \frac{P}{z-H^{\text{eff}}(z)}. \tag{B.5}$$

The above expressions refer to the evolution operator in quantum mechanics. Similar expressions can be derived in the framework of statistical physics in order to establish a connection with the Langevin's formalism.

B.2. Liouvillian mechanics

The Hilbert space of the wavefunctions of quantum mechanics moves to the Hilbert space of the operators describing the observables. The expressions defined within quantum mechanics still holds for the probabilistic approach of mechanics based on the Liouville equation. H has to be replaced by the Liouvillian L and the partition becomes [32]

$$\frac{1}{z-L} = \frac{P}{z-L^{\text{eff}}(z)} + \frac{Q}{z-L}L\frac{P}{z-L^{\text{eff}}(z)} + \frac{Q}{z-L}$$
$$+ \frac{P}{z-L^{\text{eff}}(z)}L\frac{Q}{z-L} + \frac{Q}{z-L}L\frac{P}{z-L^{\text{eff}}(z)}L\frac{Q}{z-L}. \tag{B.6}$$

P and Q are projectors ($P + Q = 1$) in the Liouville space of the operators. The z-dependent Liouvillian is the sum of the projected Liouvillian and of the level-shift operator

$$L^{\text{eff}}(z) = PLP + R(z); \qquad R(z) = PL\frac{Q}{z-L}LP. \tag{B.7}$$

$P/(z - L^{\text{eff}}(z))$ is an abbreviation for the inversion of $z - L^{\text{eff}}(z)$ in the subspace of the relevant observables . Similarly, $Q/(z - L)$ is a short-hand notation for the inverse of $z - QLQ$ in the subspace of the irrelevant (microscopic) variables. It is useful to introduce the *memory operator* (memory kernel)

$$M(z) = iR(z) \tag{B.8}$$

which permits to write the effective Liouvillian in the form

$$L^{\text{eff}}(z) = PLP - iM(z). \tag{B.9}$$

Dissipation appears through the second term in the right-hand side of (B.9). Since we are interested in the projected dynamics (subdynamics [71, 72]), one has to consider the reduced resolvent

$$\frac{1}{z-L}\,P = \frac{P}{z-L^{\text{eff}}(z)} + \frac{Q}{z-L}\,L\frac{P}{z-L^{\text{eff}}(z)} \tag{B.10}$$

and the projected resolvent

$$P\,\frac{1}{z-L}\,P = \frac{P}{z-L^{\text{eff}}(z)}\,P. \tag{B.11}$$

The Fourier–Laplace transform of the time derivative of the evolution operator (see Appendix A) is also worth of interest:

$$\frac{L}{z-L}\,P = \frac{L^{\text{eff}}(z)}{z-L^{\text{eff}}(z)} + \frac{Q}{z-L}\,L\frac{z}{z-L^{\text{eff}}} \tag{B.12}$$

$$P\,\frac{L}{z-L}\,P = \frac{L^{\text{eff}}(z)}{z-L^{\text{eff}}(z)}. \tag{B.13}$$

Expansion (B.12) derives immediately from (A.6). Instead of (B.6) one could start out of the identity

$$\frac{1}{z-L} = \frac{P}{z-L} + \frac{1}{z-L}\,QL\frac{P}{z-L} + \frac{Q}{z-L} + \frac{1}{z-L}\,PL\frac{Q}{z-L}. \tag{B.14}$$

This partitions allows to transform (B.12) as

$$\begin{aligned}
\frac{L}{z-L}\,P &= \frac{1}{z-L}\,(P+Q)LP \\
&= \frac{1}{z-L}\left(PLP + PL\frac{Q}{z-L}\,LP\right) + \frac{Q}{z-L}\,LP \\
&= \frac{1}{z-L}\,L^{\text{eff}}(z) + \frac{Q}{z-L}\,LP. \tag{B.15}
\end{aligned}$$

It can be checked that Eqs. (B.12 and B.15) are identical. One recognizes in Eq. (B.15) the three terms of the Langevin equation (see Ref. [21]). However, we emphasize that expression (B.12) has many advantages since it relates directly the complex poles of $P/(z-L^{\text{eff}}(z))$ to the various relevant microscopic and macroscopic timescales.

REFERENCES

[1] E. Brändas, Introduction to the concept of resonances, Int. J. Quant. Chem. 31 (1987) 699. Proceedings of the Uppsala Resonance Workshop.
[2] E. Brändas, E. Elander (Eds.), Resonances. The Unifying Route Towards the Formulation of Dynamical Processes. Foundations and Applications in Nuclear, Atomic and Molecular

Physics, Vol. 325: Lecture Notes in Physics, Springer-Verlag, Berlin, 1989. Proceedings of a Symposium held at Lertorpet, Värmland, Sweden, 19–26 August, 1987.

[3] V. Kukulin, V. Krasnopol'sky, J. Horáček, Theory of Resonances. Principles and Applications, Academia, Praha, 1989.

[4] Ph. Durand, J.-P. Malrieu, Effective Hamiltionians and pseudo potentials as tools for rigorous modeling, in: K.P. Lawley (Ed.), Ab Initio Methods in Quantum Chemistry I, John Wiley & Sons, New York, 1987, p. 352.

[5] P. Durand, I. Paidarová, Wave operator theory of quantum dynamics, Phys. Rev. A 58 (1998) 1867.

[6] P.-O. Löwdin, Studies in perturbation theory. X. Lower bounds to energy eigenvalues in perturbation-theory ground state, Phys. Rev. 139 (1965) A357.

[7] C. Cohen-Tannoudji, J. Dupont-Roc, G. Grynberg, Processus d'interaction entre photons et atomes, InterEditions et Editions du CNRS, Paris, 1988. English translation: Atom-Photon Interactions. Basic Processes and Applications, John Wiley & Sons, New York, 1992.

[8] Ph. Durand, I. Paidarová, F.X. Gadéa, Theory of Fano profiles, J. Phys. B At. Mol. Opt. Phys. 34 (2001) 1953.

[9] I. Paidarová, Ph. Durand, Modeling quantum resonances: I. Dynamics of interacting resonances, in: J. Maruani, R. Lefebvre, E. Brändas (Eds.), Advanced Topics in Theoretical Chemical Physics, Vol. 12: Progress in Theoretical Chemistry and Physics, Kluwer Academic, Dordrecht, 2003, p. 271.

[10] I. Paidarová, Ph. Durand, Quantum resonances: Line profiles and dynamics, Collect. Czech. Chem. Commun. 68 (2003) 529.

[11] F.X. Gadéa, P. Durand, T. González-Lezana, G. Delgado-Barrio, P. Villareal, Effective resolvent applied to interacting resonances, Eur. Phys. J. D 15 (2001) 215.

[12] Ph. Durand, I. Paidarová, G. Jolicard, F. Gemperle, Iterative determination of several interior eigenstates of large matrices: Application to the determination of light-induced resonances in H_2^+, J. Chem. Phys. 112 (2000) 7363–7373.

[13] F. Gemperle, F.X. Gadéa, Beyond Born-Oppenheimer spectroscopic study for the C state of LiH, J. Chem. Phys. 110 (1999) 11197.

[14] I. Paidarová, Ph. Durand, Effective couplings between quantum resonances: application to the resonant dissociation of the $^6Li^7Li$ molecule, Czech. J. Phys. 55 (2005) 203–216.

[15] M. Desouter-Lecomte, J. Liévin, V. Brems, Avoided resonance overlapping beyond the energy independent formalism. 1. Vibrational predissocation, J. Chem. Phys. 103 (1995) 4524.

[16] V. Brems, M. Desouter-Lecomte, J. Liévin, Avoided resonance overlapping beyond the energy independent formalism. 2. Electronic predissociation, J. Chem. Phys. 104 (1996) 2222.

[17] M. Desouter-Lecomte, J. Liévin, Memory kernels and effective Hamiltonians from time dependent methods. 1. Predissociation with a curve crossing, J. Chem. Phys. 107 (1997) 1428.

[18] V. Brems, M. Desouter-Lecomte, Memory kernels and effective Hamiltonians from time-dependent methods. II Vibrational predissociation, J. Chem. Phys. 116 (2002) 8318.

[19] U. Fano, Sullo spettro di assorbimento dei gas nobili presso il limite dello spettro darco, Nuovo Cimento 12 (1935) 154. English translation: U. Fano, G. Pupillo, A. Zannoni, C. W. Clark, On the absorption spectrum of noble gases at the arc spectrum limit, J. Res. Natl. Inst. Stand. Technol. 110 (2005) 583.

[20] P. Avan, Interacting Resonances in Atomic Spectroscopy, Ph.D. Thesis, Université de Paris VI, 1976.

[21] C. Cohen-Tannoudji, Cours au Collège de France, http://www.phys.ens.fr/cours/college-de-france/1977-78/1977-78.htm (1977).

[22] C. Mahaux, H.A. Weidenmüller, Shell Model Approach to Nuclear Reactions, North-Holland, Amsterdam, 1969.

[23] J.J.M. Verbaarschot, H. A. Weidenmüller, M. R. Zirnbauer, Grassmann integration in stochastic quantum physics — the ase of compound nucleus scattering, Phys. Rep. 129 (1985) 369.

[24] W.R. Haydock, The recursive solution of teh Schrödinger equation, in: H. Ehrenreich, F. Seitz, D. Turnbull (Eds.), Advances in Research and Applications, Vol. 35: Solid State Physics, Academic Press, New York, 1980, p. 215.

[25] E. Brändas, R.J. Bartlett, Reduced partitioning technique for configuration interaction calculations using Pade approximants and inner projections, Chem. Phys. Lett. 8 (1971) 153.

[26] J. Horáček, in T.E. Simos, G. Psihoyois, C. Tsitouras (Eds.), Determination of Resonance Parameters by Use of Pade III Approximation, Vols: 1 and 2 Numerical Analysis and Applied Mathematics, AIP Conference Proceedings, International Conference on Numerical Analysis and Applied Mathematics, Sep 18–22, 2009, Rethymno, Greece.

[27] R. Levine, Quantum Mechanics of Molecular Rate Processes, Clarendon Press, Oxford, 1969.

[28] U. Fano, Effects of configuration interaction on intensities and phase shifts, Phys. Rev. 124 (1961) 1866.

[29] E. Langmann, G. Lindblad, Fermi's golden rule and exponential decay as a RG fixed point, J. Stat. Phys. 134 (2009) 749.

[30] Th.G. Douvropoulos, C.A. Nicolaides, Nonexponential decay porpagator and its differenctial equation for real and complex energy distributions of unstable states, Phys. Rev. A 69 (2004) 032105.

[31] G. Jolicard, Effective Hamiltionian theory and molecular-dynamics, Annu. Rev. Phys. Chem. 46 (1995) 83.

[32] Ph. Durand, I. Paidarová, From effective Hamiltionians to fluctutation and dissipation, Theor. Chem. Acc. 116 (2006) 559.

[33] R. Lefebvre, O. Atabek, V. Leon, Occurrence of unit transmissivity in scattering, Phys. Rev. A 65 (2002) 042726.

[34] Ph. Durand, I. Paidarová, Theory of generalized Fano profiles, J. Phys. B At. Mol. Opt. Phys. 35 (2002) 469.

[35] Ph. Durand, I. Paidarová, Ionization of hydrogen atom: From weak to strong static electric fields, Eur. Phys. J. D 26 (2003) 253.

[36] M. Hehenberger, H.V. McIntosh, E. Brändas, Wely's theory applied to the Stark effect in the hydrogen atom, Phys. Rev. A 10 (1974) 1494.

[37] L. Landau, E. Lifshitz, Quantum Mechanics, Oxford, Pergamon, 1968, p. 257.

[38] C.A. Nicolaides, D.R. Beck, On the possibility of observing nonexponential decays in autoionizing states, Phys. Rev. Lett. 38 (1977) 683 (Addendum 1037).

[39] L.-Y. Peng, A.F. Starace, Application of Coulomb wave function disrete variable respresentation to atomic systems in strong laser fields, J. Chem. Phys. 125 (2006) 154311.

[40] A. Scrinzi, Ionization of multielectron atoms by strong static electric fields, Phys. Rev. A 61 (2000) 041402.

[41] S. Geltman, Short-time dynamics of static field excitation and ionization, J. Phys. B At. Mol. Opt. Phys. 33 (2000) 4769.

[42] J.-P. Connerade, A.M. Lane, Interacting resonances in atomic spectroscopy, Rep. Prog. Phys. 51 (1988) 1439.

[43] U. Fano, J.W. Cooper, Line profiles in the Far-UV absorption spectra of the rare gases, Phys. Rev. 137 (1965) A1364.

[44] T.Y. Wu, T. Ohmura, Quantum Theory of Scattering, Prentice-Hall, Englewood Cliffs, 1962.

[45] J.R. Taylor, Scattering Theory, John Wiley & Sons, New York, 1972.

[46] C.J. Joachain, Quantum Collision Theory, North-Holland, Amsterdam, 1975.

[47] J.N. Bardsley, F. Mandl, Resonant scattering of electrons by molecules, Rep. Prog. Phys. 31 (1968) 471.

[48] P.G. Burke, Resonances in electron scattering by atoms and molecules, Adv. At. Mol. Phys. 4 (1968) 173.

[49] W. Domcke, Theory of resonance and threshold effects in electronmolecule collisions: The projection-opperator approach, Phys. Rep. 208 (1991) 97.

[50] S.J. Buckman, C.W. Clark, Atomic negative-ion resonances, Rev. Mod. Phys. 66 (1994) 539.

[51] Ph. Durand, I. Paidarová, Modeling quantum resonances: II. Overview of collision theory, in: J. Maruani, R. Lefebvre, E. Brändas (Eds.), Advanced Topics in Theoretical Chemical Physics, Vol. 12: Progress in Theoretical Chemistry and Physics, Kluwer Academic, Dordrecht, 2003, p. 295

[52] A. Messiah, Quantum Mechanics 2, North-Holland, Amsterdam, 1966.

[53] M. Desouter-Lecomte, V. Jacques, Avoided overlap between 2 resonance energies or frequencies — formation of fast and slow decay modes, J. Phys. B At. Mol. Opt. Phys. 28 (1995) 3225.

[54] M. Müller, F.-M. Dittes, W. Iskra, I. Rotter, Level repulsion in the comlex plane, Phys. Rev. E 52 (1995) 5961.

[55] P. von Brentano, On the mixing of two bound and unbound levels: Energy repulsion and width attractions, Phys. Rep. 264 (1996) 57.

[56] J. Okołowicz, N. Płoszajczak, I. Rotter, Dynamics of quantum systems embedded in a continuum, Phys. Rep. 374 (2003) 271.

[57] F.T. Smith, Lifetime matrix in collision theory, Phys. Rev. 118 (1960) 349.

[58] K.M. Dunseath, M. Terao-Dunseath, J.-M. Launay, Shape resonances in electron-hydrogen scattering, J. Phys. B At. Mol. Opt. Phys. 33 (2000) 3037.

[59] E. Narevicius, N. Moiseyev, Non-hermitian formulation of interference effect in scattering experiments, J. Chem. Phys. 113 (2000) 6088.

[60] Ph. Durand, I. Paidarová, Towards a unified formulation of dynamics and thermodynamics I. Form microscopic to macroscopic time scales, Int. J. Quantum Chem. (2010). DOI: 10.1002/qua.22584.

[61] E.T. Jaynes, Information theory and statistical mechanics, Phys. Rev. 106 (1957) 620.

[62] M. Le Bellac, F. Mortessagne, G. Batrouni, Equilibrium and Non-equilibrium Statistical Thermodynamics, Cambridge University Press, Cambridge, 2004.

[63] E. Fick, G. Sauermann, The Quantum Statistics of Dynamic Processes, Springer, Berlin, 1990.

[64] X. Forster, Hydrodynamic, Fluctuations, Broken Symmetry, and Correlation Functions, Addison-Wesley, Reading, 1975.

[65] I. Paidarová, Ph. Durand, Towards a unified formulation of dynamics and thermodynamics II. Dissipative processes and entropy production, Int. J. Quantum Chem. (2010). DOI: 10.1002/qua.22630.

[66] D. Jou, J. Casas-Vázquez, G. Lebon, Extended Irreversible Thermodynamics, third enlarged ed. (2001), Springer, Berlin, 1993.

[67] N. Pottier, Physique statistique hors d'équilibre. Processus irréversibles linéaires, EDP Sciences, Paris, 2007.

[68] S. de Groot, P. Mazur, Non-Equilibrium Thermodynamics, North Holland, Amsterdam 1962; Dover edition, New York, 1984.

[69] P.W. Atkins, Physical Chemistry, seventh ed., W. H. Freeman, New York 1998; Oxford University Press, Oxford, 2002.

[70] F. Roddier, Distribution et Transformation de Fourier, Mc Graw-Hill, Paris, 1991.

[71] I. Prigogine, C. George, F. Henin, L. Rosenfeld, A unified formulation of dynamics and thermodynamics, Chem. Scr. 4 (1973) 5.

[72] C. Obcemea, E. Brändas, Analysis of Prigogine's theory of subdynamics, Ann. Phys. 151 (1983) 383.

Unstable States in Laser Assisted and Controlled Molecular Processes

O. Atabek[a], R. Lefebvre[a,b] and **T.T. Nguyen-Dang[c]**

Contents

[a] Institut des Sciences Moléculaires d'Orsay, Bâtiment 350, Université Paris-Sud 11 Campus d'Orsay, 91405 Orsay, France

[b] UFR de Physique Fondamentale et Appliquée, UPMC, 75005, Paris, France

[c] Département de Chimie, Université Laval, Québec, G1K 7P4, Canada

E-mail addresses: osman.atabek@u-psud.fr (O. Atabek), roland.lefebvre@u-psud.fr (R. Lefebvre), tung@chm.ulaval.ca (T.T. Nguyen-Dang)

Abstract   Many aspects of intense-field molecular dynamics rely on the concept of resonance. The chapter gives a thorough review of these aspects, bringing out the specificity of laser-induced resonances, in particular those defined in the Floquet or dressed molecule picture. The role of these resonances in the time-resolved dynamics of molecules subjected to an intense, ultrafast laser pulse is discussed and basic mechanisms of molecular fragmentation and its control are reviewed. We discuss how a thorough interpretation of two–color extreme ultraviolet (XUV) + Infra-red (IR) pump–probe experiments on the dissociative ionization of H_2 can be made in terms of adiabatic vs. non-adiabatic resonance transports (i.e., laser-induced time evolutions) and in terms of field-induced processes such as Bond-Softening (BS) and Vibrational Trapping (VT), associated with the Floquet representation or the Dynamical Dissociation Quenching (DDQ) effects associated with a time-dependent quasi-static representation. Another application of the concepts of laser-induced resonances, and of their adiabatic evolution, is devoted to laser control strategies based on Zero-Width Resonances (ZWR) and Exceptional Points (EP), the approach of which in laser parameter space corresponds to the coalescence of two laser-induced resonances. We illustrate how the concept of ZWR can be useful for the molecular cooling problem. We then show how advantage can be taken of resonance coalescence at an EP to devise new laser control strategies pertaining to vibrational energy transfer processes.

Keywords: Resonances; Multiphoton Dissociation; Floquet Theory; Attosecond Pump-Probe Spectroscopy; Zero-Width Resonances; Exceptional Points; Laser Control; Adiabaticity; Non-Adiabatic Processes.

1. INTRODUCTION

The detailed description of the interactions between a molecule and a strong electromagnetic field provides the key for the interpretation of laser-induced and laser-controlled photochemical reactions [1]. Not only can structural and dynamical properties of molecules involved in such a reaction be analyzed or the nature and the role of transient species be probed, but the

reaction itself can be optimally controlled by using appropriate sources of radiation. Intense laser fields apply forces to molecules that are strong enough to produce important distortions and offer the possibility to control both internal (total and partial dissociation rates as well as fragment kinetic and angular distributions) and external motions (angular positioning of the molecule with respect to the laser polarization vector). Resonances play an important part in the theoretical understanding of a wide variety of laser-induced molecular processes, ranging from dynamical interpretations of photofragmentation spectra [2, 3] to the depiction of basic mechanisms used as ingredients in laser control of reactivity [4–6]. These unstable states in the molecular continuous spectra are characterized by quantized complex energies, resulting from their outgoing asymptotic behavior (Siegert boundary conditions [7]). Their imaginary parts are inversely proportional to their lifetimes. Several techniques have so far been developed for their accurate calculation by solving close-coupled differential equations, with appropriate boundary conditions [4, 8]. In the context of intense laser fields, these equations describe nuclear motions on multiphoton field-dressed electronic potentials of the Floquet Hamiltonian [2, 3, 9]. Such laser-induced potentials, apart from accommodating resonances, also lead to a clear understanding of basic mechanisms. Among them, bond softening (BS) or vibrational trapping (VT) in the Above Threshold Dissociation (ATD) regime [3], acting in an antagonistic manner [5], open the way to efficient and robust control scenarios (reactivity, alignment/orientation, purification, vibrational transfer). These mechanisms have experimentally confirmed counterparts in the time domain and may considerably affect the wavepacket dynamics when referring to short pulse durations: barrier lowering and Dynamical Dissociation Quenching (DDQ) [10–13].

Highly nonlinear field-induced barrier lowering or suppression and stabilization (trapping or quenching) mechanisms both in the Visible-Ultra-Violet (Vis-UV)[3] and the Infra-Red (IR) [10–12] frequency regimes underlie chemical BS or hardening processes, respectively. Their interplay through the adequate adjustment of laser characteristics, such as laser frequency, amplitude, phase, polarization, and temporal shape, provides interesting novel control opportunities [5]. In the presence of strong fields, resonances also show highly nonlinear features. The widths increase with the field intensity in a nonperturbative way (in the cases of shape resonances) but, in some circumstances and more unexpectedly, they may saturate and even decrease (the cases of Feshbach resonances). The decrease is such that for some values of the laser parameters (frequency and intensity) one can reach strictly zero width, a counterintuitive situation where a molecule irradiated by a strong field becomes stable. A so-called bound state in a continuum or a Zero-Width Resonance (ZWR) is obtained [6, 14]. For other choices of field parameters, one can realize a coalescence of two resonances, one of the shape type and the other of Feshbach type, as a so-called Exceptional Point (EP) is reached [15].

ZWRs and EPs lead to very interesting control issues, involving molecular cooling and vibrational population transfer strategies [6, 15].

This chapter reviews these aspects of intense-field molecular dynamics and discusses their pertinence to the detailed interpretation of two-colour dissociative ionization experiments and the laser control theory. The chapter is organized as followed. The theory of laser–molecule interactions is presented in Section 2, starting from a general multicharged system considered in a semiclassical field description. The Hamiltonian of the laser-driven system is given in the length gauge [1, 16–18]. The Section continues with a thorough analysis of multichannel field-dressed molecular models within the Born–Oppenheimer (BO) approximation [19] (for the molecular part) and the Floquet formalism [9, 20] (for the radiative part). Section 3 is devoted to numerical methodologies for solving coupled equations describing the dynamics of a laser-driven two-channel (two-electronic-state) molecule, either in a time-independent frame, where emphasis is placed on field-induced resonances, or in a time-dependent context, highlighting time-resolved features. Basically, the numerical techniques that are retained are the Fox–Goodwin propagator [8] using complex rotation [21] of the spatial coordinate (time-independent approach) or the split-operator formula coupled to Fast Fourier Transform algorithms [22] adequately modified to take advantage of Volkov-type solutions [23] in asymptotic regions (time-dependent approach). Dynamical processes with their underlying mechanisms and control strategies are presented in Section 4.

As a first application of the theory, concepts, and methodologies of Sections 2 and 3, we discuss the dissociative ionization dynamics of the molecular ion H_2^+ under two-colour extreme Ultraviolet (XUV) + Infra-red (IR) pump–probe ultrafast, intense laser excitations. In Section 5 the results of wavepacket dynamics simulations, done within a theory/experiment collaboration [24, 25], are compared to experimental data, aiming at a thorough interpretation in terms of resonances and basic mechanisms. In one series of experiments using IR pulses that are shorter than the vibrational period of H_2^+, de-phasing and re-phasing of the vibrational wavepacket that is formed in H_2^+ upon ionization of the neutral molecule by the XUV pulse are observed. This observation is interpreted in terms of a laser–molecule synchronization similar to that of the DDQ mechanism [10–12]. In experiments where the duration of the IR pulse exceeds the vibrational period of H_2^+, a pronounced dependence of the H^+ kinetic energy (KE) distribution on XUV-IR delay is observed that can be explained in terms of the adiabatic propagation of the H_2^+ wavepacket and the BS mechanism on field-dressed potential energy curves.

The second application, considered in Section 6, is devoted to laser control strategies based on ZWRs and EPs [26]. A semiclassical model helps in determining, for a given wavelength, the laser intensity at which a ZWR is produced. The ZWR is shown to be useful for vibrational purification

processes and thus ultimately for molecular cooling control. Finally, it is also shown how an appropriate choice of laser parameters may provoke the approach of an EP leading to the coalescence of two resonances (complex eigenenergies and wavefunctions). We show how advantage can be taken of such a situation in devising innovative laser control strategies pertaining to vibrational energy transfer processes.

2. GENERAL THEORY OF LASER–MOLECULE INTERACTIONS

2.1. Molecular Hamiltonian in the presence of a laser field

Many forms of the Hamiltonian operator describing a system interacting with a radiation field are currently in use [1, 4, 17, 18]. These are defined within either of two descriptions: One is fully quantized and treats both the laser field and the molecular system quantum mechanically. The other is semiclassical and assumes at the outset a classical field while the charged particles are treated quantum mechanically. We recall here the expression of the Hamiltonian of a laser-driven molecule written in the semiclassical description; this will serve to lay the ground work for the construction of the models encountered in the subsequent Sections. It is to be recalled also that many equivalent forms of the radiative interaction exist, corresponding to different choices of the electromagnetic field's gauge. We will systematically refer to the so-called Coulomb length gauge in writing the interaction between a charged particle of a molecule and a radiation field. Also, only electric dipole interactions are considered within the so-called long-wavelength approximation.

2.2. Multichannel molecular models

For a complete treatment of a laser-driven molecule, one must solve the many-body, multidimensional time-dependent Schrödinger equation (TDSE). This represents a tremendous task and direct wavepacket simulations of nuclear and electronic motions under an intense laser pulse is presently restricted to a few bodies (at most three or four) and/or to a model of low dimensionality [27]. For a more general treatment, an approximate separation of variables between electrons (fast subsystem) and nuclei (slow subsystem) is customarily made, in the spirit of the BO approximation. To lay out the ideas underlying this approximation as adapted to field-driven molecular dynamics, we will consider from now on a molecule consisting of N_n nuclei (labeled α, β, ...) and N_e electrons (labeled i, j, ...), with position vectors $\mathbf{R}_\alpha$ and $\mathbf{r}_i$ respectively, defined in the center of mass (rotating) body-fixed coordinate system, in a classical field $\mathbf{E}(t)$ of the form $\mathbf{E}_0 f(t) \cos(\omega t)$. The full semiclassical length gauge Hamiltonian is written, for a system of electrons and nuclei, as [4]

$$H(t) = H_{el}(t) + T_N - \boldsymbol{\mu}_N(\{\mathbf{R}_\alpha\}) \cdot \mathbf{E(t)} \tag{1}$$

with

$$H_{el}(t) = \sum_i \frac{\mathbf{p}_i^2}{2m} + V(\{\mathbf{r}_i\},\{\mathbf{R}_\alpha\}) + e \sum_i \mathbf{r}_i \cdot \mathbf{E}(t) \tag{2}$$

where T_N denotes the KE and $\boldsymbol{\mu}_N(\{\mathbf{R}_\alpha\})$ is the dipole moment operator associated with the nuclei. This gauge has the advantage of giving a simple form for the close-coupled equations, as is clarified hereafter.

In the electronic Hamiltonian $H_{el}(t)$, the potential function $V(\{\mathbf{r}_i\},\{\mathbf{R}_\alpha\})$ comprises all Coulomb interactions between the charges, i.e., it is the sum of V_{en}, the attraction between electrons and nuclei, V_{ee}, the Coulomb repulsion between the electrons, as well as V_{nn}, the repulsion between the various nuclei of the molecular system. The sum of $V(\{\mathbf{r}_i\},\{\mathbf{R}_\alpha\})$ and the electronic KE defines the field-free electronic Hamiltonian, H_{el}^0:

$$H_{el}^0 = \sum_i \frac{\mathbf{p}_i^2}{2m} + V(\{\mathbf{r}_i\},\{\mathbf{R}_\alpha\}). \tag{3}$$

Its eigenfunctions

$$H_{el}^0 \Xi_I(\{\mathbf{r}_i\};\{\mathbf{R}_\alpha\}) = \epsilon_I(\{\mathbf{R}_\alpha\}) \Xi_I(\{\mathbf{r}_i\}; \{\mathbf{R}_\alpha\}), \tag{4}$$

which are supposedly orthonormal by construction, constitute a complete basis in terms of which the total molecular wavefunction can be expanded:

$$\Omega(\{\mathbf{r}_i\},\{\mathbf{R}_\alpha\},t) = \sum_I \Psi_I(\{\mathbf{R}_\alpha\},t) \Xi_I(\{\mathbf{r}_i\}; \{\mathbf{R}_\alpha\}). \tag{5}$$

It is to be noted that the dependence of the electronic basis wavefunctions $\Xi_I(\{\mathbf{r}_i\}; \{\mathbf{R}_\alpha\})$ on the nuclear coordinates $\{\mathbf{R}_\alpha\}$ is a parametric one. Since the field-free electronic Hamiltonian is time independent, the basis set is independent of time. Yet, the expansion coefficients $\Psi_I(\{\mathbf{R}_\alpha\},t)$ in this basis are time-dependent and have to obey the reduced coupled Schrödinger equations:

$$i\hbar \frac{\partial \Psi_I(\{\mathbf{R}_\alpha\}, t)}{\partial t} = [T_N + \epsilon_I(\{\mathbf{R}_\alpha\}) - \boldsymbol{\mu}_N(\{\mathbf{R}_\alpha\}) \cdot \mathbf{E}(t)] \Psi_I(\{\mathbf{R}_\alpha\}, t)$$
$$- \mathbf{E}(t) \cdot \sum_J \langle \Xi_I | (-e \sum_i \mathbf{r}_i) | \Xi_J \rangle \Psi_J(\{\mathbf{R}_\alpha\}, t) + \sum_J \mathcal{C}_{I,J} \Psi_J(\{\mathbf{R}_\alpha\}, t), \tag{6}$$

where $\mathcal{C}_{I,J}$ are non-adiabatic coupling operators, the exact form of which depends on the choice of nuclear coordinates. When the field is turned off

(i.e., $\mathbf{E}(t) = 0$), neglect of the nonradiative (i.e., non-adiabatic) coupling terms on the third line of this equation yields the celebrated BO approximation [19]: Since no coupling then exists any longer between the various Ψ_I's, the expansion of Eq. (5) reduces to a single term denoting an approximate separation of nuclear and electronic variables. While the electronic part is described by Eq. (4), an effective Schrödinger equation describes the nuclear motions viewed as occurring on a single potential energy surface (PES), a single *electronic channel*, described by the electronic energy $\epsilon_I(\{\mathbf{R}_\alpha\})$ which now plays the role of a potential energy function. In field-free molecular dynamics, the neglect of non-adiabatic couplings is usually justified, at least in part, by the disparity between the nuclear and the electronic masses. Here, their neglect is justified by the observation that they are dominated by the strong couplings between the electronic states or the *channels* as induced by the intense laser field. Thus, neglecting these nonradiative couplings [the last sum in Eq. (6)] to concentrate on field-induced effects, we obtain

$$i\hbar \frac{\partial \Psi_I(\{\mathbf{R}_\alpha\}, t)}{\partial t} = [T_N + \epsilon_I(\{\mathbf{R}_\alpha\}) - \boldsymbol{\mu}_N(\{\mathbf{R}_\alpha\}) \cdot \mathbf{E}(t)] \Psi_I(\{\mathbf{R}_\alpha\}, t)$$
$$- \mathbf{E}(t) \cdot \sum_J \langle \Xi_I | (-e \sum_i \mathbf{r}_i) | \Xi_J \rangle \Psi_J(\{\mathbf{R}_\alpha\}, t). \tag{7}$$

This is the start of the construction of multichannel models of laser-driven molecules. In practice, one restricts to a finite number, N_{ch}, of electronic states, selected on the basis of physical relevance and Eq. (7) defines an N_{ch}-channel molecular model system. The "electronic" Hamiltonian is, in this model, described by the operator

$$H_{el}(\{\mathbf{R}_\alpha\}, t) = \sum_{I,J} [\epsilon_I(\{\mathbf{R}_\alpha\})\delta_{IJ} - \mathbf{E}(t) \cdot \boldsymbol{\mu}_{IJ}(\{\mathbf{R}_\alpha\})] | \Xi_I \rangle \langle \Xi_J |, \tag{8}$$

where

$$\boldsymbol{\mu}_{IJ}(\{\mathbf{R}_\alpha\}) = \langle \Xi_I | (-e \sum_i \mathbf{r}_i) | \Xi_J \rangle \tag{9}$$

is the transition dipole moment between the field-free electronic states $| \Xi_I \rangle$ and $| \Xi_J \rangle$. In matrix form, H_{el} is represented by

$$\tilde{\mathbf{W}}(\{\mathbf{R}_\alpha\}; t)$$
$$= \begin{pmatrix} \epsilon_1 - \boldsymbol{\mu}_{11} \cdot \mathbf{E}(t) & -\boldsymbol{\mu}_{12} \cdot \mathbf{E}(t) & .. & .. & .. \\ -\boldsymbol{\mu}_{21} \cdot \mathbf{E}(t) & \epsilon_2 - \boldsymbol{\mu}_{22} \cdot \mathbf{E}(t) & -\boldsymbol{\mu}_{23} \cdot \mathbf{E}(t) & .. & .. \\ .. & -\boldsymbol{\mu}_{32} \cdot \mathbf{E}(t) & \epsilon_3 - \boldsymbol{\mu}_{33} \cdot \mathbf{E}(t) & -\boldsymbol{\mu}_{34} \cdot \mathbf{E}(t) & .. \\ .. & .. & .. & .. & .. \end{pmatrix} \tag{10}$$

and, gathering the nuclear amplitudes $\Psi_I(\{\mathbf{R}_\alpha\}, t)$ into a column vector $\Psi(\{\mathbf{R}_\alpha\}, t)$, Eq. (7) reads

$$i\hbar \frac{\partial \Psi(\{\mathbf{R}_\alpha\}, t)}{\partial t} = \left[T_N \mathbf{1} + \tilde{\mathbf{W}}(\{\mathbf{R}_\alpha\}; t) \right] \Psi(\{\mathbf{R}_\alpha\}, t). \quad (11)$$

2.3. Floquet theory

When the external field is a continuous wave (cw) field,

$$\mathbf{E}(t) = \mathbf{E}_0 \cos \omega t \quad (12)$$

the various Hamiltonians given above, in Eqs. (1, 2) or in Eq. (11), are time-periodic of period $T = 2\pi/\omega$, i.e., $H(t + T) = H(t)$. Owing to this time-periodicity, the Floquet theorem [20] is applicable to the TDSE associated with that Hamiltonian. We recall here the main concepts of Floquet theory as applied to the Schrödinger equation

$$i\hbar \frac{\partial \mid \Psi(t) \rangle}{\partial t} = H(t) \mid \Psi(t) \rangle, \quad (13)$$

for any of the time-periodic Hamiltonians referred to above (specialization to a specific form of this Hamiltonian will be made later). Floquet theorem states that this TDSE admits solutions of the form:

$$\mid \Psi_E(t) \rangle = \mathrm{e}^{-i\frac{Et}{\hbar}} \mid \Phi_E(t) \rangle, \quad (14)$$

with $\mid \Phi_E(t + T) \rangle = \mid \Phi_E(t) \rangle$, which constitute a complete basis for a full description of the dynamics.[1] Introduction of the Floquet form into the wave equation produces for $\mid \Phi_E(t) \rangle$ the equation:

$$\left[H(t) - i\hbar \frac{\partial}{\partial t} \right] \mid \Phi_E(t) \rangle = E \mid \Phi_E(t) \rangle. \quad (15)$$

The operator acting on $\mid \Phi_E(t) \rangle$ is called the Floquet Hamiltonian,

$$H_F(t) = H(t) - i\hbar \frac{\partial}{\partial t}, \quad (16)$$

and the time in this is to be treated as an additional dynamical variable so that Eq. (15) determines eigenvalues and eigenstates of the Floquet

---

[1] The theorem applies to scattering and bound states with a real energy and to resonance states with a complex energy. When the energy is quantized (bound and resonance states), it is called a quasi-energy, for reasons to be developed below.

Hamiltonian in an extended space, the direct product of the usual molecular Hilbert space, and the space of periodic functions of $t \in [0,T]$. This extension of the Hilbert space can be made somewhat more transparent by introducing a new time-like variable, to be distinguished from the actual time variable t. This new time variable can be defined through the arbitrary phase of the continuous (periodic) field, as done in Ref. [28, 29]. A variant of the idea is found in the (t, t') method developed by Peskin and Moiseyev [30] and applied to the photodissociation of H_2^+ [31, 32]. We will continue with the more traditional and simpler formulation of Floquet theory here, as this is sufficient to bring out ideas of laser-induced resonances in the dressed molecule picture.

In all strong-field molecular dynamics problems, the Hamiltonian $H(t)$ can be split into a time-independent part, denoting the field-free molecule, and a time-dependent one representing the matter–field interaction:

$$H(t) = H_0 + V(t). \tag{17}$$

The time-periodic part $| \ \Phi_E(t)\rangle$ of the Floquet eigenvector and the time dependent interaction 'potential'[2] $V(\mathbf{r}, t)$ can be written in the form of a discrete Fourier series,

$$V(\mathbf{r},t) = \sum_n V_n(\mathbf{r})e^{in\omega t}, \tag{18}$$

and:

$$| \ \Phi_E(t)\rangle = \sum_n | \ U_n\rangle e^{in\omega t} \tag{19}$$

with n going from $-\infty$ to $+\infty$. In the case of Eq. (19) for the Floquet wavefunction $| \ \Phi_E(t)\rangle$, we are in fact expanding it in the complete orthonormal basis of periodic functions of the new dynamical variable t, $e^{in\omega t}$. Substituting these expansions into the Floquet eigenvalue equation (Eq. (15)) results in an elimination of the time variable to give a system of coupled *time-independent* equations:

$$[H_0 + V_0(\mathbf{r})] | \ U_n\rangle + \sum_{n' \neq n} V_{n-n'}(\mathbf{r}) | \ U_{n'}\rangle = (E - n\hbar\omega) | \ U_n\rangle. \tag{20}$$

In the case of a matter–field interaction of the form

$$V(\mathbf{r}, t) = -\boldsymbol{\mu}(\mathbf{r}) \cdot \mathbf{E}(t) = -\frac{1}{2}\boldsymbol{\mu}(\mathbf{r}) \cdot \mathbf{E}_0[e^{i\omega t} + e^{-i\omega t}], \tag{21}$$

---

[2] To fix the idea, we shall henceforth consider the case this interaction term depends on $\mathbf{r}$, as in the length gauge Hamiltonian.

as found in Eqs. (1 and 2) with a cosine electric field, $V(t)$ has only two non-zero Fourier components

$$V_{\pm 1} = -\frac{1}{2}\boldsymbol{\mu}(\mathbf{r}) \cdot \mathbf{E}_0, \tag{22}$$

so that the coupled Eq. (20) reduce to

$$(H_0 + n\hbar\omega) \mid U_n \rangle - \frac{1}{2}\boldsymbol{\mu}(\mathbf{r}) \cdot \mathbf{E}_0 (\mid U_{n+1} \rangle + \mid U_{n-1} \rangle) = E \mid U_n \rangle. \tag{23}$$

A number of basic properties of the Floquet states $\mid \Psi_E(t) \rangle$ can be infered easily from Eqs. (14 and 19). First, if E_i is a quasi-energy, i.e., an eigenvalue of H_F associated with an eigenstate $\mid \Phi_{E_i}(t) \rangle$, then

$$E_{i,k} = E_i + k\hbar\omega \tag{24}$$

is also an eigenvalue, i.e., it also belongs to the Floquet energy spectrum. The eigenvector associated with this eigenvalue is obtained by multiplying $\mid \Phi_{E_i}(t) \rangle$ with $e^{ik\omega t}$ as can be verified by substituting the new periodic function $e^{ik\omega t} \mid \Phi_{E_i}(t) \rangle$ into Eq. (19). Accordingly, the Fourier indices n labeling the components $\mid U_n \rangle$ are shifted by $-k$, i.e, $\mid U_n^{E+k} \rangle = \mid U_{n-k}^E \rangle$. Thus quasi-energies are defined modulo an integer multiple of $\hbar\omega$ and should therefore be identified by at least two indices, as evoked in Eq. (24): Together with i, the index k defines a quasi-energy level in a definite Brillouin zone, which is specified by k alone. This is in complete analogy with the situation met in crystals, where the Floquet theorem also applies, but this time as a result of the spatial periodicity of the potential, and is called Bloch theorem [33]. It is known that the Floquet states belonging to a single zone constitute a complete basis set [34], in the case where the quasi-energy spectrum is discrete. Extension to cases involving continua and resonance states can be made heuristically by invoking a continuum discretization procedure.

Second, the properties of Floquet eigenstates are such as to produce a very simple *stroboscopic* way of following the motion of a general wavepacket of the time-dependent laser-driven system: Consider the evolution operator $\mathcal{U}(t + T, t)$ between times t and $t + T$. Starting at time t from a Floquet state

$$\mid \Psi_i(t) \rangle = e^{-i\frac{E_i t}{\hbar}} \mid \Phi_i(t) \rangle, \tag{25}$$

we have after time T:

$$\mathcal{U}(t + T, t) \mid \Psi_i(t) \rangle = e^{-i\frac{E_i(t+T)}{\hbar}} \mid \Phi_i(t+T) \rangle = e^{-i\frac{E_i(t+T)}{\hbar}} \mid \Phi_i(t) \rangle. \tag{26}$$

In particular if $t = 0$:

$$\mathcal{U}(T, 0) \mid \Psi_i(0) \rangle = e^{-i\frac{E_i T}{\hbar}} \mid \Phi_i(T) \rangle = e^{-i\frac{E_i T}{\hbar}} \mid \Phi_i(0) \rangle. \tag{27}$$

This shows that the time evolution is exactly like that of a stationary state of a time-independent Hamiltonian, provided the probing is limited to T, or any multiple of T. Since $|\Psi_i(0)\rangle$ is equal to $|\Phi_i(0)\rangle$, Eq. (27) also shows that $\exp(-iE_iT/\hbar)$ is an eigenvalue of the evolution operator over one period of the field. Suppose now that we wish to follow the development in time of an arbitrary initial wavepacket $|\eta(0)\rangle$. We can expand it over the complete set of Floquet eigenfunctions of a given Brillouin zone at time $t = 0$:

$$| \eta(0)\rangle = \sum_i | \Phi_i(0)\rangle\langle\Phi_i(0) | \eta(0)\rangle. \tag{28}$$

At time $t = NT$, the wavepacket has evolved into

$$| \eta(NT)\rangle = \sum_i e^{-i\frac{E_iNT}{\hbar}} | \Phi_i(0)\rangle\langle\Phi_i(0) | \eta(0)\rangle. \tag{29}$$

This relation emphasizes again the similarity between the properties of Floquet eigenfunctions and the ordinary stationary eigenfunctions (see Ref. [35] for more details). Although it has been proven here only for stroboscopic times, Eq. (29) may be written more generally by changing NT into an arbitrary t.

2.4. Dressed molecule picture and laser-induced resonances

Without the coupling term linear in μ in Eq. (23), the components $| U_n\rangle$ would solely be governed by the field-free Hamiltonian H_0 augmented by $n\hbar\omega$, the energy of n-photon. One can take Eq. (23) as defining the dressed molecule picture within this semiclassical description, and $| U_n\rangle$ is the amplitude (wavefunction) of the n-photon dressed (diabatic) channel. The field interaction $(1/2)\mu(\mathbf{r}) \cdot \mathbf{E}_0$ couples these diabatic channel amplitudes together. Diagonalizing the potential part of the full Floquet Hamiltonian matrix defined by Eq. (23), i.e., containing these diabatic channel couplings, one gets an equivalent picture, called the adiabatic Floquet scheme, with channel crossings in the diabatic representation becoming avoided crossings where adiabatic amplitudes $| U_n^{(adia)}\rangle$ are now coupled together by strongly localized field-induced non-adiabatic couplings.

To illustrate the above concepts, we consider a two-electronic-state molecular model system, corresponding to keeping just two terms in the sum on the right-hand side (rhs) of Eq. (5), so that $\Psi(\{\mathbf{R}_\alpha\}, t)$ in Eq. (11) is a two-dimensional column vector and $\tilde{\mathbf{W}}(\{\mathbf{R}_\alpha\}; t)$, a (2×2) matrix. A representative of this class of models is the one-electron diatomic H_2^+ molecule described in a two-electronic-state approximation.

Using the notations defined in Section (2.2), the position vectors in the center-of-mass frame of the two nuclei in this specific case are

$\mathbf{R}_1 = + \mathbf{R}/2$, $\mathbf{R}_2 = - \mathbf{R}/2$, where $\mathbf{R}$ is the relative position vector, and considering the system in interaction with a linearly polarized field, the full molecular Hamiltonian for this one-electron system is

$$H(t) = H_{\text{el}}^0 + T_N + eE_0 \cos(\omega t)\, \boldsymbol{\epsilon} \cdot \mathbf{r} \tag{30}$$

with H_{el}^0 defined by

$$H_{\text{el}}^0 = \frac{\mathbf{p}^2}{2m} + V(\mathbf{r}, \mathbf{R}), \tag{31}$$

$V(\mathbf{r}, \mathbf{R})$ being the sum of Coulomb interactions among the three particles. The two relevant electronic states of the H_2^+ molecule are the ground state of symmetry $^2\Sigma_g^+$, described by the wavefunction

$$\Xi_1(\mathbf{r}, \mathbf{R}) = 1s\sigma_g(\mathbf{r}, \mathbf{R}), \tag{32}$$

and the first excited state that is accessible via an electronic dipole allowed transition, of symmetry $^2\Sigma_u^+$, and described by[3]

$$\Xi_2(\mathbf{r}, \mathbf{R}) = 2p\sigma_u(\mathbf{r}, \mathbf{R}). \tag{33}$$

The $\mathbf{R}$-dependent electronic energies of these two states are noted $\epsilon_g(R)$ and $\epsilon_u(R)$. Note that, if the z axis of the molecule-fixed center-of-mass coordinate system is chosen to lie along the internuclear axis, then these depend explicitly on $R = |\mathbf{R}|$ only, as indicated. The time-dependent statefunction $\Omega^L(\mathbf{r}, \mathbf{R}, t)$ of the system expanded in the truncated basis of the two electronic wavefunctions is then

$$\Omega^L(\mathbf{r}, \mathbf{R}, t) = \Psi_1(\mathbf{R}, t)\Xi_1(\mathbf{r}, \mathbf{R}) + \Psi_2(\mathbf{R}, t)\Xi_2(\mathbf{r}, \mathbf{R}). \tag{34}$$

With this two-component state, applying the Floquet ansatz consists of writing

$$\begin{pmatrix} \Psi_1(\mathbf{R}, t) \\ \Psi_2(\mathbf{R}, t) \end{pmatrix} = e^{-i\frac{Et}{\hbar}} \begin{pmatrix} \Phi_1(\mathbf{R}, t) \\ \Phi_2(\mathbf{R}, t) \end{pmatrix}, \tag{35}$$

---

[3] Note that in designating the molecular orbitals representing these two electronic states as above, the $1s$ and $2p$ symbols refer to the united-atom limit.

and the general Floquet eigenvalue equation (15) takes on the following particular form:

$$i\hbar\frac{\partial \Phi_1(\mathbf{R}, t)}{\partial t} = [T_N + \epsilon_g(R) - E]\Phi_1(\mathbf{R}, t) - E_0\mu_{gu}(R)\cos\theta\cos(\omega t)\Phi_2(\mathbf{R}, t),$$

$$i\hbar\frac{\partial \Phi_2(\mathbf{R}, t)}{\partial t} = [T_N + \epsilon_u(R) - E]\Phi_2(\mathbf{R}, t) - E_0\mu_{ug}(R)\cos\theta\cos(\omega t)\Phi_1(\mathbf{R}, t),$$

$$(36)$$

where θ is the angle between the molecular internuclear axis and the direction of the polarization vector $\boldsymbol{\epsilon}$ and $\mu_{gu}(R)$ is the matrix element

$$\mu_{gu}(R) = \langle \Xi_1(\mathbf{r}, \mathbf{R})|(-ez)|\Xi_2(\mathbf{r}, \mathbf{R})\rangle_{\mathbf{r}} = \mu_{ug}(R) \qquad (37)$$

defined in the body-fixed system. The subscript $\mathbf{r}$ is to recall that the integration implied in this matrix element is made only over the electronic coordinates. Note that diagonal matrix elements of $-ez$ vanish for a homonuclear system such as H_2^+, owing to the inversion symmetry of the field-free molecule. We note that, in a complete treatment of the laser-driven dynamics, the relative nuclear KE operator T_N in Eq. (36) is the sum of a radial and an angular parts, $\mathbf{T}_R$, $\mathbf{T}_{\theta,\varphi}$, respectively, as exhibited and defined in Eqs. (56–58). However, the essential features of the Floquet representation of this two-state system are best illustrated by considering a one-dimensional, rotationless molecule, for which $T_N = \mathbf{T}_R$ and $\cos\theta = 1$ corresponding to the situation of a perfect alignment of the molecular axis along the laser polarization. We will briefly discuss the role of rotations, i.e., of angular dynamics within this Floquet scheme in Section 4.

Returning to Eq. (36), each of the functions $\Phi_k(\mathbf{R}, t)$, $k = 1, 2$, being time-periodic, it is expressible in the form

$$\Phi_k(\mathbf{R}, t) = \sum_{-\infty}^{+\infty} e^{in\omega t}\Psi_{k,n}(\mathbf{R}) \qquad (38)$$

corresponding to the general Eq. (19), i.e., $\Psi_{k,n}$, $k = 1, 2$, are the two components of $|U_n\rangle$ in the two-state field-free electronic basis. Introduction of these developments into the above coupled equations (36) leads to

$$\left[T_N + \epsilon_g(R) + n\hbar\omega\right]\Psi_{1,n} - \frac{E_0}{2}\mu_{gu}(R)[\Psi_{2,n-1} + \Psi_{2,n+1}] = E\Psi_{1,n}$$

$$\left[T_N + \epsilon_u(R) + n\hbar\omega\right]\Psi_{2,n} - \frac{E_0}{2}\mu_{gu}(R)[\Psi_{1,n-1} + \Psi_{1,n+1}] = E\Psi_{2,n} \qquad (39)$$

This pair of equations, which in fact represents an infinite set of coupled equations as n varies from $-\infty$ to $+\infty$, corresponds to the general Eq. (23).

In this specific case, the radiative couplings follow a parity selection rule that arises from the fact that $\mu_{kk} = 0$, $k = 1, 2 \leftrightarrow g, u$, in the model considered here. Once a parity of the Fourier indices ('numbers of photons') n associated with channel 1 is chosen, the nuclear amplitudes $\Psi_{1,n}$ supported by this channel (dressed by 'n photons') are coupled only to amplitudes $\Psi_{2,n'}$ supported by channel 2 with a number n' of opposite parity. The type of dressed picture that emerges from this is illustrated in Figure 2.1, for the dressing by a $\lambda = 532$ nm field of a rotationless two-state H_2^+ molecule, with even values of n associated with channel 1, and odd ones with channel 2. The corresponding R-dependent channel energies, i.e., $\epsilon_g(R)$ and $\epsilon_u(R)$, dressed by $n\hbar\omega$ according to this n-parity convention, exhibit, at specific R, crossings with $|\Delta n| = 1, 3, 5, \ldots$ that have been interpreted as corresponding to local electronic transitions $^2\Sigma_g \longrightarrow {}^2\Sigma_u$ with absorption of $1, 3, 5, \ldots$ photons, respectively.

If we ignore the nuclear kinetic operator T_N in Eq. (39), then the resulting equation defines Floquet eigenstates of the two-state electronic system considered at a fixed R. These local electronic Floquet eigenstates and energies can thus be obtained simply by diagonalizing the local electronic Floquet Hamiltonian matrix. The results are shown in dashed lines on Figure 2.1. Doing this leaves the problem of determining the full molecular Floquet states unsolved, however, as the electronic Floquet Hamiltonian matrix and its eigenvectors do not commute with the nuclear KE operator.
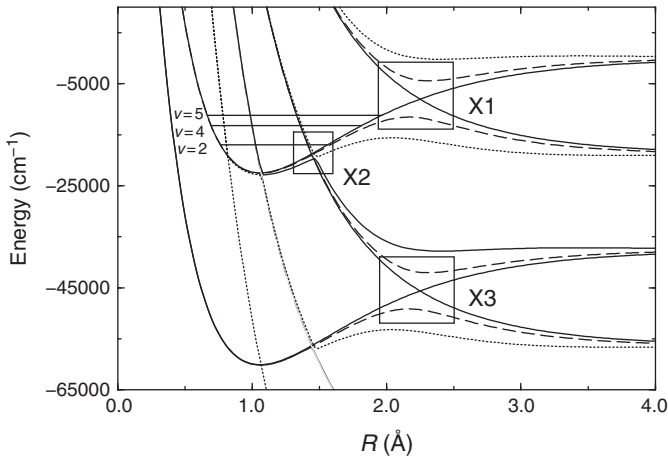
Figure 2.1 Field-dressed potential energy curves of H_2^+ ($\lambda = 532$ nm), in the diabatic (solid lines) and adiabatic (broken lines for $I = 10^{13}$ W/cm^2 and dotted lines for $I = 5 \times 10^{13}$ W/cm^2) frames. Curve-crossing regions are outlined by rectangular boxes X1, X2, and X3. The energies of the $v = 2, 4, 5$ vibrational levels are indicated by thin horizontal lines.

At best, the local electronic Floquet eigenvectors can be taken as a new basis, an adiabatic one, on which the total molecular Floquet states can be expanded. The channel amplitudes in this basis are coupled by kinetic non-adiabatic couplings, arising from the commutator between T_N and $H_F^{el}(R)$.

The dressed channels represented by the potentials traced in solid lines in Figure 2.1 are coupled to each other by diabatic couplings that increase linearly with E_0, i.e., with the field intensity and that are also delocalized in R, as, for H_2^+, μ_{gu} diverges as $R/2$. In contrast, non-adiabatic couplings in the dressed adiabatic picture decrease as E_0 increases and are localized in the neighborhood of avoided crossings created at the one-, three-, five-... photon crossings of the diabatic dressed scheme. This confers to the adiabatic representation some advantages in interpretations, i.e., in the qualitative readings of calculated dynamics. In particular, laser-induced resonances, i.e., metastable Floquet states, of two sorts can clearly be identified on the adiabatic dressed potential energy curves of Figure 2.1. These are defined by the avoided crossing created at the intersection of the $\epsilon_g + n\hbar\omega$ and the $\epsilon_u + (n-1)\hbar\omega$ curves, for any n, i.e., the one-photon crossing. The lower of the pair of adiabatic potentials associated with this avoided crossing supports resonances of shape type, while the upper one supports resonances of Feschbach type.

Shape resonances are responsible for the so-called BS dissociation process for resonances lying below the barrier created at the one-photon crossing, and for Above-The-Barrier dissociation in the opposite situation. Feshbach resonances give rise to the VT phenomenon, also called Bond-Hardening process. The positions and the widths of these resonances vary with the field intensity. In particular, the widths of shape and Feshbach resonances vary in opposite directions as the field strength increases: While shape resonances become more and more unstable, the barrier to dissociation of the lower adiabatic potential being lowered with increasing E_0, Feshbach resonances are stabilized in the same conditions, as non-adiabatic couplings that are responsible for their decays into the continua in which they are embedded are lowered as E_0 increases.

2.5. Adiabatic time development

2.5.1. Adiabatic Floquet representation:

Rigorously, the above Floquet representation is valid only when the field is periodic. Imagine now that the field amplitude $\mathbf{E}_0$ in Eq. (12) carries a time dependence that denotes a slow modulation of the cosine field which oscillates with a frequency ω in the UV-Vis spectral range. Without the amplitude modulation, the dynamics under the UV-Vis field is well captured by the Floquet representation. If the amplitude modulation is slow,

the Floquet ansatz can still be applied to the TDSE with this locally periodic field, albeit approximately. This can be seen as followed: Within some time interval $[\bar{t} - \Delta t, \bar{t} + \Delta t]$, $\Delta t = T_L/N$ around $\bar{t}$ ($T_L = 2\pi/\omega$ is the laser-field period), with N large enough so that the variations of the pulse envelope over $2\Delta t$ can be neglected, but still ensuring that some oscillations of the high-frequency carrier wave do occur during that time interval, the laser field $\mathbf{E}(t)$ can be considered of constant amplitude, i.e., it can be written $\mathbf{E}(t) = \mathbf{E}_0 \cos \omega t$ with $\bar{\mathbf{E}}_0 := \mathbf{E}_0(\bar{t})$. The eigenstates of the instantaneous Floquet Hamiltonian $H_F^{(\bar{t})}(t) = H^{(\bar{t})}(t) - i\hbar\frac{\partial}{\partial t}$ associated with this local periodic field define a basis for the expansion of the actual wavepacket of the system as it evolves during this time interval from some initial condition. If this initial condition, which is nothing else than the wavepacket evolved up to time $\bar{t} - \Delta t$, projects unitarily (or at least mainly) on a single state of this local basis, i.e., a single Floquet state, then it will remain in this state during the whole time interval. Imagine now that the laser pulse duration is divided up into N_t time slices of width Δt_n centered on $\bar{t} = t_n$, $n = 0, 1, 2, \ldots. N_t$. If the actual time evolution across the full pulse width is essentially the transport of a single Floquet resonance state or a group of quasi-degenerate Floquet states from one time slice to another, then the Floquet dynamics is said adiabatic. This definition represents the extension, to Floquet states, of the concept of adiabatic transport of eigenstates of time-dependent Hamiltonian as expressed by the celebrated adiabatic theorem [36]. Its precise formulation within Floquet theory has been given in different forms by many authors [29, 30, 37–39]. We will not be concerned with these formal aspects, but only use the concept of Floquet adiabatic or non-adiabatic dynamics mostly for interpretative purposes. In the adiabatic situation, not only do resonances' properties vary smoothly in time, as the slowly varying field envelope modulates the adiabatic energy barrier height and width, and the energy gap at the main (one-photon) avoided crossing of the dressed potentials, but resonances (or degenerate groups of these) are also transported smoothly, in a one-to-one manner, from one time slice to another. Thus, if the field–molecule interaction is switched on smoothly, then an initial eigenstate of the field-free molecule will be transported adiabatically onto a single resonance and will remain in this resonance (whose properties change slowly with time), at all subsequent times, until the end of the pulse. We will also encounter situations where the field–molecule interaction is switched on suddenly, at a time within the pulse width, when a noticeable field-intensity is already attained, defining resonance states that already differ markedly from field-free molecular eigentstates. Although the preparation of the molecule in an instantaneous Floquet wavepacket is sudden in this case, subsequent evolution of each component of this wavepacket, i.e., of Floquet resonances, may be adiabatic within the remaining part of the laser pulse. In all instances, whenever the transport of Floquet resonance states is adiabatic, their time-integrated widths are meaningful as a

measure of their decay probabilities. Much of the discussion to be found in the next sections are based on this adiabatic Floquet picture. The understanding of the distinction between adiabatic and non-adiabatic Floquet dynamics is central to the interpretation of recent experimental findings in the ultra-fast pump–probe spectroscopy of dissociative ionization of dihydrogen (see Section 5).

Care must be exercised to distinguish the concept of adiabatic Floquet dynamics introduced here, which refers to an adiabatic time-evolution, or to the slow variations of the Floquet basis with time, from the concept of adiabatic representation defined in the previous section, which refers to the slow variations of the electronic Hamiltonian (Floquet or not) with respect to nuclear motions (i.e., the noncommutativity of the electronic Hamiltonian H_{el} and the nuclear KE operator T_N). Where confusion is possible and to be avoided, we shall refer to this concept of adiabaticity related to the BO approximation as the R-adiabaticity, while adiabaticity in actual time evolution will be termed t-adiabaticity. Non-adiabatic effects in time evolution are due to a fast variation of the (Floquet) Hamiltonian with time, causing Floquet states to change rapidly in time, to the extent that in going from one time slice to another, a resonance may be projected onto many new resonances as well as diffusion (continuum) states [40], and the Floquet analysis breaks down completely. We will see in Section 5 how one can take advantage of such effects to image nuclear motions by an ultrafast pump–probe process.

2.5.2. Adiabaticity in non-Floquet representations

An instance in which the Floquet representation breaks down, in the sense of becoming impractical, even though the field is genuinely periodic, is when the field frequency is small, as compared with the Bohr frequency of the first electronic transition at small R. The one-photon crossing is then brought to a large distance and Floquet blocks and zones are so close to each other that resonance overlaps are numerous. In such a case, it is more appropriate to discuss the dynamics in terms of the adiabatic transport of instantaneous eigenstates of the time-dependent (non-Floquet) Hamiltonian of the molecule, as this varies slowly in time [10, 41]. The diagonalization of the electronic part $H_{el}(R, t)$ of the time-dependent Hamiltonian in Eqs. (30 and 36) yields potential energy curves which fluctuate in time as shown in Figure 2.2. The lower adiabatic surface is now characterized by a barrier that moves in time, both in position and in height and width. Note that these PESs refer to an electronic representation that is both adiabatic with respect to time and with respect to nuclear motions, reflecting the two timescales, that of electronic motions, much faster, and that of the slower field oscillations that would be comparable also to the nuclear motions' timescale. The lower adiabatic potential energy curve in Figure 2.2 supports instantaneous nuclear eigenfunctions which correspond to resonances of the
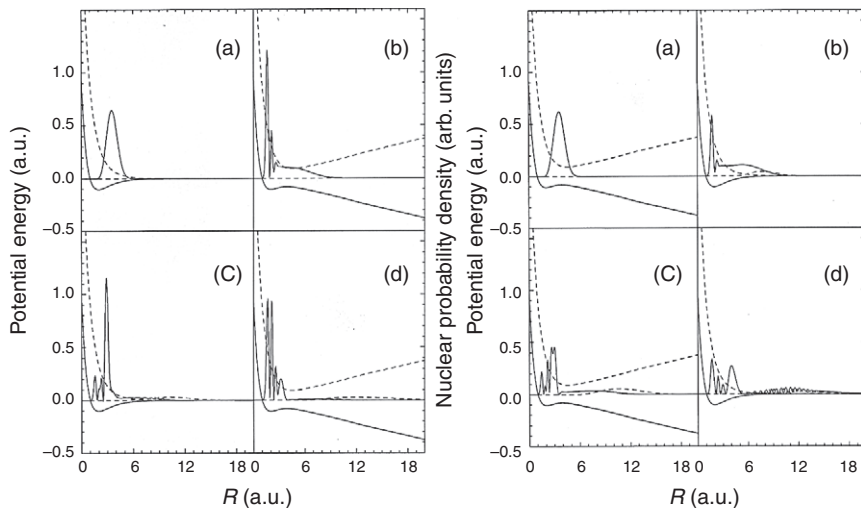
Figure 2.2   Nuclear probability distributions associated with the wavepacket supported by the adiabatic channels $W_{\pm}(R,t)$ formed under a $\omega = 943.3\ \mathrm{cm}^{-1}$, $I = 5 \times 10^{13}\ \mathrm{W/cm}^2$ laser pulse with $\delta = 0$ on the left panel and $\delta = \pi/2$ on the right panel. The wavepackets are taken at four times within the first optical cycle: (a) $t = 1/4T$; (b) $t = 1/2T$; (c) $t = 3/4T$; (d) $t = T$.

shape type and, if desired, the nuclear actual wavepacket dynamics may be described and discussed in terms of these resonances. However, due to the comparable timescales of the field oscillations and the nuclear motions, it is more useful to analyze these directly in terms of the synchronization of the time-dependent wavepacket with the moving barrier found on this lower potential energy curve. This is the framework of the analysis originally given [10] to the DDQ effect in the laser-driven dissociation of small diatomic molecules, as reviewed in Section 4.

3. NUMERICAL METHODOLOGIES

As seen above, laser assisted and controlled photofragmentation dynamics can conceptually be viewed in two different ways. The time-dependent viewpoint offers a realistic time-resolved dynamical picture of the basic processes that are driven by an intense, short laser pulse. For pulses characterized by a long duration (as compared to the timescales of the dynamics), the laser field can be considered periodic, allowing the (quasi-) complete elimination of the time variable through the Floquet formalism, giving rise to a time-independent viewpoint. This formalism not only offers a useful and important interpretative tool in terms of the stationary field

dressed molecular states but also provides a more direct and accurate way to calculate the resonances involved in various laser-induced processes. We first review, in the next Section (40), the computational method to actually calculate Floquet resonances in this time-independent approach as applied to the dressed H_2^+ (rotationless) molecule. The methodology used for the calculations of wavepackets in the complementary time-dependent approached will then be reviewed in Section (41).

3.1. Time-independent calculations of Floquet resonances

We present the numerical methodology for solving Eqs. (39), resulting from the application of the Floquet formalism to the semiclassical Hamiltonian of the molecule plus field system. For this purpose, we present Eqs. (39) in the generic form of a system of a finite number of closed-coupled equations

$$[T_N \mathbf{1} + \epsilon(R))] \Psi(R) = E \mathbf{1} \Psi(R), \tag{40}$$

where, with p two-channel Floquet blocks being kept to give $N = 2p$ coupled dressed channels, $\epsilon(R)$ is the $(N \times N)$ potential matrix appearing on the left-hand-side (lhs) of Eqs. (39), with elements

$$[\epsilon]_{n,n'} = \epsilon_\kappa(R) + n\hbar\omega - \frac{E_0}{2}\mu_{ug}(R)[\delta_{n',n-1} + \delta_{n',n+1}], \quad \kappa = \begin{cases} g \leftrightarrow & n = 2k \\ u \leftrightarrow & n = 2k+1 \end{cases}$$

and $\mathbf{1}$ is the $(N \times N)$ unit matrix. The method is presented for the one-dimensional version of these coupled equations as befit the calculations of laser-induced resonances in a diatomic (rotationless) molecule perfectly aligned along the laser polarization.

Molecular channels appearing in Eqs. (39) belong to one of the following two classes. For a given energy E, if $E - \epsilon_{g(u)}(R) - (N-n)\hbar\omega$ goes to a positive limit $E_n = E - (N-n)\hbar\omega$ as $R \to \infty$, then the channel is open. This means that the two nuclei can separate from each other, with a relative KE $E_n = \hbar^2 k_n^2/2\mathcal{M}$, k_n being the associated wave number given by

$$k_n = \frac{1}{\hbar}[2\mathcal{M}(E - (N-n)\hbar\omega)]^{\frac{1}{2}}. \tag{41}$$

If the limit is negative, then the channel is closed and the nuclei remain bounded to each other. The form of the solutions of the coupled equations, Eqs. (39 or 40), depends on the imposed boundary conditions. Consider first the case where there is at least one open channel. Scattering boundary conditions consist of imposing, for an open channel n, a combination of incoming ($\exp[-ik_n R]$) and outgoing ($\exp[+ik_n R]$) waves, while all closed channel functions are constrained to vanish asymptotically. In the case

of a molecular dissociation, because of the strong interatomic repulsion prevailing at short internuclear distances, all channel functions must decay to zero as $R \longrightarrow 0$. Scattering solutions then exist with a real arbitrary energy above a certain threshold. They describe, for example, a situation where the nuclei approach each other with a given number of photons in the field, and then separate from each other with the same number (elastic scattering) or a different number (inelastic scattering) of photons. The scattering situation is, however, not the type of problem of interest in this review. When the molecule is supposed to be initially in a state belonging to a closed channel (e.g., a vibrational state of the ground electronic state), half-collision (or Siegert-type) boundary conditions are more appropriate. We then impose to the amplitudes associated with open channels to be asymptotically of the outgoing type only [7], while closed channel functions must vanish asymptotically as in the scattering case. This type of solution is only possible if the (quasi-)energy is quantized and complex of the form $E = E_R - i\Gamma/2$. Such an energy characterizes a resonance. Note that the closed or open character of a given channel as defined above must be decided using the real part of the energy. The total rate of dissociation is given by $\mathcal{K} = \Gamma/\hbar$. This can be seen from the behavior of the associated Floquet wavefunction as imparted by the exponential factor containing its quasi-energy. Since a probability is calculated with the squared modulus of the wavefunction, this factor produces

$$\left| \exp\left[-i\frac{Et}{\hbar} \right] \right|^2 = \exp\left[-\frac{\Gamma t}{\hbar} \right] = \exp[-\mathcal{K}t]. \tag{42}$$

Siegert boundary conditions also imply that the open-channel wave numbers are complex, since Eq. (41) is now used with a complex energy. Thus k_n can be written as

$$k_n = k_{n0} - ik_{n1}, \tag{43}$$

with both k_{n0} and k_{n1} positive. Since the wavefunction in open channel n goes asymptotically as $\exp[ik_nR]$, we have

$$\exp[ik_nR] = \exp[ik_{n0}R]\exp[k_{n1}R], \tag{44}$$

which diverges at infinity. The interpretation of this fact is the following: when measuring the outgoing flux at a distant position from the source, we are in fact interrogating the system at some time in the past. Since the source is decaying, the more distant we are from it, the more active was the source at the time of emission.

It is possible to implement explicitly Siegert boundary conditions in the determination of the multichannel wavefunction. An alternative approach is to transform the reaction coordinate R into a complex one $R = \rho \exp(i\vartheta)$

[21]. The complex wave number k_n can also be written $\kappa \exp(-i\beta)$ with β positive. With this, the new channel function asymptotically goes to

$$\exp[ik_n R] = \exp[i\kappa\rho \exp(i(\vartheta - \beta))] \tag{45}$$
$$= \exp[i\kappa\rho \cos(\vartheta - \beta)] \exp[-\kappa\rho \sin(\vartheta - \beta)].$$

If the condition $0 < (\vartheta - \beta) < \pi$ is fulfilled, the second exponential factor in the last form of $\exp[ik_n R]$ goes to zero as $\rho = |R| \longrightarrow \infty$. The channel function then behaves as that of a bound state. It is also important to note that this complex transformation of the coordinate does not affect the decreasing asymptotic behavior and the square integrability of a bound state wavefunction. This means that any method available for bound state calculations can be used for resonance calculations. A variant of the complex rotation method consists in transforming the reaction coordinate only after some value, say R_0. The form given to the coordinate is then $R_0 + (R - R_0)\exp(i\vartheta)$. This procedure is called exterior scaling [42, 43].

For the propagation of the multichannel wavefunction $\Psi(\mathbf{R})$, in real or complex-scaled coordinates, an efficient algorithm is furnished by the Fox-Goodwin–Numerov method [8, 44], which results from a discretization of the differential operator T_N appearing in Eqs. (39). Given adjacent points $R - h$, R, and $R + h$ on the grid, we define an inward matrix (labeled i) and an outward matrix (labeled o) as:

$$\mathbf{P}^i(R) = \mathbf{Q}^i(R + h)[\mathbf{Q}^i(R)]^{-1}, \tag{46}$$

$$\mathbf{P}^o(R) = \mathbf{Q}^o(R - h)[\mathbf{Q}^o(R)]^{-1}, \tag{47}$$

where $\mathbf{Q}^i(\mathbf{Q}^o)$ is a matrix of independent vector solutions of the coupled-channel equations satisfying boundary conditions for inward or outward propagation respectively. The Fox-Goodwin–Numerov method actually propagates these $\mathbf{P}$ matrices on the grid. If $R - h_1$, R, and $R + h_2$ are three adjacent points on the grid, either all real or all complex or mixed, define the following (Numerov) matrices:

$$\boldsymbol{\alpha}(R) = h_2 \left[1 + \frac{1}{12}(h_1^2 + h_1 h_2 - h_2^2)(E\mathbf{1} - \boldsymbol{\epsilon}(R)) \right], \tag{48}$$

$$\boldsymbol{\beta}(R) = (h_1 + h_2) \left[1 - \frac{1}{12}(h_1^2 + 3h_1 h_2 + h_2^2)(E\mathbf{1} - \boldsymbol{\epsilon}(R)) \right], \tag{49}$$

$$\boldsymbol{\gamma}(R) = h_1 \left[1 + \frac{1}{12}(-h_1^2 + h_1 h_2 + h_2^2)(E\mathbf{1} - \boldsymbol{\epsilon}(R)) \right]. \tag{50}$$

Then, the propagation is done with the two equations:

$$\mathbf{P}^i(R - h_1)) = [\boldsymbol{\beta}(R) - \boldsymbol{\alpha}(R + h_2)\mathbf{P}^i(R)]^{-1}\boldsymbol{\gamma}(R - h_1), \tag{51}$$

$$\mathbf{P}^o(R + h_2) = [\boldsymbol{\beta}(R) - \boldsymbol{\alpha}(R - h_1)\mathbf{P}^o(R)]^{-1}\boldsymbol{\gamma}(R + h_2). \tag{52}$$

Let R_m and $R_m + h$ be the two points chosen for the matching of the inward and outward solutions. The matching condition has the form:

$$\det|\mathbf{P}^i(R_m) - (\mathbf{P}^o(R_m + h))^{-1}| = 0. \tag{53}$$

The fulfillment of Eq. (53) generates a complex energy if the inward matrix incorporates outgoing boundary conditions (with a real coordinate) or bound state boundary conditions (with a complex rotated coordinate).

Once the complex Floquet eigenenergy has been determined from an iterative resolution of the implicit energy-dependent Eq. (53), the multichannel wavefunction written as a column vector $\Psi(R)$ can be calculated at the matching point because it satisfies the set of homogeneous linear equations:

$$[\mathbf{P}^i(R_m) - (\mathbf{P}^o(R_m + h))^{-1}]\Psi(R_m) = 0. \tag{54}$$

The wavefunction at the other grid points can be obtained recursively from $\Psi(R_m)$ using

$$\begin{aligned}\Psi(R + h) &= (\mathbf{P}^o(R + h))^{-1}\Psi(R),\\ \Psi(R - h) &= (\mathbf{P}^i(R - h))^{-1}\Psi(R).\end{aligned} \tag{55}$$

3.2. Time-dependent wavepacket propagation

We now turn to the time-dependent wavepacket calculations, i.e., to techniques used for solving directly the nuclear TDSE (cf. Eq. (11)), which for a diatomic multichannel molecule is

$$i\hbar\frac{\partial}{\partial t}\Psi(R,\theta,\varphi;t) = \left[\mathbf{T}_R + \mathbf{T}_{\theta,\varphi} + \tilde{\mathbf{W}}(R, \theta; t)\right]\Psi(R, \theta, \varphi; t), \tag{56}$$

where R, θ, φ are the spherical coordinates of the internuclear vector $\mathbf{R}$ in the laboratory frame. The KE operators in Eq. (56) are given by

$$\mathbf{T}_R = -\frac{\hbar^2}{2\mathcal{M}}\frac{\partial^2}{\partial R^2}, \tag{57}$$

$$\mathbf{T}_{\theta,\varphi} = -\frac{\hbar^2}{2\mathcal{M}R^2}\left\{\frac{1}{\sin\theta}\frac{\partial}{\partial\theta}(\sin\theta\frac{\partial}{\partial\theta}) + \frac{1}{\sin^2\theta}\frac{\partial^2}{\partial\varphi^2}\right\}. \tag{58}$$

The potential energy part $\tilde{\mathbf{W}}(R, \theta; t)$ is as defined in Eq. (10) for a general N-channel system. We will consider the specific case of a two-channel system, with the two coupled electronic states designated by g and u.

Equation (56) is typically solved by writing

$$\Psi(R,\theta,\varphi;t + \delta t) = \mathbf{U}(\delta t)\Psi(R, \theta, \varphi; t)$$

$$= \exp\left[-\frac{i}{\hbar}[\mathbf{T}_R + \mathbf{T}_{\theta,\varphi} + \tilde{\mathbf{W}}(R, \theta; t)]\delta t\right]$$

$$\times \Psi(R, \theta, \varphi; t)$$

and by using a split-operator representation of the short-time propagator $U(\delta t)$:

$$U(\delta t) = \exp\left[-\frac{i}{\hbar}[\mathbf{T}_R + \mathbf{T}_\theta + \tilde{\mathbf{W}}(t)]\delta t\right]$$

$$= \exp\left[-\frac{i}{\hbar}\tilde{\mathbf{W}}\delta t/2\right]\exp\left[-\frac{i}{\hbar}\mathbf{T}_{\theta,\varphi}\delta t/2\right]$$

$$\times \exp\left[-\frac{i}{\hbar}\mathbf{T}_R\delta t\right]\exp\left[-\frac{i}{\hbar}\mathbf{T}_{\theta,\varphi}\delta t/2\right]$$

$$\times \exp\left[-\frac{i}{\hbar}\tilde{\mathbf{W}}\delta t/2\right] + O(\delta t^3).$$

All propagators appearing on the rhs of Eq. (59) are treated using the Feit–Fleck technique [22], except the one involving $\mathbf{T}_{\theta,\varphi}$, which is approximated by Cayley's formula [45]:

$$\exp\left[-\frac{i}{\hbar}\mathbf{T}_{\theta,\varphi}\delta t/2\right] = [1 + (\frac{i}{\hbar})\mathbf{T}_{\theta,\varphi}\delta t/4]^{-1}$$

$$\times [1 - (\frac{i}{\hbar})\mathbf{T}_{\theta,\varphi}\delta t/4]$$

$$+ O(\delta t^3),$$

which maintains unitarity ($\mathbf{T}_{\theta,\varphi}$ being self-adjoint) and is further implemented in a way that avoids matrix inversion.

The exponential operator containing the potential energy is straightforwardly evaluated in the coordinate representation. A prediagonalization of the instantaneous multichannel potential matrix $\tilde{\mathbf{W}}(R, \theta; t)$ is needed and naturally brings one to the (both $t-$ and $R-$) adiabatic representation described in the previous section. Fourier-transform methodology [22, 46] and, for the angular variables, a method employing either spherical harmonics basis-sets expansions [47] or grid techniques [45] are then used to represent the exponential operators involving the radial and angular kinetic energies in

Eq. (59). In particular, the last reference gave a significantly improved grid approach with an implementation of the above unitary Cayley scheme for $T_{\theta,\varphi}$, combined with a split operator technique using a cosine Fourier transform, resulting in a recursion formula. Apart from avoiding the numerical instabilities associated with the division by $\sin\theta$ in this angular KE term, the major advantage of this approach is the absence of matrix element evaluations and multiplications, the computational task being basically fast Fourier transforms.

Until very recently the calculations of dissociation fragments' KE spectra involved wavepacket propagations over very large grids, during the total pulse duration. A much restricted grid may be used if the wavepackets are splitted into an internal and an asymptotic part [48]:

$$\Psi_j(R, \theta; t_i) = \Psi_j^I(R, \theta; t_i) + \Psi_j^A(R, \theta; t_i) \quad (j = 1,2) \tag{59}$$

(I for inner and A for asymptotic). The inner part is calculated by the numerical procedure described above using the restricted grid. As for the asymptotic part, the angular KE operator $T_{\theta,\varphi}$ can be omitted thanks to the R^{-2} factor it contains which tends to zero as R goes to infinity. The asymptotic region, which is the support of Ψ_j^A, is also where the field-free potential energy curves become degenerate and are flat, while the transition dipole moment between the two charge-resonant states goes as $\mu(R > R_S) \to \frac{1}{2}eR$. Because of these asymptotic behaviors of the potential matrix, the asymptotic two-state electronic system can be decoupled by an appropriate time-independent unitary transformation. The resulting decoupled equations describing field-driven nuclear motions in the asymptotic region are formally analog to the ones describing the motion of a free electron in an electric field and admit Volkov-type analytical solutions [17]. This implies that, after Fourier transforming, the asymptotic wavepackets Ψ_j^A can be propagated analytically, avoiding the use of an extended grid, even during the field interaction [23, 49].

A much more detailed account for the split operator method and the accompanying asymptotic analysis is given in Ref. [4].

4. PROCESSES AND MECHANISMS FOR MOLECULAR FRAGMENTATIONS IN IR AND UV-VIS FREQUENCY REGIMES

4.1. General ideas

Many effects and nonlinear processes induced by a laser field have been uncovered through the study of the simplest molecular system, the one-electron homonuclear diatomic H_2^+ molecule. The scope of these findings is larger though, as manifestations of these effects may be found in more complex molecules, including polyatomic systems.

The nature of these effects, the concepts required for their understanding depend on the spectral range to which the frequency of the laser field belongs. Nowadays, modern laser technology gives access to a wide range of frequencies, from IR, to Vis, up to UV domains. Achievable peak intensities (up to tens of TW/cm^2) correspond to forces of the same order or even larger than those of the Coulomb forces that ensured the cohesion of stable molecular structures. Fields of such intensity can induce effects that are basically of two types: multiphoton effects, i.e., molecular excitations accompanying the absorptions and/or emissions of a finite number of photons, and profound modifications of molecular internal force fields. These effects have different consequences in terms of underlying mechanisms that can be exploited in control problems, for example, depending on the frequency domain which is addressed.

In the *UV-Vis regime* (wavelengths within 750 to 40 nm), the photon energy (a few electron-volts) is resonant with electronic transitions at some particular molecular geometry. Typically a single photon brings enough energy for the dissociation to occur, but due to the high intensity of the field, the molecule continues to absorb photons above its dissociation threshold (multiphoton ATD mechanism). The subsequent dynamics leads to fragmentation into different channels characterized by different kinetic energies associated with the absorptions of different numbers of photons. As the photon frequency (larger than 5×10^{14} Hz) is high as compared to that of molecular internal motions (vibration or rotation), the molecule feels a time-averaged strong radiative field that modifies its field-free Coulomb force field. These modifications are well captured by the dressed molecule picture associated with the Floquet representation. They give rise to the softenings of some chemical bonds (barrier suppression, BS mechanism), while others are hardened (confinement or VT mechanism). New scenarios for the control of molecular reactivity can be designed by exploiting the interplay between these antagonistic mechanisms.

In the *IR regime* (wavelengths within 750 nm to 0.1 cm), the photon energy (less than one electron-volt) is typically resonant with nuclear vibrational motions. A single photon is not energetic enough to induce electronic excitation and/or dissociation. These processes are highly multiphotonic, requiring the accumulation of the energy of a large number of individual photons. In contrast with the UV-Vis regime, the IR laser frequency (10^{14} Hz) being comparable to internal vibrational frequencies, the molecule follows, in a time-resolved manner, the oscillations of the electromagnetic field. When properly synchronized with a vibrational mode, the laser can be used as a tool for controlling dissociation through new BS or stabilization mechanisms that are proper to the IR frequency regime. Finally, it is worthwhile to note that IR laser frequencies remain high with respect to rotational motions. This gives the possibility of controlling the angular distributions of laser-driven

molecules through time-averaged pendular states which govern alignment dynamics.

4.2. A simple model system

The general ideas outlined above are best illustrated with the example of electronic excitations and concomitant large-amplitude nuclear motions in the molecular ion H_2^+ under a UV-Vis and IR laser pulse. The two-channel model introduced in Section 2.4, which will be recalled briefly below, is of widespread use for its ability to capture in its simplicity the essence of strong field molecular dynamics. Furthermore, the discussion can be conducted by first considering a one-dimensional model ($\theta = 0$) representing a strictly aligned (i.e., rotationless) molecule. We thus solve the nuclear TDSE to generate wavepackets moving on the BO potential energy curves associated with two electronic states labeled g (ground, $^2\Sigma_g^+$) and u (excited, $^2\Sigma_u^+$),

$$i\hbar \frac{\partial}{\partial t} \left[\begin{array}{c} \psi_g(R,t) \\ \psi_u(R,t) \end{array} \right] = \hat{H} \left[\begin{array}{c} \psi_g(R,t) \\ \psi_u(R,t) \end{array} \right]. \tag{60}$$

where the Hamiltonian $\hat{H}$ is as given in Eq. (56) and involves a two-by-two potential operator matrix which depends on the internuclear distance R and is given by.

$$\hat{W}(R,t) = \left(\begin{array}{cc} \epsilon_g(R) & -E_0 f(t)\mu(R)\cos\omega t \\ -E_0 f(t)\mu(R)\cos\omega t & \epsilon_u(R) \end{array} \right), \tag{61}$$

where E_0, $f(t)$, and ω are, respectively, the maximum amplitude, temporal pulse shape, and carrier-wave frequency of a field explicitly taken as:

$$E(t) = E_0 f(t)\cos(\omega t + \delta). \tag{62}$$

The molecular dipole moment μ, which is the transition dipole between states g and u, does not contain any permanent part μ_0 for this homonuclear ion and is parallel to $\mathbf{R}$. The polarizability α is not explicitily introduced as, for the intensity range we are referring to, the model can be, within good approximation, strictly limited to the lowest two BO states.

Using the wavepacket propagation methodology outlined in Section 3.2, the wavepacket components $\psi_{g,u}$ are generated at a given time t, from some initial state defined at $t = 0$, which will be specified later. Various observables can be calculated from the wavepackets at the current time, among which the total instantaneous probabilities for the ion to remain in bound vibrational states of the ground electronic state, i.e.,

$$P_{\text{bound}}(t) = \sum_v \left| \langle v | \psi_g(t) \rangle \right|^2. \tag{63}$$

The dissociation probability is then simply given by

$$P_{\text{diss}}(t) = 1 - P_{\text{bound}}(t). \tag{64}$$

Another observable of interest is the final probability distribution for fragments specified by their momentum k and, in two-dimensional calculations that include rotational motions, angular position θ:

$$\mathcal{P}(k) = \sum_{n=g,u} \left| \tilde{\psi}_n^A(k; t \to \infty) \right|^2, \tag{65}$$

where $\tilde{\psi}_{g,u}^A$ represents the Fourier transform of the asymptotic-region wavepacket components of the g and u channels, respectively.

4.3. Multiphoton dissociation in the IR regime

In the IR regime, the field amplitude varies typically over the same time scale as molecular vibrational motions so that a synchronization between the nuclear motion and the laser oscillations is possible [10, 11] . This requires the definition of a time t_0 (or a related phase δ) when the field amplitude first reaches its maximum after the promotion of the initial wavepacket onto the excited electronic state,

$$\cos\left[\omega\left(t - t_0\right)\right] = \cos\left(\omega t + \delta\right). \tag{66}$$

For $t_0 = \delta = 0$, the initial wavepacket is considered to be prepared instantaneously at maximum intensity. In contrast, if t_0 is set equal to $T/4$ ($T = 2\pi/\omega$), corresponding to $\delta = \pi/2$, the initial state preparation occurs at the start of an optical cycle, i.e., at zero-field intensity. The two situations result into completely different dynamics, the former leading to dissociation quenching, while the latter is monitored by a barrier suppression mechanism. This distinction can best be understood by viewing the dynamics as taking place on the time-dependent adiabatic potential surfaces $W_{\pm}(R,t)$ which arise from diagonalizing the potential energy operator of Eq. (61).

Figure 2.2 illustrates the dynamics of $W_{\pm}$ and of the associated nuclear probability distributions. For $\delta = 0$ the field is at its peak intensity at $t = 0$, when the initial wavepacket is prepared on the inner repulsive edge of the attractive potential W_- (close to ϵ_g in this region). Only its tail penetrates the gap region ($R \sim 4$ a.u.) which, at that time, is widely open between W_+ and W_-. At $t = T/4$, the wavepacket components reach the gap region with a gap now closed due to the vanishing field amplitude, preventing thus any

escape toward the asymptotic region. At $t = T/2$, the wavepacket is reflected back toward the inner region and the gap is open again but without any consequence with respect to an eventual escape. During the next half cycle the wavepacket motion follows the same pattern and all this leads to a stabilization of the system with respect to dissociation, which is seen to be a consequence of the bound vibrational motion being perfectly synchronized with the opening and closing of the potential gap. This is the dynamical quenching mechanism (DDQ). A completely different wavepacket motion is associated with the case $\delta = \pi/2$. Every time the wavepacket reaches the right end of the binding potential ϵ_g, the gap is open and permits the escape of an important part of the wavepacket toward the asymptotic dissociative limit. This is the barrier lowering (and/or suppression) mechanism.

It is worthwhile to note that the field–molecule synchronization can be achieved by tuning the laser frequency and adjusting its intensity. This means that a quantitative knowledge of δ is not necessary. In particular, a two-pulse (UV + IR) scheme can be proposed with a given time delay. If an intense ultrashort UV pulse is turned on at a definite time t_0 after the onset of the long IR pulse, it will instantaneously prepare well-aligned H_2^+ ions from H_2 in its ground state. A variation of the frequency of the IR laser pulse would then allow the desired synchronization to occur [12].

Full 2D calculations (including rotations) have shown that molecular alignment is not among the necessary conditions for DDQ to be sharply observed [12]. In the case where the molecule is allowed to rotate during its interaction with the field, the efficiency of DDQ is only slightly affected. A control can thus be exerted on the system by adequately combining the laser intensity (which controls the position, the width, and the spatial spread of the gap) and frequency (which controls the gap opening and closing motions' period).

4.4. ATD dynamics in the UV-Vis regime

In the UV-Vis regime, the field oscillations are so fast as compared to nuclear motion that the molecular system only feels time-averaged radiatively dressed adiabatic potentials. A transparent multiphoton interpretation to be made for the two nonlinear mechanisms affecting the chemical bond (which are the analogs of the barrier suppression and DDQ of the IR regime) results from the Floquet expansion and time averaging of the molecule-plus-field Hamiltonian, valid for pulses long enough to lead to near periodic lasers. The relatively large photon energy of a UV-Vis field not only matches the electronic transition of the molecule in a modestly elongated configuration but also separates well the Floquet blocks [$(g,n);(u,n + 1)$ with varying n] from each other. Only a few Floquet blocks are actually needed (for a given intensity) for a converged calculation on the network of field-dressed diabatic potentials ($\epsilon_l + n\hbar\omega$) exhibiting one-, three-photon curve crossings at

short internuclear distances. This is to be contrasted with the case of an IR excitation for which the Floquet picture is rather inappropriate, as one-photon crossings occur at large distances, close to the dissociative limit, and a multitude of high-order crossings are densely produced in the inner region of the molecular potentials. Figure 2.1 shows the field-dressed potential energy curves involved in the two main Floquet blocks in the diabatic and adiabatic representations, for a typical UV-Vis filed at $\lambda = 532$ nm. Recall that the (R-)adiabatic representation, featuring avoided curve crossings, results from the diagonalization of the radiative interaction at fixed molecule–field orientations ($\theta = 0$ or π, which maximizes the couplings) and varying R. Two strong field intensities are considered, namely 10^{13} and 5×10^{13} W/cm^2, at a wavelength of 532 nm, corresponding to experimental conditions [50]. The curve crossing regions upon which the interpretation of the dynamics rests are indicated by rectangular boxes: X1 and X3 correspond to one-photon crossings, between the dressed states $|g, n >$ and $|u, n - 1 >$, and between $|g, n-2 >$ and $|u, n-3 >$, respectively, while X2 arises from the three-photon crossing between the ground and the two-photon channels, and X3 between $|g, n >$ and $|u, n - 3 >$. Three initial vibrational states v are also shown at the level of the X1 box, with energies above ($v = 5$) or below ($v = 2$) the laser-induced barrier for both intensities or in the energy gap between the lower and the upper adiabatic channel ($v = 4$).

Looking more closely at box X1, it is seen that the lowering of the laser-induced barrier at $I = 5 \times 10^{13}$ W/cm^2 is such that H$_2^+$ in a vibrational state $v \geq 4$ will dissociate almost exclusively by tunneling through the one-photon BS channel and leads to low energy photons. This mechanism has been abundantly discussed in the literature and experimentally verified [3, 50–53]. The counterpart of BS is the VT mechanisms the upper adiabatic channel may accommodate long-lived resonances [54, 55]. In particular, a very narrow resonance (of zero width, in a semiclassical estimate) may arise when a diabatic dressed vibrational level, defined on the lower diabatic dressed PES ($\epsilon_l + n\hbar\omega$), is close to a level created on the upper adiabatic PES [56]. Such coincidences may be obtained at will by just properly adjusting the laser wavelength (i.e., the relative energy positioning of the potentials) and intensity (i.e., the strength of the coupling) [54]. When the molecule is properly prepared (by an adiabatic excitation, using a pulse with a sufficiently long rise time) in such a resonance state, good stabilization is expected [55]. Early works even proposed an isotope separation scenario in a H$_2^+$/D$_2^+$ mixture based on this VT mechanism [54]. The scheme relies on the great sensitivity of the aforementioned diabatic–adiabatic level coincidences with respect to the laser and molecular characteristics. A coincidence that has been obtained for a molecule-plus-field system would no longer hold when one proceeds to an isotopic substitution, because of mass-related energy shifts. A detailed account of this mechanism will be given in Section 6. It is to be emphasized that the two stabilization mechanisms in consideration, here and in

the previous subsection, have completely different origins: The DDQ effect in the IR regime is based on a dynamical effect, whereas the VT effect in the UV-Vis regime is a pure stationary process. These basic mechanisms not only help in controlling molecular dissociation and understanding fragments KE distributions, but they can also be referred to for the interpretation of angular distributions of fragments in the strong-field photodissociation process.

To this end, it would be necessary to relax the restriction to a one-dimensional model and allow for rotational motion described by the angles θ and φ. In fact, for a linearly polarized field, the time-dependent Hamiltonian has axial symmetry and only the angular variable θ needs to be considered explicitly. Figure 2.3 presents 3D graphs of the (two-dimensional) adiabatic PESs in the region of the X1 and X3 avoided crossings. Imagine an initial wavepacket prepared on the short-range repulsive limit of the surface pictured in Figure 2.3a. It will be propagated toward the X1 region where the adiabatic potential barrier height is modulated by the angle-dependent laser-molecule coupling, i.e., to $\mu E_0 \cos \theta$. For a given field strength, this lowering is more pronounced for $\cos \theta \sim 1$ ($\theta \sim 0$ or π). For $\cos \theta \sim 0$ ($\theta \sim \pi/2$) the higher potential barrier is hardly penetrable. Under the effect of the torque exerted by the laser on the molecule, the wavepacket skirts around the potential barrier and follows the minimum energy pathway of the dissociative valley (that is for directions close to $\theta = 0$ or π) resulting in aligned fragments when the BS mechanism is operative [49]. Figure 2.3b represents, in the X3 region, the adiabatic surface leading to dissociation corresponding to the net absorption of two photons. To reach this surface, a large portion of the initial wavepacket has to undergo a non-adiabatic transition at X2. The non-adiabatic coupling responsible for the dissociation is sharply peaked around the avoided crossing position X2 with a strength that is much larger
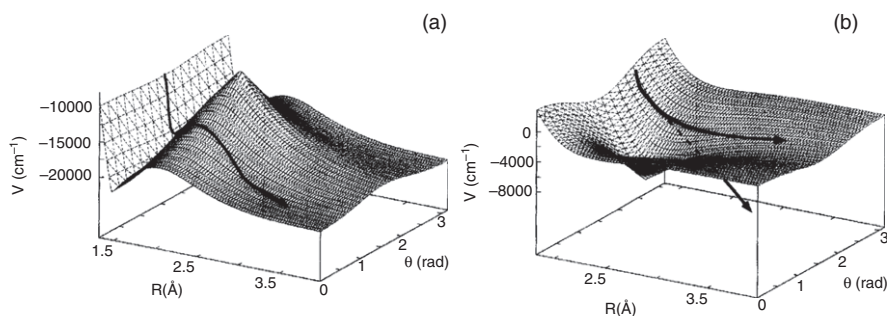
Figure 2.3 Three-dimensional graphs of adiabatic surfaces for $I = 10^{13}$ W/cm^2 in the region of the X1 (a) or X3 (b) avoided crossings. The arrows give an illustration of the minimum energy pathway on each surface.

for $\theta \approx \pi/2$ (there is no coupling at $\theta = \pi/2$) than for $\theta = 0$ or π [49]. The wavepacket prepared on this surface presents an angular distribution more pronounced around $\theta \sim \pi/2$. Subsequent dissociation dynamics on this surface also favors the $\theta \sim \pi/2$ direction as this corresponds to a potential valley. Finally, less aligned fragments are expected when non-adiabatic transitions are responsible for the dissociation of an initially trapped configuration.

We continue in the next two sections with two separate applications of the basic mechanisms discussed here: (i) A thorough interpretation of a recent pump–probe study of the dissociative ionization of H_2 and (ii) A study of control scenarios for molecular cooling and vibrational population transfer using ZWRs and the related concept of EPs.

5. XUV+IR PUMP–PROBE SPECTROSCOPY OF MOLECULAR DISSOCIATIVE IONIZATION

5.1. Introduction

With recent advances in laser technology, in particular with the generation of attosecond laser pulses as a spin-off of research on High-Harmonic generation (HHG), the real-time imaging of ultrafast molecular phenomena has become accessible. Just as femtosecond laser pulses led to the development of transition state spectroscopy and femtosecond chemistry [57], the advent of attosecond pulses [58] has given rise to endeavors where it is the even faster electronic motion that is probed in a time-resolved manner [59]. An important concern in these experiments is the question as to which extent the structure and dynamics of the molecule under investigation are influenced by the presence of the intense infrared (IR) laser field that drives the HHG process [60]. In the previous section, we have evoked the use of an ultrafast UV or XUV (pump) pulse to trigger the ionization of a molecule such as H_2 within the width of a longer IR (probe) pulse, which would cause the dissociation, or the VT, of the molecular ion depending on the delay between the two pulses and the frequency of the IR pulse, in a possible direct experimental study of the DDQ effects. A similar set of experiments has been performed recently, but with the probe pulse being in the near IR rather ($\lambda = 750$ nm) for which the Floquet dressed molecule picture still applies, so that instead of monitoring the DDQ type control, these experiments rather map out the degree of adiabaticity of the Floquet dynamics under the probe near-IR pulse (henceforth referred to as the IR pulse). We now review these experimental results and the accompanying theoretical interpretations [24, 25], and discuss the roles of different type of resonances associated with the Floquet representation in the very rich dynamics reflected in these results.

5.2. Experimental context

Two experiments were performed using an XUV attosecond pump pulse ($\hbar\omega \simeq 35\,\text{eV}$), 140 *as* Full-Width at Half Maximum (FWHM), which creates an initial vibrational wavepacket on the H_2^+ ($1s\sigma_g^+$) potential by means of a single-photon ionization of H_2. This (XUV) pump pulse thus serves to accurately define the time of ionization of the molecule, with respect to which subsequent dissociation of the H_2^+ ion is clocked, with the initial H_2^+ geometry reflecting that of the neutral ground state. The two experiments differ primarily in terms of the properties of the near IR field ($\lambda = 750\,\text{nm}$) that is used. In one experiment, henceforth called experiment A, the IR pulse is significantly shorter than the H_2^+ vibrational period (7 fs FWHM). In contrast, in experiment B, the duration of the IR laser pulse (35 fs FWHM) is comparable to (slightly longer) than the H_2^+ vibrational period, meaning that the IR field is present during the propagation of the wavepacket before dissociation, which, depending on the XUV-IR delay, τ, may or may not include the time at which the ionization by the XUV took place. In both cases, this delay is defined as the time separating the crest of the IR pulse from the peak of the XUV pulse, so that $\tau > 0$ denotes the situation where the XUV pulse precedes the IR pulse.[4]

Figure 2.4 shows a comparison of how the H^+ fragment KE distributions measured in experiments A and B varies as a function of the delay τ. In experiment A, the yield of fragments with energies below 1.2 eV exhibits a beating pattern with a main period of about 27 fs. A closer analysis of
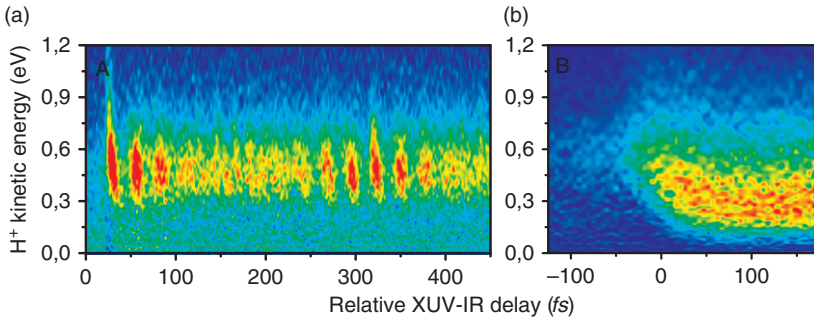
Figure 2.4   Measured time-dependent H^+ kinetic energy distributions for two-colour XUV+IR dissociative ionization of H_2, with 7 fs IR laser pulses (a) and 35 fs IR laser pulses (b).

---

[4] Note that the IR pulse generated high harmonics that were used to make the attosecond XUV pulses. As a consequence, in the case of the 35 fs IR field, one has a train of a finite number of attosecond pulses serving as the XUV pump, rather than a single one. We will ignore this distinction in the following.

this pattern, visible even at the most coarse-grained level, as obtained by integrating the experimental H$^+$ KE distribution over the energy range of 0–1.2 eV, as shown in Figure 2.5 [panel (a) of this figure shows this integrated signal as a function of τ, while panel (b) shows its Fourier transform], reveals that the oscillatory signal arises from the beating of a number of frequencies that are basically the Bohr frequencies between adjacent field-free vibrational
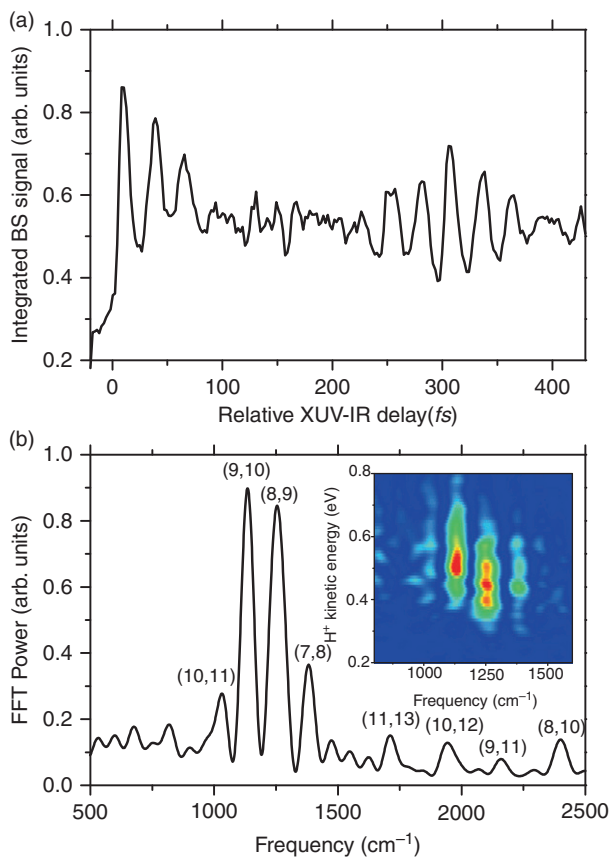

Figure 2.5   (a) Time-dependence of the H$^+$ fragment yield (obtained by integrating the measured KE distribution between 0 and 1.2 eV) as a function of the XUV-IR delay. The fragment yield shows oscillations resulting from the motion of the vibrational wavepacket on the $1s\sigma_g^+$ potential. Clear indications of wavepacket de-phasing and re-phasing are observed; (b) Fourier transform of the measurement shown in (a), revealing the two-level beats that are responsible for the observed time-dependence. The inset shows a KE-resolved Fourier transformation of the experimental results and reveals a correlation between the fragment KE release and the vibrational level occupied prior to dissociation.

levels around $v = 9$. This experiment A thus seems to be imaging just the vibrational content of the initial wavepacket. The results for experiment B, where the IR pulse duration is somewhat longer than the vibrational period of the H_2^+ molecule, are radically different. In this case, the proton kinetic energy distribution evolves smoothly as a function of τ. The most important feature in this smooth τ-dependence is the red shift of the center of gravity of the spectrum as τ increases past the interval denoting XUV-IR pulse overlap, to stabilize at a low level of 0.25 eV, for all positive values of τ denoting the situation where the IR pulse clearly follows the XUV pulse ($\tau > 20$ fs). No oscillatory pattern is seen in the experimental results for this case.

5.3. Theoretical simulations

In order to simulate the experimental results, concentrating on the dissociation of H_2^+ after its preparation by the XUV pulse, the one-dimensional two-channel model described in previous sections was used. We thus consider the H_2 parent molecule, originally in its ground vibrational and electronic state, to be ionized by the XUV pulse at time $t = 0$ and that the ionization is merely a Franck–Condon (FC) vertical promotion of the $v = 0$ vibrational state of the parent molecule onto the ground electronic state $|1s\sigma_g^+\rangle$ of the molecular ion. Subsequent nuclear wavepacket motions then develop on the two electronic manifolds of the molecular ion H_2^+, the ground state $|1s\sigma_g^+\rangle$ and the first excited electronic state $|2p\sigma_u^+\rangle$. The molecule is assumed to be aligned along the laser polarization. This is justified not only by our wish to concentrate on the essential feature of the dynamics but also by the fact that experimentally, the angle-resolved H^+ detection allows one to selectively observe fragments along the polarization axis, and it was found that none of the observations reported, and summarized in Figure 2.4 depends very strongly on the ejection angle of the H^+ fragment with respect to the polarization axis. As for the results shown in the preceding section, the wavepacket propagation procedure described in Section 3.2, but restricted to just the radial dimension, is used, and the proton kinetic spectra is extracted from the relative momentum k distribution defined in Eq. (65). The calculations are repeated for an extensive range of values of τ (more details on the calculations can be found in Ref. [25]) and produced the results shown in Figure 2.6, which displays the theoretical proton KE distributions as a function of τ for the same IR pulse durations as in experiments A and B, at intensities of 1×10^{13} and 3×10^{13} W/cm^2, respectively, which corresponds to the estimated peak intensities in the experiments. The calculations give spectra with much better detailed structures than the experiment. However, the main observations of the experimental Figure 2.4, as detailed above, are well brought out: In the case of the shorter IR pulse (experiment A), the same beating pattern, though much better resolved, is found when the KE spectrum is viewed as a function of the delay τ. Again this is in marked contrast with the results of the
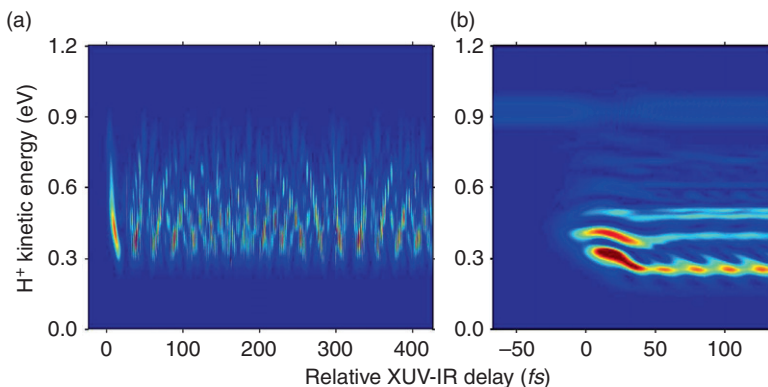
Figure 2.6 Comparison of the time-dependent kinetic energy distributions resulting from model calculations for two-colour XUV+IR dissociative ionization of H_2, making use of a 7 fs IR pulse (a) and a 35 fs IR pulse (b).

calculations for the longer IR pulse, which give a much smoother variation of the various features in the proton KE spectrum as a function of τ, although the lowest energy band does show a residual beating pattern. Of note again is the global red shift of the whole spectrum as τ increases from zero to ca. 20 fs.

5.4. Adiabatic vs. non-adiabatic Floquet resonance dynamics

In the condition of experiment A, as long as τ is larger than the width of the IR pulse so that no pulse overlap is possible and the IR pulse clearly follows the XUV pulse, the coherent superposition of vibrational states of H_2^+ prepared by this pump pulse (the Franck–Condon wavepacket) evolves under essentially field-free conditions, oscillating back and forth and spreading out on the $1s\sigma_g^+$ potential, before encountering the IR pulse. The shortness of the IR pulse evokes a limiting situation (a "sudden" dissociation limit), where the laser–molecule interaction merely opens, for a very brief instant (around the peak of the already short IR probe pulse), a "gate" to dissociation at some internuclear distance. The dissociation yield at any (half-collision) energy, measured essentially by the squared moduli of the wavepackets evaluated at this gate, thus depends on a synchronization between the wavepacket and the opening of this gate at the maximum of the IR field. This synchronization is a result of the coherence between the various vibrational components of the initial wavepacket and the dissociation yield necessarily reflects that coherence in this case. The dominant, coarse-grained behavior of the KE spectrum as a function of τ, the beating pattern reflecting the coherence of the initial vibrational wavepacket, i.e., field-free vibrational states, carries no

or little specific information on laser-induced resonances, as the adiabatic Floquet picture breaks down completely for such a short IR pulse. The wavepacket/gap synchronization evoked above is rather reminiscent of the DDQ effect, denoting a dynamical effect rather than a static, structural one.

Turning now to the case the H_2^+ vibrational wavepackets interact with a longer, 35 fs FWHM, IR pulse (experiment B), a behavior denoting a somewhat more adiabatic Floquet dynamics is expected, and little or no dependence of the KE spectrum on the time delay τ should be found as long as the XUV pulse precedes the IR without overlapping. This is what is indeed observed at time delays $\tau > 20$ fs. The residual oscillatory found in the computed τ-dependent spectrum indicates that t-non-adiabatic effects are present though, and this is hardly surprising as the 35 fs IR pulse features strong modulation of this laser's intensity over a time scale that is only about ten times the period of the carrier wave. For $\tau < 20$ fs, the fragment KE spectrum is strongly delay dependent, curving up smoothly as τ decreases to reach energy values similar to those encountered in the experiment A near zero delay.

This dependence of the H^+ KE on the XUV-IR delay in this case of the longer, 35 fs FWHM, IR pulse can be understood in terms of the adiabaticity of the Floquet dynamics underlying the dissociation processes, and the way that the IR intensity affects both the preparation and the propagation of the Floquet components of the wavepackets. More precisely, the IR probe pulse projects the various vibrational components of the wavepacket onto Floquet resonances, whose widths vary with the intensity of the IR pulse. We recall that these resonances are of two types: Shape resonances supported by the lower adiabatic potential defined at the one-photon crossing between the dressed (g, n), (u, n') channels and leading to efficient dissociation through the BS mechanism, or Feshbach resonances, vibrationally trapped in the upper adiabatic potential well.

When the IR pulse follows the XUV pulse without overlapping (i.e., $\tau > 20$ fs) as shown in Figure 2.7a, individual field-free vibrational states v^+ of the ion are, at first, transported adiabatically onto corresponding Floquet resonances. Each resonance gives rise to a characteristic line in the proton KE spectrum. The magnitude of the KE is determined by the nonperturbative laser-induced modification of the dressed potential energy curves. On the way toward dissociation, the ion experiences the increasing in time of the IR pulse amplitude and therefore sees a lowering of the BS barrier. The lowest barrier height is reached at mid-pulse time (maximum of intensity), resulting in most efficient dissociation when the lowest energy shape resonance can still tunnel through before the barrier rises. Most protons contributing to the spectrum have a KE of about 0.3 eV corresponding to the shape resonance issued from $v^+ = 8$. Higher energy shape resonances are also dissociative, but are not significantly populated by the XUV ionization step (through FC mapping of the vibrationless ground state of H_2).

This situation is to be contrasted with the case where the IR and XUV pulses are overlapping ($\tau < 10\,\text{fs}$), i.e., the H_2^+ ion is prepared at a moment when the IR field already has an appreciable intensity, and Floquet resonances defined by that field already differ markedly from field-free vibrational states. In this case, it can be said that the vibrational states of the ion are shaken up by this sudden intense IR excitation and are all instantly projected onto a superposition of shape and Feshbach resonances and these now appear in the wavepacket with weighting coefficients that may differ noticeably from those characterizing the FC wavepacket in terms of field-free states. In particular, higher energy resonances may temporarily be populated and take an important part in the dissociation step. Afterward, as shown in Figure 2.7b, the ion experiences the falling edge of the IR pulse with a rising BS barrier which quenches the dissociation of low-energy shape resonances. High-energy over-the-barrier shape resonances, more populated than in the previous adiabatic case, are the ones which contribute most to the dissociation. This explains the blue-shift of the protons KE distribution when τ decreases, bringing the XUV pulse closer to the maximum of the IR probe,
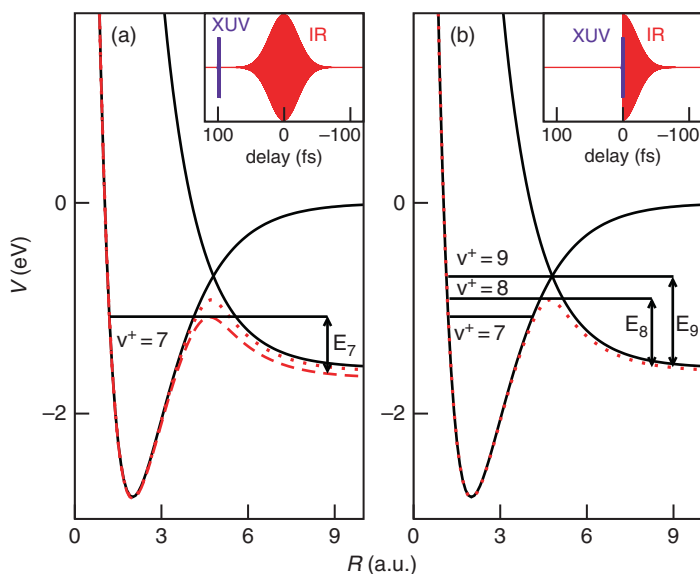
Figure 2.7 Potential energy curves of H_2^+ in a 750 nm laser-dressed diabatic representation (black solid lines). Are also indicated the lower adiabatic curves resulting from the diagonalization of the radiative interaction for two intensities ($I = 3 \times p10^{13}\,\text{W/cm}^2$ reached at mid-pulse time, in red dashed line and $I = 10^{13}\,\text{W/cm}^2$ in doted red line). E_7, E_8, and E_9 represent the kinetic energies issued from $v^+ = 7$, 8, and 9 for the typical XUV-IR delays [about 100 fs (a) and 0 fs (b)].

with the increasing role played by resonances issued from $v^+ = 9,10$ leading to a spectrum centered at about 0.5 eV.

To obtain a better, quantitative experiment versus theory agreement would require the relaxation of some of the assumptions inherent in our model. Among these approximations are a phenomenological description of the XUV ionization step[61], the neglect of rotational degrees of freedom [62] and also of the neglect of such realistic effects as laser focal volume averaging [62]. Nevertheless, the analysis just given shows how the dynamics of the two-colour dissociative ionization of H_2 under the influence of an XUV+IR pump–probe pulse sequence depends considerably on the adiabaticity of both the initial Floquet wavepacket preparation and the Floquet states' transport under the IR pulse. The present work represents a departure from most intense-field dynamics work. Ordinarily, adiabatic laser excitation regimes result in spectral observables with finely resolved peak structures that can be interpreted in terms of isolated, non-overlapping resonances [63], while a sudden and strong laser excitation normally induces overlapping of large width resonances, erasing specific dynamical information (leading to structureless and less informative spectral data). Rather, the two experimental situations described here and their interpretations illustrate how the richness of the structural determination of molecules, their imaging, and possible control in these situations rest on the sudden (non-adiabatic) or gradual (adiabatic) character of the strong IR excitations.

6. ZWRS AND EPS IN MOLECULAR PHOTODISSOCIATION

6.1. Introduction

We consider again a (diatomic) molecule with a ground electronic state represented by an attractive BO potential energy curve and a first excited state represented by a repulsive potential. The H_2^+ model system considered in the preceding sections is a typical example of such a system. Imagine first the molecule exposed to a continuous wave (cw) laser field. Within the Floquet formalism, the photodissociation rate can then be calculated quantum mechanically by the Fox-Goodwin–Numerov algorithm, as described in Section 3.1, for a realistic $N = 2p$-channel, p-Floquet-block model, but it can also be obtained with a semiclassical approach whenever the intensity is such as to justify for a two-channel approximation. The semiclassical approach has been originally developed to treat predissociation [56] and has been useful in showing that under some particular circumstances the predissociation rate could be vanishingly small. In the semiclassical theory of predissociative systems, their occurrence can be traced back to the existence of two kinds of zeroth-order states with energies which come in close coincidence. The disposition of the potential energy curves in the dressed

molecule picture is similar to that of a predissociative system and thus can give rise to ZWRs. It has been shown [6, 14, 54] that it is indeed possible, for a given wavelength and for a given resonance issued from a vibrational state of the field-free molecule, to find a laser intensity at which the resonance width and hence the photodissociation rate vanishes. We call such an intensity a critical intensity. The flexibility in choosing laser frequency and intensity conditions to tune predissociation-like couplings and curve crossing is at the origin of another interesting phenomenon: Resonance coalescence, i.e., the coincidence of the complex energies and wavefunctions of two resonances, which is attainable for specific laser wavelengths and intensities, leading to the so-called EPs. Such points are present in many areas of physics, with examples in classical physics [64, 65], as well as in quantum physics [66, 67]. We give here a review of these ideas, starting with the semiclassical expression of the condition for the appearance of a ZWR, the physical definition of the EP, before illustrating the two concepts and their use in vibrational control problems. We will be showing results of two types of calculations: Explicit intensity-dependent resonance energies and widths are obtained by the time-independent approach detailed in Section 3.1 applied to the Floquet N-channel closed-coupled equations, Eqs. (39 or 40), $N = 2, 4$, or 6, corresponding to keeping one, two, or three Floquet blocks. Results of wavepacket calculations for adiabatic, long pulses will also be shown to verify predictions made based on just the resonance properties, in particular on those of ZWR and EP. These results are obtained with the time-dependent wavepacket propagation procedure detailed in Section 3.2, mainly in the one-dimensional version, i.e., with just the radial dimension, ignoring rotational effects.

6.2. Semiclassical theory

Semiclassical theory of predissociation of a diatomic molecule [56, 68] states very clearly the conditions for the occurrence of ZWRs. This formalism is also applicable to laser-induced resonances given the analogy between the potentials describing predissociation and those of Figure 2.8 arising from the dressing of a two-channel molecule by a field. The potentials involved in the semiclassical treatment are indicated in the right panel of Figure 2.8. For predissociation the interchannel coupling is a property of the molecule. For intense-field photodissociation, the parameters controlling the couplings are those of the external field and, in principle, can be tuned at will. The semiclassical formalism provides analytic formulas for the resonance width. It predicts [56, 68] that if the energy is such that the two following conditions are simultaneously satisfied

$$\int_{R_+}^{R_0} dR \, k_+(R,E) + \int_{R_0}^{R_t} dR k_+(R,E) + \chi = (\tilde{v}_+ + \frac{1}{2})\pi \qquad (67)$$
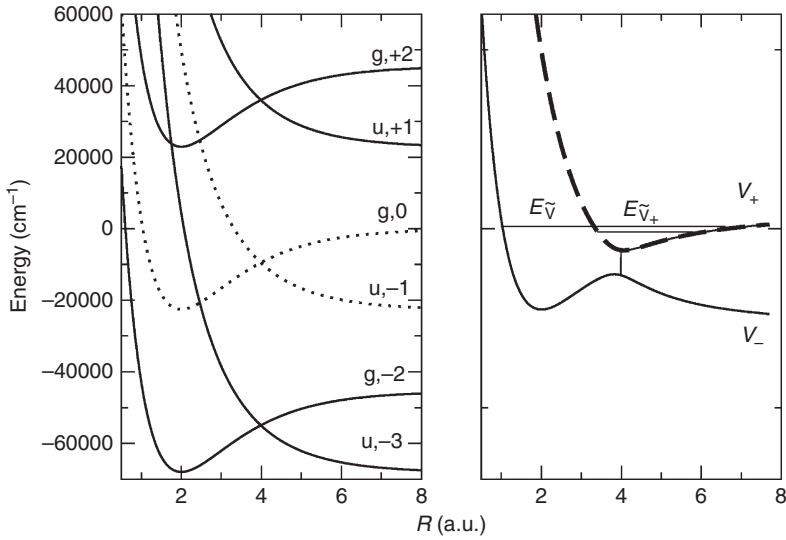
Figure 2.8 Diabatic (left panel) and adiabatic (right panel) potentials of H_2^+ for a wavelength $\lambda = 440$ nm and a field intensity 10^{13} W/cm². The excited state potential has been lowered by $\hbar\omega$. $E_{\tilde{v}}$ and E_{v_+} are representative of energies associated with the modified diabatic and the modified upper adiabatic potentials, respectively.

and

$$\int_{R_-}^{R_0} dR\, k_-(R,E) + \int_{R_0}^{R_t} dR k_+(R,E) = (\tilde{v} + \frac{1}{2})\pi \tag{68}$$

with $\tilde{v}_+$ and $\tilde{v}$ some integers, then the outgoing scattering amplitude in the lower (open) adiabatic channel is zero, with the consequence that the predissociation is quenched. In Eqs. (67, 68) the energy-dependent wave numbers are $k_\pm(R,E) = \hbar^{-1}[2\mathcal{M}(E - V_\pm(R)]^{1/2}$, $\mathcal{M}$ being the nuclear reduced mass. $R_\pm$ are the left turning points of the lower and upper adiabatic potentials $V_\pm(R)$, whereas R_t is the right turning point of $V_+(R)$. These conditions are nothing but Bohr–Sommerfeld quantization conditions. They mean that there is coincidence of two energy levels: $E_{\tilde{v}_+}$ supported by the upper adiabatic potential, affected by a phase correction χ, which is $-\pi/4$ in the weak coupling limit[68], and $E_{\tilde{v}}$ supported by a diabatic-like potential presenting a discontinuity and defined as follows: On the left of the diabatic crossing point R_0 this potential is the lower adiabatic potential, while beyond this point it is the upper adiabatic potential. For a weak coupling, this is practically the diabatic attractive potential. We call these two kinds of energies the "modified" diabatic and adiabatic energies, respectively. The coincidence condition can then be appreciated with the expression for the resonance

width Γ_v which emphasizes the role of the proximity of the two kinds of energies [68]:

$$\Gamma_v = \frac{2\pi}{\hbar} \frac{e^{2\pi v}(e^{2\pi v} - 1)\omega\omega_+}{(\omega_+ + (e^{2\pi v} - 1)\omega)^3}(E_{\tilde{v}} - E_{\tilde{v}_+})^2, \tag{69}$$

where ω and ω_+ are local energy spacings of the modified diabatic and adiabatic potentials. v is the coupling parameter, which, in a Landau–Zener type of approximation, is given in the laser-induced photodissociation problem, represented by a single Floquet block, by

$$v = \frac{\mu^2(R_0)\mathcal{E}_0^2}{\hbar\overline{v}|\Delta F|}, \tag{70}$$

$\overline{v}$ and ΔF are the classical velocity and the difference of slopes of the diabatic potentials at the diabatic crossing point R_0. $\mu(R_0)$ is the electronic transition moment at the diabatic crossing point and $\mathcal{E}_0$ the electric field amplitude of the laser field.

In the predissociation problem the coincidence can only be accidental since the potentials and the coupling cannot be modified. For a diatomic molecule submitted to an electromagnetic field, the wavelength and the intensity of the field are two external parameters which allow one to produce at will such coincidences. This explains the occurrence of ZWRs in laser-induced photodissociation. Such a flexibility can also be exploited to produce the EPs occurring in this context.

6.3. ZWRs and coalescence at an EP

Figure 2.9 displays the rates as a function of intensity for two resonances issued, respectively, from the field-free vibrational states $v = 8$ and $v = 9$, for a wavelength $\lambda = 255.255$ nm. Of note is the existence of an intensity where the rates, i.e., the imaginary part of the two resonance energies, approach each other. This signals the existence of an EP in the laser parameter (intensity, frequency) space. The left panel is a zoom of the curves near the EP. Similar features are found in many other areas of physics including optics, atomic physics, electron–molecule collisions, superconductors, quantum phase transitions in systems of interacting bosons, electric field oscillations in microwave cavities, to, more recently, molecular physics [26]. We note that the rate of the resonance $v = 9$ can shoot up to very high values. This has been interpreted [69] as due to the shape character of such resonances, which in zeroth order (in the channel couplings), are associated with energies marked as $E_{\tilde{v}}$ in Figure 2.8. The resonances associated with energies marked as $E_{\tilde{v}_+}$ are interpreted as having a Feshbach-like character. Their widths go asymptotically to zero, since the coupling of the upper diabatic potential with the lower one decreases as the intensity increases.
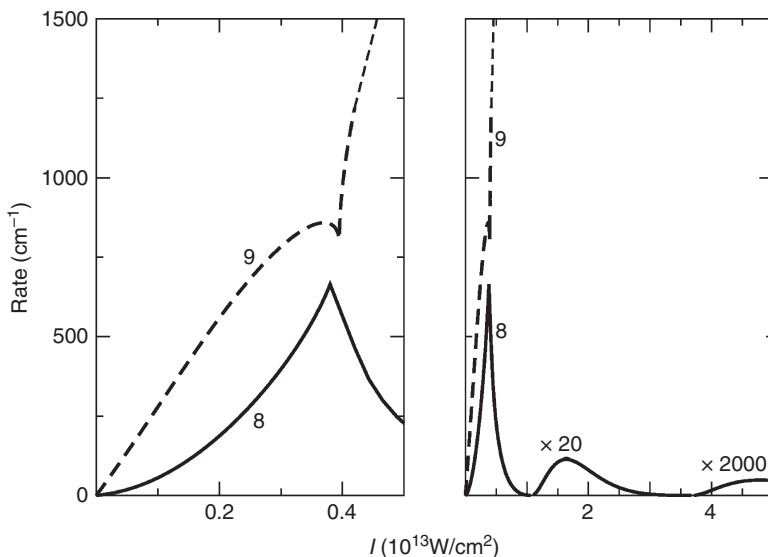
Figure 2.9   The rates versus intensity for the resonances issued from the vibrational states $v = 8$ and $v = 9$ for a wavelength $\lambda = 255.255$ nm. The left panel zooms the region showing how the rates approach each other for an intensity $I = 0.395 \, 10^{13}$ W/cm². The right panel shows that at two intensities the rate passes through a zero value. An amplification is needed because when the intensity increases, the coupling between the two adiabatic potential decreases and the bound states of the upper adiabatic potential become very good approximations.

The right panel of Figure 2.9 shows that the rate of level $v = 8$ reaches zero twice. This multiple occurrence of the zero-width phenomenon has been related to the possibility to produce several times a diabatic–adiabatic coincidence as the intensity increases [69]. This is so because the adiabatic (vibrational) levels goes up faster than the diabatic ones and therefore a given adiabatic level can cross several diabatic levels as the intensity increases. It is to be noted that resonance coalescence, i.e., the existence of an (EP), requires an appropriate choice of both frequency and intensity, while a ZWR would show up at some critical intensity(ies), irrespective of the choice of the wavelength, for all resonances of Feshbach type. One must keep in mind that the classification into shape and Feshbach depends strongly on the wavelength.

6.4. Vibrational purification using ZWR

At $\lambda = 420$ nm, the resonances $v = 8$ and $v = 10$ can acquire a zero width as, with increasing intensity, they tend to merge each into some bound state of the upper adiabatic potential, actually with states given, respectively, by

quantum numbers $\tilde{v}_+$ equal 0 and 1. In contrast, resonances 7 and 9, which are of shape type, can acquire very large widths when the intensity increases, due to the progressive lowering of the barrier of the lower adiabatic potential. Figure 2.10 shows (lower panel) how the rates of these four resonances actually vary as an function of time, considered a parameter in correspondence with the instantaneous electric field of the pulsed laser shown in the top panel. Clearly the width of resonance 8 goes through zero twice, while the laser intensity never got large enough throughout the pulse for the rate of resonance 10 to go to zero. It is interesting to compare at this point results of time-dependent wavepacket calculations starting from field-free vibrational states with $v = 7 - 9$, with those predicted by accumulating the widths of the above Floquet resonances over time, assuming a pure adiabatic transport of these resonances under the pulse shown in Figure 2.10. The observable considered here, the probability for the system to remain bound, while it adiabatically evolves as a pure Floquet resonance v (which, at zero-field, correlates with the vibrational state of the same v) under a pulse of total duration t_f is [6]:
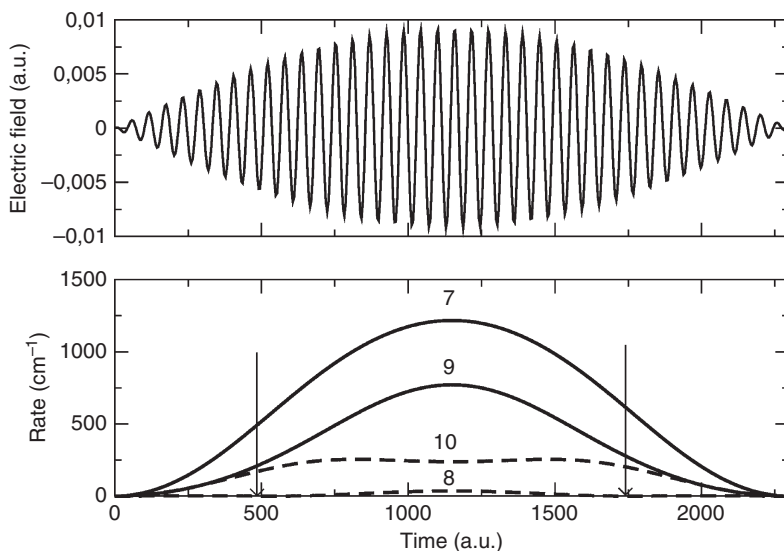
Figure 2.10 Time variation of the rates of various resonances followed adiabatically during the pulse shown in the upper panel. The wavelength is $\lambda = 420$ nm. The mid-pulse intensity $I = 0.3\ 10^{13}$ W/cm² is large enough for the width of the resonance $v = 8$ to pass twice through a null value at times depicted by the vertical arrows of the lower panel, but not large enough for resonance $v = 10$ to reach a zero width. Resonances $v = 7$ and $v = 9$ belong to the class reaching high values of the rates because of their shape nature.

$$P_b(v; t_f) = \exp\left[- \int_0^{t_f} \Gamma_v(t')dt' \right].$$

(71)

On the other hand, in the direct time-dependent approach, the survival probability, i.e., the probability for the system to remain bound at the end of the pulse, adapting Eq.(63), is [6]

$$P_{\text{bound}}(v; t_f) = \sum_{v'} p_{\text{bound}}(v, v'; t_f),$$

(72)

where

$$p_{\text{bound}}(v, v'; t_f) = \frac{|\langle v'|\psi_g^{(v)}(t_f)\rangle|^2}{|\langle \psi_g^{(v)}(t_f)|\psi_g^{(v)}(t_f)\rangle|^2 + |\langle \psi_u(t_f)|\psi_u(t_f)\rangle|^2}.$$

(73)

The sum is taken over all the discrete vibrational levels v' of state $|g\rangle$. $\psi_g^{(v)}(t)$ is the component of the wavepacket on the g channel evolved up to time t from the field-free vibrational state $|v >$ prepared at time $t = 0$. Note that $P_{\text{bound}}(v; t_f)$ actually represents the total bound state population at any time after t_f, since no further decay is then possible, the laser being turned off at such a time. It is clear that Eq. (71) gives a useful approximation for the result of a full time-dependent wavepacket evolution, [Eq. (73)], only if the assumption of an adiabatic transport of Floquet states is valid.

Figure 2.11 gives an example of such a comparison, considering specifically the evolution of the molecule out of the $v = 7$ state, under a $\lambda = 420$ nm, $I = 0.05 \times 10^{13}$ W/cm^2, 56 fs long pulse of the same form as shown in Figure 2.10. An excellent agreement is note. In fact, this agreement holds not only for the final value of the probability for the molecule to remain bound after the pulse is over but also for the survival probability evaluated at any time during the pulse.

Figure 2.12 further compares the results of the two types of calculations for a series of resonances at a higher peak intensity of the same pulse. Two conclusions emerge. First, the adiabatic Floquet formalism is again validated by the rather good agreement. Second, as expected, the state which is best protected against dissociation is $v = 8$, this being clearly related to the fact that only this state benefits, in this example, from a width which does vanish at least once while the pulse is on. A different way to check how the different states react to the field is to start from a coherent combination of vibrational functions and to follow in time the evolution of this combination. The initial wavepacket is taken as $|\tilde{\psi}(t = 0) >= 3^{-\frac{1}{2}}[|7 > +|8 > +|9 >]$. For the pulse used for this level-by-level study, shown in Figure 2.10, upper panel, we obtain now for the probability to find the system remaining bounded at the end of the pulse, the total value of

$$P_{\text{bound}} = 0.2960,$$

(74)
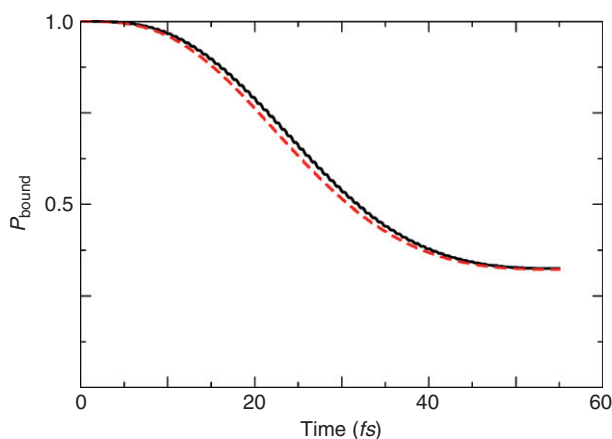
Figure 2.11 Time variation of the probability to remain bound for the resonance labeled $v = 7$. The wavelength is $\lambda = 420$ nm. The mid-pulse intensity is $I = 0.05 \times 10^{13}$ W/cm². The pulse duration is 56 fs. The dashed curve is for the adiabatic Floquet treatment while the solid curve is for the time-dependent calculation.
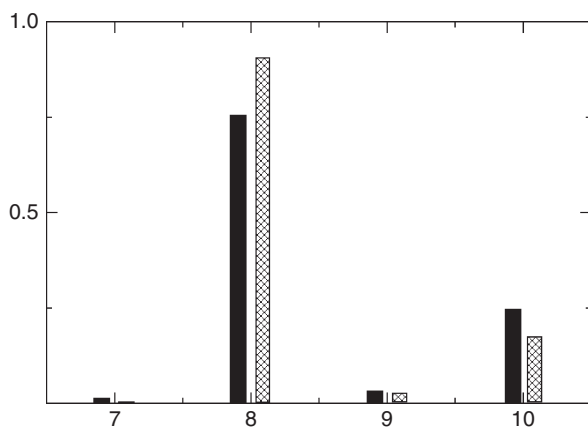
Figure 2.12 Comparison of survival probabilities for the resonances 7–10 calculated either from a time-dependent wavepacket propagation or from the adiabatic Floquet formalism with the same laser parameters as in Figure 2.10 and for a light pulse duration of $t_f = 56$ fs, corresponding to about 40 optical cycles. For each initial state, the wavepacket propagation result is given by the left histograms (full boxes), while the adiabatic Floquet result is represented by the right histograms (hatched boxes). Only the state 8 shows a large survival probability because, as shown on Figure 2.10, its rate passes twice through a null value.

with the following breakdown into three dominant contributions that are

$$P_{\text{bound}}(7; t_f) = | < 7|\tilde{\psi}(t_f) > |^2 = 0.0021, \tag{75}$$

$$P_{\text{bound}}(8; t_f) = | < 8|\tilde{\psi}(t_f) > |^2 = 0.2852, \tag{76}$$

$$P_{\text{bound}}(9; t_f) = | < 9|\tilde{\psi}(t_f) > |^2 = 0.0044. \tag{77}$$

It is thus the resonance issued from the level $v = 8$ that contributes most to the survival probability, which is not surprising as the resonance's width goes twice through a zero value during the pulse.

A ZWR may also offer an original isotope separation technique. A coincidence of the "modified" diabatic $E_{\tilde{v}}$ and adiabatic $E_{\tilde{v}_+}$ energies such as those involved in Eq. (69), supposedly ensured for a given molecule-plus-laser system, would no longer hold when one proceeds to an isotopic substitution. The feasibility, selectivity, and efficiency of an isotope separation in a mixture of D_2^+ / H_2^+ is proven in Figure 2.13 [54]. For a laser wavelength of 120 nm we examined the $v = 2$ resonance for both D_2^+ and H_2^+. A ZWR for D_2^+ is reached at an intensity of about 1.1 $\times$ 10 ^{13} W/cm^2. It is important to note that while the width attains a minimum (which is actually a zero) for D_2^+, it acquires a rather large value, Γ_2=600 cm^{-1} for H_2^+ (the rates of Figure 2.13 are twice the corresponding widths). We have thus shown that with a specific choice of the laser wavelength and intensity, D_2^+ dissociation may completely be suppressed,
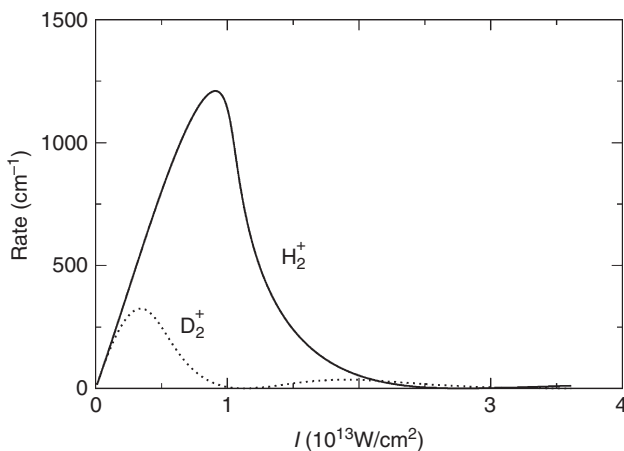
Figure 2.13 Rates as a function of laser intensity for D_2^+ (dotted line) and H_2^+ (solid line). The laser wavelength is taken as 120 nm and the resonance under consideration is $v = 2$.

whereas for the same field H_2^+ is still strongly dissociative: This is an original isotope separation scheme by laser-induced purification of D_2^+ in a mixture of D_2^+/H_2^+.

6.5. Vibrational transfer around an EP

We turn now to an exploitation of the other feature of Figure 2.9. We have seen that it is possible to make a choice of laser intensity and frequency which produces a near coalescence of two resonance energies. Because of the numerical character of the exploration, it is difficult to be accurately on the EP. However, there is a property of such a point which can be checked even when its position is known with a limited accuracy: Driving adiabatically the system along a closed loop encircling an EP should produce a resonance transfer. Starting from one of the resonances involved in the EP, the final result is that the molecule must end up in the other resonance [15, 26, 70]. We illustrate this property of an EP in Figure 2.14, with the initial state being $v = 9$. The loop in the parameter plane is defined by the two relations

$$\lambda = 255.25 \; 10^{-7} + 10 \; 10^{-7} \; \sin(\phi); \quad I = 0.5 \; \sin(\phi/2), \qquad (78)$$
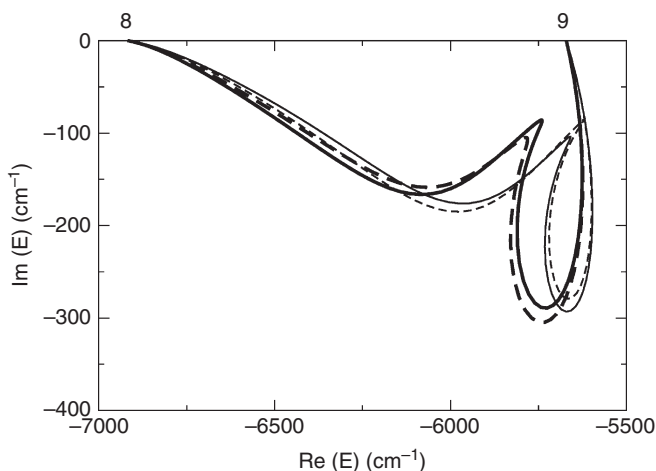
Figure 2.14   Transfer from state 9 to state 8 when following adiabatically the resonance issued from 9 around the exceptional point where the resonance energies from 8 to 9 are merging. The paths are as follows: thin solid curve, the two-channel model; thin dashed curve, four channels, with inclusion of the two lower channels of Figure 2.8; thick dashed curve, four channels, with inclusion of the two higher channels of Figure 2.8; thick solid curve, six channels, with inclusion of all channels of Figure 2.8.

The wavelength λ is in nm and the intensity I in units of 10^{13} W/cm^2. The angle ϕ goes from 0 to 2π. The loop goes around the EP with coordinates in the (intensity, wavelength) control plane estimated to be $\lambda = 255.25$ nm and $I = 0.395\ 10^{13}$ W/cm^2 for the pair $8 - 9$. The state 8 is finally reached. This is shown in Figure 2.14. We also demonstrate that this transfer is robust, i.e., it still holds when adding further channels to the basic two-channel model. Convergence is reached when, as displayed in Figure 2.14, one Floquet block is added on both sides of the reference block, that is the block of the single-photon two-channel model. However, near-convergence is already obtained with only the block above the reference block included. This shows incidentally that in all these calculations the EP is still within the loop.

Another important consequence of the occurrence of EPs is that on the EP the wavefunctions of the two resonances merge into a single one. This is illustrated in Figure 2.15 where the wavefunctions issued from 8 and 9 are shown (in dashed and in thin solid lines, respectively) at two different intensities for a wavelength $\lambda = 442.26$ nm. When the intensity is rather low ($I = 0.05\ 10^{13}$ W/cm^2), the nodal structure in the lower channel (g) is still recognizable. The resonance energies are then, respectively, $-6849.89 - i\ 9.21$
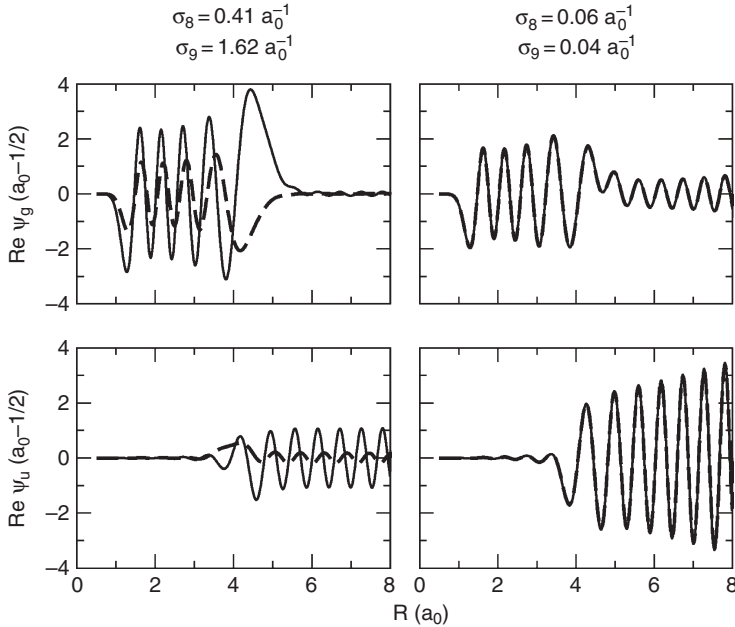
Figure 2.15 The resonance wavefunctions and their corresponding self-overlaps at two different intensities $I = 0.05\ 10^{13}$ W/cm^2 (left panels) and $I = 0.3949\ 10^{13}$ W/cm^2 (right panels). Only the real part of each channel wavefunction is displayed.

and $-5626.68 - i\, 68.06\,\text{cm}^{-1}$. For an intensity close to that of the EP, $I = 0.3949\ 10^{13}\,\text{W/cm}^2$, for which the resonance energies are still distinguishable and are $-5926.52 - i\, 391.58\,\text{cm}^{-1}$ and $-5917.11 - i\, 399.21$, the two wavefunctions become almost undistinguishable. A very interesting feature, the self-orthogonality phenomenon, occurs whenever two photodissociation resonances coalesce. This can numerically be evidenced from the so-called self-overlap σ of a given resonance solution $\Psi(R,t)$ evaluated as [26]

$$\sigma = \sum_{n=-\infty}^{n=+\infty} \int_0^\infty dR \left[\left(\psi_{g,n}(R) \right)^2 + \left(\psi_{u,n}(R) \right)^2 \right] . \qquad (79)$$

It is important to note that no complex conjugate of the Floquet components $\psi_{g,u}(R)$ appears here in the implied scalar-product, consistently with the definition of the non-hermitian c-product (see Refs. [21, 71]). The self-orthogonality phenomenon cannot be described using the standard hermitian definition where the usual complex conjugates of $\psi_{g,u}(R)$ would appear. The corresponding values are given in Figure 2.15 where one observes a significant decrease of σ_8 and σ_9 near the EP.

The occurrence of ZWRs and of EPs in the context of laser-induced photodissociation can be exploited in various ways. We have shown how ZWRs can be beneficial in purification scenarios. We have also shown that EPs can be exploited in vibrational transfer scenarios. Such scenarios could ultimately be applied for vibrational cooling strategies by depleting all vibrational levels except the ground ($v = 0$) one.

7. CONCLUSION

Intense laser-induced molecular dissociation is definitely one of the most challenging applications of Quantum Mechanics where theoretical models and their computer-based numerical simulations may help in a quantitative understanding and prediction of experimental discoveries. This has been exemplified in this review on some simple systems. Although the low-dimensional models considered may appear limited, the nature and dynamics of the unstable states (resonances) and the basic mechanisms associated with them are of wider application range than evoked and particularly in reactivity control. Strong field mechanisms, specifically barrier suppression and dynamical quenching in the IR regime or BS and VT in the UV regime, are basic tools for a detailed interpretation of experimental observations made on ATD spectra. By adjusting adequately the laser's characteristics such as its intensity, frequency, polarization, pulse shape, and phase, one can bring into competition chemical BS and/or hardening mechanisms, to obtain intense laser control scenarios of photochemical processes. Advantage can be taken of such a competition to direct the chemical

reaction toward a given channel, involving the breaking of a given bond, while the others are stabilized by laser-induced trapping or quenching mechanisms.

It is important to note that control strategies based on resonances and basic mechanisms present interesting complementarities when compared to optimal control schemes, with the advantage for the formers of a thorough understanding of the dynamics on the one hand, and robustness and transposability, on the other hand. More precisely, this complementarity can be discussed referring to three observations: (i) there is no single solution arising from optimal control scenarios (not only different criteria but also different sampling spaces for the laser parameters to be optimized would lead to different results); (ii) a careful study of the laser-induced dynamics can help to the identification (or guess) of some basic mechanisms leading to the desired observable in a very robust way (not a black-box numerical approach); (iii) by appropriately building the targets and delineating the parameter sampling space, we can help the optimal control scheme to take advantage of the mechanisms and specific behaviors of the resonances. Finally, we emphasize again that we refer to basic mechanisms or resonances only for interpretation or control purposes, or when describing strictly time-adiabatic processes, all calculations dealing with the "exact" resolution of the time-dependent Schrödinger equation.

The opposition of sudden excitations and adiabatic dynamics provides other ways of controlling and/or imaging dissociative ionization processes. This has been illustrated by quantitative theoretical interpretations of observations made in the XUV + IR pump–probe experiment discussed in Section 5, where the imaging and/or possible dynamical control of the dissociative ionization of H_2 rests on a partial breakdown of the widely common assumption of adiabatic transports of individual, isolated resonances during the laser-induced dynamics. On the other hand, it is rather within such an adiabatic regime, associated with a long pulse duration, that one encounters counterintuitive situations due to highly nonlinear behaviors in the transports and decays of single resonances induced by strong fields as exemplified by ZWRs, denoting situations where a molecule irradiated by a very strong field is stabilized with respect to dissociation. Advantage can be taken from a ZWR that is adiabatically connected with a given field-free vibrational state, as one can manage to bring all population in other vibrational states to dissociation, leaving residual bound population in the ZWR under consideration: This constitutes a vibrational purification control scheme. In the same spirit, it is possible to proceed to a separation of different chemical species (two isotopes, for instance) in a mixture merely by dissociating certain species while stabilizing others through a ZWR reached within the same laser excitation, the result being an enrichment of the mixture in the stabilized species.

At the frontier of non-adiabaticity (i.e., of the breakdown of the single resonance adiabatic transport approximation) lies the EPs that can be

reached by an appropriate combination of laser parameters (frequency and intensity). A coalescence of two resonances adiabatically connected with two different field-free vibrational states occurs at an EP. With a loop in the (frequency, intensity) plane encircling the EP, such a resonance coalescence situation is produced. As the loop is followed adiabatically, the system switches from a single resonance connected with a given vibrational level to a second resonance, and ends up in a final, different vibrational level when the laser is turned off: This is a vibrational transfer control scheme. Combining ZWRs and EPs and using appropriately chirped laser pulses, it is easily realized how a molecular cooling control objective can be attained by depleting all vibrational levels except the ground ($v = 0$) one.

An important issue concerns the robustness of the control strategies discussed presently with respect to the introduction of rotational degrees of freedom and additional electronic states. We have not addressed this issue explicitly here, but studies have been made, e.g., on rotational effects on the existence of ZWRs, and give reassuring results [6]. Even if there may be some efficiency loss upon inclusion of further channels in the model, the general strategies seem to resist to these additional degrees of freedom. Laser-induced molecular orientation, manipulation, and imaging are among the future goals of such control schemes based on laser-induced resonances and associated processes.

ACKNOWLEDGMENTS

REFERENCES

[1] A.D. Bandrauk, Quantum and semiclassical electrodynamics, in: A. D. Bandrauk (Ed.), Molecules in Laser Fields, Marcel Dekker, New York, 1994.

[2] A.D. Bandrauk, E.E. Aubanel, J.M. Gauthier, Theory of molecules in intense laser fields, in: A.D. Bandrauk (Ed.), Molecules in Laser Fields, Marcel Dekker, New York, 1994.

[3] A. Giusti-Suzor, X. He, O. Atabek, F.H. Mies, *Above-threshold dissociation of H_2^+ in intense laser fields*, Phys. Rev. Lett. 64 (1990) 515.

[4] O. Atabek, R. Lefebvre, T.T. NguyenDang, Control theory and quantum dynamics, in: T.G. Ciarlet, J.L. Lyons, C. Lebris (Ed.), Handbook of Numerical Analysis, Vol. X, Elsevier, 2003.

[5] C. Lefebvre, T.T. Nguyen-Dang, O. Atabek, *Intense laser-controlled quenching of molecular fragmentation*, Phys. Rev. A 75 (2007) 023404.

[6] O. Atabek, R. Lefebvre, C. Lefebvre, T.T. Nguyen-Dang, *Intense-field zero-width resonances and control of molecular photodissociation*, Phys. Rev. A 77 (2008) 043413.

[7] A.F.J. Siegert, *On the derivation of the dispersion formula for nuclear reactions*, Phys. Rev. 56 (1939) 750.

[8] L. Fox, E.T. Goodwin, *The numerical solution of non-singular linear integral equations*, Philos. Trans. R. Soc., Lond. 245A (1953) 501.

[9] S.I. Chu, *Floquet theory and complex quasivibrational energy formalism for intense field molecular photodissociation*, J. Chem. Phys. 75 (1981) 2215.

[10] F. Châteauneuf, T.T. Nguyen-Dang, N. Ouellet, O. Atabek, *Dynamical quenching of field-induced dissociation of H_2^+ in intense infrared lasers*, J. Chem. Phys. 108 (1998) 3974.

[11] H. Abou-Rachid, T.T. Nguyen-Dang, O. Atabek, *Dynamical quenching of laser-induced dissociations of heteronuclear diatomic molecules in intense infrared fields*, J. Chem. Phys. 110 (1999) 4737.

[12] H. Abou-Rachid, T. Nguyen-Dang, O. Atabek, *Dynamical quenching of laser-induced dissociations of diatomic molecules in intense infrared fields: Effects of molecular rotations and misalignments*, J. Chem. Phys. 114 (2001) 2197.

[13] H. Niikura, P.B. Corkum, D.M. Villeneuve, *Controlling vibrational wave packet motion with intense modulated laser fields*, Phys. Rev. Lett. 90 (2003) 203601.

[14] O. Atabek, R. Lefebvre, F.X. Gadéa, *Zero-width resonances in intense-field molecular photodissociation*, Phys. Rev. A 74 (2006) 063412.

[15] O. Atabek, R. Lefebvre, *Laser control of vibrational transfer based on exceptional points*, J. Phys. Chem. 114 (2010) 3031

[16] F.H.M. Faisal,Theory of Multiphoton Processes, Plenum, New York, 1986.

[17] H.R. Reiss, *Effect of an intense electromagnetic field on a weakly bound system*, Phys. Rev. A 22 (1980) 1786.

[18] C. Cohen-Tannoudji, J. Dupont-Roc, G. Grynberg, Atom-Photon Interactions, Wiley-Interscience, New York, 1992.

[19] M. Born, R. Oppenheimer, *Zur Quantentheoric der Moleken*, Ann. Phys. 84 (1927) 457.

[20] G. Floquet, *Sur les équations différentielles linéaires à coefficients périodiques* Ann. de l'Ecol. Norm. Sup. 12 (1883) 47.

[21] N. Moiseyev, *Quantum theory of resonances: Calculating energies widths ans cross-sections by complex scaling*, Phys. Rep. 302 (1998) 212.

[22] M.D. Feit, J.A. Fleck, A. Steiger, *Solution of the Schrödinger equation by a spectral method*, J. Comput. Phys. 47 (1982) 410.

[23] A.Keller,*Asymptotic analysis in time-dependent calculations with divergent coupling*, Phys.Rev. A 52 (1995) 1450.

[24] F. Kelkensberg, C. Lefebvre, W. Siu, O. Ghafur, T.T. Nguyen-Dang, O. Atabek, et al., *Molecular dissociative ionization and wave-packet dynamics studied using two-color XUV and IR pump-probe spectroscopy*, Phys. Rev. Lett. 103 (2009) 123005.

[25] C. Lefebvre, Stratégies de contrôle laser de la dynamique moléculaire, Ph. D. Thesis, Université Laval, Québec and Université Paris-sud 11, Orsay, 2008.

[26] R. Lefebvre, O. Atabek, M. Šindelka, N. Moiseyev, *Resonance coalescence in molecular photodissociation* Phys. Rev. Lett. 103 (2009) 123003.

[27] S. Chelkowski, T. Zuo, O. Atabek, A.D. Bandrauk, *Dissociation, ionization, and Coulomb explosion of H_2^+ in an intense laser field by numerical integration of the time-dependent Schrödinger equation*, Phys. Rev. A 52 (1995) 2977.

[28] S. Guérin, F. Monti, J.M. Dupont, H. Jauslin, *On the relation between cavity-dressed states, Floquet states, RWA and semiclassical models*, J. Phys. A Math. Gen. 30 (1997) 7193.

[29] S. Guérin, H.R. Jauslin, *Control of quantom dynamics by laser pulses: Adiabatic Floquet theory*, Adv. Chem. Phys. 125 (2003) 147.

[30] U. Peskin, N. Moiseyev, *The solution of the time-dependent Schrödinger equation by the (t,t′) method: Theory, computational algorithm and applications*, J. Chem. Phys. 99 (1993) 4590.

[31] N. Moiseyev, M. Chrysos, R. Lefebvre, *The solution of the time-dependent Schrödinger by the (t,t′) method: application to intense field molecular photodissociation*, J. Phys. B At. Mol. Opt. Phys. 28 (1995) 2599.

[32] N. Moiseyev, O.E. Alon, V. Ryabov, *The (t,t') method and gauge transformations for two electronic potential surfaces: An application to the partial width of H_2^+*, J. Phys. B At. Mol. Opt. Phys. 28 (1995) 2611.

[33] C. Kittel, Introduction to Solid State Physics, seventh Ed., John Wiley, New York, 1996.

[34] J.M. Okuniewickz, *Quasiperiodic pointwise solutions of the periodic, time-dependent Schrödinger equation*, J. Math. Phys. 15 (1974) 1587.

[35] T.T. Nguyen-Dang, F. Châteauneuf, O. Atabek, X. He, *Time-resolved dynamics of two-channel molecular systems in cw laser fields: Wave-packet construction in the Floquet formalism*, Phys. Rev. A 51 (1995) 1387.

[36] T. Kato, *On the adiabatic theorem of quantum mechanics*, J. Phys. Soc. Jpn. 5 (1950) 435.

[37] H.P. Breuer, K. Dietz, M. Holthaus, *Berry's phase in quantum optics*, Phys. Rev. A 47 (1993) 725.

[38] H.P. Breuer, M. Holthaus, *Adiabatic control of molecular excitation and tunneling by short laser pulses*, J. Phys. Chem. 97 (1993) 12634.

[39] T.T. Nguyen-Dang, E. Sinelnikov, A. Keller, O. Atabek, *High-order adiabatic representations of quantum systems through a perturbative construction of dynamical invariants*, Phys. Rev. A 76 (2007) 052118.

[40] G. Jolicard, J.P. Killingbeck, D. Viennot, J. Buldyreva, P. Joubert, *Transitional and permanent regimes in the adiabatic Floquent approach to photodissociation processes*, J. Phys. A 41 (2008) 095303.

[41] F. Châteauneuf, Dynamique et structure moléculaire en champs laser intenses, Ph. D. Thesis, Département de chimie, Université Laval, Québec, 1997.

[42] C.A. Nicolaides, D.R. Beck, *The variational calculation of energies and widths of resonances*, Phys. Lett. A 65 (1978) 11.

[43] B. Simon, *The definition of molecular resonance curves by the method of exterior complex scaling*, Phys. Lett. A 71 (1979) 211.

[44] D.W. Norcross, M.J. Seaton, *Asymptotic solutions of the coupled equations of electron-atom collision theory for the case of some channels closed*, J. Phys. B 6 (1973) 614.

[45] C.E. Dateo, H. Metiu, *Numerical solution of the time-dependent Schrödinger equation in spherical coordinates by Fourier-transform methods*, J. Chem. Phys. 95 (1991) 7392.

[46] R. Kosloff, *Time-dependent quantum-mechanical methods for molecular dynamics*, J. Phys. Chem. 92 (1988) 2087.

[47] D.J. Kouri, R.C. Mowrey, *Close-coupling wavepacket formalism for gas phase atom-diatom collisions*, J. Chem. Phys. 80 (1987) 2578.

[48] R. Heather, H. Metiu, *An efficient procedure for calculating the evolution of the wave function by fast Fourier transform methods for systems with spatially extended wave function and localized potential*, J. Chem. Phys. 86 (1987) 5009.

[49] R. Numico, A. Keller, O. Atabek, *Laser-induced molecular alignment in dissociation dynamics*, Phys. Rev. A 52 (1995) 1298.

[50] A. Zavriyev, P.H. Bucksbaum, H.G. Muller, D.W. Schumacher, *Ionization and dissociation of H_2 in intense laser fields at 1.064 m, 532 nm, and 355 nm*, Phys. Rev. A 42 (1990) 5500.

[51] G. Jolicard, O. Atabek, *Above-threshold-dissociation dynamics of H_2^+ with short intense laser pulses*, Phys. Rev. A 46 (1992) 5845.

[52] G. Yao, S.I. Chu, *Molecular-bond hardening and dynamics of molecular stabilization and trapping in intense laser pulses*, Phys. Rev. A 48 (1993) 485.

[53] E.E. Aubanel, A. Conjusteau, A.D. Bandrauk, *Effect of rotations on stabilization in high-intensity photodissociation of H_2^+*, Phys. Rev. A 48 (1993) R4011.

[54] O. Atabek, M. Chrysos, R. Lefebvre, *Isotope separation using intense laser fields*, Phys. Rev. A 49 (1994) R8.

[55] R. Numico, A. Keller, O. Atabek, *Nonadiabatic response to short intense laser pulses in dissociation dynamics*, Phys. Rev. A 56 (1997) 772.

[56] A.D. Bandrauk, M.S. Child, *Analytic predissociation linewidths from scattering theory*, Mol. Phys. 19 (1970) 95.

[57] A.H. Zewail, *Femtochemistry: Atomic-scale dynamics of the chemical bond*, J. Phys. Chem. A 104 (2000) 5660.

[58] P.B. Corkum, F. Krausz, H. Ferenc, *Attosecond science*, Nat. Phys. 3 (2007) 381.

[59] M. Drescher, M. Hentschel, R. Kienberger, G. Tempea, C. Spielmann, G.A. Reider, et al., *X-ray Pulses Approaching the Attosecond Frontier*, Science 291 (2001) 1923.

[60] C.C. Chirila, M. Lein, *Effect of dressing on high-order harmonic generation in vibrating H_2 molecules*, Phys. Rev. A 77 (4) (2008) 043403.

[61] T.T. Nguyen-Dang, F. Châteauneuf, S. Manoli, O. Atabek, A. Keller, *Tunnel ionization of H_2 in a low-frequency laser field: A wave-packet approach*, Phys. Rev. A 56 (1997) 2142.

[62] V. Serov, A. Keller, O. Atabek, H. Figger, D. Pavicic, *Intense laser dissociation of D_2^+: From experiment to theory*, Phys. Rev. A 72 (3) (2005) 033413.

[63] K. Sändig, H. Figger, T.W. Hänsch, *Dissociation dynamics of H_2^+ in intense laser fields: Investigation of photofragments from single vibrational levels*, Phys. Rev. Lett. 85 (23) (2000) 4876.

[64] C. Dembowski, F. Gräf, H.L. Harney, A. Heine, W.D. Heiss, H. Rehfeld, et al., *Experimental observation of the topological structure of exceptional points*, Phys. Rev. Lett. 86 (2001) 787.

[65] T. Stehmann, W.D. Heiss, F.G. Scholtz, *Observation of exceptional points in electronic circuits*, J. Phys. A Math. Gen. 37 (2004) 7813.

[66] E. Navericius, N. Moiseyev, *Trapping of an electron due to molecular vibrations*, Phys. Rev. Lett. 84 (2000) 1681.

[67] H. Cartarius, J. Main, G. Wunner, *Exceptional points in atomic spectra*, Phys. Rev. Lett. 99 (2007) 173003.

[68] M.S. Child, *Predissociation and photodissociation of IBr. A case of intermediate coupling strength*, Mol. Phys. 32 (1976) 1495.

[69] O. Atabek, R. Lefebvre, *Multiple occurrence of zero-width resonances in photodissociation: Effect of laser field intensity and frequency*, Phys. Rev. A 78 (2008) 043419.

[70] R. Lefebvre, O. Atabek, *Exceptional points in multichannel resonance quantization*, Eur. J. Phys. D 56 (2010) 317.

[71] N. Moiseyev, P.R. Certain, F. Weinhold, *Resonance Properties of Complex-Rotated Hamiltonians*, Mol. Phys. 36 (1978) 1613.

Coherence Effects in Laser-Induced Continuum Structure

Ioannis Thanopulos[a] and **Moshe Shapiro**[b,c]

Contents

Abstract We review recent developments in coherence related phenomena involving metastable states embedded in (multiple) continua via the action of (strong) laser pulses. The role of *Laser-Induced Continuum Structure* (LICS)

[a] Theoretical and Physical Chemistry Institute, National Hellenic Research Foundation, Athens 11635, Greece
[b] Departments of Chemistry and Physics, The University of British Columbia, Vancouver V6T1Z1, Canada
[c] Department of Chemical Physics, The Weizmann Institute, Rehovot 76100, Israel
E-mail addresses: ithano@eie.gr (I. Thanopulos), mshapiro@chem.ubc.ca (M. Shapiro)

in a number of diverse phenomena, such as *Coherent Population Trapping*, enhancement and suppression of photo-ionization and photo-dissociation, and population transfer through manifolds of continuum states is discussed. We also discuss the effect of (natural and light induced) structured multiple continua on *Electromagnetically Induced Transparency* and the slowing down of light. We explore the relation of LICS to *Coherent Control* (CC) which makes use of interferences between several quantum pathways so as to control the branching ratios of processes involving bound-bound or bound-continuum optical transitions. As examples, we discuss the use of CC and LICS in controlling the electronic branching in the photo-dissociation of the Na_2 molecule and the photo-electron angular distribution in atoms. Finally, we discuss the *Coherently Controlled Adiabatic Passage* (CCAP) method, which combines the selectivity of CC with the robustness of *Adiabatic Passage* for executing complete population transfers from an arbitrary superposition of initial states to an arbitrary superposition of target states.

1. INTRODUCTION

The continuous parts of the spectra ("continua") of atomic and molecular systems were traditionally thought of as incoherent sinks that result in "rate-like" processes and irreversible decay. While this view may sometimes be true for continua whose coupling matrix element varies relatively slowly with energy ("flat" continua), experiments of the last two decades have demonstrated coherent behavior in many laser-mediated processes associated with continua. The "dressing" of continua by light was shown to cause coherent phenomena, such as induced transparency, nonexponential decay and recurrences, and "above-threshold" ionization and dissociation processes, involving optical transitions within continua.

Laser-induced continuum structure (LICS) [1, 2] is one such effect. LICS experiments involve using a ("dressing") laser field to strongly couple an unpopulated bound state to a continuum. A different ("probe") laser field is made to couple a second, populated, bound state to the same continuum. The result is that the transition rate to the continuum acquires a "Fano-resonance" [3]-type shape.

The LICS phenomenon was first discussed explicitly (by Heller and Popov [4]) in the 1970s. The complementary situation, in which a bound state acquires a continuum-like character, has however been studied since much earlier. Cases that fall under this category are for example broadening of spectral lines due to spontaneous emission; "shape" or Feshbach scattering resonances [5]; autoionizing resonances [3, 6, 7]; Stark resonances [8–10], where a static electric field ionizes high-lying bound atomic states; electronic (vibrational, rotational) "predissociation" where a bound state associated with a particular electronic (vibrational, rotational) manifold is coupled

to a lower lying continuum belonging to another electronic (vibrational, rotational) manifold [11, 12].

The major new feature of LICS is that in the above cases the resonance parameters are fixed by the internal Hamiltonian of the material system involved, whereas in LICS, the resonance properties, including interferences between multiple continua and line-shape asymmetries, can be tuned and adjusted by the laser fields.

Many of the developments in the early years of experimental and theoretical investigations of LICS have been summarized in the review article by Knight et al. [2]. Since then, further interesting aspects of LICS have come to light. A topic of special interest is the connection with other light–matter coherent effects, such as *electromagnetically induced transparency* (EIT) [13–19], *adiabatic passage* (AP) [20–23], and *coherent control* (CC) [24–26]. In this review we discuss these aspects, concentrating on metastable states coupled by laser fields to (multiple) continua.

In Section 2, we give a brief outline of LICS and related phenomena, from the early experiments on atoms, till recent work on molecular systems. In Section 3, we discuss the effect of natural and light-induced structured multiple continua on EIT and the slowing down of light. In Section 4, we introduce the CC methodology and the *stimulated Raman adiabatic passage* (STIRAP) technique. Both techniques are based on quantum coherence and are directly related to LICS when continua are involved. In Section 5 we discuss the use of LICS for the control of electronic branching in the photo-dissociation (PD) of the Na_2 molecule. We also discuss the *coherently controlled adiabatic passage* (CCAP) method, which combines the selectivity of CC with the robustness of STIRAP. Concluding remarks are made in Section 6.

2. A BRIEF HISTORICAL SURVEY OF LICS

In this section we present a brief historical account of LICS without going into too many details, as our main concern is aspects of quantum interferences. LICS was initially suggested by Heller and Popov [4] and by Armstrong et al. [27], who termed the effect *"pseudo-autoionization."* Early theoretical investigations on LICS focused on *coherent population trapping* [28, 29], multichannel effects [30–33], and Raman-type transitions [2, 34–40].

The early experimental studies on LICS involved polarization-rotation, frequency-up conversion, third-harmonic generation, and multiphoton ionization. The progress was hampered initially because a LICS experiment is rather demanding on resources: it requires two frequency-stable tunable lasers, at least one of which must be sufficiently intense to embed a bound state in the continuum in the presence of processes that degrade the LICS signatures, such as spontaneous emission. A difficulty associated with the observation of LICS is due to the change in the effective coupling over the

frequency span of the ionization width of the embedded state. If the width is small compared to other characteristic widths (laser line-widths, natural line-widths, etc.), then the change in transition probabilities is difficult to detect.

The first observation of LICS in photo-absorption was made by Heller et al. [41] in Cs. They employed a circularly polarized dressing laser to embed a bound state in an ionization continuum. The probe laser field was tunable and linearly polarized. Since linearly polarized light is a sum of left-handed and right-handed circular components, and only one such component dresses up the continuum, the effect could be well detected by comparing the line shape of one component relative to the other [42].

Early demonstrations of LICS were also done in frequency up-conversion [43] and third-harmonic generation [44] experiments. In such experiments it is important to distinguish between the effects of LICS and those due to "natural" autoionizing states, both affecting frequency up-conversion [27, 45, 46] and third-harmonic generation [47] in pretty much the same way [4, 48]. Experiments of LICS in three-photon ionization of Na [35, 36, 49] and Xe [50–52] have also been reported. These experiments were followed by a set of extensive studies on Na [53–58], Xe [59, 60], Cs [61, 62], Ca [63–67], Mg [68], and He [69]. LICS effects were also reported in NO [70].

Subsequent theoretical papers on LICS [71–78] included studies of LICS in presence of collisions [76, 77]; R-matrix Floquet theory in relation to multiphoton processes in LICS [78]; and the LICS-related laser-induced degenerate states [79–82].

The topics that mainly concern us in this review have to do with the connections between various coherent optical experiments and LICS. In the next section we discuss the relation between LICS and EIT, examples of which include experiments done in Rb [83, 84] and Kr [85]. We then extend the discussion to EIT with structured continua [86, 87]. We proceed by reviewing the use of LICS in the control of population transfer processes [88]; the control of PD [89]; the production of photo-electrons [90–92]; and as a means of steering population transfer processes [93]. We also discuss the connection between LICS and ultrafast methodologies [94]; generalized STIRAP techniques [95–97]; and coherent population trapping [69, 93, 98–101].

3. EIT AND ITS CONNECTION WITH LICS

The EIT phenomenon [13, 15, 18, 23, 102–106] is a quantum interference effect by which one can change the optical properties of material systems. In the original EIT scenario [13, 102], one allows two light beams to interact with a three-level material system so as to minimize, and often completely eliminate, the absorption of the same light beams as they pass through a thick sample.

The EIT phenomenon is intimately related to the formation of *resonances*, i.e., the broadening of spectral lines due to the interaction of bound states with a (radiative or nonradiative) continuum of states. When the broadening becomes comparable to the spacing between the lines, the resonances are said to *overlap*. This property can be controlled optically due to the splitting of *dressed states*, which depends on the intensity of the light field used to induce the Autler–Townes (AT) splitting [107]. Once the relative positions of the various levels are known, there is a well-established theory [3, 5, 108–110] for dealing with interferences between overlapping resonances.

It was realized early on [109], following the analysis of Fano [3], that the interference between overlapping resonances can give rise to *"dark states."* Such dark states, which are characterized by the vanishing of photoabsorption, were found experimentally a few years later [111, 112]. They feature very highly in many applications in coherent optics and in particular in "lasing without inversion" [13, 113, 114] and adiabatic passage (AP) phenomena [20–23, 115].

The emergence of dark states as a result of overlapping resonances was at the heart of the original EIT idea of Harris et al. [13, 102]. However, only limited use of the general theory of overlapping resonances has been subsequently made. In particular, the Wigner–Weisskopf approximation [116], according to which the resonance width is independent of the energy ("unstructured continuum"), was invariably assumed. The widths of the various levels were thus represented [105] as constant imaginary additions to the Hamiltonian matrix elements or, in the density-matrix description of the process, as decay and dephasing *rates*.

An immediate consequence of this approximation is the neglect of the resonance *level shifts*. The reason is that the shifts, which are given as the Hilbert transform of the level widths, vanish for a constant function. Past treatments of EIT have also neglected multichannel effects, arising when each level is coupled to a multiplicity of continua.

The above are important effects because structure and multiplicity of continua abound in molecular systems, photonic band-gap materials, and microcavities. Thus, in photonic band-gap materials, the level widths vary widely due to the presence of band gaps where decay is forbidden. In complex molecules, the levels decay indirectly due to the existence of "tier-like" coupling schemes where levels belonging to a given vibrational mode ("tier") are coupled to levels belonging to just one other tier, which are coupled to yet another limited set of levels, and so on, until one reaches the continuum tiers. The tier-like scheme thus leads to highly "structured" continua, which are in addition often coupled to one another, leading to "multichannel" scattering [108] and dissociation [117].

Within a comprehensive theory of EIT, based on the overlapping resonances concept [86], in which natural or optically induced structured

multiple continua are considered, the EIT line shapes can change and become highly asymmetric.

3.1. Elements of the theory of multichannel overlapping resonances

We start by briefly reviewing elements of "partitioning" theory [3, 5, 108–110, 118] used to treat the interference between overlapping resonances. The physical situation we address is illustrated in Figure 3.1 in which (as explained in Section 3.2) two overlapping resonances are created by optically splitting a single resonance.

Assuming that we have a situation in which bound states interact with continuum states, we define, according to this approach, two Hermitian projection operators Q and P, satisfying the equalities

$$Q^\dagger = Q \,, \ P^\dagger = P \,, \ QQ = Q \,, \ PP = P \,, \ PQ = QP = 0 \,, \ P + Q = I \,, \quad (1)$$

where I is the identity operator and the superscript † denotes the adjoint operation. The Q and P operators are chosen to project out the subspaces spanned by the bound states and the continuum states, respectively; as Eq. (1) indicates, they project onto (any) two subspaces known to be orthogonal.
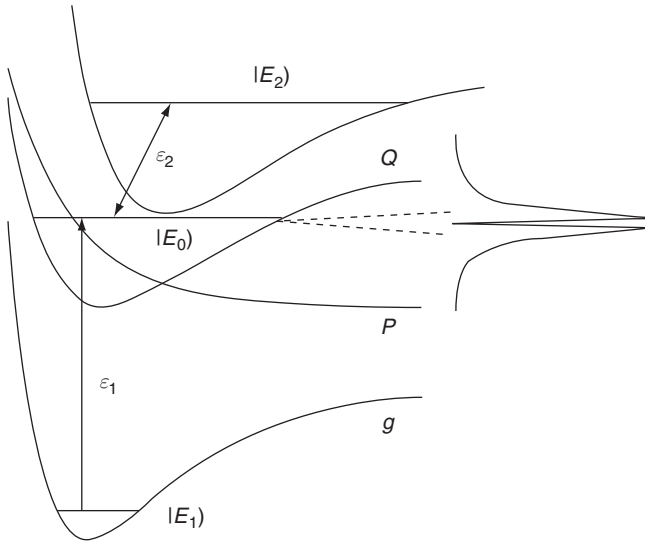
Figure 3.1   A ground state $|E_1\rangle$ is excited by a weak laser pulse ε_1 to a resonance state $|E_0\rangle \in Q$ decaying radiatively or nonradiatively to space P. The $|E_0\rangle$ state is coupled optically to a third state $|E_2\rangle$ by a strong guiding field ε_2 and undergoes as a result AT splitting. As a result of the splitting and the decay, an EIT "hole" is formed at $E = E_0$.

The full scattering incoming states $|E, \mathbf{n}^-\rangle$ are eigenstates of the Schrödinger equation

$$[E - i\epsilon - H] |E, \mathbf{n}^-\rangle = 0 \,, \tag{2}$$

where $-i\epsilon$ gives rise to "incoming" boundary conditions [108]. This equation can be rewritten as $[E - i\epsilon - H][P + Q]|E, \mathbf{n}^-\rangle = 0$, from which we obtain (using the orthogonality of P and Q) two coupled equations,

$$[E - i\epsilon - PHP] \, P|E, \mathbf{n}^-\rangle = PHQ|E, \mathbf{n}^-\rangle \tag{3}$$

$$[E - i\epsilon - QHQ] \, Q|E, \mathbf{n}^-\rangle = QHP|E, \mathbf{n}^-\rangle \,. \tag{4}$$

We define two basis sets, $|E, \mathbf{n}_1^-\rangle$ and $|\phi_s\rangle$, which are the solutions of the *homogeneous* (decoupled) parts of Eqs. (3 and 4), that is,

$$[E - i\epsilon - PHP] |E, \mathbf{n}_1^-\rangle = 0 \,, \tag{5}$$

$$[E_s - QHQ] |\phi_s\rangle = 0 \,. \tag{6}$$

Implicit in Eqs. (5 and 6) is that $|E, \mathbf{n}_1^-\rangle \in P$ and $|\phi_s\rangle \in Q$ and as such they are orthogonal to one another. We, in fact, assume that each basis set spans the entire subspace to which it belongs, hence we can write an explicit representation of Q and P as,

$$Q = \sum_s |\phi_s\rangle\langle \phi_s|, \tag{7}$$

$$P = \sum_{\mathbf{n}} \int dE|E, \mathbf{n}_1^-\rangle\langle E, \mathbf{n}_1^- | \,. \tag{8}$$

Using Eqs. (7 and 8) we can therefore write $|E, \mathbf{n}^-\rangle = [P + Q]|E, \mathbf{n}^-\rangle$ in terms of Q and P as

$$|E, \mathbf{n}^-\rangle = \sum_s |\phi_s\rangle\langle\phi_s|E, \mathbf{n}^-\rangle + \sum_{\mathbf{n}'} \int dE'|E', \mathbf{n}_1'^-\rangle\langle E', \mathbf{n}_1'^-|E, \mathbf{n}^-\rangle \,. \tag{9}$$

We now solve for $P|E, \mathbf{n}^-\rangle$ by writing it as a sum of the homogeneous solution of Eq. (5) and a particular solution of Eq. (3) obtained by inverting $[E - i\epsilon - PHP]$,

$$P|E, \mathbf{n}^-\rangle = P|E, \mathbf{n}_1^-\rangle + [E - i\epsilon - PHP]^{-1}PHQ|E, \mathbf{n}^-\rangle \,. \tag{10}$$

Substituting this solution into Eq. (4) we obtain that

$$[E - i\epsilon - Q\mathcal{H}Q] \, Q|E, \mathbf{n}^-\rangle = QHP|E, \mathbf{n}_1^-\rangle, \tag{11}$$

where

$$QHQ \equiv QHQ + QHP[E - i\epsilon - PHP]^{-1}PHQ . \tag{12}$$

Equation (11) can be solved to yield

$$Q|E, \mathbf{n}^-\rangle = [E - i\epsilon - QHQ]^{-1}QHP|E, \mathbf{n}_1^-\rangle . \tag{13}$$

An explicit representation of Eq. (13) is obtained by using the well-known identity,

$$[E - i\epsilon - PHP]^{-1} = P_v[E - PHP]^{-1} + i\pi\delta(E - PHP) , \tag{14}$$

with P_v denoting a Cauchy principal value integral, as,

$$QHQ = QHQ + QHPP_v[E - PHP]^{-1}PHQ + i\pi QHP\delta(E - PHP)PHQ . \tag{15}$$

Given Eqs. (10 and 15) we can express, via Eq. (9), the full scattering wave function $|E, \mathbf{n}^-\rangle$ in terms of $|\phi_s\rangle$ and $|E, \mathbf{n}_1^-\rangle$.

3.2. EIT as emerging from the interference between resonances

We consider the situation illustrated in Figure 3.1 in which a ground state $|E_1\rangle$ and a resonance state $|E_0\rangle$ (decaying radiatively or nonradiatively) coupled optically to a third state $|E_2\rangle$ (which can also decay radiatively or nonradiatively) by a strong guiding field

$$\mathbf{E}_2(t) \equiv \hat{\boldsymbol{\varepsilon}}_2 \, \varepsilon_2(t) = \hat{\boldsymbol{\varepsilon}}_2 \, R_e\mathcal{E}_2(t)e^{-i\omega_2 t} \tag{16}$$

is depicted, where $\hat{\boldsymbol{\varepsilon}}_2$ is the polarization vector. We probe the system by another laser pulse

$$\mathbf{E}_1(t) \equiv \hat{\boldsymbol{\varepsilon}}_1 \, \varepsilon_1(t) = \hat{\boldsymbol{\varepsilon}}_1 \, R_e\mathcal{E}_1(t)e^{-i\omega_1 t} . \tag{17}$$

We first treat $\varepsilon_1(t)$ as a perturbation and obtain the adiabatic eigenstates resulting from the $\varepsilon_2(t)$-induced interaction between the $|E_0\rangle$ and $|E_2\rangle$ states. The extension to the strong $\varepsilon_1(t)$ pulse regime is presented in Section 3.4.

Therefore, temporarily neglecting $\varepsilon_1(t)$, we can expand the system wave function in just two states,

$$|\Psi(t)\rangle = b_0(t)|E_0\rangle e^{-iE_0 t/\hbar} + b_2(t)|E_2\rangle e^{-iE_2 t/\hbar} . \tag{18}$$

Using the expansion of Eq. (18) we obtain from the time-dependent Schrödinger equation

$$i\hbar\frac{\partial \Psi(t)}{\partial t} = H\Psi(t) = [H_M + H_{MR}]\Psi(t) , \tag{19}$$

where H_M is the material Hamiltonian and H_{MR} is the matter–radiation interaction, given in the dipole approximation as

$$H_{MR} = -\vec{\mu} \cdot \mathbf{E}(t) , \tag{20}$$

the usual set of ordinary coupled differential equations for the $\underline{b} \equiv (b_0, b_2)^{\mathrm{T}}$ coefficients vector, where the superscript T designates the matrix transpose,

$$\frac{d}{dt}\underline{b} = i\underline{\underline{H}} \cdot \underline{b}(t) , \tag{21}$$

where $\underline{\underline{H}}$ is given in the "rotating-wave approximation" (RWA) [114] as

$$\underline{\underline{H}} = \begin{pmatrix} 0 & \Omega_2^*(t)e^{i\delta_2 t} \\ \Omega_2(t)e^{-i\delta_2 t} & 0 \end{pmatrix} , \tag{22}$$

with the detuning and the Rabi frequency given, respectively, as

$$\delta_2 \equiv \omega_2 - |E_0 - E_2|/\hbar , \ \ \Omega_2(t) \equiv \vec{\mu}_2 \cdot \hat{\boldsymbol{\varepsilon}}_2 \, \mathcal{E}_2(t)/\hbar . \tag{23}$$

We now transform $\underline{\underline{H}}$ to a form which does not contain the highly oscillatory $e^{-i\delta_2 t}$ terms which might invalidate the adiabatic approximation. Multiplying Eq. (21) by a diagonal matrix, $\exp\left(i\hat{\Delta}t/2\right)$, with $\hat{\Delta}$ being the diagonal detuning matrix,

$$\hat{\Delta} \equiv \begin{pmatrix} -\delta_2 & 0 \\ 0 & \delta_2 \end{pmatrix} . \tag{24}$$

We can eliminate the oscillatory terms by defining

$$\underline{c} \equiv \exp\left(i\hat{\Delta}t/2\right) \cdot \underline{b} \tag{25}$$

and obtain that

$$\frac{d}{dt}\underline{c} = i\underline{\underline{H}}' \cdot \underline{c}(t) , \tag{26}$$

where

$$\underline{\underline{H}}' = \begin{pmatrix} -\delta_2/2 & \Omega_2^*(t) \\ \Omega_2(t) & \delta_2/2 \end{pmatrix} . \tag{27}$$

We now build adiabatic solutions by diagonalizing Eq. (27) using a 2×2 unitary matrix

$$\underline{\underline{U}} = \begin{pmatrix} \cos\theta & e^{-i\phi_2}\sin\theta \\ -e^{i\phi_2}\sin\theta & \cos\theta \end{pmatrix} . \tag{28}$$

The θ and ϕ_2 angles of $\underline{U}$ are given as

$$\tan \theta = \frac{|\Omega_2(t)|}{-\left(\delta_2^2/4 + |\Omega_2(t)|^2\right)^{\frac{1}{2}} + \delta_2/2} , \tag{29}$$

with ϕ_2 being the argument of Ω_2 [Eq. (23)]. The corresponding diagonal eigenvalue matrix $\hat{\lambda}$ is composed of the two roots,

$$\lambda_{1,2}(t) = \pm\lambda(t) = \pm\left[\delta_2^2/4 + |\Omega_2(t)|^2\right]^{\frac{1}{2}} . \tag{30}$$

Operating with $\underline{U}^\dagger$, where † stands for the Hermitian adjoint operation, on Eq. (26) and defining $\underline{a} \equiv (a_1, a_2)^\mathrm{T} \equiv \underline{U}^\dagger \cdot \underline{c}$ we obtain, by neglecting the nonadiabatic coupling matrix $\underline{\underline{A}} = \underline{U} \cdot d\underline{U}^\dagger/dt$, the adiabatic approximation for $\underline{a}$,

$$\frac{d}{dt}\underline{a} = i\hat{\lambda}(t) \cdot \underline{a}(t) , \tag{31}$$

whose solution is given by

$$a_{1,2}(t) = \exp\left\{\pm i \int_0^t \lambda(t')dt'\right\} a_{1,2}(0) = \exp\left\{\pm i \int_0^t \left[\delta_2^2/4 + |\Omega_2(t')|^2\right]^{\frac{1}{2}}dt'\right\} a_{1,2}(0) . \tag{32}$$

We now introduce the (weak) $\varepsilon_1(t)$ pulse. Since $|E_1\rangle$ is the initially populated state, in the absence of $\varepsilon_1(t)$, neither the $|E_0\rangle$ or $|E_2\rangle$ states nor the $|\lambda_1\rangle$ and $|\lambda_2\rangle$ adiabatic states can ever be populated. Thus, in the absence of the $\varepsilon_1(t)$ pulse, the only effect of the $\varepsilon_2(t)$ pulse is to change the spectrum of the Hamiltonian.

Assuming that the adiabatic condition

$$|\dot{\theta}(t)| \ll |\lambda_2(t) - \lambda_1(t)| \tag{33}$$

indeed holds, the states seen by the $\varepsilon_1(t)$ pulse with $\varepsilon_2(t)$ on are the adiabatic states $|\lambda_1\rangle$ and $|\lambda_2\rangle$, rather than the $|E_0\rangle$ and $|E_2\rangle$ material states. Using the definition of $\underline{a}$ [Eqs. (25 and 28)], we can write the adiabatic states, using the identity $\underline{b} = e^{-i\hat{A}t/2} \cdot \underline{U} \cdot \underline{a}$, as

$$|\lambda_1(t)\rangle = e^{i\int_0^t \lambda(t')dt' + i\delta_2 t/2 - iE_0 t}\left\{\cos\theta|E_0\rangle + \sin\theta e^{-i\phi_2(t) - i\omega_{2,0}t}|E_2\rangle\right\},$$

$$|\lambda_2(t)\rangle = e^{-i\int_0^t \lambda(t')dt' - i\delta_2 t/2 - iE_0 t}\left\{-\sin\theta e^{i\phi_2(t)}|E_0\rangle + \cos\theta e^{-i\omega_{2,0}t}|E_2\rangle\right\} . \tag{34}$$

Here $|\lambda_1(t)\rangle$ and $|\lambda_2(t)\rangle$ are obtained by setting either $\underline{a} = (a_1, 0)^\mathrm{T}$ or $\underline{a} = (0, a_2)^\mathrm{T}$ and $\omega_{2,0} \equiv (E_2 - E_0)/\hbar$.

When $\delta_2 = 0$ (i.e., when ω_2 is exactly resonant with the $|E_2\rangle$ to $|E_0\rangle$ transition), it follows from Eq. (29) that $\theta = 3\pi/4$. If, in addition, we assume that the pulse has no chirp (i.e., that the phase of $\mathcal{E}_2(t)$, $\phi_2(t) = 0$), we have that

$$
\begin{aligned}
|\lambda_1(t)\rangle &= e^{i\int_0^t |\Omega_2(t')|dt' - iE_0 t} \left\{ |E_0\rangle - e^{-i\omega_{2,0}t}|E_2\rangle \right\} / \sqrt{2}, \\
|\lambda_2(t)\rangle &= e^{-i\int_0^t |\Omega_2(t')|dt' - iE_0 t} \left\{ |E_0\rangle + e^{-i\omega_{2,0}t}|E_2\rangle \right\} / \sqrt{2}.
\end{aligned}
\tag{35}
$$

We see that the time evolution of the $|E_0\rangle$ component of $|\lambda_1(t)\rangle$ is governed by a "quasi-energy" of $E_0 - |\Omega_2(t)|$, whereas the time evolution of the $|E_0\rangle$ component of $|\lambda_2(t)\rangle$ is governed by a "quasi-energy" of $E_0 + |\Omega_2(t)|$. We say that the two levels are "AT" split by an amount equal to $2|\Omega_2(t)|$.

We now consider the broadening of the adiabatic levels due to the decay channels considered in Section 3.1. When this broadening is comparable to or in excess of the $2|\Omega_2(t)|$ splitting (see Figure 3.3) the switch on of the $\varepsilon_1(t)$ pulse results in the simultaneous excitation of the two adiabatic eigenstates. The probability of one-photon absorption to each scattering state $|E\rangle$ is given in first-order perturbation theory as

$$
P_{\mathbf{n}}(E) = \left| 2\pi \epsilon_1(\omega_{E,1}) \mu_{1,\mathbf{n}}(E) \right|^2 ,
\tag{36}
$$

where $\mu_{1,\mathbf{n}}(E)$ are bound-free dipole matrix elements between states on the ground (g) and excited (e) electronic potential surfaces, given as,

$$
\mu_{1,\mathbf{n}}(E) = \langle E_1 | \vec{\mu}_1 \cdot \hat{\boldsymbol{\varepsilon}}_1 | E, \mathbf{n}^- \rangle .
\tag{37}
$$

In Eq. (36), $\omega_{E,1} = (E - E_1)/\hbar$ is the transition frequency between $|E_1\rangle$ and $|E\rangle$, and $\epsilon_1(\omega)$ is the temporal Fourier transform of the pulse

$$
\epsilon_1(\omega) \equiv \frac{1}{2\pi} \int dt \varepsilon_1(t) \exp\left[-i\omega(z/c - t) \right],
\tag{38}
$$

where z is the direction of propagation of the light and c is the velocity of light in vacuum. Assuming for simplicity that no direct transitions to the continuum occur, i.e., that only the Q space of Eq. (7) is coupled radiatively to $|E_1\rangle$, we have that,

$$
\mu_{1,\mathbf{n}}(E) = \sum_s \langle E_1 | \vec{\mu}_1 \cdot \hat{\boldsymbol{\varepsilon}}_1 | \phi_s \rangle \langle \phi_s | E, \mathbf{n}^- \rangle .
\tag{39}
$$

If we now identify the $|\phi_s\rangle$ bound states (which become resonances due to the interaction with the continuum) with the adiabatic states of Eq. (34), we can write that

$$
\mu_{1,\mathbf{n}}(E) = \sum_{s=1,2} \langle E_1 | \vec{\mu}_1 \cdot \hat{\boldsymbol{\varepsilon}}_1 | \lambda_s \rangle \langle \lambda_s | E, \mathbf{n}^- \rangle \equiv \sum_{s=1,2} \langle E_1 | \vec{\mu}_1 \cdot \hat{\boldsymbol{\varepsilon}}_1 | \lambda_s \rangle \ell_s(E),
\tag{40}
$$

where we have restricted the treatment to the interaction of just two resonances. Using Eq. (34) and the fact that $\langle E_2 | \hat{\boldsymbol{\varepsilon}} \cdot \vec{\mu} | E_1 \rangle = 0$, we have that

$$\mu_{1,\mathbf{n}}(E) = \mu_{1,0} e^{-iE_0 t} \left\{ \cos\theta e^{i\delta_2 t/2 + i\int_0^t \lambda(t')dt'} \ell_1(E) - \sin\theta e^{-i\delta_2 t/2 - i\int_0^t \lambda(t')dt' + i\phi_2} \ell_2(E) \right\} . \tag{41}$$

When $\omega_2 = \omega_{2,0}$, i.e., it is exactly on resonance, and $\phi_2 = 0$, this expression reduces to

$$\mu_{1,\mathbf{n}}(E) = \frac{1}{\sqrt{2}} e^{-iE_0 t} \mu_{1,0} \left\{ \ell_1(E) e^{i\int_0^t |\Omega_2(t')|dt'} - \ell_2(E) e^{-i\int_0^t |\Omega_2(t')|dt'} \right\} . \tag{42}$$

Using Eq. (13) we can write an exact expression for the amplitude of observing the $|\lambda_s\rangle$ states as

$$\ell_s(E) \equiv \langle \lambda_s | E, \mathbf{n}^- \rangle = \sum_{s'} \langle \lambda_s | [E - i\epsilon - Q\mathcal{H}Q]^{-1} | \lambda_{s'} \rangle \langle \lambda_{s'} | H | E, \mathbf{n}_1^- \rangle. \tag{43}$$

Following Ref. [109] we can write the $E - Q\mathcal{H}Q$ matrix of Eq. (15) in the two overlapping resonance case as

$$E - Q\mathcal{H}Q = \begin{pmatrix} E - E_0 - \lambda_1 - \Delta_{1,1} - i\Gamma_{1,1}/2 & -\Delta_{1,2} - i\Gamma_{1,2}/2 \\ -\Delta_{2,1} - \frac{i\Gamma_{2,1}}{2} & E - E_0 - \lambda_2 - \Delta_{2,2} - i\Gamma_{2,2}/2 \end{pmatrix} , \tag{44}$$

where

$$\Gamma_{s,s'}(E) = 2\pi \sum_{\mathbf{n}} \langle \lambda_s | H | E, \mathbf{n}_1^- \rangle \langle E, \mathbf{n}_1^- | H | \lambda_{s'} \rangle \tag{45}$$

and

$$\Delta_{s,s'}(E) = \mathrm{P}_v \int dE' \sum_{\mathbf{n}} \frac{\langle \lambda_s | H | E', \mathbf{n}_1^- \rangle \langle E', \mathbf{n}_1^- | H | \lambda_{s'} \rangle}{E - E'} . \tag{46}$$

We obtain that the inverse matrix is given as

$$[E - Q\mathcal{H}Q]^{-1} = \frac{1}{\mathcal{D}} \begin{pmatrix} a & b \\ c & d \end{pmatrix} , \tag{47}$$

with

$$a \equiv E - E_0 - \lambda_2 - \Delta_{2,2} - i\Gamma_{2,2}/2 \quad b \equiv \Delta_{1,2} + i\Gamma_{1,2}/2 \quad c \equiv \Delta_{2,1} + i\Gamma_{2,1}/2$$
$$d \equiv E - E_0 - \lambda_1 - \Delta_{1,1} - i\Gamma_{1,1}/2 \quad \mathcal{D} \equiv a\, d - c\, b. \tag{48}$$

Using Eq. (43) we obtain that

$$\ell_1(E) = \frac{1}{\mathcal{D}}\Big[a \, \langle \lambda_1 \, |H|E, \mathbf{n}_1^- \rangle + b \, \langle \lambda_2 \, |H|E, \mathbf{n}_1^- \rangle \Big]$$

$$\ell_2(E) = \frac{1}{\mathcal{D}}\Big[c \, \langle \lambda_1 \, |H|E, \mathbf{n}_1^- \rangle + d \, \langle \lambda_2 \, |H|E, \mathbf{n}_1^- \rangle \Big]. \tag{49}$$

It follows from Eq. (34) that

$$\langle \lambda_1 \, |H|E, \mathbf{n}_1^- \rangle = e^{-i \int_0^t \lambda(t')dt' - i\delta_2 t/2 + iE_0 t} \left\{ \cos\theta \, V_{0,\mathbf{n}} + \sin\theta e^{i\phi_2 + i\omega_{2,0}t} V_{2,\mathbf{n}} \right\},$$

$$\langle \lambda_2 \, |H|E, \mathbf{n}_1^- \rangle = e^{i \int_0^t \lambda(t')dt' + i\delta_2 t/2 + iE_0 t} \left\{ -\sin\theta e^{-i\phi_2} V_{0,\mathbf{n}} + \cos\theta e^{i\omega_{2,0}t} V_{2,\mathbf{n}} \right\}, \tag{50}$$

where

$$V_{0,\mathbf{n}}(E) \equiv \langle E_0 \, |H|E, \mathbf{n}_1^- \rangle, \quad V_{2,\mathbf{n}}(E) \equiv \langle E_2 \, |H|E, \mathbf{n}_1^- \rangle. \tag{51}$$

Using Eq. (50) and neglecting the terms containing the highly oscillatory $e^{\pm i\omega_{2,0}t}$ factors, we obtain from Eq. (45) that

$$\Gamma_{1,1} = \Gamma_0 \cos^2\theta + \Gamma_2 \sin^2\theta, \quad \Gamma_{2,2} = \Gamma_0 \sin^2\theta + \Gamma_2 \cos^2\theta,$$

$$\Gamma_{1,2} = (-\Gamma_0 + \Gamma_2) e^{-2i \int_0^t \lambda(t')dt' - i\delta_2 t + i\phi_2} \sin\theta \cos\theta, \tag{52}$$

where

$$\Gamma_0(E) \equiv 2\pi \sum_\mathbf{n} \left| \langle E, \mathbf{n}_1^- \, |H|E_0 \rangle \right|^2, \quad \Gamma_2(E) \equiv 2\pi \sum_\mathbf{n} \left| \langle E, \mathbf{n}_1^- \, |H|E_2 \rangle \right|^2. \tag{53}$$

In the same manner from Eq. (46)

$$\Delta_{1,1} = \Delta_0 \cos^2\theta + \Delta_2 \sin^2\theta, \quad \Delta_{2,2} = \Delta_0 \sin^2\theta + \Delta_2 \cos^2\theta,$$

$$\Delta_{1,2} = (-\Delta_0 + \Delta_2) e^{-2i \int_0^t \lambda(t')dt' - i\delta_2 t + i\phi_2} \sin\theta \cos\theta, \tag{54}$$

where

$$\Delta_i(E) \equiv \left(\frac{1}{2\pi}\right) P_v \int dE' \frac{\Gamma_i(E')}{E - E'}, \quad i = 0, 2. \tag{55}$$

Hence from Eq. (49), and after defining $I \equiv e^{-i \int_0^t \lambda(t')dt' - i\delta_2 t/2}$ and $F \equiv \frac{e^{iE_0 t}}{\mathcal{D}}$, we have

$$\ell_1(E) = F\Big[(aI \cos\theta - bI^* \sin\theta)V_{0,\mathbf{n}} + (aI \sin\theta e^{i\phi_2 + i\omega_{2,0}t} + bI^* \cos\theta e^{i\omega_{2,0}t})V_{2,\mathbf{n}} \Big],$$

$$\ell_2(E) = F\Big[(cI^* \cos\theta - dI \sin\theta)V_{0,\mathbf{n}} + (cI^* \sin\theta e^{i\phi_2 + i\omega_{2,0}t} + dI \cos\theta e^{i\omega_{2,0}t})V_{2,\mathbf{n}} \Big]. \tag{56}$$

After neglecting the highly oscillatory $e^{i\omega_{2,0}t}$ terms in Eq. (41), we further obtain

$$\mu_{1,\mathbf{n}}(E) = \frac{\mu_{1,0}V_{0,\mathbf{n}}}{\mathcal{D}}\left[E - E_0 + \lambda\cos 2\theta - (\Delta_2 + i\Gamma_2/2)\right]. \tag{57}$$

Thus, if state $|E_2\rangle$ is unstable, giving rise to the $i\Gamma_2$ term, there is no real E for which the transition dipole matrix element vanishes. In case of $\delta_2 = 0$ detuning and $\cos 2\theta = 0$, we have

$$\mu_{1,\mathbf{n}}(E) = \frac{1}{\mathcal{D}}\mu_{1,0}V_{0,\mathbf{n}}\left[E - E_0 - (\Delta_2 + i\Gamma_2/2)\right]. \tag{58}$$

When we use the explicit form of $\mathcal{D}$, as given by Eq. (48), and the values of $\Gamma_{i,j}$ as given by Eq. (52), we have

$$\begin{aligned}
\mathcal{D} = {}& \left[E - E_0 - \lambda - \Delta_0\cos^2\theta - \Delta_2\sin^2\theta - i(\Gamma_0\cos^2\theta + \Gamma_2\sin^2\theta)/2\right] \\
&\times \left[E - E_0 + \lambda - \Delta_0\sin^2\theta - \Delta_2\cos^2\theta - i(\Gamma_0\sin^2\theta + \Gamma_2\cos^2\theta)/2\right] \\
&- \left[\Delta_0 - \Delta_2 + i(\Gamma_0 - \Gamma_2)/2\right]^2\sin^2\theta\cos^2\theta.
\end{aligned} \tag{59}$$

In case we irradiate exactly on resonance, $\delta_2 = 0$, we also have that $\cos^2\theta = \sin^2\theta = 1/2$, which results in

$$\mathcal{D}(t) = \left[E - E_0 - (\Delta_0 + \Delta_2)/2 - i(\Gamma_0 + \Gamma_2)/4\right]^2 - \left[(\Delta_0 - \Delta_2)/2 + i(\Gamma_0 - \Gamma_2)/4\right]^2 - \lambda^2(t). \tag{60}$$

3.2.1. Unstructured continua

If we neglect the variation of $\Gamma_{0,2}(E)$ with energy and assume that $E \gg 0$, we have that the integrand defining $\Delta_{0,2}$ is antisymmetric about E and is essentially zero at the integration limits, hence $\Delta_i \approx 0$. Therefore

$$|\mathcal{D}(t)|^2 = \left[(E - E_0)^2 - \Gamma_0\Gamma_2/4 - |\Omega_2(t)|^2\right]^2 + \left[(E - E_0)(\Gamma_0 + \Gamma_2)\right]^2/4. \tag{61}$$

The channel-specific probability of absorption of a photon of energy $E - E_1$ from state $|E_1\rangle$ is given, using Eqs. (58, 61, and 36) (assuming $\Delta_2 = 0$), as

$$P_{\mathbf{n}}(E) = \frac{\left|2\pi\mu_{1,0}V_{0,\mathbf{n}}\epsilon_1(\omega_{E,1})\right|^2\left[(E - E_0)^2 + (\Gamma_2^2/4)\right]}{\left[(E - E_0)^2 - |\Omega_2(t)|^2 - \Gamma_0\Gamma_2/4\right]^2 + \left[(E - E_0)(\Gamma_0 + \Gamma_2)/2\right]^2}. \tag{62}$$

$P(E)$, the total probability for absorbing a photon of energy $E - E_1$ from state $|E_1\rangle$, given as $A_1(E) = \sum \mathbf{n} P_\mathbf{n}(E)$ is

$$A_1(E) = \frac{2\pi \Gamma_0 \left|\mu_{1,0}\epsilon_1(\omega_{E,1})\right|^2 \left[(E - E_0)^2 + (\Gamma_2^2/4)\right]}{\left[(E - E_0)^2 - |\Omega_2(t)|^2 - \Gamma_0\Gamma_2/4\right]^2 + \left[(E - E_0)(\Gamma_0 + \Gamma_2)/2\right]^2} , \quad (63)$$

where we have used Eq. (53), according to which $\Gamma_0 = 2\pi \sum_\mathbf{n} |V_{0,\mathbf{n}}|^2$. We see that the basic form of the total photon-absorption probability remains essentially the same as in the single continuum case, with sums over channel-specific widths and shifts replacing the single channel entities.

3.2.2. Structured continua

When the variation of $\Gamma_{0,2}(E)$ with energy cannot be neglected we cannot assume that $\Delta_{0,2}(E)$ vanish. In that case we need to compute $\mathcal{D}$ according to Eq. (59). Assuming that $\Gamma_{0,2}(E)$ can be parametrized, for example, as a sum of Lorentzian functions

$$\Gamma_i(E) = \sum_j \frac{A_{i,j}\gamma_{i,j}}{\left(E - e_{i,j}\right)^2 + \gamma_{i,j}^2/4} , \quad i = 0, 2 , \quad (64)$$

we have that

$$\begin{aligned}
\Delta_i(E) &= \frac{1}{2\pi} \mathrm{P}_v \int_{-\infty}^{\infty} dE' \frac{\Gamma_i(E')}{E - E'} \\
&= \frac{1}{2\pi} \mathrm{P}_v \int_{-\infty}^{\infty} dE' \sum_j \frac{A_{i,j}\gamma_{i,j}}{\left(E' - e_{i,j} + i\gamma_{i,j}/2\right)\left(E' - e_{i,j} - i\gamma_{i,j}/2\right)(E - E')}.
\end{aligned}$$
$$(65)$$

Writing the P_v integral as the difference between a contour integral which includes the $E' = e_i - i\gamma_{i,j}/2$ poles but avoids the $E' = E$ and $E' = e_i + i\gamma_{i,j}/2$ poles, where the straight line segment is supplemented by a large semicircle on the lower half complex plane (whose contribution vanishes as $|E'| \to \infty$ because on it the integrand is proportional to $|E'|^{-3}$) and the small semicircle contribution about the $E' = E$ pole, one has that

$$\begin{aligned}
\Delta_i(E) &= \sum_j \frac{-iA_{i,j}}{-i(E - e_{i,j} + i\gamma_{i,j}/2)} + \frac{iA_{i,j}\gamma_{i,j}}{2(E - e_{i,j} + i\gamma_{i,j}/2)(E - e_{i,j} - i\gamma_{i,j}/2)} \\
&= \sum_j \frac{A_{i,j}(E - e_{i,j})}{(E - e_{i,j})^2 + \gamma_{i,j}^2/4} .
\end{aligned}$$
$$(66)$$

An illustration of a typical case of structured continua of the dressed AT split pair of states is given in Figure 3.2. We see that the shift function is
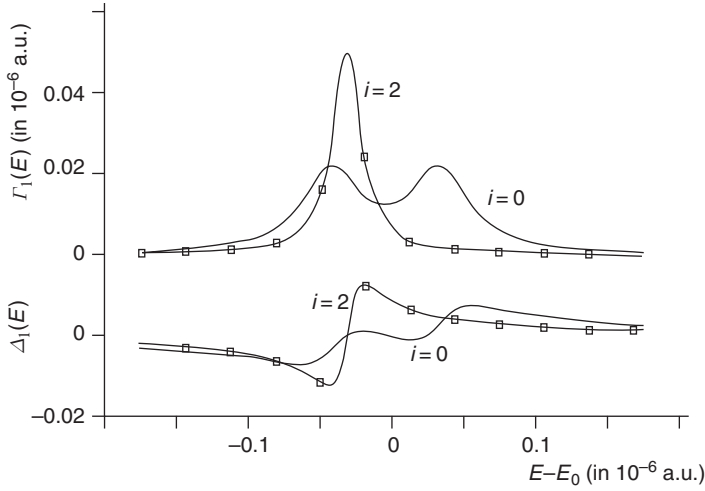
Figure 3.2   An example of the widths and shifts of a case of "highly structured" continua, characterized by $\gamma_{0,1} = \gamma_{0,2} = 0.02$, $\gamma_{2,1} = 0.01$, $e_{0,1} = 0$, $e_{0,2} = -0.03$, $A_{0,1} = A_{0,2} = 0.02$, $A_{2,1} = 0.05$, coupled to the AT split pair. Shown are $\Gamma_0(E)$, $\Gamma_2(E)$, as of Eq. (53), and $\triangle_0(E)$ and $\triangle_2(E)$, given by Eq. (55).

antisymmetric about e_i, $i = 0$, 2. As a result, the probability of absorption, given as the square of $\mu_{1,n}(E)$ of Eq. (57), is no longer symmetric about the line center. Thus the appearance of asymmetry in the EIT absorption line shape is a hallmark of a structured continuum.

3.3. Photo-absorption

We first present calculations of the photo-absorption of the probe pulse $\varepsilon_1(t)$ by the three-level system depicted in Figure 3.1. In this system the ground state $|E_1\rangle$ is electric dipole coupled to an upper state $|E_0\rangle$ that is in turn coupled by a strong optical pulse to a third state $|E_2\rangle$. The (channel-specific) photo-absorption probability from the ground state is given by $P_n(E)$ and the total photo-absorption of the ε_1 pulse by $A_1(E)$.

In Figures 3.3–3.7 we plot the absorption line shapes as a function of the detuning from the $E_1 - E_0$ resonance at different times in the history of the Gaussian pulse linking $|E_0\rangle$ to $|E_2\rangle$, with $t = 0$ being the pulse maximum. The $|E_0\rangle$ and $|E_2\rangle$ states are coupled nonradiatively to some continuum channels representing the P space.

We first analyze the situation for *unstructured continua*. Figure 3.3 shows the situation when only the $|E_0\rangle$ level (the one with the dipole allowed transition to the ground state) is broadened ($\Gamma_0 = 0.05 \times 10^{-6}$ a.u.). We assume no detuning ($\delta_2 = 0$) of the center of the strong pulse connecting the $|E_0\rangle \leftrightarrow |E_2\rangle$ states. A *perfect* EIT dip is seen to arise. In contrast, Figure 3.4
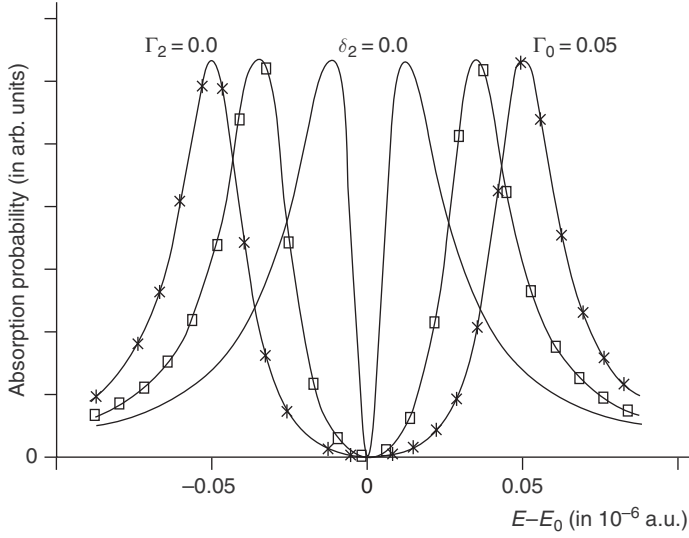
Figure 3.3   The formation of the EIT "hole" for unstructured continuum. $\Gamma_0 = 0.05 \times 10^{-6}$ a.u., $\Gamma_2 = 0$, and $\delta_2 = 0$. Shown is the line shape (Eq. (63)) at three different times, (X)—at the peak of the pulse $t = 0$, ($\Box$)—as the pulse begins to wane, $t = 0.75 \times 10^6$ a.u., and (full line)—at the tail of the pulse, $t = 1.5 \times 10^6$ a.u. A simple Gaussian pulse of the form $\mathcal{E}_2(t) = \mathcal{E}_0 e^{-t^2}$ was assumed.
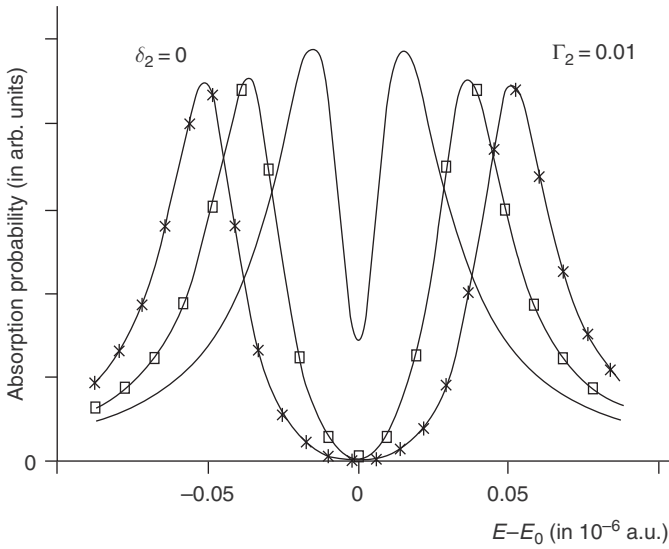
Figure 3.4   The same as in Figure 3.3 for a broadened $|E_2\rangle$ ($\Gamma_2 = 0.01$) with zero detuning ($\delta_2 = 0$).
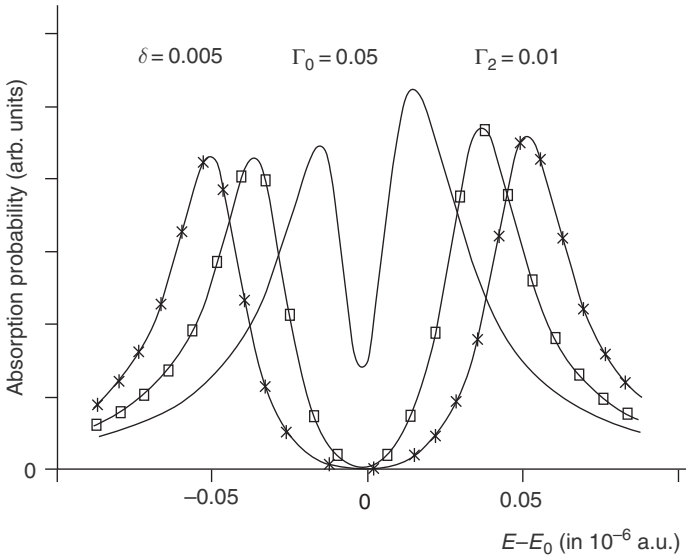
Figure 3.5   The same as in Figure 3.3 for a broadened $|E_2\rangle$ ($\Gamma_2 = 0.01$) with finite detuning ($\delta_2 = 0.005$).
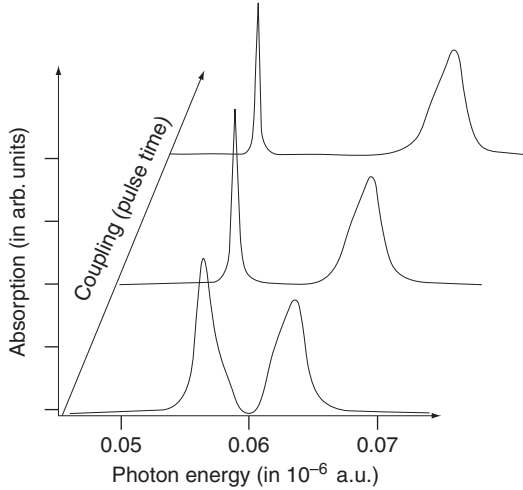
Figure 3.6   EIT for structured continuum ($A_{0,1} = 0.02$, $\gamma_{0,1} = 0.02$, $e_{0,1} = 0$, $A_{0,2} = 0.02$, $\gamma_{0,2} = 0.02$, $e_{0,2} = -0.02$, $A_{2,1} = 0.002$, $\gamma_{2,1} = 0.01$, $e_{2,1} = 0$) with no detuning ($\delta_2 = 0$) as a function of the ε_2 coupling strength (the uppermost trace corresponds to the peak of the ε_2 pulse). In the two upper traces the first peak was divided by 2. All energies and widths are expressed in 10^{-6} a.u. The absorption is given as the square $\mu_{1,n}(E)$ of Eq. (57).
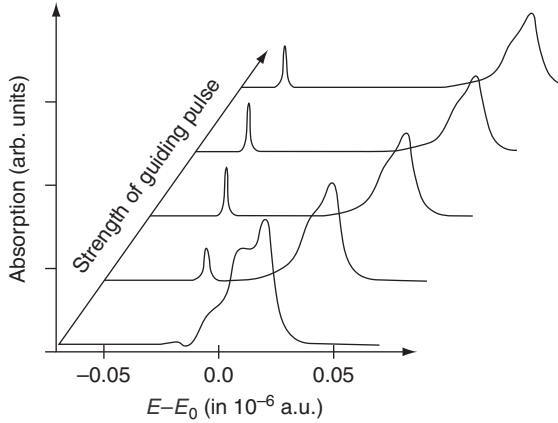
Figure 3.7   EIT for structured continuum with detuning ($\delta_2 = 0.01$) as a function of the ε_2 coupling strength (the uppermost trace corresponds to the peak of the ε_2 pulse). The continuum parameters are as in Figure 3.6. The absorption is given as the square $\mu_{1,\mathbf{n}}(E)$ of Eq. (57).

shows the zero-detuning ($\delta_2 = 0$) situation when both levels ($|E_0\rangle$ and $|E_2\rangle$) are broadened ($\Gamma_0 = 0.05 \times 10^{-6}$ a.u., $\Gamma_2 = 0.01 \times 10^{-6}$ a.u.). In this case, as clearly shown in Eqs. (62 and 63), the line shape does not dip to zero. Figure 3.5 pertains to the case when both levels ($|E_0\rangle$ and $|E_2\rangle$) are broadened ($\Gamma_0 = 0.05 \times 10^{-6}$ a.u., $\Gamma_2 = 0.01 \times 10^{-6}$ a.u.) in the presence of detuning ($\delta_2 = 0.005$). Here, the EIT does not dip to zero and the whole line shape is asymmetrically biased to the blue by an amount which depends on the intensity of the $|E_0\rangle \leftrightarrow |E_2\rangle$ coupling field.

We now turn our attention to the *structured continua* case. Figure 3.6 displays the absorption of two AT split levels for structured continua of the type displayed in Figure 3.2 with no detuning ($\delta_2 = 0$). Two asymmetric line shapes separated by an almost complete transparency "hole" are seen to form. The two parts of the line shape change, while being pushed apart, with one of them becoming much sharper as the ε_2 coupling laser intensity increases. As shown above, the sharpening of one of the peaks does not occur in the unstructured continuum case.

In Figure 3.7 we show EIT for a structured continua *with* detuning ($\delta_2 = 0.01$). The effect of the detuning in this case is quite dramatic, as it causes one of the EIT peaks to almost disappear while, as in Figure 3.6, making the line shapes change substantially with increased ε_2 coupling strengths.

3.4. The resonance description of slowing down of light by EIT

Although the slowing down of light associated with EIT [16, 119] originates, as in all dispersion phenomena, in levels which are *off-resonance* with respect

to the $\varepsilon_1(t)$ probe laser, the role of the off-resonance levels is dramatically more important in EIT than in ordinary photo-absorption line shapes. In order to see this we now go beyond the weak field limit used so far to treat the effect of the $\varepsilon_1(t)$ probe pulse, by incorporating $|E_1\rangle$ in the expansion of $\Psi(t)$—the solution of the time-dependent Schrödinger equation (Eq. (19)). We thus have that

$$|\Psi(t)\rangle = b_1(t)|E_1\rangle e^{-iE_1 t/\hbar} + \sum_{\mathbf{n}} \int dE b_{E,\,\mathbf{n}}(t)|E, \mathbf{n}^-\rangle e^{-iEt/\hbar} . \tag{67}$$

Substituting this expansion in Eq. (19) we obtain a set of ordinary differential equations (ODE) for the expansion coefficients $b_1(t)$ and $b_{E,\,\mathbf{n}}(t)$,

$$\frac{d}{dt}b_1(t) = (i/\hbar) \sum_n \int dE b_{E,n}(t)\mu_{1,\mathbf{n}}(E)\mathcal{E}_1^*(t)e^{-i(\omega_{E,1}-\omega_1)t},$$

$$\frac{d}{dt}b_{E,\,\mathbf{n}}(t) = (i/\hbar)b_1(t)\mu_{\mathbf{n},1}(E)\mathcal{E}_1(t)e^{i(\omega_{E,1}-\omega_1)t} , \tag{68}$$

where $\omega_{E,1} \equiv (E - E_1)/\hbar$. We now eliminate the continuum by solving the second part of Eq. (68) to yield

$$b_{E,\,\mathbf{n}}(t) = (i/\hbar) \int_{-\infty}^{t} dt' b_1(t')\mu_{\mathbf{n},1}(E)\mathcal{E}_1(t')e^{i\delta_E t'} , \tag{69}$$

where $\delta_E \equiv \omega_{E,1} - \omega_1$. Substituting Eq. (69) into the first part of Eq. (68) we obtain

$$\frac{d}{dt}b_1(t) = \left(\mathcal{E}_1^*(t)/\hbar\right) \int_{-\infty}^{t} dt' b_1(t')F_1(t - t')\mathcal{E}_1(t') , \tag{70}$$

where $F_1(\tau)$, the *spectral autocorrelation* function

$$F_1(\tau) \equiv -\int d\delta_E \sum_{\mathbf{n}} \left|\mu_{1,\mathbf{n}}(E)\right|^2 e^{-i\delta_E \tau} , \tag{71}$$

is just the Fourier transform of $A_1(E)$, the total absorption probability from state $|E_1\rangle$,

$$A_1(E) \equiv \sum_{\mathbf{n}} \left|\mu_{1,\mathbf{n}}(E)\right|^2 . \tag{72}$$

For an unstructured continuum we can use the explicit form of $A_1(E)$ of Eq. (63) to obtain that

$$F_1(\tau) = \frac{\left|\mu_{1,0}\right|^2}{2\pi} \int d\delta_E \frac{-\Gamma_0 \left[(E - E_0)^2 + (\Gamma_2^2/4)\right] e^{-i\delta_E \tau}}{\left[(E - E_0)^2 - |\Omega_2(t)|^2 - \Gamma_0\Gamma_2/4\right]^2 + \left[(E - E_0)(\Gamma_0 + \Gamma_2)/2\right]^2} . \tag{73}$$
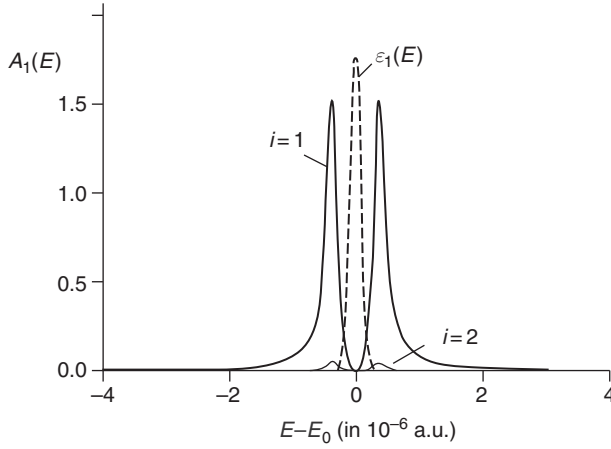
Figure 3.8 $A_2(E)$ and $A_1(E)$ for unstructured continua (Eq. (63) and its analog for $|E_2\rangle$) with $\Gamma_0 = 4 \times 10^{-6}$ a.u., $\Gamma_2 = 10^{-8}$ a.u., and $\delta_2 = 0$. Shown also is the probe laser line shape $\epsilon_1(E)$ (Eq. (38)).
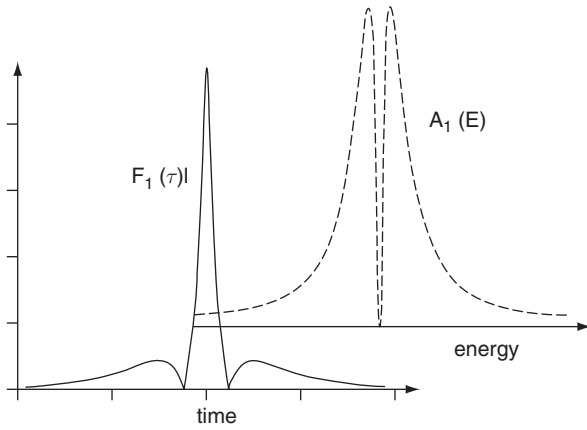
Figure 3.9 The spectral autocorrelation function $F_1(\tau)$ (full line), given by Eq. (71) and the EIT line shape (broken line) corresponding to it, as of Eq. (72).

In Figure 3.8 the $A_2(E)$ and $A_1(E)$ for unstructured continua are shown.

A sample $F_1(\tau)$ is shown in Figure 3.9, using which one obtains with the aid of Eq. (70) the $b_1(t)$ coefficient (an example of which is given in Figure 3.10). The continuum preparation coefficients $b_{E,\,\mathbf{n}}(t)$ (a sample is shown in Figure 3.11) are then readily obtained from Eq. (69).

We next turn our attention to calculating the (transient) populations of levels $|E_0\rangle$ and $|E_2\rangle$. These can be obtained using Eq. (67) as
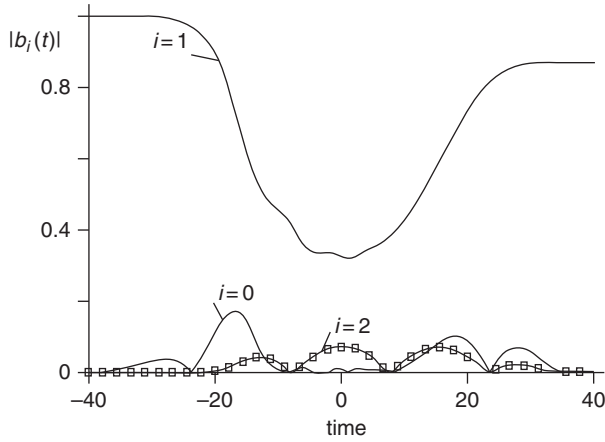
Figure 3.10   The $b_1(t)$,$b_0(t)$, and $b_2(t)$ expansion coefficients (Eqs. (70, 76, and 79)) as functions of time and energy for the EIT line shape and laser profile of Figure 3.8.
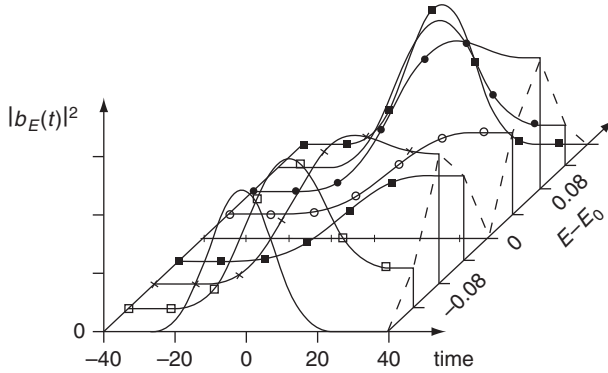
Figure 3.11 $|b_E(t)|^2$—the absolute value squared of the dressed state expansion coefficients, given by Eq. (82), as a function of time—expressed in 10^6 a.u.—and $E - E_0$—expressed in 10^{-6} a.u.

$$\langle E_0 | \Psi(t) \rangle = \sum_{\mathbf{n}} \int dE b_{E,\mathbf{n}}(t) \langle E_0 | E, \mathbf{n}^- \rangle e^{-iEt/\hbar} , \tag{74}$$

Noting that because of selection rules $|E_1\rangle$ is coupled exclusively by the dipole operator to $|E_0\rangle$, we have that

$$\mu_{1,\mathbf{n}}(E) = \mu_{1,0} \langle E_0 | E, \mathbf{n}^- \rangle . \tag{75}$$

Thus Eq. (74) can be written as

$$
\langle E_0 | \Psi(t) \rangle = \frac{1}{\mu_{1,0}} \sum_{\mathbf{n}} \int dE b_{E,\,\mathbf{n}}(t) \mu_{1,\mathbf{n}}(E) e^{-iEt/\hbar}
$$

$$
= \frac{ie^{-i(\omega_1 + E_1/\hbar)t}}{\hbar\mu_{1,0}} \int_{-\infty}^{t} dt' \mathcal{E}_1(t') b_1(t') \sum_{\mathbf{n}} \int dE \, |\mu_{\mathbf{n},1}(E)|^2 \, e^{-i\delta_E(t-t')}
$$

$$
= -\frac{ie^{-i(\omega_1 + E_1/\hbar)t}}{\mu_{1,0}} \int_{-\infty}^{t} dt' \mathcal{E}_1(t') b_1(t') F_1(t-t') \,. \tag{76}
$$

The calculation of $\langle E_2 | \Psi(t) \rangle$ is more complicated and we need to repeat the procedure adopted in calculating $\mu_{1,\mathbf{n}}(E)$. We thus write

$$
\langle E_2 | \Psi(t) \rangle = \sum_{\mathbf{n}} \int dE b_{E,\,\mathbf{n}}(t) \sum_{s=1,2} \langle E_2 | \lambda_s \rangle \ell_s(E) e^{-iEt/\hbar} \,, \tag{77}
$$

Using Eqs. (34, 52, 54, and 56) and neglecting as before the highly oscillatory terms containing the $e^{\pm i\omega_{2,0}t}$ factors, we obtain that

$$
\sum_{s=1,2} \langle E_2 | \lambda_s \rangle \ell_s(E) = \frac{V_{2,\mathbf{n}}}{\mathcal{D}} \Big[E - E_0 - \lambda \cos 2\theta - (\Delta_0 + i\Gamma_0/2) \Big] = \frac{\mu_{0,\mathbf{n}}(E)}{\mu_{2,0}} \,, \tag{78}
$$

where $\mu_{0,\mathbf{n}}(E) \equiv \langle E_0 | \vec{\mu}_2 \cdot \hat{\boldsymbol{\varepsilon}}_2 | E; \mathbf{n}^- \rangle$ and $\mu_{2,0} \equiv \langle E_2 | \vec{\mu}_2 \cdot \hat{\boldsymbol{\varepsilon}}_2 | E_0 \rangle$ and we have used the fact that the only state coupled to $|E_0\rangle$ by the $\varepsilon_2(t)$ pulse is $|E_2\rangle$. Thus,

$$
\langle E_2 | \Psi(t) \rangle = \frac{1}{\mu_{2,0}} \sum_{\mathbf{n}} \int dE b_{E,\,\mathbf{n}}(t) \mu_{0,\mathbf{n}}(E) e^{-iEt/\hbar}
$$

$$
= \frac{ie^{-i(\omega_1 + E_1/\hbar)t}}{\hbar\mu_{2,0}} \int_{-\infty}^{t} dt' \mathcal{E}_1(t') b_1(t') \sum_{\mathbf{n}} \int dE \mu_{0,\mathbf{n}}(E) \mu_{\mathbf{n},1}(E) e^{i\delta_E t'}
$$

$$
= -\frac{ie^{-i(\omega_1 + E_1/\hbar)t}}{\mu_{2,0}} \int_{-\infty}^{t} dt' \mathcal{E}_1(t') b_1(t') F_{0,1}(t-t') \,, \tag{79}
$$

where $F_{0,1}(\tau)$ is the *spectral cross-correlation* function

$$
F_{0,1}(\tau) \equiv - \int d\delta_E A_{0,1}(E) e^{-i\delta_E \tau} \,, \tag{80}
$$

where

$$
A_{0,1}(E) \equiv \sum_{\mathbf{n}} \mu_{0,\mathbf{n}}(E) \mu_{\mathbf{n},1}(E). \tag{81}
$$

We now turn our attention to the calculation of $\langle E', \mathbf{m}_1^- | \Psi(t) \rangle$—the amplitudes for populating the (radiative or nonradiative) $|E', \mathbf{m}_1^-\rangle$ continuum states, i.e., the eigenstates of PHP (see Eq. (5)), given as

$$\langle E', \mathbf{m}_1^- | \Psi(t) \rangle = \sum_{\mathbf{n}} \int dE b_{E, \mathbf{n}}(t) \langle E', \mathbf{m}_1^- | E, \mathbf{n}^- \rangle e^{-iEt/\hbar}. \tag{82}$$

With Eqs. (3, 43, and 50), neglecting the terms containing the highly oscillatory $e^{i\omega_{2,0}t}$ factor and using Eqs. (52 and 58), we have for the $\langle E', \mathbf{m}_1^- | E, \mathbf{n}^- \rangle$ amplitudes

$$\langle E', \mathbf{m}_1^- | E, \mathbf{n}^- \rangle = \frac{1}{E - i\epsilon - E'} \left\{ V_{\mathbf{m},0}(E') \mu_{1,\mathbf{n}}(E)/\mu_{1,0} + V_{\mathbf{m},2}(E') \mu_{0,\mathbf{n}}(E)/\mu_{0,2} \right\}. \tag{83}$$

Substituting in Eq. (82) and with Eq. (69) we finally have that

$$\langle E', \mathbf{m}_1^- | \Psi(t) \rangle = i e^{-i\omega_1 t} V_{\mathbf{m},0}(E')/\mu_{1,0} \int_{-\infty}^{t} dt' b_1(t') \mathcal{E}_1(t') G_1(E', t - t')$$

$$+ i e^{-i\omega_1 t} V_{\mathbf{m},2}(E')/\mu_{0,2} \int_{-\infty}^{t} dt' b_1(t') \mathcal{E}_1(t') G_{1,0}(E', t - t'), \tag{84}$$

where

$$G_1(E', \tau) \equiv \int d\delta_E e^{-i\delta_E \tau} \frac{A_1(E)}{E - i\epsilon - E'} = \int d\delta_E e^{-i\delta_E \tau} A_1(E) \left[\frac{E - E' + i\epsilon}{(E - E')^2 + \epsilon^2} \right],$$

$$G_{0,1}(E', \tau) \equiv \int d\delta_E e^{-i\delta_E \tau} \frac{A_{0,1}(E)}{E - i\epsilon - E'} = \int d\delta_E e^{-i\delta_E \tau} A_{0,1}(E) \left[\frac{E - E' + i\epsilon}{(E - E')^2 + \epsilon^2} \right]. \tag{85}$$

The contribution of the free one-photon states to the absorption for unstructured continuum is shown in Figure 3.12.

In conclusion of this section, we have thus presented a comprehensive theory of EIT in which both the structure and multiplicity of (coupled) continua are taken into account, which strongly emphasizes the fact that EIT is a manifestation of interferences in the continuum. As such, it is a property of the way the full continuum eigenfunctions are convoluted with the matter–radiation Hamiltonian and the initial bound states. The exact nature of this convolution depends on the type of spectroscopy used to probe the continuum; whether it is linear or nonlinear, the EIT line shapes and especially the EIT dips are properties of the continuum.

4. QC AND LICS

The "quantum control" (QC) problem can be phrased as finding ways of inducing complete transfer of population from an arbitrary initial wave packet of quantum states to a desired target wave packet of quantum states.
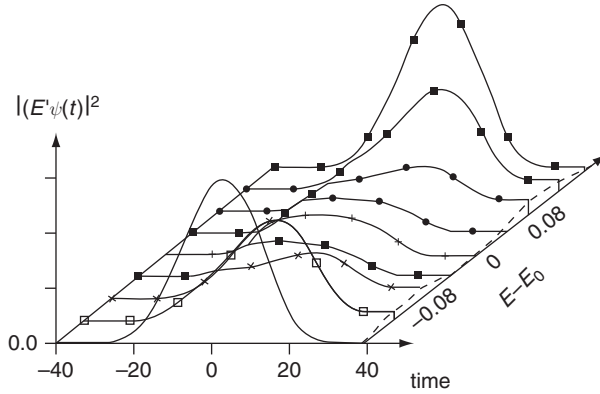
Figure 3.12 The contribution of the free one-photon states to the absorption for unstructured continuum. Plotted is $|\langle E'|\Psi\rangle|^2$ as a function of time and energy, according to Eq. (84). $\Gamma_0 = 0.4 \times 10^{-6}$ a.u., $\Gamma_2 = 0.02 \times 10^{-6}$ a.u., and $\delta_2 = 0$. The time axis (t) is expressed in 10^6 a.u. and the energy axis in 10^{-6} a.u. $|\langle E'|\Psi\rangle|$ is expressed in units of $\{1/E\}^{1/2}$ where E is expressed in a.u.

This objective can be achieved by employing a (polychromatic) set of mutually coherent light fields or, equivalently, a set of tailor-made shaped laser pulses.

In recent years QC has been realized by using a number of strategies, such as CC [24, 25], optimal control (OC) [120–124], and AP [20, 21, 125]. CC achieves final state *selectivity* using laser-controlled interferences between two and more quantum pathways. OC is a general procedure for optimizing laser pulses to achieve a desired outcome. In the ultrafast domain such optimization is performed using pulse-shaping techniques [126–130]. AP is a way of affecting population transfer between selected states via the parametric dependence of field-dressed states.

In parallel with the study of the control of atomic and molecular systems, "quantum engineering" of light itself has also been extensively investigated [114, 131, 132]. These studies have been aided by the availability of ultra-cold systems and advances in solid-state electronics. In particular, numerous nonclassical light states with squeezed fluctuations of observables have been constructed, and general methods for their preparation have been developed [133–136].

In the continuum domain, we now understand [25] that control over multiply degenerate states, leading to the final products of interest, can be attained only if we can establish an *entanglement* between the photons used to excite a material system and the material system itself. Entanglement in this context means that light-induced transition amplitudes *cannot* be factorized into products of material and radiative matrix elements. The usefulness of CC and AP is that these are general methods that can be applied to an entire

class of systems. In addition to generality, these techniques are robust, i.e., insensitive to small variations of the experimental parameters, and are based on some simple and transparent principles, thus making the underlying dynamics intuitively understandable.

4.1. Coherent control

CC [24, 25] is a method of selecting between different (energetically allowed) outcomes using multiply interfering quantum pathways. The method is most effective in dealing with degenerate quantum states, such as those associated with systems possessing multiple continua, existing in molecular dissociation, ionization, and reactive scattering processes.

Starting from initial pure quantum state one uses laser fields to control the multiplicity of quantum pathways which guide the population to different superpositions of final states of interest. By inducing constructive (destructive) interference between such quantum pathways, it is possible to enhance (suppress) desired (undesired) target states. Although CC has in the past been implemented in the perturbative regime in the combined fields, its validity has been shown to extend to the strong field regime as well [25].

Control of the interferences between different pathways may be achieved experimentally by varying the relative phase between the different laser modes used to excite the system along these pathways. Although the partial coherence of light sources combined with the fast decoherence of quantum processes in material systems, due to various scattering processes, is detrimental to the control [25], experience shows that as long as the separation of the light pulses associated with the excitation processes along different pathways is shorter than the decoherence rates, extensive control is achievable.

Many of the CC theoretical predictions, such as control of atomic and molecular processes via N versus M photon transitions [137], have been tested and demonstrated experimentally [138–146]. CC methods have also proved to be valid in the context of solid-state systems. In particular, it was shown that excitation by N and M multiphoton processes, having opposite parities, leads to symmetry breaking and the generation of DC electric currents [147–151]. These predictions have been confirmed experimentally in a number of semiconductors [152–155]. Similar techniques were shown to lead to the control of phonon emission [156] or injection of spin currents [157].

CC of photonic processes such as spontaneous emission has also been studied. Among the scenarios explored are interferences between overlapping resonances [158, 159] and direct interference between emission pathways [160–165]. The suppression of spontaneous emission in free space [160] or band-gap materials [162] results in the spectral narrowing, even the complete elimination, of the spectral lines [161, 163].

Two-photon processes can also be modified using CC. It is possible to selectively inhibit or enhance two-photon absorption by phase modulation [166–168] and other interference techniques [169, 170]. It is also possible to use CC to induce population trapping and gain in V-type systems [171, 172]. Furthermore, it has been realized that interference between one-photon and N-photon transitions results in EIT in atomic systems [173–175].

CC thus provides a satisfactory solution to quests dating back to the early 1970s of using lasers to affect selectivity. Most experiments of those days attempted to achieve selectivity by using frequency control, as afforded by narrow-band lasers. Since such lasers lead to preferential excitation of atomic and molecular levels that are in resonance with the laser lines [176, 177], the hope was that such energy selectivity will also result in selectivity of subsequent events such as ionization and dissociation. This turned out to be realizable only partly, due to the lack of high selectivity in address- ing degenerate quantum states in overlapping continua and the existence of intra-molecular vibrational redistribution [178–182], a process by which the narrow wave packet of states excited by the narrow-band laser pulses quickly disperses to many molecular vibrational modes.

4.2. Adiabatic passage

With the introduction of new laser sources in the 1980s a number of powerful population transfer techniques were developed, such as overtone pumping [183], off-resonance stimulated Raman scattering [184, 185], and stimulated emission pumping [186]. These methods resulted however in only partial population transfer between quantum states. The adoption of the AP tech- nique [20, 21, 187], operating (in contrast to CC) along a single quantum pathway, has opened the way for inducing a complete population transfer between quantum material states.

Complete population transfer in AP was shown theoretically [20] and independently implemented experimentally a few years later in a method called STIRAP [21, 187]. In this method, which is a variant of the stimu- lated Raman process, the two ("pump" and "Stokes") pulses are employed in the reverse ("counter-intuitive") order to that of the usual stimulated Raman process, namely in STIRAP the Stokes pulse precedes the pump pulse. This method designed to work with discrete states clearly comple- ments CC by being able to transfer populations completely but at the same time *not* being phase sensitive, in contrast to the CC that is typically used in continua of states in weak-field but phase-sensitive regimes. We later explore the advantages resulting from the combination of both approaches.

We now show that the counter-intuitive pulse ordering leads to the desired complete population transfer. Consider irradiating the (Λ-type) three-state system depicted in Figure 3.13 (left) by two laser pulses, a pump pulse (P) of center frequency ω_P and electric field envelope $\mathcal{E}_P(t)$ and a Stokes pulse (S)
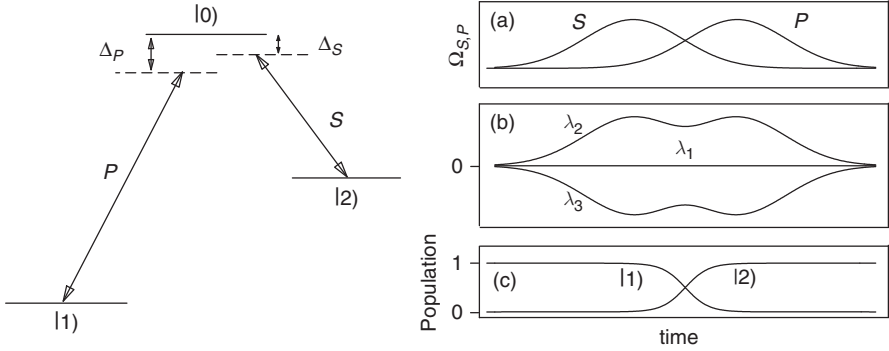
Figure 3.13 (left) The three-level Λ-configuration AP scheme. (right) The pulses (panel (a), where *P* stands for the pump and *S* for the Stokes pulse), eigenvalues (panel (b)), and populations (panel (c)) as a function of time in this AP with counter-intuitive pulse ordering.

of center frequency ω_S and field envelope $\mathcal{E}_S(t)$. We assume that the pump pulse is close to resonance with the $|1\rangle \leftrightarrow |0\rangle$ transition and the Stokes pulse is close to resonance with the $|2\rangle \leftrightarrow |0\rangle$ transition, and the two transitions have well-separated energies.

The time-dependent Hamiltonian of this radiation–matter system can be written in the Schrödinger picture as follows [114, 188]:

$$H(t) = H_M + H_I(t), \quad H_M = \sum_{i=1,0,2} E_i |i\rangle\langle i|,$$

$$H_I(t) = -\mathcal{E}_P(t)\cos(\omega_P t)\left(\mu_{0,1} |0\rangle\langle 1| + \text{h.c.}\right)$$
$$- \mathcal{E}_S(t)\cos(\omega_S t)\left(\mu_{0,2} |0\rangle\langle 2| + \text{h.c.}\right). \tag{86}$$

Here, as well as in all subsequent sections, we use the "$\mathbf{r} \cdot \mathbf{E}$" gauge of the radiation–matter interaction Hamiltonian $H_I(t)$. In Eq. (86), $\mu_{0,1}$ is the projection of the dipole matrix element for the $|1\rangle \leftrightarrow |0\rangle$ transition on the *P* polarization axis, $\mu_{2,0}$ is the projection of the dipole matrix element for the $|0\rangle \leftrightarrow |2\rangle$ transition on the *S* polarization axis, and $E_i = \hbar\omega_i$ are the free-field eigenenergies. The connection between the electric field envelope $\mathcal{E}(t)$ and the intensity of the radiation $I(t)$ is

$$\mathcal{E}(t)\,[\text{V/cm}] = 27.4682\sqrt{I(t)\,[\text{W/cm}^2]}. \tag{87}$$

We can write the time-dependent wave function, $|\Psi(t)\rangle$, solving the Schrödinger equation

$$\hbar \frac{d}{dt} |\Psi(t)\rangle = -iH(t) |\Psi(t)\rangle \,, \tag{88}$$

in the form [114, 188]

$$|\Psi(t)\rangle = \sum_{i=1,0,2} C_i(t) |i\rangle = \sum_{i=1,0,2} c_i(t) e^{-i\omega_i t} |i\rangle \,. \tag{89}$$

After substituting this $|\Psi(t)\rangle$ in Eq. (88) and performing its time derivative on the left side, we can cancel the terms associated with the free evolution in the H_M Hamiltonian. Then, its multiplication by the terms $\langle j| e^{i\omega_j t}$ gives a set of equations for the $c_i(t)$ coefficients. If we collect these coefficients in the vector $\mathbf{c}(t) \equiv (c_1(t), c_0(t), c_2(t))^{\mathrm{T}}$, then Eq. (88) can be written in the matrix form

$$\hbar \frac{d}{dt} \mathbf{c}(t) = -i \underline{\underline{H}}(t) \cdot \mathbf{c}(t) \,, \tag{90}$$

where

$$\underline{\underline{H}}(t) = \frac{\hbar}{2} \begin{pmatrix} 0 & \Omega_P^*(t)\, e^{-i\Delta_P t} & 0 \\ \Omega_P(t)\, e^{i\Delta_P t} & 0 & \Omega_S^*(t)\, e^{i\Delta_S t} \\ 0 & \Omega_S(t)\, e^{-i\Delta_S t} & 0 \end{pmatrix} \,. \tag{91}$$

This is the Schrödinger equation in the interaction representation for the problem described by the Hamiltonian in Eq. (86) [114, 188]. For its formal derivation we refer to Ref. [26].

In Eq. (91), $\Omega_\nu \equiv \mu_\alpha \mathcal{E}_\nu / \hbar$ ($\nu = P,S$; $\alpha = (0,1),(2,0)$) is the Rabi frequency for the pump (Stokes) pulse and $\Delta_\nu \equiv \omega_\nu - \omega_\alpha$ ($\nu = P,S$) its detuning relative to the transition frequency $\omega_\alpha = \omega_0 - \omega_\beta$ ($\alpha = (0,1),(2,0)$, $\beta = 1,2$) between the levels $|0\rangle$ and $|1\rangle$ ($|0\rangle$ and $|2\rangle$). Even though the Rabi frequencies are in general complex, in some of the cases discussed below we choose them, for simplicity, to be real.

In deriving the Hamiltonian $\underline{\underline{H}}(t)$, we have also employed the RWA, according to which one only keeps terms proportional to the slowly varying factors $\exp\left[\pm it\left(\omega_\nu - (E_i - E_j)/\hbar\right)\right]$, where $\omega_\nu \approx (E_i - E_j)/\hbar$, ($\nu = P,S$), while we neglect containing the rapidly oscillating factors $\exp\left[\pm it\left(\omega_\nu + (E_i - E_j)/\hbar\right)\right]$ ($\nu = P,S$). Since in all the cases studied here, the excitation fields are in resonance ($\Delta_P = \Delta_S = 0$) with all the considered states, the RWA Hamiltonian $\underline{\underline{H}}(t)$ does not possess oscillatory terms, and we can use the concept of adiabatic states [114, 188].

We now diagonalize the RWA Hamiltonian, $\underline{\underline{H}}(t) \cdot \underline{\underline{U}}(t) = \underline{\underline{U}}(t) \cdot \hat{\lambda}(t)$, where $\hat{\lambda}(t)$ is a diagonal matrix with the coefficients

$$\lambda_1 = 0, \quad \lambda_{2,3}(t) = \pm \left[|\Omega_P(t)|^2 + |\Omega_S(t)|^2 \right]^{\frac{1}{2}} \,. \tag{92}$$

The normalized eigenvector corresponding to the $\lambda_1 = 0$ null eigenvalue is

$$\underline{\underline{U}}^{(1)}(t) = \begin{pmatrix} \cos\theta(t) \\ 0 \\ -e^{i\chi(t)}\sin\theta(t) \end{pmatrix}, \quad \theta(t) = \arctan\left(\left|\frac{\Omega_P(t)}{\Omega_S(t)}\right|\right), \tag{93}$$

where $\chi(t) \equiv \phi_P(t) - \phi_S(t)$ and $\phi_i(t)$ are the phases of the Rabi frequencies, $\Omega_i(t) \equiv |\Omega_i(t)| \, e^{i\phi_i(t)}$ $(i = P,S)$, allowing the formation of null eigenvalue (dark) states described below.

We can write the dark state in the interaction representation and the bare-state basis $|i\rangle$ $(i = 1,0,2)$ as

$$|\lambda_1(t)\rangle = \cos\theta(t)\,|1\rangle - \sin\theta(t)\,e^{i\chi(t)}\,|2\rangle \tag{94}$$

and transform it to the Schrödinger picture as follows:

$$\begin{aligned} |\Lambda_1(t)\rangle &= U_0(t)\,|\lambda_1(t)\rangle \\ &= \cos\theta(t)\,e^{-i\omega_1 t}|1\rangle - \sin\theta(t)\,e^{-i\omega_2 t + i\chi(t)}\,|2\rangle, \end{aligned} \tag{95}$$

where $U_0(t) = \exp(-i H_M t/\hbar)$ (see also Ref. [26]). Since the other two dark states, $|\lambda_\nu(t)\rangle$ $(\nu = 2,3)$, turn out not to be connected at $t = 0$ to the $|1\rangle$ state, we see from Eqs. (93 and 94) that a system residing initially in state $|1\rangle$ correlates exclusively with the $|\lambda_1(t)\rangle$ dark eigenvector. Moreover, if the Stokes pulse is made to precede the pump pulse, this eigenvector executes a smooth transition from state $|1\rangle$ to state $|2\rangle$, while leaving state $|0\rangle$ unpopulated throughout the process. Thus, as illustrated in Figure 3.13 (right), we can achieve the desired complete population transfer.

In the continuous regime, where flying molecules cross mutually space-shifted light beams, STIRAP has been demonstrated for Na$_2$ [21, 187] and for Ne* atoms [189] and in the pulsed regime for NO [190] and SO$_2$ [191]. It has been demonstrated in the "ladder" configuration for Rb [192], with degenerate or nearly degenerate states [193].

Following the initial works of Bergmann and others, the properties of three-state STIRAP have been thoroughly investigated theoretically [20, 23, 115, 194]. Among the properties examined were the sensitivity of the population transfer to the delay between the Stokes and pump pulse [22] and the effect of single-photon [195] and two-photon detuning [23]. Going beyond the RWA [196, 197], parasitic effects due to losses from intermediate state [198–202] and the existence of many intermediate states [203, 204] have also been studied.

Generalizations of the three-state STIRAP to multistate chains [189, 205–209]; to adiabatic momentum transfer [189, 206, 210, 211]; and to branched-chain excitation [212–216] have been made. The extensions of the three-state

STIRAP to population transfer via a continuum of intermediate states [93, 95, 215, 217–220], which is related to LICS [2, 69, 78, 101], are discussed in detail in the next section.

Numerous novel techniques related to STIRAP have been further developed recently. Examples are the hyper-Raman STIRAP [196, 197, 221], Stark-chirped rapid adiabatic passage (SCRAP) [222, 223], adiabatic passage by light-induced potentials [224–227], and photo-associative STIRAP, as a source for cold molecules [228–231]. Some experimental implementations of these ideas, e.g., to the formation of dark states in the photo-association of an atomic Bose-Einstein Condensate (BEC) to form a molecular BEC, have already been reported [232, 233].

5. THE CONNECTION BETWEEN LICS, CC, AND AP

The focus of this section is to draw the connection between LICS, CC, and AP. We are mainly concerned with the manipulation of population transfer by laser pulse in situations involving (multichannel) continua.

5.1. Coherent population trapping via LICS

Under appropriate conditions, a strong laser field, which alone produces no ionization, can suppress the ionization by another (" probe") laser pulse. The two fields create a dressed state that is immune to photo-ionization, called a "trapped" or "dark" state [29, 234].

The first substantial ≈70% ionization suppression and population trapping in relation to LICS has been observed in atomic helium [69, 101]. Earlier experiments on LICS have observed dominantly ionization enhancement, with only a few percent recognizable ionization suppression [50–54, 56, 57, 62, 65]. The LICS in the flat photo-ionization continuum of helium is a strong and spectrally sharp resonance showing both enhancement and diminished ionization.

A schematic diagram of the states and transitions involved is shown in the left panel of Figure 3.14. A dressing pulse couples the initially unpopulated excited state $4s^1S_0$ to the ionization continuum thereby inducing the continuum structure. This is probed by a weaker laser pulse that couples the initially populated metastable state $2s^1S_0$ to the ionization continuum. When the probe laser is tuned across the two-photon resonance, between the states $2s^1S_0$ and $4s^1S_0$, a strong and spectrally narrow feature in the ionization rate, as shown in the right panel of Figure 3.14, is observed. This feature can be regarded as a $4s^1S_0$ resonance embedded in the ionization continuum by the strong dressing laser (and probed by the weak probe laser). The structure exhibits a typical asymmetric Fano profile, in which the ionization rate is controlled by appropriately tuning the probe laser frequency, thereby selecting the region of enhanced or diminished ionization. At the minimum of the
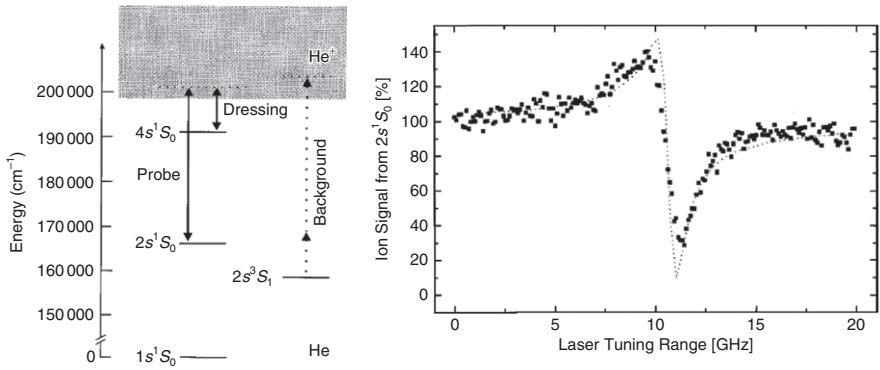
Figure 3.14   Left panel: Helium level scheme and the relevant couplings. The dressing laser ($\lambda_S = 51\,064$ nm) couples the excited state $4s^1S_0$ to the ionization continuum. The induced continuum structure is probed (at $\lambda = 5294$ nm) through ionization of the $2s^1S_0$ state. Right panel: Variations of the ionization cross section probed with a weak probe pulse, the frequency of which is tuned across the two-photon resonance between the $2s^1S_0$ and $4s^1S_0$ states. The axis of the probe laser beam (diameter 0.5 mm) coincides with the axis of the dressing laser beam (diameter 3.5 mm). There is no time delay between the pulses. The laser intensities are $I_P = 4$ MW/cm^2 and $I_D = 75$ MW/cm^2. The experimental profile (dots) is in good agreement with the result from numerical studies (dotted line), which include averaging over fluctuating laser intensities and integrating over the spatial profile of the probe laser. Taken from Ref. [69].

ionization profile the yield is reduced to less than 30% of its unperturbed value (in the absence of LICS). The figure also shows the result of numerical simulations [101]. It is also found that the position of the profile minimum varies linearly with dressing pulse intensity.

The LICS, produced by an idealized Continuous-Wave (CW) laser (steady amplitude and single-frequency laser), can differ substantially from the structure produced by a pulsed laser, since the AC Stark shifts produce time-dependent detunings relative to one- and two-photon resonance. The time-dependent pulse and frequency effects in population trapping in LICS have received attention in theoretical works [93]. Using numerical approaches, as well as approximate analytical solution, it was shown that the trapped population in realistic atomic systems can be sufficiently decreased, to the point when no population remains in the system, by the increase in laser energies. Furthermore, the use of properly chirped laser pulses not only helps to increase the trapped population but also makes the system more stable against increases in the pulse energy.

Phase control of two-channel photo-ionization rates and coherent population trapping induced by four laser fields operating on an atomic system initially in its ground state $|1\rangle$, which proceeds via a pair of intermediate bound states, $|2\rangle$ and $|3\rangle$, to a manifold of structureless continua, has also

been studied [99]. Different effects of the ϕ_g and ϕ_c phases of the lasers which, respectively, drive the $|1\rangle \leftrightarrow |3\rangle$ and $|2\rangle \leftrightarrow |3\rangle$ transitions were observed. For example, $\phi_g = \pi$ led to the formation of one unstable and two stable eigenstates, all decoupled from $|1\rangle$. In this way, an atom initially in $|1\rangle$ was protected from ionization.

Extensions to multibound state LICS have also been made. For example, atomic coherent population trapping in a multilevel model of LICS, in which a laser embeds a "Bixon–Jortner-type" quasi-continuum [235] into a structureless atomic continuum, has been investigated [236]. (The Bixon–Jortner quasi-continuum model consists of an unbounded set of levels $|j\rangle$, $j = 0, \pm 1, \pm 2,...$, of equal spacing, which are all equally coupled to a continuum.) The finding was that for large detuning the population is trapped in $|0\rangle$. Interference stabilization against one-photon ionization was shown theoretically to exist when two atomic levels are coupled by a strong two-color laser field, in two-photon Raman-type resonance [100].

5.2. STIRAP via a continuum

The first experimental demonstration of coherent population transfer by STIRAP via continuum states was reported recently [237]. It was realized, as shown in the left panel of Figure 3.15, by transferring population from the $2s^1S_0$ metastable state of He to its $4s^1S_0$ excited state by a Raman-type
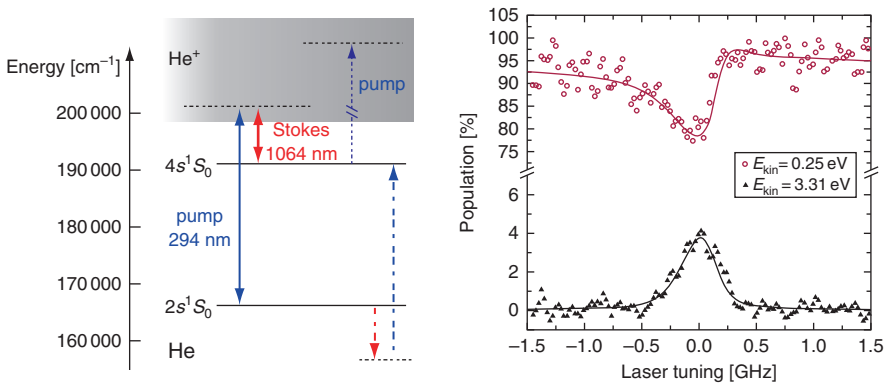
Figure 3.15 The STIRAP via a continuum experiment. Left panel: The coupling scheme in He. The pump and Stokes lasers couple the initially populated state $2s^1S_0$ to the target state $4s^1S_0$ via the ionization continuum (solid lines). Population transferred to the target state can be ionized by the pump laser (dotted line), too. An off-resonant Raman-type transition between the initial and target states is also indicated (dash-dotted lines). Right panel: The measured electron signals versus laser tuning of the pump laser in the two-photon resonance range for the counter-intuitive pulse ordering. The circles and the triangles indicate slow and fast electrons, respectively. The solid lines show numerical simulations. Taken from Ref. [237].

process involving an intermediate continuum. The He $2s^1S_0$ state was coupled to the ionization continuum by the pump laser, thereby generating slow photo-electrons whose kinetic energy is $E_{kin} = 0.25\,\text{eV}$. The Stokes laser couples the initially unpopulated state $4s^1S_0$ to the same ionization continuum. While ionization in the above process is eliminated by the formation of the STIRAP dark state, there is a second channel in which the pump laser ionizes the $4s^1S_0$ state, generating fast photo-electrons with kinetic energy of $E_{kin} = 3.31\,\text{eV}$. Since spontaneous emission losses from this state can be safely neglected, the above second channel is the main source of incoherent losses.

Theoretically, the process can be treated by adiabatically eliminating the continuum and all off-resonance bound states, as done in our discussion of partitioning theory. The result is an effective (2×2) Hamiltonian involving only the initial and target states. It has been shown [237] that in the "counter-intuitive" pulse ordering, the "dark" state of the system evolves, as in three-state STIRAP, from the initial state to the target state, provided the evolution is adiabatic.

The measured electron signals at $E_{kin} = 0.25\,\text{eV}$ (circles) and $E_{kin} = 3.31\,\text{eV}$ (triangles) versus the laser tuning of the pump laser of the two-photon resonance between the initial and final states are shown in the right panel of Figure 3.15. The pump laser is 7.5 ns delayed with respect to the Stokes laser. The signal from the slow electrons shows a pronounced asymmetric Beutler–Fano line profile [3], which indicates population trapping in a dark state of the process and thus coherent interaction via the continuum. The signal from the fast electrons is maximized when the population of the ground states, i.e., the signal of the slow electrons, approaches minimum. In this way, the population transfer from state $2s^1S_0$ to the target state $4s^1S_0$ is demonstrated. In the same panel of Figure 3.15 results of numerical simulations are also depicted.

The maximum transfer efficiency by STIRAP in systems involving continua is far less than 100%, due to dynamic Stark shifts and incoherent losses from the target state induced by the pump laser, as theory predicts [202, 215, 219, 220]. However, since techniques based on incoherent excitation via resonant continuum couplings do not usually permit any transfer at all, the STIRAP technique offers an advantage in such environments, even though the efficiency of STIRAP in such cases is far less than in purely bound systems.

Several theoretical works investigating population transfer via a continuum have been reported. In the earliest model [238], the continuum was treated as a Bixon–Jortner-type [235] unbounded set of equally spaced quasi-bound states. In such a model complete population transfer was shown to be possible [238]. Soon thereafter it was however pointed out [239] that complete population transfer via a true continuum is not generally achievable. Several works have tried to maximize the transfer efficiency, by employing structured continua; auto-ionizing states [240]; or in the case of LICS by controlling the Stark shifts, the area of laser pulses, and the effect of

the incoherent channels of ionization [202, 219, 241]. Alternatively, chirped lasers have been used in combination with STIRAP for enhancing the population transfer via the continuum [242]. In this case the highest efficiency is obtained for a particular nonzero value of the two-photon detuning between the pump and Stokes pulses.

Generalized STIRAP schemes, including more than three states, for which one state is a continuum have been studied. The bound state tripod system [243, 244] has been extended to a tripod system coupled via a continuum [95], as shown in the left panel of Figure 3.16. In this scheme, it is possible to find laser parameters which allow for ionization-free partial population transfer between the discrete states within the counter-intuitive pulse order, as shown in the right panel of Figure 3.16.

Figure 3.17 demonstrates a LICS–STIRAP scheme for maximizing the *ionization* from a discrete state coupled to a continuum by a two-photon transition via a lossy intermediate state whose lifetime is much shorter than the interaction duration [97]. As in three-level STIRAP, the counter-intuitive pulse ordering is most efficient. It achieves almost complete ionization by embedding a third discrete state into the continuum using a third control laser.

The deleterious effect of AC Stark shifts can be minimized by employing the LICS–SCRAP scheme [96], shown schematically in the right panel of Figure 3.17. This scheme uses in addition to the two-photon pump
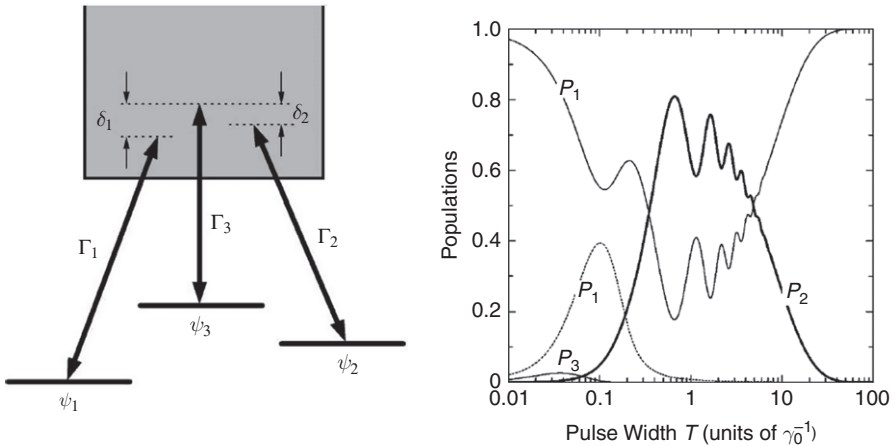
Figure 3.16   Left panel: Sketch of the tripod scheme involving three discrete states coupled via a common continuum by three lasers. Right panel: Population of the discrete states and the ionization probability versus the pulse width of the pump and Stokes pulses within the counter-intuitive pulse order. Taken from Ref. [95].
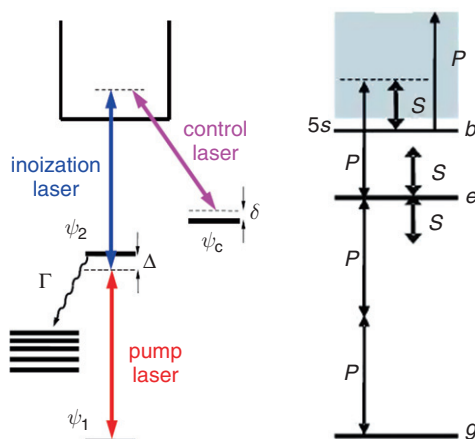
Figure 3.17   Left panel: The scheme for ionization by LICS–STIRAP. (Taken from Ref. [97].)
Right panel: The scheme for maximizing population transfer to state *e* by LICS–SCRAP. (Taken
from Ref. [96].)

laser a second field to control the dynamic Stark shifts via SCRAP, thereby
suppressing undesired photo-ionization. The proposed method is illustrated
by numerically simulating the two-photon excitation of the 2*s* metastable
state of H [96]. By carefully choosing the laser parameters (peak intensities,
pulse delay, and detuning) population transfer to the target state can be as
high as 86%.

5.3. Use of LICS in CC

The use of LICS in the control of a molecular process was first demonstrated
experimentally [89] in the branching PD process

$$Na(3s) + Na(3d) \longleftarrow Na_2^* \longrightarrow Na(3s) + Na(3p).$$

The experiment was based on theoretical predictions that LICS can give rise
to channel selectivity [245–247]. In these works it was shown that the dress-
ing of a continuum with an initially unpopulated bound state by a laser of
frequency ω_2, performed while exciting a populated bound state to the same
dressed continuum using a laser field of frequency ω_1, results in a quantum
interference whose (destructive or constructive) character depends on the
final channel. An illustration of this scenario is shown in the left panel of
Figure 3.18.
   The character of the quantum interference in the above scenario as shown
in Figure 3.18 depends on the relative frequency between the two laser fields.
Therefore, selectivity between the Na(3*s*)+Na(3*p*) and the Na(3*s*)+Na(3*d*)
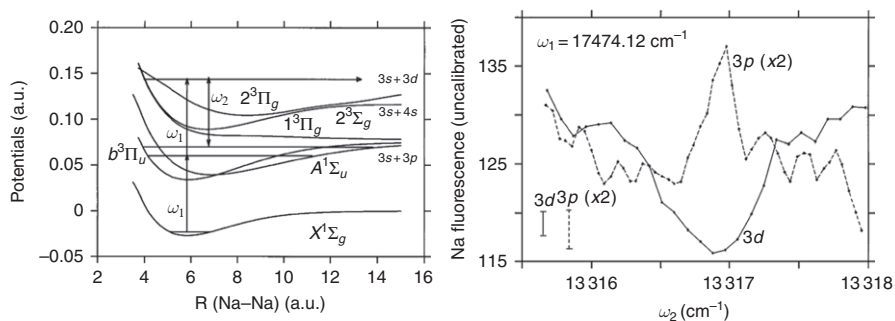
Figure 3.18 Left panel: The molecular LICS scheme for Na_2. In this scheme a $2\omega_1$-photon excitation interferes with an ω_2 photon. The two-photon process proceeds from an initial sate, assigned here as $v = 5, J = 37$, via the $v = 35, J = 36,38$ levels, belonging to the interacting $A^1\Sigma_u/^3\Pi_u$ electronic states, acting as intermediate resonances. The ω_2 photon dresses the continuum with the (initially unpopulated) $v = 93, J = 36$ and $v = 93, J = 38$ levels of the $A^1\Sigma_u/^3\Pi_u$ electronic states. Right panel: Experimental Na(3d) fluorescence (solid) and Na(3p) fluorescence (dashed) (both uncalibrated) for the $Na_2 \longrightarrow Na(3s)+$ Na(3p)/Na(3d) LICS scenario of the left panel, as a function of the ω_2 frequency. The ω_1 frequency is fixed at $17\,474.12$ cm^{-1}. Taken from Ref. [89].

channels can be achieved by varying ω_1 or ω_2. Importantly, this effect is virtually independent of the relative phase between the two light fields, i.e., the light fields need not be coherent. Thus, although the control depends on quantum interference, the interference cannot be destroyed by incoherence of the incident laser radiation.

In the right panel of Figure 3.18 the experimental Na(3d) and Na(3p) emission as a function of ω_2 at a fixed ω_1 is shown. As expected [245–247], the Na(3d) yield dips when the Na(3p) yield peaks. The controlled modulation of the Na(3p)/Na(3d) branching ratio is exceeding 30%. Theoretical calculations of the Na(3d) yield resulting from PD of a single initial Na_2 bound state are presented in the left panel of Figure 3.19 and contrasted with the experimental results. The same is done in the right panel of the same figure for the Na(3p) yield. The agreement with the experiment is obviously good. Moreover, considering the uncertainties in the theoretical potentials for the Na_2 dissociation used, the agreement of theory and experiment (in particular in the Na(3d) case) is impressive.

LICS control over branching reactions was also demonstrated in the two spin–orbit ionization continua of Xe [88]. The photo-ionization of Xe atom to yield the two spin–orbit $Xe^+ + e^-$ continua can be varied by electromagnetically embedding into the continua an atomic bound state. The dressed $^2P_{1/2}$ continuum, when probed by a three-photon absorption from the ground state, exhibits a pronounced induced structure, whereas the $^2P_{3/2}$ continuum possesses no such structure, as demonstrated
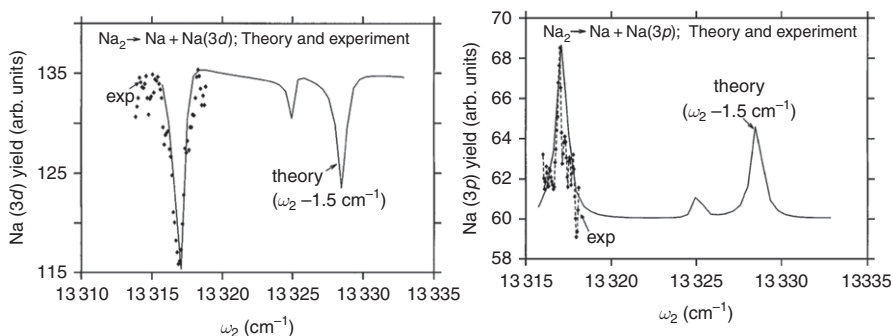
Figure 3.19 Comparison of the experimental and theoretical $Na_2 \longrightarrow Na(3s)+Na(3d)$ yields (left panel) and $Na_2 \longrightarrow Na(3s)+Na(3p)$ yields (right panel) as a function of ω_2. In the calculation, an intermediate $v = 33, J = 31,33$ resonance is used and ω_1 is fixed at $17\,720$ cm^{-1}. The intensities of the two laser fields are $I(\omega_1) = 1.72 \times 10^8$ W/cm^2 and $I(\omega_2) = 2.84 \times 10^8$ W/cm^2. The ω_2 frequency axis of the calculated results was shifted by -1.5 cm^{-1} in order to better compare the predicted and measured line shapes. Taken from Ref. [89].

by high-resolution photo-electron spectra. The ionization ratio in the $^2P_{1/2}$ and $^2P_{3/2}$ channels is controlled by the frequency of the dressing laser field.

The use of LICS in the production of spin-polarized photo-electrons has also been investigated [90]. The general theoretical results have been applied to Rb and Cs. In both cases, enhancement of a factor of $\sim$2 in the degree of spin polarization has been obtained by the introduction of a dressing laser at intensity larger than 10^9 W/cm^2.

An additional example deals with the modification of the K atom photo-electron angular distribution by a dressing laser [91]. In this scenario the branching ratio into different ionization channels is controlled by detuning the dressing laser relative to the probe laser. As a result, the electron angular distribution is altered [91]. Alternatively, the photo-electron angular distribution can be affected by varying the polarization angle between the linearly polarized probe and dressing lasers [91]. The angular distribution of atomic photo-electrons by LICS has been also theoretically studied in the ultrafast domain [92], a technique that complements CC in the frequency domain [248].

A scenario which merges the techniques of CC and AP, called CCAP, has recently been developed [26]. It enjoys the CC selectivity between competing quantum states and the completeness of the population transfer process as afforded by AP. Originally, the CCAP approach was confined to the control of bound state dynamics. It was recently extended [249] to the multicontinuum channel control.
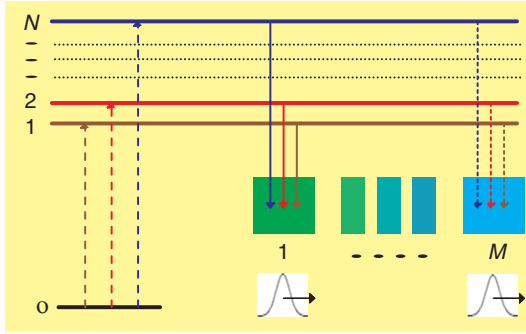
Figure 3.20 The CCAP in the continuum scheme: A multipath two-photon process links a bound state to *M* degenerate channels via *N* intermediate bound states. Taken from Ref. [249].

The CCAP solution to the multichannel quantum control (MCQC) problem [249] is based on the multipath Raman scheme shown in Figure 3.20. One couples the initial state $|0\rangle$ and the degenerate $|E^{(-\ell)}\rangle$ ($\ell = 1,...,M$) target continuum states via N nondegenerate intermediate bound levels $|k\rangle$ ($k = 1,...,N$). The laser frequencies are tuned to induce one-photon resonant transitions from $|0\rangle$ to the intermediate states and to be in one-photon resonance with the transitions from the intermediate states to the continuum energy E of the degenerate multichannel states $|E^{(-\ell)}\rangle$ ($\ell = 1,...,M$). Similar schemes have been used previously for excitation of very high-lying vibrational levels in molecules [250].

The multichannel control is complicated by the existence of uncontrollable "satellite" transitions [2, 25], i.e., transitions whose total energy differs from the target continuum energy E. Because usually only one quantum path contributes to such satellites, no control is possible [25]. These transitions inevitably degrade the effectiveness of the control mechanism, as recent studies have clearly demonstrated [237]. However, the degree of degradation may significantly vary between different systems. Nevertheless adequate control was demonstrated in such cases as the PD of the CH_3I molecule [249].

The total Hamiltonian is given as $H = H_0 + H_{int}$, where H_0 denotes the matter Hamiltonian and H_{int} is the matter–radiation interaction term. Defining the bound and continuum eigenstates of H_0 via the eigenvalue relations as $(\hbar\tilde{\omega}_k - H_0)|k\rangle = (E - H_0)|E^{(-\ell)}\rangle = 0, k = 0,...,N, \ell = 1,...,M$, we express H_{int} as

$$H_{int} = - \sum_{k=1}^{N} \left(\vec{\mu}_{0,k} \cdot \vec{\mathcal{E}}_{0,k}|0\rangle\langle k| + \sum_{\ell=1}^{M} \vec{\mu}_{k,\ell}(E) \cdot \vec{\mathcal{E}}_k|k\rangle\langle E^{(-\ell)}| + \text{h.c.} \right), \tag{96}$$

where $\vec{\mu}_{0,k}$ and $\vec{\mu}_{k,\ell}(E)$ are the electric dipole matrix elements for the bound–bound and bound–continuum transitions, respectively, and $\vec{\mathcal{E}}_{0,k} = \mathcal{R}_e\{\vec{E}_{0,k}\epsilon_{0,k}(t)e^{-i\omega_{0,k}t}\}$ and $\vec{\mathcal{E}}_k = \mathcal{R}_e\{\vec{E}_k\epsilon_k(t)e^{-i\omega_k t}\}$ are the corresponding electric field amplitudes with pulse envelopes $\epsilon_{0,k}(t)$ and $\epsilon_k(t)$.

The system wave function is expanded as $|\Psi(t)\rangle = \sum_{k=0}^{N} b_k(t)|k\rangle e^{-i\tilde{\omega}_k t} + \sum_{\ell=1}^{M} \int dE b_E^\ell(t)|E^{(-\ell)}\rangle e^{-iEt/\hbar}$. After substitution into the Schrödinger equation, $i\hbar|\dot{\Psi}\rangle = H(t)|\Psi\rangle$, invoking the RWA, and neglecting off-resonant terms, we obtain

$$\dot{b}_E^\ell = i\sum_{k=1}^{N} \Omega_{k,\ell}^{E*} b_k e^{i\Delta E_k t},$$

$$\dot{b}_0 = i\sum_{k=1}^{N} \Omega_{0,k} b_k, \tag{97}$$

$$\dot{b}_k = i\Omega_{0,k}^* b_0 + i\sum_{\ell=1}^{M} \int dE \, \Omega_{k,\ell}^E b_E^\ell e^{-i\Delta E_k t},$$

where $\Omega_{0,k} = \vec{\mu}_{0,k}\cdot\vec{E}_{0,k}\epsilon_{0,k}/2\hbar$, $\Omega_{k,\ell}^E = \vec{\mu}_{k,\ell}(E)\cdot\vec{E}_k\epsilon_k/2\hbar$, and $\Delta E_k = \omega_k-(E_k-E)/\hbar$. It follows from Eqs. (97) that

$$\frac{\partial(\dot{b}_E^\ell)}{\partial E} = i\sum_{k=1}^{N} \left(itA_{k,\ell}^E/\hbar + B_{k,\ell}^E\right) b_k e^{i\Delta E_k t}, \tag{98}$$

where $A_{k,\ell}^E \equiv \Omega_{k,\ell}^{E*}(t)$ and $B_{k,\ell}^E \equiv \Omega_{k,\ell}^{E*}(t)/\partial E$. For an unstructured ("flat") continuum, $B_{k,\ell}^E \approx 0$ is valid.

It has been shown [251, 252] that AP methods enable population transfer to/from a continuum while keeping the intermediate states essentially unpopulated, $b_k(t) \approx 0$ ($k = 1,...,N$). It follows from Eq. (98) that in this case, $|\partial(\dot{b}_E^\ell)/\partial E|$ can be very small, resulting in the *approximative* separability of the time and energy variables in the $b_E^\ell(t)$ coefficients. Thus as long as the transfer is adiabatic, which warrants that the intermediate $|k\rangle$ state population is low [251, 252], we can assume the separable form

$$b_E^\ell(t) \approx f(E)\beta_\ell(t). \tag{99}$$

We note that the $f(E)$ function obeys the normalization condition $\int dE|f(E)|^2 = 1$, and that the channel-specific $\beta_\ell(t)$ functions obey the initial $\beta_\ell(0) = 0$ condition.

Equation (99) allows us to derive an *approximate* analytic solution to the MCQC problem, which is validated below by comparing it to the numerical solution of Eqs. (97). Using Eq. (99), we can now write Eqs. (97) as

$$\dot{b}_k = i\Omega_{0,k}^* b_0 + i\sum_{\ell=1}^{M} \int dE \, \Omega_{k,\ell}^E(t)f(E)\beta_\ell(t)e^{-i\Delta E_k t}, \tag{100}$$

$$\dot{\beta}_\ell = i \sum_{k=1}^{N} \int dE\, f^*(E) \Omega_{k,\ell}^{E*}(t) b_k(t)\, e^{i\Delta E_k t} \ . \tag{101}$$

We can now solve a simplified set of first-order ODE $i\dot{\mathbf{c}}(t) = \underline{\underline{H}}(t)\,\mathbf{c}(t)$, where $\mathbf{c} \equiv (b_0, b_1, ..., b_N, \beta_1, ..., \beta_N)^{\mathrm{T}}$ and $\underline{\underline{H}}(t)$ is given as

$$\underline{\underline{H}}(t) = \begin{pmatrix} 0 & \mathbf{\Omega}_0 & 0 \\ \mathbf{\Omega}_0^\dagger & 0 & \mathbf{H}_E \\ 0 & \mathbf{H}_E^\dagger & 0 \end{pmatrix}, \ \mathbf{H}_E = \begin{pmatrix} \overline{\mathbf{\Omega}}_1 \\ \vdots \\ \overline{\mathbf{\Omega}}_N \end{pmatrix} . \tag{102}$$

The vectors that make up the $\underline{\underline{H}}(t)$ matrix are defined as

$$\mathbf{\Omega}_0 = (\Omega_{0,1}, ..., \Omega_{0,N}) , \tag{103}$$

$$\overline{\mathbf{\Omega}}_k = A(t)(\overline{\Omega}_{k,1}, ..., \overline{\Omega}_{k,M}) , \ k = 1, ..., N , \tag{104}$$

with $A(t) \equiv \int dE \exp(-i\Delta E_k t) f(E)$.

The derivation of Eqs. (102–104) invokes the slowly varying continuum approximation (SVCA) [253] ("flat" continuum approximation), according to which the Rabi frequencies $\Omega_{k,\ell}^{E}$ are approximated as $\Omega_{k,\ell}^{E} \approx \overline{\Omega}_{k,\ell} = \vec{\mu}_{k,\ell}(\bar{E}) \cdot \vec{\mathcal{E}}_k / 2\hbar$, with $\bar{E}$ being the continuum energy at the pulse center $\bar{E} = E_k/\hbar - \omega_k$.

We can achieve *complete* population transfer by choosing $M = N$ and applying the pulses in the "counter-intuitive" order (where the Stokes $\vec{\mathcal{E}}_k$ pulse precedes the pump $\vec{\mathcal{E}}_{0,k}$ pulse), *provided* $\mathbf{H}_E$ is a regular matrix. In that case $\mathcal{D} \equiv \det(\mathbf{H}_E) \neq 0$ and the Hamiltonian $\underline{\underline{H}}(t)$ has only one zero eigenvalue, whose ("null") eigenvector is given as $\mathbf{d} \equiv (1,\mathbf{0},\mathbf{x})^{\mathrm{T}}$, where $\mathbf{0}$ denotes an N-dimensional zero vector and $\mathbf{x}$ is an N-dimensional vector given as $\mathbf{x} = -\mathbf{H}_E^{-1}\mathbf{\Omega}_0^\dagger$. Direct operation by $\underline{\underline{H}}(t)$ on $(1,\mathbf{0},\mathbf{x})^{\mathrm{T}}$ confirms the identity of $\mathbf{d}$ as a null eigenvector.

Choosing the $\mathbf{\Omega}_0^\dagger$ vector of Eq. (103) to be proportional to the ℓth column of $\mathbf{H}_E$, e.g., $\Omega_{0,i}^* \propto \overline{\Omega}_{i,\ell}$, causes $\mathbf{d}$ to correlate initially (at $t = 0$) with the $|0\rangle$ state and to correlate finally with $\beta_\ell(t_{\mathrm{end}})$ of a *single* channel. Due to the linearity of our time-dependent ODE, the choice

$$\Omega_{0,i}^* \propto \sum_{k=1}^{M} a_k^* \overline{\Omega}_{i,k}, \ i = 1, ..., N \tag{105}$$

leads in creating at the end of the process the superposition state $\sum_{\ell=1}^{M} a_\ell f(E)|E^{(-\ell)}\rangle$. We also note that since the $A(t)$ factor appears during the transfer process in the $\mathbf{\Omega}_0^\dagger$ control fields, as well as in the $\mathbf{H}_E^{-1}$ matrix, it is effectively canceled out, thus rendering the transfer robust with respect to the exact functional form of $f(E)$.
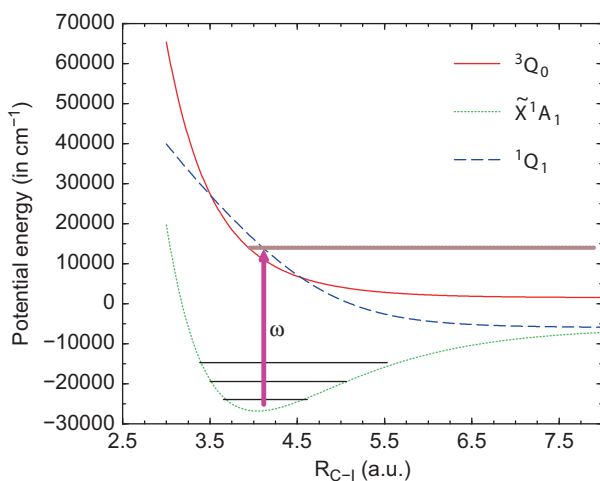
Figure 3.21 A schematic depiction of the PD of CH$_3$I: A rovibrational state of the electronic ground state $\tilde{X}^1A_1$ is excited by a photon of frequency ω to energetically degenerate continuum states of the coupled anti-binding $^1Q_1$ and $^3Q_0$ electronic states. Taken from Ref. [249].

We now demonstrate the use of Eq. (105) for the control of the PD of CH$_3$I initially in its electronic ground state $\tilde{X}^1A_1$ to yield a vibrationally excited CH$_3$ and a ground and excited iodine atom

$$\text{CH}_3(v) + \text{I}^*(^2P_{1/2}) \leftarrow \text{CH}_3\text{I} \rightarrow \text{CH}_3(v) + \text{I}(^2P_{3/2}) , \qquad (106)$$

where v denotes the CH$_3$ umbrella-mode vibration. The process takes place via the $^3Q_0$ and $^1Q_1$ excited electronic surfaces [254], as shown in Fig. 3.21, which correlate with iodine in the excited I*($^2P_{1/2}$) and ground I($^2P_{3/2}$) states, respectively.

In the calculation we have treated CH$_3$I as a pseudo-triatomic molecule [254]. It is viewed as a rotating linear molecule composed of the I, C, and H$_3$ groups, with the $\tilde{X}^1A_1$, $^3Q_0$, and $^1Q_1$ potential energy surfaces being functions of the R_{CI} bond length ("CI stretching mode") and the distance R_{CH3} of the C atom from the H$_3$ plane ("CH$_3$ umbrella mode"). In this model, we denote the states as $|J,v_{CI},v\rangle$, where J designates the total angular momentum, and v_{CI} and v are the number of vibrational quanta in the stretching and umbrella modes, respectively. All other vibrational modes are assumed frozen.

We consider the PD of CH$_3$I by a multipath two-photon process from the $|0,0,0\rangle \equiv |0\rangle$ of the $\tilde{X}^1A_1$ surface via excited states $|1,v_{CI},v\rangle$ of the same surface. The $|J,v_{CI},v\rangle$ states on the $\tilde{X}^1A_1$ surface are obtained using the potential surface of Ref. [254] within the rigid-rotor approximation; the corresponding

transition moments are calculated using an electric dipole surface obtained by *ab initio* methods. The transition moments between different electronic states are obtained as in Ref. [254]. According to our calculations, there are 10 such states with $0 < v_{CI}, v_{CH3} < 5$ that are connected to the $|0\rangle$ state by nonnegligible electric dipole matrix elements, and we use all of them as intermediate $|k\rangle$ states of the process. The dissociation of CH_3I from the $|k\rangle$ states to an overall continuum energy of $E = 38\,465\,\text{cm}^{-1}$ above E_0, the energy of the $|0\rangle$ state, takes place further. At energy E, the CH_3 can be formed in up to eight umbrella-mode vibrational states ($v_{CH3} = 0,...,7$) of each of the $^3Q_0$ and $^1Q_1$ electronic states. We also refer to Ref. [249] for further details.

We study the performance of our *approximative* analytic solution of Eq. (105) in different cases, including the presence of "satellites," by comparison to numerical solution of the "exact" Eqs. (97) within the SVCA [251],

$$
\begin{aligned}
\dot{b}_0 &= i\sum_{k=1}^{N}\Omega_{0,k}b_k, \\
\dot{b}_k &= i\Omega_{0,k}^{*}b_0 - \frac{\pi}{\hbar}\sum_{\ell=1}^{M}\sum_{m=1}^{M}G_{k,\ell}^{m}b_m, \\
b_E^{\ell}(t) &= i\sum_{k=1}^{M}\int dt'\,\Omega_{k,\ell}^{E*}(t')b_k(t')\,e^{i\Delta E_k t'},
\end{aligned}
\tag{107}
$$

with $G_{k,\ell}^{m}(t) \equiv \overline{\Omega}_{k,\ell}(t)\,\overline{\Omega}_{\ell,m}^{*}(t)$.

We first demonstrate complete and selective population transfer when the number of intermediate states $N = 10$ is equal to the number M of continuum channels $|E^{(-\ell)}\rangle$ ($\ell = 1,...,10$), ideally when all "satellites" are neglected. In doing so we can safely ignore the higher umbrella-mode $\ell = 6$–8,14–16 channels, whose transition moments from the intermediate states were computed to be much smaller [249] than for the lower $\ell = 1,...,5$ and $\ell = 9,...,13$ channels. The forms of the pump and Stokes pulses used are $\Omega_{0,k}^{max}\exp\left(-(t-\tau)^2/\tau^2\right)$ and $\Omega_{k,\ell}^{max}\exp\left(-t^2/\tau^2\right)$, respectively, with $\tau \approx 2\,\text{ns}$ and $|\Omega_{0,k}^{max}| = |\Omega_{k,\ell}^{max}| \approx 0.01\,\text{ps}^{-1}$.

The $P_\ell(t_{end}) = \int dE\,|b_E^{\ell}(E,t_{end})|^2$ ($\ell = 1,...,10$) final channel population for a control pulse given by $\Omega_{0,i}^{*} = 0.5^{\frac{1}{2}}\overline{\Omega}_{i,1} + 0.3^{\frac{1}{2}}\overline{\Omega}_{i,2} + 0.15^{\frac{1}{2}}\overline{\Omega}_{i,3} + 0.05^{\frac{1}{2}}\overline{\Omega}_{i,4}$ ($i = 1,...,N$) is shown in panel (a) of Figure 3.22. As anticipated, the final populations correspond exactly to the composition of the control pulse used, when Eq. (102) is used. In panel (c) of the same figure, we present $P_\ell(t_{end})$ ($\ell = 1,...,10$) for the same control field obtained by solving the "exact" Eqs. (97); we see that the control field derived for use with Eq. (102) performs extremely well even when the "exact" Eqs. (107) are used: the results in panel (a) and panel (c) of Figure 3.22 are practically identical.
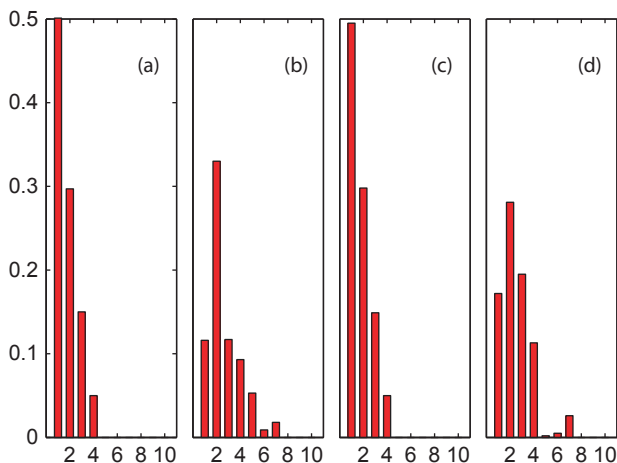
Figure 3.22   The PD of CH$_3$I at $E = 38\,465\,\text{cm}^{-1}$, with $N = 10$ and $\Omega_{0,i}^* = 0.5^{\frac{1}{2}}\overline{\Omega}_{i,1} + 0.3^{\frac{1}{2}}\overline{\Omega}_{i,2} + 0.15^{\frac{1}{2}}\overline{\Omega}_{i,3} + 0.05^{\frac{1}{2}}\overline{\Omega}_{i,4}$ $(i = 1,...,N)$. (a) $P_\ell(t_{\text{end}})$ $(\ell = 1,...,N)$, using Eq. (102), of the first five channels of the $^1Q_1$ and the first five channels of the $^3Q_0$ electronic states. (b) As in (a) but including also the $N(N-1)$ "satellites." (c–d) As in (a) and (b), respectively, using the "exact" Eqs. (107). Taken from Ref. [249].

When we take into account the strongest "satellites" related to the $N = 10$ intermediate states, which in our case correspond to $N(N-1)$ combinations of one pump photon and one Stokes photon with total energy $E \neq 38\,465\,\text{cm}^{-1}$, the degree of control is diminished. In panels (b) and (d) of Figure 3.22, we present the populations $P_\ell(t_{\text{end}})$ $(\ell = 1,...,10)$ obtained using Eq. (102) and the "exact" Eqs. (107) including the above "satellites" for the same control field as in panels (a) and (c). In both cases, the completeness and the selectivity of the transfer to the M degenerate channels are being *degraded*, with completeness being affected more than selectivity; the population transferred is diminished about 40–50% due to the presence of numerous "satellites." However, the results in panels (b) and (d) are very similar.

Lastly, we study the PD control including all $M = 16$ degenerate channels in the $^1Q_1$ and $^3Q_0$ electronic surfaces accessible from the chosen $N = 10$ intermediate states. In Figure 3.23, we present the P_ℓ $(\ell = 1,...,16)$ using Eq. (102) (panel (a)) and the "exact" Eqs. (107) (panel (c)), for $\ell = 1,...,16$ different control fields, with corresponding components $\Omega_{0,i}^* = \overline{\Omega}_{i,\ell}$ $(i = 1,...,10)$ in the absence of "satellites," where a completely filled diagonal indicates perfectly selective PD control. In both cases, the completeness and the selectivity of the transfer are adequate, but not 100% due to the fact that $N \neq M$. As before, inclusion of the $N(N-1)$ "satellites" in the transfer, shown in panels (b)
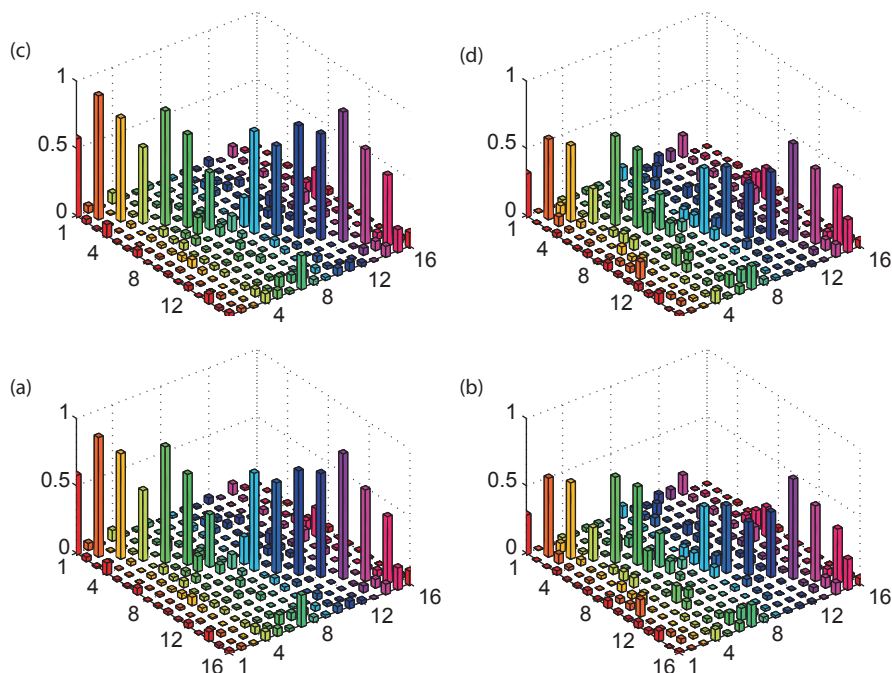
Figure 3.23 The PD of CH_3I at $E = 38\,465\ \text{cm}^{-1}$ with $N = 10$ and $M = 16$, for $\ell = 1,...,16$ control fields, with corresponding components $\Omega^*_{0,i} = \overline{\Omega}_{i,\ell}$ ($i = 1,...,10$): (a) $P_\ell(t_{\text{end}})$, using Eq. (102), for eight channels ($\ell = 1,...,8$) of the $^1Q_1$ and eight channels ($\ell = 9,...,16$) of the $^3Q_0$ electronic states. (b) As in (a) but including $N(N-1)$ "satellites" in the transfer process, as well. (c–d) As in (a) and (b), respectively, but using the "exact" Eqs. (107). Taken from Ref. [249].

and (d) of Figure 3.23 for control fields as in panels (a) and (c), degrades the completeness of the transfer further, about 50% with respect to the results of panels (a) and (c), respectively; as before, the selectivity is much less affected by the presence of the "satellites."

6. SUMMARY

In this review we have tried to demonstrate the uniformity of such phenomena as LICS, EIT, and AP via a continuum. Our focus has been on coherence effects in situation involving (multiple) structured continua. We have also discussed the merging of the CC and AP methods and their use in controlling population transfer to multi-channel continua. We have discussed

recent advances in coherent population trapping via LICS and in generalized STIRAP schemes including continua. Clearly, the research area related to (radiation-induced) structures in continua is a very active field, which is linked to various sub-disciplines in physics, chemistry, and material science.

ACKNOWLEDGMENTS

REFERENCES

[1] P.E. Coleman, P.L. Knight, K. Burnett, Laser-induced continuum structure in multi-photon ionization, Opt. Commun. 42 (1982) 171.

[2] P.L. Knight, M.A. Lauder, B.J. Dalton, Laser-induced continuum structure, Phys. Rep. 190 (1990) 1.

[3] U. Fano, Effects of configuration interaction on intensities and phase shifts, Phys. Rev. 124 (1961) 1866.

[4] Y.I. Heller, A.K. Popov, Formation of narrow nonlinear resonances in continuum, Sov. J. Quantum Electron. 6 (1976) 606.

[5] H. Feshbach, A unified theory of nuclear reactions. II, Ann. Phys. (New York) 19 (1962) 287; The unified theory of nuclear reactions : III. Overlapping resonances, 43 (1967) 410.

[6] H. Beutler, Über Absorptionsspektren aus der Anregung innerer Elektronen, Z. Phys. 86 (1933) 495.

[7] H. Beutler, Über Absorptionsserien von Argon, Krypton und Xenon zu Termen zwischen den beiden Ionisierungsgrenzen $^2P_3^{2/0}$ und $^2P_1^{2/0}$, Z. Phys. 93 (1935) 177.

[8] S. Feneneuille, S. Liberman, E. Luc-Koenig, J. Pinard, A. Taleb, Field-induced stabilisation of Stark states in the rubidium atom, J. Phys. B 15 (1982) 1205.

[9] E.B. Saloman, J.W. Cooper, D.E. Kelleher, Electric-field induced interferences in autoionizing resonances, Phys. Rev. Lett. 55 (1985) 193.

[10] G.S. Agrawal, J. Cooper, S.L. Haan, P.L. Knight, Isomorphism of dc-field-induced interference and laser-induced effects in autoionization, Phys. Rev. Lett. 56 (1986) 2586.

[11] F.H. Mies, M. Krauss, Time-dependent behavior of activated molecules. High-pressure unimolecular rate constant and mass spectra, J. Chem. Phys. 45 (1966) 4455.

[12] H. Lefebvre-Brion, R.W. Field, Perturbations in the spectra of diatomic molecules, Academic Press, London, 1986.

[13] S.E. Harris, Lasers without inversion: Interference of lifetime-broadened resonances, Phys. Rev. Lett. 62 (1989) 1033.

[14] S.E. Harris, J.E. Field, A. Immamoglu, Nonlinear optical processes using electromagnetically induced transparency, Phys. Rev. Lett. 64 (1992) 1107.

[15] M.O. Scully, From lasers and masers to phaseonium and phasers, Phys. Rep. 219 (1992) 191.

[16] L.V. Hau, S.E. Harris, Z. Dutton, C.H. Behroozi, Light speed reduction to 17 metres per second in an ultracold atomic gas, Nature 397 (1999) 594.

[17] M.M. Kash, V.A. Sautenkov, A.S. Zibrov, L. Hollberg, G.R. Welch, M.D. Lukin, et al., Ultraslow group velocity and enhanced nonlinear optical effects in a coherently driven hot atomic gas, Phys. Rev. Lett. 82 (1999) 5229.

[18] M.D. Lukin, Trapping and manipulating photon states in atomic ensembles, Rev. Mod. Phys. 75 (2003) 457.

[19] M. Fleischahuer, A. Immamoglu, J.P. Marangos, Electromagnetically induced transparency: Optics in coherent media, Rev. Mod. Phys. 77 (2005) 633.

[20] J. Oreg, F.T. Hioe, J.H. Eberly, Adiabatic following in multilevel systems, Phys. Rev. A 29 (1984) 690.

[21] U. Gaubatz, P. Rudecki, S. Sciemann, K. Bergmann, Population transfer between molecular vibrational levels by stimulated Raman scattering with partially overlapping laser fields. A new concept and experimental results, J. Chem. Phys. 92 (1990) 5363.

[22] K. Bergmann, H. Theuer, B.W. Shore, Coherent population transfer among quantum states of atoms and molecules, Rev. Mod. Phys. 70 (1998) 1003.

[23] N.V. Vitanov, M. Fleishhauer, B.W. Shore, K. Bergmann, Coherent manipulation of atoms and molecules by sequential laser pulses, Adv. At. Mol. Opt. Phys. 46 (2001) 55.

[24] P. Brumer, M. Shapiro, Control of unimolecular reactions using coherent light, Chem. Phys. Lett. 126 (1986) 541.

[25] M. Shapiro, P. Brumer, Principles of quantum control of molecular processes, Wiley-Interscience, New York, 2003.

[26] P. Král, I. Thanopulos, M. Shapiro, Coherently controlled adiabatic passage, Rev. Mod. Phys. 79 (2007) 53.

[27] L. Armstrong, Jr., B.L. Beers, S. Feneuille, Resonant multiphoton ionization via the Fano autoionization formalism, Phys. Rev. A 12 (1975) 1903.

[28] P.E. Coleman, P.L. Knight, K. Burnett, Laser-induced continuum structure in multiphoton ionisation, Opt. Commun. 42 (1982) 171.

[29] P.L. Knight, M.A. Lauder, P.M. Radmore, B.J. Dalton, Making atoms transparent—Trapped superpositions, Acta Phys. Austriaca 56 (1984) 103.

[30] P.M. Radmore, P.L. Knight, 2-photon ionization—Interference and population trapping, Phys. Lett. A 102 (1984) 180.

[31] Z. Deng, Complete population trapping in 2-photon ionization, Phys. Lett. A 105 (1984) 43; Line narrowing and photoelectron trapping in multiphoton ionization spectroscopy, J. Opt. Soc. Am. B 1 (1984) 874.

[32] G. Alber, P. Zoller, Structure of autoionizing Rydberg series in strong laser fields: A multichannel-quantum-defect-theory approach, Phys. Rev. A 29 (1984) 2290.

[33] J.F. Kelly, J.P. Hessler, G. Alber, Experimental studies of three-photon ionization of Ba: Evidence of channel interference and Raman coupling, Phys. Rev. A 33 (1986) 3913.

[34] G. Alber, P. Zoller, Spin polarization by selective laser-induced interference, Phys. Rev. A 27 (1983) 1713.

[35] R. Parzynski, Fine-splitted autoionizing-like resonance-spectrum, Phys. Lett. A 130 (1988) 476; Raman-type resonances in 2-laser multiphoton ioanization, J. Phys. B 20 (1987) 57; Raman-enhanced multiphoton ionization, 5035.

[36] B. Dai, P. Lambropoulos, Laser-induced autoionizing-like behavior, population trapping, and stimulated Raman processes in real atoms, Phys. Rev. A 36 (1987) 5205.

[37] Z. Deng, J.H. Eberly, Double-resonance effects in strong-field autoionization, J. Opt. Soc. Am. B 1 (1984) 102.

[38] S.M. Barnett, A.M. Lane, Increase of mesomolecular formation by laser-induced resonances, J. Phys. B 21 (1988) L523.

[39] B. Richie, Third-harmonic generation from a laser-induced autoionizing level, Phys. Rev. A 31 (1985) 823; Laser probe of the atomic ionization continuum: Stimulated recombination into an excited state, Phys. Rev. A, 30 (1984) 1849.

[40] M.H. Nayfeh, W. Glab, Double-resonance via continuum states—Ionization quantum beats, Phys. Rev. A 25 (1982) 1619.

[41] Y.I. Heller, V.F. Lukinykh, A.K. Popov, V.V. Slabko, Experimental-evidence for a laser-induced auto-ionizing-like resonance in continuum, Phys. Lett. A 82 (1981) 4.

[42] Y.I. Heller, A.K. Popov, Non-linear polarization resonances in a continuum, Sov. Phys.— JETP 78 (1980) 506.

[43] S.S. Dimov, L.I. Pavlov, K.V. Stamenov, G.B. Altshuller, Non-linear optical susceptibility measurement of an autoionizing-like resonance in atoms, Opt. Quantum Electron. 15 (1983) 305.

[44] L.I. Pavlov, S.S. Dimov, D.I. Metchkov, G.M. Mileva, K.V. Stamenov, G.B. Altshuller, Efficient tunable tripler of optical frequency at an autoionizing-like resonance in a continuum, Phys. Lett. A 89 (1982) 441.

[45] P.O. Sorokin, J.J. Wayne, J.A. Armstrong, R.T. Hodgson, Resonantly enhanced, non-linear generation of tunable, coherent, vacuum, ultraviolet (VUV) light in atomic vapours, Ann. N. Y. Acad. Sci. 267 (1976) 30.

[46] R.R. Freeman, G.C. Bjorklund, N.P. Economou, P.F. Liao, J.E. Bjorkholm, Generation of cw VUV coherent radiation by four-wave sum frequency mixing in Sr vapor, Appl. Phys. Lett. 33 (1978) 739.

[47] J.R Taylor, Third harmonic generation and four-wave parametric mixing in sodium vapour, Opt. Commun. 18 (1976) 504.

[48] P.E. Coleman, J.N. Elgin, P.L. Knight, K. Burnett, in: Quantum electronics, P.L. Knight (Ed.), Wiley, New York, 1983, p. 359.

[49] D. Feldman, G. Otto, D. Petring, K.H. Welge, Resonances in the multiphoton ionisation spectrum of sodium atoms induced by a second strong laser field, J. Phys. B 19 (1986) 269.

[50] M.H.R. Hutchinson, K.M.M. Ness, Laser-induced continuum structure in xenon, Phys. Rev. Lett. 60 (1988) 105.

[51] X. Tang, A. L'Huiller, P. Lambropoulos, Comment on "Laser-induced continuum structure in xenon", Phys. Rev. Lett. 62 (1989) 111.

[52] M.H.R. Hutchinson, K.M.M. Ness, Reply on comment on "Laser-induced continuum structure in xenon", Phys. Rev. Lett. 62 (1989) 112.

[53] Y.L. Shao, D. Charalambidis, C. Fotakis, J. Zhang, P. Lambropoulos, Observation of laser-induced continuum structure in ionization of sodium, Phys. Rev. Lett. 67 (1991) 3669.

[54] S. Cavalieri, F.S. Pavone, M. Matera, Observation of a laser-induced resonance in the photoionization spectrum of sodium, Phys. Rev. Lett. 67 (1991) 3673.

[55] J. Zhang, P. Lambropoulos, Laser-induced continuum structure and third-harmonic generation in sodium: Theory and calculations, Phys. Rev. A 45 (1992) 489.

[56] S. Cavalieri, R. Eramo, L. Fini, R. Buffa, Effect of incoherent processes on laser-induced continuum structures, J. Phys. B 28 (1995) L637.

[57] R. Eramo, S. Cavalieri, L. Fini, M. Matera, L.F. DiMauro, Observation of a laser-induced structure in the ionization continuum of sodium atoms using photoelectron energy spectroscopy, J. Phys. B 30 (1997) 3789.

[58] K.G.H. Baldwin, M.D. Bott, H.-A. Bachor, P.B. Chapple, Third-harmonic generation and laser-induced continuum structure in sodium, J. Opt. B 2 (2000) 470.

[59] K. Böhmer, T. Halfmann, L.P. Yatsenko, D. Charalambidis, A. Horsmans, K. Bergmann, Laser-induced continuum structure in the two ionization continua of xenon, Phys. Rev. A 66 (2002) 013406.

[60] A.N. Grum-Grzhimailo, E.V. Gryzlova, A.I. Magunov, S.I. Strakhova, Laser-induced effects for overlapping autoionizing Rydberg states of xenon, Opt. Spectrosc., 100 (2006) 517.

[61] A. Lyras, X. Tang, P. Lambropoulos, Radiation amplification in free-bound transitions through incoherent multiphoton pumping and stimulated recombination, Opt. Commun. 92 (1992) 355.

[62] S. Cavalieri, M. Matera, F.S. Pavone, J. Zhang, P. Lambropoulos, T. Nakajima, High-sensitivity study of laser-induced birefringence and dichroism in the ionization continuum of cesium, Phys. Rev. A 47 (1993) 4219.

[63] O. Faucher, D. Charalambidis, C. Fotakis, J. Zhang, P. Lambropoulos, Control of laser induced continuum structure in the vicinity of autoionizing states, Phys. Rev. Lett. 70 (1993) 3004.

[64] O. Faucher, Y.L. Shao, D. Charalambidis, Modification of a structured continuum through coherent interactions observed in third harmonic generation, J. Phys. B 26 (1993) L309.

[65] O. Faucher, Y.L. Shao, D. Charalambidis, C. Fotakis, Laser-induced modification of a structured continuum observed in ionization and harmonic generation, Phys. Rev. A 50 (1994) 641.

[66] O. Faucher, D. Charalambidis, C. Fotakis, Laser control of third-harmonic generation by means of an additional EM field, Opt. Quantum. Electron. 28 (1996) 291.

[67] D. Charalambidis, O. Faucher, N.E. Karapanagioti, Y.L. Shao, C.J.G.J. Uiterwaal, D. Xenakis, Light induced modification of continua and ionization dynamics, Phys. Scr., T72 (1997) 41.

[68] N.E. Karapanagioti, O. Faucher, C.J.G.J. Uiterwaal, D. Charalambidis, H. Bachau, I. Sanchez, et al., Investigation of a two-autoionizing-level system coupled by a strong laser field, J. Mod. Opt. 43 (1996) 953.

[69] T. Halfmann, L.P. Yatsenko, M. Shapiro, B.W. Shore, K. Bergmann, Population trapping and laser-induced continuum structure in helium: Experiment and theory, Phys. Rev. A 58 (1998) R46.

[70] O. Faucher, E. Hertz, B. Lavorel, R. Chaux, T. Dreier, H. Berger, et al., Observation of laser-induced continuum structure in the NO molecule, J. Phys. B 32 (1999) 4485.

[71] M. Dörr, R.M. Potvliege, D. Proulx, R. Shakeshaft, Multiphoton processes in an intense laser field. VI. Two-color ionization with incommensurable frequencies, Phys. Rev. A 44 (1991) 574.

[72] J.R. Kuklinski, M. Lewenstein, T.W. Mossberg, Laser-induced photonic-continuum structure, Phys. Rev. A 48 (1993) 764.

[73] R. Parzynski, A. Wojcik, J. Schmidt, Multilevel light-induced continuum structure: Strong-probe and stabilization effects, Phys. Rev. A 50 (1994) 3285; Multilevel light-induced continuum structure: limitations of adapted Fano theory, J. Opt. Soc. Am. B 11 (1994) 644.

[74] B.J. Dalton, M.E.StJ. Dutton, Laser-induced continuum structures and above-threshold ionization, J. Mod. Opt. 41 (1994) 1099.

[75] S.-M. Wang, S.-L. Cong, K.-J. Yuan, Y.-Y. Niu, Photoionization of NO molecule in two-color femtosecond pulse laser fields, Chem. Phys. Lett. 417 (2006) 164.

[76] R. Buffa, Laser-induced autoionization of transient molecules, Phys. Rev. A 46 (1992) R1171.

[77] R. Buffa, Laser-induced resonances in ionizing radiative collisions, Opt. Commun. 128 (1996) 30.

[78] N.J. Kylstra, E. Paspalakis, P.L. Knight, Laser-induced continuum structure in helium: Ab initio non-perturbative calculations, J. Phys. B 31 (1998) L719.

[79] H.W. van der Hart, R-matrix Floquet theory of multiphoton processes: VII. A two-colour approach, J. Phys. B 29 (1996) 2217.

[80] A. Cyr, O. Latinne, P.G. Burke, R-matrix Floquet theory of multiphoton processes: IX. Three-photon laser-induced degenerate states in argon, J. Phys. B 30 (1997) 659.

[81] H.W. van der Hart, L. Feng, Multiphoton ionization processes in Ar^{7+}, J. Phys. B 35 (2002) 1185.

[82] C.J. Joachain, R-matrix-Floquet theory of multiphoton processes: Concepts, results and perspectives, J. Mod. Opt. 54 (2007) 1859.

[83] S.M. Sadeghi, J. Meyer, H. Rastegar, Laser-induced transparency and dark-line effects caused by three-wave mixing in atomic systems, Phys. Rev. A 56 (1997) 3097.

[84] S.M. Sadeghi, J. Meyer, Two-field electromagnetically induced transparency and switching between ultranarrow absorption and gain features in rubidium atoms, Phys. Rev. A 59 (1998) 3998.

[85] M.P. Anscombe, R. de Nalda, I. Kucukkara, J.P. Marangos, Role of atomic coherence effects in four-wave mixing using autoionizing resonances, Phys. Rev. A 68 (2003) 043810.

[86] M. Shapiro, Electromagnetically induced transparency with structured multicontinua, Phys. Rev. A 75 (2007) 013424.

[87] A. Raczynski, M. Rzepecka, J. Zaremba, S. Zielinska-Kaniasty, Electromagnetically induced transparency and light slowdown for Λ-like systems with a structured continuum, Opt. Commun. 266 (2006) 552.

[88] S. Cavalieri, R. Eramo, L. Fini, M. Materazzi, O. Faucher, D. Charalambidis, Controlling ionization products through laser-induced continuum structure, Phys. Rev. A 57 (1998) 2915.

[89] A. Shnitman, I. Sofer, I. Golub, A. Yogev, M. Shapiro, Z. Chen, et al., Experimental observation of laser control: electronic branching in the photodissociation of Na_2, Phys. Rev. Lett. 76 (1996) 2886.

[90] T. Nakajima, L.A.A. Nikolopoulos, Role of spin-orbit interaction in the production of spin-polarized photoelectrons using a dressing laser, Phys. Rev. A 68 (2003) 013413.

[91] T. Nakajima, G. Buica, Modification of the photoelectron angular distribution through laser-induced continuum structure, Phys. Rev. A, 71 (2005) 013413; Effects of laser polarization on photoelectron angular distribution through laser-induced continuum structure, Phys. Rev. A, 72 (2005) 053416.

[92] A.N. Grumm-Grzhimailo, A.D. Kondorskiy, K. Bartschat, Controlling the angular distribution of atomic photoelectrons in the region of laser-induced continuum structure in the femtosecond time domain, J. Phys. B 39 (2006) 4659.

[93] E. Paspalakis, M. Protopapas, P.L. Knight, Time-dependent pulse and frequency effects in population trapping via the continuum, J. Phys. B 31 (1997) 775.

[94] T.-M. Yan, Y.-C. Han, K.-J. Yuan, S.-L. Cong, Steering population transfer via continuum structure of the Li_2 molecule with ultrashort laser pulses, Chem. Phys. 348 (2008) 39.

[95] R.G. Unanyan, N.V. Vitanov, B.W. Shore, K. Bergmann, Coherent properties of a tripod system coupled via a continuum, Phys. Rev. A 61 (2000) 043408.

[96] L.P. Yatsenko, V.I. Romanencko, B.W. Shore, T. Halfmann, K. Bergmann, Two-photon excitation of the metastable 2s state of hydrogen assisted by laser-induced chirped Stark shifts and continuum structure, Phys. Rev. A 71 (2005) 033418.

[97] A.A. Rangelov, N.V. Vitanov, E. Arimondo, Stimulated Raman adiabatic passage into continuum, Phys. Rev. A 76 (2007) 043414.

[98] G.-X. Li, J.-S. Peng, P. Zhou, Effects of laser phases on photoionization and coherent population trapping in a two-channel ionization system, J. Mod. Opt. 44 (1996) 505.

[99] G.-X. Li, J.-S. Peng, Coherent population trapping in multilevel laser-induced continuum structure system, Opt. Commun. 138 (1997) 59.

[100] M.V. Fedorov, N.P. Poluektov, Two-color interference stabilization of atoms, Phys. Rev. A 69 (2004) 033404.

[101] L. Yatsenko, T. Halfmann, B. Shore, K. Bergmann, Photoionization suppression by continuum coherence: Experiment and theory, Phys. Rev. A 59 (1999) 2926.

[102] S.E. Harris, J. E. Field, A. Imamoglu, Nonlinear optical processes using electromagnetically induced transparency, Phys. Rev. Lett. 64 (1990) 1107.

[103] M.D. Lukin, P. Hemmer, M.O. Scully, Resonant nonlinear optics in phase-coherent media, Adv. At. Mol. Opt. Phys. 42 (2000) 347.

[104] A.B. Matsko, O. Kocharovskaya, Y. Rostovtsev, G.R. Welch, M.O. Scully, Slow, ultraslow, stored, and frozen light, Adv. At. Mol. Opt. Phys. 46 (2001) 191.

[105] M. Fleischhauer, A. Imamoglu, J.P. Marangos, Electromagnetically induced transparency: Optics in coherent media, Rev. Mod. Phys. 77 (2005) 633.

[106] S.E. Harris, Electromagnetically induced transparency, Phys. Today 50 (1997) 36.

[107] S.H. Autler, C.H. Townes, Stark effect in rapidly varying fields, Phys. Rev. 100 (1955) 703.

[108] R.D. Levine, *Quantum Mechanics of Molecular Rate Processes,* Clarendon Press, Oxford, UK, 1969.

[109] M. Shapiro, Dynamics of dissociation. I. Computational investigation of unimolecular breakdown processes, J. Chem. Phys. 56 (1972) 2582.

[110] M. Shapiro, Uniform theory of preparation, dissociation, and product formation in the decay of overlapping resonances, J. Phys. Chem. A 102 (1998) 9570.

[111] G. Alzetta, A. Gozzini, L. Moi, G. Orriols, Experimental-method for observation of rf transitions and laser beat resonances in oriented Na vapour, Nuovo Cimento Soc. Ital. Fis. B 36 (1976) 5.

[112] E. Arimondo, G. Orriols, Non-absorbing atomic coherences by coherent 2-photon transitions in a 3-level optical pumping, Lett. Nuovo Cimento Soc. Ital. Fis. 17 (1976) 333.

[113] O.A. Kocharovskaya, Y.I. Khanin, Coherent amplification of an ultrashort pulse in a 3-level medium without a population-inversion, JETP Lett., 48 (1988) 630; M.O. Scully, S. Zhu, A. Gavrielides, Degenerate quantum-beat laser: Lasing without inversion and inversion without lasing, Phys. Rev. Lett. 62 (1989) 2813.

[114] M.O. Scully, M.S. Zubairy, Quantum Optics, Cambridge University Press, Cambridge, 1997.

[115] B.W. Shore, Examples of counter-intuitive physics, Contemp. Phys. 36 (1995) 15.

[116] V. Weisskopf, E.P. Wigner, Berechnung der natürlichen Linienbreite auf Grund der Diracschen Lichttheorie, Z. Phys. 63 (1930) 54.

[117] M. Shapiro, R. Bersohn, Theories of the dynamics of photo-dissociation, Ann. Rev. Phys. Chem. 33 (1982) 409.

[118] K.C. Friedrichs, On the perturbation of continuous spectra, Comm. Pure Appl. Math. 1 (1948) 361.

[119] M.S. Bigelow, Superluminal and slow light propagation in a room-temperature solid, Science 301 (2003) 200.

[120] D.J. Tannor, R. Kosloff, S.A. Rice, Coherent pulse sequence induced control of selectivity of reactions: Exact quantum mechanical calculations, J. Chem. Phys. 85 (1986) 5805.

[121] R. Kosloff, S.A. Rice, P. Gaspard, S. Tersigni, D.J. Tannor, Wavepacket dancing: Achieving chemical selectivity by shaping light pulses, Chem. Phys. 139 (1989) 201.

[122] S.A. Rice, M. Zhao, Optical Control of Molecular Dynamics, Wiley, New York, 2000.

[123] A.P. Peirce, M.A. Dahleh, H. Rabitz, Optimal control of quantum-mechanical systems: Existence, numerical approximation, and applications, Phys. Rev. A 37 (1998) 4950.

[124] S. Judson, H. Rabitz, Teaching lasers to control molecules, Phys. Rev. Lett. 68 (1992) 1500.

[125] D.G. Grischkowski, M.M.T. Loy, P.F. Liao, Adiabatic following model for two-photon transitions: Nonlinear mixing and pulse propagation, Phys. Rev. A 12 (1975) 2514.

[126] A.M. Weiner, J.P. Heritage, Picosecond and femtosecond Fourier pulse shape synthesis, Rev. Phys. Appl. 22 (1987) 1619.

[127] A.M. Weiner, D.E. Leiard, G.P. Wiederrecht, K.A. Nelson, Femtosecond pulse sequences used for optical manipulation of molecular-motion, Science 247 (1990) 1317.

[128] A.M. Weiner, Femtosecond pulse shaping using spatial light modulators, Rev. Sci. Instrum. 71 (2000) 1921.

[129] M. Haner, W.S. Warren, Synthesis of crafted optical pulses by time domain modulation in a fiber-grating compressor, Appl. Phys. Lett. 52 (1988) 1459.

[130] C.W. Hillegas, J.X. Tull, D. Goswami, D. Strickland, W.S. Warren, Femtosecond laser pulse shaping by use of microsecond radio-frequency pulses, Opt. Lett. 19 (1994) 737.

[131] J. Peřina, Quantum Statistics of Linear and Nonlinear Phenomena, D. Riedl, Dordrecht, Boston, 1984.

[132] C. Law, J. Eberly, Arbitrary control of a quantum electromagnetic field, Phys. Rev. Lett. 76 (1996) 1055.

[133] W. Schleich, M. Peringo, F.L. Kien, Nonclassical state from two pseudoclassical states, Phys. Rev. A 44 (1991) 2172.

[134] B. Yurke, D. Stoler, Generating quantum mechanical superpositions of macroscopically distinguishable states via amplitude dispersion, Phys. Rev. Lett. 57 (1986) 13.

[135] P. Král, Displaced and squeezed fock states, J. Mod. Opt. 37 (1990) 889.

[136] P. Král, Kerr interaction with displaced and squeezed Fock states, Phys. Rev. A 42 (1990) 4177.

[137] M. Shapiro, J.W. Hepburn, P. Brumer, Simplified laser control of unimolecular reactions: Simultaneous (ω_1,ω_3) excitation, Chem. Phys. Lett. 149 (1988) 451.

[138] C. Chen, Y.-Y. Yin, D. Elliot, Interference between optical transitions, Phys. Rev. Lett. 64 (1990) 507.

[139] Y.-Y. Yin, C. Chen, D.S. Elliott, A.V. Smith, Asymmetric photoelectron angular distributions from interfering photoionization processes, Phys. Rev. Lett. 69 (1992) 2353.

[140] S. Park, S.-P. Lu, R. Gordon, Coherent laser control of the resonance-enhanced multiphoton ionization of HCl, J. Chem. Phys. 94 (1991) 8622.

[141] S.-P. Lu, S. Park, Y. Xie, R. Gordon, Coherent laser control of bound-to-bound transitions of HCl and CO, J. Chem. Phys. 96 (1992) 6613.

[142] V. Kleiman, L. Zhu, X. Li, R. Gordon, Coherent phase control of the photoionization of H_2S, J. Chem. Phys. 102 (1995) 5863.

[143] L. Zhu, V. Kleiman, X. Li, S. Lu, K. Trentelman, R. Gordon, Coherent laser control of the product distribution obtained in the photoexcitation of HI, Science 270 (1995) 77.

[144] L. Zhu, K. Suto, J. Fiss, R. Wada, T. Seideman, R. Gordon, Effect of resonances on the coherent control of the photoionization and photodissociation of HI and DI, Phys. Rev. Lett. 79 (1997) 4108.

[145] R. Gordon, L.C. Zhu, T. Seideman, Coherent control of chemical reactions, Acc. Chem. Res. 32 (1999) 1007.

[146] X. Wang, R. Bersohn, K. Takahashi, M. Kawasaki, H. Kim, Phase control of absorption in large polyatomic molecules, J. Chem. Phys. 105 (1996) 2992.

[147] G. Kurizki, M. Shapiro, P. Brumer, Phase-coherent control of photocurrent directionality in semiconductors, Phys. Rev. B 39 (1989) 3435.

[148] R. Atanasov, A. Haché, L.P. Hughes, H.M. van Driel, J.E. Sipe, Coherent control of photocurrent generation in bulk semiconductors, Phys. Rev. Lett. 76 (1996) 1703.

[149] P. Král, D. Tománek, Laser-driven atomic pump, Phys. Rev. Lett. 82 (1999) 5373.

[150] V. Deyirmenjian, J. Sipe, Coherent control of the angular distribution of electrons photoemitted from metal surfaces, Phys. Rev. Lett. 82 (1999) 4942.

[151] P. Král, J. Sipe, Quantum kinetic theory of two-beam current injection in bulk semiconductors, Phys. Rev. B 61 (2000) 5381.

[152] B. Baranova, A. Chudinov, B.Y. Zel'dovitch, Polar asymmetry of photoionization by a field with $\langle E^3 \rangle \neq 0$. Theory and experiment, Opt. Commun. 79 (1990) 116.

[153] E. Dupont, P.B. Corkum, H.C. Liu, M. Buchanan, Z.R. Wasilewski, Phase-controlled currents in semiconductors, Phys. Rev. Lett. 74 (1995) 3596.

[154] B. Sheehy, B. Walker, L. DiMauro, Phase control in the two-color photodissociation of HD^+, Phys. Rev. Lett. 74 (1995) 4799.

[155] A. Haché, Y. Kostoulas, R. Atanasov, J.L.P. Hughes, J.E. Sipe, H.M. van Driel, Observation of coherently controlled photocurrent in unbiased, bulk GaAs, Phys. Rev. Lett. 78 (1997) 306.

[156] H. Xu, W. Pötz, Coherent manipulation of phonon emission rates in semiconductor heterostructures, Phys. Rev. Lett. 82 (1999) 3116.

[157] R. Bhat, J. Sipe, Optically injected spin currents in semiconductors, Phys. Rev. Lett. 85 (2000) 5432.

[158] E. Frishman, M. Shapiro, Complete suppression of spontaneous decay of a manifold of states by infrequent interruptions, Phys. Rev. Lett. 87 (2001) 253001.

[159] E. Frishman, M. Shapiro, Suppression of the spontaneous emission of atoms and molecules, Phys. Rev. A 68 (2003) 032717.

[160] S.-Y. Zhu, R. Chan, C. Lee, Spontaneous emission from a three-level atom, Phys. Rev. A 52 (1995) 710.

[161] S.-Y. Zhu, M. Scully, Spectral line elimination and spontaneous emission cancellation via quantum interference, Phys. Rev. Lett. 76 (1996) 388.

[162] S.-Y. Zhu, H. Chen, H. Huang, Quantum interference effects in spontaneous emission from an atom embedded in a photonic band gap structure, Phys. Rev. Lett. 79 (1997) 205.

[163] P.R. Berman, Analysis of dynamical suppression of spontaneous emission, Phys. Rev. A 58 (1998) 4886.

[164] F.-L. Li, S.-Y. Zhu, Resonance fluorescence quenching and spectral line narrowing via quantum interference in a four-level atom driven by two coherent fields, Phys. Rev. A 59 (1999) 2330.

[165] E. Paspalakis, P.L. Knight, Phase control of spontaneous emission, Phys. Rev. Lett. 81 (1998) 293.

[166] D. Yelin, D. Meshulach, Y. Silberberg, Adaptive femtosecond pulse compression, Opt. Lett. 22 (1997) 1793.

[167] N.D.B. Dayan, S.G. Faeder, Y. Silberberg, Transform-limited pulses are not optimal for resonant multiphoton transitions, Phys. Rev. Lett. 86 (2001) 47.

[168] B. Dayan, A. Pe'er, A.A. Friesem, Y. Silberberg, Two photon absorption and coherent control with broadband down-converted light, Phys. Rev. Lett. 93 (2004) 023005.

[169] J.-Y. Gao, S.-H. Yang, D. Wang, X.-Z. Guo, K.-X. Chen, Y. Jiang, et al., Electromagnetically induced inhibition of two-photon absorption in sodium vapor, Phys. Rev. A 61 (2000) 023401.

[170] G. Agarwal, W. Harshawardhan, Inhibition and enhancement of two photon absorption, Phys. Rev. Lett. 77 (1996) 1039.

[171] E. Paspalakis, S.-Q. Gong, P. Knight, Spontaneous emission-induced coherent effects in absorption and dispersion of a V-type three-level atom, Opt. Commun. 152 (1998) 293.

[172] S. Menon, G. Agarwal, Gain components in the Autler-Townes doublet from quantum interferences in decay channels, Phys. Rev. A 61 (1999) 013807.

[173] C. Ye, A. Zibrov, Y. Rostovtsev, A. Matsko, M. Scully, Three-photon electromagnetically induced absorption and transparency in an inhomogeneously broadened atomic vapour, J. Mod. Opt. 49 (2002) 2485.

[174] A. Zibrov, C. Ye, Y. Rostovtsev, A. Matsko, M. Scully, Observation of a three-photon electromagnetically induced transparency in hot atomic vapor, Phys. Rev. A 65 (2002) 043817.

[175] J. Hu, G. La Rocca, F. Basani, D. Wang, J. Gao, Electromagnetically induced one-photon and two-photon transparency in rubidium atoms, Opt. Commun. 216 (2003) 157.

[176] R.B. Kurzel, J.I. Steinfeld, Energy-transfer processes in monochromatically excited iodine molecules. III Quenching and multiquantum transfer from $v' = 43$, J. Chem. Phys. 53 (1970) 3293.

[177] K. Bergmann, W. Demtröder, Inelastic collision cross section of excited molecules. 1. Rotational energy transfer within B1IIu-state of Na_2 induced by collision with He, Z. Phys. 243 (1971) 1.

[178] F.F. Crim, Vibrationally mediated photodissociation—exploring excited state surfaces and controlling decomposition pathways, Annu. Rev. Phys. Chem. 44 (1993) 397.

[179] C. Parmenter, B. Stone, The methyl rotor as an accelerating functional group for IVR, J. Chem. Phys. 84 (1986) 4710.

[180] D. Moss, C. Parmenter, Acceleration of intramolecular vibrational redistribution by methyl internal rotation. A chemical timing study of *p*-fluorotoluene and *p*-fluorotoluene-d_3, J. Chem. Phys. 98 (1993) 6897.

[181] D. Borst, D. Pratt, Toluene: Structure, dynamics, and barrier to methyl group rotation in its electronically excited state. A route to IVR, J. Chem. Phys. 113 (2000) 3658.

[182] M. Quack, Spectra and dynamics of coupled vibrations in poly-atomic molecules, Annu. Rev. Phys. Chem. 41 (1990) 839.

[183] F.F. Crim, Selective excitation studies of unimolecular reaction dynamics, Annu. Rev. Phys. Chem. 35 (1984) 657.

[184] B.J. Orr, J.G. Haub, R. Haines, Time-resolved infrared-ultraviolet double resonance studies of rotational relaxation in D_2CO, Chem. Phys. Lett. 107 (1984) 168.

[185] W. Meier, G. Ahlers, H. Zacharias, State selective population of $H_2(v'' = 1, J'' = 1)$ and $D_2(v'' = 1, J'' = 2)$ and rotational relaxation in collisions with H_2, D_2, and He, J. Chem. Phys. 85 (1986) 2599.

[186] C. Kittrel, E. Abramson, J.L. Kinsey, S.A. McDonald, D.E. Reisner, R.W. Field, et al., Selective vibrational excitation by stimulated emission pumping, J. Chem. Phys. 75 (1981) 2056.

[187] U. Gaubatz, P. Rudecki, M. Becker, S. Schiemann, M. Külz, K. Bergmann, Population switching between vibrational levels in molecular beams, Chem. Phys. Lett. 149 (1988) 463.

[188] B.W. Shore, The theory of coherent atomic excitation, Vol. 1, John Wiley & Sons, New York, 1990.

[189] H. Theuer, K. Bergmann, Atomic beam deflection by coherent momentum transfer and the dependence on weak magnetic fields, Eur. Phys. J. D 2 (1998) 279.

[190] A. Kuhn, S. Steuerwald, K. Bergmann, Coherent population transfer in NO with pulsed lasers: the consequences of hyperfine structure, Doppler broadening and electromagnetically induced absorption, Eur. Phys. J. D 1 (1998) 57.

[191] T. Halfmann, K. Bergmann, Coherent population transfer and dark resonances in SO_2, J. Chem. Phys. 104 (1996) 7068.

[192] W. Süptitz, B.C. Duncan, P.L. Gould, Efficient 5D excitation of trapped Rb atoms using pulses of diode-laser light in the counterintuitive order, J. Opt. Soc. Am. B 14 (1997) 1001.

[193] J. Martin, B.W. Shore, K. Bergmann, Coherent population transfer in multilevel systems with magnetic sublevels. III. Experimental results, Phys. Rev. A 54 (1996) 1556.

[194] J.R. Kuklinski, U. Gaubatz, F.T. Hioe, K. Bergmann, Adiabatic population transfer in a three-level system driven by delayed laser pulses, Phys. Rev. A 40 (1989) 6741.

[195] N.V. Vitanov, S. Stenholm, Properties of stimulated Raman adiabatic passage with intermediate-level detuning, Opt. Commun. 135 (1997) 394.

[196] S. Guérin, H.R. Jauslin, Two-laser multiphoton adiabatic passage in the frame of the Floquet theory. Applications to (1+1) and (2+1) STIRAP, Eur. Phys. J. D 2 (1998) 99.

[197] L.P. Yatsenko, S. Guerin, T. Halfmann, B.W. Shore, K. Bergmann, Stimulated hyper-Raman adiabatic passage. I. The basic problem and examples, Phys. Rev. A 58 (1998) 4683.

[198] Y.B. Band, P.S. Julienne, Density matrix calculation of population transfer between vibrational levels of Na_2 by stimulated Raman scattering with temporally shifted laser beams, J. Chem. Phys. 94 (1991) 5291.

[199] Y.B. Band, P.S. Julienne, Complete alignment and orientation of atoms and molecules by stimulated Raman scattering with temporally shifted lasers, J. Chem. Phys. 96 (1992) 3339.

[200] B. Glushko, B. Kryzhanovsky, Radiative and collisional damping effects on efficient population transfer in a three-level system driven by two delayed laser pulses, Phys. Rev. A 46 (1992) 2823.

[201] M. Fleischhauer, A.S. Manka, Propagation of laser pulses and coherent population transfer in dissipative three-level systems: An adiabatic dressed-state picture, Phys. Rev. A 54 (1996) 794.

[202] N.V. Vitanov, S. Stenholm, Population transfer via a decaying state, Phys. Rev. A 56 (1997) 1463.

[203] G.W. Coulston, K. Bergmann, Population transfer by stimulated Raman scattering with delayed pulses: Analytical results for multilevel systems, J. Chem. Phys. 96 (1992) 3467.

[204] N.V. Vitanov, S. Stenholm, Adiabatic population transfer via multiple intermediate states, Phys. Rev. A 60 (1999) 3820.

[205] B.W. Shore, K. Bergmann, J. Oreg, S. Rosenwaks, Multilevel adiabatic population transfer, Phys. Rev. A 44 (1991) 7442.

[206] P. Marte, P. Zoller, J.L. Hall, Coherent atomic mirrors and beam splitters by adiabatic passage in multilevel systems, Phys. Rev. A 44 (1991) 4118.

[207] V.S. Malinovsky, D.J. Tannor, Simple and robust extension of the stimulated Raman adiabatic passage technique to N-level systems, Phys. Rev. A 56 (1997) 4929.

[208] C. Law, J. Eberly, Synthesis of arbitrary superposition of Zeeman states in an atom, Opt. Express 2 (1998) 368.

[209] T. Nakajima, Population transfer in N-level systems assisted by dressing fields, Phys. Rev. A 59 (1999) 559.

[210] T. Esslinger, F. Sander, M. Weidemüller, A. Hammerich, T.W. Hänsch, Subrecoil laser cooling with adiabatic transfer, Phys. Rev. Lett. 76 (1996) 2432.

[211] S. Kulin, B. Saubamea, E. Peik, J. Lawall, M. Leduc, C. Cohen-Tannoudji, Coherent manipulation of atomic wave packets by adiabatic transfer, Phys. Rev. Lett. 78 (1997) 4185.

[212] M.N. Kobrak, S.A. Rice, Coherent population transfer via a resonant intermediate state: The breakdown of adiabatic passage, Phys. Rev. A 57 (1998) 1158.

[213] M.N. Kobrak, S.A. Rice, Equivalence of the Kobrak-Rice photoselective adiabatic passage and the Brumer-Shapiro strong field methods for control of product formation in a reaction, J. Chem. Phys. 109 (1998) 1.

[214] M.N. Kobrak, S.A. Rice, Selective photochemistry via adiabatic passage: An extension of stimulated Raman adiabatic passage for degenerate final states, Phys. Rev. A 57 (1998) 2885.

[215] R. Unanyan, N. Vitanov, S. Stenholm, Suppression of incoherent ionization in population transfer via continuum, Phys. Rev. A 57 (1998) 462.

[216] H. Theuer, R.G. Unanyan, C. Habschied, K. Klein, K. Bergmann, Novel laser controlled variable matter wave beamsplitter, Opt. Express 4 (1999) 77.

[217] N.V. Vitanov, S. Stenholm, Population transfer by delayed pulses via continuum states, Phys. Rev. A 56 (1997) 741.

[218] C.E. Carroll, F.T. Hioe, Excitation using two lasers: Effects of continuum-continuum transitions, Phys. Lett. A 199 (1995) 145.

[219] L.P. Yatsenko, R.G. Unanyan, T. Halfmann, B.W. Shore, Population transfer through the continuum using laser-controlled Stark shifts, Opt. Commun. 135 (1997) 406.

[220] C.E. Carroll, F.T. Hioe, Selective excitation and structure in the continuum, Phys. Rev. A 54 (1996) 5147.

[221] S. Guérin, L.P. Yatsenko, T. Halfmann, B.W. Shore, K. Bergmann, Stimulated hyper-Raman adiabatic passage.II.Static compensation of dynamic Stark shifts, Phys. Rev. A 58 (1998) 4691.

[222] L. Yatsenko, B. Shore, T. Halfmann, K. Bergmann, A. Vardi, Source of metastable H(2s) atoms using the Stark chirped rapid-adiabatic-passage technique, Phys. Rev. A 60 (1999) R4237.

[223] T. Rickes, L.P. Yatsenko, S. Steurwald, T. Halfmann, B.W. Shore, N.V. Vitanov, et al., Efficient adiabatic population transfer by two-photon excitation assisted by a laser-induced Stark shift, J. Chem. Phys. 113 (2001) 534.

[224] B.M. Garraway, K.-A. Suominen, Adiabatic passage by light-induced potentials in molecules, Phys. Rev. Lett. 80 (1998) 932.

[225] S. Kallush, Y.B. Band, Short-pulse chirped adiabatic population transfer in diatomic molecules, Phys. Rev. A 61 (2000) 041401.

[226] I.R. Solá, J. Santamarría, V.S. Malinkovsky, Efficiency and robustness of adiabatic passage by light-induced potentials, Phys. Rev. A 61 (2000) 043413.

[227] M. Rodriguez, B.M. Garraway, K.-A. Suominen, Tailoring of vibrational state populations with light-induced potentials in molecules, Phys. Rev. A 62 (2000) 053413.

[228] A. Vardi, D. Abrashkevich, E. Frishman, M. Shapiro, Theory of radiative recombination with strong laser pulses and the formation of ultracold molecules via stimulated photorecombination of cold atoms, J. Chem. Phys. 107 (1997) 6166.

[229] A. Vardi, M. Shapiro, K. Bergmann, Complete population transfer to and from a continuum and the radiative association of cold Na atoms to produce translationally cold Na_2 molecules in specific vib-rotational states, Opt. Express 4 (1999) 91.

[230] J. Javanainen, M. Mackie, Probability of photoassociation from a quasicontinuum approach, Phys. Rev. A 58 (1998) R789.

[231] M. Mackie, R. Kowalski, J. Javanainen, Bose-stimulated raman adiabatic passage in photoassociation, Phys. Rev. Lett. 84 (2000) 3803.

[232] K. Winkler, G. Thalhammer, M. Theis, H. Ritsch, R. Grimm, J.H. Denschlag, Atom-molecule dark states in a Bose-Einstein condensate, Phys. Rev. Lett. 95 (2005) 063202.

[233] R. Dumke, J.D. Weinstein, M. Johanning, K. Jones, P. Lett, Sub-natural-linewidth quantum interference features observed in photoassociation of a thermal gas, Phys. Rev. A 72 (2005) 041801.

[234] E. Arimondo, Coherent population trapping in laser spectroscopy, Prog. Opt. 35 (1996) 259.

[235] M. Bixon, J. Jortner, Intramolecular radiationless transitions, J. Chem. Phys. 48 (1968) 715.

[236] G.-X. Li, J.-S. Peng, Coherent population trapping in multilevel laser-induced continuum structure system, Opt. Commun. 138 (1997) 59.

[237] T. Peters, L.P. Yatsenko, T. Halfmann, Experimental demonstration of selective coherent population transfer via a continuum, Phys. Rev. Lett. 95 (2005) 103601.

[238] C.E. Carroll, F.T. Hioe, Coherent population transfer via the continuum, Phys. Rev. Lett. 68 (1992) 3523; Selective excitation via the continuum and suppression of ionization, Phys. Rev. A 47 (1993) 571.

[239] T. Nakajima, M. Elk, J. Zhang, P. Lambropoulos, Population transfer through the continuum, Phys. Rev. A 50 (1994) R913.

[240] T. Nakajima, P. Lambropoulos, Population transfer through an autoionizing state by pulse delay, Z. Phys. D 36 (1996) 17.

[241] C.E. Carroll, F.T. Hioe, Selective excitation and structure in the continuum, Phys. Rev. A 54 (1997) 5147.

[242] E. Paspalakis, M. Protopapas, P.L. Knight, Population transfer through the continuum with temporally delayed chirped laser pulses, Opt. Commun. 142 (1997) 34.

[243] R.G. Unanyan, B.W. Shore, K. Bergmann, Laser-driven population transfer in four-level atoms: Consequences of non-Abelian geometrical adiabatic phase factors, Phys. Rev. A 59 (1999) 2910.

[244] R.G. Unanyan, M. Fleischhauer, B.W. Shore, K. Bergmann, Robust creation and phase-sensitive probing of superposition states via stimulated Raman adiabatic passage (STIRAP) with degenerate dark states, Opt. Commun. 155 (1998) 144.

[245] Z. Chen, M. Shapiro, P. Brumer, Interference control of photodissociation branching ratios. Two-color frequency tuning of intense laser fields, Chem. Phys. Lett. 228 (1994) 289.

[246] Z. Chen, M. Shapiro, P. Brumer, Interference control without laser coherence: Molecular photodissociation, J. Chem. Phys. 102 (1995) 5683

[247] Z. Chen, M. Shapiro, P. Brumer, Incoherent interference control of two-photon dissociation, Phys. Rev. A 52 (1995) 2225.

[248] M. Shapiro, P. Brumer, On the origin of pulse shaping control of molecular dynamics, J. Phys. Chem. A 105 (2001) 2897.

[249] I. Thanopulos, M. Shapiro, Enhanced selectivity and yield in multichannel photodissociation reactions: Application to CH_3I, J. Chem. Phys. 125 (2006) 133314; Coherently controlled adiabatic passage to multiple continuum channels, Phys. Rev. A 74 (2006) 031401.

[250] F. Legare, S. Chelkowski, A.D. Bandrauk, Preparation and alignment of highly vibrationally excited molecules by CARP chirped adiabatic Raman passage, Chem. Phys. Lett. 329 (2000) 469.

[251] A. Vardi, M. Shapiro, Two-photon dissociation/ionization beyond the adiabatic approximation, J. Chem. Phys. 104 (1996) 5490; Theory of radiative recombination with strong laser pulses and the formation of ultracold molecules via stimulated photorecombination of cold atoms, A. Vardi, D. Abrashkevich, E. Frishman, M. Shapiro, J. Chem. Phys. 107 (1997) 6166.

[252] G. Thalhammer, M. Theis, K. Winkler, R. Grimm, J.H. Denschlag, Inducing an optical Feshbach resonance via stimulated Raman coupling, Phys. Rev. A 71 (2005) 033403.

[253] M. Shapiro, Theory of one- and two-photon dissociation with strong laser pulses, J. Chem. Phys. 101 (1994) 3844; E. Frishman, M. Shapiro, Reversibility of bound-to-continuum transitions induced by a strong short laser pulse and the semiclassical uniform approximation, Phys. Rev. A. 54 (1996) 3310.

[254] M. Shapiro, Photophysics of dissociating methyl iodide: Resonance-Raman and vibronic photofragmentation maps, J. Phys. Chem. 90 (1986) 3644.

Theory and State-Specific Methods for the Analysis and Computation of Field-Free and Field-Induced Unstable States in Atoms and Molecules

Cleanthes A. Nicolaides[a]

Contents

[a] Theoretical and Physical Chemistry Institute, National Hellenic Research Foundation, 48 Vasileos Constantinou Avenue, Athens 11635, Greece
E-mail address: caan@eie.gr (C.A. Nicolaides)

Abstract

The chapter discusses certain formal properties of *field-free* and *field-induced unstable* (*nonstationary* or *resonance*) states in atoms and molecules which are embedded in the continuous spectrum, and corresponding methods for the practical solution of the *many-electron problem* (MEP) that accompanies the requirement of the ab initio computation of their wavefunctions and of measurable quantities. It synthesizes new material and commentary with selected published theoretical and numerical results by the author and collaborators, going back to Nicolaides, Phys. Rev. A **6**, (1972) 2078.

Because there is a central theme that pervades the formalisms and applications of this work, its framework has been given the generic name of: *The state-specific approach* (SSA) (Nicolaides, Int. J. Quantum Chem. **60**, (1996) 119; ibid, **71**, (1999) 209). According to the SSA, critical to the development of formalism which is physically helpful as well as computationally practical is, first, the choice of appropriate for each problem *forms* of the trial wavefunctions and, second, the possibility of employing corresponding function spaces that are as specific and optimal as possible for the state and property of interest. A salient feature of the SSA is that it makes the interplay between electronic structure and dynamics transparent.

At the core of the analysis and methods that are discussed in this Chapter is the consistent consideration of the fact that the form of each resonance wavefunction is $\Psi_r = a\Psi_0 + X_{as}$ (Eq. (4.1) of text). If necessary, the extension to multi-dimensional forms is obvious. Depending on the formalism, the coefficient a and the "asymptotic" part, X_{as}, are functions of either the energy (real or complex) or the time. The many-body, square-integrable, Ψ_0, represents the localized part of the decaying (unstable) state, i.e., the unstable wavepacket which is assumed to be prepared at $t = 0$. Its energy, E_0, is real and embedded inside the continuous spectrum. It is a minimum of the average value of the corresponding state-specific effective Hamiltonian that keeps all particles bound.

The frameworks used in the SSA of this chapter are either energy-dependent or time-dependent, and engage methods that solve in a practical way the

corresponding Schrödinger equations nonperturbatively. Both Hermitian and non-Hermitian formalisms have been applied, using the Coulomb or the relativistic Breit–Pauli Hamiltonians.

As regards the theme of irreversible decay, the discussion examines briefly aspects of the relevance of three time domains: (1) The regime of exponential decay (ED), $e^{-\Gamma t}$, which is the regime that defines the resonance state on the energy axis in terms of its energy, E_r, and its width, Γ. (2) The regime of pre-ED, which defines the degree of stability of $a(t)\Psi_0$ subject to interactions with $X_{as}(t)$, and (3) The regime of non-ED that starts after a duration of (normally) many lifetimes in the ED regime.

The information on the bulk of the interparticle interactions is contained in Ψ_0, even though the decay properties are obtained only after input from X_{as} has been added. It follows that its accurate and systematic computation is of prime importance. Instead of following procedures of brute-force diagonalization, the calculation of Ψ_0 for electronic structures is done directly, via the solution of state-specific Hartree–Fock (HF) equations under special orbital constraints. The practicality of this approach even for open-(sub)shell multiply excited resonances was demonstrated in the 1972 paper, thereby opening the way for later computations that start with state-specific multiconfigurational HF equations and tackle efficiently the MEP and electron correlation in the context of appropriate formalisms for resonance states.

When a Hermitian, real energy formalism is adopted, the mixing of bound-scattering components in the case of field-free resonances is computed from a multichannel (in general) K-matrix formalism, with frozen-core, term-dependent, energy-normalized HF scattering orbitals as basis sets for the continuous spectrum. On the other hand, following our work from the 1970s and early 1980s, it is shown that starting from Fano's 1961 Hermitian formalism which accounts rigorously for discrete-continuum mixing, when the appropriate boundary conditions are imposed formally on the solution of the Schrödinger equation in the vicinity of E_0, two adjoint *complex eigenvalue Schrödinger equations* (CESE) emerge naturally, whose eigenfunctions have a two-component *form*, while their eigenvalues are complex conjugate. The physically acceptable solution for a decaying state, Ψ_r, is the one with the outgoing-wave boundary condition, for which the complex energy is $z_r = E_r - (i/2)\Gamma$. Methods have been developed and applied for the *nonperturbative* solution of the corresponding state-specific CESE for both the field-free and the field-induced cases, within non-Hermitan formalisms with optimized superpositions of real and complex functions of real or complex coordinates.

In summary, the discussion includes formalism and analysis contributing to the understanding of the nature of unstable states, as well as indicative theoretical and numerical examples from applications to atoms and molecules, and related comparisons with other methods, concerning prototypical problems of autoionization, predissociation, series of isolated and overlapping resonances, structure and spectroscopy of doubly and multiply excited states, multiphoton ionization, field-induced polarization, etc.

1. BEYOND PURE FORMALISM: THE IMPORTANCE OF SOLVING EFFICACIOUSLY THE MANY-ELECTRON PROBLEM (MEP) FOR UNSTABLE (OR NONSTATIONARY, OR RESONANCE) STATES IN THE FIELD-FREE AND FIELD-INDUCED SPECTRA OF MANY-ELECTRON ATOMS AND MOLECULES

> ...The underlying physical laws necessary for the mathematical theory of a large part of physics and the whole of chemistry are thus completely known, and the difficulty is only that the exact application of these laws lead to equations much too complicated to be soluble.
>
> P. A. M. Dirac, 1929 [1]

The difficulty to which Dirac [1] refers in the above well-known quotation is here interpreted as follows: Concerning the physics of atoms and molecules, the benefits of theory must go beyond pure formalism and phenomenology and must allow two things: First, the possibility of computing systematically from first principles the physically relevant quantities to sufficient accuracy compared to measurement. Second, the possibility of applying generally applicable concepts and of facilitating the passing from the computationally simpler to the more complex, without unnecessary discounts on the required quantum mechanics (QM) for polyelectronic states.

The theme of this chapter focuses on the possibility of combining in a practical and economic way essential conceptual and formal elements of the description of *unstable* states (also referred to here as *nonstationary*, as *decaying*, or as *resonance* states) in atoms and molecules, with computational methodologies that handle the *many-electron problem* (MEP) for a variety of electronic structures, especially of excited atoms.

These states are formed inside the continuous spectra of the total Hamiltonian and are responsible for phenomena such as resonances in electron scattering from atoms or molecules, *autoionization*, *predissociation*, etc. Furthermore, in this work we also consider as unstable states those states that are constructs of the time-independent theory of the interaction of an atom (molecule) with an external field which is either static or periodic, in which case the effect of the interaction is obtained as an average over a cycle. In this framework, the "atom + field" state is inside the continuous (ionization or dissociation) spectrum, and so certain features of the problem resemble those of the unstable states of the field-free Hamiltonian. The probability of decay of these *field-induced* unstable states corresponds either to tunneling or to ionization–dissociation by absorption of one or more photons.

The conceptual framework of the treatment of the field-induced resonances of work discussed in this article follows from the one that has proven useful for the solution of the MEP for *field-free* resonances. Therefore, the

emphasis in the following sections is on the field-free case. The related formalism and computational methodology constitute the background for the theory and computation of the field-induced resonances which are discussed in Section 11.

The paper synthesizes new material and commentary with selected published theoretical and numerical results by the author and collaborators, going back to 1972 [11a]. Because there is a central theme that pervades the formalisms and applications of this work, its framework has been given the generic name of: The *state-specific approach* (SSA) [9, 10]. According to the SSA, critical to the development of formalism which is physically helpful as well as computationally practical is, first, the choice of appropriate for each problem forms of the trial wavefunctions, and second, the possibility of employing corresponding function spaces that are as specific and optimal as possible for the state and property of interest. A salient feature of the SSA is that it makes the interplay between electronic structure and dynamics transparent.

The frameworks used in the SSA of the present article are either energy-dependent or time-dependent, and engage methods that solve in a practical way the corresponding Schrödinger equations nonperturbatively. Both Hermitian and non-Hermitian formalisms have been applied, using the Coulomb or the relativistic Breit-Pauli Hamiltonians. At the core of the analysis and methods that are discussed is the consistent consideration of the fact that the form of each resonance wavefunction is $\Psi_r = a\Psi_0 + X_{as}$, (eq. 1). If necessary, the extension to multi-dimensional forms is obvious. Depending on the formalism, the coefficient a and the 'asymptotic' part, X_{as}, are functions of either the energy, (real or complex), or of time. The many-body, square-integrable, Ψ_0, represents the localized part of the decaying (unstable) state, i.e., the unstable wavepacket which is assumed to be prepared at $t = 0$. Its energy, E_0 , is real, and embedded inside the continuous spectrum. It is a minimum of the average value of the corresponding state-specific effective Hamiltonian that keeps all particles bound.

When a Hermitian, real energy formalism is adopted, the mixing of bound-scattering components in the case of field-free resonances is computed from a multichannel (in general) K-matrix formalism, with frozen-core, term-dependent, energy-normalized Hartree-Fock (HF) scattering orbitals as basis sets for the continuous spectrum. On the other hand, following our work from the 1970s and early 80s, it is shown that starting from Fano's 1961 Hermitian formalism [29] which accounts rigorously for discrete-continuum mixing, when the appropriate boundary conditions are imposed formally on the solution of the Schrödinger equation in the vicinity of, two adjoint *complex - eigenvalue Schrödinger equations* (CESE) emerge naturally, whose eigenfunctions have a two-component *form* whilst their eigenvalues are complex conjugate. The physically acceptable solution for a decaying state,, is the one with the outgoing-wave boundary condition, for which the complex

energy is $z_r = E_r - (i/2)\Gamma$. Methods have been developed and applied for the *nonperturbative* solution of the corresponding state-specific CESE for both the field-free and the field-induced cases, within non-Hermitian formalisms with optimized superpositions of real and complex functions of real or complex coordinates.

Finally, as regards the theme of irreversible decay, the discussion examines briefly aspects of the relevance of three time domains: 1) The regime of exponential decay (ED), $\exp(-\Gamma t)$, which is the regime that defines the resonance state on the energy axis in terms of its energy, E_r, and its width, Γ. 2) The regime of pre-ED, which defines the degree of stability of $a(t)\Psi_0$ subject to interactions with $X_{as}(t)$, and, 3) The regime of non-ED that starts after a duration of (normally) many lifetimes in the ED regime.

1.1. The need to combine transparent theory of unstable states with practical computational methods for the solution of the MEP in atoms and molecules

It is well known that very simple systems or simple models of polyelectronic systems are very often the basis for a variety of theoretical treatments, ranging from phenomenology to quantitative answers. For the requirements of certain problems, such approximations may suffice. However, regardless of how pleasing the visualization and the computational facility of simple models are, the fact is that atoms and molecules are not, say, textbook one-dimensional systems, nor are their properties understood by simply examining only low-lying states of, say, one- or two-electron systems. At the end of the day, theoretical work (and of course experimental one as well!) has to deal with real systems of arbitrary structures and to tackle the omnipresent MEP. Any formalism, no matter how rigorous and detailed it appears to be, whose basic structure does not facilitate the computational solution of various MEPs involving resonance states, is limited either to descriptive phenomenology (which is, of course, valuable when needed) or to special simple cases where calculation becomes feasible.

A paradigm of such a limitation is the one concerning the rigorous application of Feshbach's widely cited formalism that explains the formation and effects of resonances in nuclear reactions [2]. The faithful implementation of this formalism, as regards the use of properly defined projection operators, to resonance states of atomic systems was first demonstrated in 1965 by O'' 'Malley and Geltman [3a], albeit only for certain low-lying resonance states of two-electron atoms. The papers which ensued along these lines for two-electron systems have explored aspects of high computational accuracy, e.g., Ref. [3b]. However, as the authors of those papers in the 1960s and early 1970s pointed out, this theory-based procedure is valid and practical only for two-electron systems, since there, the target states are known exactly, the properties of the projection operators are rigorously satisfied,

and the computational algorithm is in harmony with the formalism. In order to bypass the intrinsic requirements of the Feshbach scattering formalism as regards its extension to systems with more than two electrons, modifications were advanced during the 1980s in terms of "quasi-projection operators" and applied to the lowest-lying resonances of the three-electron He$^-$ and Li [4]. A few years after the publications of Temkin and Bhatia [4a], Bylicki [5] penetrated into essential theoretical aspects of this problem in conjunction with systematic computations on three-electron resonances of He$^-$. For example, he paid attention to the choice of orbital orthogonality conditions when defining projection operators onto open and closed channels—a practical approximation originating, as Bylicki pointed out, in the polyelectronic theory of Ref. [11]. In any case, regardless of how the "quasi" Feshbach operators are chosen, the awesome difficulties of electronic structure and of the MEP which accompany the "Feshbach projection and quasi-projection" methods remain [3–5]. Therefore, the direct implementation of the Feshbach (P, Q) formalism for high-level computational purposes, which has been demonstrated in low-lying resonance states of two-electron systems, has faced practical as well as fundamental difficulties when it comes to resonance (autoionizing) atomic states of various types and energies and of any number of electrons.

In order to emphasize from a different angle the argument about computation, suppose one considers one of the rigorous results of scattering theory [6, 7], namely, that the isolated resonances in scattering cross-sections correspond to simple complex poles of the (multichannel in general) S-matrix. These complex poles define the complex energies at which the equation of Schrödinger has solutions with no incoming waves and with only outgoing waves in all channels, a result which was made explicit in Siegert's treatment of s-wave scattering by a short range potential [8a].

Well, even though the general formulas of scattering theory exist, one is entitled, many decades after the establishment of the formalism, to questions such as the following: What is the physical origin of the S-Matrix complex poles representing resonance states, and how is this reflected on the ab initio construction of the S-matrix?: How easy is it to compute accurately these S-matrix poles for, say, elastic and inelastic scattering of electrons by arbitrary N-electron atomic states, over a certain range of energies and for various symmetries? The answer given by anyone familiar with the field would not be encouraging, even for isolated states, which is the main object of the formal discussion in this chapter. For example, the electronic structures of the resonance states corresponding to the complex poles that have to be uncovered in such a scattering-type calculation may differ considerably from state to state. Furthermore, the real and the imaginary part of each pole may differ by orders of magnitude. In addition, the possible presence of pseudo-resonances complicates things.

In fact, things become much more complicated when it comes to the ab initio computation of neighboring resonances, a few of which may be overlapping. For example, such is the case of the resonance state spectra of H^- for different symmetries, which is the subject of Section 7.2.

The inevitable conclusion that follows from considering the above is that, even if all the details of formalism and of techniques of electronic structure were understood in a practical way, reliable calculations of the S-matrix and of its complex poles representing resonance states would be computationally extremely demanding, if not impossible, even with today's computers, at least if the problems were approached in the way that calculations of scattering processes have thus far been carried out.

1.2. Formalism and polyelectronic methods in the framework of the state-specific approach

The main focus in this chapter is on two themes: On the one hand, the discussion aims at presenting, without many formulae, certain critical characteristics and properties of unstable states in general, and, in particular, of states that are normally represented by multi-particle wavefunctions, such as the ones that are found in the spectra of atoms and small molecules. On the other hand, the discussion aims at demonstrating why and how it is possible to tackle, from first principles and from a many-electron point of view, a large number of problems that have to do with field-free and field-induced unstable states, for which reliable electronic structure calculations are, in principle, feasible.

Only certain issues which are considered basic to the aims of the review and to the understanding of the theory and of the computational methodology are discussed, in frameworks which include both energy-dependent and time-dependent analyses and methods. Of course, additional information on formal analysis (some of which is not friendly to computational prospects), on various theories and their implementation, on computations and on models can be found in the numerous publications that have dealt with the huge topic of resonance states. It is hoped that many of these can be found by the reader by studying the chapters of this volume.

As regards calculation and the necessity of tackling efficiently the MEP for a large variety of cases, both the herein discussed formalism and the corresponding computational methodology have been developed based on the following assertion: Especially for excited states, it is critically important to utilize state-specific forms of the trial wavefunctions, to analyze the origin and contributions of the different main parts, to represent them by different function spaces which reflect their different types of contribution to the physics of each problem, and to optimize these functions by suitable procedures. For this reason, the relevant formalisms and methodologies have been named collectively the *state-specific approach*, e.g., Refs. [9, 10].

The various analyses, examples and applications of the SSA which are presented in the sections that follow, show how reliable wavefunctions of unstable states can be obtained. These have a form which is transparent and usable regardless of whether they describe field-free or field-induced excited state systems of, say, 2, 15, or 30 electrons and of whether there is one or many open channels. In this way, additional properties and good understanding of the interplay between structure and dynamics can be (and indeed have been) obtained. The discussion, in conjunction with the corresponding references, explains how the SSA has formed the framework for the formal and computational treatment—nonperturbatively—of a variety of prototypical problems involving *field-free* as well as *field-induced* resonance states in atoms and in small molecules.

Molecular applications have thus far involved the calculation of the electronic structure and potential energy surfaces of negative ion "compound states" and of "diabatic states" in the continuous spectrum of polyelectronic diatomics and triatomics and of energies and partial widths with interchannel coupling of vibrational shape and *predissociating* resonances of diatomics. The same principles and methodologies can be applied to many more such cases.

A word about the field-induced case: This is concerned with problems where the Hamiltonian includes the time-independent or time-averaged (over a cycle) interaction of atomic or molecular ground or excited states with strong static and ac fields, where low-order perturbation theory does not suffice. Following the framework of the *decaying state* with a *complex eigenvalue* that was (is) used for the field-free case, these problems are formulated as field-induced resonance states, where the interaction mixes the field-free states, represented by function spaces with real coordinates, with the continuous spectrum, where the free electron(s) are represented by orbitals of *complex coordinates* (Section 11). A practical, non-Hermitian, complex-energy methodology has been developed and applied for the nonperturbative computation of quantities such as rates of multiphoton ionization and above-threshold ionization, double ionization with electron pair correlation at threshold, dc-field-induced ionization and hyperpolarizabilities, field-induced shifts and widths of doubly excited states (DESs), ionization control by di- or tri-chromatic fields. In addition, mention is also made of the fact that the problem of atom–strong field interaction has also been tackled in terms of *large-order perturbation theory with complex energies*, where the computation of the terms uses function spaces that can be state specific.

I close this introduction by making two comments:

(1) Aspects of the contents of this chapter have been placed in a historical context, supplemented by appropriate references. Such a chronological perspective always enhances the understanding of the significance of

the introduction of new approaches and methods. For example, up to the beginning of the 1970s, the published bound-state-type methods for approximating resonance state wavefunctions had been using single sets of bound orbitals (see Section 2 and its references). At the same time, it was not known whether it was legitimate and/or possible to solve directly the HF equations for complicated excited state structures with open (sub)shells that are in the continuous spectrum. The possibility of finding such HF solutions that are physically meaningful was first demonstrated in Ref. [11], where valid state-specific HF wavefunctions for the prototypical triply excited He$^-$ "$2s^22p$" $^2P^o$ and "$2s2p^2$" ^2D resonance states were computed, subject to *orbital constraints* of orthogonality and asymptotic behavior and to the satisfaction of the *virial theorem*, which, in combination with computational experience, secure proper convergence of the variational computation. Once such HF wavefunctions are obtained (in modern times this is done systematically, especially in terms of the solution of state-specific numerical multiconfigurational HF (MCHF) equations), the computation of electron correlation and of the multichannel continuum involves the implementation of advanced but practical methods and the use of different function spaces (see later sections in this chapter).

(2) The numerical results and the explanatory nature of parts of the following sections as regards the understanding and systematic many-electron treatment of resonances offer the opportunity for the reader to evaluate the advantages, the limitations, and the shortcomings not only of the SSA but also of other methods to which reference is made. This ought to be helpful in current research on a variety of topics on polyelectronic atoms and molecules. For example, the discussion on the direct computation of the state-specific localized component of resonance states, Ψ_0, explains how such wavefunctions can be immediately practical for use in the *state-specific expansion approach* (SSEA) which has been introduced as a general method for the nonperturbative solution of the *time-dependent Schrödinger equation* (TDSE) (see Chapter 6).

2. PRINCIPAL CHARACTERISTICS OF THE DOMINANT THEORETICAL APPROACHES TO THE COMPUTATION OF UNSTABLE STATES IN ATOMS AND MOLECULES UP TO ABOUT THE END OF THE 1960s-EARLY 1970s

The essential features of the herein discussed analyses and methods that have been developed in the framework of the SSA, evolved and diversified starting from the initial arguments and results of the 1972 publication [11]. It is for this reason that in this section I recall certain facts from that period concerning the subject of the ab initio computation and analysis of resonance

states in many-electron atoms and molecules. Of course, for a full exposition to the situation at that time regarding both theory and experiment, the reader is referred to the excellent review articles of that period that are cited below. Here, for reasons of economy, the examples which I use to refer prototypical resonance states in small atoms. In molecules, the additional degrees of freedom due to nuclear motion give rise to extra phenomena, such as dissociative attachment or predissociation. A thorough review for molecular processes involving resonances was published in 1968 by Bardsley and Mandl [12], while in 1973 Schulz [13] reviewed resonances in electron scattering from diatomics mainly from the experimental point of view.

2.1. Aspects of concepts and methods prior to [11]

It is unnecessary, and certainly not in the scope of the chapter, to review here in detail the formalisms, the computational methods, and the experimental progress that had been achieved until the end of the 1960s-early 1970s on the subject of the resonance states of atoms and molecules. It suffices to cite the reviews of Burke [14, 15], of Smith [16], of Fano and Cooper [17], of Bardsley and Mandl [12], and of Schulz [13, 18]. (See also the introduction and categorization of methods in Ref. [11a].) In addition, I note that, concerning the crucial for theory topic of resonance states of atomic negative ions (ANIs), the extensive reviews by Buckman and Clark [19] and by Andersen [20] have covered the period from the late 1960s and early 1970s [18] to 2003. It is worth noting that an analysis of computational methods of scattering theory as they were applied by the end of the 1960s, with emphasis on issues of spurious solutions and with applications to the e + H lowest resonance in the elastic channel, was published by Shimamura [21].

As it is clear from the aforementioned reviews, following the creation of QM there were only a few and sporadic contributions to elements of the physics of resonance (autoionizing) states in atoms until the early 1960s. Indeed, the systematic research activity concerning the theory and experiment on resonance states in atoms and molecules started in the early 1960s.

In the period between the 1930s and the end of the 1950s, much formal work had been carried out in the context of research on the nuclear reactions, where one of the main concepts was (is) that of the "compound state." The framework was that of scattering theory. Indeed, some of the ideas and formalisms of nuclear physics—e.g., "R-matrix" or "eigenchannel" formalisms, e.g., Ref. [22], have, in more recent decades, been taken over from the subject of nuclear reactions and have been implemented appropriately for the treatment of resonance-state problems in atomic and molecular physics, e.g., Ref. [23].

In the start of that early period, results that established fundamental concepts in the theory of unstable states in different fields were published, on the

one hand by Wentzel [24a] on the rate of the Auger effect, and on the other hand by Gamow [25] and by Gurney and Condon [26] on alpha particle tunneling. Wentzel applied first-order time-dependent perturbation theory and derived an energy-conserving golden-rule type formula expressing the transition from a bound wavefunction to a scattering state, the perturbation being formally caused by the full interelectronic interaction. Gamow, Gurney and Condon considered the (what is now standard) one-dimensional tunneling potential model. Of special interest to the present discussion is the (ad hoc) introduction by Gamow of complex energies, whose imaginary part is the decay rate of the unstable state.

The work of Wentzel [24a] served as reference point for the approaches that Rice [24b] and Rosen [24c] took toward the initial understanding of the presence of predissociating states in molecular spectra.

Thus, the essence of the description of unstable states was established in terms of the model of *bound (discrete) level with energy embedded inside a pure continuum or, to some level of approximation, inside a highly dense series of discrete levels*. The first rigorous mathematical analysis of aspects of such a situation, from the point of view of spectral theory, was published by Friedrichs in 1948 [27], and his treatment is referred to in many publications as the "Friedrichs model." Certain of its basic aims and results can also be found in the 1961 seminal work of Fano (see below).

A few years later, the strong interest in describing nuclear reactions led to the concept of the "compound state" of the $(N + 1)$ particle system and to the development, over a few decades, of various treatments of resonances in the context of scattering theory (e.g., see Refs. [2, 6, 7, 22, 23, 27–29] and references therein). Among the main theoretical results from these theories were the association of resonance states with the π-jump of the phase shift on resonance, the correspondence of poles of the S-matrix and of the resolvent operator (Green's function) to the energies and decay widths of resonances, the recognition of characteristic Breit–Wigner resonance profiles of scattering cross-sections and of related interferences, aspects of formal properties of resonance eigenfunctions, the possibility of determining, in principle, the energy positions and widths of the various resonance peaks in cross-sections, etc.

Also in that early period of nuclear physics, Siegert [8a] showed, from a simple argument for a short-range potential, that a resonance in the scattering cross-section is caused by a complex pole of the S-matrix below the real energy axis, and that the concomitant resonance eigenfunction asymptotically has the form $e^{ik_r r}$, where k_r is the complex momentum of the outgoing particle, in harmony with the previous Gamow proposal. Extensive and analytic discussions on formal aspects of the properties of resonance states, on their biorthonormality and on their use in expansions that are complete, were published in 1966 by Fonda et al. [8b] and in 1968 by Berggren [28a], and subsequently by others. An attempt to carry over to problems of atomic

(molecular) physics (where the long-range Coulomb potential is present), a formalism of resonance scattering involving outgoing boundary conditions and complex energies and bypassing the use of "arbitrary joining radius R," was published in 1964 by Herzenberg et al. [28b].

One common conceptual denominator of the various publications on resonance (nonstationary) states is the association of the appearance of a resonance with a quasi-localized single- or multi-particle wavepacket whose energy is above the fragmentation threshold. This means that, on resonance, there is an "inner" and an "outer" (asymptotic) component of the wavefunction, each contributing in a different way to the intrinsic characteristics of the state and to the quantity which is measured.

For example, Eq. (3a) below, which is a consequence of Fano's elegant and general theory of 1961 [29], expresses the fact that, on resonance, the exact scattering state in the energy continuum is almost the same as the square-integrable (inner) part, Ψ_0, with the energy dependence of the scattering state represented by the coefficient of Ψ_0.

The concept of "inner" and "outer" regions of the resonance wavefunctions can indeed be visualized and understood in terms of simple one-particle models. It can also be written formally, as a definition, as is done, e.g., in Feshbach's theory [2]. It can even be stated that Ψ_0 is an unstable wavepacket and, as such, it can formally be expanded in terms of the complete set of the system's Hamiltonian. However, such models or formal definitions do not help in practice with the solution of the MEP.

Thus, at the end of the 1950s and early 1960s, a systematic computational scheme for *many-particle systems* in arbitrary states was far from being obvious and/or accomplished. Focusing on the field of atomic and molecular physics, by the end of the 1950s the theory and the practical understanding of how to treat systematically such transient states from a many-body point of view were essentially nonexistent, in part because specific experimental results requiring interpretation had not yet appeared, and mainly because no advances had been made in combining effectively the theory of resonance states with computational many-electron methods of electronic structure which, at that time, were still restricted to simple applications on ground states of few electron systems. For example, in his classic and extensive presentation of atomic structure theory, Slater, in 1960 [30], does not discuss at all the problem of resonances (autoionizing states), while a couple of years earlier, Bethe and Salpeter [31], in their authoritative treatise on the QM of one- and two-electron atoms, state explicitly that they will not consider doubly excited states (DESs) (i.e., states that in Helium lie in the continuous spectrum and normally give rise to resonances) [31], p. 125.

Regardless of the degree of rigor of the principles on which they are based, the methods used in the 1960s for the computation of field-free resonance states had serious intrinsic and/or practical limitations, which is natural given that the field was nascent, while the requirements are very demanding,

especially regarding the handling of the MEP, and of situations of high excitations, of multichannel mixings, of resonance states with weak binding, etc.

For example, the scattering-theory method of "close-coupling," whose implementation in atomic physics with emphasis on the identification of low-lying resonances was initiated in the 1960s [14–16, 32–34], was (is) in principle capable of providing a wealth of information as a function of energy. However, as implemented, it was uneconomical and exhibited very slow convergence, even for low-lying resonances of two- or three-electron atoms, since the addition of terms for electron correlation and for closed channels increases the computational requirements immensely. Furthermore, by necessity, in order to make the overall calculation tractable, the closed channel and target wavefunctions were not consistently accurate, while the quantitative identification of resonances of high excitation (many open channels) and/or of rather narrow widths was (is) essentially outside the practical reach of the method, e.g., Refs. [14–16, 32–34].

The late 1950s and the whole of 1960s also saw the publication of methods, which were (are) based on the use of discrete basis sets (one set, without or with a variable parameter), for the diagonalization of the Hamiltonian. Their implementation was limited to the computation of the positions of resonances in selected two- and three-electron systems. From the diagonalization one obtains as many roots as it is numerically possible. The task is then to identify those that correspond to resonance states (we recall that on resonance the wavefunction is dominated by its localized component) and to determine their energies and, perhaps in simple cases, the total width. According to the computational experience and analysis that was reported by the first practitioners of this method (normally called the "stabilization method"—see below), numerical and even pictorial criteria on the behavior of the roots of the diagonalized matrices that remain reasonably stable upon variation of a parameter or upon increase of the number of basis functions are used for drawing conclusions.

A brief commentary on such approaches is given in the following paragraphs.

Already in the late 1920s–mid-1930s, owing to new findings in atomic, molecular, and nuclear physics, there were discussions and results (experimental as well as theoretical), concerning phenomena of auto-disintegration of atoms (the "Auger effect") and of nuclei (alpha particle decay), of electric field-induced tunneling, of autoionization, of predissociation, of participation of DESs in radiative processes, and of resonances in nuclear reactions, whose nature has a dynamical origin that is absent in the idealized concept of the time-independent stationary state. From the need to describe these phenomena emerged, on the one hand formalisms of resonant scattering to which I have already referred, and on the other hand conceptually simple bound state-type calculations in atomic physics, at the level of the independent particle model of DESs in the two-electron He.

The first such attempts in atomic physics involved simple approaches that did not pay attention to the continuous spectrum and its formal or computational consequences. Thus, Vinti [35] and Fender and Vinti [36], as part of their analysis of the dispersion and absorption of He, assumed simple orbital bound wavefunctions which they optimized variationally and obtained energies for the He DESs 2s2p $^{1,3}P^o$ states. No concern was expressed about the fact that these labels correspond to states that are not discrete but, instead, belong to the continuous spectrum. On the other hand, Vinti did refer explicitly to the problems from the requirement of orthogonality to all lower states of the same symmetry. These problems are real, especially in multiply excited states of N-electron systems where the existence of near-degeneracies of various electronic structures is the rule. The problem of dealing with orthogonality to lower states was tackled explicitly in the work on two-electron systems in the 1960s [3], and a practical analysis for polyelectronic excited states, which was based mainly on considerations of electronic structure and of *orbital orthogonalities*, was also reported in the SSA to resonance (autoionizing) states [11, 37b].

It is relevant to the issue of understanding the simple electronic structures of DESs to note that the variationally optimized orbital wavefunction of Ref. [36] gave the position of the 2s2p $^1P^o$ state at 61.3 eV above the ground state, in satisfactory agreement with the accurate value of 61.1 eV that was to come in the 1960s from calculations that accounted for electron correlation [3].

The problem of accurate (i.e., beyond the independent electron approximation) computation of such low-lying DESs in He and in H$^-$ was taken up in 1950 by Hylleraas [38]. Hylleraas ignored the formal and computational role of the continuous spectrum. His method consisted in diagonalizing the Hamiltonian matrix that he constructed from discrete basis sets. He discussed the problem of orthogonality to lower states of the same symmetry and he argued that the sought after solution corresponded to the second root of his secular equation for the energy. Referring to the 2s2p $^3P^o$ state he concluded that, "the existence of a second stable state of the negative hydrogen has been proved." He made this statement because the energy was lower than the H $n = 2$ threshold by about 0.29 eV. Obviously, the interpretation of this result was not stated correctly. Finding that the energy is below the H $n = 2$ threshold does not mean that the state is stable, since it can decay to the 1sεp continuum, i.e., it is a resonance state. Furthermore, Hylleraas predicted that "...it is, however, doubtful whether the 2p^2 ^3P state is stable at all for H$^-$..." Twenty years later, it was definitively shown by Drake [39] via variational calculations that this state is in fact a discrete state (stable against autoionization) since not only is its energy just below the H $n = 2$ threshold but also because symmetry does not allow its interaction with the continuum between the H $n = 1$ and $n = 2$ thresholds.

The work and conclusions of Hylleraas [38] provide evidence of the state of affairs in 1950, as regards both formal theory and understanding of even the simplest of resonance states in atomic physics and of possibilities of solving reliably Schrödinger's equation as though the problem belongs to those of the discrete spectrum.

2.1.1. The use of discrete basis sets in the late 1950s and in the 1960s

The bound-state type of approach that was followed by Hylleraas—albeit fraught with a couple of erroneous conclusions—eventually evolved in the 1960s into methods aiming at the calculation and identification of resonance states from the behavior of roots of diagonalized energy matrices constructed from discrete basis sets, as a function of a scaling parameter, or size of discrete basis sets, or size of the artificial box inside which the continuous spectrum is artificially discretized.

In fact, the diagonalization of Feshbach's "QHQ" Hamiltonian is also related, although this is the product of a rigorous approach based on scattering theory which connects the eigenvalues of "QHQ" to complex poles of the S-matrix [2–4].

The approach to the approximate calculation of energies of simple resonance states via diagonalization of Hamiltonian matrices constructed from discrete basis sets was introduced and pursued for many years by Holøien in the late 1950s and the 1960s, with application to the lowest lying ^1S resonances of He and H^- [40–43]. Holøien employed basis sets of associated Laguerre functions with single orbital exponents (the so-called Sturmian, hydrogen-like, functions), and a single scale parameter, which form a discrete, complete set that includes the continuous spectrum of the hydrogenic Hamiltonian. His stated aim was to investigate "how the configuration-interaction method works with such a basis when applied to the imperfectly quantized quasi discrete states" [41] p. 76. His approach was based on associating what appeared as "localization" (stabilization) of roots in the continuous spectrum with resonance states as a function of basis set size and of variation of the scaling parameter. In this context, Perkins [44] proposed an upper-bound variational method and stated "This conclusion is applicable to calculations of Holøien, and explains the observed stabilization of roots." The publication of Perkins led to further investigations by Holøien and Midtdal [45] on the lowest five He resonances of ^1S symmetry. In introducing the evolution of the subject, they wrote [45], p. 592

> ".... Meanwhile, it was noticed that eigenvectors associated with the corresponding stabilized roots apparently had vanishing overlap with the hydrogenic ground-state wavefunction, and the stabilization tendency of the expansion coefficients themselves were clearly demonstrated against the extension of the basis [41]. This fact has later on been stressed by other workers [46–48] ...."

I point out that the analysis in Refs. [47, 48] and, later on, the one by Hazi and Taylor [49] penetrated deeper into the understanding of the empirical behavior of roots in the continuous spectrum by paying attention to the theory of resonance scattering [2, 3] and to the properties of the scattering continuum, such as normalization and density of states.

In one way or another, the discrete-basis diagonalization methods of the 1960s attempt to provide an understanding of the behavior of roots of Hamiltonian matrices, in view of the picture of quasi-localization of resonance eigenfunctions. For example, Fels and Hazi [50] write:

> ". . . .The stabilization method for finding resonance parameters may be briefly summarized: After the choice of an appropriate basis of square-integrable functions, the complete Hamiltonian is diagonalized in successively larger bases. For sufficiently large basis sets, the presence of a "stable" root indicates a resonance, and the degree of stability of that root is a measure of the width . . . ."

In order to further develop and clarify the characteristics of the stabilization method, Taylor and Hazi published a comment that includes a proposal for the calculation of the total width [51]. An additional proposal regarding the use of L^2 basis sets for the discretization of the continuum and the calculation of widths was made by Hazi a couple of years later [52].

Even in simple systems, the pursuit of resonance states via root stabilization is not without risks. For example, the difficulty with the correct identification of the roots is reflected in the 1966 publication of Holøien [42] where, after comparison with the then new experimental results on the lowest resonance states of He, he corrects a serious error in his previous work [40]. In the abstract he states that "the error lies in the incorrect root which is associated with the state."

Indeed, the techniques of repeated diagonalization of the Hamiltonian on a large basis set and the search for resonance states from the numerical features of the roots upon variation of the function space may lead to reliable conclusions for models or for certain cases of ground *shape* resonances or of low-lying states of simple systems for which the chosen function space happens to describe the inner part of the resonance accurately. However, it was evident in the late 1960s that such methods had (have) certain limitations when it comes to the MEP in complex, polyelectronic systems. For example, for complex spectra of polyelectronic systems the root-identification criteria may not always lead to physically correct results, even qualitatively. Thus, in spite of careful (and computationally costly) examination, resonance states may be missed or roots may be wrongly attributed to resonances that do not exist.

This possibility was already mentioned above with respect to the early calculations of Holøien [42]. Additional such evidence was reported by

Eliezer and Pan [53], who had the serious experience with stabilization calculations of resonance states of He$^-$. Characteristic examples from the spectrum of He$^-$ are discussed in Sections 2.2 and 2.3.

Another drawback was that, given that the aim is the correct detection of those roots that exhibit behavior ostensibly expected only from wavefunctions at the resonance energy, it is nearly impossible to handle the MEP for the plethora of possible electronic structures of N-electron systems in such an empirical way that depends on repeated diagonalizations of Hamiltonian matrices constructed from single basis sets. Finally, as Taylor and Hazi point out [51], the procedure that was associated with the stabilization method did not allow, in principle, the calculation of partial widths in multichannel continua.

2.1.2. Introduction of state-specific many-electron methods for the treatment of resonance states

The theory and computational methods for the analysis and calculation of field-free resonances in polyelectronic atoms and molecules that are adumbrated here were initiated in 1972 [11a] as an alternative to the theoretical approaches mentioned above and in the review articles [12–16, 21], for the purpose of dealing efficiently with the MEP in arbitrary electronic structures. A complementary discussion based on the ideas in Ref. [11a] and on later publications dealing with various topics within energy-dependent and time-dependent frameworks was given a few years later [37b].

The main argument in Refs. [11a, 37] was to adopt the conceptual and formal framework of describing the *decaying states* with *complex eigenvalues*, and from there to emphasize the form of the resonance wavefuction, as is required by the asymptotic boundary conditions, and the significance of the state-specific MEP in the localized component, Ψ_0, which is a square-integrable wavefunction with a real energy, $E_0 = <\Psi_0|\mathbf{H}|\Psi_0>$. The essence of the content of the initial eqs. (1–4) of Ref. [11a] is the same as that of Eq. (1) of this chapter.

The validity of the physics that adopts the point of view of decaying states depends on the characteristics of the process of excitation-preparation. Specifically, one must assume that the duration of the pulse of excitation energy is much shorter than the lifetime of the unstable state. This implies that indeed the system is prepared in a nonstationary state at $t = 0$, i.e., in the localized state (Ψ_0, E_0), while losing memory of the excitation step. For long-lived unstable states, this is expected to be achievable easily. For short-lived unstable atomic or molecular states, say of the order of 10^{-14} s, this is also achievable, in principle, via modern pump–probe techniques with time-delays in the range of a few femtoseconds or of a couple of hundreds of attoseconds.

A consistent way of pursuing the computation of Ψ_0 could be achieved via a direct approach that keeps track of the boundary condition of square-integrability, i.e., of localization in coordinate space. In this direct approach, the objective is not to diagonalize repeatedly a Hamiltonian matrix, to obtain all the roots and to identify as resonance states those with seeming stabilization properties. Instead, the objective of the first step is to compute a state-specific zero order localized function space by solving, when possible, the relevant HF (and in later years of the MCHF) equations subject to appropriate constraints. Lack of proper convergence in such computations implies that either there is no localized state corresponding to the chosen configurations or the solution is numerically extremely difficult to obtain. The function spaces for the remaining localized electron correlation and for the asymptotically scattering channels, which are different, must then be added and optimized via techniques that are in harmony with the formal nature of the resonance states. The substance of these techniques is discussed in subsequent sections.

2.2. Particular examples I: Question marks on results of calculations on resonances of He$^-$ and of H^{2-}

As a short supplement to the above, I recall specific results from the period of the 1960s to early 1970s concerning the search for resonance states in the scattering of electrons from He and from H$^-$. This subject, which became convenient experimentally as soon as the resolution was improved drastically [18], is at a higher threshold of complexity compared to that of the extensively investigated few low-lying resonance states in the two-electron He and H$^-$, due mainly to the multitude of possible electronic structures and couplings of the three-electron states of He$^-$ and H^{2-} as excitation energy increases and to the inevitable very weak binding (if present at all) in these systems, especially of course in H^{2-}. Therefore, these systems, even though they have only three electrons, provide opportunities for testing the fidelity of resonance state theories and their computational implementation under more stringent conditions than those normally encountered in low-lying DESs of He or of pseudo two-electron atoms and positive ions where nuclear attraction is strong. In other words, the success of a many-electron theory and computational approach that may work for excited states where the attractive Coulomb interaction dominates need not be a good criterion for establishing their generality and accuracy.

Eliezer and Pan [53] reviewed the techniques and numerical results of calculations on He$^-$ scattering resonances, indicating cases of agreement, of uncertainties and of controversies. For example, in their discussion of resonances from the low-energy excitation of the two electrons to the $n = 2$ shell, they pointed out that the 2^2P^o (19.45 eV) resonance which had been observed

in the experiments of Kuyatt et al. [54], was missing in the "most reliable calculations to-date of Burke and co-workers [55] who used the close-coupling method," while their own calculations a "rather poorly stabilized" root was obtained at 19.6 eV. Hence they concluded that "the existence of this state is unclear." On the other hand, the calculations of Ref. [53] clearly indicated the presence of stable roots at 57.1 and 58.2 eV, corresponding to the "$2s^2 2p$" $^2P^o$ and "$2s2p^2$" ^2D resonances [54]. This identification was again confirmed quantitatively 2 years later by the SSA computations [11] and their main wavefunction characteristics were reported by Schulz in his review [18], p. 406.

One might think that, after the above results, the existence of these prototypical triply excited compound states would be recognized. However, it is a sign of the subtlety that computations of highly excited correlated states sometimes have, the fact that the existence of the "$2s2p^2$" ^2D resonance was doubted in the literature of the following years. The related opposing views constituted the impetus for the recent systematic calculations and extensive discussion of Ref. [56], where a number of arguments and results were used to demonstrate the reality of this resonance.

The aforementioned cases highlight the difficulties that theoretical methods had faced by the early 1970s in identifying and computing certain resonance states in even the "simple" three-electron He^-. The following two examples of three-electron systems, also from the period up to the early 1970s, provide additional evidence that for the reliable treatment of resonance states, regardless of the degree to which the effects of the scattering continuum are incorporated (if at all) into a calculation, it is crucial to account accurately for the details of electronic structures and electron correlation in the localized ("inner") component of the wavefunction.

The first case is the prediction, based on a scattering formalism, by Herzenberg and Lau [57] of a resonance in $e - He$ scattering at the very high energy of 73.5 eV with a width of 2.2 eV. This result, which was interpreted as originating from the implication of the exclusion principle, did not (still does not) fit any experimental data nor any electronic structure picture. Therefore, the validity of the theoretical model adopted in Ref. [57] remains in question.

The second case has to do with the intriguing possibility of resonance state formation in $e - H^-$ collisions, i.e., with possible resonances of H^{2-}. The question first arose in 1970, with the publication of absolute cross-sections for $e - H^-$ scattering by Walton et al. [58]. They reported a structure at 14.5 eV, which they attributed to the formation of a resonance state with a lifetime of the order of 10^{-15} s. This publication led to the theoretical work by Taylor and Thomas [59] who applied the stabilization method and interpreted their results as showing the existence of a H^{2-} "$2s^2 2p$" $^2P^o$ resonance state at 14.8 eV with a width of about 1 eV. In addition, following the experimental

finding of Peart and Dolder [60] of a second resonance at 17.2 ± 0.35 eV with "an apparent width of order 0.4 eV," Thomas [61] analyzed the previous computational results [59] and concluded that they reveal a second resonance state, labeled by $2p^3\ ^2p^o$, at 17.26 eV. These results were generally accepted at the time. However, having carried out trial calculations in the spirit of Ref. [11], a few years later, in two short comments [37b, p. 462] and [62, p. 1984], strong skepticism was expressed as to the existence of states of H^{2-} labeled by these two configurations. Our conclusion was based on the failure of the relevant analytic HF equations to converge properly beyond the effective charge of $Z = 1.6$. Even if a better calculation were attempted (say an MCHF one by today's criteria), the breakdown point of $Z = 1.6$ is too far from the physical $Z = 1$ to permit any optimism as to the valid convergence to a square-integrable solution with energy inside the continuous spectrum. Two decades later, the same conclusions were reached by Robicheaux et al. [63] according to extensive R-matrix and configuration interaction calculations. Furthermore, the theoretical conclusions [37b, 62, 63] as to the nonexistence of these resonances were corroborated by the negative experimental results of Refs. [64, 65].

The story of the calculations and results on the H^{2-} resonances is briefly reviewed in Ref. [66]. The importance of this chapter is the announcement of the reliable calculation of two complex eigenvalues of the complex-coordinate-rotated Hamiltonian for H^{2-} using large and flexible basis functions, a requirement that is absolutely necessary for the definitive solution of this problem.

The computational use of complex scaling of coordinates in the Hamiltonian is normally called the "complex coordinate rotation" (CCR) method. A brief reference to it is given in Sections 3.3 and 5.1, with references to related review articles.

The two complex eigenvalues that were identified in Ref. [66] were of $^4S^0$ symmetry. Although for such a doubly negative system the hydrogenic shell model is on shaky grounds, reasonable configurational labels are "$2p^3$" and "$3p^3$" correspondingly. The first state is located at 1.43 eV above the $n = 2$ H threshold with a width of 1.69 eV, and the second is located at 0.46 eV above the $n = 3$ threshold with a much smaller width, 0.29 eV. The result for the first resonance agrees with the one published by Sommerfeld et al. [67], who also used the CCR method, but disagrees with that of Morishita et al. [68], who calculated potential curves via the hyperspherical coordinate method and concluded that there is no resonance in H^{2-} since there was no local minimum on the potential curves. The interesting and intriguing result of the complex eigenvalue with a width that is larger than the energy above the threshold was commented upon in Ref. [66] as regards its physical significance and possible experimental observation.

2.3. Particular examples II: Negative ion bound state just below threshold or resonance state just above threshold?

The total energy of a ground state of an N-electron neutral atom or molecule relative to that of an $(N + 1)$-electron negative ion state defines the nature of the negative ion state. If the energy separation is large and clearly determined, then normally there is no difficulty in the qualitative characterization of the (N+1) state either as a bound state $(E(N+1) < E(N))$ or as a resonance state $(E(N + 1) > E(N))$. However, if this separation is small then it poses a serious challenge to theory and to the reliability of the corresponding calculations, since accuracy is obviously of fundamental importance as regards the understanding of the physics and of the means of observation.

A discussion of the importance of treating the continuous spectrum properly in such cases and of the difficulty that conventional methods of quantum chemistry may have in making accurate predictions is given in Ref. [10]. Here I recall an early example from the 1960s, having to do with the spectrum of He⁻.

In 1967, Holøien and Geltman [69], based on their results from discrete basis variational calculations, predicted that He⁻ has two bound nonrelativistic states: The 1s2s2p $^4P^o$ at about 0.033 eV below the He 1s2s ^3S threshold, and the 1s2p² ^4P at about 0.20 eV below the He 1s2p $^3P^o$ threshold. In the 1970s, two experimental papers [70, 71] reported measurements that were interpreted as suggesting the existence of yet another bound state, the 1s2p² ^2P. Perturbative calculations by Safronova and Senashenko [72] led them to the conclusion that the 1s2p² ^2P state is indeed bound but that the 1s2p² ^4P state is not. (For the 1s2p² ^2P and 1s2p² ^4P states to be bound, their energy must lie below that of the He 1s2p $^3P^o$ threshold, which is 20.96 eV above the 1s² ground state of He).

The SSA analysis and calculations of 1981 [73] showed that neither of these He⁻ states (1s2p² ^4P, ^2P) is bound. Instead, they are *shape* resonances. In fact, it was concluded that the nonrelativistic discrete spectrum of He⁻ consists of only two states, the 1s2s2p $^4P^o$ at 19.74 eV above the He ground state and the newly found triply excited 2p³ $^4S^o$ at about 59.33 eV above the He ground state. The 1s2p² ^4P shape resonance was predicted to exist about 10–11 meV above its threshold [73]. This SSA prediction is in agreement with the result of Hazi and Reed [74], which they obtained at the same time from very large CI computations as part of a calculation of the photodetachment cross-section, and with the very accurate laser-spectroscopic measurements produced in 1994 by Walter et al. [75].

Needless to add that situations such as the prototypical ones referred to above, where the state of interest is very close (above or below) its threshold, are present in the spectra of other atomic and molecular systems. The reliable quantification of their identity and properties is a theoretically and computationally demanding task [10].

3. FIELD-FREE HAMILTONIAN: THE FORM OF WAVEFUNCTIONS FOR RESONANCE STATES IN THE CONTEXT OF TIME- AND OF ENERGY-DEPENDENT THEORIES AND ITS USE FOR PHENOMENOLOGY AND COMPUTATION

At the center of the edifice of any theory of resonances in the continuous spectrum of a many-particle Hamiltonian, regardless of what type of process produces their excitation, is the concept of transient wavefunction localization in the N-particle configuration space, which takes place as the reaction proceeds from the stationary states (reactants) at $t = -\infty$ to the stationary states (products) at $t = \infty$.

The formal reduction of this transient state to a time-dependent resonance state whose initial condition is set at $t = 0$ presupposes the normally occurring situation that the duration of its preparation is much smaller than its lifetime, in which case the assumption of decoupling between excitation and decay is valid. Otherwise, when the time-scales of preparation and decay are comparable, it is necessary to resolve the coherent time evolution by solving the TDSE in the range $-\infty < t < \infty$, e.g., Ref. [76] and Chapter 6.

By making this fundamental decoupling assumption, which is intrinsic to all theories dealing directly with unstable states rather with a scattering process where $-\infty < t < \infty$, the present theory assumes the computability of a square-integrable many-electron wavefunction, $\Psi_0(r_1, \ldots, r_N)$, which vanishes as any one of its coordinates goes to ∞, while its energy, $E_0 = <\Psi_0|\mathbf{H}|\Psi_0>$, attains a local minimum in the space of square-integrable functions which is inside the continuous spectrum of the N-electron system (Operators are symbolized by bold letters).

This $\Psi_0(r_1, \ldots, r_N)$ is assumed to be identical in two descriptions: In the decaying state description where it represents the initial state (at $t = 0$) of the decay process, and in the description in terms of a scattering process as "target plus projectile," where it represents the localized N-electron wavepacket that is created transiently.

The present analysis focuses on wavefunction *forms*. To this purpose, it suffices to consider *isolated resonances*. The case of *overlapping resonances* complicates things as regards phenomenology and computation, but does not alter the argument regarding the concepts and principles which are discussed here. Numerically accurate results for overlapping resonances in the spectra of H^- are presented in Section 7.2.

Much of the phenomenology of unstable states and of resonances as a function of energy was placed on firm foundations in the 1930s via the works of Breit and Wigner (see in Refs. [6, 7]) and in the late 1950s and early 1960s through the works of Feshbach [2] and of Fano [29], in which the concept of channel radius is avoided. The latter two assumed the theoretical possibility of the existence of separate function spaces that are allowed to mix through the interparticle interactions. Feshbach formally employed

projection operators operating on exact target states, while Fano assumed separation of the full space in terms of prediagonalized discrete and scattering zero-order basis. A complementary picture containing some of the results of Ref. [2, 29] is obtained from the time-dependent framework of decaying states [6, 11a, 37].

As far as the present discussion on understanding and computing wavefunctions and properties of unstable states of polyelectronic systems is concerned, the crucial point is how to define and compute Ψ_0 and, subsequently, how to determine its correct superposition with the function space that represents the open channels, thereby leading to the formation of resonance in the vicinity of E_0. The practical success of this quest is dependent on the choice of forms of trial resonance wavefunctions and of corresponding matrices that appear in the formalism.

The fundamental argument underlying the work which is discussed in this chapter is that, whether in wavefunction or in operator-matrix representation, the physically and computationally appropriate symbolic form that must transcent theoretical approaches to the understanding of resonance states is

$$\Psi_r = a\Psi_0 + X_{\text{as}} \tag{1}$$

Depending on the formalism, the coefficient a and the "asymptotic" part, X_{as}, are functions of either the energy (real or complex) or of time.

In the following sections, I discuss basic elements of formalisms for these three cases, i.e., the description involves either real energy, or complex energy, or time. Their proper consideration provides insight into the formal aspects of the QM of resonances and into the problem of how to compute them efficiently.

3.1. Real energy hermitian approaches. Extension of Fano's K-matrix, configuration interaction theory

In Fano's [29] formal theory of resonance states, the energy-dependent wavefunctions are stationary, the energies are real, and the formalism is Hermitian. The observable quantities, such as the photoabsorption cross-section in the presence of a resonance, are energy-dependent and the theory provides them in terms of computable matrix elements involving prediagonalized bound and scattering N-electron basis sets. The serious MEP of how to compute and utilize in a practical way these sets for arbitrary N-electron systems is left open.

Noting the fact that the exact representation of the bound (representing the "inner region") and of the scattering ("outer region") components of the superposition defining an isolated resonance state may differ formally as well as practically from one theoretical approach to another, here I use Ψ_0 as the localized component of the superposition

$$\Psi_r(q,E) = a(E)\Psi_0(q) + \int b_E(E')U(q,E')dE' \tag{2}$$

$\Psi_r(q,E)$ is the stationary scattering solution of the Schrödinger equation at each value of energy in the neighborhood of the continuous spectrum with an isolated resonance and one open channel. The superposition consists of two orthogonal function spaces. q stands for all the coordinates collectively.

It is important to keep in mind that, in solving for the expansion coefficients, $a(E)$ and $b_E(E')$, the Fano-type of analysis uses standing waves (real waves) for the description of the prediagonalized states of the continuum.

The conclusion that one may draw from the real-energy treatment [29] is that, in the neighborhood of a resonance whose exact energy is E_r, we have a pair of critical equations, both of which exhibit the significance of (Ψ_0, E_0):

$$\Psi_r(E) \approx a(E)\Psi_0, \text{ for } E \approx E_0, \tag{3a}$$

$$\frac{\pi}{2}|a(E_r)|^2 = \tau \text{ mean lifetime} \tag{3b}$$

It should be added that the exact energy of Ψ_r is defined by $E_r = E_0 + \Delta$, where Δ is the energy shift (it can be a positive or a negative number) that is caused by the remaining interactions involving the open channels (Eq. (11)).

Although the numerical value of Δ depends on how Ψ_0 is computed, and although it differs for each physical problem, it is normally expected that, in most cases, when a good calculation of Ψ_0 and E_0 has been achieved, Δ is very small, with $|\Delta| << |E_0|$. Indeed, this was computed explicitly in the early work on DESs of Helium [3, 4]. However, I point out that in the Auger energies of inner-hole states of large atoms, where certain subshells are relatively close to each other and there are many electrons interacting, the value of Δ is much larger, as it can be inferred from the early quantitative demonstration of the significance of the *hole-filling* correlations of the type of *symmetric exchange of orbital symmetry* (SEOS) (Section 9). On the other hand, not all contributions from the *hole-filling* correlations necessarily go into Δ. As it is discussed in Section 8, some of the contributions from the states of the continuous spectrum produce components of Ψ_0 and E_0. (See Section 8 and Refs. [56, 77].)

The information contained in $\Psi_r(q,E)$ refers to the energy representation. At the value $E_r = E_0 + \Delta$, the corresponding information in the time representation is the exponential decay (ED) distribution, $e^{-\Gamma t}$, where Γ is the rate of decay and $1/\Gamma \equiv \tau$ is the corresponding lifetime, Eq. (3b) (in atomic units).

3.1.1. Profile of the rate of resonance–resonance electric dipole transitions

As the title of his paper indicates, Fano's contribution aimed at explaining the phenomenology of photoabsorption from a discrete state to the region of the

continuous spectrum where an autoionizing state is located. The result was the formula that bears his name: *The Fano profile* [29]. It contains the effect of interference on the photoionization cross section that the form (2) can have as a final state.

Since the 1960s, advances in all types of spectroscopy have been made, especially in those using lasers. Because of them, the possibility exists of field-induced resonance–resonance transitions in the continuous spectrum. Komninos and Nicolaides [78] derived the general expression for the energy-dependent cross section of the transition between two resonant states, provided the field is weak and does not affect the atomic wavefunctions and spectrum. The profile is expressed in terms of a symmetric, an asymmetric and a background component, and is cast in a form containing as limiting cases the discrete–discrete Lorentzian profile and the discrete—resonance Fano profile. The formula for the cross section published in Ref. [78] Eq. (11) is

$$I(\varepsilon) \approx \text{background} - \frac{1}{\pi \Gamma_+} B_+^2 + \frac{1}{\pi \Gamma_+} B_+^2 \frac{(Q+\varepsilon)^2}{1+\varepsilon^2} \tag{4}$$

with

$$\varepsilon = \frac{\hbar\omega - \Delta E}{\Gamma_+}, Q = \frac{G_+(E_1, E_2)}{B_+(E_1, E_2)} \tag{4a}$$

The symbols are expressed in terms of matrix elements [78]. In the limit of a bound-resonance transition, Q reduces to the Fano q-parameter, while the second term of Eq. (16) cancels the background term.

The theory was implemented numerically from first principles, by the SSA methods, on the transition He "2s2p" $^1P^o \rightarrow$ "2p3p"^1D for tunable radiation around 3.4 eV. It was found that the Q parameter for this transition has the value 8.27, while the oscillator strength from the bound–bound part of the transition is 0.0347. The initial $^1P^o$ state at 60.15 eV can be reached from the ground state $2s^2\ ^1S$ by synchrotron radiation.

3.1.2. Valence-Rydberg-continuum mixing and a unified treatment of discrete and continuous spectra in polyelectronic atoms

Here I simply mention the application of the form (1) in its multi-state version, in the context of real-energy scattering (reaction (K)-matrix) theory. This subject is broad and very sophisticated from the point of view of formalism as well as computation, and there is no room here for a detailed discussion. The reader will be helped by the cited references. Basic results and conclusions of the theory are presented in the article by Mercouris, Komninos and Nicolaides, Chapter 6.

For the single channel case, the form (2) has been solved formally by Fano [29]. The first numerical application for this case was done by Altick and Moore [79].

On the other hand, the symbolism (2) also includes the generalization to a multi-state discrete spectrum interacting with a multichannel continuous one. This case was also admirably tackled by Fano formally [17, 29], albeit only for the continuous spectrum, without the inclusion of the closed channels.

Along those lines, Cordes and Altick [80] also implemented multichannel CI theory with a basis set of hyperspherical coordinates for the determination of properties of the He (3,3b) ^{1}S resonance. The first CI multichannel implementation of Fano's formalism was done by Ramaker and Schrader [81] with application to the He $(n\ell^2)$ ^{1}S autoionizing states.

In order to unify, in the spirit of quantum defect theory, the treatment of discrete and continuous spectra in the presence of discrete Rydberg and valence states and of resonances, Komninos and Nicolaides [82, 83] developed K-matrix-based CI formalism that includes the bound states and the Rydberg series, and where the state-specific correlated wavefunctions (of the multi-state Ψ_0) can be obtained by the methods of the SSA. The validity and practicality of this unified CI approach was first demonstrated with the He ^{1}P^o Rydberg series of resonances very close to the $n = 2$ threshold [76], and subsequently in advanced and detailed computations in the fine-structure spectrum of Al using the Breit–Pauli Hamiltonian [84, 85], which were later verified by experiment (See the references in Ref. [85]).

Furthermore, spin-offs of this type of framework have found application in the study of the effects of Rydberg series on resonances at threshold [86] or in sensitive calculations with Rydberg series-scattering state mixing and radiative transitions between resonance states [87]. The latter application demonstrated the subtle effects that exist in the photoionization cross section of Sr $5d17\ell$ ($\ell \approx 12$) Rydberg level which is autoionizing, in agreement with experiment [88].

In all cases, the agreement with experimental data was achieved without any fitting of parameters for energies, matrix elements, or potentials.

3.2. Complex energy non-Hermitian approaches

As we shall see in Section 5, it is also possible to put together the substance contained in the two equations (3a) and (3b) as one equation. This is achieved by non-Hermitian formalisms which yield the resonance energy and decay rate as a complex number:

$$z_r = E_r - i\frac{\Gamma}{2} \tag{5}$$

The notion of complex energies in quantum physics was introduced ad hoc, via a simple model, by Gamow [25], soon after the establishment of the well-known Hilbert-space QM developed for the discrete spectra. This notion was in radical departure from the Hermitian character of QM, whose normal

structure and calculus involve stationary states and real energies, for which time evolution is represented by a unitary transformation parametrized by a continuous parameter, which is the time, $-\infty < t < +\infty$.

The complex energy, z_r, of Eq. (5) is normally understood in the context of resonance scattering theory as the complex pole in the Breit–Wigner amplitude, or in the S-matrix, or in the "optical potential of Feshbach's theory," or in the Green's function, e.g., Refs. [2, 6–8].

In our work, given our argument that the main emphasis as regards computations in many-electron systems ought to be on the reliable and systematic calculation of (Ψ_0, E_0), we have focused on the following two approaches: In the first, it is demonstrated, by appealing to Fano's formalism [29], that Eq. (5) is an eigenvalue of the Schrödinger equation, with all interactions present, provided the outgoing-wave asymptotic boundary conditions are imposed on the real-energy scattering state of Eq. (2). The second approach applies the time-dependent theory of decaying states [6, 11a, 37, 89]. In either case, the form (1) remains basic.

Below, I recall relevant results from the theory of decaying states. In Section 5, I show how the complex eigenvalue as well as the corresponding form of the resonance eigenfunction can be extracted from Fano's real energy Hermitian treatment, by invoking the outgoing-wave boundary condition that corresponds to the decaying state. In other words, the model of "discrete level interacting with a continuous spectrum" [24, 27, 29] can also yield the complex eigenvalue and the exact form of the resonance eigenfunction, provided the physically appropriate boundary conditions are imposed.

3.3. Decaying state theory and complex poles of the resolvent

In the context of the theory of decaying states for time-independent Hamiltonians [6, 37, 89], the time-dependent wavefunction is in harmony with the form (1),

$$\Psi(t) = a(t)\Psi_0 + X_{as}(t) \qquad (6)$$

where $X_{as}(t)$ represents the products of decay, and $a(t)$ is the amplitude of the "survival probability," $|a(t)|^2$, defined as ($\hbar = 1$),

$$a(t) = \ <\Psi_0|e^{-iHt}|\Psi_0> \ = \ \frac{-1}{2\pi i} \oint_{\text{spectrum}} <\Psi_0\Big|\frac{1}{z - H}\Big|\Psi_0> e^{-izt} dz \qquad (7)$$

In the general case, the contour for the complex variable $z = E \pm i\eta$ surrounds the spectrum of H counterclock-wise on the first Riemann sheet of E, in which case it is valid for $t > 0$ and for $t < 0$. However, in the case of the decay of an unstable state of a field-free Hamiltonian, rigor implies that the following physically constraints must be imposed on the integration of Eq. (7): $E \geq 0$ and $t \geq 0$ [37, 89].

Equation (7) expresses the time-dependent quantum mechanical motion of the system to all orders. As it turns out formally and computationally, for an isolated unstable state decaying irreversibly into a pure continuum, there are three principal regions of time duration that distinguish the behavior of $|a(t)|^2$, e.g., Refs. [6,7,37,89,94 and chapters 7 and 9 in this volume]:

(1) The pre-exponential decay (pre-ED) regime, in a state-specific, very small time interval, $[0,\delta t]$, where the system starts experiencing the effects of the bound-continuum mixing, but has not taken yet the avenue of irreversible exponential decay. Both formally and computationally for real, many-electron systems [94a], the dependence of $|a(t)|^2$ on time in this regime is proportional to t^2, with a "stationarity coefficient" that expresses the degree of initial stability of the state [94] and Section 4.
(2) The ED regime, where $|a(t)|^2 = e^{-\Gamma t}$. The well-known quantity of the energy width of the Lorentzian distribution, with Γ representing the decay rate of the unstable state, acquires legitimacy in this regime. The Fourier transformation to the energy axis of the exponentially decaying $|a(t)|^2$, or of $a(t)$, reveals the corresponding complex energy pole with which the resonance state is associated in the stationary picture.
(3) The long-time non-exponential decay (NED) regime, whose magnitude and physical significance (if any), depend primarily on the type of the energy distribution characterizing the unstable state and on the magnitude of the ratio E/Γ with respect to the energy at threshold [37,89] and Section 3.4.

Let us symbolize the identity operator by $I = \sum |n><n| + \int |E><E| dE$. I is a Hermitian projection operator defined in terms of the complete set of discrete, $|n>$, and scattering, $|E>$, stationary states of the system for each symmetry. Insertion of I into the amplitude $<\Psi_0|e^{-iHt}|\Psi_0>$ leads to the expansion

$$a(t) = \sum_n |<\Psi_0|n>|^2 e^{-iE_n t} + \int |<\Psi_0|E>|^2 e^{-iEt} dE \tag{8}$$

The problem of resonance states, or of decaying states, normally involves only the continuous spectrum, in which case the energy distribution is, according to the above use of the Hermitian I, a real function, given by $|<\Psi_0|E>|^2 dE = |a(E)|^2 dE$. The explicit form of this distribution in terms of computable matrix elements is given by Fano's theory or by decaying-state theory, as

$$|a(E)|^2 = \frac{1}{2\pi} \frac{\Gamma(E)}{((E - E_0 - \Delta(E))^2 + \Gamma^2(E)/4} \tag{9}$$

where, the energy-dependent width and shift functions, $\Gamma(E)$ and $\Delta(E)$, respectively, are given by

$$\Gamma(E) = 2\pi |<\Psi_0|\mathbf{H}|U(E)>|^2 \equiv 2\pi |V(E)|^2 \tag{10}$$

$$\Delta(E) = p.v. \int \frac{|V(E')|^2}{E - E'} dE' \equiv \frac{1}{2\pi} p.v. \int \frac{\Gamma(E')}{E - E'} dE' \tag{11}$$

p.v. stands for principal value, and $U(E)$ is the energy-normalized scattering function of the prediagonalized set.

The value of $\Gamma(E)$ is always positive, but $\Delta(E)$ may be positive or negative. If the behavior of the function $\Gamma(E)$ is smooth and the position of the resonance is far from threshold, the *p.v.* integration in (11) is expected to give a value for the energy shift which is of the same order of magnitude as that of the energy width.

From Eq. (9) it is seen that at $E \approx E_r$ it is the energy-dependence of $\Gamma(E)$ that affects, in principle, the spectral concentration. The standard assumption is that for narrow resonances $\Gamma(E)$ is a constant, whose value at the exact resonance energy is $\Gamma(E_r) \equiv \Gamma = \frac{\hbar}{\tau}$, where τ is the mean *lifetime*, Eq. (3b). The distribution is then an exact Lorentzian. The dependence on energy of τ in the neighborhood $E \approx E_r$ thus follows the Lorentzian distribution, $\frac{1}{\pi} \frac{\Gamma/2}{(E-E_r)^2 + \Gamma^2/4}$ ($\hbar = 1$). On the other hand, the energy-dependence of $\Gamma(E)$ (and, in general, of the *self-energy* of the autoionizing state, see below) may indeed become important formally as well as computationally, and so its evaluation is often necessary, e.g. Ref. [77]. The ED is driven by the complex pole of $|<\Psi_r(E)|\Psi_0>|^2$ just below the real energy axis, i.e., by z_r of Eq. (5).

There is also a conjugate pole of $|<\Psi_r(E)|\Psi_0>|^2$ above the real energy axis, resulting from the contribution of the *time-reversed* state, which represents the adjoint system. Per se, for irreversible decay processes, the time-reversed state corresponding to the conjugate pole does not have physical meaning for $t > 0$, since it then represents a "growing" and not a decaying state (see Eq. (25)).

The complex energy pole and the associated complex energy distribution result from the analysis of Eq. (7) and the constraint $t \geq 0$ (see Section 3.4). Since the resolvent function, $<\Psi_0|\frac{1}{z-\mathbf{H}}|\Psi_0> \equiv <\Psi_0|R(z)|\Psi_0>$, is analytic on the first Riemann sheet, any of its possible complex poles, such as the normal one of Eq. (5), must appear on the second sheet. Rearrangement of $<\Psi_0|R(z)|\Psi_0>$ leads to the implicit for z equation [6, 37]

$$z - E_0 - <\Psi_0|\mathbf{A}(z)|\Psi_0> = 0 \tag{12}$$

whose physically acceptable complex-valued solution gives Eq. (5).

$\mathbf{A}(z)$ is the *self-energy* operator for the decaying state, given by $<\Psi_0|\mathbf{V}R_0(z)\mathbf{V}|\Psi_0>$, where R_0 is the resolvent for the unperturbed Hamiltonian, $\mathbf{H}_0$, and $\mathbf{V}$ is the perturbation operator. In terms of projection operators, if $\mathbf{Q} = |\Psi_0><\Psi_0|$ and $\mathbf{P} = 1 - \mathbf{Q}$, then $\mathbf{H}_0 = \mathbf{QHQ} + \mathbf{PHP}$ and $\mathbf{V} = (\mathbf{H} - \mathbf{H}_0) = \mathbf{QHP} + \mathbf{PHQ}$.

In other words, as discussed in Ref. [37b], the required resonance complex pole of $R(z)$ is the complex eigenvalue, z_r, of the non-Hermitian matrix

$$\bar{\mathbf{M}}(z) = \bar{\mathbf{H}}_0 + \bar{\mathbf{A}}(z) \tag{13}$$

in a space of square-integrable functions, for which: (a) $\mathrm{Im}\bar{\mathbf{A}}(z_r) < 0$, and (b) $|\mathrm{Im}\bar{\mathbf{A}}(z_r)| =$ smallest of other possible poles.

Here I may note that the above definition implies that the pole is reasonably isolated. If this is not the case, then, just as in the case of diagonalization of real matrices for the discrete spectrum, the effects of mixing (interaction) among states with neighboring (even overlapping) complex poles should in principle acquire physical significance. An example of ab initio computation of closely lying or essentially overlapping resonances in a real system (the negative ion of Hydrogen), in terms of a practical method that employs the form (13) with superpositions of real and complex functions in the framework of the CESE theory is discussed in Section 7.2. The analogy is explained below.

3.3.1. From Eqs. (12 and 13), to computational methods such as the CESE, the "exterior complex scaling" and the "complex absorption potential" methods

The matrix $\bar{\mathbf{M}}(z)$ consists of two parts, in correspondence with the form (1). The solution of Eq. (12) or the diagonalization of $\mathbf{M}(z)$ implies the accurate construction and handling of the complex self-energy matrix $\bar{\mathbf{A}}(z)$, which is the same as the complex quantity in the resonance formula in Feshbach's theory [2a, p. 367, 2b, p. 304]. For a many-electron system, such a goal is very difficult to achieve rigorously. Therefore, one has to search for a practical computational method which produces the resonance wavefunction and the corresponding complex energy.

In the article [37b] from the 1978 Sanibel conference on complex scaling, it is pointed out [37b, p. 503] that an equivalent form to that of Eq. (13) can be obtained by rearranging the complex, non-Hermitian Coulomb Hamiltonian matrix, $\mathbf{H}(re^{i\theta})$, whose complete diagonalization produces the discrete, the scattering, and the resonance states [107–114]. (As it turns out, this holds for other types of interactions as well.) The complex eigenvalues of $\mathbf{H}(re^{i\theta})$ are the same as the solutions of Eq. (12) for physical resonance states. The rearrangement that was suggested in Ref. [37b] is

$$\mathbf{H}(re^{i\theta}) = \mathbf{H}(r) + (e^{-2i\theta} - 1)\mathbf{T} + (e^{-i\theta} - 1)\mathbf{V} \tag{14a}$$

$$= \mathbf{H}(r) + \mathbf{K}(re^{i\theta}),\ \mathbf{K}(r) = 0 \tag{14b}$$

This form, which is analogous to that of Eq. (13), exhibits symbolically the fact that only the second part, i.e., a complex operator (matrix), represents the non-Hermitian nature of the problem in a complete function space of square-integrable functions, where the state-specific expectation value of $\mathbf{H}(r)$ is the real E_0 and that of $\mathbf{K}(re^{i\theta})$ is the complex self-energy. Translated into the language of function spaces, it is evident that diagonalization of the real $\mathbf{H}(r)$ on a space of real square-integrable functions yields (Ψ_0, E_0). It is then necessary to find a practical way to incorporate into the complete calculation the equivalent to the effects of the complex operator (matrix) $\mathbf{K}(re^{i\theta})$.

One way of doing this is to focus on the choice of two function spaces on which to project and diagonalize the total Hamiltonian, $\mathbf{H}$ (real coordinates). One would consist of real functions and one would involve a complex basis set that would represent the asymptotic part of the resonance and would allow the contribution of the self-energy to be computed. This spirit is represented by the CESE approach which is discussed in Sections 5 and 6. E.g., see eq. (7.7) of Ref. [37b].

Corresponding to the above idea are methods that implement the regularization technique of "exterior complex scaling" (ECS), which was introduced to atomic physics in Ref. [92b]—see also Refs. [95, 96], and which is discussed in Section 4.3.

A method which attempts to take into account the effects of the form (14b) via brute-force diagonalization is the "complex absorption potential" (CAP) method [193]. In essence, in this method, the complex quantity $\mathbf{K}(re^{i\theta})$ of Eq. (14b) is replaced by an artificial complex function, such as $i\beta r^6$, acting mainly in the outer region of space (β is an adjustable parameter). The papers [193] also discuss the connection between the CAP and the ECS methods, the essence of which is in harmony with that of Eq. (14).

As regards the efficiency and accuracy of the aforementioned methods, it is worth citing a recent study by Meng et al. [194], who used very large B-spline basis sets and a complex coordinate-scaled Hamiltonian, and obtained complex Stark energies for low-lying excited states of Hydrogen and of Lithium. They compared their results with those from previous CESE computations by Themelis and Nicolaides [187] and from CAP computations by Sahoo and Ho [195]. In cases where there are discrepancies between the CESE and the CAP results, the Meng et al. calculations agree with those of Ref. [187]. (Ref. [194], p. 7 and section with conclusions).

The CESE theory and methodology for states perturbed by external fields is discussed in Section 11.

3.4. Non-exponential decay (NED), energy distribution, and time asymmetric dynamics

In standard QM, the reversibility in time is a manifestation of a Hermitian (self-adjoint) system with stationary states and is reflected in the unitarity of the S-matrix. Unitarity entails the inclusion of the contribution of time-reversed states. In other words, for a stationary state, invariance under time-reversal implies that if $\Phi(q)$ is a stationary wavefunction, then so is $\Phi^*(q)$. A major tool for deriving results in the framework of a Hermitian formalism, explicitly or implicitly, is the resolution of the identity operator, $\boldsymbol{I}$, on the real axis, which is a Hermitian projection operator.

In accordance with the Hermitian formalism is the fact that the energy distribution of an unstable state, $|a(E)|^2 dE$, is a real function. In this case, the survival probability, $P(t) \equiv |a(t)|^2$, decays purely exponentially if, and only if, the following conditions are simultaneously satisfied:

(1) The functions $\Gamma(E)$ and $\Delta(E)$ are assumed to be independent of energy in the neighborhood of the position of the resonance. This is a valid assumption for the normally encountered narrow resonances far from threshold.

(2) The lower limit of energy is taken as $-\infty$, rather than finite, contrary to the fact of the existence of the lower bound of the energy of the material system. Most of the formal work on $P(t)$ assumes that the lower limit of the energy integral is $-\infty$ and/or that the discrete spectrum does not contribute. Nevertheless, requirements of corrections to these assumptions may arise when the resonance state is very near the threshold of the continuous spectrum, in which case the time-dependent curve of $P(t)$ acquires, at long-times, a tail of NED [6, 37], see also Refs. [86, 89] and Chapters 7 and 9 of this volume.

Until the mid-1970s, the issue of NED of unstable states had been tackled exclusively in the context of nuclear and particle physics, either via pure formalism or via simple one-dimensional models. The standard approach was to assume a model function for $|a(E)|^2 dE$. The established wisdom was that in isolated quantum systems decaying into a purely continuous spectrum, long-time NED is just too small to be observed, regardless of the method of measurement.

In 1976–1978, we examined the issue of NED in the context of the real spectra of atoms, focusing on the decay of autoionizing states [37]. Our analysis aimed at understanding favorable conditions for observability of NED. We pointed out that a crucial parameter is the ratio E/Γ, and we introduced the idea of searching for states with *threshold proximity*. The importance of this idea to the appearance of NED was actually demonstrated in real many-electron unstable states in 1996, via the ab initio solution of the TDSE [89b].

In addition to the question of observability, our attention also turned to the fundamentals of the theory of decaying states as regards the computation of $P(t)$. Specifically, it was pointed out [37], and explained again a few years ago [89], that, if the theory starts directly from Eq. (7), without first introducing the Hermitian spectral resolution as in Eq. (8), then, in addition to the constraint of $E \geq 0$, there is the constraint imposed by the singular point at $t = 0$, which separates, in the theory of decaying states, time evolution for $t \geq 0$ from that for $t < 0$. This is connected to the fact that the real function $|a(E)|^2 dE$ separates into two *complex conjugate energy distributions*, say $a(E)$ and $a^*(E)$. Of the two, the physics of decay implies that only $a(E)$ produces the decay for $t \geq 0$. Now, the mathematical structure of the problem of computing $a(t)$ in terms of $a(E)$ becomes non-Hermitian. The assumption of the physical significance of the point $t = 0$, which is basic to the definition and analysis of decaying states, adds a source term $i\delta(t)$ (δ is the delta function) in the solution of the TDSE as a boundary condition [37b, 89]. The requirement for decay is to choose the complex energy distribution for only the $t \geq 0$ case. This breaks the unitary structure of S-matrix QM via which the formalism incorporates the contribution of time-reversed stationary states, and allows *time-asymmetric dynamics* at the quantum level [37, 89].

Both the real energy distribution (Hermitian treatment of decay) and the complex energy distribution (non-Hermitian treatment of decay) were considered in Refs. [37, 89] in connection with the problem of NED and the *quantum arrow of time*. It was demonstrated that, although the complex pole characterizing the unstable state and its exponential decay is the same for both distributions, the quantitative result for the NED in each case is different. As it was stated in my Physical Review paper [89a], these facts "raise the issue of the nature of the energy distribution in the description of irreversibility at the quantum level, and its possible manifestation"… [89a, p. 2].

> If, in the future, it becomes possible to measure with great accuracy the NED of an isolated unstable state, for which accurate calculations of the same quantity could also exist within the two frameworks discussed in this paper (real and complex energy distributions), significant information as to the physical relevance of long-time NED should emerge.
>
> [89a, p. 6]

A proposal for a pump–probe experiment for the possible detection of long-time NED of an isolated unstable state has been published in Refs. [94a, 94c]. It involves the following excitation scheme:

He$^-$ 1s2s2p ^{4}P^o $\xrightarrow{pump}$ He$^-$ 1s2p^2 ^{4}P $\xrightarrow{probe}$ He 1s2p^3 P^o + e where He$^-$ 1s2p^2 ^{4}P labels a shape resonance 10 meV above the He 1s2p^{3}P^o threshold.

Aspects of the theme of long-time NED and its exploration in terms of models are discussed in the articles by Garcia-Calderon, Chapter 7, and by Torrontegui et al., Chapter 9.

4. ASPECTS OF THE NATURE AND OF THE PREPARATION OF Ψ_0 AND OF ITS CONNECTION TO THE RESONANCE EIGENFUNCTION

As I have already mentioned, when the treatment of unstable (resonance) states in many-particle systems is attempted not in terms of model potentials with, say, easily recognizable wells and repulsive regions, but in terms of formalism that uses the exact kinetic and potential operators, it becomes impossible to separate the total Hamiltonian into two explicitly written parts, one providing as real eigenvalues and eigenfunctions the "zero-order discrete spectrum" embedded in the continuum and the other providing the continuous spectrum of the scattering states that are rigorously decoupled from the discrete states. Such an uncoupled form is meaningful only for resonance states that are produced upon the interaction of a weak external field with the atom (molecule), in which case both the zero-order Hamiltonian and the full perturbation can be written explicitly.

The concomitant fundamental problem is how to understand physically and how to define and compute the state of the system which is assumed to be localized at $t = 0$. If attention is turned to features of function spaces rather than to forms of operators, then the degree and type of mixing, due to all couplings present in the Hamiltonian, between localized and scattering components for an assumed separation of the total function space plays a crucial role. In addition, I emphasize that the mode of excitation of the system under examination in the energy region of the continuous spectrum where the resonance exists is also of paramount importance. For example, it is a standard prerequisite for the validity of the preparation of Ψ_0 that yields the complex pole and the associated exponential decay that the energy width of the well-defined excitation pulse is larger than $\hbar/\tau$, where τ is the mean lifetime of the unstable state [6, 7]. Finally, given the system "atom plus excitation pulse," the relative magnitude of the excitation matrix elements to the assumed Ψ_0 and to the scattering continuum associated with it must also be considered.

In the following paragraphs of this section, I elaborate briefly on aspects of the theory of resonance states in many-electron atoms and molecules that have to do with the above comments.

Let us assume that the Born–Oppenheimer (B–O) approximation works extremely well, although this is certainly not guaranteed for highly excited

molecular states. Then, without loss of the conceptual generality, the formal and computational focus is on the N-electron atomic or B–O Hamiltonian, which, in the nonrelativistic and in the relativistic (Dirac–Breit–Pauli), formulation consists of one- and two-electron operators,

$$\mathbf{H} = \sum_{i=1}^{N} f_i + \sum_{i>j}^{N} g_{ij}.$$

Since for a given symmetry, nonrelativistic or relativistic, $\mathbf{H}$ has only a continuous spectrum above the first ionization threshold, it is impossible to write an explicit form of a local operator of which Ψ_0 is an eigenfunction. On the other hand, any approximate (model) Hamiltonian which is separable as the sum of one-electron operators, such as the hydrogenic or the HF, may produce discrete eigenvalues inside the continuous spectrum. However, such models for choosing Ψ_0, i.e., the "exact" discrete state embedded in the continuum, are computationally unrealistic, since the interelectronic interactions are never switched off physically. Therefore, for the purpose of quantitative understanding, the difficult task is how to obtain Ψ_0 and E_0 that refer to an effective nonseparable Hamiltonian, $\mathbf{H}_0$, so as to account for all the contributions to the initial stability of the state. This question was the main object of discussion in Refs. [11a, 37b]. For example, in Refs. [37b, p. 461] the following statement is written:

> Equation $(\mathbf{QHQ} - E_0)|\Psi_0> = 0$ (where $\mathbf{Q}$ is defined by $\mathbf{Q} = |\Psi_0><\Psi_0|$), has the character of a self-consistent equation, like an ordinary HF equation. This is so because $\mathbf{QHQ}$ depends on the wave function on which it operates, which in turn can depend implicitly on the eigenvalue E_0. Its solution is effected by successively expanding the function space spanned by the trial $\tilde{\Psi}_0$ and looking for a maximal square-integrable Ψ_0 still satisfying the above equation.....

In the case of a relativistic system, as a first (and useful) approximation, the zero-order spectrum can be taken as the nonrelativistic one, with $\mathbf{H}_0$ defined explicitly as the Coulomb Hamiltonian. Then, the perturbation $\mathbf{V}$ is also written explicitly as the relativistic Breit–Pauli operators, and it is this perturbation that turns the initially discrete state into a resonance. For example, this type of advanced calculation, with multichannel coupling included, has been shown to explain quantitatively the positions and lifetimes of the relativistic levels of metastable states in negative ions [90]. However, if the more accurate four-component relativistic Dirac treatment for each electron is invoked for cases of high effective nuclear charge, then the stability against autoionization implies not only the exclusion of components representing decay to

the adjacent electronic continuum but also, in principle, the exclusion of the mixing of positive–negative energy components that may cause dissipation into the "positron sea." In any case, the concepts discussed herein as to the importance of appropriate boundary conditions on wavefunctions that can be used in the problem of computing wavefunctions and properties of resonance states in nonrelativistic or in relativistic Hamiltonians are generally applicable.

In Ref. [11a], the physical meaning and the possibility of accurate computation of Ψ_0 was placed at the center of the quest for a practical theory of resonance states. Thus, in the defining equations (1–4) of Ref. [11a], the Gamow-Siegert boundary conditions for the resonance eigenfunction, $\Psi_r(z_r)$ (henceforth Ψ_r), and for Ψ_0 (asymptotically vanishing) were considered, together with the finite projection $<\Psi_0|\Psi_r>$ which implies the form (1) in the energy representation.

The development of the theory [11, 37b] used as reference point the difference between Ψ_0 and Ψ_r in terms of the change of the boundary condition asymptotically.

This is in harmony with the notion that, in configuration space, for all practical purposes Ψ_0 represents the resonance eigenfunction in the inner region, beyond which the components of Ψ_r connected to the open channels describe the state.

It was emphasized that, irrespective of what type of formalism is used, the practical and essential question is how to define Ψ_0, whose energy E_0 is embedded in the continuous spectrum of **H**, how to compute it systematically in real, polyelectronic systems, and how to continue the computation in order to obtain Ψ_r and its properties. This is because, although the phenomenology resulting from resonance scattering theory or from decaying state theory is satisfied by the mere adoption of any bound wavefunction (i.e., a model of discrete-continuum state mixing leading to a complex pole below the real energy axis and to the concomitant ED), two important questions remain:

(1) Does the formal definition of Ψ_0 as a bound wavefunction have an optimal correspondence with the description of the resonance state in terms of an initially localized wavepacket?
(2) How can the computation of Ψ_0 be carried out systematically for a many-electron Hamiltonian, **H**?

The second question is the subject of Section 8, while a sample of relevant applications is given in Section 7. Here, I briefly comment on the first question.

Formally, the proximity, but not equality, between the resonance state and Ψ_0 was defined in the context of time evolution of a nonstationary state as [94b, 37b],

$$\lim_{t \to 0} |\Psi(t) > = |\Psi_0 > \tag{15}$$

with

$$|\Psi(t) > = \exp[-(i/\hbar)\mathbf{H}t]|\Psi_0>, \quad |\Psi_0(t) > = \exp[-(i/\hbar)\mathbf{H}_0 t]|\Psi_0 > \tag{16}$$

Let

$$u(t) \equiv \Psi(t) - \Psi_0(t) \tag{17}$$

By considering the infinitesimal unitary transformation such that

$$||\lim_{t \to 0} u(t)|| = \min, \tag{18}$$

the result which emerges is that, formally, the optimal $|\Psi_0 >$ must satisfy the following relation involving the energy variance,

$$<\Psi_0|(\mathbf{H}- <\mathbf{H}>)^2|\Psi_0> \equiv (\Delta E)^2 = \min \tag{19}$$

Obviously, if Ψ_0 were a real stationary state, i.e., an eigenstate of $\mathbf{H}$, Eq. (19) would be zero.

The relevance of matrices of $(\mathbf{H} - <\mathbf{H}>)^2$ constructed in terms of real basis functions has been invoked either in the context of time-independent formalism or ad hoc, in analogy with calculations on discrete states, for the computation and certain analysis of simple unstable atomic states [91].

The time-dependent considerations of the previous paragraphs [94b, 37b] provide a justification for Eq. (19) at a fundamental level which is based on the notion of time-dependent *stationarity* of unstable states in the regime of $t \approx 0$.

A generalized version of Eq. (19), suitable for complex matrices and producing both energies and widths of resonances, has also been introduced and applied in the framework of the present theory [37b, 92, 93]. As it was pointed out in Refs. [37b, p. 487], "This variational principle was first given with the Gamow functions in mind [92]. However, given the equivalence demonstrated (in Ref. [37b]), it is obvious that a completely analogous principle holds for $\mathbf{H}(\theta)$." $\mathbf{H}(\theta)$ is the complex Hamiltonian with scaled coordinates, $r \to re^{i\theta}$, see Section 5.1).

It was in response to criticism of the method proposed in Ref. [92a] (and implemented in Ref. [93]) as regards the practical computation of matrix elements with resonance wavefunctions that the integration technique later called "ECS" was suggested—see Section 4.3 below. Its conceptual background is the form (1).

4.1. A comment on preparation of time-dependent nonstationary states with initial state Ψ_0 and of energy-dependent stationary states in the form of Eq. (2)

Given the normal formulation of QM in terms of stationary states, including the case of resonances in the continuous spectrum (see the superposition wavefunction of Eq. (2)), and the corresponding expressions which are measured on the energy axis, the question arises as to how easy it is to prepare unstable states in polyelectronic atoms and molecules and to observe their time-dependence. The answer involves more than one components. The most frequently mentioned is to consider the magnitude of the lifetime (provided, of course, that it is known) relative to the duration of the excitation process. Obviously, if the former is much longer than the latter, the concept of a decaying state is valid.

However, a related issue that has to be addressed is the fact that, in the energy representation, there are only stationary scattering states in the continuum. So it is important to explore and understand the components of the excitation mechanism which lead to the preparation of the decaying state, rather than of the stationary state, Eq. (2). Obviously, one parameter is indeed the duration of the excitation interaction. At the same time, of fundamental significance is the magnitude of the excitation matrix elements to the components of the wavefunction in the form of Eq. (2). Their knowledge implies a quantitative understanding of the interplay between the characteristics of the interaction and the electronic structure and spectrum of the atom.

The following examples of photoabsorption into the continuous spectrum demonstrate the argument: Consider the interaction of two atomic ground states, the He $1s^2\ ^1S$ and the Be $1s^2 2s^2\ ^1S$ state, with photons in the vicinity of 60.1 eV for the former and of 125 eV, and slightly above, for the latter. For the sake of this discussion, I will not consider electron correlation (see Sections 8 and 9).

In the first case, the energy corresponds to the position of the doubly excited resonance state, He "2s2p" $^1P^o$. The energy-dependent, stationary state description of the excitation is

$$\text{He } 1s^2\ ^1S \xrightarrow{h\nu\ \approx\ 60.1\,\text{eV}} \Psi(E) = \left[a(E)(2s2p) + \int_0^\infty d\varepsilon\, b_E(\varepsilon)(1s\varepsilon p) \right]\ ^1P^o.$$

For a given duration of the photon pulse, the probability of raising the system to the bound component (2s2p) or to the scattering component $(1s\varepsilon p)$, in the vicinity of $E = E_0$, depends on the magnitude of the electric dipole-coupled matrix elements, $|{<}1s^2|r|2s2p{>}| = |{<}1s|r|2p{>}| \times |{<}1s|2\bar{s}{>}|$ and $|{<}1s^2|r|1s\varepsilon p{>}| = |{<}1s|r|\varepsilon p{>}| \times |{<}1s|1\bar{s}{>}|$. I point out that the orbitals $(1\bar{s}, 2\bar{s})$ are obtained from their own state-specific potential and, therefore,

are not orthonormal to the HF 1s orbital of the ground state. This implies that even in this independent electron description with state-specific HF functions, the overlap $|<1s|2\bar{s}>|$ is finite rather than zero, and the double excitation is allowed even without the addition of correlation configurations, see Section 9.3. In fact, even before electron correlation is considered, because of the large magnitude of $|<1s|r|2p>|$, the excitation by a short pulse of the (2s2p) component (representing the unstable state) is expected to be considerable but, of course, not exclusive, since the direct ionization matrix element, $|<1s|r|\varepsilon p>| \times |<1s|1\bar{s}>|$ is also important. The preceding conclusions do not change when electron correlation is included in the computation of the wavefunctions of the initial state and of the localized Ψ_0. In other words, this is a case where a pulse in the range of femtoseconds or shorter can excite the unstable state ("2s2p") with high probability, but the scattering components,1sεp, are also simultaneously excited and contribute to the quick formation, via the Coulomb interaction, of the stationary superposition. For the first ab initio computations of the time-dependent excitation and decay of this resonance state and of the time-resolved formation of its profile on the energy axis, the reader is referred to Refs. [171b, 171c].

The second case chosen above, that of Be, is even more characteristic of the decisive role that is played by the excitation matrix elements in preparing overwhelmingly the unstable state, which now is an inner-hole autoionizing state. Specifically, since the binding energy of the 1s electron in Be $1s^2 2s^2$ ^1S is about 123.7 eV [149a], the absorption of a photon with, say, $h\nu = 125$ eV or slightly higher, gives rise to the following two possibilities of ionization to the same continuum, whose probability amplitudes interfere to some degree.

(1) Preparation of an inner-hole unstable state:

Be $1s^2 2s^2$ ^1S $\xrightarrow{h\nu \approx 125\,eV}$ [Be$^+$ $1s2s^2$ $^2S + \bar{\varepsilon}p]^1P^o$, where $\bar{\varepsilon}p \approx 1.3$ eV and the autoionizing state, Be$^+$ $1s2s^2$ ^2S, whose width is 0.023 eV [149a], decays to Be^{++} $1s^2{}^1S$ by emitting an $\bar{\varepsilon}s$ electron of energy 96.2 eV [149a].

(2) Double electron ejection from the valence shell:

Be $1s^2 2s^2$ ^1S $\xrightarrow{h\nu \approx 125\,eV}$ [Be^{++} $1s^2$ $^1S + (\varepsilon's, \varepsilon p)]$ $^1P^o$, where the sum of the energies of the two electrons, $(\varepsilon's + \varepsilon p)$, is equal to 125 eV—[$E(Be^{++}_{1s^2}) - E(Be_{1s^2 2s^2})$] ≈ 97.5 eV.

In the vicinity of the energy of the unstable state, ("1s2s^2"), the stationary state is the superposition $[a(E)(1s2s^2) + \int_0 d\varepsilon's b_E(\varepsilon')(1s^2\varepsilon's)]$.

The excitation matrix elements for the processes (1) and (2), for each value of the free-electron energies, involve all four electron coordinates, even without electron correlation—see Section 9.3. These are (squared),

$$(1) \ |<1s2s^2|1\bar{s}2\bar{s}^2>|^2 \times |<1s|r|\bar{\varepsilon}p>|^2 \ \approx \ |<1s|r|\bar{\varepsilon}p>|^2.$$

$$(2) \ |<1s^2|1\bar{s}^2>|^2 \times |<1s|\varepsilon's>|^2 \times |<1s|r|\varepsilon p>|^2 \approx 0$$

The zero for case (2) is caused by the squared overlap, $| < 1s|\varepsilon's > |^2$, where the two orbitals are essentially orthogonal. It follows that, upon photoexcitation by a pulse in the region of photon energies above 125 eV (and before the next channel opens), Be will be driven exclusively to the unstable state of Be^+, the $('1s2s^{2'}) \ ^2S$.

4.2. Formal and quantitative properties in the pre-exponential decay regime of duration $[0, \delta t]$

The assumption of the preparation of the localized wavefunction Ψ_0 at $t = 0$ is of paramount importance to the theoretical-mathematical description of decaying (resonance) states. It is only then that notions and observations such as irreversible fragmentation of unstable states or interference effects in transition processes involving the continuous spectrum can be understood conceptually and quantitatively.

For example, when a spectroscopic measurement is carried out along the energy axis that covers the energy continuum of stationary states and an isolated resonance peak is observed having a particular profile, it is through the Feshbach-Fano formalism of bound-scattering mixing in the continuum that its details can be explained in terms of coupling matrix elements. In other words, without the complete formation over an energy range and rigorous analysis of the spectral peak (profile) on the energy axis in the region of (Ψ_0, E_0), no accurate description of a resonance state in terms of its exact position, E_r, and of its rate of decay, Γ, can be deduced from an energy measurement. The most characteristic example is the detailed description of the asymmetric peaks in photoabsorption experiments which was introduced by Fano [29].

In this section, I turn my attention to the question of what happens from the point of view of time when the description refers to a very short time duration, $[0, \delta t]$, just after the point $t = 0$ at which Ψ_0 is prepared and *before* ED (which corresponds to the complex pole in the resolvent that constitutes the definition of the resonance state on the energy axis), starts. Of course, this question has clear meaning when the combination of the characteristics of the unstable state and of the corresponding excitation process justify the assumption of the distinct preparation of Ψ_0 at $t = 0$, which is the point in time that the mixing with the adjacent continuum starts.

I will refer to three themes. Two of them have already been investigated in terms of the ab initio solution of the TDSE for real, many-electron unstable states of atoms. The third is, admittedly, rather speculative and is awaiting measurement or detailed computation.

(1) The first theme refers to the computation of the *survival probability*, $|a(t)|^2 = |<\Psi_0|e^{-i\mathbf{H}t}|\Psi_0>|^2$, Eq. (7), in the time domain $t \approx 0$. Given its computational advantages, the SSA has allowed the calculation of related quantities, from first principles, of three different types of unstable states with different structures and lifetimes: The He$^-$ 1s2p^2 ^4P shape resonance, the *Ca KLM*3d5p $^3F^o$ Coulomb autoionizing state, and the He$^-$ 1s2s2p $^4P^o_{5/2}$ metastable state which decays via spin–spin interactions [94a].

(2) The second theme refers to the recent demonstration, from first principles, of the time-dependent formation of the photoabsorption Fano profile of the He 2s2p $^1P^o$ resonance, i.e., of the time-resolved dynamics of the formation of a stationary state in the region of a resonance [171b, 171c].

(3) The third theme has a hypothetical element, in that no quantitative results exist yet. In this case, the assertion is made that, upon the initiation of the discrete-continuum level interaction at $t = 0$ and during the pre-ED period, $[0,\delta t]$, a time-dependent progression of energy shift is also initiated and accumulates from the value zero at $t = 0$, when the initial value of the energy is E_0, to the final amount Δ, which is the energy shift of the energy-dependent resonance or of the decaying state theories, in which $E_r = E_0 + \Delta$.

Theme (1): The appearance of the variance $(\Delta E)^2$ in Eq. (19) is a principal result of the consideration of the $t \rightarrow 0$ limit of the decaying state. In addition to the possibility of using it as a computational constraint, e.g., Ref. [91], its significance has to do with the nature of unstable states. Because of this, in Ref. [94a] it was named the *stationarity coefficient*. This quantity, together with the conventional quantity of the mean lifetime corresponding to the ED regime, constitutes an intrinsic property of each unstable state.

The stationarity coefficient, $(\Delta E)^2$, emerges formally upon the expansion in series of the time evolution operator, $e^{-i\mathbf{H}t}$, as the coefficient of t^2 in the first-order expansion of $|a(t)|^2$. Specifically, $|a(t)|^2 \approx 1 - (\Delta E)^2 t^2 + \ldots$. In fact, this easily derived formal, and model-independent, result, i.e., the t^2 - dependence for a time interval $[0,\delta t]$, was first verified and quantified in real many-electron systems in 2001, via the ab initio solution of the TDSE for the unstable atomic states mentioned above, for which it was found that indeed it characterizes the regime of pre-exponential decay of $|a(t)|^2$ for $[0,\delta t]$ of the order of decades to hundreds of atomic units of time (1 a.u. = 24.2 as) [94a]. The magnitudes of $(\Delta E)^2$ differ considerably from state to state. For example, for the He$^-$ 1s2p^2 ^4P state it is 1.9×10^{-7}, while the lifetime is about 5200 a.u.. For the *Ca KLM*3d5p $^3F^o$ state, the magnitude of $(\Delta E)^2$ is 1.1×10^{-5}, while the lifetime is about 1450 a.u. [94a].

Theme (2): The assertion as to the physical significance of the pre-ED period, $[0,\delta t]$, is supported by the recently obtained, from the ab initio

solution of the TDSE, time-resolved formation of the resonance (Fano) profile in doubly excited and in inner-hole states, within short periods of a few thousand attoseconds [171b, 171c, 76]. For example, figure 3 of Ref. [171b] shows the various phases of the formation of the resonance photoionization profile as a function of time (in the hundreds of atomic units) upon excitation of the He ground state by a laser pulse of 60.1 eV (which is the position of the resonance). Specifically, after about 450 a.u. the profile is essentially symmetric, meaning that the effects of interference from the discrete-continuum mixing are still weak and far from being complete. The completion of the build up of the stationary state in the neighborhood of (Ψ_0, E_0) takes about 4000–5000 atomic units of time. Its characteristics (Fano q parameter, energy position and width), agree with those that are known from energy-dependent theory and experiment [171b].

These results imply that, since the complete description of the resonance state must account for all the effects of interaction and of interference before it can be recognized as such on the energy axis, it is indeed possible to time-resolve a short period of stationarity before the exponential decay starts, during which the unstable state acquires its observable intrinsic characteristics.

Theme (3): I now make the following assertion, the essence of which first appeared in the discussion of Ref. [11a] (see quotation below) and continued with the analysis presented in Ref. [94b]: Assume that the excitation interaction leads the system overwhelmingly to $|\Psi_0 >$ at $t = 0$. Given the existence of the pre-ED period $[0, \delta t]$, one may assume that this time duration represents the preparation stage for the complete formation of the stationary resonance state, since it is the subsequent ED and the corresponding complex pole that ought to define the resonance state in the energy representation. In other words, the variance $(\Delta E)^2$ expresses the degree of stability (instability) of the initially ($t = 0$) localized state, $|\Psi_0 >$, upon mixing with the adjacent continuum, and the assertion is made that it is during this short period, that the energy shift, Δ, acquires cumulatively along the time axis its final constant value, so as to have the subsequent ED with a mean lifetime $\tau = 1/\Gamma$ and an exact energy, $E_r = E_0 + \Delta$.

Accordingly, if the contribution to the total shift, Δ, at each point of time in the range of $[0, \delta t]$ is $v(t)$, then Δ is of the order of $\int_0^{\delta t} v(t)dt$. Presumably, $v(t)$ is proportional to (real) $<a(t)\Psi_0|\mathbf{H}|X(t)>$, evaluated at each t in the pre-ED period $[0, \delta t]$. When the state has entered into the ED time regime, $v(t)$ should go to zero for $t > \delta t$, and remain so for all t in $(\delta t, \infty)$. It is in the ED regime that the state is recognized as a resonance on the energy axis, whose intrinsic properties are E_r and Γ.

The above assertion could be tested via ultra fast, time-delay, pump-probe experiments which would measure the energy of the probed resonance as

it is being "dressed" by the continuum for a very short period of time after the preparation of (Ψ_0, E_0). It first appeared as a descriptive hypothesis in 1972 [11a], at a time when it was unthinkable to consider the ab initio solution of the TDSE or the measurement of hyper-short time-resolved processes. I quote:

> Furthermore, due to the coupling with the continuum, the initial energy suffers a shift Δ which in principle ought to be time (energy) dependent. One may then imagine that for $t \sim (0, \delta t)$ the energy changes by small increments $\varepsilon(t)$ until an extremum is reached at which $\frac{\partial E(t)}{\partial t}\big|_{t \geq t'} = 0$, $[\varepsilon(t') = 0]$, and the state of the system is in the resonant state $|\Psi >$ with energy E. . . .

> [11a, p. 2084]

A complementary result which is along the spirit of this speculative description as regards the significance of the stationarity regime of $t \approx 0$ was published a few years later [94b] in terms of $(\Delta E)^2$ and of the concepts expressed via Eqs. (15–19).

4.3. Exterior complex scaling

Equation (1), and the fact that Ψ_0 represents the bulk of the characteristics of the state and of the interparticle interactions, imply that the optimal route to the calculation of the total $\Psi_r = a\Psi_0 + X_{as}$ goes through a two-step procedure, each step requiring the application of specific methods and correspondingly appropriate functions spaces. Following the picture of decaying states, the first step is the direct and state-specific calculation of Ψ_0, containing the information from the interaction inside the main volume. This is followed by a different type of calculation of X_{as} in the presence of Ψ_0, leading to the determination of the total Ψ_r.

This idea is at the root of the ECS technique for the regularization of matrix elements between resonance wavefunctions, which was written explicitly in Ref. [92b] (see Eq. (20) below) and was used in Ref. [95] for various potentials. The name ECS was later given by Simon [96], who proposed the same scheme for handling difficulties with the calculation of molecular resonances in the B–O approximation.

Specifically, in Ref. [92b], in response to earlier criticism by Bransden as to the validity of our proposed variational method for resonances [92a, 93], we commented on certain properties of resonance states, emphasizing that what is important is to have a consistent definition of matrix elements. We focused on the argument that the essence of the difference between the resonance function and Ψ_0 lies in the change of the boundary conditions asymptotically [11, 37]. Thus, given a wavefunction calculation of any type in a finite region of configuration space of radius R, it was argued that matrix

elements could still be defined consistently provided the following regularization procedure for the resonance wavefunction is followed (eq. (3) of Ref. [92b]),

$$\int\limits_{\text{all space}} \psi^2 dr = \int\limits_{0}^{R} \psi^2 dr + \int\limits_{C} \psi^2 ds \qquad (20)$$

where the contour C is defined based on the intrinsic characteristics of the resonance and $R < \text{Re}\, s < \infty$.

In Ref. [92b] we wrote: "Construction (20) shows that, as the resonance width tends to zero, the contour integral is brought to the real axis and the integral $\int_{\text{all space}}$ is finite on the real line because it is taken over bound states..."

The ECS technique has attracted interest and has found applications in a number of areas. For example, it has been used for the calculation of resonances in molecular states with finite barriers [95, 97], or for the solution of numerically demanding scattering problems [98], or for the solution of the TDSE via grid methods [99]. It has also been invoked for practical connections to the CAP method [193]-see discussion in Section 3.3.

5. THE FORM OF THE RESONANCE EIGENFUNCTION AND THE COMPLEX EIGENVALUE SCHRÖDINGER EQUATION

When remonstrating Gamow in the library, I went so far as to express doubt whether Gamow wavefunctions, with their infinite norm, could at all be regarded as solutions of a Schrödinger equation. Pauli happened to overhear this rather wild statement: "They are certainly solutions" he interjected, "but whether they are allowed in quantum mechanics, this is questionable". Gamow looked at us with an expression of wonder in his face: "But my solution," he said, "just represents a damped resonance process; the exponential increase at large distances has a simple interpretation, and after all I get the decay constant and an improved Geiger-Nuttal law. What else do you want?". "Anyhow," Pauli concluded as he went away, "it was great fun to see the flood of papers your theory let loose."

[100]

As first proposed by Gamow [25] via a model for alpha particle decay (tunneling of the so-called "shape" resonances), and later again by Siegert [8a] in the context of scattering theory, the complex eigenvalue is the result of the physical notion of a wavefunction with only an outgoing component. The corresponding complex eigenfunction of the time-independent Schrödinger equation is not square-integrable and does not belong to Hilbert space.

On the other hand, Fano's theory [29] has a Hermitian structure where only real energies appear. At the same time, it contains all the information regarding the problem of mixing of bound and scattering components of resonance states. So the following question arises: Where is the complex eigenvalue and how can one extract it from Fano's formalism together with the corresponding form of the resonance eigenfunction?

This question was answered some time ago in Ref. [101], where we showed how the corresponding *complex eigenvalue Schrödinger equation* (CESE) is derived via the appropriate consideration of boundary conditions. The concomitant results justify the computation of resonance states in terms of non-Hermitian, complex-energy formalism via the use of superpositions of square-integrable real and complex functions.

Specifically, instead of solving the problem of uncovering the resonance state by using the appropriate superposition of Ψ_0 with stationary scattering wavefunctions for each value of the energy in the continuous spectrum, this description is achieved directly in terms of the CESE. The CESE is obtained after the boundary conditions on the Fano scattering function, $\Psi(E)$, have been changed from those of a standing wave to those of an outgoing wave only. The first such derivation [101] involved short range and Coulomb potentials, together with a corresponding variational principle. Subsequently, the same idea was applied for the understanding of the creation of resonance eigenfunctions in the LoSurdo-Stark problem as well as of the necessary coordinate transformations that render these eigenfunctions square-integrable [102].

The crucial idea is the imposition of the appropriate asymptotic boundary conditions on the real-energy scattering wavefunction in order to render it a resonance eigenfunction. To this purpose, let us return to Fano's standing wave approach. In order to solve for the expansion coefficients, $a(E)$ and $b_E(E')$, in Eq. (2), Fano followed Dirac's method ([103a] and section 50 of Ref. [103b]), whereby inverting $(E - E')$ along the real axis of the continuous spectrum introduces an unknown function, $\lambda(E)$, which is determined by the boundary conditions. Thus, he obtained the real function

$$\lambda(E) \rightarrow Z(E) = \frac{E - E_0 - \Delta(E)}{|V(E)|^2}, \tag{21}$$

The reality of $Z(E)$ in Eq. (21) is the manifestation of the time-symmetric, Hermitian structure of the theory. On the other hand, it was shown [101] that $\lambda(E)$ becomes imaginary if the outgoing boundary conditions are imposed on the asymptotic form of $\Psi_r(E)$, whereby the problem becomes non-Hermitian and time-asymmetric, and described by two adjoint CESEs, one of which corresponds to the physically relevant solution of the decaying state.

Specifically, suppose, for the sake of simplicity in the symbolism, we consider the case of a short-range potential. Using the asymptotically standing

wave scattering function of the free particle which enters in the antisymmetric N-electron wavefunction $U(E)$ of Eq. (2), $u_{r\to\infty}(r;E) \sim \sqrt{\frac{2}{\pi k}} \sin(kr + \delta)$, it is possible to rearrange the asymptotic form of the Fano solution into the form (energy and momentum are real, $E = \frac{1}{2}k^2$),

$$\Psi_{r\to\infty}(E) \sim -\sqrt{\frac{\pi}{2k}} Va(E)\left[\left(1 - \frac{\lambda(E)}{i\pi}\right)e^{iN} + \left(1 + \frac{\lambda(E)}{i\pi}\right)e^{-iN}\right] \qquad (22)$$

where $N \equiv (kr + \delta)$ and $\lambda(E)$ is to be determined by the boundary conditions which we impose.

The form (22) is the sum of an incoming (e^{-iN}) and of an outgoing (e^{iN}) wave. For $t > 0$, the outgoing wave corresponds to a decaying state and the incoming wave to a "growing" (unphysical for $t > 0$) state. In order for only one or the other to survive, $\lambda(E)$ must take one of the two values:

$$\lambda(E) = -i\pi, \text{ for outgoing wave boundary condition} \qquad (23a)$$

$$\lambda(E) = +i\pi \text{ for incoming wave boundary condition} \qquad (23b)$$

From Eqs. (21 and 23) it follows that, corresponding to the real energy which results from the Hermitian treatment, there exist two conjugate complex energies:

$$\text{For } \lambda(E) = -i\pi, E \to z_r = E_r - i\frac{\Gamma}{2} \qquad (24a)$$

$$\text{For } \lambda(E) = +i\pi, E \to z_r^* = E_r + i\frac{\Gamma}{2} \qquad (24b)$$

Furthermore, since for $E = E_r$ the coefficient $a(E)$ has the value $a(E_r) = -\frac{\sin(\pi/2)}{\pi V} = -\frac{1}{\pi V}$, the asymptotic forms for the two solutions at the energy E_r are the complex functions

$$\Psi_{r\to\infty}^d(z_r) \sim \sqrt{\frac{2}{\pi k_r}} e^{i(k_r r + \delta)} \; k_r = \sqrt{2z_r}, \text{decaying state for } t > 0 \qquad (25a)$$

$$\Psi_{r\to\infty}^g(z_r^*) \sim \sqrt{\frac{2}{\pi k_r^*}} e^{-i(k_r^* r + \delta)} \; k_r^* = \sqrt{2z_r^*}, \text{growing state for } t > 0 \qquad (25b)$$

The above results show how, from Fano'sHermitian (time-symmetric) treatment of discrete-continuum level interaction, which is based on the real-energy Schrödinger equation and the scattering stationary-state normalization

$$\mathbf{H}\Psi_r(E) = E\Psi_r(E), \; <\Psi_r(E)| \Psi_r(E')> = \delta(E - E') \qquad (26)$$

it is possible to extract two adjoint, non-Hermitian CESEs, whose solutions have the form (1), with asymptotic boundary conditions given by Eqs. (25). In other words, Eqs. (23–25) reflect the fact that the Hamiltonian describing a decaying system is not self-adjoint, due to the special asymptotic boundary conditions. Instead, there are two adjoint solutions which are different functions and produce conjugate complex energies.

Note that, on resonance, the forms (25) are the traveling-wave-equivalent of the standing wave real function, with the same normalization factor. The new insight is that the discrete-continuum interaction which is taken into account in the Fano treatment turns the momentum into a complex number with physical significance, while the two solutions correspond to the two directions of time. Of these, only one is physically acceptable as a decaying state, namely the one with outgoing wave conditions:

$$(\mathbf{H} - z_r)\Psi(r; z_r) = 0 \quad \text{CESE with outgoing wave conditions} \qquad (27)$$

A basic characteristic of (27), which is in harmony with the implicit character of Eq. (12), is that the solution of (27) depends on the complex eigenvalue.

In conclusion, it was shown that from the Hermitian treatment of resonances on the real energy axis [29], two adjoint CESEs emerge, having as complex eigenvalues z_r and z_r^* of (24). This is achieved by separating the form obtained by Fano using standing wave asymptotic boundary conditions into the sum of two forms corresponding to incoming and outgoing-wave boundary solutions. Considered separately, each solution is a manifestation of nonunitarity, brought about by the fact that there is a cut of $(E - \mathbf{H})^{-1}$ on the real axis, or, equivalently, by the fact that, when the TDSE is employed for the description of resonances, there is a singularity at $t = 0$ which in fact adds a source term, $i\delta(t)$, on the TDSE ([37b], eq. (3.4)). Only the solution of Eq. (27) is acceptable since its adjoint state is unphysical for $t \geq 0$.

5.1. Norms, attenuation factors and the Dykhne-Chaplik regularization in terms of complex scaling

Crucial to all types of computation is the possibility of defining and computing consistently matrix elements. According to standard QM, for the stationary scattering state of real energy, $\Psi(q,E,t) = \Psi(q,E)e^{-iEt}$, the norm is equal to one for all times:

$$<\Psi(t)|\Psi(t)> \; = \iint \Psi^*(q,E)e^{iEt}\Psi(q,E)e^{-iEt}dqdE = 1 \qquad (28)$$

On the other hand, the following norms are obtained when considering the pair of the adjoint complex wavefunctions with asymptotic behavior (25).

(1) If the solution for the decaying state is used, then the particle-number probability is not conserved since decay takes place (i.e., the system is open). This is seen by assuming the form of the time-dependent resonance eigenfunction to be defined in terms of its complex pole (24a) and of the requirement of satisfying the TDSE:

$$\Psi(q,z_r,t) = \Psi(q,z_r)e^{-iz_rt} \ t \geq 0 \tag{29}$$

Then,

$$\int \Psi^*(q,z_r,t)\Psi(q,z_r,t)dq = (\exp{[(z_r^* - z_r)it]})\int \Psi^*(q,z_r)\Psi(q,z_r)dq$$

$$= e^{-\Gamma t}\int \Psi^*(q,z_r)\Psi(q,z_r)dq \tag{30}$$

I.e., there is time-dependence for this norm. Therefore, the form (29) is, indeed, in harmony with the assumption that a consistent definition of the resonance (decaying) state must be associated with exponential decay.

(2) The second type of norm is the one that has to show conservation for the whole (closed) system, just like the conventional norm (28) does. Following the line of argument about the correspondence between the solution on the real energy axis and the two adjoint solutions in the complex energy plane, it is evident that the norm which conserves the number of particles in the whole system must involve both the decaying state and its adjoint, $\Psi^\dagger(q,z_r^*)$. In this case,

$$\int [\Psi^\dagger(q,z_r^*,t)]^*\Psi(q,z_r,t)dq = (\exp{[(z_r - z_r)it]})\int \Psi(q,z_r)\Psi(q,z_r)dq$$

$$= \int \Psi(q,z_r)\Psi(q,z_r)dq \tag{31}$$

which is time-independent. Hence, it is the use of the two adjoint eigenfunctions, which are characterized by the conditions of Eqs. (23–25), that produces a constant norm for the whole system.

Equation (31) shows a characteristic feature of the resonance wavefunctions, namely that the integral over radial space (not over the spherical harmonics), involves the square of the function itself and not of its absolute value. However, due to the asymptotic behavior (25a), the integral (31) (as well as the one of Eq. (30)), is infinite, since the integrant goes like e^{2ar}, where a is the imaginary part of the complex momentum of the free Gamow orbital.

The lack of square-integrability of $\Psi(q,z_r)$, recognized of course by Gamow and his contemporaries, reduced for many decades the possibility and/or the interest in tackling problems of resonance states (in conjunction with

the requirements of the many-body problem for real systems), in terms of methods that would employ such trial functions.

Kemble, in his 1937 book on QM (section 31 of Ref. [104]), briefly discusses this issue, wondering about the possibility of defining a new norm by introducing the attenuation factor e^{-br^n}. In his study of formal aspects of resonance functions, Berggren [28a] examined this possibility systematically, following earlier work by Zel'dovich [105] on the subject of regularizing the divergent integral by using the above attenuation factor.

In fact, a simple and practical solution to the norm problem was provided in 1961 by Dykhne and Chaplik [106], who obtained the result of Zel'dovich by extending integration into the upper half of complex coordinate plane, i.e., by changing r to $re^{i\theta}$. This reference was first cited and brought to the attention of the community of researchers in complex scaling in 1980–1981 by Nicolaides et al. [101], as soon as we discovered it. Dykhne and Chaplik used the s-wave short-range potential model and concluded that, upon the above transformation, "in spite of the fact that the wave functions vanish at infinity, the energy values are complex because of the non-Hermitian character of the Hamiltonian in V" (the volume of integration).

The above statement from [106] contains the essence of the theory and computations in terms of scaled, non-Hermitian Hamiltonians with complex coordinates that started a decade later. It is remarkable that the simple, one-page paper of Dykhne and Chaplik was not cited in the literature discussing the early developments of the theory of complex scaling of Hamiltonians, until 1981 [101].

Indeed, in the early 1970s, complex scaling of coordinates, $r \rightarrow re^{i\theta}$, was used in a mathematical context and language which analyzed the spectral properties of the non-Hermitian Coulomb Hamiltonian $\mathbf{H}(re^{i\theta}) \equiv e^{-2i\theta}\mathbf{T} + e^{-i\theta}\mathbf{V}$ in the Hilbert space of L^2 functions [107, 108]. It was shown that, for the "dilatationally analytic" Coulomb Hamiltonian, the complex eigenvalues of $\mathbf{H}(re^{i\theta})$ correspond to the second sheet complex poles of the resolvent, normally associated with resonance states, while the discrete states appear as poles on the real energy axis. Soon afterwards, this mathematical result attracted the attention of theoretical chemists and physicists, mainly because of the conceptual simplicity that it entails. Of course, the MEP remains. The practical computational problem is how to diagonalize $\mathbf{H}(re^{i\theta})$ in the complete Hilbert space of states of polyelectronic systems. The CCR method which ensued has to do with finding the complex eigenvalues of $\mathbf{H}(re^{i\theta})$ by following the convergence of the "θ-trajectories" [109, 110]. Although the initial mathematical results concerned the Coulomb operators, empirical evidence with calculations of the Stark resonances suggested that the use of $\mathbf{H}(re^{i\theta})$ is relevant for other types of potential which are not dilatationally analytic [111, 112]. Thus, since its introduction in the 1970s, the CCR has become a practical computational tool for the computation and analysis of resonances in a variety of simple Hamiltonians.

For reviews of the CCR and its applications, and of various aspects of the theory of resonances in general, the reader could consult [113, 114] and articles in the volume on "Resonances" edited by Brändas and Elander [115].

6. COMPUTATION VIA THE CESE SSA. MANY-BODY EXPANSION AND PARTIAL WIDTHS WITH INTERCHANNEL COUPLING

In spite of its conceptual simplicity, the CCR method, i.e., the repeated direct diagonalization of $\mathbf{H}(re^{i\theta})$ on a single function space of L^2 functions and the corresponding identification of stable complex roots, is not capable of producing partial widths, with or without interchannel coupling. This was recognized since the first applications to two-electron atoms started in the 1970s. For example, it is stated explicitly in the review published in 1983 by Ho [113 a].

Furthermore, and most important, the CCR method is not suitable for the solution of the MEP, just like the direct diagonalization of $\mathbf{H}(r)$ on a single set of basis functions is not a practical method for solving the Schrödinger equation for even the ground states of polyelectronic atoms or molecules (More discussion is given in Sections 7 and 8.)

The facts to which the above two paragraphs refer, suggest that, at least concerning the use of square-integrable functions for the calculations of resonance states, alternative theories are needed. Indeed, the CESE-SSA, whose basic elements and characteristics are reviewed here, is structured so as to allow the practical and efficient computation of the MEP in electronic structures, the multichannel continuum and partial widths, and, in general, the production of easily usable wavefunctions that contain the information that is relevant to the state and property of interest.

For example, as regards efficiency, a comparison between the method of CCR and that of the CESE-SSA was published in Ref. [116], concerning the three-electron He$^-$ 2s2p^2 ^{4}P resonance state and the resonances of the system "Hydrogen atom plus magnetic field." The results show that the CESE method is much more efficient.

In addition, as it will be seen below with unique results on the resonance spectrum of H$^-$ (Tables 4.2 and 4.3), it is also very accurate for even the most subtle and difficult to handle cases of interelectronic interactions in the continuous spectrum.

Furthermore, the CESE approach was proven convenient and very efficient when r_{ij}- dependent basis sets are used. Specifically, Bednarz and Bylicki [117] published results of their computations on the He 2s^2 ^{1}S resonance, where they followed the CESE procedures with explicitly correlated basis functions. In explaining their work, these authors pointed out that "…one should realize that the r_{ij}- dependent basis functions are not capable of repairing the slow radial convergence of the CCR method."

According to the CESE approach, one of the main computational bottle-necks regarding the implementation of the CCR method, namely the need to diagonalize directly and repeatedly $\mathbf{H}(re^{i\theta})$ on a space of functions constructed from a single basis set, is bypassed by using trial functions of the form (1). Without going into the background, I mention that the form of the trial complex wavefunctions is guided by the arguments given previously as regards the significance of Ψ_0, by results that are discussed in Ref. [37b] as to the invariance of certain matrix elements with respect to complex scaling, and by the derivation of the CESE where the emphasis is on asymptotic boundary conditions.

In the CESE approach, the coordinates of the Hamiltonian are real. Special attention is given to the accurate, state-specific, single- or multi-state calculation of Ψ_0. Complex coordinates are used only in certain orbitals of the function space, which is chosen appropriately so as to follow the two-part form of the resonance eigenfunction discussed above. We have called these orbitals "Gamow orbitals." They may be chosen to have particular forms in harmony with the corresponding open channels, or they can be expanded in standard forms, such as the one of Slater orbitals, albeit with a complex coordinate. Specifically, in the case of one-electron decay, the simplest version of the SSA square-integrable resonance wavefunction for an N-electron atom is (r symbolizes collectively the real coordinates of the bound orbitals),

$$\Psi(r_{N-1}, \rho^*) = \alpha(\theta)\Psi_0(r) + \sum_n \beta_n(\theta)u_n(r_{N-1}, \rho^*), \tag{32}$$

$$\rho^* = re^{-i\theta}, \, |\alpha(\theta)|^2 + \sum_n |\beta_n(\theta)|^2 = 1 \tag{32a}$$

The complex functions $u_n(r_{N-1}, \rho^*)$ are properly symmetrized products of basis functions that have real coordinates for the bound part of the channel and complex coordinates for the outgoing particle in that channel. They are optimized at different values of θ with respect to variation of parameters.

The use of the form (32), in the single- or in the multi-state version, for the solution of the CESE, has been applied in the context of the SSA to a variety of problems. Its extension to problems involving the interaction with external fields is discussed in Section 11.

One of the useful consequences of the CESE approach, in conjunction with the related many-electron analysis, is the fact that it solves in a simple way the problem of computing partial decay widths, without or with inter-channel coupling. In order to see this, I draw from the theory published in Refs. [37b, 101, 118–121].

Even though the computation of Ψ_0 has not been discussed yet, let us assume that a state-specific HF solution, $\Phi_{HF}(r)$, of a configuration with energy in the continuous spectrum of a polyelectronic atom, has been

obtained. Then, it is possible to write a symmetry-adapted cluster expansion corresponding to the exact resonance wavefunction of Eq. (32) in the symbolic form:

$$\Psi(r_{N-1}, \rho^*) = \Phi_{HF}(r) + \Phi_{HF}^{-1}(r_{N-1})\sigma + \Phi_{HF}^{-2}(r_{N-2})\pi + \Phi_{HF}^{-3}(r_{N-3})\tau + \ldots \tag{33}$$

The symbols $\Phi_{HF}^{-1}(r_{N-1})$, $\Phi_{HF}^{-2}(r_{N-2})$, $\Phi_{HF}^{-3}(r_{N-3})$, etc., stand for the HF configurations with one, two, three, etc. electrons missing from the initial one.

σ, π, τ...stand for the corresponding correlation functions of one, two, three, etc. electrons. They are symmetry-adapted and so they correspond directly to observable exit channels, if they are open. The dominant ones are the single and, especially, the pair correlations. However, for inner-hole states, depending on the subshell where the hole is made, the relative importance of higher order correlations increases [122], and of course, if energy is high enough, there is probability for more than one electrons to be emitted.

The coordinates in all the HF configurations with bound electrons are real. The coordinates of the electrons in the correlation functions are real, r, or complex, ρ^*, depending on whether they belong to the space of Ψ_0, thus contributing to the stability of the wavepacket, or whether they are variables for the Gamow orbitals of the open channels through which decay takes place. Each correlation function has, in general, both the "localized" and the "asymptotic" components. For single electron emission it is sufficient to a good approximation to keep the first three terms of Eq. (33). Thus, I write symbolically for the single and pair correlation functions,

$$\sigma \rightarrow \sigma_{loc}(r_1) + \sigma_{as}(\rho_1^*) \tag{34a}$$

$$\pi \rightarrow \pi_{loc}(r_1, r_2) + \pi_{as}(r_1, \rho_2^*) \tag{34b}$$

In the above orthogonal separation into localized (*loc*) and asymptotic (*as*) correlations, $\sigma_{as}(\rho_1^*)$ is zero for closed channel resonances (the so-called *Feshbach resonances*). This term is non-zero and physically significant in the cases of open channel resonances (the so-called *shape resonances*), see Section 8.3.

The two-electron π functions are the most significant contributors to the real as well as to the imaginary parts of the resonance energy for the normal cases of autoionizing states. The $\pi_{as}(r_1, \rho_2^*)$ part is responsible for the Auger rearrangement of two correlating electrons in the presence of all the others. To a good approximation, each π, and therefore each $\pi_{as}(r_1, \rho_2^*)$, can be calculated independently of all the others. This constitutes the "independent channel approximation." However, once this part of the calculation is done, the whole wavefunction can be put together, and from a total diagonalization the final results for energies and partial widths, which include interchannel coupling, are obtained.

Specifically, by diagonalizing an appropriately constructed non-Hermitian Hamiltonian matrix and by producing the final solution in the form of an expansion over configurations with complex coefficients,

$$\Psi_r = a\Psi_0 + \sum_i b_i X^i_{as} \tag{35}$$

the partial widths to all orders of interchannel coupling are given by

$$\gamma_i = -2\, \mathrm{Im} \left(\frac{b_i}{a} < \Psi_0\, |\mathbf{H}|\, X^i_{as}> \right), \Gamma = \sum_i \gamma_i \tag{36}$$

The wavefunctions X^i_{as} represent the open channels. They are obtained as symmetry-adapted products between localized core functions of real coordinates and channel-dependent complex orbitals that are square-integrable.

The method expressed in terms of Eqs. (35 and 36) has also been applied to prototypical cases in atoms and molecules, such as,

- The computation of the five partial widths in the nine-electron Ne^+ $1s2s^22p^6$ ^2S Auger state (about 870.3 eV above the Ne ground state) [118, 119].
- The computation and analysis of partial widths in a series of doubly excited autoionizing states in He and in He^- [120].
- The ab initio calculation of the partial widths of the predissociating $2^2\Sigma^+$ excimer state of HeF which decays via radial and rotational couplings (computed from first principles), to the repulsive $X^2\Sigma^+$ and $1^2\Pi$ states [121].

7. TWO EXAMPLES OF RESULTS FROM THE APPLICATION OF THE CESE APPROACH

The possibilities of test, and the scope and scale of the first applications of the Hermitian and non-Hermitian methods that we were developing in the 1970s for the computation of resonance states, were seriously limited in that period by lack of access, in Athens, to the necessary decent computational facilities. Progress on the computational front became more comfortable in the 1980s and 1990s. In addition, two young scientists, namely Yannis Komninos and Theodoros Mercouris, started collaborating with the author on such problems. It thus became possible to work on formalism and applications more efficiently. As regards the application of the CESE-SSA, which is how the results that follow were produced, when the memory and speed of the accessible computers increased we were able to use reasonably flexible expansions and to acquire better numerical experience about the choice, the sizes and

the optimization of the function spaces for the two parts of Eq. (35), $a\Psi_0$ and $\sum_i b_i X^i_{as}$.

The previously published results which are quoted here are:

(1) The energy and partial and total widths of the Ne^+ $1s2s^2 2p^6$ ^2S Auger state. The results are taken from [118, 119].
(2) The resonance spectrum of H^-. The results are taken from [123] (see also [124]).

These results were obtained in different time periods using different types of function spaces and of optimization, which, in general, depend on the system under examination. The reader will find the details of the calculations in the original papers.

7.1. The energy and decay widths of the $Ne^+ 1s2s^2 2p^6$ ^2S Auger state

This is a nine electron system, which autoionizes into the following five available open channels: $1s - 2p^2$ ^1D, $1s - 2p^2$ ^1S, $1s - 2s2p^3$ P^o, $1s - 2s2p^1$ P^o and $1s - 2s^2$ ^1S. As written symbolically, each of these electron rearrangements is represented by the corresponding "asymptotic" symmetry-adapted pair function, $\pi_{as}(r_1, \rho_2^*)$.

The total energy of this state is calculated as 870.3 eV, in very good agreement with experiment [118]. The achievement of such accuracy has been possible exactly because of the emphasis on the separate, state-specific calculation of Ψ_0 by methods of the SSA [9, 10, 122].

As regards the autoionization widths, Table 4.1 contains the CESE results and the results of two previous theoretical ones that were obtained at some level of approximation using real-energy methods [125, 126]. The experimental ones are the ones quoted in Ref. [125].

The calculations of Ref. [118, 119] still remain the only ones in which complex scaling and square-integrable complex functions have been employed for the determination of the complex eigenvalue and its breakdown in its partial widths, without and with interchannel coupling, of an inner-hole resonance state of a system with many interacting electrons.

We point out that since the structure of the CESE-SSA is such that it requires well-defined matrix elements and computations that are practical and economic, its first-principles implementation has been extended to prototypical cases, such as the determination of partial and total autoionization widths in series of high-lying DESs [120] and Section 9.4, and of partial widths with interchannel coupling for the predissociation of excimer molecules [121].

Table 4.1 Auger partial and total widths (in 10^{-2} a.u.) for the Ne 1s hole state. The CESE results from [118] are without interchannel coupling and those from [119] include interchannel coupling

Transition	Theory CESE		[126]	Experiment [125]		As quoted in Ref. [125]
	[118]	[119]		Hartree-Fock basis set	"Transition State" basis set	
1s-2p^2 ^{1}D	0.560	0.565	0.493	0.606	0.550	0.604 ± 0.06
1s-2p^2 ^{1}S	0.048	0.040	0.077	0.095	0.083	0.089 ± 0.009
1s-2s2p ^{3}P^o	0.029	0.032	0.049	0.101	0.070	0.063 ± 0.006
1s-2s2p ^{1}P^o	0.154	0.165	0.137	0.195	0.150	0.174 ± 0.017
1s-2s^2 ^{1}S	0.044	0.043	0.049	0.060	0.045	0.060 ± 0.006
Total	0.835	0.844	0.805	1.057	0.898	0.990 ± 0.099

7.2. The complete resolution of the resonance spectrum of H$^-$. Unperturbed and perturbed series, overlapping, "loner," and "shape" resonances

The normal difficulties that are associated with the MEP originate from the number of electrons, the complexity of excited state electronic structures and the possible strong mixing of the open channels. This was the case with the example of the Ne^+ Auger state.

On the other hand, extreme theoretical and computational difficulties may also be caused in cases of resonance states whose fundamental cause is the very weak binding and the concomitant enhancement of the significance of the details of interelectronic interactions, regardless of the number of the system'selectrons. In such cases, it is difficult to identify and to compute with accuracy the correct Ψ_0s. For example, investigations of such cases in resonances of He$^-$ have been reported in Refs. [127, 128].

It is easily understood that weak binding is likely to appear in states of ANIs. Except in few cases where the electrons occupy the same space, as in the case of the previously discussed, almost unique, "2p^3" $^4S^o$ resonance of H^{2-} with its relatively large width (Section 2.2), resonance states of ANIs are likely to have small to very small widths as one of the electrons is distancing itself from the others—provided there is some physically significant transient binding.

These two facts, namely weak binding and resonances with extremely small widths, constitute serious tests for the theory and the methods of locating resonances, and of identifying and computing reliably the main

spectral characteristics that originate from the correlated motion of the electrons. For example, there are electronic structures of resonances of ANIs where it is necessary to compute Ψ_0s that are very diffuse. Indeed this is the case of the resonance states of H^-, which are discussed below, where the Ψ_0s were computed up to about 8000 a.u..!

The widths of many of the resonances of H^- that were calculated by the CESE method go down to $1 \times 10^{-8} - 1 \times 10^{-9}$ a.u., which is orders of magnitude smaller than the values of widths which have been computed by other methods.

The work and analysis reported in Refs. [123, 124], took the scope and the accuracy of the theory and computation of electron-atom (molecule) scattering resonances to an unprecedented level for the standards of the field, in order to achieve the first definitive resolution and interpretation of the spectrum of the complex poles representing the resonance states of H^-.

Specifically, in Ref. [123], the identification of 76 H^- resonance states of $^1P^o$, $^1D^o$ and $^1F^o$ symmetries up to the $n = 4$ threshold, was reported, with widths down to about $1 \times 10^{-8} - 1 \times 10^{-10}$ a.u., depending on symmetry and threshold. In Ref. [124], 70 states of ^1S and ^1D symmetries, and 83 states of $^3P^o$ symmetry were identified, having widths down to about 1×10^{-9} a.u.

The results were classified according to the predictions of the model of "dipole resonances" [129], and it was found for the first time that, for this special dipole potential, there are unperturbed as well as perturbed series, in analogy with the Rydberg spectra of the Coulomb potential in atoms and positive ions. For the unperturbed series, the agreement with the predictions of Gailitis and Damburg [129] as to the relationship of the extent of the outer orbital and of the energies and widths of states is excellent. On the other hand, there are also perturbed series, which result from interchannel coupling and the remaining electron correlation. One of the effects is the existence of *overlapping resonances* on the real energy axis, of "loner" states (i.e., not belonging to any series), and of *shape* resonances.

As is well-known, the two-electron system $e + H$ has been attracting theoretical attention for decades, with a large number of reports on the identification and nature of its resonances. Hence, it is possible to compare the CESE results of Ref. [123, 124] with those published by other groups, who applied large scale R-matrix methods [130–132], or the CCR method [133–136], or specially improved close-coupling methods [137], or implementation of Feshbach's formalism. The related references are cited in Refs. [123, 124] and below.

This comparison shows that the combined results of all previously applied methods since the 1960s, had identified only 35 resonances for the $^1P^o$, $^1D^o$ and $^1F^o$ symmetries, 32 resonances for the ^1S and ^1D symmetries, and 13 resonances for the $^3P^o$ symmetry, with only very few cases having a level of accuracy comparable to that of the CESE calculations. The limited number of

those resonances uncovered before the CESE results of Ref. [123, 124] could not provide definitive conclusions as to the nature of the resonance spectra in H⁻, regardless of the level of accuracy of the calculated positions and widths that were available then.

In order to support the above, it suffices to recall here only a subset of the results that were published in Refs. [123, 124]. To this purpose, I chose the resonances of H⁻ in the energy region below the $n = 3$ threshold, for the $^1P^o$, $^1D^o$ and $^1F^o$ symmetries. The CESE results [123] are listed in Tables 4.2 and 4.3, together with those obtained from large scale computations using the R-matrix method [130–132], or the CCR method [133–136].

Finally, needless to add, I point out that the same CESE approach can be applied for the calculation of the details of the resonance spectra corresponding to various thresholds of He, Li^+, etc. In fact, such calculations would be much simpler than the ones in H⁻, since the presence of the Coulomb attraction would reduce the conceptual and computational requirements. Indeed, except for very high-lying DESs (see Sections 9.4 and 9.5), a percentage of the resonances in He, Li^+, etc., below the low-lying thresholds can also be computed reliably by methods such as the CCR and standard basis sets.

8. THE STATE-SPECIFIC CALCULATION OF Ψ_0

In Section 4, I discussed aspects of the formal meaning and significance of Ψ_0. Here I turn to the essence of the SSA as regards the computation of Ψ_0.

8.1. Simple arguments regarding the significance of the SSA to problems in polyelectronic atomic and molecular physics

Over the many decades of the development and the implementation of methods for the computation of bound electronic structures and/or of properties associated with the continuous spectrum (e.g., resonances), the standard approach has been the use of formalisms that in practice utilize a single set of orthonormal basis sets for the calculation of relevant matrices, wavefunctions, etc. (e.g., Gaussian or Slater functions, or B-splines, etc). However, regardless of the level of sophistication of the formalism, when it comes to the solution of MEPs or of difficult problems such as the ones discussed in the previous sections, this approach has serious practical limitations regarding both efficiency and interpretation.

The argument of the SSA is that forms and state-specific function spaces do matter in a critical way, and that it is advantageous to develop or adopt formalism that can be implemented in terms of optimized function spaces, whether in numerical or analytic form, or both [9, 10, 122] and references therein.

Table 4.2 Energies and widths of H⁻ ¹Pᵒ resonances below the $n = 4$ threshold, as identified from the implementation of different theories for field-free resonances. The number in brackets, x, implies multiplication of the preceding number by 10^{-x}

	R matrix		CCR				CESE	
	Pathak et al. [130]		Ho [133]		Lindroth [134]		Bylicki and Nicolaides [123]	
State	$-E$ (a.u.)	Γ (a.u.)	$-E$ (a.u.)	Γ (a.u.)	$-E$ (a.u.)	Γ (a.u.)	$-E$ (a.u.)	Γ (a.u.)
(1)	0.0371305	1.245 [3]	0.03717945	1.0336 [3]	0.03718	1.03 [3]	0.0371794	1.03428 [3]
(2)	0.034289	1.80 [5]	0.03429405	1.83 [5]	0.03430	1.84 [5]	0.03429397	1.8328 [5]
(3)	0.032324	2.25 [4]	0.0323525	2.44 [4]	0.03235	2.4 [4]	0.032350629	2.4152 [4]
(4)	0.032192	8.0 [6]	0.0321985	7.7 [6]	0.03220	7.7 [6]	0.032198287	7.9216 [6]
(5)	0.0316025		0.031613	5.95 [6]	0.03161	6.6 [6]	0.031613080	5.958 [6]
(6)	0.0315535	4.65 [5]	0.031562	3.15 [6]	0.03156	2.2 [6]	0.03155516	2.716 [6]
(7)	0.0313515		0.0314975	6.47 [5]	0.03150	6.3 [5]	0.03149750	7.550 [5]
(8)							0.031349759	8.718 [7]
(9)	0.0313115		0.031315	1.2 [4]			0.03132298	1.13866 [4]
(10)	0.0313045				0.03131	1.5 [5]	0.031304250	1.1694 [5]
(11)							0.031282674	2.86 [7]
(12)							0.0312645831	2.614 [7]
(13)							0.0312627480	2.5110 [6]
(14)							0.031260682	9.4 [8]
(15)							0.0312535114	3.24 [8]
(16)							0.03125293164	5.788 [7]
(17)							0.0312511519	1.054 [8]

(18)	0.03125067253	1.338 [7]
(19)	0.03125053534	9.50 [9]
(20)	0.0312503765	3.80 [9]
(21)	0.0312501542	3.10 [8]
(22)	0.031250120	3.4 [9]
(23)	0.0312500159	1.34 [9]
(24)	0.0312500172	1.8 [8]

Table 4.3 Energies and widths of H^{-1}D^0 and ^{1}F^0 resonances below the $n = 3$ threshold, as identified from the implementation of different theories for field-free resonances. The number in brackets, ×, implies multiplication of the preceding number by $10^{-\times}$

| | *R* matrix | | | | CCR | | | | CESE | |
| | Pathak et al. [130] | | Odgers et al. [132] | | Bhatia and Ho [135] | | Ho [136] | | Bylicki and Nicolaides [123] | |
State	$-E$ (a.u.)	Γ (a.u.)	$-E$ (a.u.)	Γ (a.u.)	$-E$ (a.u.)	Γ (a.u.)	$-E$ (a.u.)	Γ (a.u.)	$-E$ (a.u.)	Γ (a.u.)
$^1D^0$										
(1)	0.0594095	2.755 [4]	0.05943	2.645 [4]	0.059431007	2.49901 [4]			0.059430923	2.4991 [4]
(2)									0.0555997787	2.6768 [6]
(3)									0.055556101835	3.3034 [8]
$^1F^0$										
(1)	0.056558	5.5 [6]	0.056875				0.0565588	5.02 [6]	0.0565587519	5.0068 [6]
(2)									0.05565771162	5.5402 [7]
(3)									0.05556643170	5.972 [8]
(4)									0.055556720982	6.408 [9]
(5)									0.0555556809	6.8 [10]

For example, consider the following two cases:

(1) Suppose one is interested in computing the 10th, say, excited state of *s*-symmetry of Hydrogen. One way, which is obviously not the recommended one, is to follow the expansion approach in a basis set, say Gaussian or Slater or "Sturmian" orbitals, and diagonalize the hydrogenic Hamiltonian. A huge basis set will be needed in order to reach a high level of accuracy for the energy as well as for the wavefunction of the tenth root of the diagonalized matrix. This is certainly an inefficient way of solving the problem. Furthemore, if one wants to use the resulting wavefunction for further analysis and calculation of properties, this approach becomes seriously uneconomical and lacks physical transparency.

On the other hand, the state-specific way is to solve directly for the eigenvalue and eigenfunction of the 10th state, something which is of course practical since the Schrödinger equation is solved exactly in the case of hydrogen.

Therefore, in this simple and easily understood example, one wavefunction, computed analytically or numerically, is equivalent to an expansion over a basis set which mathematically has to be infinite. The choice is obvious.

(2) Let me repeat the above argument, using the hydrogenic Hamiltonian with complex coordinates, which is the hallmark of the CCR method. According to mathematical analysis [107, 108], the poles of the hydrogenic $\mathbf{H}(re^{i\theta})$ are real and correspond to the discrete spectrum below threshold. As θ increases from zero, these poles must remain at their initial positions on the real energy axis.

Now suppose we want to obtain the ground state energy of Hydrogen— (let alone the energy of the 10th excited state). According to the CCR, which is a characteristic example of the use of single basis sets for the diagonalization of matrices, in order to obtain the single number that is trivially known from the exact solution, one would have to diagonalize an infinite (in principle) matrix in some complete basis set.

Instead, Nicolaides and Beck [37b, p. 506] considered the exactly solvable problems of the harmonic oscillator and of hydrogen and found that in fact, a single function can diagonalize $\mathbf{H}(re^{i\theta})$. This is the rotated function of the unrotated solution, i.e., $[\mathbf{H}(re^{i\theta}) - \varepsilon_n]\varphi_n(re^{i\theta}) = 0$, for each state $|n >$ and real ε_n. (The proof is straight-forward). In fact, we stated two "theorems" that are basic to the development of the practical implementation of the CESE-SSA [37b, p. 505], since, in practice, they allow the difficult electron correlation calculations to be done only once on the real axis, and then continue the computation in the complex energy plane where the Gamow orbitals are optimized until the complex energy is stabilized.

Theorem 1: The (normalized) N-electron, M-nuclei function $\Psi_0(\theta) \equiv \Psi_0(re^{i\theta}, Re^{i\theta})$ will leave the expectation value $E_0 = <\Psi_0(0)|\mathbf{H}(0)|\Psi_0(0)>$ invariant under rotation in the θ-plane.

Theorem 2: For a Coulomb Hamiltonian, in an actual configuration-interaction -type calculation with one-particle square-integrable, analytic functions as basis sets, all overlap, one- and two-particle integrals remain invariant under transformations of the type $u(r) \rightarrow e^{i3/2}u(re^{i\theta})$, $U(R) \rightarrow e^{i3/2}(Re^{i\theta})$.

In the above, R symbolizes the nuclear coordinates considered as variables. Such possible calculations, where no B–O approximation is applied, might be more attractive nowadays than 30 years ago.

As an example, and in support of the above arguments, I quote from [37b]:

> ...we diagonalized the hydrogenic $\mathbf{H}(re^{i\theta})$ in a basis set of ten unrotated, real hydrogenic functions, $|ns>$, i.e., we obtained complex eigenvalues for the expansion $\sum_{n=1}^{10} a_n(\theta)|ns>$. As θ increased, the coefficients $a_n(\theta)$, $n > 1$, increased rapidly in magnitude and the width of the ground state was larger than typical resonance widths after $\theta > 4^o$. [Of course this is wrong, since the width of a discrete state is zero]. This shows the origin of the slow convergence of the coordinate rotation method, where up to now only fixed, large basis sets have been used. I.e., an arbitrarily chosen set of square-integrable functions may be a good representation on the real axis, but in the θ-plane they need not.
>
> [37b, p. 506]

If the one-electron problem exhibits such difficulties when, instead of the state-specific solution, which is this case is known exactly, the expansion in a basis set is adopted, one can immediately understand that things become much more complicated or impossible for a number of MEPs if states and the related matrix elements are to be obtained in terms of methods that depend on the use of basis sets that are common to all parts of the system under investigation.

8.2. The direct HF or MCHF solution as the zero-order approximation to Ψ_0.

The MEP in resonance states of many-electron atoms (molecules) complicates things not only computationally but also conceptually and formally. For example, the resonance state is in the continuous spectrum, with an infinity of lower states of the same symmetry. Its localized part, Ψ_0, and its energy E_0, do not obey rigorously a variational minimum principle to all orders. Instead, in a variational calculation, what one expects is a correct convergence to a local energy minimum, secured by the anticipated localization of the state. In addition, there are complications from possible

near-degeneracies with other resonance states of the same symmetry, and, of course, from the mixing of scattering components.

In certain extreme and rare cases, such as the one of the H^- dipole resonances, it was necessary to create the function space of the Ψ_0 states out to very large radial distances by adding judiciously extended bound functions [123, 124]. However, this is not the way to the systematic solution of the MEP.

The proposal and demonstration in Refs. [11, 37] was that, given the correspondence decaying state $\leftrightarrow$ resonance state, the MEP of the field-free polyelectronic Hamiltonian, $\mathbf{H}$, for the computation of Ψ_0, is best solved by adjusting and adapting formalism and advanced computational methods that were in the process of being developed in the 1960s (and are still used) for the lowest-lying discrete states.

Accordingly, instead of expecting to obtain Ψ_0 say from a somehow identifiable root of a diagonalized $\mathbf{H}$ matrix constructed from a large basis set of orthonormal functions or B-splines, Ψ_0 for an isolated state was computed directly in the form

$$\Psi_0 = \Phi_0 + X_{loc} \tag{37}$$

Φ_0 stands for the state-specific HF or MCHF solution. X_{loc} stands for "localized" correlation and represents those parts of the one-, two-, three-, etc., electron correlation function space that contributes, together with Φ_0, to the stability of the state, e.g., Refs. [9–11, 37, 56, 77, 122, 128, 138, 139].

One of the advantages of the state-specific calculation of Φ_{MCHF} is that this wavefunction accounts in an efficient way for the self-consistently adjusting major correlations that contribute to localization, including a few that incorporate parts of the open-channel continuous spectrum, which we have named the "open-channel-like" (OCL) configurations [56, 77]—see below.

Indeed, apart from the fact that the dominant electronic structure features are exhibited directly and reliably, the use of a state-specific Φ_{MCHF} helps convergence in the overall calculational scheme of resonance states immensely. For example, we have published a number of papers where it is demonstrated that only a few self-consistently optimized configurations can provide accurate descriptions of Ψ_0 for polyelectronic resonance states of various structures. Such state-specific calculations show that, quite often, there is significant dependence of the zero-order orbitals and their electron correlation on symmetry and on spin couplings. An example from simple structures is relevant here. Unpublished results [140] on the He $(2s2p)^{3,1}P^o$ resonances show that the HF solutions give the averages for the HF orbitals as $<r>_{2s} = 3.45$ a.u. for $^3P^o$ and 4.43 a.u. for $^1P^o$, a rather large difference. For the total HF wavefunctions, $<r_{12}> = 5.21$ a.u. for $^3P^o$ and 4.67 a.u. for $^1P^o$. When the Φ_{MCHF} wavefunctions (a few configurations) are used, the expectation value reflecting angular correlation, $<\cos\vartheta_{12}>$, reveals a qualitative

difference: -0.37 a.u. for the $^3P^o$ state (the two electrons are, on the average, at opposite sides of the nucleus), and 0.03 a.u. for the $^1P^o$ state.

The differences that are noted above imply that if an electron-correlation calculation were carried out using the same basis sets for the wavefunctions of these two spectroscopic terms, then the size requirements would be very large, simply in order to correct for the inadequacy of the zero-order wavefunctions.

The sensitivity of properties to the numerical level of accuracy at the zero-order approximation, which is evident from the above example, constitutes an additional reason for the slow convergence of methods that use a basis set common to various terms of the same configurations, let alone of different configurations.

In contradistinction, a SSA calculation, by obtaining state-specific zero-order orbitals and corresponding optimized correlation configurations, immediately reduces the magnitude of calculation while increasing considerably its accuracy. Specifically, the calculation of X_{loc} involves the proper construction of symmetry-adapted configurations consisting of MCHF and of virtual orbitals, and their variational optimization, separately (if needed), and via the minimization into a local minimum of the total energy, E_0, using orthonormal or nonorthonormal configuration-interaction techniques [9, 122].

In view of the existing publications to which the reader may refer for extensive discussions and applications of Eqs. (1 and 37), here I focus briefly on the following three points.

(1) For many cases, the task of computing Φ_{MCHF} correctly requires considerable care. For example, it requires stability and high numerical accuracy for large radial distances, the satisfaction of the virial theorem (which is a condition of localization), as a guiding tool for accepting the solution that has converged into a local energy minimum, the attention to the major features of the radial characteristics and of the satisfaction of asymptotically vanishing boundary conditions, the satisfaction of proper orbital orthogonalities, the inclusion of nearly-degenerate and OCL configurations, the application of appropriate orbital rotations, etc. Related discussions can be found in Refs. [9, 10, 56, 77, 127, 128].

(2) In current times, it may seem that the calculation of highly excited atomic states via the solution of the numerical MCHF scheme is as straight forward as it is for ordinary ground or low-lying discrete excited states, in view of the existence of published computer programs such as the one of Froese-Fischer ([141] and later versions). This is not so, except for some of the cases of well-localized states, as are the normal Auger states, and it certainly was not the case in the early 1970s when [11] was published. For example, in 1978 Froese-Fischer [141], in the preface of her publication, writes: "…Since bound states in the continuum interact most strongly

with continuum states, a multi-configuration calculation for such states cannot be performed with this program."

The possibility of state-specific HF computation of even difficult cases of resonance states and the development of theory in the spirit of Eqs. (1) and (37), was first demonstrated in Ref. [11], by applying the analytic HF method of Roothaan [142a] through the slight modification and judicious use of the computer program written by Roos et al. [142b]. At that time, HF theory for multideterminantal structures with many-open sub-shells, where new vector-coupling coefficients and Lagrange multipliers enter, had been applied only to low-lying discrete states. The only previous HF calculations on states that are in the continuous spectrum, albeit without any theory or computations of electron correlation and of scattering contributions, were those of Bagus [143] for certain ns-hole states of the single determinantal Ne-like and Ar-like ions.

The publication of Ref. [11a] reported reasonably accurate calculations of the (Ψ_0, E_0) of the then challenging lowest triply excited resonances with open (sub)shells of He$^-$, the $'2s^2 2p'\ ^2P^o$ and $'2s2p^{2'}\ ^2D$ states, as well as of inner-hole states of larger systems, such as the $F'1s^2 2s2p^{6'}\ ^2S$ autoionizing state, which is characterized mainly by *hole-filling* correlations that correspond to the mixing of the valence configuration with channels of Rydberg and scattering orbitals of s and of d symmetry.

Since 1972, this approach has been understood better as regards the computation of both Φ_0 and X_{loc}, and has been applied to various problems involving different electronic structures, from resonances in negative ions to open (sub)shell Auger states, e.g., Ref. [144]. One such improvement has to do with the fact that, starting in the mid-1970s, upon the appropriate adaptation of the code published by Froese-Fischer [141], the SSA for atomic structures has been using the numerical MCHF method for the calculation of Φ_0.

In cases of lack of convergence or of false convergence, which are often distinguished because of the appearance of an unlikely orbital with positive energy, or of oscillatory solutions or of "solutions" for which the orbital becomes overextended, etc, care must be exercised, as already mentioned. When proper convergence is absolutely impossible, judgment must be exercised as to whether the resonance exists at all, since there is no localization at this level. For example, for cases such as the high-lying dipole resonances of H$^-$ which were discussed in Section 6, it is certain that the HF or MCHF equations cannot converge to a bound solution.

(3) The strategy of initializing the calculation of autoionizing states with a state-specific MCHF wavefunction allows the major configurational features of, say, a multiple excited state, to emerge clearly and quantitatively, while the MCHF energy is reasonably close to E_0. A class of configurations that are very useful, and many times absolutely necessary

components of Φ_{MCHF}, are the OCL-type [56,77]. Their presence accounts for a part of the contribution from the continuum of a lower lying threshold which does not destroy the square-integrability of the zeroth-order function. For example, for the resonance in He$^-$ whose label is $2p^3\ ^2D^o$, such an OCL configuration is the MCHF $(2s2p)^3P^{o'}3d'\ ^2D^o$, which incorporates part of the open channel $[He(2s2p)^3P^o + \varepsilon d]\ ^2D^o$.

The computational "phenomenon" of the OCL MCHF configurations can be understood from formal considerations as follows, [37b, p. 463] and [77].

Suppose we consider a hydrogenic or a HF solution to an electronic structure that labels an autoionizing state. Let the symbol for this zero-order wavefunction be φ_0 with energy ε_0. Either from Schrödinger or from Wigner-Brillouin perturbation theory, the expansion of the exact function shows that there are integrals of the form $\int \frac{<\varphi_0|H|E><E|}{\varepsilon_0 - E} dE$ over the continuum. So there is a singularity at $\varepsilon_0 = E$. If we exclude a small part of the continuous spectrum around, ε_0, say $\varepsilon_0 \pm \delta$, as a principal value integral, the wavefunction remains square-integrable because the terms $\int_{-\infty}^{\varepsilon_0 - \delta} \frac{|<\varphi_0|H|E>|^2}{\varepsilon_0 - E} dE$ and $\int_{\varepsilon_0 + \delta}^{\infty} \frac{|<\varphi_0|H|E>|^2}{\varepsilon_0 - E} dE$ are finite. A converged MCHF solution means that essentially the effect of the continuum comes from contribution of integrals such as the above. Convergence becomes generally easier as the effective nuclear charge is increased, even though a number of channels may still remain open. When the solution is achieved, the correlating virtual bound orbital having the orbital angular momentum of the open channel has picked up just the portion of the channel which contributes to the stability of the wavepacket.

The above situation is more easily achieved when the mixing of correlating configurations is relatively weak, or when the potential seen by the electron is enhanced by the angular momentum barrier, or when the effective nuclear charge is strong. For example, this is often the case with calculations of inner-hole Auger states if the hole is such that there are no strongly mixing configurations corresponding to core-electron rearrangements. This is why researchers in modern times, who have been using more recent versions of Froese-Fischer's code [141], find HF or MCHF solutions for Auger states satisfying such criteria, evidently without serious difficulties.

On the other hand, if for some type of electronic structure it is impossible to obtain valid convergence of the state-specific MCHF equations because of the presence of correlating configurations whose structure corresponds to open channels, then the calculation of Φ_{MCHF} and of Ψ_0 should exclude them. For example, this is the case of He$^-$ $2s2p^2\ ^2S$ which interacts with the $[He(2s^2) + \varepsilon s]\ ^2S$ continuum. Their effect is then incorporated from principal value integrals over purely scattering function spaces.

8.3. The division into "Feshbach" and "shape" resonances in polyelectronic atoms and molecules

Since the 1960s, it has become customary among many researchers studying and/or discussing resonances to divide them into two categories: 1) "*Shape*" or "*open channel*" resonances and, 2) "*Feshbach*," or "*closed channel*" resonances (e.g., see the reviews by Burke [15] and by Buckman and Clark [19]).

In general, this division is guided by criteria of energy: When the picture of scattering of a particle from a target is adopted, then, if the resonance state can be associated, via an assumed criterion, with a scattering channel which is open (i.e., accessible) energetically, then it has been considered appropriate to name it "shape" (i.e., it follows from the "shape" (i.e., characteristics) of the scattering potential), or "open channel" resonance. On the contrary, if the channel to which the resonance is attributed as a result of its coupling is energetically closed, the name "Feshbach," or "closed channel" is used.

In addition, when it comes to problems involving electronic structures, the two categories are understood in terms of those configurations that label, in zero order, the $(N+1)$-particle resonance state and the N-particle target states.

In order to illustrate the above, I recall a simple example: When electrons scatter elastically off the Be $1s^2 2s^2\ {}^1S$ ground state, a shape resonance of ${}^2P^o$ symmetry can be formed, to which the zero-order configurational label of $1s^2 2s^2\ \widehat{p}\ {}^2P^o$ is assigned, e.g., Ref. [19]. The symbol $\widehat{p}$ represents the open channel orbital of p symmetry, whose phase shift at a particular energy reveals the presence of a resonance. (As regards its characteristics, it may resemble, up to a point, a bound 2p orbital, since this is the nearest empty one. However, in general, for negative ion states of atoms and molecules, given the lack of an attractive Coulomb potential and the complexity of open (sub)shell structures, the a priori assignment of the orbital of the extra electron of shape resonances to easily identifiable empty orbitals of the target state loses credibility). On the other hand, upon inelastic scattering of electrons by Be $1s^2 2s^2\ {}^1S$, a negative ion resonance state labeled by Be$^-$ $1s^2 2s 2p^2\ {}^2D$ can be prepared, with an energy below that of the Be $1s^2 2s 2p\ {}^3P^o$ state and decaying into the $1s^2 2s^2\ {}^1S + \varepsilon d$ continuum. Therefore, it can conventionally be considered as a Feshbach resonance, where the closed channel is represented by the Be $1s^2 2s 2p\ {}^3P^o$ threshold.

At certain periods of the development and application of resonance scattering theory to atoms and molecules, the notions of "Feshbach" and "shape" resonances have occasionally been elevated to the level of an important issue. Characteristic discussions as to the relative merits of theoretical methods and as to the relevance of this issue can be found in the literature on doubly and triply excited resonances of the prototypical three-electron system, He$^-$, e.g., Refs. [4a, 4b, 5b, 11b, 56, 73, 77]. For example, normally, if the

scattering theory of Feshbach is followed, which is based on the choice of a unique projection operator, $\mathbf{P}$, in the asymptotic region, then, use of the projection operators $\mathbf{P}$ and $\mathbf{Q} = 1 - \mathbf{P}$ may not allow the recognition of a shape resonance in a particular problem, since the open channel to which the resonance belongs is, in principle, projected out of such a computation.

The purpose of this subsection is to point out that the theoretical and computational relevance of this division is rather particular to certain low-lying structures and that, at least in multiparticle systems, it may lose validity, especially when open subshell electronic structures are involved where spin and angular momentum couplings acquire importance as to the nature of resonance states. In particular, the delineation between the concepts "Feshbach" and "shape" is not very useful or meaningful when the $(N + 1)$ resonance state is associated with multiply excited threshold states of the N-electron atom (molecule), and/or when coupling takes place when two target channels are energetically very close and the energy of the resonance state is in between. This ambiguity is absent when the resonance states are treated according to the present theory, since the concept of target states is not even raised (as it is in a scattering theory framework). In fact, the information about the neighboring thresholds and corresponding channels is contained in the components of Ψ_0, such as the OCL configurations which I mentioned earlier. For example, in a publication on triply excited resonances of He$^-$ and in the context of this issue, we have written:

> This approach renders the question of "Feshbach" vs "shape" resonance without computational or physical significance. Consideration of a nearby threshold enters only for establishing whether it contributes to the width or not. On the other hand, if the desire exists, it is still possible to understand the character of the state under examination by analyzing the major configurations in conjunction with the energy results.
>
> ([77b], p. 3586])

In other words, once the SSA for the computation of resonance states according to Eqs. (1 and 37) has been adopted and the computation of the Ψ_0 and E_0 of interest has been carried out, the concomitant knowledge of the configurational constitution of Ψ_0 reveals the dominant character of the resonance in terms of the coupled thresholds, while the exact energy, $E_r = E_0 + \Delta$, shows its position relative to these thresholds. More discussion and SSA results on this issue can be found in Refs. [11, 56, 77, 127, 128, 144].

As examples of the use and analysis of state-specific Ψ_0 to this purpose, and of comparisons with earlier results and conclusions, I refer to the prototypical triply excited resonances of He$^-$ with all three electrons in the $n = 2$ or $n = 3$ shells, [56, 77b], and to the He$^-$ 1s2s2p ^{2}P$^{\text{o}}$ resonance [4a, 4b, 77a].

The latter one is one of the earliest cases which attracted attention and was discussed in the context of "understanding" resonances in terms of "Feshbach vs shape." Specifically, the He$^-$ 1s2s2p ^{2}P^o resonance, is found between the He 1s2s ^3S and the 1s2s ^1S thresholds at 19.8 and 20.6 eV respectively, and decays to the [(He 1s2s $^3S)\varepsilon p$] and [(He 1s^2 $^1S)\varepsilon' p$] channels. Because of its position and its zero-order electronic structure, certain publications focused on the accurate computation, the nature and the classification of this resonance, e.g., Ref. [4, 5, 77a].

Our work, [77a], demonstrated the efficiency and transparency that come with the SSA computation of Ψ_0. In particular, it was demonstrated that just a two-term, properly coupled, state-specific He$^-$ MCHF wavefunction, computed as $0.995(1s2s2p) - 0.099(1s^2 2p)$ with energy -2.1503 a.u., which is below the energy of the He 1s2s ^1S threshold at -2.14597 a.u., reveals the dominant Feshbach character of the resonance, with smaller parts that can be expanded in terms of the wave functions of the open channels [(He 1s2s $^3S)\varepsilon p$] and [(He 1s^2 $^1S)\varepsilon' p$]. Starting with this fact and including additional localized as well as scattering function spaces, the SSA results showed that, in essential agreement with experiment, the resonance is revealed via a broad, non-Lorentzian peak in the inelastic electron scattering cross-section, and is characterized by $E_r = 20.26$ eV and $\Gamma = 0.60$ eV [77a].

Finally, I bring to attention the fact that, in constructing and carrying out the solution of the MCHF equations for such open (sub)shell systems, the choice of interelectronic spin and angular momentum coupling is of paramount importance in obtaining those state-specific MCHF solutions that can provide the proper zero-order descriptions of the Ψ_0s of highly excited resonances [56, 77, 127, 128]. For example, I quote from our publication on the He$^-$ 1s2s2p ^{2}P^o resonance [77a]:

> In computing Φ and later X, we chose the coupling to be in the $n = 2$ shell, where the interactions are greatest. The more common [six references] coupling between the 1s and the 2s electrons, He$^-$ (1s2s)$^{3,1}S$2p ^{2}P^o, is less desirable for computational reasons. On the other hand, in order to establish correspondence between the physics of the scattering experiment and the $n = 2$ coupling, one can develop the 1s2s2p ^{2}P^o configuration as a linear combination of (1s2s)^1S2p and (1s2s)^3S2p with coefficients $\sqrt{3}/2$ and $-1/2$, respectively. The presence of the 1s^{2}2p component prevents an energy collapse and allows for a proper convergence, in analogy with the better known case of the HF solution for the He 1s2s ^1S state.
>
> ([77a] p. 1867)

A more extensive analysis concerning the interpretation of the components of Ψ_0 for a more complex situation, namely the He$^-$ 2s2p^2 ^2P triply excited resonance, is given in section VI of Ref. [77b].

8.4. Calculations of state-specific $\Psi_0 s$ and of the corresponding potential energy surfaces of negative ion resonances and of diabatic states in molecules

The calculation of $\Psi_0 s$ of resonance states that are based on the separation (37) hinges on the capacity of first producing a valid state-specific HF or MCHF solution, or approximately so. Once this has been accomplished, useful conclusions may be drawn already at this level and, of course, it becomes possible to proceed with the computation of those parts of X_{loc} that are deemed important for the problem under investigation.

It is in this spirit that a priori constructed and calculated "diabatic" molecular states crossing a vibrational or an electronic continuum were obtained in Refs. [138, 145]. The direct state-specific calculation avoids, in the first case the coupling towards predissociation and in the second case the coupling towards autoionization.

Specifically, in Ref. [145] state-specific HF calculations allowed the understanding of formation and the consequences of excited states in the tri-atomic molecules HeH_2, NeH_2 and ArH_2, which are formed transiently in the dissociative continua of the ground state.

Similarly, the computation of a prototypical diabatic state, the He_2^+ $1\sigma_g 1\sigma_u^2$ $^2\Sigma_g^+$ valence state, and its energy curve that crosses as a function of the internuclear distance the Rydberg series $He_2^+ 1\sigma_g^2 n\sigma_g$, $n = 2,3, 4, \ldots$, and the ionization threshold into the $(He_2^{2+}$ $1\sigma_g^2$ $^1\Sigma_g^+ + \varepsilon\sigma_g)$ continuum, was reported in Ref. [138]. This computation resulted from the state-specific methodology that is described in Ref. [146], in which Φ_{MCHF} is obtained numerically by the use of the code published by McCullough [147].

Finally, the SSA and methodology for the computation of the electronic structures with electron correlation of states of diatomic molecules [138, 146] was applied to the elucidation of resonance state problems in the spectrum of the negative ion He_2^- [139]. Specifically, it was determined that the He_2^- $(1\sigma_g^2 1\sigma_u 2\pi_u 1\delta_g)$ $^4\Phi_g$ state is a "Feshbach" resonance, lying below the parent He_2 $(1\sigma_g^2 1\sigma_u 2\pi_u)$ $^3\Pi_g$ and $(1\sigma_g^2 1\sigma_u 1\delta_g)$ $^3\Delta_u$ excited states, and autoionizing into the continuum of He_2 $(1\sigma_g^2 1\sigma_u 1\pi_u)$ $^3\Pi_g$ by the two-orbital rearrangement $2\pi_u 1\delta_g \rightarrow 1\pi_u \varepsilon\delta_g$ or $1\pi_u \varepsilon\gamma_g$ (in $\sigma, \pi, \delta, \varphi, \gamma \ldots$ notation). Furthermore, it was recognized that the localized solution for the $(1\sigma_g^2 1\sigma_u 1\delta_g 1\varphi_u)$ $^4 I_g$ state ought to give rise to a *shape* resonance above the He_2 $(1\sigma_g^2 1\sigma_u 1\delta_g)$ $^3\Delta_u$ state.

9. UNDERSTANDING THE ELECTRONIC STRUCTURES OF RESONANCES AND THEIR EFFECTS ON SPECTRA IN THE FRAMEWORK OF THE SSA

One of the important benefits of the SSA has been the possibility of justifying and understanding, through formalism and advanced many-electron

calculations, properties of various types of autoionizing states by establishing and analyzing just the localized $\Psi_0 s$, where the zero-order description is obtained by solving numerically the MCHF equations with the appropriate for each problem configurations. By the word "appropriate" I mean those self-consistently-obtained bound configurations whose superposition allows an optimal and economic zero-order description of the resonance wavefunction and at the same time secures proper solution and convergence to the correct local energy minimum.

As examples, this section discusses briefly four subjects where, in conjunction with suitable theoretical support, consideration of just the $\Psi_0 s$ has provided quantitative as well as semiquantitative general understanding of the nonrelativistic MEP in a variety of autoionizing (Auger) states across the Periodic Table and of the interplay between their electronic structures on the one hand, and energy, photoionization or autoionization spectra on the other.

9.1. Effects of "hole-filling" electron correlations

The calculation of the Φ_{HF} or of the Φ_{MCHF} representing the zero-order description of Ψ_0, normally has one or more inner holes below the highest occupied orbitals, except when it describes a negative-ion *shape* resonance above the ground state of the neutral atom or molecule. If, for reasons of convenience, a single configuration is used to label the state, then it follows that those electron correlations where the electron rearrangement is such that the hole is filled, play a dominant physical and computational role. The same holds with possible structures where there are more than one holes. We have named these correlations "hole-filling." Normally, they are dominated by symmetry-adapted pair correlations. However, as energy and subshell near-degeneracies increase in certain states of medium to heavy atoms, the relative importance of electron correlations among three and four electrons also increases [122].

The reliable computation of the contribution of the *hole-filling* correlations together with other types, is quite a demanding MEP. On the other hand, in the past even advanced calculations on, say, Auger states, did not even consider them, with the result that serious discrepancies between theory and experiment remained, a situation which was corrected via calculations that applied methods of the SSA [148, 149b]. For example, more than 25 years ago, the abstract of Ref. [148] reads "We show that the large discrepancies between single- and multiconfigurational Dirac-Fock calculations and experiment recently obtained for certain binding and Auger energies of *Ar*, *K*, *Kr*, *Rb*, *Sr* and *Xe*, can be removed by including easily computed (SEOS) correlations." (The SEOS correlations constitute a subset of *hole-filling* correlations).

The fact that *hole-filling* correlations are important is associated with either strong off-diagonal interactions, or with new couplings of the hole(s) with

valence electrons, or with heavy mixings from near-degeneracies, or with all three. This occurs regardless of the size of the atom or of whether the state is discrete or autoionizing [122] and references therein. The result is that they most often constitute an important component of the total wavefunction and so they leave conspicuous signs on spectra.

In this context, the discussions in Refs. [149b, 122, 148, 150] (and in their references), present quantitative results as well as summaries of arguments regarding the a priori recognition and computation of those parts of $\Psi_0 s$ which influence in an essential way the preparation and the consequences of resonance states during photoabsorption by polyelectronic systems. This type of understanding has also allowed the deduction of simple rules as to types of configurational mixing that affect spectra the most. For example, if a $5p$ electron in the actinides (say Uranium) is sent to the continuum by photoabsorption, the SEOS pair correlation $df \leftrightarrow pg$ alters the single-particle picture significantly. The radials of the occupied orbitals $5p$, $5d$ and $4f$ or $5f$ are either of the HF or, more appropriately, of the Dirac-Fock type, while the g orbital is virtual [148].

The rules for the a priori recognition of electron correlations in excited states (in addition to those of the ground state), that affect significantly the photoionization and autoionization spectra have been listed in Ref. [150].

A recent investigation by Kučas et al. [151] verified the exceptional significance of SEOS correlations of the type $4p^5 4d^{n+1} \leftrightarrow 4p^6 4d^{n-1} 4f$ in the photoexcitation and emission spectra of isoelectronic sequences.

9.2. "Collective excitations" related to "giant resonances" in photoabsorption

Because of strong electron correlations, mostly connected to the *hole-filling* type, it is possible to have exceptional cases whereby photoabsorption transitions to the continuum into which inner-hole autoionizing states are embedded, have an unusually large probability within a certain energy range. This possible phenomenon was first discussed in atomic and molecular physics during the 1960s and 1970s from different points of view, and with different interpretations, some of which borrowed the language and formalism from other fields [152] and references therein.

In the work of Ref. [152] we adopted the arguments of the SSA and assumed that electron correlation for highly excited inner-hole states can be understood from the many-electron analysis of the wavefunctions in the form of Eq. (37). Specifically, we adopted the language of superposition of configurations, assuming, for the sake of simplifying the formalism, that the main interacting correlation configurations are represented by bound functions. We then showed that there is a direct connection between electronic structure and the dynamics of excitations for which oscillator strength is

reduced drastically from the single electron excitations and is concentrated exclusively on a narrow range of the spectrum. This may be understood in terms of conditions that connect configuration-interaction mixing coefficients of the excited state (resonance) wavefunction, let us here call it ψ_R, to photoexcitation transition amplitudes to each of its components [152]. To first order, the principal condition is, (Eq. (11) of Ref. [152]),

$$\frac{E_R - E_n}{<\phi_R|\mathbf{H}|\phi_n>} = \frac{<\phi_R|\mathbf{D}_z|\psi_i>}{<\phi_n|\mathbf{D}_z|\psi_i>} \qquad (38)$$

where $\mathbf{D}_z$ is the zth component of the electric dipole operator, $|\psi_i>$ is the initial state, and the matrix elements can be understood from the approximate form of the total (correlated) wavefunction of the resonance state:

$$\psi_R = a_R|\phi_R> + \sum_n a_n|\phi_n>$$

The $|\phi_n>$ may contain contributions from the scattering continuum of the same channel. We concluded that "it is reasonable to expect that in reality these optimum conditions cannot be satisfied exactly and thus physical spectra must contain some single-particle excitation character even in regions where the spectrum is characterized mainly by a single, strongly absorbing peak" [143, p. L262].

9.3. Properties of multiply excited states

The topic of *multiply excited states* (MESs) has attracted both experimental and theoretical interest over the last few decades. In a series of publications, we have produced results of SSA calculations for a variety of MESs, based on the analysis and computations of their $\Psi_0 s$. By the word "multiply" I mean not only the normally examined DESs of He-like systems (Section 9.4), but also novel structures where three or four electrons occupy higher-lying subshells [153–156] and references therein.

The MESs offer opportunities for challenging investigations concerning the correlations of electrons, the difficult to determine details of the MEP, and the interplay of structure and dynamics. In the context of the first step of the SSA, which concerns the efficient computation of electronic structure features and of electron correlation according to the form of Eq. (37), it has proven possible since 1972 to reduce the magnitude of computational problems, to produce quantitative results for properties, and to acquire physical insight of general validity. As regards the latter, I cite two related themes:

9.3.1. Nonorthonormality in photoabsorption and autoionization
The first theme is the significance of *nonorthonormality* (NON) between separately optimized state-specific wavefunctions of the form of Eq. (37). One

of the effects of NON is the allowance of multielectron radiative transitions when no correlation is included, contrary to recycled statements in the literature. In other words, according to rigorous electronic structure theory, the transition matrix elements are always integrals over N-electron coordinates. Hence, transition matrix elements to multiply excited resonance states even with only HF wavefunctions that are specific for initial and final states need not give a null result, provided the orbital symmetries are such that the dipole selection rule is satisfied, e.g., Ref. [153]. In fact, in many cases, computation with just state-specific HF wavefunctions provides a semiquantitative and economic way of predicting the radiative probabilities of such transitions.

As an example of the above, let me consider the one-photon, three-electron transitions from the $n = 2$ to the $n = 3$ shell in Carbon,

$$C\ 1s^2\ 2s^2\ 2p^2\ {}^3P \xrightarrow{\text{one photon}} 1s^2\ 2s\ 3p^3\ {}^3D^o,\ {}^3P^o,\ {}^3S^o$$
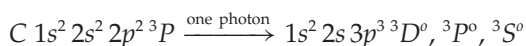
for which the transition energies are computed to be approximately 50.7 eV ($^3D^o$), 51.8 eV ($^3P^o$) and 52.0 eV ($^3S^o$). No experimental measurements exist.

In the late 1980s, this three-electron excitation was cited by other researchers as a heuristic case to argue that, "as far as we can tell, a multiply excited state such as $3p^3$ is virtually inaccessible by single-photon absorption." Yet, small-size (for reasons of economy) SSA calculations show that the state-specific HF result, which is of course obtained from an independent electron model with no electron correlation, produces nonzero values for the probabilities of the three transitions. Furthermore, the order of magnitude of the HF transition probabilities is the same as that from computations that include some part of electron correlation. Specifically, the results of the SSA calculations for the oscillator strengths, using only approximate wavefunctions for the $\Psi_0 s$, are:

	HF	HF plus electron correlation:
$^3P \rightarrow {}^3D^o$	0.99×10^{-4}	0.88×10^{-4}
$^3P \rightarrow {}^3P^o$	0.58×10^{-4}	0.16×10^{-4}
$^3P \rightarrow {}^3S^o$	0.76×10^{-4}	0.94×10^{-4}

In other words, a result which in another kind of theory that uses a single basis set would appear as a high-order correlation effect (e.g., I recall that algorithms such as the Random Phase Approximation cannot handle multi-electron transitions), in fact it is a zero-order effect when computed according

to the SSA. The significance of this conclusion lies both in the simplicity of the calculation and in the physical insight that it provides.

Obviously, NON plays a similar role in the calculation of autoionization matrix elements. For example, see [127, 155] for its contribution to the understanding of the mechanism of autoionization.

9.3.2. Regularities in electronic geometries and spectra

The second theme is the discovery of the existence of remarkable regularities that are common to classes of doubly, triply, and quadruply excited states, in specific total angular momentum and spin symmetries. For example, for the intrashell state of lowest energy, there are regular series for the DESs which shows that the two electrons on the average tend to the linear geometry as the two-electron threshold is approached. For the three-electron case, it is the equilateral triangle geometry that is reached. And for the four-electron case of $^5S^o$ symmetry, it is the tetrahedron geometry that is approached at the four-electron fragmentation threshold [154] and references therein.

Here, I focus on the results of the most complex case, that of the quadruply excited states in Be of $^5S^o$ symmetry. In Ref. [154] we found via theory and its implementation in terms of correlated wavefunctions obtained by solving the MCHF equations for the intrashell configurations, regularities in the geometry of electron distribution and in the energy spectrum.

(1) *Geometry*: As a result of the mixing of many intrashell configurations with self-consistently obtained orbitals, the average angle between the electrons opens up as the manifold quantum number, n, increases, tending to that of a tetrahedron. Specifically, for $n = 2$, where the wavefunction is essentially the HF 2s2p^3 $^5S^o$, the interelectronic average angle, $<\theta_{12}>$, is 99.5^o. As n increases, the state-specific wavefunction has been calculated at the MCHF level for the lowest root of an expansion with all $n_1 = n_2 = n_3 = n_4 = n$ configurations [154]. For $n = 3$, the main configuration, 3s3p^3, has a weight of 0.90, while $<\theta_{12}> = 103.3^o$. For $n = 6$, the wavefunction is highly correlated, having the MCHF composition of 0.77 (6s6p^3) + 0.48 (6s6p6d^2) + 0.23 (6s6f6d^2) − 0.28 (6d6f6p^2) + 0.13 (6p6d6f^2) − 0.11(6f6d^3). Now, the average angle has already opened to $<\theta_{12}> = 106.0^o$, while the character of the wavefunction exhibits a broad distribution over orbital angular momenta, with main configuration, (6s6p^3), having a weight of only 0.59. In this case, doubly, triply, as well as quadruply excited correlation configurations with respect to what appears as the main label, i.e., the (nsnp^3) configuration, contribute to the wavefunction significantly. As n increases further, there is a shift of configurational weights, towards the intrashell configurations other than the (nsnp^3).

(2) *Energy spectrum*: For these intrashell states of the lowest energy, as energy increases the energy spectrum becomes clearly a simple function of the quantum number of each manifold, n, having the same (hydrogenic) form with those of analogous doubly and triply excited states (C is essentially

constant):

$$E_n = -A_n \frac{n(n-1)}{<r_n>^2} \tag{39a}$$

and since computations showed that $<r_n> \sim n^2$ and that A_n varies slowly with $<r_n>$,

$$E_n = -C\frac{1}{n^2}, \text{ for large } n \tag{39b}$$

In other words, two results from the physics of the hydrogen atom, the $1/n^2$ dependence of the energy spectrum and the $<r_n> \sim n^2$ proportionality, were shown to be valid also in special classes of quadruply excited states. The same result holds for classes of doubly and triply excited states. For example, in Ref. [156]. we demonstrated quantitatively for the first time the existence of a "hyper-ridge" for triply excited states in *Li*, with the following property: As the three-electron fragmentation threshold is approached, the ion core and the three electrons tend to lie in a plane, with equilateral triangular geometry, and with the average values for the electron radii satisfying, $< r_1 > = < r_1 > = < r_1 >$.

I emphasize that the geometrical-dynamical properties mentioned above have emerged from analysis that is based on first-principles quantum mechanical considerations and calculations. The common feature of these MESs is that they represent situations where, for each value of n, the interelectronic correlations are maximal, regardless of the number of electrons.

A descriptive analysis of triply excited states of $^4S^o$ symmetry whose geometric assumptions depend on the findings in Ref. [156] can be found in Ref. [157]. For recent theoretical work on quadruply excited states of Be, see the paper by Poulsen and Madsen [158]. For experimental progress in the study of "hollow" states of Be, see the Letter by Hasegawa et al. [159].

9.4. Series of DESs of H⁻ and of He. Electron correlation and the classification according to the (*F,T*) scheme of quantum numbers

The research on the formal and quantitative understanding of MESs that was briefly described in the previous subsection started with theory and results on DESs. In this subsection I discuss properties of such states in H⁻ and in He that are deduced solely from the computation and analysis of the localized component, Ψ_0. In the next subsection, results from the computation of partial and total widths from the CESE method are also discussed.

In 1983, Fano [160] published a review on aspects of the physics of DESs with emphasis on their analysis in terms of hyperspherical coordinates. In this framework, his attention was mainly towards descriptively connecting features of the DESs with Wannier's threshold scattering "law" for two electrons, which is obtained from classical mechanics. Fano also referred to the pioneering work of Herrick and Sinanoğlu [161, 162] on the classification

of DESs according to new quantum numbers, (K,T), derived and applied within the hydrogenic model from group-theoretic (algebraic) analysis. He commented as follows:

> The initial Herrick- Sinanoðlu paper appeared unrealistic in projecting the Hamiltonian on a single hydrogenic $((N,n))$ manifold...thus recovering any hybridization of radial quantum numbers and related aspects of correlations.... However, the numerical work is now understood to have actually included some of this hybridization whereby the close approach of eigenvalues $E(K,T)$ to observed levels no longer need cause surprise.
>
> [160, p. 119]

A reading of Fano's paper under the prism of quantitative knowledge for DESs of high excitation (e.g., experimentally verifiable numbers for their positions, partial and total widths and excitation probabilities), suggested to us that such an understanding was a desideratum. Therefore, we embarked upon a research program for the investigation of such problems in terms of appropriate state-specific calculations of electronic structure and of electron correlation. The results have been published in a series of papers by Komninos and Nicolaides and their graduate students Chrysos and Themelis, e.g., Refs. [120, 163–168], and include analysis of correlated wavefunctions for different symmetries, energies and corresponding regularities, oscillator strengths to the states of the "Wannier two-electron ionization ladder" (TEIL), autoionization widths, geometrical location of the two-electrons, a new classification scheme for high excitation, etc.

For example, by computing the correlated wavefunctions up to very high quantum numbers, i.e., up to the manifold $N = 25$ [166–168], it became clear that a new classification scheme, based on the (F,T) quantum numbers, is much closer to the accurate description than the (K,T) scheme is, as the two-electron threshold is approached, i.e., as the relative importance of electron correlations increases.

After an experience of a 2–3 years period with the ab initio SSA computations of high-lying DESs of the TEIL category, up to about the $N = 10$ manifold, e.g., Refs. [163–165], Komninos and Nicolaides turned to the examination of the goodness of the (K,T) scheme as a function of the excitation energy, since it was evident that the effects of electron correlation and of configurational mixing ought to become more significant as threshold is approached. The result of this search was the introduction in 1993 by Komninos et al. [166] of the F number, as a combination of N and K, neither of which is now a good number. Specifically, F is defined by $F = N - K - 1$ where K goes from $-N - 1 - T$ to $N - 1 - T$ in steps of 2.

The breakdown of the "goodness" of the numbers N and K (but not of T) has to do with the increased relative importance, as the excitation energy

(i.e., as N) increases, of electron correlations beyond those included in the hydrogenic intrashell "doubly excited symmetry basis" (DESB) of Herrick and Sinanoğlu. Having recognized this fact, we stated explicitly that the cause of the breakdown of the (K, T) representation is to be found mainly in the importance of double excitations from the near-degenerate hydrogenic manifold [166, p. 405]. Furthermore, we proceeded with the implementation of practical computational methods for the calculation of correlated wavefunctions and energies of TEIL states of ^1S and $^1P^o$ symmetry as a function of excitation up to the manifold $N = 15$.

Eventually, wavefunctions for more than one roots for each N were computed and analyzed. E.g., one of the results in Ref. [168] was obtained via the ab initio computation of the angular probability density, $\rho(\theta_{12})$, for states in the range of the $N = 10$–25 manifolds, and shows explicitly how the angle between the two electrons opens towards 180° as excitation increases.

"…. Another result in Refs. [167, 168] for the DESs of $^1P^o$ symmetry is that, among the four lowest states of each manifold, in all cases in H$^-$ and in most cases in He, the three are of the intrashell type and one is of the intershell type with $(F,T) = (0,0)$. The lowest intrashell states and the lowest intershell states exhibit a wide angle geometry tending to 180° as $N \rightarrow \infty$…."

[167]

Other consequences of the goodness of the F number are mentioned in Refs. [167, 168].

One of the keys of the initial Komninos–Nicolaides work was the recognition that the state-specific MCHF orbitals for these DESs were represented almost exactly by natural orbitals that can be obtained from bases of hydrogenic orbitals [166]. Therefore, for very high excitation where the state-specific MCHF method breaks down numerically, one can use diagonalization with judiciously chosen hydrogenic orbitals in order to produce results whose accuracy is expected to be very good [166–168]. Once this fact is realized, the approach of using CI with hydrogenic functions has the advantage that the use of the exact hydrogenic functions makes it feasible to carry out computations with systematically chosen singly and doubly excited configurations, while excluding open channels of states of Rydberg series and of scattering continua.

The computation of these CI wavefunctions and their projection of the suitably constructed wavefunctions in the (K, T) (DESB basis) and the (F, T) representations are discussed and demonstrated in Refs. [166–168]. It is important to note that whereas the DESB vectors are the same for all Z, the FT ones are not. The quality of the (F, T) classification scheme depends on the system, and the theory of Ref. [166–168] permits its investigation via ab initio numerical calculation.

I close by quoting the conclusions from [168] on the $^1P^o$ DESs in H$^-$ and in He:

(1) The (F, T) scheme expresses the character of the DESs much better than the (K, T) scheme, in both the intrashell, T = 1, and the intershell, T = 0, cases, for H$^-$ as well as for He.
(2) In H$^-$, where the relative importance of electron correlation is greater, the deterioration of the (K, T) classification is rapid for all four states. In contrast, the purity of the (F, T) scheme for the lowest intrashell state (i.e., the TEIL state (F, T) = (1, 1)), and for the lowest intershell state (F, T) = (0, 0), remains very high and stable up to N = 25. This is probably due to the fact that, for the lowest energy states the CI calculations usually incorporate a larger part of the electron correlation.
(3) For He, the difference between the (K, T) and the (F, T) purities of the four states increases more slowly than for H$^-$ as N increases. It is interesting that there appears a maximum of purity at low N for the three higher intrashell DESs, both with the (K, T) scheme and with the (F, T) scheme.

Finally, it is worth pointing out that the *F* number of the (*F*,*T*) scheme was recently recognized as being significant in the classification of complex spectra of DESs in He. Specifically, it was utilized appropriately by Jiang et al. [196a] and by Eiglsperger and Madroñero [196b], in order to provide explanations of experimental photoionization cross-sections for DESs in He and of corresponding theoretical results. For example, in their abstract, Jiang et al state "The fact that all spectra are dominated by principal Rydberg series is explained by the observation that the quantity $F = N - K$, representing angular motion, is an approximate quantum number for a large fraction of states. . . " [196a, abstract].

9.5. Series of DESs of H$^-$ and of He. Regularities in their wavefunctions, energies and decay widths

The SSA allows calculations and quantitative analysis of DESs of polyelectronic systems irrespective of their symmetry and of the nature of their inner core. Such situations constitute MEPs which are rather difficult-if not impossible- to solve within the framework of hyperspherical coordinates reviewed by Fano [160]. A prototypical such system which is amenable to economic computations is the three-electron negative ion, He$^-$, in states that are labeled by configurations with one electron in the 1s shell. For example, the DESs $'1sn\ell^{2'}$ of He$^-$can be recognized as the three electron analogue of the DESs $'n\ell^{2'}$ of H$^-$. The 1s orbital screens the outer electrons while producing effects of spin-coupling that are expected to diminish as the quantum number $n$increases. I stress that the labels $'1sn\ell^{2'}$ or $'n\ell^{2'}$ imply correlated wavefunctions that are dominated by the intrashell configurations at each manifold n.

In this context, I recall two sets of results on properties of the TEIL states of ^2S [165] and of ^4P [120] symmetry.

In the latter case [120], the previously unknown TEIL states of the $He^{-\prime}1sn\ell^{2\prime}$ ^4P and of $H^{-\prime}n\ell^{2\prime}$ ^3P systems were studied from first principles within the SSA, and the results for $n = 3 - 8$ were compared. These had to do with their wavefunction constitution, the energies, the widths, the partial widths, and the trends of energetics and of decay dynamics as n increases. For information and analysis, the reader is referred to [120]. Here, I can mention two related conclusions:

(1) When the total width is broken down into partial widths, the closest threshold contributes the most to the decay dynamics.
(2) Upon analysis of the correlated wavefunctions, it becomes clear that, for both the $He^{-\prime}1sn\ell^{2\prime}$ ^4P and the $H^{-\prime}n\ell^{2\prime}$ ^3P systems, up to $n = 5$ the dominant configuration is the np^2. For higher n, the principal weights shift to nd^2 and to higher ℓ^2. In fact, analysis showed that the probability of finding a given value of ℓ peaks at $\ell_{max} = \frac{\sqrt{3}}{2}\sqrt{n}$ [120].

In the former case, our results were the first ab initio quantum mechanical predictions, and they were verified by the experimental resonance spectrum measured by Buckman and Newman [169]. By computing conditional probabilities, it was explicitly demonstrated [165] for the first time that as energy increases, the two-electrons in the $'1sn\ell^{2\prime}$ ^2S intrashell states of He^- that have the lowest energy in each shell reach the two-electron ionization threshold with the Wannier geometry of $r_1 = r_2$ and $\theta_{12} = 180^o$.

Table 4.4 lists the theoretical predictions for the positions of the $He^{-\prime}1sn\ell^{2\prime}$ ^2S TEIL states [165] and the experimental energies [169] which confirmed them (in eV). These are calculated with respect to the two-electron ionization threshold of 24.588 eV.

Table 4.4 Theoretical and experimental energies (in eV) of the He^- $'1sn\ell^{2\prime}$ ^2S TEIL states, measured from the two-electron ionization limit of 24.588 eV. The numbers in parenthesis give the experimental uncertainties

n	Theory, SSA [165]	Experiment [169]
3	2.156	2.137 (10)
4	1.180	1.153 (10)
5	0.745	0.738 (10)
6	0.511	0.508 (10)
7	0.375	0.371 (10)
8	0.287	0.281 (10)
9	0.227	0.201 (10)
10	0.184	

Table 4.5 Comparison of total energies (in a.u.) of the TEIL states He^{-} $'1sn\ell^{2\prime}$ ^2S and H^{-} $'n\ell^{2\prime}$ ^1S, according to the SSA of Ref. [165]. For He^{-}, the He^{+} 1s energy is subtracted. As n increases, they converge toward each other, in accordance with intuition that the spectra are dominated by the correlations of the two outer electrons

n	He^{-} $'1sn\ell^{2\prime}$ ^2S	H^{-} $'n\ell^{2\prime}$ ^1S
3	−0.07923	−0.06927
4	−0.04337	−0.03997
5	−0.02738	−0.02595
6	−0.01877	−0.01814
7	−0.01378	−0.01344
8	−0.01056	−0.01035
9	−0.00835	−0.00823
10	−0.00677	

Table 4.5 compares the total energies (in a.u) of the He^{-} $'1sn\ell^{2\prime}$ ^2S TEIL states with those of H^{-} $'n\ell^{2\prime}$ ^1S. The wavefunctions are correlated according to the SSA to these DESs. For He^{-}, the $He^{+}1s$ energy is subtracted [165]. The results are quantitative and demonstrated what is expected intuitively, namely, that as threshold is approached the behavior of the pair of electrons in the two systems is similar and that the energy spectra tend to converge to each other.

10. THE USE OF Ψ_0s AND OF SCATTERING WAVEFUNCTIONS IN THE SSEA FOR THE SOLUTION OF THE TDSE

The possibility of obtaining compact and usable square-integrable wavefunctions Ψ_0s that represent the localized part of the resonance states accurately, has been critical in developing and implementing the SSEA for the solution of the polyelectronic TDSE [76, 170, 171], and Chapter 6 of this volume by Mercouris et al. This is because, for polyelectronic atoms and molecules the resonance states are always present in the continuous spectrum and may cause critically important contributions. Therefore, as the continuous spectrum is being probed experimentally more efficiently and accurately, the ability of accounting computationally for the time-dependence of multielectron excitations or of the coherent creation and decay of autoionizing (Auger) states becomes necessary.

11. FIELD-INDUCED QUANTITIES OBTAINED AS PROPERTIES OF RESONANCE STATES IN THE FRAMEWORK OF THE CESE-SSA

11.1. The MEP for field-induced quantities

During the past three decades or so, steady advances in the technology of production of strong dc- and, especially, ac-fields, and in the concomitant spectroscopies for atoms and molecules, have provided the impetus for the development of new and effective theories for treating the problem of matter-field interaction beyond "lowest order perturbation theory" (LOPT). The literature on the multifarious subject of the formalism and calculation of phenomena and properties resulting from the interaction of atomic (molecular) states with strong fields is extensive, and, of course, it is outside the scope of this article to review it. A useful background for the material to which I refer below can be obtained from the well-written book of Faisal [172] and from the 1988 conference volume on "Atoms in Strong Fields" [173].

Of interest here are the effects of static electric and magnetic fields and of cycle-averaged interaction with ac-fields. I do not discuss the theme of interaction with time-dependent pulses, for which the theoretical requirement is the proper time-dependent solution of the polyelectronic TDSE (see Chapter 6).

The essence of the theoretical and computational problems that have to be solved can be understood and formulated as follows:

Assume that the strength of the external field does not exceed the forces inside the atom, and that therefore, the notion of atomic states and electronic structures is still valid, albeit perturbed. In general, the characterization of the field strength is done relative to the binding strength of the state(s) with which it interacts. The new total Hamiltonian is $\mathbf{H} = \mathbf{H} + V$, where V represents the atom–field interaction operator(s). Now, the ensuing MEPs are field-dependent and the level of their formal and computational complexity and difficulty is often much higher than that of the field-free cases.

For example, the interaction engages all states of electric dipole-allowed symmetries from both the discrete and the continuous spectrum, each of which contributes to some degree (from significant to negligible), to the properties under investigation. Indeed, special physical importance is acquired by the infinitely degenerate continuous spectrum, since the strong perturbation inevitably couples it, directly or indirectly, to the initial state. For dc fields, the coupling leads to energy shift and to electron tunneling, normally seen as energy broadening, as a function of field strength. For ac fields, apart from the energy shift, transitions to and within the continuous spectrum also occur, via absorption of one or more photons. As frequency tends to zero, ionization is conceived as tunneling whose magnitude is strongly dependent on the field strength. In general, the magnitudes of the measurable quantities depend on the parameters of the field in relation to the system of interest.

One direction of theoretical research for going beyond LOPT that has attracted attention, albeit with applications thus far only to one-electron systems, where, of course no electron correlations (i.e., the effects of the two-electron operators in **H**), exist, is the possibility of going to high order and of summing the full perturbation theory (PT) series by some technique. The book [172] and the articles by Silverstone and by Silverman and Nicolaides in Ref. [173] discuss such approaches, via which both energies and ionization rates can be obtained.

It must be stressed that most of the published high-order PT calculations that have obtained field-induced energies and widths are based on methods that are limited intrinsically to one-electron atoms. One exception is the formalism published by Silverman and Nicolaides [173, 174], which is based on matrices that can be constructed for many-electron systems as well. However, although the method has been successful not only with the normally studied ground state of hydrogen but also with some of its excited states, no calculations on a many-electron system have been carried out yet.

The alternative to trying to go beyond LOPT via the calculation of higher order terms of the PT, is the possibility of implementing nonperturbative methods, which, provided that they use sufficiently accurate function spaces, are equivalent to the all-orders PT.

With the aim of computing tunneling rates induced by strong static electric fields and of multiphoton transition rates induced by strong ac fields, Reinhardt and coworkers [111, 112, 175–177] carried out the first nonperturbative calculations in the framework of the CCR method. Their calculations were carried out for the dc-field induced tunneling of the $n = 1$, 2 states of Hydrogen and of the $^1P^o$ shape resonance of H^-, and for the ac-field induced few-photon ionization of the $n = 1$ state of Hydrogen. As regards the ac-field problem, the papers by Chu and Reinhardt [176] and by Maquet et al. [177] justify the semiclassical use of the time-independent interaction Hamiltonian. In particular, by invoking Shirley's [178] basic work on ac-fields interacting with atomic spectra, they explain how, by using a "Floquet" formalism, a symbolic form of the atom–field Hamiltonian in the dipole approximation that is averaged over a cycle can be written in terms of the field strength, with the presence of creation ($a_\omega^\dagger$)-annihilation (a_ω) operators allowing for the book-keeping of the construction of the field-dressed Hamiltonian matrix.

The "Floquet formalism" is reviewed in Chapter 2 by Atabek et al.

In analogy to the field-free problem, the "Stark CCR" and the "Floquet CCR" methods have serious limitations with respect to the MEP. The way out was proposed in the late 1980s, when ideas and the general methodology of the SSA for the field-free resonances that solves state-specific CESEs were adapted so as to achieve the nonperturbative solution of problems of interaction of strong dc-and ac- electric fields and static magnetic fields with atomic (molecular) ground or excited states in terms of non-Hermitian formulations, e.g., Refs. [103, 179–190].

Following the analysis and justification of the CESE-SSA, the Hamiltonians for the ac field and the static electric and magnetic fields have real and not complex coordinates. However, the trial function space is partitioned according to the form of Eq. (35) (see below). Hence, the resulting non-Hermitian Hamiltonian matrices have a different form than that of the standard "Stark" or "Floquet" CCR matrices. As a consequence, the field-dressed CESE-SSA can be, and has been, applied efficiently to polyelectronic problems in terms of many-electron methods. Again, state-specific complex eigenvalues are obtained, with the effects of ac-field interaction assumed to be averaged over a cycle. The real part of the field-dependent complex eigenvalue includes the field-induced energy shift, from which polarizabilities and hyperpolarizabities can be obtained. The imaginary part represents the decay rate into the continuum, either via tunneling or via ionization by absorption of one or more photons, or via both.

The subject is broad and open as regards computational possibilities and applications, and so the reader is referred to the original papers. Below, I simply outline certain formal procedures and quote some results as examples.

11.2. The CESE-SSA to the ab initio calculation of states interacting with strong electric static or ac-fields

Let us consider the static electric field problem, for which the perturbed Hamiltonian is (in a.u.),

$$\mathbf{H} = \mathbf{H} + \sum_{i=1}^{N} \vec{r}_i \cdot \vec{F} \tag{40}$$

The spectrum of this operator is unbounded and continuous. Yet, because of the existence of the discrete or of the resonance states of the field-free $\mathbf{H}$, what happens is that at their positions there is high spectral concentration, in direct correspondence with the problems of decaying states and of the mixing of discrete-continuous spectra, elements of which were outlined in Sections 3–6. In other words, we have to do with a decaying state problem in which the clearly defined initial discrete, Φ_n, or autoionizing, $\Psi_r(E)$, states (they are eigenstates of $\mathbf{H}$), mix via V with the continuous spectrum. The perturbation changes the asymptotic boundary conditions for the acceptable solution of the Schrödinger equation, and produces a CESE, in analogy with the resonance state problem discussed in Section 5. The form of the resonance eigenfunctions for the linear potential and procedures for its regularization, were treated in Ref. [103].

The same concept holds when the time-independent Hamiltonian for the ac-field interaction is considered, only that now, there is also dependence on the frequency and on the electric dipole excitations-de-excitations caused by the a_ω and $a_\omega^\dagger$ operators.

In the CESE procedure, the coordinates of the Hamiltonian (40) are left real. The total function space is formally divided into two multi-dimensional parts of N-electron wavefunctions, say Q and P, not necessarily orthonormal between them. The Q space is fixed by considering judiciously the electronic structure and spectrum of the system under study. The P space is not completely fixed. It contains parameterized configurations with real as well as complex orbitals representing contributions from the multichannel high Rydberg and scattering states. It is the variational optimization of this space via the diagonalization of the matrix

$$\underline{\mathbf{H}} = \begin{bmatrix} H_{QQ} & H_{QP} \\ H_{PQ} & H_{PP} \end{bmatrix} \tag{41}$$

that allows the tuning of the concerted effect of field-induced state mixing and of electron correlation, and leads to the determination of the width and shift of the perturbed state. $\underline{\mathbf{H}}$ is diagonalized repeatedly with respect to changes in the nonlinear parameters in the basis set of the P space and in the rotation angle, until the root having the maximum overlap with (Ψ_0, E_0) is stabilized. It should be noted that due to difficulties of numerical origin, resonances induced by very weak fields are not calculable in this way, since the widths become very small exponentially. Instead, in such cases the calculation can be based on a golden rule-type formula, even within the semiclassical approximation [187].

The case of the ac field is treated in an analogous way. Following the discussions in Refs. [176–178], the N-electron Hamiltonian for a one-color linearly polarized field of field strength F_o (1 a. u. $= 5.14 \times 10^9$ V/cm) and of frequency ω (see [188, 189] for calculations with two and three colors), is chosen as ($\hbar = 1$).

$$\mathbf{H}_{ac} = \mathbf{H} + \omega \alpha_\omega^\dagger \alpha_\omega - \frac{F_o}{2} \sum_i^N z_i(\alpha_\omega^\dagger + \alpha_\omega) \tag{42}$$

For the study of the interaction that causes single-electron ionization (two-electron ionization has also been computed [190]), the trial wavefunction is constructed in terms of symmetry-adapted MCHF and correlation configurations that are grouped into two parts:

$$Q: \{\Psi_i(r_N); n\} \tag{43a}$$

$$P: \left\{X_j(r_{N-1}, \rho^*); n\right\} \equiv \left\{\Psi_j(r_{N-1}) \otimes \varepsilon \ell(\rho^*); n\right\} \tag{43b}$$

The index j assigns electronic wavefunctions with bound orbitals whose coordinates are real. The index n denotes the photon states. This bookkeeping number ranges, in principle, from $-\infty$ to $+\infty$, changing in units ± 1. In practice, its maximum value determines the number of the "photon blocks" and of the angular momenta states in the continuous spectrum. The $X_j(r_{N-1}, \rho^*)$ denote the open channel states represented by the symmetry-adapted product of the bound core wavefunctions, $\Psi_j(r_{N-1})$, with complex L^2 Gamow functions, $\varepsilon\ell(\rho^*)$, which are normally chosen as (more flexible forms are possible),

$$\text{Radial of } \varepsilon\ell = r^m e^{-a\rho^*}, \; \rho^* = re^{-i\theta} \tag{44}$$

The number of angular momenta for $\varepsilon\ell$ depends on the problem, and its final choice is made by following the convergence of the overall calculation. For the systems that we have studied, ℓ ranges from 0 up to about 10.

Given the basis (43 and 44), it is straight forward to obtain the form of the matrix elements of H_{ac}, Eq. (42). The corresponding complex Hamiltonian matrix has the form

$$\underline{H}_{ac} = \begin{bmatrix} \cdot & & & & & & \\ & \underline{A} + 2\omega\underline{I} & \underline{V} & & 0 & & \\ & \underline{V} & \underline{A} + \omega\underline{I} & \underline{V} & & & \\ & & \underline{V} & \underline{A} & \underline{V} & & \\ & & & \underline{V} & \underline{A} - \omega\underline{I} & \underline{V} & \\ & & & & \underline{V} & \underline{A} - 2\omega\underline{I} & \\ & 0 & & & & & \cdot \end{bmatrix} \tag{45}$$

where $\underline{A}$ contains the free-atom matrix elements within the same photon number, and $\underline{V}$ is the matrix of the interaction operator, $-\frac{F_o}{2}\sum_i^N z_i(\alpha_\omega^\dagger + \alpha_\omega)$. The photon states differ by ± 1.

The complex eigenvalue problem is solved iteratively by the method explained in Refs. [181, 182]. The parameters $(a, \theta,)$, $0 < \theta < \pi/2$, of (44) are varied until stability in the result of the eigenvalue is observed.

The solution, namely the complex eigenvalue of the field-induced resonance state, is a function of the frequency and strength of the field. For normal cases where there are no serious field-induced near-degenaracies, it is connected smoothly to the unperturbed energy E_0:

$$z_r(\omega, F_o) = E_0 + \Delta(\omega, F_o) - \frac{i}{2}\Gamma(\omega, F_o) \tag{46}$$

The final form of the field-induced complex eigenfunction is the superposition

$$\Psi(r_{N-1}, \rho^*) = \sum_{i,n} \alpha_{i,n}(\theta_r)|\Psi_i(r_N); n > + \sum_{j,n} \beta_{j,n}(\theta_r)|X_j(r_{N-1}, \rho^*); n > \qquad (47)$$

Projection onto scattering states provides additional information concerning the continuous spectrum, such as the understanding of "above threshold ionization" (ATI) in the presence of a dc field [183] or of angular distributions of the emitted electron.

There have been many applications of the CESE-SSA to the solution of prototypical problems created by the interaction of strong static and dynamic fields with discrete or autoionizing states. The reader may consult the references. Here, I mention only three types as examples.

11.2.1. Static and dynamic polarizabilities and hyperpolarizabilities

From the expansion of $\Delta(\omega, F_o)$ in Taylor series for as small values of F_o as computationally possible, it is possible to obtain cycle-averaged quantities corresponding to measurable polarizabilities and hyperpolarizabilities, of ground, excited and autoionizing states, e.g., Refs. [182, 186]. Specifically, the computed energy shift for atomic states is written as

$$\Delta(static) = -\frac{1}{2!}\alpha F_o^2 - \frac{1}{4!}\gamma F_o^4 - \frac{1}{6!}\delta F_o^6 - \dots \qquad (48a)$$

$$\Delta(\omega) = -\frac{1}{2!}\alpha(\omega)\overline{(F_o \cos \omega t)^2} - \frac{1}{4!}\gamma(\omega)\overline{(F_o \cos \omega t)^4} - \dots$$

$$== -\frac{1}{2!}\alpha(\omega)\left(\frac{1}{2}\right)F_o^2 - \frac{1}{4!}\gamma(\omega)\left(\frac{3}{8}\right)F_o^4 - \dots \qquad (48b)$$

The expansion coefficients are then obtained via least-squares fitting. This procedure can be (and has been) implemented directly to the ab initio calculation of the frequency-dependent polarizabilities and hyperpolarizabilities.

As an example, I bring the problem of computing these quantities for the ^1S ground state of the negative ion of Li. Such a four-electron system is challenging not only because of the $2s^2 \leftrightarrow 2p^2$ near-degeneracy in the ^1S state but also because its wavefunction is relatively diffuse while the ionization (detachment) threshold is only 0.617 eV and so the continuous spectrum acquires increased importance.

By the end of the 1980s, state of the art methods of quantum chemistry, such as coupled cluster, configuration interaction, fourth order perturbation theory (MP4), second-order polarization propagator (SOPPA, multiconfigurational linear response (MCLR) etc., had been applied to the calculation of

the static polarizability of Li^-. In spite of the magnitude of such calculations, there was considerable disparity in their results. This fact was pointed out by Ågren et al. [191] and also by us, Table 1 of Ref. [182]. There were no results for frequency-dependent polarizabilities, and this was rectified by the work of Ågren et al. [191] as well as of Nicolaides et al. [182] whose results were published at about the same time.

The calculations of Ågren et al. employed the MCLR theory and exact full configuration interaction and are of much larger scale than those of the CESE-SSA. Yet, the agreement between the two sets of results is very good. For example, for $\omega = 0.02$ a.u. Ågren et al. give $\alpha(\omega) = 1208$ a.u. (Table III of Ref. [191]), while our result was 1098.5 a.u. (Table 4 of Ref. [182], a difference of 9%. On the other hand, I point out that the results of Ågren et al. [191] go only up to about $\omega = 0.022$ a.u., i.e., the frequencies reach up to the detachment threshold of Li^-, whereas it was possible for the CESE-SSA calculations to cover the continuum of $Li + e$ as well, producing results in the range of frequencies $0.000\, a.u. < \omega < 0.102\, a.u.$.

Furthermore, our CESE-SSA work dealt with the much more difficult problem of nonlinear polarization, and produced the first static and frequency—dependent results for the hyperpolarizability, $\gamma(\omega)$, for the same range of frequencies. As far as I know, our results on $\gamma(\omega)$ of a polyelectronic negative ion [182] are still the only ones in the literature.

A brief description of the wavefunctions used in the CESE-SSA calculations is as follows: The first step is to obtain a reliable initial state wavefunction, with a good description of the asymptotic region. Our $Li^{-1}S$ ground state wavefunction contained 43 terms, of which the zeroth order was obtained numerically at the MCHF level as

$$\Psi_0^{\text{MCHF}}(\text{Li}^-) = 0.939(1s^2 2s^2) + 0.360(1s^2 2p^2)$$

whereas the remaining correlation vectors were obtained by minimizing the total energy as a function of the nonlinear parameters of the analytic correlation orbitals [9]. The total energy thus obtained is $E_0 = -7.455364$ a.u., and compares well with the configuration interaction result of Weiss [192], -7.4553 a.u..

The $1s^2 2s\,^2S$ and the $1s^2 2p\,^2P^o$ state-specific wavefunctions were included in the many-electron, many-photon (MEMP) matrix (Eq. (45)), as the two Li thresholds. The coupling of the initial (ground) state, Ψ_0, through the dipole field and the corresponding excited configurations were as follows:

$$\Psi_0 \xrightarrow{F_z} 1s^2 2s\varepsilon\ell,\ \ell = 0, 1, \ldots \ldots 10,\ \varepsilon\ell = r^n \exp\left(-\alpha r e^{-i\theta}\right)$$

$\alpha = $ parameter, $\pi/2 < \theta < 0$

$$\Psi_0 \xrightarrow{F_z} 1s^2 2p\varepsilon s\ ^1P^o,\ 1s^2\, 2p\varepsilon\, p\ ^1S,\ ^1P,\ ^1D,\ 1s^2 2p\varepsilon d\ ^1P^o,\ ^1D^o,\ ^1F^o$$

It is stressed that the nonperturbative MEMP CESE-SSA calculations have shown that it is important to include in the continuous spectrum many partial waves. This necessity can be easily handled by the MEMP CESE-SSA.

11.2.2. Dependence of the ionization rate on the phase difference of a dichromatic field

The structure of the formalism of the MEMP theory outlined above, allows the easy computation from first principles of the effects of polychromatic fields with commensurate frequencies. This type of information is useful for the quantitative understanding of possibilities of control of ionization as a function of the parameters of the fields. For example, for a weak dichromatic field, we have demonstrated that the ionization rate, Γ, has the following dependence on the relative phase φ [188, 189] and references therein. For even harmonics, $\omega = (2k)\omega_2$,

$$\Gamma = A + B\cos(2\varphi) + C\cos^2(2\varphi) + \ldots \tag{49a}$$

and for odd harmonics, $\omega = (2k + 1)\omega_2$,

$$\Gamma = A + B\cos(\varphi) + C\cos^2(\varphi) + \ldots \tag{49b}$$

The coefficients A, B, C, … are quantities that depend on the field strengths and on the frequencies, and constitute the components of the rate that correspond to the interference of paths to the ionization continuum of various orders.

11.2.3. AC-field-induced stabilization of resonances and destabilization of discrete states

Since the theory can handle all types of electronic structures (and not just those of ground states), it has been applied to doubly excited resonances in order to demonstrate the effects of field-induced coupling between bound and resonance states, i.e., the variation of the real and the complex poles of the field-free resolvent as a function of ac- or of dc-field strengths [184].

Specifically, we considered the spectrum of H^- at about $10\,eV$ above the ground state, where the discrete state $2p^2\,^3P$, at $10.195\,eV$, and the resonance state

"$2s2p$"$^3P^o$ at $9.74\,eV$ exist. The width of the "$2s2p$"$^3P^o$ state is due to the Coulomb interaction with the $H^-[1s + \varepsilon p]$ channel. Using the methods discussed in the earlier sections, and without large wavefunction expansions, this width was found to be 6.5 meV, in agreement with previous theoretical and experimental investigations. The energy difference between the states is $\Delta E \simeq 0.457\,eV$, which corresponds to radiation of 27 100 Å. The two states are allowed to interact via a tunable ac–field, on- and off- resonance with the transition frequency. By truncating the hydrogen thresholds to $n = 1$ and

$n = 2$, we solved the fully coupled problem with the following 15 scattering channels mixing with the two DESs either through the atomic Hamiltonian or through the electric dipole operator: ($1s\varepsilon p$, $2p\varepsilon s$, $2s\varepsilon p$, $2p\varepsilon d$) $^3P^o$, $2p\varepsilon d$ $^3D^o$ ($1s\varepsilon f$, $2s\varepsilon f$, $2p\varepsilon d$) $^3F^o$ ($1s\varepsilon s$, $2s\varepsilon s$, $2p\varepsilon p$) ^3S, $2p\varepsilon p$ ^3P ($1s\varepsilon d$, $2s\varepsilon d$, $2p\varepsilon p$) ^3D.

The results of the ac-field calculation showed that indeed there is a physically detectable *transfer of width* as a function of frequency and strength of the field. On the transition frequency ($\omega \simeq 0.0165$ a.u.), and for intensity of 1.4×10^7 W/cm^2, the discrete state has a width of 0.20×10^{-6} a.u., while for intensity 5×10^8 W/cm^2 the width becomes 1.30×10^{-4} a.u.. On the other hand, for a small range of intensities the autoionizing state is stabilized by a factor of two [184].

Finally, when the "2s2p" $^3P^o$ autoionizing state interacts only with the dc field, its width starts widening only after the strength becomes larger than 3.5×10^{-4} a.u. $\simeq 1.8$ MV/cm. This is an order of magnitude larger than that which was found necessary in the CCR calculations of Ref. [175] to initiate the broadening of the $^1P^o$ shape resonance.

12. CONCLUSION AND SYNOPSIS

Atoms and molecules and their ions have both discrete and continuous energy spectra. Inside the otherwise smooth continuum of free electrons or of free nuclei, a number of spectroscopies reveal the presence of structures ("peaks"), whose profile within a narrow energy region may be symmetric or asymmetric. Depending on the experimental arrangement and the type of measurement, as well as on the theoretical framework for their treatment, such states have been (are) called either "resonance," or "autoionizing," or "predissociating," or "compound," or "Auger" states. The point of view that permeates this chapter is that the basic understanding and the possibility of ab initio computation of their properties and of their impact on dynamical processes at the quantum level can be understood in *energy-dependent* or in *time-dependent* frameworks where they are treated as "decaying" (*unstable*) states.

In the same spirit, problems that involve the cycle-averaged interaction of static or ac fields with atoms and molecules in the ground or in excited states have been formulated and solved here within a time-independent, stationary-state framework, as problems of *field-induced decaying* (*unstable*) states.

The discussion of the previous 11 sections included introductory-historical remarks that are related to the work described here, and focused, on the one hand on certain aspects of formal properties of *field-free* and *field-induced unstable* states (mainly Sections 3–5, 11), and on the other hand, on the theory and methodology for the systematic computation and

use of their wavefunctions in many-electron atoms and small molecules (mainly Sections 6–11). A minimum of energy- or of time-dependent formalism was used, starting with the arguments in the 1972 paper [11] (see also [37, 92, 101]), where the picture of the decaying state was invoked for the description and computation of properties of autoionizing states in many-electron atoms and molecules.

In presenting the "why and the how" of the work reviewed here, emphasis was placed on the significance of identifying and implementing the appropriate *forms* of basic equations, the fundamental one being Eq. (1). For example, I discussed the importance of the term $a\Psi_0$ both in the energy (Sections 3–11) and in the time domain (Sections 3–5) and the importance of handling in practical way the asymptotic behavior of the term X_{as} (Sections 3–7, 11).

In both the energy-dependent and the time-dependent frameworks, it was demonstrated that it is of paramount importance to be able to understand quantitatively the *state-specific* nature of the localized component, Ψ_0. For example, for atoms and diatomics this has been demonstrated on prototypical systems, via systematic construction and optimization under constraints of many-electron wavefunctions, whose zero-order approximation is computed directly either from the HF or the MCHF equations, that are specific to the assumed zero-order electronic structure of the unstable state. In this context, in several sections of this review, I pointed out that, as regards excited electronic structures, the approaches which were (and still are) followed before the introduction of the ones described here [9, 10, 11], i.e., diagonalization approaches that use single basis sets for computations either on the real energy axis or in the complex energy plane (e.g., the "CCR method), are limited in practice when it comes to solving the MEP in arbitrary, open (sub)shell electronic structures representing different levels of energy excitation.

As regards the theoretical framework, the *form* of the resonance eigenfunction according to Eq. (1) constitutes a reference point. Eq. (1) is related to time-dependent analysis (Eq. (6) and subsequent discussion) or to Hermitian K-matrix computations that depend on real values of the energy (Sections 3.1.1 and 3.1.2 and Chapter 6) or to computations that depend on complex energies and non-Hermitian constructions (Sections 3–7, 11). As regards the computational framework, Eq. (1), is implemented in terms of wavefunctions of the form of Eqs. (32, 35, 37, and 48).

For example, this form is in harmony with the superposition of energy states in Eq. (2), whose coefficients have been obtained formally by Fano [29]. Although, for the solution of particular problems involving unstable states, we have implemented, in conjunction with the methods of the SSA, the real-energy, Hermitian, CI in the continuum formalism that characterizes Fano's theory, e.g., Refs. [78, 82–87] and Chapter 6, in this chapter I focused on the theory and the nonperturbative method of solution of the *complex eigenvalue Schrödinger equation* (CESE), Eq. (27).

Specifically, I demonstrated formally, as it was first done in 1981 [101], how the CESE is obtained by first invoking Fano's solution, where all quantities are given in terms of computable matrix elements, and then by applying the physically necessary outgoing-wave boundary condition that characterizes the decaying states. By understanding the meaning and significance of the form of the CESE state-specific solution (Section 5), it is possible to carry out advanced nonperturbative computations in the complex energy plane with *square-integrable functions of real and of complex coordinates*, by invoking the 1961 regularization technique of Dykhne and Chaplik $r \rightarrow re^{i\theta}$ [106] (see Sections 5–7, 11 and Tables 4.1–4.3). In the *state-specific CESE* approach, only the "Gamow" orbitals are complex, representing the outgoing $\ell-$ dependent waves. The coordinates of the Hamiltonian are real.

The continuous spectrum is also present, both in physical processes and in the quantum mechanical formalism, when an atomic (molecular) state is made to interact with an external electromagnetic field of appropriate frequency and strength. In conjunction with energy shifts, the normal processes involve ionization, or electron detachment, or molecular dissociation by absorption of one or more photons, or electron tunneling. Treated as stationary systems with time-independent atom + field Hamiltonians, these problems are equivalent to the CESE scheme of a decaying state with a complex eigenvalue. For the treatment of the related MEPs, the implementation of the CESE approach has led to the state-specific, non-perturbative *many-electron, many-photon* (MEMP) theory [179–190] which was presented in Section 11. Its various applications include the ab initio calculation of properties from the interaction with electric and magnetic fields, of multiphoton above threshold ionization and detachment, of analysis of path interference in the ionization by di- and tri-chromatic ac-fields, of cross-sections for double electron photoionization and photodetachment, etc.

The overall methodology of theoretical analysis and computational implementation that characterizes our work has been given the generic name of the *SSA*. The crucial idea in the SSA as applied to unstable states is the following: If, in conjunction with suitable computational methods, attention is given to the form of the resonance wavefunctions which is dictated by the concept of decaying states and outgoing-wave boundary conditions, and to the state-specific choice and optimization of the relevant function spaces, the accuracy of the description of all types of electronic structure increases considerably. At the same time, there is significant reduction of the complexity of the MEP to a size which is economic and physically transparent for systems with many electrons and with arbitrary electronic structures. Such facts allow the consistent understanding of the interplay between properties or processes and major features of electronic structure and of the multichannel continuous spectrum in N-electron atoms and small molecules.

In the framework of the SSA, the basic difficulties of the MEP are present in the localized component, Ψ_0, which in molecules can also represent a diabatic state. As it was argued in Ref. [11] and was further expanded in subsequent publications cited here, the Ψ_0 for electronic structures can be computed directly via methods of open-(sub)shell polyelectronic theory that until the early 1970s had been restricted to ground states or to a few low-lying excited discrete states. Specifically, it is possible as well as economic to start the overall computation by computing directly the state-specific zero order localized wavefunctions of various electronic structures as solutions under special constraints of HF or of appropriately constructed multicon-figurational HF (MCHF) equations. The electronic structures solved directly via the MCHF equations may label "shape" or "Feshbach" resonances. (This standard categorization loses meaning in highly excited states where there is more than one relevant nearby thresholds).

To the bound HF or MCHF solutions, the remaining of the interelectronic interactions contributing to the stability of the state are added variationally, and so is obtained the square-integrable wavefunction, Ψ_0. Examples of the practical use of the $\Psi_0 s$ were given in Sections 2.2, 7–10, and in Tables 4.1, 4.4, and 4.5. On the other hand, for resonance states that are transiently bound extremely weakly, such as the series of the "dipole resonances" in H^-, there are no HF solutions. In those rare cases, appropriate alternatives have been followed as regards the optimal choice of the trial Ψ_0 (and of X_{as}), allowing an essentially complete (the first of its kind) resolution and understanding of the resonance spectra of this three-particle system [123, 124], Section 7.2, and Tables 4.2 and 4.3.

The contribution of the open channels is then taken into account by appropriate methods that employ different function spaces, symbolized here by X_{as} (as = asymptotic) (Eq. (1)). These methods are based either on K-matrix theory and numerically computed scattering orbitals for atoms and diatomics (real energy-dependent) (see [17, 29, 79–87]), or via diagonalization of the non-Hermitian matrices of the CESE-SSA for field-free or field-induced resonances.

The numerical results which are listed in Tables 4.1–4.5 were obtained from nonperturbative, time-independent calculations. Tables 4.1–4.3 contain results of energies, partial, and total widths that were obtained by the herein discussed non-Hermitian CESE-SSA. Tables 4.4 and 4.5 contain only the real energies corresponding to the (Ψ_0, E_0) of the present theory (For partial and total widths of such series of DESs see [120]).

In addition, several examples of application were cited. These include phe-nomena such as, ac field-induced stabilization of resonances, or long-time NED and its relation to issues of irreversibility at the quantum level, or the profile of photoabsorption cross-sections for resonance to resonance tran-sitions, or the time-dependent coherent excitation and multichannel decay of multiply and inner-hole excited states, or aspects of the physics of the

pre-ED regime, or the time-dependence of the formation of the profile of the photo-excitation cross-section, or properties of doubly and of multiply excited states, or linear and nonlinear frequency-dependent polarizabilities.

In conclusion, the discussion, the results, and the accompanying references of this chapter have documented, explained, and justified a set of formalisms and methods that can be used for the ab initio computation of time-independent and time-dependent polyelectronic wavefunctions and for the quantitative understanding of basic quantities connected to a variety of field-free and field-induced unstable states (resonances) in the continuous spectra of atoms and molecules.

REFERENCES

[1] P.A.M. Dirac, Quantum mechanics of many-electron systems, Proc. R. Soc. Lond. A123 (1929) 714.

[2a] H. Feshbach, A unified theory of nuclear reactions. I, Ann. Phys. (N.Y.) 5 (1958) 357.

[2b] H. Feshbach, A unified theory of nuclear reactions. II, Ann. Phys. (N.Y.) 19 (1962) 287.

[3a] T.F. O''Malley, S. Geltman, Compound-atom states for tow-electron systems, Phys. Rev. 137 (1965) A1344.

[3b] A.K. Bhatia, P.G. Burke, A. Temkin, Calculation of the $^1P^o$ ($2s2p$) autoionization state of He with a pseudostate nonresonant continuum, Phys. Rev. A 8 (1973) 21.

[4a] A. Temkin, A.K. Bhatia, Projection and quasi-projection operators for electron impact resonances on many-electron atomic targets, in: A. Temkin (Ed.), Autoionization, Plenum Press, New York, 1985.

[4b] A.K. Bhatia, A. Temkin, Lowest inelastic He^- autodetachment state ($^2P^o$) in a Feshbach resonance, Phys. Rev. A 23 (1981) 3361.

[4c] A. Berk, A.K. Bhatia, B.R. Junker, A. Temkin, Projection-operator calculations of the lowest $e^- - He$ resonance, Phys. Rev. A 34 (1986) 4591.

[5a] M. Bylicki, Generalized saddle-point method for Feshbach resonances, Phys. Rev. A 39 (1989) 3316.

[5b] M. Bylicki, Feshbach-projection calculation of inelastic resonances in He^-, Phys. Rev. A 41 (1990) 2386.

[5c] M. Bylicki, Reply to "Comment on 'Generalized saddle-point method for Feshbach resonances'", Phys. Rev. A 41 (1990) 4093.

[5d] M. Bylicki, Feshbach-type projection calculations of triply excited resonances in He^-, Phys. Rev. A 45 (1992) 2079.

[6] M.L. Goldberger, K.M. Watson, Collision Theory, John Wiley & Sons, New York, 1964.

[7] R.G. Newton, Scattering Theory of Waves and Particles, second ed., Springer-Verlag, Berlin, 1982.

[8a] A.J.F. Siegert, On the derivation of the dispersion formula for nuclear reactions, Phys. Rev. 56 (1939) 750.

[8b] L. Fonda, G.C. Ghirardi, T. Weber, A. Rimini, Analytic properties of resolvents and completeness, J. Math. Phys. 7 (1643) 1966.

[8c] R.M. More, E. Gerjuoy, Properties of resonance wave functions, Phys. Rev. A 7 (1973) 1288.

[9] C.A. Nicolaides, The state-specific approach to the solution of problems of electronic structure and dynamics involving excited states, Int. J. Quantum Chem. 60 (1996) 119.

[10] C.A. Nicolaides, On the application of conventional quantum chemistry methods of computation to states perturbed by the continuous spectrum, Int. J. Quantum Chem. 71 (1999) 209.

[11a] C.A. Nicolaides, Theoretical approach to the calculation of energies and widths of resonant (autoionizing) states in many-electron atoms, Phys. Rev. A 6 (1972) 2078.

[11b] C.A. Nicolaides, Hole-projection, saddle points and localization in the theory of autoionizing states, Phys. Rev. A 46 (1992) 690.

[12] J.N. Bardsley, F. Mandl, Resonant scattering of electrons by molecules, Rep. Prog. Phys. 31 (1968) 471.

[13] G.J. Schulz, Resonances in electron impact on diatomic molecules, Rev. Mod. Phys. 45 (1973) 423.

[14] P.G. Burke, Resonances in electron scattering and photon absorption, Adv. Phys. 14 (1965) 521.

[15] P.G. Burke, Resonances in electron scattering by atoms and molecules, Adv. At. Mol. Phys. 10 (1968) 173.

[16] K. Smith, Resonant scattering of electrons by atomic systems, Rep. Prog. Phys. 29 (1966) 373.

[17] U. Fano, J.W. Cooper, Spectral distribution of atomic oscillator strength, Rev. Mod. Phys. 40 (1968) 441.

[18] G.J. Schulz, Resonances in electron impact on atoms, Rev. Mod. Phys. 45 (1973) 378.

[19] S.J. Buckman, C.W. Clark, Atomic negative-ion resonances, Rev. Mod. Phys. 66 (1994) 539.

[20] T. Andersen, Atomic negative ions: Structure, dynamics and collisions, Phys. Rep. 394 (2004) 157.

[21] I. Shimamura, Resonances and pseudoresonances in the Kohn variational method and the Feshbach method, J. Physcal. Soc. Japan 31 (1971) 852.

[22a] A.M. Lane, R.G. Thomas, R-matrix theory of nuclear reactions, Rev. Mod. Phys. 30 (1958) 257.

[22b] R.F. Barrett, L.C. Biedenharn, M. Danos, P.P. Delsanto, W. Greiner, H.G. Wahsweiler, The eigenchannel method and related theories for nuclear reactions, Rev. Mod. Phys. 45 (1973) 44.

[23] P.G. Burke, K.A. Berrington (Eds.), Atomic and Molecular Processes: An R-Matrix Approach, Institute of Physics Publishing, Bristol, 1993.

[24a] G. Wentzel, Die unperiodischen Vorgängein der Wellenmechanik, Phys. Z. 29 (1928) 321.

[24b] O.K. Rice, On the quantum mechanics of chemical reactions: Predissociation and unimolecular decompositions, Phys. Rev. 34 (1929) 1451.

[24c] N. Rosen, Lifetimes of unstable molecules, J. Chem. Phys. 1 (1933) 319.

[25] G. Gamow, Zur Quantentheorie des Atomkernes, Z. Phys. 51 (1928) 204.

[26] R.W. Gurney, E.U. Condon, Quantum mechanics and radioactive disintegration, Phys. Rev. 33 (1929) 127.

[27] K.O. Friedrichs, On the perturbation of continuous spectra, Commun. Pure Appl. Math. 1 (1948) 361.

[28a] T. Berggren, On the use of resonant states in eigenfunction expansions of scattering and reaction amplitudes, Nucl. Phys. A 109 (1968) 265.

[28b] A. Herzenberg, K.L. Kwok, F. Mandl, Resonance scattering theory, Proc. Phys. Soc. 84 (1964) 477.

[29] U. Fano, Effects of configuration interaction on intensities and phase shifts, Phys. Rev. 124 (1866) 1961.

[30] J.C. Slater, Quantum Theory of Atomic Structure, Vols. I, II, McGraw-Hill, New York, 1960.

[31] H.A. Bethe, E.E. Salpeter, Quantum Mechanics of One- and Two-Electron Atoms, Springer-Verlag, Berlin, 1957.

[32] P.G. Burke, The convergence of the close coupling expansion, Proc. Phys. Soc. Lond. 82 (1963) 443.

[33] P.G. Burke, A.J. Taylor, The excitation of He^+ by electron impact, J. Phys. B 2 (1969) 44.

[34] P.G. Burke, J.W. Cooper, S. Ormonde, Low-energy scattering of electrons by Helium, Phys. Rev. 183 (1969) 245.

[35] J.P. Vinti, The dispersion and absorption of Helium, Phys. Rev. 42 (1932) 632.

[36] F.G. Fender, J.P. Vinti, Doubly-excited states in Helium, Phys. Rev. 46 (1934) 77.

[37a] C.A. Nicolaides, D.R. Beck, On the possibility of observing nonexponential decays in autoionizing states, Phys. Rev. Lett. 38 (1977) 683; Addendum: 1037.

[37b] C.A. Nicolaides, D.R. Beck, Time dependence, complex scaling, and the calculation of resonances in many-electron systems, Int. J. Quantum Chem. 14 (1978) 457.

[38] E. Hylleraas, A new stable state of the negative hydrogen ion, Astrophys. J. 111 (1950) 209.

[39] G.W.F. Drake, Second bound state for the hydrogen negative ion, Phys. Rev. Lett. 24 (1970) 126.

[40a] E. Holøien, The $(2s^2)\,^1S$ state solution of the non-relativistic Schrödinger equation for Helium and the negative Hydrogen ion, Proc. Phys. Soc. A 71 (1958) 357.

[40b] E. Holøien, On the $2p^2\,^1S$ state solution of the non- relativistic Schrödinger Helium equation, Proc. Phys. Soc. A 72 (1958) 141.

[41] E. Holøien, An investigation of quasi stationary states of the two-electron atomic systems with a special study of negative atomic ions, Phys. Norvegica 1 (1961) 53.

[42] E. Holøien, Energy calculation of ^1S autoionizing states of He and H^-, Proc. Phys. Soc. 88 (1966) 538.

[43] E. Holøien, J. Midtdal, New investigations of the ^1S autoionizing states of He and H^-, J. Chem. Phys. 45 (1966) 2209.

[44] J.F. Perkins, Variational-bound method for autoionization states, Phys. Rev. 178 (1969) 89.

[45] E. Holøien, J. Midtdal, Tests of the multiconfiguration energy-bound method for Feshbach-type autoionizization states of two-electron atoms I. Application to He states below the $n = 2$ threshold, J. Phys. B 3 (1970) 592.

[46] L. Lipsky, A. Russek, Auto-ionizing states in Helium, Phys. Rev. 142 (1966) 59.

[47] W.H. Miller, Resonances in the scattering of electrons from atoms, Phys. Rev. 152 (1966) 70.

[48] H.S. Taylor, G.V. Nazaroff, A. Golebiewski, Qualitative aspects of resonances in electron-atom and electron-molecule scattering, excitation and reactions, J. Chem. Phys. 45 (1966) 2872.

[49] A.U. Hazi, H.S. Taylor, Stabilization method of calculating resonance energies: Model problem, Phys. Rev. A 1 (1970) 1109.

[50] M.F. Fels, A.U. Hazi, Calculation of energies and widths of compound-state resonances in elastic scattering: Stabilization method, Phys. Rev. A 4 (1971) 662.

[51] H.S. Taylor, A.U. Hazi, Comment on the stabilization method: Variational calculation of the resonance width, Phys. Rev. A 14 (1976) 2071.

[52] A.U. Hazi, A purely L^2 method for calculating resonance widths, J. Phys. B 11 (1978) L259.

[53] I. Eliezer, Y.K. Pan, Calculations on some excited states of He^-, Theor. Chim. Acta (Berlin) 16 (1970) 63.

[54] C.E. Kuyatt, J.A. Simpson, S.R. Mielczarek, Elastic resonances in electron scattering from He, Ne, Ar, Kr, Xe and Hg, Phys. Rev. 138 (1965) A385.

[55] P.G. Burke, J.W. Cooper, S. Ormonde, Electron-impact excitation of $n = 2$ states in He, Phys. Rev. Lett. 17 (1966) 345.

[56a] C.A. Nicolaides, N.A. Piangos, State-specific approach and computation of resonance states: Identification and properties of the lowest $^2p^{\rm o}$ and ^2D triply excited states of He^-, Phys. Rev. A 64 (2001) 052505.

[56b] C.A. Nicolaides, N.A. Piangos, Existence and characterization of $n = 3$ triply excited resonances of He^-, J. Phys. B 34 (2001) 99.

[57] A. Herzenberg, H.S. Lau, Resonances and exchange in the scattering of electrons by helium atoms II. Correlated Helium wave function, J. Phys. B 1 (1968) 33.

[58] D.S. Walton, B. Peart, K. Dolder, Structure observed during detailed measurements of detachment from H^- by electron impact, J. Phys. B 3 (1970) L148.

[59] H.S. Taylor, L.D. Thomas, Short-lived resonant state of H^{2-}, Phys. Rev. Lett. 28 (1972) 1091.

[60] B. Peart, K.T. Dolder, Measurements which indicate the existence of a second short-lived state of H^{2-}, J. Phys. B 6 (1973) 1497.

[61] L.D. Thomas, Identification of a second resonant state of H^{2-}, J. Phys. B 7 (1974) L87.

[62] C.A. Nicolaides, D.R. Beck, Electronic structure and oscillator strengths of highly excited states: Resonances in He^-, Li and Be, J. Chem. Phys. 66 (1982) 1977.

[63] F. Robicheaux, R.P. Wood, C.H. Greene, Simplest doubly charged negative ion: Nonexistence of H^{2-} resonances, Phys. Rev. A 49 (1866) 1994.

[64] L.H. Andersen, D. Mathur, H.T. Schmidt, L. Vejby-Christensen, Electron-impact detachment of D^-: Near-threshold behavior and the nonexistence of D^{2-} resonances, Phys. Rev. Lett. 74 (1995) 892.

[65] T. Tanabe, I.I. Katayama, H. Kamegaya, K. Chida, T. Watanabe, Y. Arakaki, et al., Search for H^{2-} resonances in the detachment of H^- by electron impact with a high-resolution cooler ring, Phys. Rev. A 54 (1996) 4069.

[66] M. Bylicki, C.A. Nicolaides, The H^{2-} $^4S^o$ spectrum has at least two resonance states, J. Phys. B 31 (1998) L685.

[67] T. Sommerfeld, U.V. Riss, H.-D. Meyer, L.S. Cederbaum, Evidence for a metastable state of the fundamental dianion H^{2-}, Phys. Rev. A 55 (1903) 1997.

[68] T. Morishita, C.D. Lin, C.G. Bao, Nonexistence of resonances in H^{2-}, Phys. Rev. Lett. 80 (1998) 464.

[69] E. Holøien, S. Geltman, Variational calculations for quartet states of three-electron atomic systems, Phys. Rev. 153 (1967) 81.

[70] R.A. Baragiola, E.R. Salvatelli, Formation of negative Helium ions by electron capture from ground-state Helium atoms, J. Phys. B 8 (1975) 382.

[71] K.F. Dunn, B.J. Gilmore, F.R. Simpson, H.B. Gilbody, $He(2^1 S)$ and He^- formation in fast charge-changing collisions and evidence for a long-lived doublet state of He^-, J. Phys. B 11 (1797) 1978.

[72] V.I. Safronova, V.S. Senashenko, Metastable autoionizing states of the negative Helium ion, Phys. Lett. 55A (1976) 401.

[73] C.A. Nicolaides, Y. Komninos, D.R. Beck, Bound states and decay mechanisms of He^-, Phys. Rev. A 24 (1981) 1103.

[74] A.U. Hazi, K. Reed, Theoretical photodetachment cross-section for He^- ($^4P^o$), Phys. Rev. A 24 (1981) 2269.

[75] C.W. Walter, J.A. Seifert, J.R. Peterson, Reexamination of the He^- $1s2p^2$ ^4P shape resonance: Details of its properties and precise electron affinity for the He $2^3 S$, Phys. Rev. A 50 (1994) 664.

[76] Th. Mercouris, Y. Komninos, C.A. Nicolaides, Time-resolved hyperfast processes of strongly correlated electrons during the coherent excitation and decay of multiply excited and inner-hole excited states, Phys. Rev. A 76 (2007) 033417.

[77a] Y. Komninos, G. Aspromallis, C.A. Nicolaides, Resonance scattering theory: Application to the broad He^- $1s2s2p$ $^2P^o$ resonance, Phys. Rev. A 27 (1865) 1983.

[77b] C.A. Nicolaides, N.A. Piangos, Y. Komninos, Theory and computation of triply excited resonances: Application to states of He^-, Phys. Rev. A 48 (1993) 3578.

[78] Y. Komninos, C.A. Nicolaides, Theory and computation of the profile of the free-free transition probability between autoionizing (resonant) states, J. Phys. B 30 (1997) L237.

[79] P.L. Altick, E.N. Moore, Configuration interaction in the Helium continuum, Phys. Rev. 147 (1966) 59.

[80] D. Cordes, P.L. Altick, Application of the multichannel configuration-interaction theory to the characteristics of the $(3,3b)^1 S$ state of He, Phys. Rev. A 41 (1990) 5213.

[81] D.E. Ramaker, D.M. Schrader, Multichannel configuration-interaction theory: Application to some resonances in Helium, Phys. Rev. A 9 (1980) 1974.

[82] Y. Komninos, C.A. Nicolaides, Multi-channel reaction matrix theory and configuration-interaction in the discrete and in the continuous spectrum. Inclusion of closed channels and derivation of quantum defect theory, Z. Phys. D 4 (1987) 301.

[83] Y. Komninos, C.A. Nicolaides, Many-electron approach to atomic photoionization: Rydberg series of resonances and partial photoionization cross sections in Helium, around the $n = 2$ threshold, Phys. Rev. A 34 (1986) 1995.

[84] Y. Komninos, G. Aspromallis, C.A. Nicolaides, Theory and computation of perturbed spectra: Application to the Al relativistic spectrum, J. Phys. B 28 (1995) 2049.

[85] Y. Komninos, C.A. Nicolaides, Quantum defect theory for Coulomb and other potentials in the framework of configuration interaction, and implementation to the calculation of $^2 D$ and $^2 F^o$ perturbed spectra of Al, J. Phys. B 37 (1817) 2004.

[86] Y. Komninos, C.A. Nicolaides, Effect of the Rydberg states on the time evolution of non-stationary states below or just above the ionization threshold, Phys. Rev. A 72 (2005) 032716.

[87] Y. Komninos, C.A. Nicolaides, Effects of configuration interaction on photoabsorption spectra in the continuum, Phys. Rev. A 70 (2004) 042507.

[88] U. Eichmann, T.F. Gallagher, R.M. Konik, Fano like shapes reconsidered: Symmetric photoionization peaks from pure continuum excitation, Phys. Rev. Lett. 90 (2003) 0233004.

[89a] C.A. Nicolaides, Physical constraints on nonstationary states and nonexponential decay, Phys. Rev. A 66 (2002) 022118.

[89b] Th.G. Douvropoulos, C.A. Nicolaides, Time-dependent tunneling via path integrals. Connection to results of the quantum mechanics of decaying states, J. Phys. B 35 (2002) 4453.

[89c] C.A. Nicolaides, Th. Mercouris, On the violation of the exponential decay law in atomic physics: Ab initio calculation of the time-dependence of the $He^- 1s2p^2\,^4P$ nonstationary state, J. Phys. B 29 (1996) 1151.

[89d] Th. Mercouris, C.A. Nicolaides, Time dependence and properties of nonstationary states in the continuous spectrum of atoms, J. Phys. B 30 (1997) 811.

[90] G. Aspromallis, C. Sinanis, C.A. Nicolaides, The lifetimes of the fine structure levels of the $Be^- 1s^2 2s 2p^2\,^4P$ metastable state, J. Phys. B 29 (1996) L1.

[91a] A. Russek, H.C. Wu, J. Owens, Bounds on energy levels and lifetimes of autoionizing states, Phys. Rev. 180 (1969) 6.

[91b] F.H. Read, New applications of the least-squares method: Unbound states of Helium and asymptotically correct bound states, Chem. Phys. Lett. 12 (1972) 549.

[91c] P. Froelich, E. Brändas, Variational principle for quasibound states, Phys. Rev. A 12 (1975) 1.

[92a] C.A. Nicolaides, D.R. Beck, A variational method for calculating the energies and widths of resonances, Phys. Lett. A 60 (1977) 92.

[92b] C.A. Nicolaides, D.R. Beck, The variational calculation of energies and widths of resonances, Phys. Lett. A 65 (1978) 11.

[93] C.A. Nicolaides, H.J. Gotsis, On the calculation of the complex energies of resonances, J. Phys. B 25 (1992) L171.

[94a] Th. Mercouris, C.A. Nicolaides, Stationarity coefficients and short-time deviations from exponential decay in atomic resonance states, Phys. Rev. A 65 (2001) 012112.

[94b] C.A. Nicolaides, D.R. Beck, Comment on the mean-square deviation formula for autoionizing states, Phys. Rev. A 15 (1787) 1977.

[94c] C.A. Nicolaides, Time asymmetry, non-exponential decay, and complex eigenvalues in the theory and computation of resonancestates, Int. J. Quantum Chem. 89 (2002) 94.

[95] C.A. Nicolaides, H.J. Gotsis, M. Chrysos, Y. Komninos, Resonances and exterior complex scaling, Chem. Phys. Lett. 168 (1990) 570.

[96] B. Simon, The definition of molecular resonance curves by the method of exterior complex scaling, Phys. Lett. A 71 (1979) 211.

[97] R. Lefebvre, Resonances of the double-well potential of the $B''\bar{B}$ state of H_2, Chem. Phys. Lett. 451 (2008) 14.

[98] C.W. McCurdy, M. Baertschy, T.N. Rescigno, Solving the three-body Coulomb breakup problem using exterior complex scaling, J. Phys. B 37 (2004) R137.

[99a] F. He, C. Ruiz, A. Becker, Absorbing boundaries in numerical solutions of the time-dependent Schrdinger equation on a grid using exterior complex scaling, Phys. Rev. A 75 (2007) 053407.

[99b] L. Tao, W. Vanroose, B. Reps, T.N. Rescigno, C.W. McCurdy, Long-time solution of the time-dependent Schrödinger equation for an atom in an electromagnetic field using complex coordinate contours, Phys. Rev. A 80 (2009) 063419.

[100] L. Rosenfeld, Quantum theory in 1929: Recollections from the first Copenhagen conference Nordita reprint 387, Rhodos, Copenhagen (1971)

[101] C.A. Nicolaides, Y. Komninos, Th. Mercouris, Theory and calculation of resonances using complex coordinates, Int. J. Quantum Chem. Symp. 15 (1981) 355.

[102] C.A. Nicolaides, S.I. Themelis, Theory of the resonances of the LoSurdo-Stark effect, Phys. Rev. A 45 (1992) 349.

[103a] P. Dirac, Über die Quantenmechanik der Stossvorgänge, Z. Phys. 44 (1927) 585.

[103b] P.A.M. Dirac, The Principles of Quantum Mechanics, fourth ed., Oxford University Press, Oxford, 1958.

[104] E.C. Kemble, The Fundamental Principles of Quantum Mechanics, McGraw- Hill, New York, 1937.

[105] Ya.B. Zel'dovich, On the theory of unstable states, Sov. Phys.-JETP 12 (1961) 542.

[106] A.M. Dykhne, A.V. Chaplik, Normalization of the wave functions of quasistationary states, Sov. Phys.-JETP 13 (1961) 1002.

[107] J. Aguilar, J.M. Combes, A class of analytic perturbations for one-body Schrödinger Hamiltonians, Commun. Math. Phys. 22 (1972) 268.

[108] E. Balslev, J.M. Combes, Spectral properties of many-body Schrödinger operators with dilatation-analytic interactions, Commun. Math. Phys. 22 (1972) 280.

[109] G.D. Doolen, A procedure for calculating resonance eigenvalues, J. Phys. B 8 (1975) 525.

[110] G.D. Doolen, Complex scaling: An analytic model and some new results for e^+- H resonances, Int. J. Quantum Chem. 14 (1978) 523.

[111a] W.P. Reinhardt, Method of complex coordinates: Application to the Stark effect in Hydrogen, Int. J. Quantum Chem. Symp. 10 (1976) 359.

[111b] C. Cerjan, R. Hedges, C. Holt, W.P. Reinhart, K. Scheibner, J.J. Wendoloski, Complex coordinates and the Stark effect, Int. J. Quantum Chem. 14 (1978) 393.

[112] E. Brändas, P. Froelich, Continuum orbitals, complex scaling problem, and the extended virial theorem, Phys. Rev. A 16 (1977) 2207.

[113a] Y.K. Ho, The method of complex coordinate rotation and its application to atomic collision processes, Phys. Rep. 99 (1983) 1.

[113b] M. Bylicki, Methods involving complex coordinates applied to atoms, Adv. Quantum Chem. 32 (1998) 207.

[114a] B. R. Junker, Recent computational developments in the use of complex scaling in resonance phenomena, Adv. At. Mol. Phys. 18 (1982).

[114b] N. Moiseyev, Quantum theory of resonances: Calculating energies, widths and cross-sections by complex scaling, Phys. Rep. 302 (1998) 211.

[115] E. Brändas, N. Elander (Eds.), Resonances. The Unifying Route Towards the Formulation of Dynamical Processes. Foundations and Applications in Nuclear, Atomic and Molecular Physics, Lecture Notes in Physics, Springer-Verlag, Berlin, 1989, p. 325.

[116] M. Bylicki, C.A. Nicolaides, Computation of resonances by two methods involving the use of complex coordinates, Phys. Rev. A 48 (1993) 3589.

[117] E. Bednarz, M. Bylicki, Fast convergent approach for computing atomic resonances, Int. J. Quantum Chem. 90 (2002) 1021.

[118] C.A. Nicolaides, Th. Mercouris, Y. Komninos, Many-electron theory for autoionizing states using complex coordinates: The position and the partial and total widths of the Ne^+ $1s$ hole state, Int. J. Quantum Chem. 26 (1984) 1017.

[119] C.A. Nicolaides, Th. Mercouris, Partial widths and interchannel coupling in autoionizing states in terms of complex eigenvalues and complex coordinates, Phys. Rev. A 32 (1985) 3247.

[120] S.I. Themelis, C.A. Nicolaides, Energies, widths and l- dependence of the H^- ^3P and He^- ^4P TEIL states, J. Phys. B 28 (1995) L379.

[121] I.D. Petsalakis, Th. Mercouris, G. Theodorakopoulos, C.A. Nicolaides, Theory and ab-initio calculations of partial widths and interchannel coupling in predissociation diatomic states. Application to HeF, Chem. Phys. Lett. 182 (1991) 561.

[122] C.A. Nicolaides, On calculations of correlated wave functions with heavy configurational mixing, Int. J. Quantum Chem. 102 (2005) 250.

[123] M. Bylicki, C.A. Nicolaides, Theoretical resolution of the H^- resonance spectrum up to the $n = 4$ threshold. I. States of $^1P^o$, $^1D^o$, and $^1F^o$ symmetries, Phys. Rev. A 61 (2000) 052508.

[124a] M. Bylicki, C.A. Nicolaides, Theoretical resolution of the H^- resonance spectrum up to the $n = 4$ threshold. II. States of ^1S and ^1D symmetries, Phys. Rev. A 61 (2000) 052509.

[124b] M. Bylicki, C.A. Nicolaides, Theoretical resolution of the H^- resonance spectrum up to the $n = 5$ threshold: States of $^3P^o$ symmetry, Phys. Rev. A 65 (2002) 012504.

[125] G. Howat, T. Åberg, O. Goscinski, Relaxation and final-state channel mixing in the Auger effect, J. Phys. B 11 (1978) 1575.

[126] H.P. Kelly, K Auger rates calculated for Ne^+, Phys. Rev. A 11 (1975) 556.

[127] N.A. Piangos, C.A. Nicolaides, Weakly bound resonances: Electronic structure and partial decay widths of a new He^- triply excited resonance, J. Phys. B 34 (2001) L633.

[128] N.A. Piangos, Y. Komninos, C.A. Nicolaides, He^- ^2D weakly bound triply excited resonances: Interpretation of previously unexplained structures in the experimental spectrum, Phys. Rev. A 66 (2002) 032721.

[129] M. Gailitis, R. Damburg, The influence of close coupling on the threshold behaviour of cross sections of electron-hydrogen scattering, Proc. Phys. Soc. Lond. 82 (1963) 192.

[130] A. Pathak, A.E. Kingston, K.A. Berrington, Resonances in H^- associated with the n = 2, 3 and 4 hydrogenic thresholds, J. Phys. B 21 (1988) 2939.

[131] H.R. Sadeghpour, C.H. Greene, M. Cavagnero, Extensive eigenchannel R-matrix study of the H^- photodetachment spectrum, Phys. Rev. A 45 (1992) 1587.

[132] B.R. Odgers, M.P. Scott, P.G. Burke, Analysis of the resonant states of H^- associated with the N = 2 and 3 thersholds of atomic hydrogen, J. Phys. B 28 (1995) 2973.

[133] Y.K. Ho, High-lying doubly exited $^1P^o$ states of H^-, Phys. Rev. A 45 (1992) 148.

[134] E. Lindroth, Photodetachment of H^- and Li^-, Phys. Rev. A 52 (1995) 2737.

[135] A.K. Bhatia, Y.K. Ho, $^3D^o$ shape-resonant state of H^- lying above the hydrogen N = 3 threshold, Phys. Rev. A 50 (1994) 4886.

[136] Y.K. Ho, F-wave shape resonances in e^- $-$ H scattering above the hydrogen N = 3 threshold, Phys. Lett. A 189 (1994) 374.

[137] M. Venuti, P. Decleva, Convergent multichannel continuum states by a general config-
uration interaction expansion in a B-spline basis: Application to H^- photodetachment,
J. Phys. B 30 (1997) 4839.

[138] C.A. Nicolaides, N.C. Bacalis, Y. Komninos, Theory for the direct construction of diabatic
states and application to the He_2^+ $^2\Sigma_g^+$ spectrum Chem. Phys. Lett. 192 (1992) 486.

[139] N.C. Bacalis, Y. Komninos, C.A. Nicolaides, Toward the understanding of He_2^- excited
states, Chem. Phys. Lett. 240 (1995) 172.

[140] N.A. Piangos, C.A. Nicolaides, unpublished

[141] C. Froese-Fischer, A general multi-configuration Hartree-Fock program, Comput. Phys.
Commun. 14 (1978) 145.

[142a] C.C.J. Roothaan, Self-consistent field theory for open shells of electronic systems, Rev.
Mod. Phys. 32 (1960) 179.

[142b] B. Roos, C. Salez, A. Veillard, E. Clementi, A general program for calculation of atomic
SCF orbitals by the expansion method, IBM technical report RJ 518 (1968)

[143] P.S. Bagus, Self-consistent-field wave functions for hole states of some Ne-like and
Ar-like ions, Phys. Rev. 139 (1965) A619.

[144] C. Sinanis, G. Aspromallis, C.A. Nicolaides, Electron correlation in the Auger spectra of
the Ne^+ $K2s2p^5$ $(^{1,3}P^o)$ $3p^2S$ satellites, J. Phys. B 28 (1995) L423.

[145] C.A. Nicolaides, A. Zdetsis, Theory of chemical reactions of vibronically excited H_2
$(B^1\Sigma_u^+)$. II: Noble gas dihydrides, J. Chem. Phys. 80 (1984) 1900.

[146] N.C. Bacalis, Y. Komninos, C.A. Nicolaides, State-specific theory and method for the
computation of diatomic molecules: Application to He_2^{2+} $^1\Sigma_g^+$, Phys. Rev. A 45 (1992)
2701.

[147] E.A. McCullough, Numerical Hartree-Fock methods for diatomic molecules: A partial-
wave expansion approach, Comput. Phys. Rep. 4 (1986) 265.

[148] D.R. Beck, C.A. Nicolaides, Specific correlation effects in inner-electron photoelectron
spectroscopy, Phys. Rev. A 26 (1982) 857.

[149a] C.A. Nicolaides, Y. Komninos, Theory of Auger energies in free-atoms: Application to
the alkaline earths, D.R. Beck, Phys. Rev. A 27 (1983) 3044.

[149b] D.R. Beck, C.A. Nicolaides, Theory of Anger energies in free-atoms: Application to the
alkaline earths, Phys. Rev. A 33 (1986) 3885.

[150] C.A. Nicolaides, The state-specific theory of atomic structure and aspects of the dynam-
ics of photoabsorption, in: Connerade J.P., Esteva J.P., Karnatak R.C. (Eds.), Giant
Resonances in Atoms, Molecules and Solids, Plenum Publishing, New York, 1987,
p. 213.

[151] S. Kučas, R. Karazija, V. Jonauskas, A. Momkauskaíté, Interaction of $4p^54d^{n+1}$ and
$4p^64d^{n-1}4f$ configurations and its influence on the photoexcitation and emission spectra
in the isoelectronic and isonuclear sequences, J. Phys. B 42 (2009) 205001.

[152] C.A. Nicolaides, D.R. Beck, On 'collective excitations' in atoms and molecules, J. Phys.
B 9 (1976) L259.

[153] C.A. Nicolaides, Multielectron radiative transitions, J. Phys. B 26 (1993) L291.

[154] Y. Komninos, C.A. Nicolaides, Electron correlation, geometry and energy spectrum of
quadruply excited states, Phys. Rev. A 50 (1994) 3782.

[155] Y. Komninos, N. Makri, C.A. Nicolaides, Electronic structure and the mechanism of
autoionization for doubly excited states, Z. Phys. D 2 (1986) 105.

[156] Y. Komninos, M. Chrysos, C.A. Nicolaides, Hyperridge of triply excited states, Phys.
Rev. 38 (1988) 3182.

[157] C.-G. Bao, Possible modes of angular motion in ^4S triply excited states, J. Phys. B 25
(1992) 3725.

[158] M.D. Poulsen, L.B. Madsen, Pyramidal atoms: Beryllium-like hollow states, Phys. Rev.
A 71 (2005) 062502.

[159] S. Hasegawa, F. Yoshida, L. Matsuoka, F. Koike, S. Fritzsche, S. Obara, et al, Photoexci-
tation of K-shell and L-shell hollow Beryllium, Phys. Rev. Lett. 97 (2006) 023001.

[160] U. Fano, Correlations of two excited electrons, Rep. Prog. Phys. 46 (1983) 97.

[161] O. Sinanoğlu, D. Herrick, Group theoretic prediction of configuration mixing effects due to Coulomb repulsions in atoms with applications to doubly- excited spectra, J. Chem. Phys. 62 (1975) 886.

[162] D. Herrick, O. Sinanoğlu, Comparison of doubly-excited helium energy levels, iso-electronic series, autoionization lifetimes, and group-theoretical configuration-mixing predictions with large configuration-interaction calculations and experimental spectra, Phys. Rev. A 11 (1975) 97.

[163] Y. Komninos, C.A. Nicolaides, The Wannier two-electron ionization ladder in many-electron systems: The $He\ ^1P^o$ doubly excited states, J. Phys. B 19 (1701) 1986.

[164] C.A. Nicolaides, Y. Komninos, Wannier two-electron ionization ladder of $^1P^o$ symmetry in H^-, He and Li^+, Phys. Rev. A 35 (1987) 999.

[165] Y. Komninos, M. Chrysos, C.A. Nicolaides, The two-electron ionization ladder for $He^{-2}S$ and $H^{-1}S$, J. Phys. B 20 (1987) L791.

[166] Y. Komninos, S.I. Themelis, M. Chrysos, C.A. Nicolaides, Properties of the two-electron ionization ladder and related good quantum numbers, Int. J. Quantum Chem. Symp. 27 (1993) 399.

[167] S. Themelis, Y. Komninos, C.A. Nicolaides, Properties of doubly excited states of H^- and He associated with the manifolds from $N = 6$ up to $N = 25$, Eur. Phys. J. D 18 (2002) 277.

[168] C.A. Nicolaides, S.I. Themelis, Y. Komninos, Degrees of validity of models for the description of doubly excited states of H^- and He, J. Phys. B 35 (1831) 2002.

[169] S.J. Buckman, D.S. Newman, A further study of highly excited resonances in He^-, J. Phys. B 20 (1987) L711.

[170] Th. Mercouris, Y. Komninos, S. Dionissopoulou, C.A. Nicolaides, Computation of strong-field multiphoton processes in polyelectronic atoms. State-specific method and application to H and Li^-, Phys. Rev. A 50 (1994) 4109.

[171a] Y. Komninos, Th. Mercouris, C.A. Nicolaides, Ab initio calculation of time-dependent control dynamics in polyelectronic systems involving bound and resonance states: Application to a quartet spectrum of He^-, Phys. Rev. A 77 (2008) 013412.

[171b] Th. Mercouris, Y. Komninos, C.A. Nicolaides, Time-dependent formation of the profile of the $He\ 2s\ 2p\ ^1P^o$ state excited by a short laser pulse, Phys. Rev. A 75 (2007) 013407.

[171c] C.A. Nicolaides, Th. Mercouris, Y. Komninos, The time-dependent formation of the profile of resonance atomic states and its dependence on the duration of ultra-short pulses from free-electron lasers, Phys. Rev. A 80 (2009) 055402.

[172] F.H.M. Faisal, Theory of Multiphoton Processes, Plenum Press, New York, 1987.

[173] C.A. Nicolaides, C.W. Clark, M.H. Nayfeh (Eds.), Atoms in Strong Fields, Plenum Press, New York, 1990.

[174] J.N. Silverman, C.A. Nicolaides, Complex Stark eigenvalues for excited states of hydrogenic ions from analytic continuation of real variationally based large-order perturbation theory, Chem. Phys. Lett. 164 (1991) 321.

[175] J.J. Wendoloski, W.P. Reinhardt, Effects of external electric field on $^1P^o$ resonances of H^-, Phys. Rev. A 17 (1978) 195.

[176] S.-I. Chu, W.P. Reinhardt, Intense field multiphoton ionization via complex dressed states: Application to the H atom, Phys. Rev. Lett. 39 (1977) 1195.

[177] A. Maquet, S.-I. Chu, W.P. Reinhardt, Stark ionization in dc and ac fields: An L^2 complex-coordinate approach, Phys. Rev. A 27 (1983) 2946.

[178] J.H. Shirley, Solution of the Schrödinger equation with a Hamiltonian periodic in time, Phys. Rev. 138 (1965) B979.

[179] Th. Mercouris, C.A. Nicolaides, Polyelectronic theory of atoms in strong laser fields. CO_2-laser seven-photon ionisation of H^-, J. Phys. B 21 (1988) L285.

[180] C.A. Nicolaides, Th. Mercouris, Multiphoton ionization of negative ions in the presence of a dc-field. Application to Li^-, Chem. Phys. Lett. 159 (1989) 45.

[181] Th. Mercouris, C.A. Nicolaides, Laser ionization of H^- in the presence of a DC field, J. Phys. B 23 (1990) 2037.

[182] C.A. Nicolaides, Th. Mercouris, G. Aspromallis, Many-electron, many- photon theory of nonlinear polarizabilities, J. Opt. Soc. Am. B 7 (1990) 494.

[183] Th. Mercouris, C.A. Nicolaides, Above threshold ionization in the presence of a DC field, J. Phys. B 24 (1991) L57.

[184] Th. Mercouris, C.A. Nicolaides, Computation of the widths of doubly excited states coupled by external ac or dc fields, J. Phys. B 24 (1991) L557.

[185] M. Bylicki, S.I. Themelis, C.A. Nicolaides, State-specific theory and computation of a polyelectronic atomic state in a magnetic field. Application to doubly excited states of H^-, J. Phys. B 27 (1994) 2741.

[186] S.I. Themelis, C.A. Nicolaides, Dipole polarizabilities and hyperpolarizabilities of excited valence states of *Be*, Phys. Rev. A 52 (1995) 2439.

[187a] S.I. Themelis, C.A. Nicolaides, Complex energies and the polyelectronic Stark problem, J. Phys. B 33 (2000) 5561.

[187b] S.I. Themelis, C.A. Nicolaides, Complex energies and the polyelectronic Stark problem: II. The Li n = 4 levels for weak and strong fields, J. Phys. B 34 (2001) 2905.

[188] Th. Mercouris, C.A. Nicolaides, Solution of the many-electron many- photon problem for strong fields: Application to Li^- in one- and two-color laser fields, Phys. Rev. A 67 (2003) 063403.

[189] Th. Mercouris, C.A. Nicolaides, Controllable surfaces of path interference in the multiphoton ionization of atoms by a weak trichromatic field, J. Opt. B 7 (2005) S403.

[190] C.A. Nicolaides, C. Haritos, Th. Mercouris, Theory and computation of electron corre- lation in the continuous spectrum: Double photoionization cross- section of H and He near and far from threshold, Phys. Rev. A 55 (1997) 2830.

[190] H. Ågren, J. Olsen, H. Jørgen, P. Jørgensen, Accurate static and dynamic polarizabilities of Li^-, Phys. Rev. A 40 (1989) 2265.

[192] A.W. Weiss, Theoretical electron affinities for some of the alkali and alkaline-earth elements, Phys. Rev. 166 (1968) 70.

[193a] G. Jolicard, E.J. Austin, Optical potential method of calculating resonance energies and widths, Chem. Phys. 103 (1986) 295.

[193b] U.V. Riss, H.-D. Meyer, The transformative complex absorbing potential method: a bridge between complex absorbing potentials and smooth exterior scaling, J. Phys. B 31 (1998) 2279.

[193c] H.O. Karlsson, Accurate resonances and effective absorption of flux using smooth exterior scaling, J. Chem. Phys. 109 (1998) 9366.

[193d] Y. Sajeev, M. Sindelka, N. Moiseyev, Reflection-free complex absorbing potential for electronic structure calculations: Feshbach type autoionization resonance of Helium, Chem. Phys. 329 (2006) 307.

[194] H.-Y. Meng, Y.-X. Zhang, S. Kang, T.-Y. Shi, M.-S. Zhan, Theoretical complex Stark ener- gies of lithium by a complex scaling plus the B-spline approach, J. Phys. B 41 (2008) 155003.

[195a] S. Sahoo, Y.K. Ho, The complex absorbing potential method (CAP) to study the Stark effect in hydrogen and lithium, J. Phys. B 33 (2000) 2195.

[195b] S. Sahoo, Y.K. Ho, Stark effect on the low-lying excited states of the hydrogen and the lithium atoms, J. Phys. B 33 (2000) 5151.

[196a] Y.H. Jiang, R. Püttner, D. Delande, M. Martins, G. Kaindl, Explicit analysis of chaotic behavior in radial and angular motion in doubly excited helium, Phys. Rev. A 78 (2008) 021401(R).

[196b] J. Eiglsperger, J. Madroñero, Highly doubly excited states of planar helium: Fluctua- tions in photoionization cross section, Phys. Rev. A 80 (2009) 022512.

Quantum Theory of Reactive Scattering in Phase Space

Arseni Goussev[a], **Roman Schubert**[a], **Holger Waalkens**[a,b], and **Stephen Wiggins**[a]

Contents

[a] School of Mathematics, University of Bristol, University Walk, Bristol BS8 1TW, UK
[b] Johann Bernoulli Institute for Mathematics and Computer Science, University of Groningen, PO Box 407, 9700 AK Groningen, The Netherlands
E-mail addresses: Arseni.Goussev@bristol.ac.uk (A. Goussev), Roman.Schubert@bristol.ac.uk (R. Schubert), H.Waalkens@rug.nl (H. Waalkens), S.Wiggins@bristol.ac.uk (S. Wiggins)

Abstract   We review recent results on quantum reactive scattering from a phase space perspective. The approach uses classical and quantum versions of Poincaré–Birkhoff normal form theory and the perspective of dynamical systems theory. Over the past 10 years the classical normal form theory has provided a method for realizing the phase space structures that are responsible for determining reactions in high-dimensional Hamiltonian systems. This has led to the understanding that a new (to reaction dynamics) type of phase space structure, a *normally hyperbolic invariant manifold* (or NHIM), is the "anchor" on which the phase space structures governing reaction dynamics are built, e.g., it is the classical analogue of the chemists notion of the "activated complex" and it is essential for the construction of a surface that divides reactants from products which has the "no-recrossing" property for trajectories and minimal flux. The quantum normal form (QNF) theory provides a method for quantizing these phase space structures through the use of the Weyl quantization procedure. We show that this approach provides a solution of the time-independent Schrödinger equation leading to a (local) S-matrix in a neighborhood of the saddle point governing the reaction. These results can be obtained for any dimension system for which an accurate normal form can be computed, and it does *not* require numerical solution of the Schrödinger equation or the generation of any classical trajectories. It follows easily that the quantization of the directional flux through the dividing surface with the properties noted above is a flux operator that can be expressed in a "closed form." Moreover, from the local S-matrix we easily obtain an expression for the cumulative reaction probability (CRP), which is the essential ingredient for the computation of microcanonical reaction rates and thermal reaction rates. Significantly, the expression for the CRP can be evaluated without the need to compute classical trajectories. This is a by-product of the quantization of classical phase space structures that govern "exact" classical dynamics. The quantization of the NHIM is shown to lead to the activated complex, and the lifetimes of quantum states initialized on the NHIM correspond to the Gamov–Siegert resonances. We apply these results to the collinear nitrogen exchange reaction and a three degree-of-freedom system corresponding to an Eckart barrier coupled to two Morse oscillators. We end by describing some further challenges that are topics of current research, but where some preliminary results are known: corner-cutting tunneling, state-to-state reaction rates, the flux–flux autocorrelation function formalism, and the convergence of the QNF. We emphasize that this dynamical system, phase space approach to quantum reactive scattering through the QNF provides a completely new approach to the computation of the relevant

quantum scattering quantities (e.g., CRP, resonances) which shows promise in leading to computationally efficient methods for "high-dimensional" systems.

1. INTRODUCTION

Over the past 50 years the computation of quantities describing quantum reactive scattering processes has been a topic of great interest in the chemistry and physics community, see the Perspective article of Miller [1] for background and history. The interest in this topic continues to grow as a result of the need to include quantum effects in order to understand the behavior of certain biomolecules and molecular materials [2]. These contemporary applications are concerned with "large systems," and quantum mechanical calculations are notorious for their consumption of computational resources as the number of degrees of freedom (DoFs) grows. As noted in Ref. [3], the Nobel Prize winner Walter Kohn has identified the problem as the exponential wall of difficulty when one tries to perform numerical calculations in the traditional manner using the rules of quantum mechanics. In this review we discuss a new (phase space) approach to quantum reactive scattering that allows us to bypass the traditional computational difficulties for certain types of physically relevant quantities.

Our purpose here is not to review the entire field of quantum reactive scattering. That would be a huge task that is beyond the scope of this review. Rather, we begin by describing the standard quantities that are computed to describe quantum reactive scattering processes and the issues associated with their computation. Our description follows the excellent review of Miller [4].

The quantity that contains a great deal of detailed information about a particular quantum reactive scattering process is the **S**-matrix. The **S**-matrix, $\{S_{n_p, n_r}(E, J)\}$ as a function of total energy E and total angular momentum J, can be obtained by solving the Schrödinger equation with scattering boundary conditions. From the **S**-matrix state-to-state differential scattering cross sections can be computed as follows:

$$\sigma_{n_p \leftarrow n_r}(\theta, E) = |(2ik_{n_r})^{-1} \sum_J (2J + 1) d^J_{m_p, m_r}(\theta) S_{n_p, n_r}(E, J)|^2, \tag{1}$$

where n_r (n_p) labels the reactant (product) rotational and vibrational states, θ is the scattering angle between the relative velocity vectors of reactants and products, m_r (m_p) is the projection of total angular momentum onto the relative velocity vector of the reactants (products), and $d^J_{m\,m'}(\theta)$ is the Wigner rotation matrix.

For many chemical reactions a sufficient description is provided by the *rate constant*, either the canonical rate constant characterized by the temperature, $k(T)$, or the microcanonical rate constant characterized by the total energy, $k(E)$. These rate constants can be obtained using appropriate averages of the state-to-state differential cross sections. This averaging process yields the *cumulative reaction probability* (CRP):

$$\mathcal{N}(E) = \sum_J (2J + 1) \sum_{n_p, n_r} |S_{n_p, n_r}(E, J)|^2, \qquad (2)$$

which is used to compute the microcanonical and canonical rate constants, as follows:

$$k(E) = [2\pi \hbar \rho_r(E)]^{-1} \mathcal{N}(E), \qquad (3)$$

$$k(T) = [2\pi \hbar Q_r(T)]^{-1} \int_{-\infty}^{\infty} dE e^{-\beta E} \mathcal{N}(E). \qquad (4)$$

where $\beta = (kT)^{-1}$, ρ_r is the density of reactant states, and Q_r is the reactant partition function.

Miller has pointed out [4] that if one is interested only in the rate, then solving the Schrödinger equation to obtain the **S**-matrix from which the state-to-state differential scattering cross section (1) is computed, and then subsequently averaged to obtain the CRP (2), is an extremely inefficient process in the sense that a great deal of the detailed information obtained through the computation of the **S**-matrix is "thrown away" in the averaging process. Instead, Miller [4] discusses a *direct* way to compute $\mathcal{N}(E)$, or $k(T)$, i.e., a method that avoids first computing the **S**-matrix, that is also *correct* in the sense that the expressions for $\mathcal{N}(E)$ or $k(T)$ are exact, i.e., no approximations are involved. These expressions are given as follows [4]:

$$\mathcal{N}(E) = 2\pi \hbar \, \mathrm{Tr} \left(\delta(E - \hat{H}) \hat{F} P_r \right), \qquad (5)$$

$$k(T) = Q_r(T)^{-1} \, \mathrm{Tr} \left(e^{-\beta \hat{H}} \hat{F} P_r \right), \qquad (6)$$

where $\hat{H}$ is the Hamilton operator, $\hat{F}$ is a flux operator, P_r is the long time limit of the quantum mechanically time-evolved Heaviside function, and $\mathrm{Tr}(\cdot)$ denotes the trace operation. Schatz and Ratner [5] point out that there are three possibilities for the use of Eqs. (5 and 6) for computing rates. The first is to evaluate the trace of the operators in a basis, the second is to develop semiclassical theories for the rate constants [2, 6], and the third is to use the expressions to develop a version of quantum transition state theory [7].

An alternative approach is to express Eqs. (5 and 6) in terms of a form of flux–flux autocorrelation function [8, 9], and we discuss this approach in some detail in Section 6.3. A recent survey of methods for computing reaction rates is given in Ref. [10].

Our approach is firmly rooted in phase space, both the classical and quantum theories. The classical phase space theory forms the "skeleton" on which our quantum theory of reactive scattering in phase space is built. The classical theory of reaction dynamics in phase space is reviewed in Section 2. Certainly there has been earlier work on classical reaction dynamics in phase space. In particular, we note the seminal work of Pechukas, Pollak, Child, and McLafferty from the 1970s and early 1980s on two DoF Hamiltonian systems [11–18] where the notion of a periodic orbit dividing surface (PODS) was introduced. The PODS bound a two-dimensional dividing surface (in the three-dimensional energy surface) having the "no-recrossing" property and minimal flux. This work did not generalize to more than two DoFs. The generalization has required a new concept—the notion of a *normally hyperbolic invariant manifold*, or NHIM. This was introduced in the study of phase space transport in Hamiltonian systems with three or more DoFs in Ref. [19] and was subsequently used in the study of chemical reaction dynamics in Ref. [20]. For a d DoF Hamiltonian system, the NHIM has the structure of a $2d − 3$ dimensional sphere in the $2d − 1$ dimensional energy surface (so for $d = 2$, the NHIM has the structure of a one-dimensional sphere, or periodic orbit). Conceptually, the NHIM is a fundamentally new dynamical object. It is a *manifold* of "saddle-type stability" that exists in phase space. In Section 2 we discuss in more detail why this is the mathematical manifestation of the chemists notion of the *activated complex*. Later, it was shown in Ref. [21] that the NHIM played the role of the PODS for systems with three or more DoFs in the sense that the NHIM is the boundary of a dividing surface having the "no-recrossing" property and minimal flux.

This approach to phase space reaction dynamics for three or more DoF Hamiltonian systems did not receive a great deal of applications throughout the 1990s. One reason for this was that there was not a computational method for realizing NHIMs in specific Hamiltonian systems (with three or more DoFs). This changed as a result of the work in Refs. [22, 23] where it was shown that the classical Poincaré–Birkhoff normal form theory could be used to compute a coordinate system where the NHIM could be realized, along with a variety of associated phase space structures. Software was developed that enabled the computation of the classical (CNF) and quantum normal forms (QNF), and this allowed the realization of these phase space structures in specific examples.[1] This enabled

---

[1] The software, along with documentation, is freely available for download at
http://lacms.maths.bris.ac.uk/publications/software/index.html.

the application of this approach to classical phase space reaction dynamics to HCN isomerization [24], computation of the volume of points in an energy surface corresponding to reactive trajectories (the "reactive volume," [25, 26]), and a realization of Thiele's [27] notion of "gap times" and reaction rates [28].

The generalization of this approach to the quantum setting has been carried out in Refs. [29–31]. The essential tools that make this possible are a quantum mechanical generalization of the classical Poincaré–Birkhoff normal form (described in Appendix A.2) and the Weyl quantization procedure. This firmly establishes a phase space approach to quantum mechanics. Our development and understanding of classical phase space structures associated with reaction dynamics is essential because one sees precisely their quantum mechanical manifestations. For example, in the classical setting the normal form is integrable in a (phase space) neighborhood of a particular saddle point that is relevant to the reaction of interest (in a way that we precisely describe in Section 2). This property is manifested quantum mechanically by yielding a Hamilton operator in QNF that factors into separate one-dimensional problems that can be solved exactly. This, in turn, gives rise to a block diagonal local **S**-matrix that can easily be computed and analyzed. This is described in some detail in Section 4.1. This is a significant result because the implication is if the relevant QNF for a system can be computed, then *regardless of the size of the system*, the local **S**-matrix can be calculated. In other words, our approach leads to an expression for the **S**-matrix that does *not* require a solution of the Schrödinger equation. In Section 4.1 we show that the classical flux through a dividing surface in phase space having the no-recrossing and minimal flux properties is directly related to the quantum mechanical CRP. We apply this approach to computing the CRP for the collinear nitrogen exchange reaction in Section 4.2 and coupled Eckart–Morse–Morse oscillators in Section 4.3. In Section 5 we show that quantum resonances are related to the time of decay of quantum states initialized on the activated complex. We conclude in Section 6 by considering four developing areas of the theory: "corner-cutting" tunneling trajectories, state-to-state reaction rates, the flux–flux autocorrelation formalism, and convergence of the QNF.

2. PHASE SPACE STRUCTURES UNDERLYING REACTION DYNAMICS

In this section we describe the dynamics and geometry associated with phase space structures governing reaction dynamics. While the emphasis in this review is on quantum mechanics, the phase space structure that we describe forms the classical mechanical "skeleton" on which the quantum mechanical theory is supported. Here we merely summarize the basic results,

more details can be found in the references given in the introduction. Our exposition here follows Ref. [32].

We consider a Hamiltonian system with d DoFs, phase space coordinates $(\tilde{q}, \tilde{p}) \in \mathbb{R}^d \times \mathbb{R}^d$, and Hamiltonian function H. We assume that $(\tilde{q}_0, \tilde{p}_0)$ is an equilibrium point of Hamilton's equations which is of saddle–center–$\cdots$–center stability type.[2] By adding a constant term to the Hamiltonian function (which does not change the dynamics) we can, without loss of generality, assume that $H(\tilde{q}_0, \tilde{p}_0) = 0$. Moreover, for simplicity of exposition, we can assume that the coordinates have been suitably translated so that the relevant equilibrium point $(\tilde{q}_0, \tilde{p}_0)$ is at the origin. For much of the discussion below, we will consider isoenergetic geometrical structures belonging to a single positive energy surface $\Sigma(E) := H^{-1}(E)$ for some constant $E > 0$. However, we note that in Ref. [33] essentially the same "picture" of phase space structures governing reaction dynamics has been shown to occur for constant temperature dynamics governed by the Hamiltonian isokinetic thermostat.

We construct geometric structures in a neighborhood of the equilibrium point. We emphasize that by "neighborhood" we mean a neighborhood in phase space, not just on a fixed energy surface. We denote this neighborhood of the equilibrium point by $\mathcal{L}$. We will defer until later a discussion of the constraints on the size of this neighborhood; suffice it to say for now that the region is chosen so that a new set of coordinates can be constructed (the normal form coordinates) in which an accurate nonlinear approximation of the Hamiltonian can be expressed (the normal form Hamiltonian) such that it provides an integrable approximation to the dynamics, as well as an algorithmic procedure for realizing phase space structures to within a given desired accuracy.

Before describing the dynamics in normal form coordinates, as well as the realization of the phase space structures in normal form coordinates that govern "reaction," i.e., trajectories in a phase space neighborhood of the saddle–center–$\cdots$–center equilibrium point (henceforth, referred to as a "saddle"), we describe the relevant geometric structures that have been developed in the references given above. We emphasize that although the normal form procedure provides a specific method for realizing these geometric structures in a given coordinate system, their existence is independent of any specific set of coordinates.

---

[2] We will define this more precisely shortly. However, briefly, it means that the matrix associated with the linearization of Hamilton's equations about this equilibrium point has two real eigenvalues of equal magnitude, with one positive and one negative, and $d - 1$ purely imaginary complex conjugate pairs of eigenvalues. We will assume that the eigenvalues satisfy a nonresonance condition that we will describe more fully in the following.

Locally, the $(2d - 1)$-dimensional energy surface $\Sigma(E)$ has the structure of $\mathbb{S}^{2d-2} \times \mathbb{R}$, i.e., the Cartesian product of a $(2d - 2)$-dimensional sphere and a line, in the $2d$-dimensional phase space. The energy surface $\Sigma(E)$ is split locally into two components, "reactants" and "products," by a $(2d - 2)$-dimensional "dividing surface" that is diffeomorphic to $\mathbb{S}^{2d-2}$ and which we therefore denote by $S_{ds}^{2d-2}(E)$. The dividing surface that we construct has the following properties:

- The only way that trajectories can evolve from reactants to products (and vice versa), without leaving the local region $\mathcal{L}$, is through $S_{ds}^{2d-2}(E)$. In other words, initial conditions (ICs) on this dividing surface specify all reacting trajectories.
- The dividing surface that we construct is free of local recrossings; any trajectory which crosses it must leave the neighborhood $\mathcal{L}$ before it might possibly cross again.
- The dividing surface that we construct minimizes the flux, i.e., the directional flux through the dividing surface will increase upon a generic deformation of the dividing surface (see Ref. [21] for details).

The fundamental phase space building block that allows the construction of a dividing surface with these properties is a particular NHIM which, for a fixed positive energy E, will be denoted $S_{\text{NHIM}}^{2d-3}(E)$. The NHIM is diffeomorphic to $\mathbb{S}^{2d-3}$ and forms the natural *dynamical equator* of the dividing surface: The dividing surface is split by this equator into $(2d - 2)$-dimensional hemispheres, each diffeomorphic to the open $(2d - 2)$-ball, B^{2d-2}. We will denote these hemispheres by $B_{ds,f}^{2d-2}(E)$ and $B_{ds,b}^{2d-2}(E)$ and call them the "forward reactive" and "backward reactive" hemispheres, respectively. $B_{ds,f}^{2d-2}(E)$ is crossed by trajectories representing "forward" reactions (from reactants to products), while $B_{ds,b}^{2d-2}(E)$ is crossed by trajectories representing "backward" reactions (from products to reactants).

The $(2d - 3)$-dimensional NHIM can be viewed as the energy surface of an (unstable) invariant subsystem which as mentioned above, in chemistry terminology, corresponds to the "activated complex," which as an oscillating "supermolecule" is located between reactants and products.

The NHIM is of saddle stability type, having $(2d - 2)$-dimensional stable and unstable manifolds $W^s(E)$ and $W^u(E)$ that are diffeomorphic to $\mathbb{S}^{2d-3} \times \mathbb{R}$. Being of co-dimension[3] one with respect to the energy surface,

---

[3] Briefly, the co-dimension of a submanifold is the dimension of the space in which the submanifold exists, minus the dimension of the submanifold. The significance of a submanifold being "co-dimension one" is that it is one less dimension than the space in which it exists. Therefore it can "divide" the space and act given it is invariant as a separatrix, or barrier, to transport.

these invariant manifolds act as separatrices, partitioning the energy surface into "reacting" and "nonreacting" parts as will explain in detail in Section 2.2.

2.1. Dynamics and phase space structures near the saddle in normal form coordinates

As mentioned in the previous section, reaction type dynamics is induced by equilibrium points of saddle×center× · · · ×center stability type. These are equilibria for which the matrix associated with the linearization of Hamilton's equations has eigenvalues which consist of a pair of real eigenvalues of equal magnitude and opposite sign, $(+\lambda, -\lambda)$, $\lambda \in \mathbb{R}$, and $(d-1)$ pairs of complex conjugate purely imaginary eigenvalues, $(+i\omega_k, -i\omega_k)$, $\omega_k \in \mathbb{R}$, for $k = 2, \dots, d$.

The phase space structures near equilibria of this type exist independently of a specific coordinate system. However, in order to carry out specific calculations we will need to be able to express these phase space structures in coordinates. This is where Poincaré–Birkhoff normal form theory is used. This is a well-known theory and has been the subject of many review papers and books, see, e.g., Refs. [34–40]. For our purposes it provides an algorithm whereby the phase space structures described in the previous section can be realized for a particular system by means of the normal form transformation which involves making a nonlinear symplectic change of variables,

$$(q, p) = T(\tilde{q}, \tilde{p}),\tag{7}$$

into *normal form coordinates* (q, p) which, in a local neighborhood $\mathcal{L}$ of the equilibrium point, "decouples" the dynamics into a "reaction coordinate" and "bath modes." The coordinate transformation T is obtained from imposing conditions on the form of H expressed by the new coordinates (q, p),

$$H_{\mathrm{CNF}}(q, p) = H\big(T^{-1}(q, p)\big) = H(\tilde{q}, \tilde{p}).\tag{8}$$

These conditions are chosen such that H_{CNF} and the resulting equations of motions assume a simple form in which the reaction coordinate and bath modes "decouple." This decoupling is one way of understanding how we are able to construct the phase space structures, in the normal form coordinates, that govern the dynamics of reaction.

In fact, we will assume that a (generic) nonresonance condition holds between the eigenvalues, namely that

$$k_2\omega_2 + \cdots + k_n\omega_d \neq 0\tag{9}$$

for all non-vanishing integer vectors $(k_2, \ldots, k_d) \in \mathbb{Z}^{d-1}$.[4] When such a condition holds, the CNF procedure, see Appendix A.1, yields an explicit expression for the normalized Hamiltonian H_{CNF} truncated at order N as a function of d integrals of motion:

$$H_{\mathrm{CNF}}^{(N)} = K_{\mathrm{CNF}}^{(N)}(I, J_2, J_3, \ldots, J_d)$$

$$= E_0 + \lambda I + \sum_{k=2}^{d} \omega_k J_k + \sum_{n=2}^{\lfloor N/2 \rfloor} \sum_{|\alpha|=n} \kappa_{n,\alpha} I^{\alpha_1} J_2^{\alpha_2} \ldots J_d^{\alpha_d}. \tag{10}$$

Note that the normal form is expressed as a polynomial in the action integrals I and J_k, $k = 2, \ldots, d$, corresponding to a "reaction coordinate" and $(d - 1)$ "bath modes," respectively. In Eq. (10) E_0 denotes the energy of the system at the equilibrium point and the expansion coefficient $\kappa_{n,\alpha}$ is obtained by the CNF algorithm presented in Appendix A; here, $\alpha = (\alpha_1, \ldots, \alpha_d)$ with $\alpha_k \in \mathbb{N}_0$ for $k = 1, \ldots, d$, and $|\alpha| = \sum_k \alpha_k$. In Appendix A we show that the normal form algorithm generates a polynomial at each step, where the normalization algorithm at a certain order does not modify the normalized terms at lower order. However, in practice it is necessary to stop the algorithm at a given order. In this sense the normal form is an approximation to the original Hamiltonian in a neighborhood of the saddle, which we have denoted by $\mathcal{L}$. Certainly, it is essential that the approximation is accurate enough to yield useful information. Numerous examples have show this to be the case, and we discuss this issue more fully in Section 2.5.

The integral, I, corresponds to a "reaction coordinate" (saddle-type DoF):

$$I = q_1 p_1. \tag{11}$$

We note that there is an equivalent form of the reaction coordinate: making the linear symplectic change of variables $q_1 = (P_1 - Q_1)/\sqrt{2}$ and $p_1 = (P_1 + Q_1)/\sqrt{2}$ transforms the above into the following form, which may be more familiar to many readers:

$$I = q_1 p_1 = \frac{1}{2}\left(P_1^2 - Q_1^2\right). \tag{12}$$

Geometrically speaking, one can move freely between these two representations by considering the plane (q_1, p_1) and rotating it by angle $\pi/4$ to give (Q, P).

---

[4] We note that the inclusion of $\pm\lambda$ in a nonresonance condition would be vacuous; one cannot have a resonance of this kind between a real eigenvalue, $\pm\lambda$, and purely imaginary eigenvalues, $\pm i\omega_k$, $k = 2, \ldots, d$.

The integrals J_k, for $k = 2, \ldots, d$, correspond to "bath modes" (center-type DoF)[5]:

$$J_k = \frac{1}{2}\left(p_k^2 + q_k^2\right), \quad k = 2, \ldots, d. \tag{13}$$

In the new coordinates, Hamilton's equations have a particularly simple form:

$$\dot{q}_1 = \frac{\partial H_{\mathrm{CNF}}}{\partial p_1} = \Lambda(I, J_2, \ldots, J_d)q_1,$$

$$\dot{p}_1 = -\frac{\partial H_{\mathrm{CNF}}}{\partial q_1} = -\Lambda(I, J_2, \ldots, J_d)p_1,$$

$$\dot{q}_k = \frac{\partial H_{\mathrm{CNF}}}{\partial p_k} = \Omega_k(I, J_2, \ldots, J_d)p_k$$

$$\dot{p}_k = -\frac{\partial H_{\mathrm{CNF}}}{\partial q_k} = -\Omega_k(I, J_2, \ldots, J_d)q_k, \tag{14}$$

for $k = 2, \ldots, d$, where we denote

$$\Lambda(I, J_2, \ldots, J_d) := \frac{\partial K_{\mathrm{CNF}}(I, J_2, \ldots, J_d)}{\partial I}, \tag{15}$$

$$\Omega_k(I, J_2, \ldots, J_d) := \frac{\partial K_{\mathrm{CNF}}(I, J_2, \ldots, J_d)}{\partial J_k}, \quad k = 2, \ldots, d. \tag{16}$$

The integrals provide a natural definition of the term "mode" that is appropriate in the context of reaction, and they are a consequence of the (local) integrability in a neighborhood of the equilibrium point of saddle–center– $\cdots$ –center stability type. Moreover, the expression of the normal form Hamiltonian in terms of the integrals provides us a way to partition the "energy" between the different modes. We will provide examples of how this can be done in the following.

---

[5] Throughout our work we use, somewhat interchangeably, terminology from both chemical reaction dynamics and dynamical systems theory. This is most noticeable in our reference to the integrals of motion. I is the integral related to reaction and in the context of dynamical systems theory it is related to hyperbolic behavior. The term "reactive mode" might also be used to describe the dynamics associated with this integral. The integrals $J_2, \ldots, J_d$ describe the dynamics associated with "bath modes." In the context of dynamical systems theory, the dynamics associated with these integrals is referred to as "center-type dynamics" or "center modes." A key point here is that integrals of the motion provide us with the natural way of defining and describing the physical notion of a "mode." The nature of the mode is defined in the context of the specific application (i.e., chemical reactions) or, in the context of dynamical systems theory, through its stability properties (i.e., hyperbolic or center).

The normal form transformation T in (7) can be computed in an algorithmic fashion. One can give an explicit expression for the phase space structures discussed in the previous section in terms of the normal form coordinates, (q, p). This way the phase space structures can be constructed in terms of the normal form coordinates, (q, p), and for physical interpretation transformed back to the original "physical" coordinates, $(\tilde{q}, \tilde{p})$, by the inverse of the transformation T.[6]

In summary, the "output" of the normal form algorithm is the following:

- A symplectic transformation $T(\tilde{q}, \tilde{p}) = (q, p)$ and its inverse $T^{-1}(q, p) = (\tilde{q}, \tilde{p})$ that relate the normal form coordinates (q, p) to the original "physical" coordinates $(\tilde{q}, \tilde{p})$.
- An expression for the normalized Hamiltonian: in the form H_{CNF}, in terms of the normal form coordinates (q, p), and in the form K_{CNF}, in terms of the integrals $(I, J_2, \ldots, J_d)$.
- Explicit expressions for the integrals of motion I and J_k, $k = 2, \ldots, d$, in terms of the original "physical" coordinates by means of the symplectic transformation $T(\tilde{q}, \tilde{p}) = (q, p)$.

2.2. Explicit definition and construction of the phase space structures in the normal form coordinates

As indicated in the previous section it is straightforward to construct the local phase space objects governing "reaction" in the normal form coordinates (q, p). In this section, we will define the various structures in the normal form coordinates and discuss briefly the consequences for the original dynamical system.

2.2.1. The structure of an energy surface near a saddle point

For $E < 0$, the energy surface consists of two disjoint components. The two components correspond to "reactants" and "products." The top panel of Figure 5.1 shows how the two components project to the various planes of the normal form coordinates. The projection to the plane of the saddle coordinates (q_1, p_1) is bounded away from the origin by the two branches of the hyperbola, $q_1 p_1 = I < 0$, where I is given implicitly by the energy equation with the center actions J_k, $k = 2, \ldots, d$, set equal to zero: $K_{\text{CNF}}(I, 0, \ldots, 0) = E < 0$. The projections to the planes of the center coordinates (q_k, p_k), $k = 2, \ldots, d$, are unbounded.

At $E = 0$, the formerly disconnected components merge (the energy surface bifurcates), and for $E > 0$, the energy surface has locally the structure of

---

[6] The original coordinates $(\tilde{q}, \tilde{p})$ typically have an interpretation as configuration space coordinates and momentum coordinates. The normal form coordinates (q, p), in general, do not have such a physical interpretation since both q and p are nonlinear functions of both $\tilde{q}$ and $\tilde{p}$.
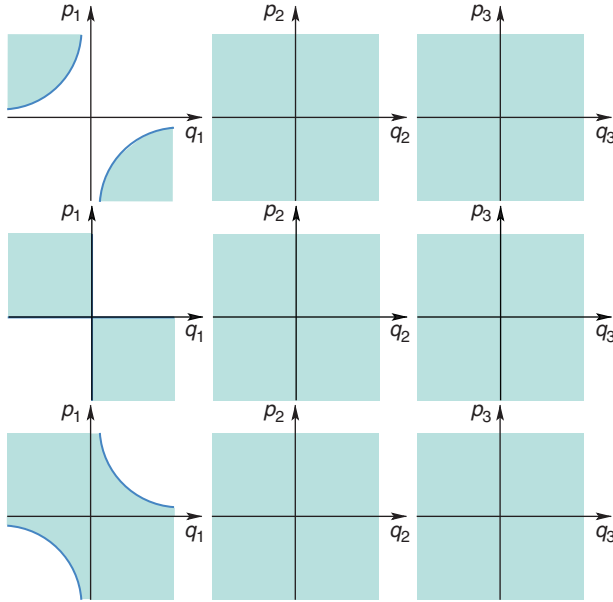
Figure 5.1 Projection of energy surfaces (turquoise regions) to the planes of the normal form coordinates. The energy surfaces have energy $E < 0$ (top panel), $E = 0$ (middle panel), $E > 0$ (bottom panel).

a spherical cylinder, $\mathbb{S}^{2d-2} \times \mathbb{R}$. Its projection to the plane of the saddle coordinates now includes the origin. In the first and third quadrants it is bounded by the two branches of the hyperbola, $q_1 p_1 = I > 0$, where I is again given implicitly by the energy equation with all center actions equal to zero, but now with an energy greater than zero: $K_{\mathrm{CNF}}(I, 0, \ldots, 0) = E > 0$. The projections to the planes of the center coordinates are again unbounded. This is illustrated in the bottom panel of Figure 5.1.

2.2.2. The dividing surface, and reacting and nonreacting trajectories

On an energy surface with $E > 0$, we define the dividing surface by $q_1 = p_1$. This gives a $(2d - 2)$ sphere which we denote by $S_{\mathrm{ds}}^{2d-2}(E)$. Its projection to the saddle coordinates simply gives a line segment through the origin which joins the boundaries of the projection of the energy surface, as shown in Figure 5.2. The projections of the dividing surface to the planes of the center coordinates are bounded by circles $(p_k^2 + q_k^2)/2 = J_k$, $k = 2, \ldots, d$, where J_k is determined by the energy equation with the other center actions, J_l, $l \neq k$, and the saddle integral, I, set equal to zero. The dividing surface divides the energy surface into two halves, $p_1 - q_1 > 0$ and $p_1 - q_1 < 0$, corresponding to reactants and products.
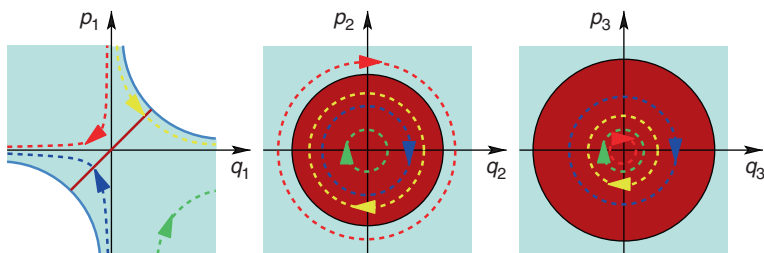
Figure 5.2 Projection of the dividing surface and reacting and nonreacting trajectories to the planes of the normal form coordinates. In the plane of the saddle coordinates, the projection of the dividing surface is the dark red diagonal line segment, which has $q_1 = p_1$. In the planes of the center coordinates, the projections of the dividing surface are the dark red discs. Forward and backward reactive trajectories (yellow and blue) project to the first and third quadrants in the plane of the saddle coordinates, respectively, and pass through the dividing surface. The red and green curves mark nonreactive trajectories on the reactant side ($p_1 - q_1 > 0$) and on the product side ($p_1 - q_1 < 0$) of the dividing surface, respectively. The turquoise regions indicate the projections of the energy surface.

As mentioned above, trajectories project to hyperbolae in the plane of the saddle coordinates and to circles in the planes of the center coordinates. The sign of I determines whether a trajectory is nonreacting or reacting, see Figure 5.2. Trajectories which have $I < 0$ are nonreactive and for one branch of the hyperbola $q_1 p_1 = I$ they stay on the reactants' side and for the other branch they stay on the products' side; trajectories with $I > 0$ are reactive, and for one branch of the hyperbola $q_1 p_1 = I$ they react in the forward direction, i.e., from reactants to products, and for the other branch they react in the backward direction, i.e., from products to reactants. The projections of reactive trajectories to the planes of the center coordinates are always contained in the projections of the dividing surface. In this, and other ways, the geometry of the reaction is highly constrained. There is no analogous restriction on the projections of nonreactive trajectories to the center coordinates.

2.2.3. The NHIM and its relation to the "activated complex"

On an energy surface with $E > 0$, the NHIM is given by $q_1 = p_1 = 0$. The NHIM has the structure of a $(2d - 3)$ sphere, which we denote by $S_{\text{NHIM}}^{2d-3}(E)$. The NHIM is the equator of the dividing surface; it divides it into two "hemispheres": the *forward dividing surface*, which has $q_1 = p_1 > 0$, and the *backward dividing surface*, which has $q_1 = p_1 < 0$. The forward and backward dividing surfaces have the structure of $(2d - 2)$-dimensional balls, which we denote by $B_{\text{ds, f}}^{2d-2}(E)$ and $B_{\text{ds, b}}^{2d-2}(E)$, respectively. All forward reactive trajectories cross $B_{\text{ds, f}}^{2d-2}(E)$; all backward reactive trajectories cross $B_{\text{ds, b}}^{2d-2}(E)$. Since $q_1 = p_1 = 0$ in the equations of motion (14) implies that $\dot{q}_1 = \dot{p}_1 = 0$, the NHIM is an invariant manifold, i.e., trajectories started in the NHIM stay in the NHIM

for all time. The system resulting from $q_1 = p_1 = 0$ is an invariant subsystem with one DoF less than the full system. In fact, $q_1 = p_1 = 0$ defines the center manifold associated with the saddle–center-$\cdots$–center equilibrium point, and the NHIM at an energy E greater than the energy of the equilibrium point is given by the intersection of the center manifold with the energy surface of this energy E [21, 23].

This invariant subsystem with one DoF less than the full system is the "activated complex" (in phase space) located between reactants and products. The NHIM can be considered to be the energy surface of the activated complex. In particular, all trajectories in the NHIM have $I = 0$.

The equations of motion (14) also show that $\dot{p}_1 - \dot{q}_1 < 0$ on the forward dividing surface $B_{\mathrm{ds,f}}^{2d-2}(E)$ and $\dot{p}_1 - \dot{q}_1 > 0$ on the backward dividing surface $B_{\mathrm{ds,b}}^{2d-2}(E)$. Hence, except for the NHIM, which is an invariant manifold, the dividing surface is everywhere transverse to the Hamiltonian flow. This means that a trajectory, after having crossed the forward or backward dividing surface, $B_{\mathrm{ds,f}}^{2d-2}(E)$ or $B_{\mathrm{ds,b}}^{2d-2}(E)$, respectively, must leave the neighborhood of the dividing surface before it can possibly cross it again. Indeed, such a trajectory must leave the local region in which the normal form is valid before it can possibly cross the dividing surface again.

The NHIM has a special structure: due to the conservation of the center actions, it is filled, or *foliated*, by invariant $(d − 1)$-dimensional tori, $\mathbb{T}^{d-1}$. More precisely, for $d = 3$ DoFs, each value of J_2 implicitly defines a value of J_3 by the energy equation $K_{\mathrm{CNF}}(0, J_2, J_3) = E$. For three DoFs, the NHIM is thus foliated by a one-parameter family of invariant 2-tori. The end points of the parameterization interval correspond to $J_2 = 0$ (implying $q_2 = p_2 = 0$) and $J_3 = 0$ (implying $q_3 = p_3 = 0$), respectively. At the end points, the 2-tori thus degenerate to periodic orbits, the so-called Lyapunov periodic orbits.

2.2.4. The stable and unstable manifolds of the NHIM forming the phase space conduits for reactions

Since the NHIM is of saddle stability type, it has stable and unstable manifolds, $W^{\mathrm{s}}(E)$ and $W^{\mathrm{u}}(E)$. The stable and unstable manifolds have the structure of spherical cylinders, $\mathbb{S}^{2d-3} \times \mathbb{R}$. Each of them consists of two branches: the "forward branches," which we denote by $W_f^{\mathrm{s}}(E)$ and $W_f^{\mathrm{u}}(E)$, and the "backward branches," which we denote by $W_b^{\mathrm{s}}(E)$ and $W_b^{\mathrm{u}}(E)$. In terms of the normal form coordinates, $W_f^{\mathrm{s}}(E)$ is given by $q_1 = 0$ with $p_1 > 0$, $W_f^{\mathrm{u}}(E)$ is given by $p_1 = 0$ with $q_1 > 0$, $W_b^{\mathrm{s}}(E)$ is given by $q_1 = 0$ with $p_1 < 0$, and $W_b^{\mathrm{u}}(E)$ is given by $p_1 = 0$ with $q_1 < 0$, see Figure 5.3. Trajectories on these manifolds have $I = 0$.

Since the stable and unstable manifolds of the NHIM are of one less dimension than the energy surface, they enclose volumes of the energy surface. We call the union of the forward branches, $W_f^{\mathrm{s}}(E)$ and $W_f^{\mathrm{u}}(E)$, the *forward reactive spherical cylinder* and denote it by $W_f(E)$. Similarly, we define the *backward*
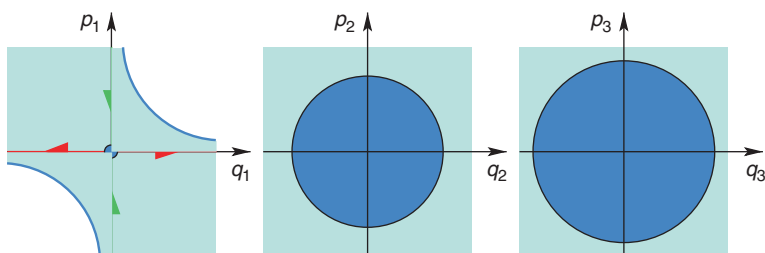
Figure 5.3 The projection of the NHIM and the local parts of its stable and unstable manifolds, $W^s(E)$ and $W^u(E)$, to the planes of the normal form coordinates. In the plane of the saddle coordinates, the projection of the NHIM is the origin marked by the blue bold point, and the projections of $W^s(E)$ and $W^u(E)$ are the p_1-axis and q_1-axis, respectively. $W^s(E)$ consists of the forward and backward branches $W_f^s(E)$ and $W_b^s(E)$, which have $p_1 > 0$ and $p_1 < 0$, respectively; $W^u(E)$ consists of $W_f^u(E)$ and $W_b^u(E)$, which have $q_1 > 0$ and $q_1 < 0$, respectively. In the plane of the center coordinates, the projection of the NHIM, $W^s(E)$ and $W^u(E)$ (the blue circular discs), coincide with the projection of the dividing surface in Figure 5.2. The turquoise regions mark the projections of the energy surface.
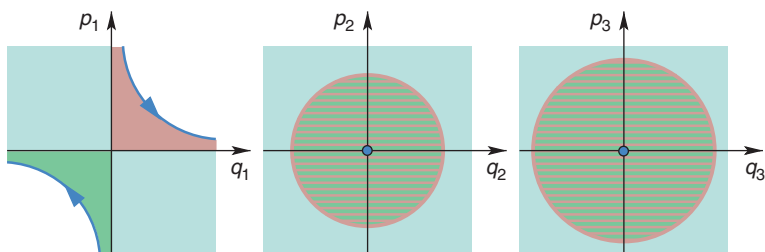
Figure 5.4 Projections of the reactive volumes enclosed by the forward and backward reactive spherical cylinders, $W_f(E)$ and $W_b(E)$, and the forward and backward reactions paths to the planes of the normal form coordinates. The volumes enclosed by $W_f(E)$ and $W_b(E)$ project to the dark pink and green regions in the first and third quadrants in the plane of the saddle coordinates, respectively. These volumes project to the dark green/dark pink brindled discs in the planes of the center coordinates, where their projections coincide with the projection of the NHIM and the dividing surface in Figures 5.2 and 5.3. The forward and backward reaction paths project to the two branches of a hyperbola marked blue in the first and third quadrants in the plane of the saddle coordinates, respectively, and to the origins (bold blue points) in the planes of the center coordinates. The turquoise regions mark the projections of the energy surface.

reactive spherical cylinder, $W_b(E)$, as the union of the backward branches, $W_b^s(E)$ and $W_b^u(E)$.

The reactive volumes enclosed by $W_f(E)$ and $W_b(E)$ are shown in Figure 5.4 as their projections to the normal form coordinate planes. In the plane of the saddle coordinates, the reactive volume enclosed by $W_f(E)$ projects to the

first quadrant. This projection is bounded by the corresponding hyperbola $q_1 p_1 = I$, with I obtained from $K_{\mathrm{CNF}}(I, 0, \ldots, 0) = E$. Likewise, $W_\mathrm{b}(E)$ projects to the third quadrant in the (q_1, p_1) plane. $W_\mathrm{f}(E)$ encloses *all* forward reactive trajectories; $W_\mathrm{b}(E)$ encloses *all* backward reactive trajectories. *All* nonreactive trajectories are contained in the complement.

2.3. The foliation of the reaction region by Lagrangian submanifolds

The existence of the d integrals of motion, $(I, J_2, \ldots, J_d)$, induces phase space structures which lead to further constraints on the trajectories in addition to the ones described above. In order to describe these structures and the resulting constraints it is useful to introduce the so-called momentum map, $\mathcal{M}$ [41, 42], which maps a point $(q_1, \ldots, q_d, p_1, \ldots, p_d)$ in the phase space $\mathbb{R}^d \times \mathbb{R}^d$ to the d integrals evaluated at this point:

$$\mathcal{M}: \mathbb{R}^d \times \mathbb{R}^d \to \mathbb{R}^d, \quad (q_1, \ldots, q_d, p_1, \ldots, p_d) \mapsto (I, J_2, \ldots, J_d). \tag{17}$$

The preimage of a value for the constants of motion $(I, J_2, \ldots, J_d)$ under $\mathcal{M}$ is called a *fiber*. A fiber thus corresponds to the common level set of the integrals in phase space.

A point $(q_1, \ldots, q_d, p_1, \ldots, p_d)$ is called a *regular point* of the momentum map if the linearization of the momentum map, $\mathrm{D}\mathcal{M}$, has full rank d at this point, i.e., if the gradients of the d integrals $I, J_k, k = 2, \ldots, d$, with respect to the phase space coordinates (q, p) are linearly independent at this point. If the rank of $\mathrm{D}\mathcal{M}$ is less than d then the point is called irregular. A fiber is called regular if it consists of regular points only. Otherwise, it is called an irregular fiber. In fact almost all fibers are regular. They are d-dimensional manifolds given by the Cartesian product of an hyperbola $q_1 p_1 = I$ in the saddle plane (q_1, p_1) and $d - 1$ circles $\mathbb{S}^1$ in the center planes (q_k, p_k), $k = 2, \ldots, d$. Since the hyperbola $q_1 p_1 = I$ consists of two branches each of which have the topology of a line $\mathbb{R}$, the regular fibers consist of two disjoint *toroidal cylinders*, $\mathbb{T}^{d-1} \times \mathbb{R}$, which are the Cartesian products of a $(d - 1)$-dimensional torus and a line. We denote these toroidal cylinders by

$$\Lambda^+_{I, J_2, \ldots, J_d} = \left\{ (q, p) \in \mathbb{R}^{2d} : p_1 q_1 = I, \frac{1}{2}\left(p_2^2 + q_2^2\right) = J_2, \ldots, \frac{1}{2}\left(p_d^2 + q_d^2\right) = J_d, q_1 > 0 \right\} \tag{18}$$

and

$$\Lambda^-_{I, J_2, \ldots, J_d} = \left\{ (q, p) \in \mathbb{R}^{2d} : p_1 q_1 = I, \frac{1}{2}\left(p_2^2 + q_2^2\right) = J_2, \ldots, \frac{1}{2}\left(p_d^2 + q_d^2\right) = J_d, q_1 < 0 \right\}. \tag{19}$$

$\Lambda^+_{I, J_2, \ldots, J_d}$ and $\Lambda^-_{I, J_2, \ldots, J_d}$ are *Lagrangian manifolds* [43]. The Lagrangian manifolds consist of all trajectories which have the same constants of motion. In particular the Lagrangian manifolds are invariant, i.e., a trajectory with IC on

a Lagrangian manifold will stay in the Lagrangian manifold for all time. For $I < 0$, the Lagrangian manifolds $\Lambda^-_{I,J_2,\ldots,J_d}$ and $\Lambda^+_{I,J_2,\ldots,J_d}$ consist of nonreactive trajectories in the reactant resp. product components of the energy surface. For $I > 0$, $\Lambda^+_{I,J_2,\ldots,J_d}$ consists of forward reactive trajectories and $\Lambda^-_{I,J_2,\ldots,J_n}$ consists of backward reactive trajectories.

2.4. The directional flux through the dividing surface

A key ingredient of transition state theory and the classical reaction rate is the directional flux through the dividing surface defined in Section 2.2. Given the Hamiltonian function in normal form expressed as a function of the integrals (10) and a fixed energy E above the energy of the saddle–center-$\cdots$–center, E_0, it is shown in Ref. [21] that the directional flux through the dividing surface is given by

$$f(E) = (2\pi)^{d-1}\mathcal{V}(E), \tag{20}$$

where $\mathcal{V}(E)$ is the volume in the space of the actions $(J_2, \ldots, J_d)$ enclosed by the contour $K_{\text{CNF}}(0, J_2, \ldots, J_d) = E$. This is a significant result because it enables the computation of the directional flux *without computing trajectories*. Moreover, it directly connects the directional flux to the NHIM, i.e., the activated complex. In Figure 5.5 we illustrate the volume $\mathcal{V}(E)$ for the case of a three DoF system: here $\mathcal{V}(E)$ is given by the area in the (J_2, J_3) plane enclosed by the light blue line corresponding to the NHIM.

We also note here that the dimensionless quantity

$$\mathcal{N}_{\text{Weyl}}(E) = \frac{f(E)}{(2\pi\hbar)^{d-1}}, \tag{21}$$
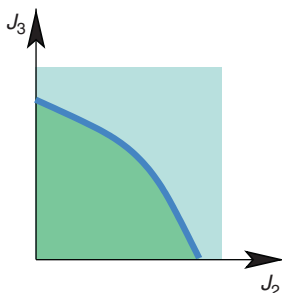
Figure 5.5   Contour $K_{\text{CNF}}(0, J_2, \ldots, J_d) = E$ (blue line) in the space of the center integrals $(J_2, \ldots, J_d)$ for $d = 3$ DoFs. Up to the prefactor $(2\pi)^{d-1}$, the area $\mathcal{V}(E)$ of the enclosed region (marked green) gives the directional flux through the dividing surface, see Eq. (20). The green region is the projection of the $I > 0$ piece of the energy surface on the (J_2, J_3) plane.

where $2\pi\hbar$ is Planck's constant, is Weyl's approximation of the integrated density of states or equivalently the mean number of quantum states of the activated complex with energies less than or equal to E (see, e.g., Ref. [44]). It is shown in Ref. [30] that $\mathcal{N}_{\mathrm{Weyl}}(E)$ can be interpreted as the mean number of open quantum "transition channels" at energy E.

In the case where we only take into account the quadratic part of the normal form, or, equivalently, if we linearize Hamilton's equations, we have $K_{\mathrm{CNF}}(I, J_2, \ldots, J_d) = \lambda I + \sum_{k=2}^{d} \omega_k J_k$ and the energy surface $K_{\mathrm{CNF}}(0, J_2, \ldots, J_d) = E$ encloses a simplex in $(J_2, \ldots, J_d)$ whose volume leads to the well-known result [45]

$$f(E) = \frac{E^{d-1}}{(d-1)!} \prod_{k=2}^{d} \frac{2\pi}{\omega_k} . \tag{22}$$

This shows, e.g., that the flux scales with E^{d-1} for energies close to the saddle energy. The key advantage of the normal form coordinates resulting from the normal form algorithm is that it allows one to include the nonlinear corrections to (22) to any desired order.

2.5. Effect of truncation of the normal form algorithm

The normalization procedure proceeds via formal power series manipulations whose input is a Taylor expansion of the original Hamiltonian, H, necessarily up to some finite order, N, in homogenous polynomials. For a particular application, this procedure naturally necessitates a suitable choice of the order, N, for the normalization, after which one must make a restriction to some local region, $\mathcal{L}$, about the equilibrium point in which the resulting computations achieve some desired accuracy. Hence, the accuracy of the normal form as a power series expansion truncated at order N in a neighborhood $\mathcal{L}$ is determined by comparing the dynamics associated with the normal form with the dynamics of the original system. There are several independent tests that can be carried out to verify accuracy of the normal form. Straightforward tests that we use are the following:

- Examine how the integrals associated with the normal form change on trajectories of the full Hamiltonian (the integrals will be constant on trajectories of the normal form).
- Check invariance of the different invariant manifolds (i.e., the NHIM and its stable and unstable manifolds) with respect to trajectories of the full Hamiltonian.

Both of these tests will require us to use the transformations between the original coordinates and the normal form coordinates. Specific examples where N, $\mathcal{L}$, and accuracy of the normal forms are considered can be found in Refs. [24–26, 46, 47].

2.6. "Globalizing" the geometrical structures in the reaction region

As we have shown, the normal form transformation to normal form coordinates provides a method for providing a complete understanding of the geometry of reaction dynamics in a neighborhood $\mathcal{L}$ (in phase space) of the saddle–center-$\cdots$–center equilibrium point of Hamilton's equations. By this, we mean that in the normal form coordinates we can give an explicit equation for the surfaces and, as a result of the "simple" structure of Hamilton's equations in the normal form coordinates, we can describe precisely the influence of these geometrical structures on trajectories of Hamilton's equations. In Table 5.1 we summarize the results obtained thus far by providing a list of the different surfaces that control the evolution of trajectories from reactants to products in the neighborhood $\mathcal{L}$.

However, it must be kept in mind that all of these surfaces, and associated dynamical phenomena, are only "locally valid" in the neighborhood $\mathcal{L}$. The next step is to understand their influence on the dynamics outside of $\mathcal{L}$, i.e., their influence on the dynamics of reaction throughout phase space in the original coordinates (as opposed to the normal form coordinates). In order to do this we will need the normal form transformation discussed in Appendix A, to order N (where N is determined according to the desired accuracy following the discussion in Section 2.5).

Table 5.1 Table of phase space surfaces influencing reaction dynamics and their representations in normal form coordinates on an energy surface of energy greater than the energy of the saddle equilibrium point

Geometrical structure	Equation in normal form coordinates
Dividing surface, $S_{ds}^{2d-2}(E)$	$q_1 = p_1$
Forward reactive hemisphere, $B_{ds,f}^{2d-2}(E)$	$q_1 = p_1 > 0$
Backward reactive hemisphere, $B_{ds,b}^{2d-2}(E)$	$q_1 = p_1 < 0$
NHIM, $S_{NHIM}^{2d-3}(E)$	$q_1 = p_1 = 0$
Stable manifold of the NHIM, $W^s(E)$	$q_1 = 0, p_1 \neq 0$
Unstable manifold of the NHIM, $W^u(E)$	$p_1 = 0, q_1 \neq 0$
Forward branch of $W^s(E)$, $W_f^s(E)$	$q_1 = 0, p_1 > 0$
Backward branch of $W^s(E)$, $W_b^s(E)$	$q_1 = 0, p_1 < 0$
Forward branch of $W^u(E)$, $W_f^u(E)$	$p_1 = 0, q_1 > 0$
Backward branch of $W^u(E)$, $W_b^u(E)$	$p_1 = 0, q_1 < 0$
Forward reactive spherical cylinder $W_f(E) \equiv W_f^s(E) \cup W_f^u(E)$	$p_1 q_1 = 0, p_1, q_1 \geq 0, q_1 \neq p_1$
Backward reactive spherical cylinder $W_b(E) \equiv W_b^s(E) \cup W_b^u(E)$	$p_1 q_1 = 0, p_1, q_1 \leq 0, q_1 \neq p_1$

In Appendix A we discuss the necessary transformations of the original physical coordinates required to transform the Hamiltonian into normal form. In particular, we translate the saddle–center-· · · –center equilibrium point to the origin, we "simplify" the linear part of Hamilton's equations (what "simplify" precisely means is described in the Appendix), then we iteratively construct a sequence of nonlinear coordinate transformations that successively "simplify" the order $3, 4, \ldots, N$ terms of the Hamiltonian according to the algorithm described in Appendix A. We can invert each of these transformations to return from the normal form coordinates to the physical coordinates.

2.6.1. Computation of $W_b^u(E)$ and $W_f^u(E)$

Our approach to computing the stable and unstable manifolds of a NHIM is, in principle, the same as for computing the stable and unstable manifolds of a hyperbolic trajectory (however, the practical implementation of the algorithm in higher dimensions is a different matter and one that deserves much more investigation).

We describe the computation of $W_f^u(E)$ as follows.

- In the normal form coordinates, choose a distribution of ICs on the NHIM and displace these ICs "slightly" in the direction of the forward branch of $W^u(E)$ ($p_1 = 0, q_1 = \varepsilon > 0, \varepsilon$ "small").
- Map these ICs back into the physical coordinates using the inverse of the normal form transformation.
- Integrate the ICs forward in time using Hamilton's equations in the physical coordinates, for the desired length of time (typically determined by accuracy considerations) that will give the manifold of the desired "size." Since the ICs are in the unstable manifold they will leave the neighborhood $\mathcal{L}$ in which the normal form transformation is valid (which is why we integrate them in the original coordinates with respect to the original equations of motion).

The backward branch of $W^u(E)$ can be computed in an analogous manner by displacing the ICs on the NHIM in the direction of the backward branch of $W^u(E)$ ($p_1 = 0, q_1 = \varepsilon < 0, \varepsilon$ "small").

2.6.2. Computation of $W_b^s(E)$ and $W_f^s(E)$

The forward and backward branches of $W^s(E)$ can be computed in an analogous fashion, except the ICs are integrated *backward* in time.

2.6.3. Practical considerations

By their very definition, invariant manifolds consist of trajectories, and the common way of computing them, and visualizing them, that works well in low dimensions is to integrate a distribution of ICs located on the invariant manifold (hence, this illustrates the value of the normal form coordinates

and transformation for locating appropriate ICs). In high dimensions there are numerical and algorithmic issues that have yet to be fully addressed. How does one choose a mesh on a $(2d - 3)$-dimensional sphere? As this mesh evolves in time, how does one "refine" the mesh in such a way that the evolved mesh maintains the structure of the invariant manifold?

Examples where this "globalization" of phase space structures in the reaction region has been carried out can be found in Refs. [24–26, 46]. However, there is tremendous scope for future work in this direction, both from the point of view of mathematical and computational techniques and applications to chemical dynamics.

3. QUANTUM NORMAL FORM REPRESENTATION OF THE ACTIVATED COMPLEX

In this section we present an extension of the CNF theory to quantum mechanics. Leaving all technical details for Appendix A we only consider here key aspects and results of the theory.

The QNF theory[7] provides an explicit algorithmic procedure that allows one to approximate the Hamiltonian operator $\hat{H}$, corresponding to a reactive system with a generally *nonintegrable* classical Hamiltonian, by a "simpler" Hamiltonian operator $\hat{H}_{QNF}$, having an *integrable* classical counterpart. The operator $\hat{H}_{QNF}$ takes the form of a power series expansion in reactive and nonreactive (bath-mode) action operators and the effective Planck's constant. The (generally infinite) power series can then be terminated at any desired order N dictated by the desired accuracy of the approximation. This leads to an Nth order QNF approximation $\hat{H}_{QNF}^{(N)}$ of the original Hamiltonian $\hat{H}$:

$$\hat{H}_{QNF}^{(N)} = K_{QNF}^{(N)}(\hat{I}, \hat{J}_2, \hat{J}_3, \ldots, \hat{J}_d)$$

$$= E_0 + \lambda\hat{I} + \sum_{k=2}^{d} \omega_k\hat{J}_k + \sum_{n=2}^{\lfloor N/2 \rfloor} \sum_{|\alpha|+j=n} \kappa_{n,\alpha,j} \hat{I}^{\alpha_1}\hat{J}_2^{\alpha_2} \ldots \hat{J}_d^{\alpha_d} \hbar_{eff}^{j}. \tag{23}$$

This approximation holds locally, in the vicinity of a single *equilibrium* point of the Hamiltonian function of the corresponding d-dimensional classical system (see Appendix A for details). It is this equilibrium point whose phase space neighborhood is traversed by reactive trajectories on their way from the valley of reactants to the valley of products. The equilibrium point is considered to be of saddle–center-· · ·–center stability type, meaning that the $2d \times 2d$ matrix associated with the linearized Hamilton's equations of motion

---

[7] See Ref. [30] for a comprehensive review of the mathematical theory, or consult Appendix A for a concise summary.

has two real eigenvalues, $\pm\lambda$, and $d-1$ purely imaginary complex conjugate pairs of eigenvalues, $\pm i\omega_k$ with $k = 2,\ldots, d$. The linear frequencies ω_k are further assumed to be rationally independent, so that the condition $m_2\omega_2 + \cdots + m_d\omega_d = 0$ implies $m_2 = \cdots = m_d = 0$ for all integers $m_2,\ldots, m_d$. Other quantities entering Eq. (23) include (i) the energy E_0 of the system at the equilibrium point, (ii) parameters $\kappa_{n,\alpha_1,\ldots,\alpha_d,j}$ obtained from the QNF expansion procedure, (iii) an effective (scaled) Planck's constant $\hbar_{\text{eff}}$, which in atomic units is given by the inverse of the square root of the reduced mass of the system and plays the role of a "small parameter," (iv) an action integral operator

$$\hat{I} = \frac{1}{2}\left(\hat{q}_1\hat{p}_1 + \hat{p}_1\hat{q}_1\right) \tag{24}$$

corresponding to the reactive mode, and (v) action integral operators

$$\hat{J}_k = \frac{1}{2}\left(\hat{q}_k^2 + \hat{p}_k^2\right), \qquad k = 2,\ldots, d, \tag{25}$$

of the bath modes. Here, the "position" and "momentum" operators, $\hat{q}_k$ and $\hat{p}_k$ respectively, satisfy the commutation relations

$$[\hat{q}_k, \hat{q}_l] = [\hat{p}_k, \hat{p}_l] = 0, \qquad [\hat{q}_k, \hat{p}_l] = i\hbar_{\text{eff}}\,\delta_{kl}, \tag{26}$$

where $k,l = 1,\ldots,d$, and δ_{kl} is the Kronecker's delta. The operators $\hat{q}_1, \hat{p}_1, \ldots,$ $\hat{q}_d, \hat{p}_d$ are given by the Weyl quantization of classical phase space coordinates $q_1, p_1, \ldots, q_d, p_d$ that in turn are obtained from the original "physical" phase space coordinates by way of a nonlinear canonical transformation [30]. Thus, $\hat{q}_1$ and $\hat{p}_1$ correspond to the reaction coordinate, while $\hat{q}_k$ and $\hat{p}_k$ correspond to the kth bath mode with $k = 2,\ldots, d$.

It sometimes proves convenient to work in a phase space coordinate basis $(Q_1, P_1, q_2, p_2, \ldots, q_d, p_d)$ (which we further refer as to "QP-basis") that is "rotated" at an angle $\pi/4$ with respect to the basis $(q_1, p_1, q_2, p_2, \ldots, q_d, p_d)$ (further referred as to "qp-basis"), i.e.,

$$\hat{Q}_1 = \frac{1}{\sqrt{2}}\left(\hat{q}_1 - \hat{p}_1\right), \qquad \hat{P}_1 = \frac{1}{\sqrt{2}}\left(\hat{q}_1 + \hat{p}_1\right). \tag{27}$$

In the QP-basis, the action integral operator corresponding to the reaction coordinate reads

$$\hat{I} = \frac{1}{2}\left(\hat{P}_1^2 - \hat{Q}_1^2\right). \tag{28}$$

The main advantage of having the original Hamiltonian $\hat{H}$ approximated by a polynomial in the operators $\hat{I}$ and $\hat{J}_k$, $k = 2,\ldots, d$, is that the eigenstates of

the QNF operator $\hat{H}^{(N)}_{\text{QNF}}$ can be chosen to be simultaneously the eigenstates of the operators $\hat{I}$ and $\hat{J}_k$, whose spectral properties are well known. Indeed,

$$\hat{H}^{(N)}_{\text{QNF}}|I, n_2, \ldots, n_d\rangle = E|I, n_2, \ldots, n_d\rangle \tag{29}$$

with

$$|I, n_2, \ldots, n_d\rangle = |\psi_I\rangle \otimes |\psi_{n_2}\rangle \otimes \cdots \otimes |\psi_{n_d}\rangle, \tag{30}$$

where

$$\hat{I}|\psi_I\rangle = I|\psi_I\rangle, \qquad\qquad I \in \mathbb{R}, \tag{31a}$$

$$\hat{J}_k|\psi_{n_k}\rangle = \hbar_{\text{eff}}(n_k + 1/2)|\psi_{n_k}\rangle, \qquad n_k \in \mathbb{N}_0, \tag{31b}$$

and

$$E = K^{(N)}_{\text{QNF}}\Big(I, \hbar_{\text{eff}}(n_2 + 1/2), \ldots, \hbar_{\text{eff}}(n_d + 1/2)\Big). \tag{32}$$

And, after having explicitly described the eigenstates $|\psi_I\rangle$ and $|\psi_{n_k}\rangle$ of the reaction and bath DoFs, respectively, one obtains a complete (approximate) eigensystem for the original reactive scattering problem.

Two independent solutions of Eq. (31a), in the q_1 representation, are given by

$$\langle q_1|\psi_I^{(o,r)}\rangle = \Theta(-q_1)(-q_1)^{-1/2+iI/\hbar_{\text{eff}}}, \tag{33a}$$

$$\langle q_1|\psi_I^{(o,p)}\rangle = \Theta(q_1)q_1^{-1/2+iI/\hbar_{\text{eff}}}, \tag{33b}$$

where Θ is the Heaviside step function, the superscript "o" stands for "outgoing to," and "r" and "p" stand for "reactants" and "products," respectively. The motivation for this notation is clear from viewing the solutions given by Eq. (31) as Lagrangian states, i.e., by writing

$$\langle q_1|\psi_I^{(o,r/p)}\rangle = A_I^{(o,r/p)}(q_1) \exp\left(\frac{i}{\hbar_{\text{eff}}}\varphi_I^{(o,r/p)}(q_1)\right), \tag{34}$$

where the purely real amplitude and phase functions are given by

$$A_I^{(o,r/p)}(q_1) = \Theta(\mp q_1)|q_1|^{-1/2}, \qquad \varphi_I^{(o,r/p)}(q_1) = I\ln|q_1|, \tag{35}$$

respectively. This way one can associate the one-dimensional Lagrangian manifolds

$$\Lambda_I^{(o,\,r)} = \left\{ (q_1, p_1) = \left(q_1, \frac{\mathrm{d}}{\mathrm{d}q_1} \varphi_I^{(o,\,r)}(q_1) \right) = \left(q_1, \frac{I}{q_1} \right) : q_1 < 0 \right\}, \tag{36a}$$

$$\Lambda_I^{(o,\,p)} = \left\{ (q_1, p_1) = \left(q_1, \frac{\mathrm{d}}{\mathrm{d}q_1} \varphi_I^{(o,\,p)}(q_1) \right) = \left(q_1, \frac{I}{q_1} \right) : q_1 > 0 \right\} \tag{36b}$$

with the states $|\psi_I^{(o,r)}\rangle$ and $|\psi_I^{(o,p)}\rangle$. From the presentation of $\Lambda_I^{(o,r)}$ and $\Lambda_I^{(o,p)}$ in Figure 5.6 one sees that for $q_1 \to -\infty$ the wave function $\langle q_1|\psi_I^{(o,r)}\rangle$ represents a state outgoing to reactants, and for $q_1 \to +\infty$ the wave function $\langle q_1|\psi_I^{(o,p)}\rangle$ represents a state outgoing to products.

Another pair of independent solutions of Eq. (31a), $\langle q_1|\psi_I^{(i,r)}\rangle$ and $\langle q_1|\psi_I^{(i,p)}\rangle$, corresponding to states "incoming from" reactants and products, respectively, is obtained by requiring their momentum representations to be given by

$$\langle p_1|\psi_I^{(i,r)}\rangle = \langle \psi_I^{(o,p)}|q_1\rangle \big|_{q_1=p_1}, \qquad \langle p_1|\psi_I^{(i,p)}\rangle = \langle \psi_I^{(o,r)}|q_1\rangle \big|_{q_1=p_1}. \tag{37}$$

The corresponding position representations are obtained by way of Fourier transform,

$$\langle q_1|\cdot\rangle = \frac{1}{\sqrt{2\pi\,\hbar_{\mathrm{eff}}}} \int e^{iq_1 p_1/\hbar_{\mathrm{eff}}} \langle p_1|\cdot\rangle \,\mathrm{d}p_1, \tag{38}$$
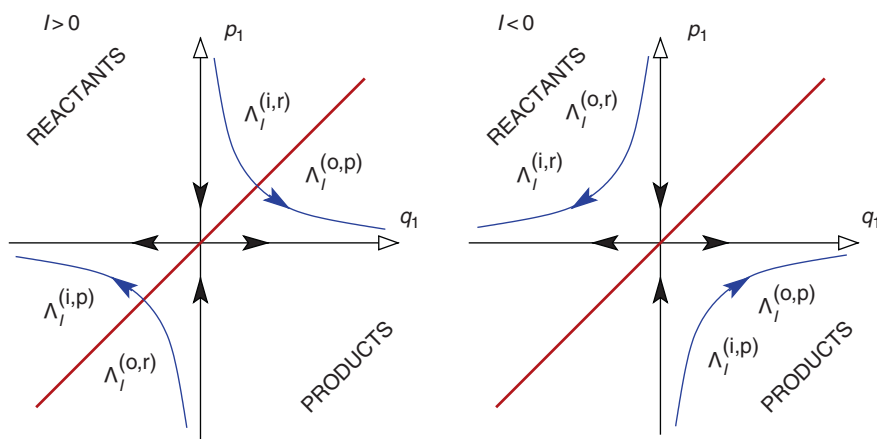
Figure 5.6 The blue lines show the Lagrangian manifolds $\Lambda_I^{(i,r)}$, $\Lambda_I^{(i,p)}$, $\Lambda_I^{(o,r)}$, and $\Lambda_I^{(o,p)}$ associated with the $\hat{I}$ eigenstates $|\psi_I^{(i,r)}\rangle$, $|\psi_I^{(i,p)}\rangle$, $|\psi_I^{(o,r)}\rangle$, and $|\psi_I^{(o,p)}\rangle$, respectively. The arrows indicate the classical Hamiltonian vector fields generated by $I = p_1 q_1$. The red thick line corresponds to the dividing surface $s(q_1, p_1) = q_1 - p_1$.

of $\langle p_1|\psi_I^{(i,r)}\rangle$ and $\langle p_1|\psi_I^{(i,p)}\rangle$ defined in Eq. (37), namely

$$\langle q_1|\psi_I^{(i,r)}\rangle = \frac{1}{\sqrt{2\pi\hbar_{\text{eff}}}} \int_0^\infty e^{iq_1p_1/\hbar_{\text{eff}}} \, p_1^{-1/2-iI/\hbar_{\text{eff}}} \, \mathrm{d}p_1 \,, \tag{39a}$$

$$\langle q_1|\psi_I^{(i,\,p)}\rangle = \frac{1}{\sqrt{2\pi\hbar_{\text{eff}}}} \int_{-\infty}^0 e^{iq_1p_1/\hbar_{\text{eff}}} \, (-p_1)^{-1/2-iI/\hbar_{\text{eff}}} \, \mathrm{d}p_1 \,. \tag{39b}$$

The integrals in (39) are not absolutely convergent, but can be defined as oscillatory integrals. The motivation for defining incoming states according to Eq. (37) becomes clear from considering the stationary phase contributions to the integrals (39). These come from p_1 satisfying the stationary phase condition

$$\frac{\mathrm{d}}{\mathrm{d}p_1}(-I\ln|p_1| + q_1p_1) = 0\,, \tag{40}$$

i.e., $p_1 = I/q_1$, where $p_1 > 0$ for $\langle q_1|\psi_I^{(i,r)}\rangle$ and $p_1 < 0$ for $\langle q_1|\psi_I^{(i,p)}\rangle$. This way one can associate the Lagrangian manifolds

$$\Lambda_I^{(i,r)} = \left\{(q_1,p_1) = \left(q_1, \frac{I}{q_1}\right) : p_1 > 0\right\},$$

$$\Lambda_I^{(i,p)} = \left\{(q_1,p_1) = \left(q_1, \frac{I}{q_1}\right) : p_1 < 0\right\} \tag{41}$$

with the incoming states. These manifolds are also shown in Figure 5.6. One sees that for $p_1 \to +\infty$ the wave function $\langle q_1|\psi_I^{(i,r)}\rangle$ represents a state incoming from reactants, and for $p_1 \to -\infty$ the wave function $\langle q_1|\psi_I^{(i,p)}\rangle$ represents a state incoming from products. Finally, calculating the Fourier integrals in Eq. (39) [30], one obtains expressions

$$|\psi_I^{(i,r)}\rangle = \frac{e^{i\left(\frac{\pi}{4}-\frac{I}{\hbar_{\text{eff}}}\ln\hbar_{\text{eff}}\right)}}{\sqrt{2\pi}}\Gamma\left(\frac{1}{2}-i\frac{I}{\hbar_{\text{eff}}}\right)\left(e^{\frac{\pi}{2}\frac{I}{\hbar_{\text{eff}}}}|\psi_I^{(o,p)}\rangle - ie^{-\frac{\pi}{2}\frac{I}{\hbar_{\text{eff}}}}|\psi_I^{(o,r)}\rangle\right), \tag{42a}$$

$$|\psi_I^{(i,p)}\rangle = \frac{e^{i\left(\frac{\pi}{4}-\frac{I}{\hbar_{\text{eff}}}\ln\hbar_{\text{eff}}\right)}}{\sqrt{2\pi}}\Gamma\left(\frac{1}{2}-i\frac{I}{\hbar_{\text{eff}}}\right)\left(e^{\frac{\pi}{2}\frac{I}{\hbar_{\text{eff}}}}|\psi_I^{(o,r)}\rangle - ie^{-\frac{\pi}{2}\frac{I}{\hbar_{\text{eff}}}}|\psi_I^{(o,p)}\rangle\right) \tag{42b}$$

that relate the incoming states to the outgoing ones [48].

The equation for eigenstates of the action operator $\hat{I}$, Eq. (31a), can also be solved in the Q_1 representation [49, 50]. The two independent solutions are

$$\langle Q_1|\psi_I^{(\mathrm{i,r})}\rangle = \frac{1}{\pi}(2\hbar_{\mathrm{eff}})^{-\frac{3}{4}}\,e^{\frac{\pi}{4}\frac{I}{\hbar_{\mathrm{eff}}}}\,\Gamma\left(\frac{1}{2}-i\frac{I}{\hbar_{\mathrm{eff}}}\right)D_{-\frac{1}{2}+i\frac{I}{\hbar_{\mathrm{eff}}}}\left(e^{-i\frac{\pi}{4}}\sqrt{\frac{2}{\hbar_{\mathrm{eff}}}}Q_1\right),\quad (43\mathrm{a})$$

$$\langle Q_1|\psi_I^{(\mathrm{i,p})}\rangle = \frac{1}{\pi}(2\hbar_{\mathrm{eff}})^{-\frac{3}{4}}\,e^{\frac{\pi}{4}\frac{I}{\hbar_{\mathrm{eff}}}}\,\Gamma\left(\frac{1}{2}-i\frac{I}{\hbar_{\mathrm{eff}}}\right)D_{-\frac{1}{2}+i\frac{I}{\hbar_{\mathrm{eff}}}}\left(e^{i\frac{3\pi}{4}}\sqrt{\frac{2}{\hbar_{\mathrm{eff}}}}Q_1\right),\quad (43\mathrm{b})$$

where D_ν is the parabolic cylinder function of order ν [51]. The outgoing states, $|\psi_I^{(\mathrm{o,r})}\rangle$ and $|\psi_I^{(\mathrm{o,p})}\rangle$, are then obtained from Eq. (42). Figure 5.7 shows the Lagrangian manifolds $\Lambda_I^{(\mathrm{i,r})}$, $\Lambda_I^{(\mathrm{i,p})}$, $\Lambda_I^{(\mathrm{o,r})}$, and $\Lambda_I^{(\mathrm{o,p})}$ in the (Q_1, P_1) coordinates.

Finally, we note that the incoming and outgoing eigenstates of the $\hat{I}$ operator are orthogonal and satisfy the completeness relations [49, 50]

$$\int_{\mathbb{R}}\left(|\psi_I^{(\mathrm{i,r})}\rangle\langle\psi_I^{(\mathrm{i,r})}| + |\psi_I^{(\mathrm{i,p})}\rangle\langle\psi_I^{(\mathrm{i,p})}|\right)\mathrm{d}I = \hat{\mathbb{1}}\,,\qquad (44\mathrm{a})$$

$$\int_{\mathbb{R}}\left(|\psi_I^{(\mathrm{o,r})}\rangle\langle\psi_I^{(\mathrm{o,r})}| + |\psi_I^{(\mathrm{o,p})}\rangle\langle\psi_I^{(\mathrm{o,p})}|\right)\mathrm{d}I = \hat{\mathbb{1}}\,,\qquad (44\mathrm{b})$$

where $\hat{\mathbb{1}}$ stands for the identity operator.

Generally speaking, the q_1 and Q_1 representations of the eigenstates of the $\hat{I}$ operator are completely equivalent, and the choice of a representation is
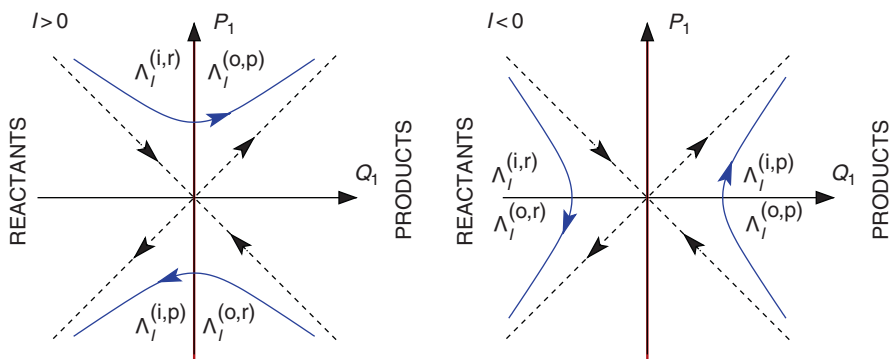
Figure 5.7   The blue lines show the Lagrangian manifolds $\Lambda_I^{(\mathrm{i,r})}$, $\Lambda_I^{(\mathrm{i,p})}$, $\Lambda_I^{(\mathrm{o,r})}$, and $\Lambda_I^{(\mathrm{o,p})}$ associated with the $\hat{I}$ eigenstates $|\psi_I^{(\mathrm{i,r})}\rangle$, $|\psi_I^{(\mathrm{i,p})}\rangle$, $|\psi_I^{(\mathrm{o,r})}\rangle$, and $|\psi_I^{(\mathrm{o,p})}\rangle$, respectively. The arrows indicate the classical Hamiltonian vector fields generated by $I = (P_1^2 - Q_1^2)/2$. The red thick line corresponds to the dividing surface $s(Q_1, P_1) = Q_1 = 0$.

usually dictated by a particular problem. For example, in order to determine the total probability flux corresponding to the eigenstates $|\psi_I^{(i,r/p)}\rangle$ through the dividing surface it is convenient to adopt the Q_1 representation. Indeed, in the QP-basis the operator corresponding to the flux through the dividing surface $s(Q_1, P_1) = Q_1$ is [30]

$$\hat{F} = \frac{i}{\hbar_{\text{eff}}}[\hat{I}, \Theta(\hat{Q}_1)] = \frac{1}{2}\left(\hat{P}_1\delta(\hat{Q}_1) + \delta(\hat{Q}_1)\hat{P}_1\right).\tag{45}$$

Thus, the expectation value of $\hat{F}$ with respect to the incoming states is given by

$$\langle\psi_I^{(i,r/p)}|\hat{F}|\psi_I^{(i,r/p)}\rangle = \hbar_{\text{eff}}\,\text{Im}\left(\langle\psi_I^{(i,r/p)}|Q_1\rangle\frac{\mathrm{d}}{\mathrm{d}Q_1}\langle Q_1|\psi_I^{(i,r/p)}\rangle\right)\Bigg|_{Q_1=0}$$

$$= \pm\frac{1}{2\pi\,\hbar_{\text{eff}}}\frac{1}{1 + \exp\left(-2\pi I/\hbar_{\text{eff}}\right)}.\tag{46}$$

The operators $\hat{J}_k$, defined by Eq. (25) and corresponding to the action integrals of the bath modes, are the Hamiltonian operators of one-dimensional harmonic oscillators with unit frequency. Therefore, the wave function representing the eigenstates in Eq. (31b) are given by

$$\langle q_k|\psi_{n_k}\rangle = \frac{1}{\sqrt{2^{n_k}(n_k!)}}\left(\frac{1}{\pi\,\hbar_{\text{eff}}}\right)^{1/4}H_{n_k}\left(\frac{q_k}{\sqrt{\hbar_{\text{eff}}}}\right)\exp\left(-\frac{q_k^2}{2\hbar_{\text{eff}}}\right),\tag{47}$$

where H_n denotes the nth-order Hermite polynomial [51].

Here we note that the QNF Hamiltonian can be interpreted as representing the activated complex. As it has been shown above, the QNF Hamiltonian has only continuous spectrum, and so there are no bound states associated with the activated complex. Physically this corresponds to the fact that the activated complex has a finite lifetime. The latter is determined by the Gamov–Siegert resonances which we discuss in detail in Section 5.

4. THE CUMULATIVE REACTION PROBABILITY

4.1. General formulation

The incoming and outgoing eigenstates of $\hat{I}$ defined in Section 3 are related to one another by Eq. (42). Therefore, each solution $|\psi_I\rangle$ of Eq. (31a) can be written as a linear combination of $|\psi_I^{(o,r/p)}\rangle$ or $|\psi_I^{(i,r/p)}\rangle$:

$$|\psi_I\rangle = \alpha_{\text{p}}|\psi_I^{(o,p)}\rangle + \alpha_{\text{r}}|\psi_I^{(o,r)}\rangle = \beta_{\text{p}}|\psi_I^{(i,p)}\rangle + \beta_{\text{r}}|\psi_I^{(i,r)}\rangle.\tag{48}$$

These representations are connected by the (one-dimensional) S-matrix,

$$\begin{pmatrix} \alpha_p \\ \alpha_r \end{pmatrix} = \mathcal{S}(I) \begin{pmatrix} \beta_p \\ \beta_r \end{pmatrix}. \tag{49}$$

The entries of the S-matrix can be read off directly from Eq. (42) yielding

$$\mathcal{S}(I) = \frac{e^{i\left(\frac{\pi}{4} - \frac{I}{\hbar_{\text{eff}}} \ln \hbar_{\text{eff}}\right)}}{\sqrt{2\pi}} \Gamma\left(\frac{1}{2} - i\frac{I}{\hbar_{\text{eff}}}\right) \begin{pmatrix} -ie^{-\frac{\pi}{2}\frac{I}{\hbar_{\text{eff}}}} & e^{\frac{\pi}{2}\frac{I}{\hbar_{\text{eff}}}} \\ e^{\frac{\pi}{2}\frac{I}{\hbar_{\text{eff}}}} & -ie^{-\frac{\pi}{2}\frac{I}{\hbar_{\text{eff}}}} \end{pmatrix}. \tag{50}$$

Using the relation $\Gamma(1/2 + iy)\Gamma(1/2 - iy) = \pi / \cosh(\pi y)$ it is easy to see that $\mathcal{S}(I)^* \mathcal{S}(I) = \mathbb{1}$ implying that the S-matrix is unitary.

The transmission coefficient corresponding to the scattering matrix $\mathcal{S}(I)$ reads

$$\mathcal{T}(I) = |\mathcal{S}_{12}(I)|^2 = \frac{e^{\pi \frac{I}{\hbar_{\text{eff}}}}}{e^{\pi \frac{I}{\hbar_{\text{eff}}}} + e^{-\pi \frac{I}{\hbar_{\text{eff}}}}} = \frac{1}{1 + e^{-2\pi \frac{I}{\hbar_{\text{eff}}}}} \tag{51}$$

and the reflection coefficient

$$\mathcal{R}(I) = |\mathcal{S}_{11}(I)|^2 = \frac{e^{-\pi \frac{I}{\hbar_{\text{eff}}}}}{e^{\pi \frac{I}{\hbar_{\text{eff}}}} + e^{-\pi \frac{I}{\hbar_{\text{eff}}}}} = \frac{1}{1 + e^{2\pi \frac{I}{\hbar_{\text{eff}}}}}. \tag{52}$$

As required, one has $\mathcal{T}(I) + \mathcal{R}(I) = 1$. The characteristic action scale is given by the effective Planck's constant: $\mathcal{T}$ tends to 1 if $I \gg \hbar_{\text{eff}}$ and to 0 if $I \ll -\hbar_{\text{eff}}$.

In accordance with Eqs. (30 and 31), the incoming and outgoing scattering states of the d-dimensional reactive system at energy E are given by

$$|\Psi^{(i,r/p)}\rangle = |\psi_I^{(i,r/p)}\rangle \otimes |\psi_{\mathbf{n}}\rangle, \tag{53a}$$

$$|\Psi^{(o,r/p)}\rangle = |\psi_I^{(o,r/p)}\rangle \otimes |\psi_{\mathbf{n}}\rangle, \tag{53b}$$

where $\mathbf{n} = (n_2, \ldots, n_d) \in \mathbb{N}_0^{d-1}$ is a $(d-1)$-dimensional vector of scattering quantum numbers, and

$$|\psi_{\mathbf{n}}\rangle = |\psi_{n_2}\rangle \otimes \cdots \otimes |\psi_{n_d}\rangle \tag{54}$$

are the eigenstates of a $(d-1)$-dimensional harmonic oscillator corresponding to the bath modes. Here, I and $\mathbf{n}$ are not independent, but related by Eq. (32). For energies E close to the equilibrium point energy E_0 this equation can be resolved for the reactive coordinate action, yielding a single-valued function $I = I_{\mathbf{n}}(E)$. Then, the S-matrix connecting the scattering states $|\Psi^{(i,r/p)}\rangle$ and $|\Psi^{(o,r/p)}\rangle$ is block-diagonal and given by

$$S_{\mathbf{n},\mathbf{m}}(E) = \delta_{\mathbf{n},\mathbf{m}} \mathcal{S}(I_{\mathbf{n}}(E)), \tag{55}$$

where $\delta_{\mathbf{n},\mathbf{m}}$ is the multidimensional Kronecker symbol, and $\mathcal{S}(I)$ is given by Eq. (50).

The transmission matrix T can be defined as a diagonal matrix with the diagonal elements equal to the modulus squared of the (1, 2)-components of the matrices $\mathcal{S}(I)$ in Eq. (55), i.e.,

$$T_{\mathbf{n},\mathbf{m}}(E) = \delta_{\mathbf{n},\mathbf{m}} \left| \mathcal{S}_{1,2}(I_{\mathbf{n}}(E)) \right|^2 = \delta_{\mathbf{n},\mathbf{m}} \left[1 + \exp\left(-2\pi \frac{I_{\mathbf{n}}(E)}{\hbar_{\mathrm{eff}}} \right) \right]^{-1}. \tag{56}$$

The CRP $\mathcal{N}(E)$ is then defined as (see, e.g., Ref. [4])

$$\mathcal{N}(E) = \mathrm{Tr}\left\{ T(E) \right\}, \tag{57}$$

where Tr stands for the trace. Thus, using Eq. (56) one obtains

$$\mathcal{N}(E) = \sum_{\mathbf{n}} T_{\mathbf{n},\mathbf{n}}(E) = \sum_{\mathbf{n}} \left[1 + \exp\left(-2\pi \frac{I_{\mathbf{n}}(E)}{\hbar_{\mathrm{eff}}} \right) \right]^{-1}. \tag{58}$$

The CRP $\mathcal{N}(E)$ is the quantum analogue of the classical flux $f(E)$ through the dividing surface or, more precisely, of the dimensionless quantity $f(E)/(2\pi\hbar_{\mathrm{eff}})^{d-1}$. To see this one should consider $\mathcal{N}(E)$ in the semiclassical limit $\hbar_{\mathrm{eff}} \to 0$, where

$$\lim_{\hbar_{\mathrm{eff}} \to 0} \left[1 + \exp\left(-2\pi I/\hbar_{\mathrm{eff}} \right) \right]^{-1} = \Theta(I), \tag{59}$$

where Θ is the Heaviside function. This means that the transmission coefficients $T_{\mathbf{n},\mathbf{n}}(E)$ in Eq. (58) are characteristic functions, i.e., in the semiclassical limit, $T_{\mathbf{n},\mathbf{n}}(E)$ is 0 or 1 if $I_{\mathbf{n}}(E)$ is negative or positive, respectively. This way the CRP can be considered to be a counting function. For a given energy E, it counts how many of the solutions $I_{\mathbf{n}}$ of the equations $K_{\mathrm{QNF}}(I_{\mathbf{n}}, \hbar_{\mathrm{eff}}(n_2+1/2), \ldots, \hbar_{\mathrm{eff}}(n_d+1/2)) = E$ with scattering quantum numbers $\mathbf{n} = (n_2, \ldots, n_d) \in \mathbb{N}_0^{d-1}$ are positive. In other words, $\mathcal{N}(E)$ can be considered to count the number of open "transmission channels," where a transmission channel with quantum numbers $\mathbf{n}$ is open if the corresponding transmission coefficient $T_{\mathbf{n},\mathbf{n}}(E)$ is close to 1.

Graphically $\mathcal{N}(E)$ can be interpreted as the number of grid points $(\hbar_{\mathrm{eff}}(n_2+1/2), \ldots, \hbar_{\mathrm{eff}}(n_d + 1/2))$ in the space of action integrals $(J_2, \ldots, J_d) \in [0,\infty)^{d-1}$ that are enclosed by the contour $K_{\mathrm{QNF}}(0, J_2, \ldots, J_d) = E$, see Figure 5.8. The number of grid points is approximately given by the volume in the space of $(J_2, \ldots, J_d) \in [0,\infty)^{d-1}$ enclosed by $K_{\mathrm{QNF}}(0, J_2, \ldots, J_d) = E$ divided by $\hbar_{\mathrm{eff}}^{d-1}$. Using the fact that for $\hbar_{\mathrm{eff}} \to 0$, K_{QNF} becomes the function K_{CNF} which gives the classical energy as a function of the classical integrals $(I, J_2, \ldots, J_d)$ we find
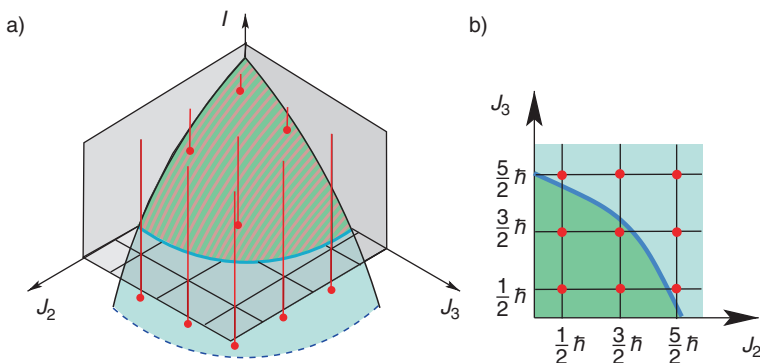
Figure 5.8 (a) Lines $(I, \hbar_{\mathrm{eff}}(n_2 + 1/2), \ldots, \hbar_{\mathrm{eff}}(n_d + 1/2))$, $I \in \mathbb{R}$, $n_k \in \mathbb{N}_0$, $k = 2, \ldots, d$, in the space $(I, J_2, \ldots, J_d) \in \mathbb{R} \times [0, \infty)^{d-1}$ for $d = 3$ and their intersections with the surface $K_{\mathrm{QNF}}(I, J_2, J_3) = E$. (b) Grid points $(\hbar_{\mathrm{eff}}(n_2 + 1/2), \ldots, \hbar_{\mathrm{eff}}(n_d + 1/2))$ in the space $(J_2, \ldots, J_d)$ for $d = 3$. The blue line marks the contour $K_{\mathrm{QNF}}(0, J_2, \ldots, J_d) = E$. In this plot only the scattering states for which the quantum numbers (n_2, n_3) have the values $(0, 0)$, $(0, 1)$, $(1, 0)$, or $(1, 1)$ correspond to "open transmission channels," see text.

that the volume in the space of $(J_2, \ldots, J_d)$ enclosed by $K_{\mathrm{CNF}}(0, J_2, \ldots, J_d) = E$ is given by the classical flux $f(E)$ divided by $(2\pi)^{d-1}$, see Eq. (20), and the CRP $\mathcal{N}(E)$ is thus approximately given by $\mathcal{N}_{\mathrm{Weyl}}(E) = f(E)/(2\pi\hbar)^{d-1}$ defined in Eq. (21). This way we verify our statement in Section 2.4 that $\mathcal{N}_{\mathrm{Weyl}}(E)$ gives the mean number of open transmission channels. In fact, as mentioned in Section 2.4, the classical flux $f(E)$ can be considered to be the phase space volume enclosed by the energy contour of energy E of the invariant subsystem which has one DoF less than the full scattering system and which as the so-called activated complex is located between reactants and products. $\mathcal{N}_{\mathrm{Weyl}}(E)$ counts how many elementary quantum cells of volume $(2\pi\hbar_{\mathrm{eff}})^{d-1}$ fit into this phase space volume and this way gives the Weyl approximation of the CRP $\mathcal{N}(E)$.

It is important to note here that like the flux in the classical case the CRP is determined by local properties of the Hamilton operator $\hat{H}$ in the neighborhood of the equilibrium point only.

4.2. Nitrogen exchange reaction

In this section we focus on the QNF theory as a tool for the computation of the CRP and the thermal reaction rate constant. To demonstrate the efficiency and capability of the QNF method and to compare it with other existing methods we follow Ref. [31] and address the CRP and the thermal rate in a collinear triatomic reaction, namely the nitrogen exchange reaction

$$\mathrm{N} + \mathrm{N}_2 \rightarrow \mathrm{N}_2 + \mathrm{N}. \tag{60}$$

The collinear version of Eq. (60) corresponds to a two DoF reactive system with the Hamiltonian operator of the form

$$\hat{H} \equiv H(\hat{\tilde{q}}_1, \hat{\tilde{q}}_2, \hat{\tilde{p}}_1, \hat{\tilde{p}}_2) = \frac{1}{2}\left(\hat{\tilde{p}}_1^2 + \hat{\tilde{p}}_2^2\right) + V(\hat{\tilde{q}}_1, \hat{\tilde{q}}_2),\tag{61}$$

where $V(\tilde{q}_1, \tilde{q}_2)$ gives the Born–Oppenheimer potential energy surface, and $\tilde{q}_1$ and $\tilde{q}_2$ are the Delves mass-scaled coordinates [52]. The effective Planck's constant is given by $\hbar_{\text{eff}} = \mu^{-1/2}$, where μ is the dimensionless reduced mass of the triatomic system (given in units of the electronic mass). For the case of the nitrogen exchange reaction $\mu \approx 1.47 \times 10^4$ yielding $\hbar_{\text{eff}} \approx 8.2 \times 10^{-3}$. We further adopt the London–Eyring–Polanyi–Sato potential energy surface [53] that possesses a single saddle point governing the reaction from the asymptotic reactant and product states.

Following the algorithmic procedure presented in Section 3 and Appendix A we compute the Nth order approximation

$$\hat{H}_{\text{QNF}}^{(N)} = K_{\text{QNF}}^{(N)}(\hat{I}, \hat{J}_2)\tag{62}$$

of the original Hamiltonian operator $\hat{H}$. The CRP is then given by

$$\mathcal{N}(E) = \sum_{n_2=0}^{\infty}\left[1 + \exp\left(-2\pi\frac{I_{n_2}(E)}{\hbar_{\text{eff}}}\right)\right]^{-1}\tag{63}$$

with $I_{n_2}(E)$ solving

$$K_{\text{QNF}}^{(N)}\left(I, \hbar_{\text{eff}}(n_2 + 1/2)\right) = E.\tag{64}$$

The resulting CPR-vs-energy curves computed for energies in the range between 1.3 and 1.7 eV are shown in Figure 5.9. The solid color curves (blue, green, and red) correspond to different orders N of the QNF approximation (2, 4, and 6, respectively). The $\mathcal{N}(E)$ curves obtained with the 4th and 6th order QNF are essentially indistinguishable for most of the energy range; this fact signals the rapid convergence of the QNF expansion for the given value of the effective Planck's constant. The vertical dashed line shows the saddle point energy, E_0, of the London–Eyring–Polanyi–Sato potential energy surface.

The circular data points in Figure 5.9 represent the "exact" value of the CRP obtained through the full *reactive quantum scattering* calculation [54, 55]. The latter were performed by integrating the coupled multichannel Schrödinger equation in hyperspherical coordinates [54, 55] from the strong interaction region to the asymptotic reactant and product configurations. The log-derivative matrix method of Manolopoulos and Gray [56] together with the six-step symplectic integrator of McLachlan and Atela [57] was used to
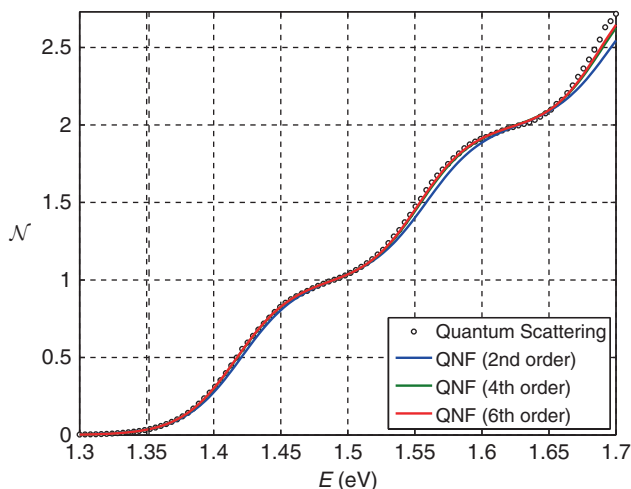
Figure 5.9   CRP as a function of the total energy, $\mathcal{N}(E)$, for the collinear nitrogen exchange reaction (60). The effective Planck's constant is $\hbar_{eff} \approx 8.2 \times 10^{-3}$. The $\mathcal{N}(E)$ curves obtained with the 4th and 6th order QNF are essentially indistinguishable for most of the energy range. The vertical dashed line shows the saddle point energy, E_0.

integrate the radial Schrödinger equation. It is evident from Figure 5.9 that the quantitative agreement of the exact and QNF values of $\mathcal{N}(E)$ well extends up to energies of 1.5 eV.[8]

We finally note that the QNF calculation of the CRP requires significantly less computational time than the corresponding full quantum reactive scattering calculation. For example, the 6th order QNF computation of the nitrogen exchange CRP curve in Figure 5.9 took about 10 min on a 2.6 GHz processor, 2 GB RAM computer, while the corresponding full quantum reactive scattering computation took more than 12 h on the same machine. The QNF approach becomes even more advantageous for treating chemical systems of atoms heavier than nitrogen: the expense of the full quantum computations rapidly grows with the number of asymptotic channels (and, therefore, with mass) [58], while the QNF expansion only becomes more rapidly convergent making the corresponding analysis computationally cheaper.

---

[8] It is interesting to note that the QNF curves in Figure 5.9 seem to converge to a result that slightly differs from the exact CRP curve at high energies: a small discrepancy starts to show up at energies around 1.5 eV and becomes more pronounced at energies above 1.65 eV. This discrepancy may be attributed to the growing importance of corner-cutting tunneling at high energies. We discuss the phenomenon of the corner-cutting tunneling in relation to the normal form theory in Section 6.1.

We now discuss the straightforward extension of the QNF approach to computation of the thermal reaction rate constant, $k(T)$, defined as [59]

$$k(T) = \frac{1}{2\pi Q_\mathrm{r}(T)} \int_0^\infty dE \exp\left(-\frac{E}{k_\mathrm{B}T}\right) \mathcal{N}(E), \tag{65}$$

where T stands for the absolute temperature, $Q_\mathrm{r}(T)$ is the partition function of the reactant, and k_B is the Boltzmann constant. To this end, we use the CRP data for the nitrogen exchange reaction, Eq. (60), presented in Figure 5.9. The data allow us to compute $k(T)$ in the range of temperatures between 600 and 700 K, for which the integrand in the right-hand side of Eq. (65) is well localized to the energy interval between 1.3 and 1.7 eV. Figure 5.10 provides a comparison of $k(T)$ calculated from $\mathcal{N}(E)$ obtained using the QNF of orders 2, 4, 6 (color solid lines) and the "exact," reactive quantum scattering technique (black line with circles). The inset in the figure shows the ratio, $k_\mathrm{QNF}/k_\mathrm{QS}$, of the thermal rate computed using the QNF of orders 2, 4, 6 to the one obtained
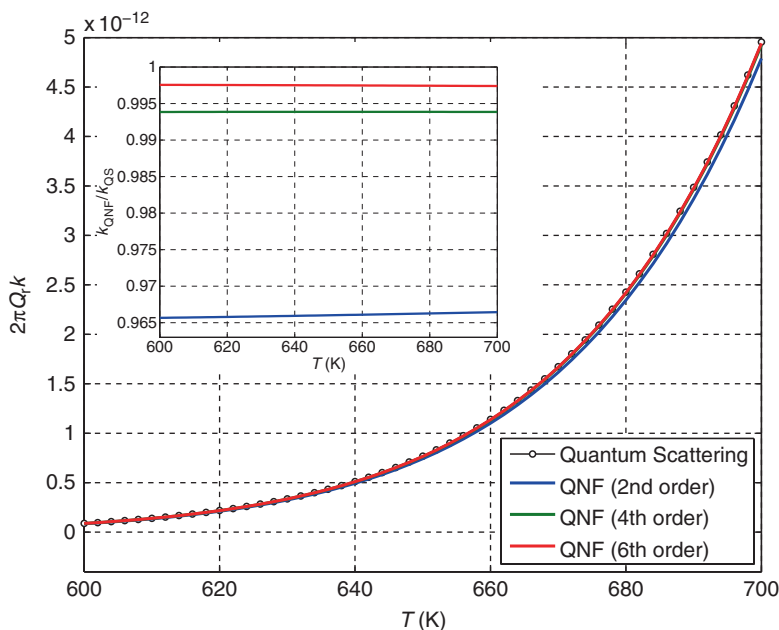
Figure 5.10 The thermal rate constant (multiplied by the reactant partition function) as a function of temperature for the collinear nitrogen exchange reaction (60). The curves obtained with the 4th and 6th order QNF are essentially indistinguishable for most of the energy range. The inset shows the ratio, $k_\mathrm{QNF}/k_\mathrm{QS}$, of the thermal rate constant computed using the QNF of orders 2, 4, 6 to the one obtained from the quantum scattering data.

from the quantum scattering data. One can clearly see that the thermal rate constant computed with the QNF method rapidly approaches its exact value as the approximation order N is increased.

4.3. A three degree-of-freedom reactive system

In order to illustrate the utility of the QNF technique for the computation of reaction rates in higher dimensional systems we consider a three DoF model system consisting of an Eckart barrier in the (physical) $\tilde{q}_1$ direction that is coupled to Morse oscillators in the $\tilde{q}_2$ direction and in the $\tilde{q}_3$ direction. The Hamiltonian operator is

$$\hat{H} = \frac{1}{2}(\hat{p}_1^2 + \hat{p}_2^2 + \hat{p}_3^2) + V_{\mathrm{E}}(\hat{\tilde{q}}_1) + V_{\mathrm{M;2}}(\hat{\tilde{q}}_2) + V_{\mathrm{M;3}}(\hat{\tilde{q}}_3) + \epsilon \hat{H}_c. \tag{66}$$

Here,

$$V_{\mathrm{E}}(q) = A\frac{\exp\left((q + q_0)/a\right)}{1 + \exp\left((q + q_0)/a\right)} + B\frac{\exp\left((q + q_0)/a\right)}{[1 + \exp\left((q + q_0)/a\right)]^2}, \tag{67}$$

with positive real parameters a, A, and B, and

$$q_0 = a\ln\frac{B + A}{B - A} \tag{68}$$

is the Eckart potential. For $B > A \geq 0$ it possesses a maximum at $q = 0$; the potential value at the maximum is $V_{\mathrm{E}}(0) = (A + B)^2/(4B)$. The Morse potentials, given by

$$V_{\mathrm{M;}k}(q) = D_{e;k}\left[\exp\left(-2a_{\mathrm{M;}k}\,q\right) - 2\exp\left(-a_{\mathrm{M;}k}\,q\right)\right], \tag{69}$$

are parameterized by $D_{e;k}$ and $a_{\mathrm{M;}k}$, for $k = 2,3$, respectively. For $\hat{H}_c$ we choose the mutual kinetic coupling

$$\hat{H}_c = \hat{p}_1\,\hat{p}_2 + \hat{p}_2\,\hat{p}_3 + \hat{p}_3\,\hat{p}_1. \tag{70}$$

The strength of the coupling is controlled by the parameter ϵ in Eq. (66). The vector field generated by the corresponding classical Hamilton function has an equilibrium point at $(\tilde{q}_1, \tilde{q}_2, \tilde{q}_3, \tilde{p}_1, \tilde{p}_2, \tilde{p}_3) = 0$. For $|\epsilon|$ sufficiently small (for given values of parameters of the Eckart and Morse potentials), the equilibrium point is of saddle–center–center stability type.

In the uncoupled case, $\epsilon = 0$, it is easy to calculate the exact CRP, $\mathcal{N}_{\mathrm{exact}}(E)$, of the Eckart–Morse–Morse system analytically. Indeed, in accordance with Eq. (58),

$$\mathcal{N}_{\mathrm{exact}}(E) = \sum_{n_2=0}^{\infty}\sum_{n_3=0}^{\infty}T_{\mathrm{exact}}\left(E - E_{\mathrm{M;2},n_2} - E_{\mathrm{M;3},n_3}\right), \tag{71}$$

where T_{exact} denotes the exact transmission coefficient for the Eckart barrier and is given by [60]

$$T_{\text{exact}}(E) = 1 - \frac{\cosh(2\pi(\alpha - \beta)) + \cosh(2\pi\delta)}{\cosh(2\pi(\alpha + \beta)) + \cosh(2\pi\delta)}, \tag{72}$$

with

$$\alpha = \frac{1}{2}\sqrt{\frac{E}{C}}, \quad \beta = \frac{1}{2}\sqrt{\frac{E - A}{C}}, \quad \delta = \frac{1}{2}\sqrt{\frac{B - C}{C}}, \quad C = \frac{\hbar_{\text{eff}}^2}{8a^2}. \tag{73}$$

In Eq. (71), $E_{M;k,n_k}$ (with $k = 2,3$) are the energy levels of the one-dimensional Morse oscillators,
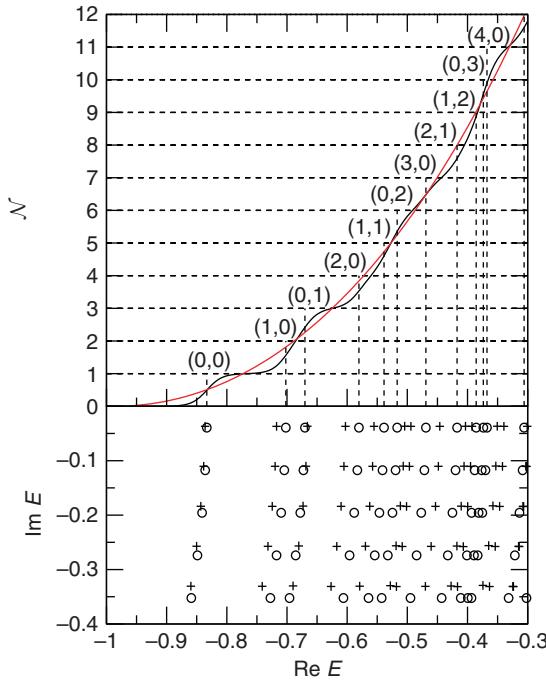
Figure 5.11 The top panel shows the cumulative reaction probabilities $\mathcal{N}_{\text{exact}}(E)$ (black oscillatory curve) and $\mathcal{N}_{\text{Weyl}}(E)$ (red smooth curve) for the Eckart–Morse–Morse reactive system with the Hamiltonian given by Eq. (66) with $\epsilon = 0$. It also shows the quantum numbers (n_2, n_3) of the Morse oscillators that contribute to the quantization steps. The bottom panel shows the resonances in the complex energy plane marked by circles for the uncoupled case $\epsilon = 0$ and by crosses for the strongly coupled case $\epsilon = 0.3$. The parameters for the Eckart potential are $a = 1$, $A = 0.5$, and $B = 5$. The parameters for the Morse potential are $D_{e;2} = 1$, $D_{e;3} = 1.5$, and $a_{M;2} = a_{M;3} = 1$. Also, $\hbar_{\text{eff}} = 0.1$.

$$E_{M;k,n_k} = -\frac{1}{2}a_{M;k}^2\, \hbar_{\text{eff}}^2 \left(n_k + \frac{1}{2} - \frac{\sqrt{2D_{e;k}}}{a_{M;k}\,\hbar_{\text{eff}}} \right)^2, \qquad n_k = 0, 1, 2, \ldots . \tag{74}$$

The graph of $\mathcal{N}_{\text{exact}}(E)$, obtained from Eqs. (71–74), is shown by the black oscillatory curve in the top panel of Figure 5.11. Here, the parameters for the Eckart potential are $a = 1$, $A = 0.5$, and $B = 5$; the parameters for the Morse potential are $D_{e;2} = 1$, $D_{e;3} = 1.5$, and $a_{M;2} = a_{M;3} = 1$; and the effective Planck's constant $\hbar_{\text{eff}} = 0.1$.

The QNF computation of the CRP for the Eckart–Morse–Morse system gives

$$\mathcal{N}_{\text{QNF}}(E) = \sum_{n_2=0}^{\infty}\sum_{n_3=0}^{\infty} \left[1 + \exp\left(-2\pi \frac{I_{n_2,n_3}(E)}{\hbar_{\text{eff}}} \right) \right]^{-1}, \tag{75}$$

with $I_{n_2,n_3}(E)$ solving

$$K_{\text{QNF}}^{(N)}\big(I, \hbar_{\text{eff}}(n_2 + 1/2), \hbar_{\text{eff}}(n_3 + 1/2)\big) = E . \tag{76}$$

The high quality of the QNF approximation of the CRP is illustrated in Figure 5.12, which shows $|\mathcal{N}_{\text{QNF}} - \mathcal{N}_{\text{exact}}|$ as a function of the energy E for different order N of the QNF. It is evident that the CRP computed with the QNF method rapidly approaches its exact value as the approximation order is increased.
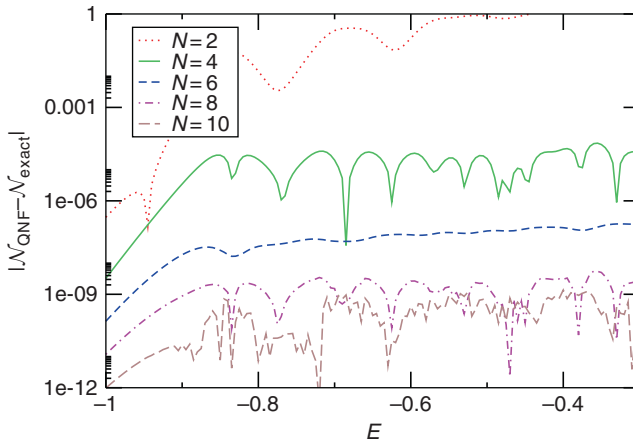
Figure 5.12 Errors $|\mathcal{N}_{\text{QNF}} - \mathcal{N}_{\text{exact}}|$ for the CRP as a function of energy E of the Eckart–Morse–Morse system for different order N of the QNF.

5. GAMOV–SIEGERT RESONANCES

As we have discussed in Section 2 in classical mechanics the transition state is represented by a lower dimensional invariant subsystem, the center manifold. In the quantum world, due to Heisenberg's uncertainty principle, we cannot localize quantum states entirely on the center manifold, so there cannot be any invariant quantum subsystem representing the transition states. Instead we expect a finite lifetime for the transition state. The lifetime of the transition state is determined by the Gamov–Siegert resonances, whose importance in the theory of reaction rates has been emphasized in the literature [61, 62].

Intuitively, a resonance is a complex eigenvalue of a Hamiltonian,

$$\hat{H}|\psi_{\text{res}}\rangle = E|\psi_{\text{res}}\rangle, \tag{77}$$

where the imaginary part has to satisfy $\text{Im} \, E \leq 0$. The time evolution of a resonance state is

$$|\psi_{\text{res}}(t)\rangle = e^{-iEt/\hbar_{\text{eff}}}|\psi_{\text{res}}\rangle = e^{-\text{Im} \, Et/\hbar_{\text{eff}}} e^{-i\,\text{Re} \, Et/\hbar_{\text{eff}}}|\psi_{\text{res}}\rangle,$$

and so we see that a resonance state decays in time with lifetime given by

$$T = \frac{\hbar_{\text{eff}}}{|\text{Im} \, E|}.$$

Notice that since $\hat{H}$ is self-adjoint, a resonant state with complex energy cannot be square integrable.

In order to see how the resonances can be computed from the QNF Hamiltonian, consider first the example of a one-dimensional system described by the Hamilton operator

$$\hat{I} = \frac{1}{2}(\hat{q}\hat{p} + \hat{p}\hat{q}). \tag{78}$$

We easily see that $|n\rangle$ defined by $\langle q|n\rangle = q^n$ is a resonance eigenstate

$$\hat{I}|n\rangle = -i\hbar_{\text{eff}}(n + 1/2)|n\rangle, \tag{79}$$

with complex eigenvalue

$$E_n = -i\hbar_{\text{eff}}(n + 1/2), \quad n = 0, \dots, N. \tag{80}$$

These are the resonances of the operator $\hat{I}$. Notice that compared to the scattering states $|I\rangle$ which depend on a continuous parameter I, the resonance states are quantized and depend on a discrete parameter $n \in \mathbb{N}_0$. Using this simple example we can now directly determine the resonances and the

corresponding resonance states for a Hamilton operator in QNF $\hat{H}_{\text{QNF}} = K_{\text{QNF}}(\hat{I}, \hat{J}_2, \ldots, \hat{J}_d)$. Let ψ_{n_k} denote the n_k^{th} harmonic oscillator eigenfunction (see Eq. (47)). For $n = (n_1, \ldots, n_d) \in \mathbb{N}_0^d$, set

$$|n_1, n_2, \ldots, n_d\rangle = |n_1\rangle \otimes |\psi_{n_2}\rangle \otimes \cdots \otimes |\psi_{n_d}\rangle, \tag{81}$$

then we have

$$\hat{H}_{\text{QNF}}|n_1, n_2, \ldots, n_d\rangle$$
$$= K_{\text{QNF}}\big(-i\hbar_{\text{eff}}(n_1 + 1/2), \hbar_{\text{eff}}(n_2 + 1/2), \ldots, \hbar_{\text{eff}}(n_d + 1/2)\big)|n_1, n_2, \cdots, n_d\rangle, \tag{82}$$

and so the resonances of $\hat{H}_{\text{QNF}}$ are given by

$$E_{n_1, n_2, \ldots, n_d} = K_{\text{QNF}}\big(-i\hbar_{\text{eff}}(n_1 + 1/2), \hbar_{\text{eff}}(n_2 + 1/2), \ldots, \hbar_{\text{eff}}(n_d + 1/2)\big). \tag{83}$$

The bottom panel of Figure 5.11 shows the resonances in the complex energy plane that have been computed using Eq. (83) for the case of the coupled Eckart–Morse–Morse reactive system discussed in Section 4.3.

The resonances computed from the QNF describe the lifetime of the activated complex. To see this in more detail consider a state localized at time $t = 0$ on the center manifold, i.e., the dependence on the local normal form reaction coordinate q_1 is of the form

$$\langle q_1|\varphi_0\rangle = \frac{1}{(\pi \hbar_{\text{eff}})^{1/4}} e^{-\frac{1}{\hbar_{\text{eff}}} \frac{q_1^2}{2}}, \tag{84}$$

which is a minimal uncertainty state. In the bath coordinates we take the state to be given by harmonic oscillator eigenfunctions ψ_{n_k}, so that

$$|\Psi\rangle = |\varphi_0\rangle \otimes |\psi_{n_2}\rangle \otimes \cdots \otimes |\psi_{n_d}\rangle \tag{85}$$

for some fixed quantum numbers $n_2, \ldots, n_d \in \mathbb{N}_0$. Then, expanding $|\Psi\rangle$ into the basis of Eq. (81) we obtain the time-evolved state

$$|\Psi(t)\rangle = \frac{1}{(\pi \hbar_{\text{eff}})^{1/4}} \sum_{n=0}^{\infty} \frac{1}{n!} \frac{(-1)^n}{(2\hbar_{\text{eff}})^n} e^{-iE_{2n, n_2, \ldots, n_d} t/\hbar_{\text{eff}}} |2n, n_2, \ldots, n_d\rangle. \tag{86}$$

A suitable quantity for measuring the lifetime of a state like (85) is the decay of the autocorrelation function

$$|\langle\Psi|\Psi(t)\rangle|^2. \tag{87}$$

For the Hamiltonian in QNF the overlap reads

$$\langle\Psi|\Psi(t)\rangle = \left(\frac{2}{\pi}\right)^{1/2}\sum_{n=0}^{\infty}\frac{\Gamma(n+1/2)}{n!}(-1)^n e^{-iE_{2n,\,n_2,\,\ldots,\,n_d}t/\hbar_{\text{eff}}}.\tag{88}$$

The leading term in this sum for $t \to \infty$ is given by the smallest resonance with $n = 0$. Hence,

$$|\langle\Psi|\Psi(t)\rangle|^2 \sim 2e^{2\,\text{Im}\,E_{0,\,n_2,\,\ldots,\,n_d}t/\hbar_{\text{eff}}},\tag{89}$$

and this determines the maximal lifetime of a quantum state of the activated complex, i.e., a state initially localized near the classically invariant subsystem given by the center manifold.

For small $\hbar_{\text{eff}}$ the QNF is dominated by its quadratic part and that gives

$$2\,\text{Im}\,E_{0,\,n_2,\,\ldots,\,n_d}/\hbar_{\text{eff}} \approx -\lambda,\tag{90}$$

and therefore for small $\hbar_{\text{eff}}$

$$|\langle\Psi|\Psi(t)\rangle|^2 \sim 2e^{-t\lambda}.\tag{91}$$

Thus, the quantum lifetime of the activated complex is in leading order for small $\hbar_{\text{eff}}$ given by the reciprocal value of the classical Lyapunov exponent associated with the saddle equilibrium point.

6. FURTHER CHALLENGES

6.1. Corner-cutting tunneling

The approach based on normal forms is designed to give an accurate description of the dynamics near the saddle or near the transition state. If the reaction is influenced by processes which avoid the neighborhood of the saddle then the normal form is unlikely to capture them. One such process is corner-cutting tunneling. We want to point out that the results derived from the QNF, like the computation of the S-matrix and CRP, contain tunneling contributions, but these are related to tunneling paths which are close to the saddle. One strength of our approach is that it describes uniformly the transition from energies below the saddle energy, where only tunneling is possible, to energies above the saddle energy.

But there are situations where other tunneling contributions have a large effect. If the reaction path (e.g., the minimum energy path) in configuration space is strongly curved in the regions where it connects reactants and products, then the reactant valley and the product valley can have a small angle relative to each other. In this situation there can be quite short tunneling paths which connect reactants and products and which do not go near the

saddle region. So these tunneling paths "cut the corner." The contribution from such trajectories play an important role, in particular for hydrogen exchange reactions at room temperature and lower [63].

In these situations the normal form approach has to be combined with multidimensional semiclassical tunneling calculations.

6.2. State-to-state reaction rates

It is important to emphasize again that, so far, our approach to quantum reaction dynamics has been local, i.e., it is derived completely from the properties of the QNF that is valid in the neighborhood of the saddle–center-$\cdots$–center equilibrium point. The property of the resulting S-matrix in (55) being block-diagonal reflects the fact that the QNF is integrable in the sense that the basis of scattering states can be chosen in the product form (53). In a different basis the matrix will lose this feature, and phenomena like mode mixing are related to how other incoming and outgoing scattering states are related to this special basis. It is natural to embed the study of this phenomenon in a study of the global dynamics which we will describe in this section. The global formalism is in particular required in order to compute general state-to-state reaction rates.

Let us start by describing the scattering or reaction process in classical mechanics by using Poincaré sections. Recall that a Poincaré section at energy E is given by a smooth hypersurface $\Sigma(E)$ of the energy surface with energy E which is transversal to the flow ($\Sigma(E)$ is allowed to have several components). If we have two such Poincaré sections $\Sigma_1(E)$ and $\Sigma_2(E)$ such that all the flow lines intersecting $\Sigma_1(E)$ intersect at a later time $\Sigma_2(E)$, too, then moving along the flow from $\Sigma_1(E)$ to $\Sigma_2(E)$ defines a Poincaré map

$$P^{(2,1)}(E):\Sigma_1(E) \to \Sigma_2(E). \tag{92}$$

Such Poincaré maps can be composed. If $\Sigma_3(E)$ is another Poincaré section which lies behind $\Sigma_2(E)$ in the sense that the flow lines that intersect $\Sigma_2(E)$ also intersect $\Sigma_3(E)$ at a later time, and if $P^{(3,2)}(E):\Sigma_2(E) \to \Sigma_3(E)$ is the corresponding Poincaré map, then the Poincaré map

$$P^{(3,1)}(E):\Sigma_1(E) \to \Sigma_3(E) \tag{93}$$

is given by

$$P^{(3,1)}(E) = P^{(3,2)}(E) \circ P^{(2,1)}(E). \tag{94}$$

Using this construction we can describe transport through phase space regions by a sequence of maps. Given some Poincaré section $\Sigma_{\text{initial}}(E)$ located in the area of initial points in the reactants region where we prepare the system and a Poincaré section $\Sigma_{\text{final}}(E)$ in the products region where we measure the outcome, a succession of Poincaré maps

$$\Sigma_{\text{initial}}(E) \to \Sigma_1(E) \to \Sigma_2(E) \to \cdots \to \Sigma_{\text{final}}(E) \tag{95}$$

tells us how the initial points are transported through the system.[9]

The advantage of subdividing the flow into a sequence of maps lies in the fact that different regions in phase space might need different techniques to compute the flow. In our case of interest Poincaré sections can be constructed to the products and reactants side of a saddle–center-· · ·–center equilibrium point. The dynamics "across" this equilibrium point can then be described by the normal form while the dynamics between neighborhoods of different saddle points can be obtained from integrating the original equations of motions [47, 65, 66]. Moreover, the phase space structures obtained from the local normal form can be "globalized" following the discussion in Section 2.6.

A similar procedure can be developed in the quantum case. The Poincaré maps

$$P^{(j,\,i)}(E) : \Sigma_i(E) \to \Sigma_j(E) \tag{96}$$

are symplectic maps and as such can be quantized using the theory of Fourier integral operators. The quantizations will be unitary operators which we interpret as local S-matrices,

$$S^{(j,\,i)}(E) : L^2_{\Sigma_i(E)} \to L^2_{\Sigma_j(E)} \ , \tag{97}$$

where $L^2_{\Sigma(E)}$ is a Hilbert space obtained by geometric quantization of $\Sigma(E)$, see, e.g., Ref. [67]. This is similar to the quantization developed in Ref. [68]. As in classical dynamics we can compose these matrices to obtain a global S-matrix

$$S^{(\text{final, initial})}(E) = S^{(\text{final, } n)}(E)S^{(n,\,n-1)}(E) \cdots S^{(1,\,\text{initial})}(E), \tag{98}$$

which tells us how initial states in $L^2_{\Sigma_{\text{initial}}(E)}$ are transformed into final states in $L^2_{\Sigma_{\text{final}}(E)}$. The reasons for introducing this splitting of the S-matrix are the same as in the classical case. We can employ different techniques for computing the S-matrices according to different local properties of the system. Near equilibrium points the dynamics can be described by the QNF we developed in this chapter. Notice that the neighborhoods of the saddle–center-· · ·–center equilibrium points are the regions where we expect quantum effects to be of most importance due to partial reflection at and tunneling through the barriers associated with saddle points. The quantum transport between neighborhoods of different equilibrium points can be described by a standard van Vleck-type formalism using, e.g., *initial value representations* which are very common in theoretical chemistry (see, e.g., Refs. [4, 69]).

---

[9] We here ignore the difficulties involved in constructing global Poincaré sections (see, e.g., Ref. [64]); we assume that the sequence of Poincaré sections (95) is intersected transversally by the trajectories with initial points from a suitable open subset in the reactants region.

6.3. Flux–flux autocorrelation function formalism

In this section we discuss the flux–flux autocorrelation function approach to computation of reaction rates in both classical and quantum theories.

6.3.1. Classical formulation

The directional flux through the dividing surface that determines the classical reaction rate, see Section 2.4, can be written as [4, 8, 9]

$$f(E) = \int_{\mathbb{R}^{2d}} \delta(E - H(z))F(z)P_r(z)\,dz\,. \tag{99}$$

The dynamical meaning of Eq. (99) is as follows. First, $z = (q_1, p_1, \ldots, q_d, p_d)$ is a point in the system's phase space, and the function $\delta(E - H(z))$ restricts the integration to the energy surface of energy E under consideration. The flux factor F is given by

$$F(z) = \left.\frac{d}{dt}\Theta(s(z_t))\right|_{t=0}, \tag{100}$$

where z_t is the Hamiltonian flow satisfying the IC $z_{t=0} = z$. The dividing surface is defined as the zero level set of the function s, i.e., $\{z \in \mathbb{R}^{2d} : s(z) = 0\}$. It is assumed that this surface divides the phase space into two components: the region given by $s(z) < 0$ corresponds to reactants, while the region given by $s(z) > 0$ corresponds to products. Finally, the projection function P_r is defined as

$$P_r(z) = \lim_{t \to \infty} \Theta(s(z_t)) \tag{101}$$

and equals unity (zero) if a trajectory starting at z ends up in the product (reactant) region for infinitely long times.

In order to explain the relation of Eq. (99) to Eq. (20) we first rewrite the projection function as

$$P_r(z) = \Theta(s(z_{t_0})) + \int_{t_0}^{\infty} \frac{d}{dt}\Theta(s(z_t))\,dt\,, \tag{102}$$

where we choose $t_0 = -\epsilon$ with $\epsilon \to 0^+$. At this stage it is important to note that since the flux factor $F(z)$ is proportional to $\delta(s(z))$ the integral in Eq. (99) is effectively restricted to the dividing surface.[10] But, using such properties

---

[10] More precisely, since in addition to the flux factor F one also has to take into account the function $\delta(E - H)$ the integral in Eq. (99) is a $(2d - 2)$-dimensional integral over the intersection of the dividing surface with the energy surface of energy E.

of the dividing surface that it is (i) recrossing-free and (ii) transverse to the Hamiltonian flow, we have

$$\lim_{\epsilon \to 0^+} \Theta\big(s(z_{-\epsilon})\big) = 1 - P_r(z) \tag{103}$$

for z on the dividing surface. Then, substituting Eqs. (100) and (103) into Eq. (102) and solving for the projection function P_r we obtain

$$P_r(z) = \frac{1}{2} + \lim_{\epsilon \to 0^+} \frac{1}{2} \int_{-\epsilon}^{\infty} F(z_t)\,dt \tag{104}$$

for z on the dividing surface. Finally, substituting Eq. (104) into Eq. (99) and taking into account the fact that the total flux through the dividing surface is zero, i.e.,

$$\int_{\mathbb{R}^{2d}} \delta(E - H(z))F(z)\,dz = 0, \tag{105}$$

we arrive at the expression for the directional flux,

$$f(E) = \lim_{\epsilon \to 0^+} \frac{1}{2} \int_{-\epsilon}^{\infty} C_F(t)\,dt \tag{106}$$

as a time integral of the *flux–flux autocorrelation function*

$$C_F(t) = \int_{\mathbb{R}^{2d}} \delta(E - H(z))F(z)F(z_t)\,dz . \tag{107}$$

We now explicitly calculate the time dependence of the function C_F using the CNF theory. To this end we first express the flux factor F in the normal form coordinates $(Q_1, P_1, q_2, p_2, \ldots, q_d, p_d)$, see Section 2.1, in which the dividing surface is given by $s(z) = Q_1$:

$$F(z) = \frac{d}{dt}\Theta\big(Q_1(t)\big)\Big|_{t=0} = \delta(Q_1)\frac{d}{dt}Q_1(t)\Big|_{t=0} = \delta(Q_1)\Lambda P_1, \tag{108}$$

where

$$\Lambda = \frac{\partial}{\partial I}H_{\mathrm{CNF}}(I, J_2, \ldots, J_d), \tag{109}$$

and H_{CNF} is the normal form Hamiltonian as a function of the action integrals $I = (P_1^2 - Q_1^2)/2$ and $J_k = (p_k^2 + q_k^2)/2$, $k = 2, \ldots, d$. Equation (107) then reads

$$C_F(t) = \int_{\mathbb{R}^{2d}} \delta(E - H_{\mathrm{CNF}})\delta(Q_1)\delta\big(Q_1(t)\big)\Lambda^2 P_1 P_1(t)\,dz . \tag{110}$$

The product of the δ-functions of Q_1 and the corresponding time-evolved coordinate $Q_1(t)$ signals that only the infinitesimally short time scales $t \to 0$ give a nonvanishing contribution to the integral. Linearization of the time evolution of z_t around $t = 0$ yields

$$C_\mathrm{F}(t) = \delta(t) \int_{\mathbb{R}^{2d}} \delta(E - H_\mathrm{CNF})\delta(Q_1)\Lambda |P_1|\, dz$$

$$= 2\delta(t)(2\pi)^{d-1} \int_{\mathbb{R}^d_+} \delta(E - H_\mathrm{CNF})\frac{\partial H_\mathrm{CNF}}{\partial I}\, dI dJ_2 \dots dJ_d$$

$$= 2\delta(t)(2\pi)^{d-1} \int_{I(E, J_2, \dots, J_d)>0} dJ_2 \dots dJ_d. \tag{111}$$

The last integral in Eq. (111) is nothing but the volume $\mathcal{V}(E)$ in the action space $(J_2, \dots, J_d)$ enclosed by the contour $H_\mathrm{CNF}(0, J_2, \dots, J_d) = E$, and illustrated in Figure 5.5, that defines the directional flux through the dividing surface, see Eq. (20). Thus, we obtain

$$C_\mathrm{F}(t) = 2\delta(t)(2\pi)^{d-1}\mathcal{V}(E) = 2\delta(t)f(E), \tag{112}$$

which is in agreement with Eq. (106). Finally, we note that in view of Eq. (112) one can rewrite Eq. (106) as

$$f(E) = \frac{1}{2}\int_{-\infty}^{+\infty} C_\mathrm{F}(t)\, dt. \tag{113}$$

6.3.2. Quantum formulation

In the quantum version of the flux–flux autocorrelation function approach Eq. (99) for the directional flux is replaced by a corresponding equation for the CRP,

$$\mathcal{N}(E) = 2\pi\hbar_\mathrm{eff} \operatorname{Tr}\left\{\delta(E - \hat{H})\hat{F}\hat{P}_\mathrm{r}\right\}. \tag{114}$$

Here, the flux factor operator $\hat{F}$ is given by

$$\hat{F} = \frac{d}{dt}\left(e^{i\hat{H}t/\hbar_\mathrm{eff}}\widehat{\Theta(s)}e^{-i\hat{H}t/\hbar_\mathrm{eff}}\right)\bigg|_{t=0} = \frac{i}{\hbar_\mathrm{eff}}[\hat{H},\widehat{\Theta(s)}], \tag{115}$$

where $\widehat{\Theta(s)}$ is a quantization of the composition of the Heaviside function with a function s defining the dividing surface. The projection operator $\hat{P}_\mathrm{r}$ is defined as

$$\hat{P}_\mathrm{r} = \lim_{t\to\infty} e^{i\hat{H}t/\hbar_\mathrm{eff}}\widehat{\Theta(s)}e^{-i\hat{H}t/\hbar_\mathrm{eff}}. \tag{116}$$

Then, as shown in Ref. [4], Eq. (114) can be written in close analogy with its classical counterpart Eq. (106):

$$\mathcal{N}(E) = (2\pi\,\hbar_{\mathrm{eff}})\,\frac{1}{2}\int_{-\infty}^{+\infty}\mathcal{C}_{\mathrm{F}}(t)\,\mathrm{d}t, \tag{117}$$

where

$$\mathcal{C}_{\mathrm{F}}(t) = \mathrm{Tr}\left\{\delta(E-\hat{H})\hat{F}\mathrm{e}^{i\hat{H}t/\hbar_{\mathrm{eff}}}\hat{F}\mathrm{e}^{-i\hat{H}t/\hbar_{\mathrm{eff}}}\right\} \tag{118}$$

is the quantum flux–flux autocorrelation function.

As we have shown above the classical flux–flux autocorrelation function C_{F} can be explicitly analyzed within the framework of the CNF theory. The following natural question arises: Can one obtain the time dependence of the quantum flux–flux autocorrelation function $\mathcal{C}_{\mathrm{F}}$ using the methods of the QNF theory? Of course, the QNF technique provides one with an approximation of the original Hamiltonian operator. This approximation is only accurate in the vicinity of the equilibrium saddle point in phase space, so one should not expect a perfect agreement between the QNF flux–flux autocorrelation function and the exact one to hold up to infinitely long times. Instead, the QNF theory will provide an approximation of the exact flux–flux autocorrelation function in a certain time interval whose length will depend on the effective Planck's constant among other parameters.

6.4. Convergence of QNF

Both the CNF and the QNF have the form of power series where each successive term is constructed via an iterative technique. Consequently, in general, we will only be able to compute a finite number of terms of the normal form. Therefore the obvious question that arises is how many terms of the normal form are required in order that the quantities derived from the normal form are accurate? A discussion, as well as some references with specific examples, was given in Section 2.5 for the CNF. In this section we are concerned with the behavior of the QNF, for which there has been essentially no work from this point of view.

First, we begin with a brief background discussion. Since the CNF and QNF, are given as series representations of the Hamiltonian function and Hamilton operator, respectively, a natural question to ask is do these series converge? In the classical setting there has been previous work on this question. However, practically speaking, from the point of view of using the results of the theory, there are three related questions: (1) convergence of the series representing the normal form Hamiltonian, (2) convergence of the transformation from the original coordinate to the normal form coordinates, and (3) convergence of any integrals of the motion that arise from

the normalization procedure. A recent discussion of these issues, as well as a discussion of earlier results for the classical Hamiltonian normal form setting, can be found in Ref. [70]. Briefly, the situation with respect to convergence for Hamiltonian systems with three or more DoFs is not optimistic. Generically, divergence is the expected behavior in normal form theory for classical Hamiltonian systems. However, the situation is not so pessimistic as one may initially believe. There are many examples of divergent series which still yield useful information in an asymptotic sense. Resummation techniques and Pade approximation techniques can be used to find an optimal number of terms that yield a desired accuracy. For classical Hamiltonian normal forms these issues have been examined in Refs. [71–74]. These issues have yet to be explored in the QNF setting.

It is useful to note that the case of two DoF Hamiltonian systems is special. In this case a classical result of Ref. [75] (see also Ref. [76]) gives convergence results for the classical Hamiltonian normal form in the neighborhood of a saddle-center equilibrium point. Recently, the first results on convergence of the QNF have appeared. In Ref. [77] convergence results for a one and a half DoF system (i.e., time-periodically forced one DoF Hamiltonian system) have been given. It is not unreasonable that these results can be extended to the QNF in the neighborhood of a saddle–center equilibrium point of a two DoF system.

In the following we provide a qualitative discussion of the convergence of the QNF based on our calculations performed for the triatomic collinear reactions. In this situation the QNF approximates the Hamiltonian of the reacting system in a phase space neighborhood of the saddle–center equilibrium point. Thus, for instance, in computing the CRP one only expects this approximation to render reliable results in a certain energy range around the saddle point energy E_0 of the potential energy surface under consideration. The energy difference $(E - E_0)$ may therefore be considered as one small parameter in the QNF expansion. The role of the other small parameter is played by the effective Planck's constant, $\hbar_{\mathrm{eff}}$. It is the convergence of the QNF with respect to this second small parameter that we focus on in this section.

We proceed by considering the right-hand side of Eq. (23), i.e., the QNF, at $I = 0$, corresponding to no "energy" in the reaction coordinate, and $n_2 = 0$, giving the zero-point "vibrational energy" of the transverse DoF. Then, Eq. (23) becomes

$$E = E_0 + \sum_{n=1}^{\lfloor N/2 \rfloor} c_n \hbar_{\mathrm{eff}}{}^n. \tag{119}$$

For the case of the collinear hydrogen exchange reaction, $H + H_2 \to H_2 + H$, on the Porter–Karplus potential energy surface the first five expansion coefficients were obtained in Ref. [31]: $c_1 = 0.161982$, $c_2 = 1.193254$, $c_3 = 14.90023$,

$c_4 = 378.7950$, and $c_5 = 1227.035$. As $N \to \infty$ the radius of convergence $\hbar_{\text{eff}}^{(0)}$ of the sum in Eq. (119) is given by

$$\hbar_{\text{eff}}^{(0)} = \lim_{n \to \infty} \frac{c_n}{c_{n+1}}. \tag{120}$$

Here, we make a crude estimate of $\hbar_{\text{eff}}^{(0)}$ by only considering the first five expansion coefficients in Eq. (120), i.e., c_n with $n = 1, \ldots, 5$; then, the radius of convergence is given by $\hbar_{\text{eff}}^{(0)} \sim 0.04$.

The estimated value of $\hbar_{\text{eff}}^{(0)}$ sheds light on the seeming inefficiency of the QNF theory for CRP computations in light atom reactions. Indeed, the ^{1}H exchange reaction, see Figure 5.13a, is characterized by $\hbar_{\text{eff}} = 3.07 \times 10^{-2}$.
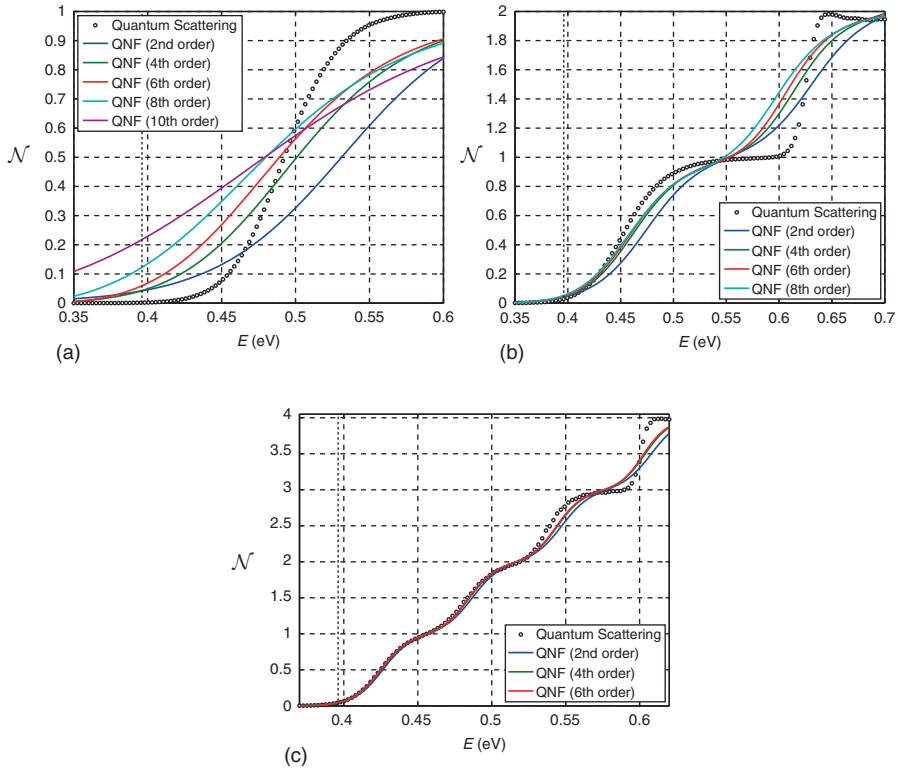
Figure 5.13 CRP as a function of the total energy, $\mathcal{N}(E)$, for the collinear hydrogen exchange reaction. Figure (a) corresponds to ^{1}H isotope characterized by $\hbar_{\text{eff}} = 3.07 \times 10^{-2}$, (b) corresponds to ^{3}H isotope characterized by $\hbar_{\text{eff}} = 1.77 \times 10^{-2}$, and (c) corresponds to a hypothetical ^{20}H "isotope" characterized by $\hbar_{\text{eff}} = 6.9 \times 10^{-3}$. The vertical dashed line shows the saddle point energy E_0.

This value being close to $\hbar_{\text{eff}}^{(0)}$ signals that the corresponding QNF expansion converges very slowly, if at all, and, possibly, terms of orders far beyond $N = 10$ are needed for a reliable CRP prediction in Figure 5.13a.

In the case of the ^{3}H exchange reaction the effective Planck's constant is $\hbar_{\text{eff}} = 1.77 \times 10^{-2}$ and is thus smaller than $\hbar_{\text{eff}}^{(0)}$. This fact is in agreement with the apparent speedup of the convergence of the CRP values, see Figure 5.13b, in comparison with the ^{1}H case. Finally, the convergence is very fast and pronounced for the case of the heavy (hypothetical) ^{20}H atoms, see Figure 5.13c, for which $\hbar_{\text{eff}} = 6.9 \times 10^{-3}$ which is much smaller than the estimated convergence radius.

Clearly, there is a great deal of scope for further studies of convergence aspects of the QNF as well as related optimal truncation and resummation techniques.

7. CONCLUSIONS

We have reviewed a new dynamical system, phase space approach to quantum reactive scattering. The quantum theory arises from an underlying classical theory that reveals the geometrical structures in phase space that govern trajectories' evolution from reactants to products in the reaction region. The classical theory is valid for any number of DoFs, and the new concept which has led to this is the introduction of the notion of a NHIM into classical reaction dynamics. The NHIM is the key phase space structure that leads to the construction of a surface dividing reactants from products having the no (local) recrossing and minimal flux properties. Moreover, the stable and unstable manifolds of the NHIMs have one less dimension than the energy surface (i.e., they are "co-dimension one") and they bound regions of the energy surface (being invariant manifolds, or "impenetrable barriers") which contain *all* reacting trajectories. These phase space structures are realized in specific systems through the use of the classical Poincaré–Birkhoff normal form. Quantization is carried out through an analogous QNF theory and the Weyl quantization procedure. The related structure of the CNF and QNF theories makes the quantum manifestation of the classical phase space structures transparent. The phase space structures in the classical case define the "landscape" in the *energy surface* which constrain the location and evolution of reacting trajectories, and this renders the need for the calculation of trajectories to evaluate, e.g., classical flux across the dividing surface unnecessary. This characteristic is inherited in the quantum setting in the sense that quantum expressions governing reaction are expressed in terms of quantities that can be computed from the QNF without the need to compute classical trajectories. Thus this phase space approach to quantum reactive scattering provides a completely new approach to the computation of quantities

describing quantum reactive scattering which may prove to be fruitful in the study of "large" quantum systems.

APPENDIX

A. THE NORMAL FORM ALGORITHM: CLASSICAL AND QUANTUM

In Section 2 we mentioned that the crucial point to realize the phase space structures governing reaction dynamics is to choose a suitable set of phase space coordinates in terms of which the Hamilton function assumes a very simple form. Similarly, the description of the activated complex in Section 3 leading to the explicit expressions for the cumulative reaction probabilities and the Gamov–Siegert resonances as explained in Sections 4.1 and 5, respectively, relied on expressing the Hamilton operator in a suitable basis. Both the canonical (or equivalently *symplectic*) transformation of the phase space coordinates and the corresponding transformation of the Hamilton function in the classical case and the unitary transformation of the basis set together with the corresponding transformation of the Hamilton operator in the quantum case can be constructed in an algorithmic fashion. The algorithms are based on a CNF in the classical case and on an analogous QNF in the quantum mechanical case. In the following we give a brief description of the algorithms to compute these normal forms. We describe the algorithms in such a way that the similarities between both algorithms become apparent. For rigorous mathematical statements, proofs, and further details we refer to Ref. [29, 30].

A.1. The CNF algorithm

We begin by considering a Hamiltonian system with phase space $\mathbb{R}^d \times \mathbb{R}^d$ with phase space coordinates $\tilde{\mathbf{q}} = (\tilde{q}_1, \tilde{q}_2, \ldots, \tilde{q}_d)$ and $\tilde{\mathbf{p}} = (\tilde{p}_1, \tilde{p}_2, \ldots, \tilde{p}_d)$ which we group in the $2d$-dimensional vector $\tilde{\mathbf{z}} = (\tilde{\mathbf{q}}, \tilde{\mathbf{p}})$ and a Hamilton function $H(\tilde{\mathbf{q}}, \tilde{\mathbf{p}})$. For convenience, we can use atomic units. This imposes no restriction. However, it has the advantage that the phase space coordinates become dimensionless. We will now assume that Hamilton's equations associated with $H(\mathbf{q}, \mathbf{p})$ have a (single) equilibrium point, $\tilde{\mathbf{z}}_0 \equiv (\tilde{\mathbf{q}}_0, \tilde{\mathbf{p}}_0)$, of saddle–center–$\cdots$–center stability type. By this we mean that the matrix associated with the linearization of Hamilton's equations about this equilibrium point has two real eigenvalues, $\pm\lambda$, of equal magnitude and opposite sign and $d-1$ purely imaginary complex conjugate pairs of eigenvalues $\pm i\omega_k$, $k = 2, \ldots, d$. If the Hamilton function is of the form of kinetic energy plus potential energy then this type of equilibrium point of Hamilton's equations corresponds to an index one saddle point of the potential energy.

The CNF procedure consists of a sequence of canonical (or equivalently *symplectic*) transformations changing the phase space coordinates $\tilde{\mathbf{z}} = (\tilde{\mathbf{q}}, \tilde{\mathbf{p}})$ in a phase space neighborhood of the equilibrium point $\tilde{\mathbf{z}}_0$. This is accomplished order by order according to the sequence

$$\tilde{\mathbf{z}} \equiv \mathbf{z}^{(0)} \rightarrow \mathbf{z}^{(1)} \rightarrow \mathbf{z}^{(2)} \rightarrow \mathbf{z}^{(3)} \rightarrow \cdots \rightarrow \mathbf{z}^{(N)}, \tag{A.1}$$

where $\mathbf{z}^{(n)}$ is obtained from $\mathbf{z}^{(n-1)}$ by means of a symplectic transformation

$$\mathbf{z}^{(n-1)} \mapsto \mathbf{z}^{(n)} = \phi_{W_n} \mathbf{z}^{(n-1)} \tag{A.2}$$

generated by a homogenous polynomial $W_n(\mathbf{z})$ of order n, i.e.,

$$W_n \in \mathcal{W}_{\text{cl}}^n := \text{span} \left\{ q_1^{\alpha_1} \ldots q_d^{\alpha_d} p_1^{\beta_1} \ldots p_d^{\beta_d} : |\alpha| + |\beta| = n \right\}. \tag{A.3}$$

More precisely, the ϕ_{W_n} in Eq. (A.2) denote the time-one maps of the flows generated by the Hamiltonian vector fields corresponding to the polynomials W_n (see Ref. [30] for details). The maximum order N in Eq. (A.1) is the desired order of accuracy at which the expansion will be terminated and truncated.

Expressing the Hamilton function H in the coordinates $\mathbf{z}^{(n)}$, $n = 1, \ldots, N$, we get a sequence of Hamilton functions $H^{(n)}$,

$$H \equiv H^{(0)} \rightarrow H^{(1)} \rightarrow H^{(2)} \rightarrow H^{(3)} \rightarrow \ldots \rightarrow H^{(N)}, \tag{A.4}$$

where for $n = 1, \ldots, N$, and $H^{(n)}(\mathbf{z}^{(n)}) = H^{(n-1)}(\mathbf{z}^{(n-1)}) = H^{(n-1)}(\phi_{W_n}^{-1} \mathbf{z}^{(n)})$, i.e.,

$$H^{(n)} = H^{(n-1)} \circ \phi_{W_n}^{-1}. \tag{A.5}$$

To avoid a proliferation of notation we will in the following neglect the superscripts (n) for the phase space coordinates.

In the first transformation in Eq. (A.1) we shift the equilibrium point $\tilde{\mathbf{z}}_0$ to the origin, i.e., $\mathbf{z} \mapsto \phi_{W_1}(\mathbf{z}) := \mathbf{z} - \tilde{\mathbf{z}}_0$. This gives

$$H^{(1)}(\mathbf{z}) = H^{(0)}(\mathbf{z} + \tilde{\mathbf{z}}_0). \tag{A.6}$$

The next steps of the CNF algorithm rely on the power series expansions of $H^{(n)}$,

$$H^{(n)}(\mathbf{z}) = E_0 + \sum_{s=2}^{\infty} H_s^{(n)}(\mathbf{z}), \tag{A.7}$$

where the $H_s^{(n)}$ are homogenous polynomials in $\mathcal{W}_{\text{cl}}^s$ given by

$$H_s^{(n)}(\mathbf{z}) = \sum_{|\alpha|+|\beta|=s} \frac{H_{\alpha_1, \ldots, \alpha_d, \, \beta_1, \ldots, \beta_d}^{(n)}}{\alpha_1! \ldots \alpha_d! \beta_1! \ldots \beta_d!} q_1^{\alpha_1} \ldots q_d^{\alpha_d} p_1^{\beta_1} \ldots p_d^{\beta_d}, \tag{A.8}$$

with $\alpha_k, \beta_k \in \mathbb{N}_0, |\alpha| = \sum_k \alpha_k, |\beta| = \sum_k \beta_k$. For $n = 1$, the coefficients in Eq. (A.8) are given by the Taylor expansion of $H^{(1)}$ about the origin,

$$H^{(1)}_{\alpha_1,\dots,\alpha_d, \beta_1,\dots,\beta_d} = \prod_{k,l=1}^{d} \frac{\partial^{\alpha_k}}{\partial q_k^{\alpha_k}} \frac{\partial^{\beta_l}}{\partial p_l^{\beta_l}} H^{(1)}(\mathbf{z})\Bigg|_{\mathbf{z}=0}. \tag{A.9}$$

For $n \geq 3$, the coefficients in Eq. (A.8) are obtained recursively. For $n = 2$, i.e., the second step in the sequence of transformations (A.1), the coefficients in Eq. (A.8) are determined by a linear transformation of the phase space coordinates according to

$$\mathbf{z} \mapsto \phi_{W_2}(\mathbf{z}) := M\mathbf{z}. \tag{A.10}$$

Here, M is a symplectic $2d \times 2d$ matrix which is chosen in such a way that the second-order term of the transformed Hamilton function

$$H^{(2)}(\mathbf{z}) = H^{(1)}(M^{-1}\mathbf{z}) \tag{A.11}$$

assumes the particularly simple form

$$H^{(2)}_2(\mathbf{z}) = \lambda q_1 p_1 + \sum_{k=2}^{d} \frac{\omega_k}{2}(q_k^2 + p_k^2). \tag{A.12}$$

Section 2.3 of Ref. [30] provides an explicit procedure for constructing the transformation matrix M.

For the first two steps in the sequence (A.1), we actually did not give explicit expressions for the generating functions W_1 and W_2. For conceptual reasons (and to justify the notation) we mention that such expressions can be determined (see Ref. [30]) but since it is not necessary for the computation we do not discuss these generating functions here. The situation is different though for the next steps in Eq. (A.1) which rely on the explicit computation of the generating functions W_n with $n \geq 3$. In order to deal with these higher order transformations we introduce the Poisson bracket of two functions $A(\mathbf{z})$ and $B(\mathbf{z})$ which for convenience, we write as

$$\{A,B\} = A \sum_{j=1}^{d} \left(\frac{\overleftarrow{\partial}}{\partial q_j} \frac{\overrightarrow{\partial}}{\partial p_j} - \frac{\overleftarrow{\partial}}{\partial p_j} \frac{\overrightarrow{\partial}}{\partial q_j} \right) B. \tag{A.13}$$

In this notation the arrows indicate whether the partial differentiation acts to the left (on A) or to the right (on B). With the Poisson bracket we associate the adjoint operator

$$\text{ad}_A : B \mapsto \text{ad}_A B \equiv \{A,B\}. \tag{A.14}$$

The transformation (A.2) then leads to a transformation of the Hamilton function $H^{(n-1)}$ to $H^{(n)}$ with $n \geq 3$ which in terms of the adjoint operator (A.14) reads

$$H^{(n)} = \sum_{k=0}^{\infty} \frac{1}{k!} [\mathrm{ad}_{W_n}]^k H^{(n-1)}. \tag{A.15}$$

Inserting the power series for $H^{(n-1)}$ (see Eqs. (A.7) and (A.8)) in Eq. (A.15) and ordering terms one finds for the sth order term of the power series of $H^{(n)}$

$$H_s^{(n)} = \sum_{k=0}^{\lfloor \frac{s}{n-2} \rfloor} \frac{1}{k!} [\mathrm{ad}_{W_n}]^k H_{s-k(n-2)}^{(n-1)}, \tag{A.16}$$

where $\lfloor \cdot \rfloor$ gives the integer part of a number, i.e., the "floor" function.

Using Eq. (A.16) one can show that the transformation defined by Eq. (A.15) satisfies the following important properties for $n \geq 3$. First, at step n, $n \geq 3$, the terms of order less than n in the power series of the Hamilton function are unchanged, i.e.,

$$H_s^{(n)} = H_s^{(n-1)}, \quad \text{for} \quad s < n, \tag{A.17}$$

so that, in particular, $H_2^{(n)} = H_2^{(2)}$. Defining

$$\mathcal{D} \equiv \mathrm{ad}_{H_2^{(2)}} = \{H_2^{(2)}, \cdot\}, \tag{A.18}$$

we get for the terms of order n,

$$H_n^{(n)} = H_n^{(n-1)} - \mathcal{D}W_n. \tag{A.19}$$

This is the so-called homological equation which will determine the generating functions W_n for $n \geq 3$ from requiring $\mathcal{D}H_n^{(n)} = 0$ or equivalently $H_n^{(n)}$ to be in the kernel of the restriction of $\mathcal{D}$ to $\mathcal{W}_{cl}^n$. In view of Eq. (A.19) this condition yields

$$H_n^{(n-1)} - \mathcal{D}W_n \in \mathrm{Ker}\, \mathcal{D}|_{\mathcal{W}_{cl}^n}. \tag{A.20}$$

Section 3.4.1 of Ref. [30] provides the explicit procedure of finding the solution of Eq. (A.20). In the generic situation where the linear frequencies $\omega_2, \ldots, \omega_d$ in Eq. (A.12) are rationally independent, i.e., $m_2\omega_2 + \cdots + m_d\omega_d = 0$ implies $m_2 = \cdots = m_d = 0$ for all integers $m_2, \ldots, m_d$, it follows that for odd n, $H_n^{(n)} = 0$, and for even n,

$$H_n^{(n)} \in \mathrm{span}\left\{ I^{\alpha_1} J_2^{\alpha_2} J_3^{\alpha_3} \ldots J_d^{\alpha_d} : |\alpha| = n/2 \right\}, \tag{A.21}$$

where $I = q_1 p_1$ and $J_k = (q_k^2 + p_k^2)/2$, with $k = 2, \ldots, d$.

Applying the transformation (A.15), with the generating function defined by Eq. (A.20), for $n = 3, \ldots, N$ and truncating the resulting power series at order N, one arrives at the Nth order CNF

$$H_{\mathrm{CNF}}^{(N)}(\mathbf{z}) = E_0 + \sum_{s=2}^{N} H_s^{(N)}(\mathbf{z}).$$

(A.22)

We stress that $H_{\mathrm{CNF}}^{(N)}$ represents an Nth order approximation of the original Hamiltonian H obtained from expressing H in terms of the phase space coordinates

$$\mathbf{z}^{(N)} = \phi(\tilde{\mathbf{z}}) := (\phi_{W_N} \circ \phi_{W_{N-1}} \circ \cdots \circ \phi_{W_2} \circ \phi_{W_1})(\tilde{\mathbf{z}})$$

(A.23)

(see Eq. (A.1)). Truncating the power series expansion of $\mathbf{z}^{(N)}$ at order N we get the transformation to the *normal form coordinates* $\mathbf{z} = (\mathbf{q}, \mathbf{p}) = T(\tilde{q}, \tilde{p})$ which we introduced in Eq. (A.7). The neighborhood $\mathcal{L}$ of validity of the CNF is now defined as a neighborhood of the equilibrium $\tilde{\mathbf{z}}_0$ in which the difference between $H^{(N)}$ and $H_{\mathrm{CNF}}^{(N)}$, i.e., the remainder term consisting of the nonnormalized tail of terms of order greater than N, and also the difference between the normal form coordinates $\mathbf{z}$ and their untruncated version $\mathbf{z}^{(N)}$ can be considered to be sufficiently small for the application under consideration (see the comments in Section 2.5).

By construction the CNF Hamilton function $H_{\mathrm{CNF}}^{(N)}$ is a polynomial of order $N/2$ in the functions I and J_k, see Eq. (A.10). We thus have

$$\dot{I} = \{I, H_{\mathrm{CNF}}^{(N)}\} = 0, \quad \dot{J}_k = \{J_k, H_{\mathrm{CNF}}^{(N)}\} = 0, \quad k = 2, \ldots, d,$$

(A.24)

i.e., I and J_k, $k = 2, \ldots, d$, are constants of the motion or *integrals* for Hamilton's equation with Hamiltonian function $H_{\mathrm{CNF}}^{(N)}$. As discussed in Section 2 it is the conservation of these integrals which allows one to construct the phase space structures governing reaction dynamics in the neighborhood of the saddle equilibrium point $\tilde{\mathbf{z}}_0$. We emphasize that the full algorithm to compute $H_{\mathrm{CNF}}^{(N)}$ and the corresponding coordinate transformation is algebraic in nature and can be implemented on a computer.

A.2. The QNF algorithm

In the quantum mechanical case we start with a Hamilton operator $\hat{H}$ which we assume to be obtained from the Weyl quantization of a classical Hamilton function $H(\tilde{\mathbf{q}}, \tilde{\mathbf{p}})$. Like in the previous section, $\tilde{\mathbf{q}} = (\tilde{q}_1, \tilde{q}_2, \ldots, \tilde{q}_d)$ and $\tilde{\mathbf{p}} = (\tilde{p}_1, \tilde{p}_2, \ldots, \tilde{p}_d)$ denote the canonical coordinates and momenta, respectively, of a Hamiltonian system with d DoFs. For convenience, we again choose atomic units, so that $\tilde{\mathbf{q}}$ and $\tilde{\mathbf{p}}$ are dimensionless. We denote the

corresponding operators by $\hat{\tilde{\mathbf{q}}} = (\hat{\tilde{q}}_1, \hat{\tilde{q}}_2, \ldots, \hat{\tilde{q}}_d)$ and $\hat{\tilde{\mathbf{p}}} = (\hat{\tilde{p}}_1, \hat{\tilde{p}}_2, \ldots, \hat{\tilde{p}}_d)$. In the coordinate representation their components correspond to multiplication by $\tilde{q}_j$ and the differential operators $\hat{\tilde{p}}_j = -i\hbar_{\mathrm{eff}} \, \partial/\partial\tilde{q}_j$. Here $\hbar_{\mathrm{eff}}$ is a dimensionless parameter which corresponds to a scaled, effective Planck's constant (see the discussion in Section 3).

Like in the classical case we will now assume that $H(\mathbf{q}, \mathbf{p}; \hbar_{\mathrm{eff}})$ (i.e., the classical Hamilton function) has an equilibrium point, $\tilde{\mathbf{z}}_0 \equiv (\tilde{\mathbf{q}}_0, \tilde{\mathbf{p}}_0)$, of saddle–center–$\cdots$–center stability type. Similar to the classical case the idea of the QNF procedure is to approximate the original Hamilton operator $\hat{H}$ by a simpler Hamilton operator where the approximation is valid in a "neighborhood of the equilibrium $\tilde{\mathbf{z}}_0$." In the classical case this simplification is achieved by a symplectic transformation leading to a specific choice of the phase space coordinates. In the quantum mechanical case the simplification will be achieved by a unitary transformation to a suitable choice of a basis for the eigenstates. The basis for computing such unitary transformation is the Wigner–Weyl symbol calculus. The crucial point of the symbol calculus is that it allows one to identify an operator with its Weyl symbol which is a (in general $\hbar_{\mathrm{eff}}$-dependent) phase space function. This way the QNF theory provides a systematic procedure to obtain a local approximation, $\hat{H}_{\mathrm{QNF}}$, of the Hamiltonian $\hat{H}$ in a phase space neighborhood of the equilibrium point $\tilde{\mathbf{z}}_0$ in order to facilitate further computation of various quantities, such as the CRP, of the reaction system under consideration, which only depend on properties of $\hat{H}$ near the equilibrium $\tilde{\mathbf{z}}_0$. From a computational point of view the symbol calculus is extremely beneficial since the resulting phase space functions can be dealt with in a similar way as in the classical case described in the previous section.

The Weyl symbol of an operator $\hat{H}$ is defined as

$$H(\tilde{\mathbf{q}}, \tilde{\mathbf{p}}; \hbar_{\mathrm{eff}}) = \int \mathrm{d}\mathbf{x} \, \langle \tilde{\mathbf{q}} - \mathbf{x}/2 | \hat{H} | \tilde{\mathbf{q}} + \mathbf{x}/2 \rangle \, e^{i\tilde{\mathbf{p}}\mathbf{x}/\hbar_{\mathrm{eff}}}. \tag{A.25}$$

The map $\hat{H} \mapsto H(\tilde{\mathbf{q}}, \tilde{\mathbf{p}}; \hbar_{\mathrm{eff}})$ leading to Eq. (A.25) is also called the Wigner map. It is the inverse of the transformation which yields a Hamilton operator $\hat{H}$ from the Weyl quantization, $\mathrm{Op}[H]$, of a phase space function H (the Weyl map) which, using Dirac notation, is given by

$$\hat{H} = \mathrm{Op}[H] = \iint \frac{\mathrm{d}\tilde{\mathbf{q}}\,\mathrm{d}\tilde{\mathbf{p}}}{(2\pi\,\hbar_{\mathrm{eff}})^d} H(\tilde{\mathbf{q}}, \tilde{\mathbf{p}}; \hbar_{\mathrm{eff}}) \int \mathrm{d}\mathbf{x} | \tilde{\mathbf{q}} - \mathbf{x}/2 \rangle e^{-i\tilde{\mathbf{p}}\mathbf{x}/\hbar_{\mathrm{eff}}} \langle \tilde{\mathbf{q}} + \mathbf{x}/2 |. \tag{A.26}$$

Accordingly, $H(\tilde{\mathbf{q}}, \tilde{\mathbf{p}}; \hbar_{\mathrm{eff}})$ in Eq. (A.25) agrees with the classical Hamilton function $H(\tilde{\mathbf{q}}, \tilde{\mathbf{p}})$ in our case. The argument $\hbar_{\mathrm{eff}}$ is introduced for convenience since the Weyl symbol of the unitarily transformed Hamilton operator we will deal with below will in general explicitly depend on $\hbar_{\mathrm{eff}}$.

Analogous to the classical case we will now construct a sequence of unitary transformations which will simplify the Hamilton operator order by order in the neighborhood of the equilibrium point z_0. These unitary transformations will be of the form

$$\hat{U}_n = e^{-i\hat{W}_n}, \tag{A.27}$$

where $\hat{W}_n$ is the Weyl quantization $\mathrm{Op}\,[W_n]$ of a symbol W_n which is a homogenous polynomial in the space

$$\mathcal{W}^n_{\mathrm{qm}} := \mathrm{span}\left\{q_1^{\alpha_1}\ldots q_d^{\alpha_d}p_1^{\beta_1}\ldots p_d^{\beta_d}\hbar_{\mathrm{eff}}{}^j : |\alpha| + |\beta| + 2j = n\right\}. \tag{A.28}$$

The main difference between the symbols W_n and the generating functions defining the symplectic transformations in the classical case in Eq. (A.2) is that the W_n in Eq. (A.27) are polynomials in the phase space coordinates $(\mathbf{q}, \mathbf{p})$ *and* $\hbar$ where for the definition of the order the power of $\hbar$ counts double.

Using unitary transformations of the form (A.27) we get the sequence of Hamilton operators

$$\hat{H} \equiv \hat{H}^{(0)} \to \hat{H}^{(1)} \to \hat{H}^{(2)} \to \hat{H}^{(3)} \to \cdots \to \hat{H}^{(N)}, \tag{A.29}$$

where

$$\hat{H}^{(n)} = \hat{U}_n\hat{H}^{(n-1)}\hat{U}_n^*. \tag{A.30}$$

Expressing the sequence (A.29) in terms of symbols we get a sequence

$$H \equiv H^{(0)} \to H^{(1)} \to H^{(2)} \to H^{(3)} \to \cdots \to H^{(N)} \tag{A.31}$$

which will be the direct analogue of the classical sequence (A.4). As we will see below, in terms of the symbols the unitary transformations (A.27) can be viewed as $\hbar$-dependent transformations of the phase space coordinates.

The first two steps of the transformations (A.31) are identical to the classical case. The first step serves to shift the equilibrium point $\tilde{\mathbf{z}}_0$ to the origin according to

$$H^{(1)}(\mathbf{z}; \hbar_{\mathrm{eff}}) = H^{(0)}(\mathbf{z} + \tilde{\mathbf{z}}_0; \hbar_{\mathrm{eff}}). \tag{A.32}$$

The higher order transformations then work on power series expansions of the symbol of the form

$$H^{(n)}(\mathbf{z}; \hbar_{\mathrm{eff}}) = E_0 + \sum_{s=2}^{\infty} H_s^{(n)}(\mathbf{z}; \hbar_{\mathrm{eff}}), \tag{A.33}$$

where

$$H_s^{(n)}(\mathbf{z}; \hbar_{\text{eff}}) = \sum_{|\alpha|+|\beta|+2j=s} \frac{H_{\alpha_1,\dots,\alpha_d,\,\beta_1,\dots,\beta_d,\,j}^{(n)}}{\alpha_1!\dots\alpha_d!\beta_1!\dots\beta_d!j!} q_1^{\alpha_1}\dots q_d^{\alpha_d} p_1^{\beta_1}\dots p_d^{\beta_d}\,\hbar_{\text{eff}}^{\,j} \in \mathcal{W}_{\text{qm}}^s\,.$$

(A.34)

For $n = 1$, the coefficients in Eq. (A.34) are again given by the Taylor expansion of $H^{(1)}$ about the origin

$$H_{\alpha_1,\dots,\alpha_d,\,\beta_1,\dots,\beta_d,\,j}^{(1)} = \left(\prod_{k,l=1}^{d} \frac{\partial^{\alpha_k}}{\partial q_k^{\alpha_k}} \frac{\partial^{\beta_l}}{\partial p_l^{\beta_l}}\right) \frac{\partial^j}{\partial \varepsilon^j} H^{(n)}(\mathbf{z}; \varepsilon)|_{(\mathbf{z};\,\varepsilon)=(0;\,0)}$$

(A.35)

where we included powers of $\hbar$ only for completeness (i.e., for the type of starting classical Hamilton functions in this chapter $H^{(1)}$ does not have terms with nonzero powers of $\hbar$). Like in the classical case the second step of the sequence of transformations (A.31) consists of a linear transformation of the phase space coordinates by a symplectic $2d \times 2d$ matrix M such that the second-order term of the symbol

$$H^{(2)}(\mathbf{z}; \hbar_{\text{eff}}) = H^{(1)}(M^{-1}\mathbf{z}; \hbar_{\text{eff}})$$

(A.36)

takes the form

$$H_2^{(2)}(\mathbf{z}; \hbar_{\text{eff}}) = \lambda q_1 p_1 + \sum_{k=2}^{d} \frac{\omega_k}{2}(q_k^2 + p_k^2)\,.$$

(A.37)

The required matrix M is identical to the classical case.

The reason for the equality of the classical transformations and the quantum transformations to second order is the commutativity of the Weyl quantization and affine linear symplectic transformations. For the nonlinear transformations corresponding to steps $n \geq 3$ the commutativity ceases to exist and the symbol calculus develops its full power.

In order to simplify the terms of order $n \geq 3$ we have to introduce the notion of the *Moyal bracket*. Given two symbols $A(\mathbf{z}; \hbar_{\text{eff}})$ and $B(\mathbf{z}; \hbar_{\text{eff}})$, corresponding to operators $\hat{A}$ and $\hat{B}$, respectively, the Moyal bracket is defined as

$$\{A,B\}_{\text{M}} = \frac{2}{\hbar_{\text{eff}}} A \sin\left[\frac{\hbar_{\text{eff}}}{2} \sum_{j=1}^{d} \left(\frac{\overleftarrow{\partial}}{\partial q_j} \frac{\overrightarrow{\partial}}{\partial p_j} - \frac{\overleftarrow{\partial}}{\partial p_j} \frac{\overrightarrow{\partial}}{\partial q_j}\right)\right] B\,.$$

(A.38)

The Moyal bracket gives the Weyl symbol of the operator $i[\hat{A},\hat{B}]/\hbar_{\text{eff}}$, where $[\,\cdot\,,\,\cdot\,]$ denotes the commutator. Like in Eq. (A.13) the arrows in Eq. (A.38)

indicate whether the partial differentiation acts to the left (on A) or to the right (on B). Equation (A.38) implies that for $\hbar_{\text{eff}} \to 0$,

$$\{A, B\}_{\text{M}} = \{A, B\} + \mathcal{O}(\hbar_{\text{eff}}^2), \tag{A.39}$$

i.e., for $\hbar_{\text{eff}} = 0$, we recover the classical Poisson bracket. Moreover, if at least one of the functions A, B is a second-order polynomial in the variables $(\mathbf{q}, \mathbf{p})$ then $\{A, B\}_{\text{M}} = \{A, B\}$. Analogous to the adjoint operator associated with the Poisson bracket in the classical case (see Eq. (A.14)) we now define a Moyal adjoint operator associated with the Moyal bracket:

$$\text{Mad}_A : B \mapsto \text{Mad}_A B \equiv \{A, B\}_{\text{M}}. \tag{A.40}$$

The symbol of $\hat{H}^{(n)}$ obtained from a unitary transformation of $\hat{H}^{(n-1)}$ according to Eq. (A.30) is then given by

$$H^{(n)} = \sum_{k=0}^{\infty} \frac{1}{k!} [\text{Mad}_{W_n}]^k H^{(n-1)}. \tag{A.41}$$

Inserting the power series of $H^{(n-1)}$ and ordering terms one finds for the sth order terms of the powers series of $H^{(n)}$

$$H_s^{(n)} = \sum_{k=0}^{\lfloor \frac{s}{n-2} \rfloor} \frac{1}{k!} [\text{Mad}_{W_n}]^k H_{s-k(n-2)}^{(n-1)}, \tag{A.42}$$

where $\lfloor \cdot \rfloor$ again denotes the floor function. Equation (A.42) looks formally the same as Eq. (A.16) in the classical case. The only difference is the occurrence of the Moyal adjoint operator instead of the adjoint operator associated with the Poisson bracket. This difference however is significant, as the Moyal bracket will in general introduce $\hbar$-dependent terms although the original symbol we started with (i.e., the classical Hamilton function) had no $\hbar$ dependence. Still, the Moyal bracket has similar properties as the Poisson bracket. Using Eq. (A.42) we see analogously the classical case that at each step $n \geq 3$, the terms of order less than n remain unchanged:

$$H_s^{(n)} = H_s^{(n-1)}, \quad \text{for} \quad s < n, \tag{A.43}$$

so that we in particular again have $H_2^{(n)} = H_2^{(2)}$ like in the classical case. Defining

$$\mathcal{D} \equiv \text{Mad}_{H_2^{(2)}} = \{H_2^{(2)}, \}. \tag{A.44}$$

we find for the terms of order n

$$H_n^{(n)} = H_n^{(n-1)} - \mathcal{D}W_n. \tag{A.45}$$

This is the *quantum homological equation* which analogous to the classical case is used to determine the symbols W_n that lead to the unitary transformations $\hat{U}_n$ defined in Eq. (A.27). Similar to the classical case we determine the W_n by requiring $\mathcal{D}H_n^{(n)} = 0$ or equivalently $H_n^{(n)}$ to be in the kernel of the restriction of $\mathcal{D}$ to $\mathcal{W}_{qm}^n$. In view of Eq. (A.45) this condition yields

$$H_n^{(n-1)} - \mathcal{D}W_n \in \operatorname{Ker}\mathcal{D}|_{\mathcal{W}_{qm}^n}. \tag{A.46}$$

Section 3.4.1 of Ref. [30] provides the explicit procedure of finding the solution of Eq. (A.46). Provided the linear frequencies $\omega_2, \ldots, \omega_d$ in Eq. (A.37) are rationally independent it again follows that for odd n, $H_n^{(n)} = 0$, and for even n,

$$H_n^{(n)} \in \operatorname{span}\left\{ I^{\alpha_1} J_2^{\alpha_2} J_3^{\alpha_3} \ldots J_d^{\alpha_d} \hbar_{\mathrm{eff}}^{\ j} : |\alpha| + j = n/2 \right\}, \tag{A.47}$$

where $I = q_1 p_1$ and $J_k = (q_k^2 + p_k^2)/2$, with $k = 2, \ldots, d$, are the analogues of the classical integrals.

Applying the transformation (A.41), with the symbol defined by Eq. (A.46), for $n = 3, \ldots, N$, and truncating the resulting power series (A.33) at the Nth order one arrives at the Weyl symbol $H_{\mathrm{QNF}}^{(N)}$ corresponding to the Nth order QNF of the Hamiltonian $\hat{H}$,

$$H_{\mathrm{QNF}}^{(N)}(\mathbf{z}; \hbar_{\mathrm{eff}}) = E_0 + \sum_{s=2}^{N} H_s^{(N)}(\mathbf{z}; \hbar_{\mathrm{eff}}). \tag{A.48}$$

We thus see that the computation of the symbol of the QNF operator is very similar to the classical case. The major difference is the use of the Moyal bracket in the quantum case which is more complicated than the Poisson bracket in the classical case. What remains to be done to get the Nth order QNF operator is to compute the Weyl quantization of the symbol $H_{\mathrm{QNF}}^{(N)}(\mathbf{z}; \hbar_{\mathrm{eff}})$:

$$\hat{H}_{\mathrm{QNF}}^{(N)} = \operatorname{Op}\left[H_{\mathrm{QNF}}^{(N)}\right]. \tag{A.49}$$

The Weyl quantization of the classical integrals I and J_k, $k = 2, \ldots, d$, are

$$\hat{I} \equiv \operatorname{Op}[I] = \frac{1}{2}(\hat{q}\hat{p} + \hat{p}\hat{q}), \tag{A.50}$$

$$\hat{J}_k \equiv \operatorname{Op}[J_k] = \frac{1}{2}(\hat{q}_k^2 + \hat{p}_k^2), \quad k = 2, \ldots, d. \tag{A.51}$$

Using Eq. (A.37) and the linearity of the Weyl quantization we get

$$\hat{H}_2^{(2)} = \lambda \hat{I} + \sum_{k=2}^{d} \omega_k \hat{J}_k . \qquad (A.52)$$

Since the higher order terms in Eq. (A.48) are polynomials in I and J_k, $k = 2, \ldots, d$ (see Eq. (A.47)), we need to know how to quantize powers of I and J_k. As shown in Ref. [30] this can be accomplished using the recurrence relations

$$\mathrm{Op}\left[I^{n+1}\right] = \hat{I}\,\mathrm{Op}\left[I^n\right] - \left(\frac{\hbar}{2}\right)^2 n^2 \mathrm{Op}\left[I^{n-1}\right] \qquad (A.53)$$

and

$$\mathrm{Op}\left[J_k^{n+1}\right] = \hat{J}_k\,\mathrm{Op}\left[J_k^n\right] + \left(\frac{\hbar}{2}\right)^2 n^2 \mathrm{Op}\left[J_k^{n-1}\right] \qquad (A.54)$$

for $k = 2, \ldots, d$. Hence, $\hat{H}_{\mathrm{QNF}}^{(N)}$ is a polynomial function of the operators $\hat{I}$ and $\hat{J}_k$ of the form Eq. (A.23). The coefficients $\kappa_{n,\alpha,j}$ are systematically obtained by the QNF procedure to compute the symbol $H_{\mathrm{QNF}}^{(N)}$, as described above, and the recurrence relations (A.53) and (A.54). So like in the case of the CNF the full procedure to compute $\hat{H}_{\mathrm{QNF}}^{(N)}$ is algebraic in nature and can be implemented on a computer. Our software for computing the QNF as well as the CNF which is recovered for $\hbar_{\mathrm{eff}} = 0$ is publicly available at http://lacms.maths. bris.ac.uk/publications/software/index.html.

In summary the Nth order QNF operator $\hat{H}_{\mathrm{QNF}}^{(N)}$ is obtained from conjugating the original Hamiltonian $\hat{H}$ by the unitary transformation

$$\hat{U} = \mathrm{e}^{-\mathrm{i}\hat{W}_1/\hbar_{\mathrm{eff}}}\mathrm{e}^{-\mathrm{i}\hat{W}_2/\hbar_{\mathrm{eff}}} \cdots \mathrm{e}^{-\mathrm{i}\hat{W}_N/\hbar_{\mathrm{eff}}}, \qquad (A.55)$$

where we used the fact that the first two steps in the sequence (A.31) can also be implemented using suitable generators $\hat{W}_1$ and $\hat{W}_2$ (see Ref. [30] for more details). It is an Nth order approximation in the sense that the symbol corresponding to the conjugated operator is truncated at order N where the order is defined according to Eq. (A.28). Using arguments based on the symbol calculus the remainder term consisting of the Weyl quantization of the unnormalized tail $H^{(N)} - H_{\mathrm{QNF}}^{(N)}$ is small "in a neighborhood of the equilibrium point $\tilde{\mathbf{z}}_0$." The local approximation given by the QNF is ideally suited to compute the CRP which is directly related to properties of the Hamilton operator in the neighborhood of $\tilde{\mathbf{z}}_0$ because of the simple structure of $\hat{H}_{\mathrm{QNF}}^{(N)}$. Since $\hat{H}_{\mathrm{QNF}}^{(N)}$ is a polynomial function of $\hat{I}$ and $\hat{J}_k$, $k = 2, \ldots, d$, we have

$$[\hat{I}, \hat{H}_{\mathrm{QNF}}^{(N)}] = 0, \quad [\hat{J}_k, \hat{H}_{\mathrm{QNF}}^{(N)}] = 0, \quad k = 2, \ldots, d, \qquad (A.56)$$

which is the quantum analogue of the invariance of the classical integrals in Eq. (A.24). The commutativities (A.56) imply that the eigenstates of $\hat{H}_{\mathrm{QNF}}^{(N)}$ are product states of the one-dimensional eigenstates of $\hat{I}$ and $\hat{J}_k$. As we demonstrated in Sections 4.1 and 5 the simplicity of the spectral properties of $\hat{I}$ and $\hat{J}_k$ upon which the QNF is built can be exploited to give an efficient procedure to compute the CRP and the Gamov–Siegert resonances associated with the equilibrium $\tilde{\mathbf{z}}_0$.

ACKNOWLEDGMENTS

REFERENCES

[1] W.H. Miller, Using classical mechanics in a quantum framework, perspective on "Semiclassical description of scattering" by Ford K.W., Wheeler J.A. (1959) Ann. Phys. (NY) 7: 259, Theor. Chem. Acc. 103 (2000) 236–237.

[2] W.H. Miller, The initial value representation of semiclassical theory: A practical way of adding quantum effects to classical molecular dynamics simulations of complex molecular systems, in: K.K. Phua, A. Zewail, (Eds.), Physical Biology–From Atoms to Cells, 51st Conference on Chemical Research, London, UK, 2008. Imperial College Press, London, UK, 2008, pp. 505–525.

[3] BESAC, Directing matter and energy: five challenges for science and the imagination. A Report from the Basic Energy Sciences Advisory Committee, US Department of Energy, December 20, 2007.

[4] W.H. Miller, "Direct" and "correct" calculation of canonical and microcanonical rate constants for chemical reactions, J. Phys. Chem. A 102 (5) (1998) 793–806.

[5] G.C. Schatz, M.A. Ratner. Quantum Mechanics in Chemistry. Dover, Mineola; New York, 2002.

[6] C. Venkataraman, W.H. Miller, Chemical reaction rates using the semiclassical Van Vleck initial value representation, J. Chem. Phys. 126 (2007) 094104.

[7] W.H. Miller, Quantum mechanical transition state theory amd a new semiclassical model for reaction rate constants, J. Chem. Phys. 61 (5) (1974) 1823–1833.

[8] T. Yamamoto, Quantum statistical mechanical theory of the rate of exchange chemical reactions in the gas phase, J. Chem. Phys. 33 (1) (1960) 281–289.

[9] W.H. Miller, S.D. Schwartz, J.W. Tromp, Quantum mechanical rate constants for bimolecular reactions, J. Chem. Phys. 79 (1983) 4889–4898.

[10] R. Collepardo-Guevara, I.R. Craig, D.E. Manolopoulos, Proton transfer in a polar solvent from ring polymer reaction rate theory, J. Chem. Phys. 128 (2008) 144502.

[11] P. Pechukas, F.J. McLafferty, On transition-state theory and the classical mechanics of collinear collisions, J. Chem. Phys. 58 (1973) 1622–1625.

[12] P. Pechukas, E. Pollak, Trapped trajectories at the boundary of reactivity bands in molecular collisions, J. Chem. Phys. 67 (12) (1977) 5976–5977.

[13] P. Pechukas, E. Pollak, Transition states, trapped trajectories, and classical bound states embedded in the continuum, J. Chem. Phys. 69 (1978) 1218–1226.

[14] E. Pollak, P. Pechukas, Unified statistical model for "complex" and "direct" reaction mechanisms: A test on the collinear $H + H_2$ exchange reaction, J. Chem. Phys. 70 (1) (1979) 325–333.

[15] P. Pechukas, E, Pollak, Classical transition state theory is exact if the transition state is unique, J. Chem. Phys. 71 (5) (1979) 2062–2068.

[16] E. Pollak, M.S. Child, P. Pechukas, Classical transition state theory: A lower bound to the reaction probability, J. Chem. Phys. 72 (1980) 1669–1678.

[17] M.S. Child, E. Pollak, Analytical reaction dynamics: Origin and implications of trapped periodic orbits, J. Chem. Phys. 73 (9) (1980) 4365–4372.

[18] E. Pollak, M.S. Child, Classical mechanics of a collinear exchange reaction: A direct evaluation of the reaction probability and product distribution, J. Chem. Phys. 73 (9) (1980) 4373–4380.

[19] S. Wiggins, On the geometry of transport in phase space I. Transport in k-degree-of-freedom Hamiltonian systems, $2 \leq k < \infty$, Physica D 44 (1990) 471–501.

[20] R.E. Gillilan, G.S. Ezra, Transport and turnstiles in multidimensional Hamiltonian mappings for unimolecular fragmentation: Application to van der Waals predissociation, J. Chem. Phys. 94 (4) (1991) 2648–2668.

[21] H. Waalkens, S. Wiggins, Direct construction of a dividing surface of minimal flux for multi-degree-of-freedom systems that cannot be recrossed, J. Phys. A: Math. Gen. 37 (2004) L435–L445.

[22] S. Wiggins, L. Wiesenfeld, C. Jaffe, T. Uzer. Impenetrable barriers in phase-space, Phys. Rev. Lett. 86 (24) (2001) 5478–5481.

[23] T. Uzer, C. Jaffe, J. Palacian, P. Yanguas, S. Wiggins, The geometry of reaction dynamics, Nonlinearity 15 (2002) 957–992.

[24] H. Waalkens, A. Burbanks, S. Wiggins, A computational procedure to detect a new type of high-dimensional chaotic saddle and its application to the 3D Hill's problem, J. Phys. A: Math. Gen. 37 (2004) L257–L265.

[25] H. Waalkens, A. Burbanks, S. Wiggins, Efficient procedure to compute the microcanonical volume of initial conditions that lead to escape trajectories from a multidimensional potential well, Phys. Rev. Lett. 95 (2005) 084301.

[26] H. Waalkens, A. Burbanks, S. Wiggins, A formula to compute the microcanonical volume of reactive initial conditions in transition state theory, J. Phys. A: Math. Gen. 38 (2005) L759–L768.

[27] E. Thiele, Comparison of the classical theories of unimolecular reactions, J. Chem. Phys. 36 (6) (1962) 1466–1472.

[28] H. Waalkens, G.S. Ezra, S. Wiggins, Microcanonical rates, gap times, and phase space dividing surfaces, J. Chem. Phys. 130 (2009) 164118.

[29] R. Schubert, H. Waalkens, S. Wiggins, Efficient computation of transition state resonances and reaction rates from a quantum normal form, Phys. Rev. Lett. 96 (2006) 218302.

[30] H. Waalkens, R. Schubert, S. Wiggins, Wigner's dynamical transition state theory in phase space: Classical and quantum, Nonlinearity 21 (1) (2008) R1–R118.

[31] A. Goussev, R. Schubert, H. Waalkens, S. Wiggins, The quantum normal form approach to reactive scattering: The cumulative reaction probability for collinear exchange reactions, J. Chem. Phys. 131 (2009) 144103.

[32] H. Waalkens, S. Wiggins, Geometrical models of the phase space structures governing reaction dynamics, Regul. Chaotic Dyn. 15 (1) (2010) 1–39.

[33] G.S. Ezra, S. Wiggins, Impenetrable barriers in phase space for deterministic thermostats, J. Phys. A: Math. Theor. 42 (2009) 042001.

[34] A. Deprit, Canonical transformations depending on a small parameter, Celestial Mech. 1 (1969) 12–30.

[35] K.R. Meyer, Normal forms for Hamiltonian systems, Celestial Mech. 9 (1974) 517–522.

[36] A.J. Dragt, J.M. Finn, Lie series and invariant functions for analytic symplectic maps, J. Math. Phys. 17 (1976) 2215–2227.

[37] V.I Arnold, V.V. Kozlov, A.I Neishtadt, Mathematical Aspects of Classical and Celestial Mechanics, Vol. III: Dynamical Systems, Springer-Verlag, New York; Heidelberg; Berlin, 1988.

[38] K.R. Meyer, A Lie transform tutorial ii, In: K.R. Meyer, D.S. Schmidt, (Eds.), Computer Aided Proofs in Analysis, Vol. 28: The IMA Volumes in Mathematics and its Applications, Springer-Verlag, New York: Heidelberg; Berlin, 1991, pp. 190–210.

[39] K.R. Meyer, G.R. Hall, Introduction to Hamiltonian Dynamical Systems and the N-Body Problem, Vol. 90: Applied Mathematical Sciences, Springer-Verlag, Berlin; Heidelberg; New York, 1992.

[40] J. Murdock, Normal Forms and Unfoldings for Local Dynamical Systems, Springer-Verlag, New York; Heidelberg; Berlin, 2003.

[41] V. Guillemin, Moment Maps and Combinatorial Invariants of Hamiltonian T^n-spaces, Birkhauser, Boston, 1994.

[42] J.E. Marsden, T.S. Ratiu, Introduction to Mechanics and Symmetry, Second ed., Springer-Verlag, New York; Heidelberg; Berlin, 1999.

[43] V.I Arnold, Mathematical Methods of Classical Mechanics, Springer-Verlag, New York; Heidelberg; Berlin, 1978.

[44] M. Gutzwiller, Chaos in Classical and Quantum Mechanics, Springer-Verlag, New York; Heidelberg; Berlin, 1990.

[45] R.S. MacKay, Flux over a saddle, Phys. Lett. A 145 (1990) 425–427.

[46] H. Waalkens, A. Burbanks, S. Wiggins, Phase space conduits for reaction in multidimensional systems: HCN isomerization in three dimensions, J. Chem. Phys. 121 (13) (2004) 6207–6225.

[47] H. Waalkens, A. Burbanks, S. Wiggins, Escape from planetary neighborhoods, Mon. Not. R. Astron. Soc. 361 (2005) 763–775.

[48] Y. Colin de Verdière, B. Parisse, Équilibre instable en régime semi-classique I, Commun. Partial Diff. Eqns. 19 (1994) 1535–1563.

[49] D. Chruściński, Quantum mechanics of damped systems, J. Math. Phys. 44 (2003) 3718–3733.

[50] D. Chruściński, Quantum mechanics of damped systems: II. Damping and parabolic barrier, J. Math. Phys. 45 (2003) 841–854.

[51] M. Abramowitz, I.A. Stegun, Handbook of Mathematical Functions with Formulas, Graphs, and Mathematical Tables, Dover, New York, 1965.

[52] L.M. Delves, Tertiary and general-order collisions, Nucl. Phys. 9 (1959) 391–399.

[53] A. Lagana, E. Garcia, L. Ciccarelli, Deactivation of vibrationally excited nitrogen molecules by collision with nitrogen atoms, J. Phys. Chem. 91 (1987) 312–314.

[54] G. Hauke, J. Manz, J. Römelt, Collinear triatomic reactions described by polar Delves coordinates, J. Chem. Phys. 73 (1980) 5040–5044.

[55] A. Kuppermann, J.A. Kaye, J.P. Dwyer, Hyperspherical coordinates in quantum mechanical collinear reactive scattering, Chem. Phys. Lett. 74 (1980) 257–262.

[56] D.E. Manolopoulos, S.K. Gray, Symplectic integrators for the multichannel Schrödinger equation, J. Chem. Phys. 102 (1995) 9214–9227.

[57] R.I. McLachlan, P. Atela, The accuracy of symplectic integrators, Nonlinearity 5 (1991) 541–562.

[58] R.B. Walker, J.C. Lights, Reactive molecular collisions, Ann. Rev. Phys. Chem. 31 (1980) 401–433.

[59] T. Seideman, W.H. Miller, Transition state theory, Siegert eigenstates, and quantum mechanical reaction rates, J. Chem. Phys. 95 (1991) 1768–1780.

[60] C. Eckart, The penetration of a potential barrier by electrons, Phys. Rev. 35 (1930) 1303–1309.

[61] T. Seideman, W. H. Miller, Transition state theory, Siegert eigenvalues, and quantum mechanical reaction rates, J. Chem. Phys. 95 (1991) 1768–80.

[62] R.N. Zare, Resonances in reaction dynamics, Science 311 (2006) 1383–1385.

[63] W.H. Miller, Semiclassical methods in chemical physics, Science, 233 (1986) 171–177.

[64] H.R. Dullin, A. Wittek, Complete Poincaré sections and tangent sets, J. Phys. A: Math. Gen. 28 (1995) 7157–7180.

[65] S.C. Creagh, Classical transition states in quantum theory, Nonlinearity 17 (2004) 1261–1308.

[66] S.C. Creagh, Semiclassical transmission across transition states, Nonlinearity 18 (2005) 2089–2110.

[67] A.A. Kirillov, Geometric quantization, Vol. IV: Dynamical Systems, Encyclopaedia of Mathematical Sciences, Springer-Verlag, New York; Heidelberg; Berlin, 2001.

[68] E.B. Bogomolny, Semiclassical quantization of multidimensional systems, Nonlinearity 5 (1992) 805–866.

[69] W.H. Miller, Spiers Memorial Lecture. Quantum and semiclassical theory of reaction rates, Farad. Discuss. 110 (1998) 1–21.

[70] R. Pérez-Marco, Convergence or generic divergence of the Birkhoff normal form, Ann. Math. 157 (2003) 557–574.

[71] M. Kaluza, M. Robnik, Improved accuracy of the Birkhoff-Gustavson normal form and its convergence properties, J. Phys. A: Math. Gen. 25 (1992) 5311–5327.

[72] M. Robnik, On the Padé approximations to the Birkhoff-Gustavson normal form, J. Phys. A: Math. Gen. 26 (1993) 7427–7434.

[73] G. Contopoulos, C. Efthymiopoulos, A. Giorgilli, Non-convergence of formal integrals of motion, J. Phys. A: Math. Gen. 36 (2003) 8639–8660.

[74] C. Efthymiopoulos, A. Giorgilli, G. Contopoulos, Nonconvergence of formal integrals: II. Improved estimates for the optimal order of truncation, J. Phys. A: Math. Gen. 37 (2004) 10831–10858.

[75] J. Moser, On the generalization of a theorem of A. Liapounoff, Comm. Pure Appl. Math. 11 (1958) 257–271.

[76] A. Giorgilli, Unstable equilibria of Hamiltonian systems, Discr. Cont. Dyn. Sys. (DCDS-A) 7 (4) (2001) 855–871.

[77] A. Anikin, Normal form of a quantum Hamiltonian with one and a half degrees of freedom near a hyperbolic fixed point, Regul. Chaotic Dyn. 13 (2008) 377–402.

The State-Specific Expansion Approach to the Solution of the Polyelectronic Time-Dependent Schrödinger Equation for Atoms and Molecules in Unstable States

Theodoros Mercouris[a]**, Yannis Komninos**[a]**,** and **Cleanthes A. Nicolaides**[a]

Contents

[a] Theoretical and Physical Chemistry Institute, National Hellenic Research Foundation, 48 Vasileos Constantinou Avenue, Athens 11635 Greece

E-mail addresses: thmerc@eie.gr (T. Mercouris), ykomn@eie.gr (Y. Komninos), caan@eie.gr (C. A. Nicolaides)

Abstract   Important problems in chemical physics require the ab initio computation
                of the nonstationary many-electron wavefunction that solves the time-de-
                pendent Schrödinger equation (TDSE) for time-independent and, especially,
                for time-dependent Hamiltonians. This chapter reviews the state-specific
                expansion approach (SSEA) to the solution of a variety of time-dependent
                many-electron problems (TDMEPs) in atoms and small molecules. Because of its
                structure, the SSEA places emphasis on the efficient computation of state-spe-
                cific wavefunctions in the discrete and in the continuous spectrum. Therefore,
                the review covers, apart from the methodology of solving the TDSE, the the-
                ory for the solution of the many-electron problem in two broad subjects of
                modern research: One which refers to isolated discrete and resonance states
                and one which refers to the series of states just below and just above the frag-
                mentation threshold. Thus, it is also concerned with the theory of the quantum
                defect and of related issues. The applications which are mentioned or are dis-
                cussed briefly involve either the ab initio computation of the time-resolved
                decay of autoionizing states or, especially, prototypical TDMEPs of absorption
                of one or of many photons by atoms, by negative ions, and by diatomics. In
                the latter case, we demonstrate how the "multipolar" interaction expressing
                the *full* atom–field interaction (and not just the electric dipole approximation)
                can be incorporated into a practical computational methodology.

1. INTRODUCTION

1.1. The many-electron problem in a stationary-state framework

Since the emergence of quantum mechanics (QM) in the 1920s, what is referred to as the *many-electron problem* (MEP) for atoms and molecules normally implies the fundamental difficulty of solving to a high degree of accuracy the *time-independent Schrödinger equation* (TISE) due to the presence in the Hamiltonian operator of terms representing interelectron interactions of purely nonrelativistic (Coulomb) or of nonrelativistic plus relativistic (Breit or Pauli) origin. In fact, the publications in quantum chemistry that are relevant to this MEP have dealt, in overwhelming numbers, with the formalism and the computation of the ground state—for molecules in the framework of the Born–Oppenheimer approximation.

On the other hand, the much broader and more challenging area of the *excited electronic states* in the discrete and in the continuous spectrum is still largely unexplored quantitatively, in spite of theoretical and computational developments that have laid the foundations for the understanding and practical computation of many of the related properties and phenomena.

Indeed, when the focus shifts to excited states, the formal and practical nature of the MEP changes, becoming more complicated theoretically and more demanding computationally. This statement is especially relevant to excited states that are found in the continuous spectrum and are *unstable*. Such unstable states ("resonances") decay into open scattering channels, with the continuum representing either free electrons (autoionization) or free atoms and ions (molecular autodissociation).

In addition, when a time-independent Hamiltonian describing the addition of static electric or magnetic fields, or of the cycle-averaged interaction of external sinusoidal electromagnetic fields (EMFs), is used, the processes of ionization (dissociation) or of tunneling can be treated rigorously, even for strong fields, within stationary-state theories which aim at defining and computing *field-induced* unstable states. In such cases, the MEP is again time-independent (but depends on energy and on field parameters), and quantities of physical relevance, such as rates of transition, are either constant with time or represent appropriate averages over time [1].

Here, we call the MEP for situations involving isolated or series of unstable states that are treatable within *stationary-state formalisms*, the "time-independent MEP" (TIMEP).

As developed in the framework of the standard Hermitian QM, the fundamental characteristic of a *stationary state* is captured by the expression ($\hbar = 1$),

$$\Psi_E(q, t) = e^{-iEt}\Psi_E(q), \tag{1}$$

The symbol q stands collectively for the space coordinates. Equation (1) contains time only in the phase and separates the *time-dependent Schrödinger*

equation (TDSE), thereby producing the TISE. It holds on the real energy axis for

1. *Bound* states of the discrete spectrum of the atomic (molecular) Hamiltonian, $\mathbf{H}_{A,M}$, in which case E is the total energy, which is one of the real eigenvalues of the TISE, say E_n. (Bold letters symbolize operators.)
2. *Scattering* states of the continuous spectrum of $\mathbf{H}_{A,M}$, in which case the total energy E is any real number corresponding to the kinetic energy of free particle(s).

On the other hand, when it comes to field-free or field-induced unstable states (in the spirit mentioned above and explained in Ref. [1]), there is also a way of describing them in analogy to Eq. (1), within non-Hermitian resonance state theories, where E is a complex eigenvalue, z_n, of the total Hamiltonian:

$$\Phi_n(q, z_n; t) = e^{-iz_n t}\Phi_n(q, z_n), \quad t \geq 0, \tag{2}$$

$z_n = E_n - \dfrac{i}{2}\Gamma_n$, where Γ_n is the rate of decay of the unstable state into the continuous spectrum. The Φ_n are not square-integrable and do not belong to a Hilbert space. Issues regarding the effective normalization of the Φ_n and their ab initio treatment are covered in Ref. [1]. The complex z_n results from the outgoing-wave boundary condition on the appropriate solution of the TISE. On such a domain of functions, the Hamiltonian is not self-adjoint (not Hermitian).

The form (2) describes *resonance* states in the continuous spectrum of the total time-independent Hamiltonian. It is evident that if this form is adopted as a property of the resonance state, then, when considering the physics from a time-dependent point of view, i.e., as being caused by a decaying state, it yields exponential decay for all $t \geq 0$.

1.2. The time-dependent MEP

On the other hand, there are many dynamic phenomena whose quantitative description cannot be achieved via a stationary-state formalism, whose hallmark, as already indicated, is the form of Eq. (1) or (2) for the eigenfunction. In other words, now, the complete solution of the TDSE for all t cannot be written as a product of two terms, one of which is the phase that contains time and the other is a time-independent eigenfunction in coordinate space. In these cases, in most real situations one faces a genuine *time-dependent many-electron problem* (TDMEP), whose solution must be based on the quantitative knowledge of time-dependent, *nonstationary* (unstable) states, $\Psi(q, t)$.

Now, the only significant and rigorous expression that can be associated with $\Psi(q, t)$ is the TDSE (atomic units are used),

$$\mathbf{H}(q, t)\Psi(q, t) = i\frac{\partial}{\partial t}\Psi(q, t), \tag{3}$$

where, depending on the problem, the Hamiltonian is either time dependent, $\mathbf{H}(q,t)$, or time independent, $\mathbf{H}(q)$.

In this chapter, we turn to problems of quantum chemistry and of many-electron atomic and molecular physics for which the desideratum is the quantitative knowledge and easy conceptual understanding of dynamical processes and phenomena that depend explicitly on time. We focus on a theoretical and computational approach which computes $\Psi(q,t)$ by solving *nonperturbatively* the many-electron TDSE for unstable states of atoms and small molecules. The time evolution of these states is caused either by the time-independent Hamiltonian, $\mathbf{H}_{A,M}$ (e.g., case of time-resolved autoionization—see below) or by the time-dependent Hamiltonian, $H(t) = \mathbf{H}_{A,M} + \mathbf{V}_{ext}(t)$, where $\mathbf{V}_{ext}(t)$ is the sum of the identical one-electron operators that couple the field of a strong pulse of radiation to the electronic and nuclear moments of N-electron atomic or molecular states of interest, thereby producing, during and at the end of the interaction, final states in the ionization or the dissociation continua.

1.3. Basic equations expressing the formal solution of the TDSE for problems of unstable states

The foundational elements of the theory and formalism necessary for the perturbative or nonperturbative treatments of the TDSE for isolated non-stationary (unstable) states of atoms and molecules have been known for decades and have been included in books. We recommend the classic treatises of Heitler [2] and of Goldberger and Watson [3]. Also, a recent textbook by Tannor [4] contains much useful information for a broad spectrum of methods and phenomena that require consideration of the solutions $\Psi(t)$ of the TDSE. In the following paragraphs, we focus on certain formal results in order to recall the fact that, although formalism is often available in elegant forms, its practical implementation for the solution of TDMEPs in real systems remains a desideratum.

1.3.1. Time-independent operators
We distinguish two cases:

$$\mathbf{H}(t) \to \mathbf{H} = \mathbf{H}_{A,M} \tag{4}$$

or

$$\mathbf{H}(t) \to \mathbf{H} = \mathbf{H}_{A,M} + \mathbf{V}_{ext}, \tag{5}$$

$\mathbf{V}_{ext}$ is an external static electric or magnetic field. For $\mathbf{H}_{A,M}$ we will assume the Born–Oppenheimer approximation, which allows the decoupling of the motion of electrons from those of the nuclei.

In order to describe the time-resolved dynamics of an unstable state in terms of the Hamiltonian **H**, it is necessary that the initial state, say at $t = 0$, *not be* an eigenstate of **H**. Otherwise the system would be stable [i.e., would have the form of Eq. (1)]. Now, instead of Eq. (1), the formal "solution" of the TDSE is given by ($\hbar = 1$)

$$\Psi(t) = e^{-i\mathbf{H}t} |\Psi(0)\rangle . \tag{6a}$$

1.3.1.1. Case of Eq. (4). The time-resolved decay of many-electron autoionizing states

For the case of Eq. (4), there is conceptual and computational difficulty in choosing the initial state wavefunction. The energy E_0 of $\Psi(0)$ is inside the continuous spectrum of the atomic or molecular system and is not an eigenfunction of an explicitly constructed local operator. Therefore, care and justification are needed when applying standard computational methods which have been developed for ground or low-lying discrete states. When the problem is about electronic spectra, $\Psi(0)$ is a many-electron, square-integrable wavepacket at $t = 0$, whose definition and systematic computation in the framework of the *state-specific theory* are discussed in Ref. [1].

The computation of Eq. (6a) implies the possibility of determining reliably the result of the action of the evolution operator $e^{-i\mathbf{H}t}$ on $|\Psi(0)\rangle$ for all t. Obviously, if the problem has to do with many-electron **H** and $|\Psi(0)\rangle$, we have a serious and insoluble TDMEP since a direct algebraic computation is not practical, and one must employ efficient methods of representation and evaluation of the propagator $e^{-i\mathbf{H}t}$ as it acts on the wavepacket $|\Psi(0)\rangle$. For purely nuclear motion, much work has been done on the efficient propagation of wavepackets on Born–Oppenheimer potential energy surfaces (PESs). (Mostly, only one PES has been considered, that of the ground state, and only a few degrees of freedom have been handled in practice.) The subject of nuclear wavepacket propagation is reviewed in, e.g., Refs. [4–8]. Aspects of it are covered and discussed by Atabek et al. in chapter 2 of this book.

On the other hand, Eq. (6a) may be handled formally in special but important cases of unstable states where the "motion" and correlations of electrons need not be taken into account explicitly. One such case is concerned with semiquantitative phenomenology. It involves the transformation of Eq. (6a) in terms of the energy spectral resolution of the atom or molecule and the derivation of formulae for the time evolution. Isolated unstable states inside a purely continuous spectrum decay exponentially, with deviations at very short and very long times (in general), whose explicit form and magnitude depend on the assumed form of the energy distribution. [The topic of decaying states is discussed in **Chapters 4** (Ref. [1]), 7, and 9 of this book]. However, if $\Psi(0)$ belongs to a system that does not have a continuous spectrum but only discrete levels, however dense, its decay curve is distorted from the exponential form, in ways which depend on the type of the spectrum and of the interaction.

For an isolated decaying state, there are alternative ways of writing Eq. (6a), which connect time evolution to the spectral properties of **H**. The first is straight forward to obtain: By inserting the spectral resolution of identity, the energy–time Fourier transformation emerges

$$\Psi(t) = \int_0^\infty dE \, |\Psi_E\rangle \, \langle \Psi_E \, |\Psi(0)\rangle \, e^{-iEt} \equiv \int_0^\infty dE c(E) e^{-iEt} \, |\Psi_E\rangle \, . \tag{6b}$$

Expression (6b) does not include the discrete spectrum—if it exists. This is the normal assumption when the irreversible decay of $\Psi(0)$ into the continuum is examined. However, there are exceptional cases of extreme proximity of $\Psi(0)$ to the threshold of the spectrum of a Coulomb potential where the Rydberg series accumulate. A study of the time evolution in this case is reported in Ref. [9].

A mathematically richer expression emerges when the *resolvent* of the Hamiltonian, $\mathbf{R}(z) \equiv 1/(z - \mathbf{H})$, $z = E \pm i\eta$, $\eta \to 0$, is used:

$$\Psi(t) = e^{-i\mathbf{H}t} \, |\Psi(0)\rangle \, = \frac{-1}{2\pi i} \oint_{\text{spectrum}} \mathbf{R}(z) e^{-izt} dz \, |\Psi(0)\rangle \, . \tag{6c}$$

Aspects of analysis of decaying states based on Eq. (6c) can be found in Refs. [3, 10, 11]. The basic formal theory concerning the connection between the time-evolution operator and the resolvent of the Hamiltonian goes back to the 1951 publication of Schönberg [2, 12].

When the contour surrounds the spectrum of **H** on the first Riemann sheet of E, the integral (6c) is valid for $t > 0$ and for $t < 0$. Since $R(z)$ is analytic on the first Riemann sheet, any of its possible simple complex poles must appear on the second sheet. Indeed, Eq. (6c) leads naturally to the identification of the isolated unstable state corresponding to $\Psi(0)$ with a complex energy of Eq. (2) that is identical to a complex pole of $\langle\Psi(0)| \mathbf{R}(z) |\Psi(0)\rangle$ on the second Riemann sheet below the real axis, for $t > 0$ [1, 3, 10, 11].

Inspection and consideration of Eqs. (6b and 6c) lead to the conclusion that computation of the physically relevant amplitude, $\langle\Psi(0) \, | \, \Psi(t)\rangle$ (or of any other amplitude involving the overlap of $\Psi(t)$ with a final state), which gives the time evolution of decay, implies knowledge of either the coefficients $c(E)$ or of the matrix element (Green's function) $\langle\Psi(0)| \mathbf{R}(z) |\Psi(0)\rangle$. If the problem requires the determination of this Green's function for a many-electron system in terms of its electronic states, then such a calculation from first principles remains to be done. On the other hand, it is possible to compute it for unstable physical systems that are solvable along the fragmentation coordinate. A recent such example is the ab initio calculation of the positions and the autodissociation widths of the five vibrational levels of the intrinsically unstable molecule He_2^{++} $^1\Sigma_g^+$, which were obtained accurately by calculating

the complex poles of the semiclassical Green's function via a path integral formulation [13].

As regards the TDMEP in computing the $\Psi(t)$ of nonstationary atomic or molecular electronic states, the purpose of this review is to explain how the *state-specific expansion approach* (SSEA), which was introduced and first applied in 1993–1994 as an alternative to the *grid method* that was then restricted to effectively one-electron problems (see Section 2), *does not* start from Eq. (6a). Rather, it deals with the differential form (3), which is transformed into a set of coupled integro-differential equations by expanding $\Psi(t)$ in terms of state-specific many-electron stationary wavefunctions for the discrete as well as for the energy-normalized continuous spectrum. In this context, apart from the requirement of a robust numerical technique for integrating over time the TDSE, the basic aim is the reliable computation of state-specific wavefunctions for that part of the discrete and continuous spectrum which is physically significant and to compute accurately the bound–bound, bound–scattering, and scattering–scattering matrix elements involving the coupling operators (see Sections 4 and 6).

In one case of its implementation during the 1990s, the SSEA was applied to the numerical computation from first principles of the process of autoionization from a time-dependent point of view. This application produced the first theoretical results—which are still the only ones—on the time-resolved decay, for very short to very long times t, of prototypical unstable states of $\mathbf{H}_{A,M}$ of polyelectronic atoms and negative ions, decaying via Coulomb or via Breit–Pauli relativistic couplings [14–16]. The regimes of exponential and of nonexponential decay were thus revealed for each state in a quantitative way. It is worth noting that the time dependence of the decay of an autoionizing atomic state was first measured in 2002, in an XUV pump–laser probe experiment by Drescher et al. [17]. However, only the exponential regime was registered.

1.3.1.2. Case of Eq. (5). The time-resolved ionization by a static electric field

For the case of Eq. (5), the initial state, $\Psi(0)$, is normally in the discrete spectrum and so it is easily recognized as a single-energy eigenstate of $\mathbf{H}_{A,M}$. The computation of such a state can be achieved according to methods of standard quantum chemistry, especially if it is the ground state. The application of say an external static electric field, which is assumed to be done suddenly, introduces, in combination with the atomic Coulomb attraction, an effective potential with a barrier, whose shape depends on the strength of the field. This fact allows the field-dependent mixing of the discrete state with the continuous spectrum, thereby turning it into an unstable state, whose energy not only is shifted from the unperturbed position but also has a width. This width represents the rate of ionization either via the direct mechanism of over the barrier transition or via tunneling through the barrier.

The problem of determining rates of the ionization processes induced by an external electric static field was for decades limited to one-electron or to model one-electron systems and semiempirical approaches. In the late 1980s and 1990s, publications where the time-independent *complex eigenvalue Schrödinger equation* (CESE) approach was applied [1], showed how the problem can be handled nonperturbatively for polyelectronic states, for electric, e.g., Refs. [18–20] as well as for magnetic fields [21]. Comparisons with extensively used semiclassical and semiempirical one-electron models, for weak and for strong fields, were presented in Refs. [20, 22]. From our calculations, as well as from independent calculations on He by Scrinzi [23], the advantages and limitations of these models (see Ref. [20]) were recognized quantitatively. It is worth noting that recent computations by Parker et al. [24], of intense field ionization of He in the static-field limit via the time-dependent solution of the TDSE by a full-dimensionality two-electron *grid method*, led to the same conclusions as the ones published in Refs. [20, 22, 23].

When time resolution is required, then it is time-dependent probabilities rather than rates (= probability per unit of time) that have to be computed. For the case of the static field, the SSEA has not been applied yet. However, for the one-electron hydrogen atom, the problem of the time-resolved evolution of its ground and its first excited states was tackled a few years ago, first by Geltman [25], who used an expansion method (the TDSE turns into a set of coupled equations), with a box-normalized discretized continuum, and then, more extensively, by Durand and Paidarová [26], who approached the problem in terms of Eq. (6c) and the complex coordinate rotation method. In addition to their numerical results, the publications [25, 26] contain interpretations and critical remarks on aspects of the dynamics.

1.3.2. Time-dependent operators
This is the case whose treatment via the SSEA is discussed in this review. The total Hamiltonian has the form

$$H(t) = \mathbf{H}_{A,M} + \mathbf{V}_{\text{ext}}(t), \tag{7}$$

where the time-dependent interaction $\mathbf{V}_{\text{ext}}(t)$ is assumed to have a temporal envelop, normally resembling a Gaussian or a $\sin^2$ function.

From a rigorous point of view, it is clear that the solution of the TDSE with $H(t)$ of Eq. (7) (we discuss the explicit form of $\mathbf{V}_{\text{ext}}(t)$ in Sections 4 and 6) constitutes a serious TDMEP with conceptual as well as computational questions. In fact, the appropriate approach depends not only on the nature of the initial state of $\mathbf{H}_{A,M}$ but also on the characteristics of $\mathbf{V}_{\text{ext}}(t)$ in connection with the discrete and continuous spectrum of $\mathbf{H}_{A,M}$.

Thus, for a pulse whose field strength is considered weak for the problem in question, an approach based on first-order, time-dependent perturbation

theory (TDPT) may suffice. For example, recent publications on pump–probe excitation of triply excited states, or on the time-dependent preparation of the profile of an autoionizing state, present analytic results in the framework of first-order TDPT [27, 28].

On the other hand, a variety of interesting and challenging experimental situations exist where the coupling is due to a time-dependent pulse which is strong, and, therefore, the many-electron TDSE must be solved to all orders of TDPT or, equivalently, directly and nonperturbatively.

In order to illustrate the magnitude of the computational difficulty for the case of strong fields, we recall that the formal solution of the TDSE on the interval $(0,t)$ is obtained as a time-ordered infinite perturbation series, the Dyson series [3, 4, 29]:

$$\Psi(t) = \sum_{n=0}^{\infty} \frac{(-i)^n}{n!} \int_0^t dt_n \int_0^t dt_{n-1} \dots \int_0^t dt_2 \int_0^t dt_1 \mathbf{T}\{\mathbf{H}(t_n)\dots\mathbf{H}(t_2)\mathbf{H}(t_1)\} |\Psi(0)\rangle ,$$

(8a)

which is equivalent to the integrated expression

$$\Psi(t) = \mathbf{T} e^{-i\int_0^t \mathbf{H}(t')dt'} |\Psi(0)\rangle ,$$

(8b)

$|\Psi(0)\rangle$ is now an eigenfunction of $\mathbf{H}_{A,M}$ and $\mathbf{T}$ is the *time-ordering operator* [3, 4, 29]. The operators $\mathbf{H}(t')$ and $\mathbf{H}(t'')$ (defined at different times) do not commute. The operation of $\mathbf{T}$ enforces causality, i.e., $\mathbf{T}\{\mathbf{H}(t'')\mathbf{H}(t')\} = 0$ for $t'' < t'$.

The rigorous implementation of Eqs. (8) is not a computationally practical approach to the solution of TDMEPs to all orders. Indeed, no calculations exist which apply Eqs. (8), or other possible rearrangement of TDPT, in order to solve the TDMEP to all orders for a polyelectronic atom or molecule interacting with a time-dependent strong radiation pulse. The fundamental difficulty has to do with the requirement of accounting for the interelectronic interactions.

On the other hand, approximations to Eq. (8) and time-integration techniques, suitable especially for time-independent Hamiltonians, under the requirement of only a few degrees of freedom and short-time evolution, have been developed and applied extensively in connection with grid-type techniques (see Section 2), by focusing on appropriate algebraic expansions of the exponential form. For example, such a approach is effected by the *split-operator* method [4] and references there in.

The approach to the solution of the TDSE that is presented in this review does not focus on the handling of the time-evolution operator and on its various approximate expressions acting on a wavefunction defined on a lattice of points in configuration space. Instead, it focuses on the appropriate

calculation of $\Psi(t)$ via its time-dependent expansion in terms of state-specific many-electron stationary states. Based on a series of characteristic calculations since 1993–1994, in the following sections it will be argued that the SSEA, which constitutes a direct implementation of basic QM provided the MEP can be dealt with efficiently, can provide reliable and transparent solutions to a variety of TDMEPs.

The review covers, apart from the methodology of solving the TDSE, the theory for the solution of the MEP in two broad subjects of modern research: One which refers to isolated discrete and resonance states, and one which refers to the series of states just below and just above the fragmentation threshold. Thus, it is also concerned with the theory of the quantum defect and of related issues. The applications which are mentioned or are discussed briefly, involve either the ab initio computation of the time-resolved decay of autoionizing states, or, especially, prototypical TDMEPs of absorption of one or of many photons by atoms, by negative ions and by diatomics. In the latter case, we demonstrate how the 'multipolar' interaction expressing the *full* atom-field interaction, (and not just the electric dipole approximation), can be incorporated into a practical computational methodology.

2. ON THE NONPERTURBATIVE SOLUTION OF THE TDSE FOR PROBLEMS WHERE A GROUND OR AN EXCITED STATE OF AN ATOM (MOLECULE) INTERACTS WITH A STRONG ELECTROMAGNETIC PULSE OF SHORT DURATION

Starting in the 1970s and, more extensively, in the 1980s, it became possible, scientifically and technologically, to generate static and, especially, dynamic EMFs at different frequencies, with the following main characteristic: When used to probe atomic and molecular systems in the ground state or in excited states, the corresponding coupling is strong enough that the concomitant phenomena and properties *cannot* be explained, let alone described quantitatively, by applying standard time-independent or TDPT to lowest order. For example, such cases occur with multiphoton processes that lead either to ionization or to dissociation or to both. When the field is strong relative to the system under consideration, free–free transitions coupling many states of different angular momenta become important. The results of such transitions are phenomena like *above-threshold ionization* (ATI) or *above-threshold dissociation* or *high-harmonic generation* (HHG).

By the end of the 1980s and early 1990s, the literature on the various aspects and directions of the general theme of atoms (molecules) interacting with strong EMFs was already extensive. (We recall that the atomic unit of radiation intensity is $\cong 3.5 \times 10^{16} \text{W} / \text{cm}^2$). Since the scope of the present article is concerned mainly with computation-oriented theory (rather than with phenomenology), that is capable of handling nonperturbatively the TDMEP in real systems, we cite three books published around 1990, rather

than the large number of related articles published in scientific journals. The first is the 1987 monograph by Faisal [30]. The second is the book edited by Nicolaides et al. [31], which contains the lectures at a NATO ASI that took place on Kos, Greece, in 1988. The subjects of the articles refer to dynamic as well as to static fields. The third is the 1992 book edited by Gavrila [32], which contains invited papers that focus on a variety of phenomena and on stationary as well as time-dependent methods involving dynamic fields.

The well-understood fact of the breakdown of "lowest-order perturbation theory" (LOPT) in the area of atom (molecule)—EMF interactions ushered theoretical research into a new age, whose substantial progress depends, apart from establishing the fundamentals of phenomenology, on the transparency and efficiency of theoretical approaches to handle the multifarious MEP within computational schemes that go beyond the LOPT. These fall into two types of frameworks: One which employs, where appropriate, stationary-state formalism (e.g., see Refs. [1, 30–32]), and another in which the aim is the computation of $\Psi(t)$ by solving the TDSE.

It is the latter case with which the present review is concerned, especially as regards the possibility of tackling efficiently a variety of TDMEPs. These TDMEPs are consequences of a great number of current or future experimental possibilities that use radiation pulses whose wavelengths can range from the microwave to the X-ray spectrum, and whose duration can be in the range of femtoseconds (1fs $= 10^{-15}$ sec) or even attoseconds (1 as $= 10^{-18}$ sec). This means that when the corresponding matter–field interaction takes place, it may induce single or multiphoton ionization and dissociation processes involving either outer or inner electrons, or Rydberg levels, or negative ions, or vibrational levels and bond fragmentation, or atomic collisions. The pulses are assumed to be not only strong but also short, so that the atom–field interaction has a temporal shape expressing the rise, the maximum, and the decline of its strength, with the number of field cycles ranging, according to experimental conditions, from one half to a few hundreds.

2.1. Two approaches to the solution of problems of time-dependent processes induced by strong pulses

2.1.1. The grid method

The first results on real (not model) atoms, specifically on H, He, and Xe, for the time-dependent multiphoton ionization induced by strong laser pulses were published by Kulander and co-workers [33–38] who implemented the *grid method*, e.g., Refs. [4, 6, 33] and references therein. Use of the grid method is the approach that remains popular among many researchers working on problems of pulse–atom (molecule) interactions, even though it cannot handle the plethora of cases involving arbitrary polyelectronic structures which would require the possibility of propagating the solution of the Schrödinger partial differential equation on multidimensional grids while accounting for interelectronic couplings.

In this approach, one looks at the TDSE as a parabolic differential equation and attempts a direct numerical integration by propagating $\Psi(t)$ (the wavepacket) on a grid of points in time and in a space of suitable coordinates, i.e., on a multidimensional lattice, subject to proper initial boundary conditions, up to a distance that is assumed to be sufficiently large. The reflection of the flux at the end of the boundary is avoided in practice by using some form of "absorbing potential." Although time–space pictures of the wavepacket reveal aspects of the physics, the quantitative information about properties must be obtained from the projection of the solution onto relevant stationary states.

The first implementation of the grid method to the time-dependent ionization by a laser pulse was done on a simple one-dimensional model in 1978 by Goldberg and Shore [39]. In 1987, Kulander [34] introduced it to the study of the time-dependent ionization of H by a laser pulse. His grid-method publications continued in 1988 with applications to He and to Xe in the framework of the independent electron model (IEM) [35, 36]. Specifically, Kulander's original [34–36] and subsequent papers, e.g., Refs. [33, 37, 38], produced the first quantitative information about time-dependent multiphoton ionization and new phenomena, such as HHG. However, those computations were restricted to simple cases of independent one-electron time-dependent quantum mechanical motion, with the initial state being a single determinant. The first such application was to He [35] and involved the single determinantal time-dependent Hartree–Fock (TDHF) approximation. The second application was based on the practical concept of the *single active-electron approximation* (SAEA), where the time-dependent wavefunction of only one-electron moving in an average local atomic potential is computed [36]. It was applied to the multiphoton ionization of Xenon, where again, the initial state was approximated by a single determinant.

The grid-implemented SAEA has been restricted to closed-shell, single determinantal initial states. In general, it should be expected to have advantages and disadvantages similar to those that characterize the IEM in various time-independent problems. In other words, it is a computationally tractable approach which is the first step toward the understanding of processes and phenomena that are associated with the ionization of atoms and molecules by intense laser pulses. Its physical relevance depends on the level of accuracy at which a particular phenomenon and/or quantity need to be known. For example, when considering the multiphoton ionization of the noble gases at certain wavelengths, certain gross features of ionization probabilities, of ATI or of HHG, are obtainable in the framework of the SAEA. Yet, one must bear in mind that, even for the noble gases beyond Neon, i.e., even for simple closed-shell ground states (let alone arbitrary open-shell zero-order wavefunctions), the SAEA misses features of electronic structure and of concomitant excitations that may be important when accurate quantitative information is desired. Such a statement is based on theoretical and

computational analysis and experience on the more conventional problem of the rates of one-photon transitions due to weak interactions [40, 41]. (See also Ref. [42] and its references.)

Specifically, theoretical and computational results from the late 1960s to the 1970s indicate that, regardless of whether the perturbing field is weak or strong, the electronic structure of the initial state in atoms other than He and Ne and in many molecules at geometries away from equilibrium, even in closed-shell ground molecular states, requires the adoption of a multiconfigurational zero-order *Fermi-Sea* wavefunction [40–42]. This concept and its implementation creates conditions for important electronic excitation amplitudes, whose basis is both *nonorthonormality* and *electron correlation*, and which are different than those predicted by simple models such as the mean–field IEM or the algorithm of the *random phase approximation* [40–42].

Since Kulander's early work, the grid method for laser pulse-induced time-dependent electron excitation has been used, in one form or another, by a number of researchers. Of major concern has been the development of efficient techniques for propagating the solution in three-dimensional lattices, e.g., Refs. [43, 44]. Furthermore, in order to account for interelectronic interactions in closed-shell systems beyond the one-electron models, two types of developments have received attention, both based on algorithms that need access to powerful computers in order to make them practical even for two-electron closed-shell systems. In one development, the direct integration of the TDSE for the two electrons in a fully dimensional scheme has been achieved at different laser frequencies for the He ground state [23, 45]. In the other development, the single determinantal TDHF method is replaced by time-dependent multiconfigurational self-consistent field methods, where both orbitals and mixing coefficients are time-dependent, e.g., Refs. [7, 46–48].

In spite of notable advances in techniques in conjunction with hugely increased computational power, it is a moot question whether it will be made possible and economic to render these computation-intensive, grid-dependent methods applicable in a practical way to the solution of laser-induced TDMEPs with arbitrary electronic structures.

2.1.2. The method of expanding $\Psi(t)$ in terms of the stationary states

In the textbook discussions of the phenomenology of the interaction between quantized matter and an external EMF, the standard approach for developing the formalism (e.g., TDPT or schemes of two- or three-level systems), is the expansion of the full solution of the TDSE, $\Psi(t)$, in terms of the eigenstates of the unperturbed $\mathbf{H}_{A,M}$, say Φ_n, with time-dependent mixing coefficients, $b_n(t)$. According to the rules of QM, $|b_n(t)|^2$ (or $|b_E(t)|^2 dE$ for a state of the continuous spectrum) is the probability for a measurement to find the system in a stationary state $|\Phi_n >$ at the time t (e.g., see chapter IV of Heitler [2]).

The TDMEPs that are of concern in this review acquire their serious difficulty not only from the fact that the eigenfunctions of the states of real systems, Φ_n, have many-electron structures and are not solvable one-electron models but also from the fact that many discrete states may be involved while the multichannel continuous spectrum, including resonances with multiply excited structures, becomes critically important.

The task of understanding and of solving reliably such TDMEPs is much more complicated and demanding than that where the goal is simply to deduce only the phenomenology. Instead, the ultimate goal is, or ought to be, the ab initio quantitative computation of time-dependent quantities and the physical transparency of the calculations, in which case phenomenology can also be tested when possible, and vice versa. However, now the final states in these TDMEPs are, in general, in the ionization or in the dissociation continuum. Therefore, what is required according to the expansion approach mentioned above is the possibility of computing and using both the Φ_n and the $b_n(t)$, for both the discrete and the continuous spectra, where the values of the complex $b_n(t)$ depend on the characteristics of the time-dependent interaction.

Although it appears from the literature that the *grid method* has attracted the overwhelming part of attention by a large number of researchers, we argue that the *expansion method*, if properly implemented, is more flexible as regards the variety of problems that it can handle, at least for atoms and small molecules, in initially ground or excited states. Proper implementation implies that one must capitalize on the theory and the computational know-how of computing wavefunctions for ground and excited stationary states that contain all the crucial for each problem features of electronic structure and of electron correlations.

The SSEA, which is the subject of this review, was introduced in 1993–1994 with the purpose of exploring the potential and the efficiency of using state-specific wavefunctions in solving from first principles TDMEPs related to laser pulse-induced properties and phenomena. In a large number of applications since then, it has been demonstrated that this fundamental, yet conceptually simple, approach to such TDMEPs can indeed be realized computationally.

Furthermore, if the spirit of the SSEA is followed, there are benefits of transparency and of economy for the following reason: By paying attention to the choice of the function space entering into the calculation of the wavefunctions that represent the states of physical and computational significance, one can easily acquire a feeling of the overall calculation as regards the importance and the degree of contribution of the various states, or sets of states, for each problem of interest.

By "state-specific" we mean that the expansion consists of wavefunctions that are as close as possible, considering the requirements of each problem, to the exact eigenfunctions of the spectrum on the real energy axis (see also

Ref. [1]). For example, this is easily understood for exactly solvable potentials (analytically or numerically), ranging from models to, say, the systems of the Morse molecule, of the hydrogen atom or of the H_2^+ molecule. In fact, in such cases, even the standard approach of quantum chemistry which obtains eigenfunctions via the diagonalization of the relevant Hamiltonian over a basis set may provide a practical way of obtaining identifiable and usable representations of the stationary states comprising the discrete and the continuous spectrum. For example, since in such systems where there is no electronic structure and interchannel mixings and the continuum is smooth, as, e.g., is the case with the multiphoton dissociation of diatomics, the use of a box-normalized basis set may be sufficient for the purposes of a corresponding problem (see examples of Section 3).

However, the "diagonalization-on-a-large-basis-set" approach to the computation of the stationary states of the whole spectrum loses its usefulness when it comes to the requirement of solving in a manageable way the TDSE for TDMEPs in polyelectronic systems. Indeed, when it comes to electronic continua of multielectronic atoms (molecules) that open in ionization processes by strong laser pulses, then the issue of their proper representation is certainly critical to calculation of quantities such as ionization probabilities, angular distributions of emitted electrons, HHG. As we will show in the following sections, in this case, as well as in cases of dissociation by strong fields where the free–free transitions in the continuum play a heavier role, the appropriate (more reliable) choice according to the SSEA is to use energy-normalized scattering wavefunctions, computed separately for each value of energy on a dense energy mesh.

In the following sections, the examples and the discussions on the theory and methodology of the SSEA have been apportioned according to the relative significance of the continuous spectrum.

Specifically, in Section 3 we cite four examples from our early work on the solution of the TDSE for TDMEPs, which focused on novel molecular processes in diatomic molecules [49–52]. These were computed from first principles, in terms of configuration interaction (CI) wavefunctions, corresponding energies, and coupling matrix elements, within the Born–Oppenheimer approximation. For the vibrational motion and the corresponding continuum, a box-normalized trigonometric basis set was used [50, 51]. On the other hand, this approximation is rectified in the example of multiphoton dissociation of the Morse molecule by low-frequency strong fields. In this case, it is preferable that the free–free coupling matrix elements be computed systematically and accurately, and so the SSEA is applied in a rigorous way, in terms of energy-normalized scattering states of the Morse potential [53].

Starting with Section 4, we describe the essentials of the SSEA for the systematic treatment of various electronic processes in atoms and diatomics. In Section 5 we focus on the theory and computation of the state-specific Φ_n for

atoms and negative ions (indicating its possible extension to diatomics), of the free–free matrix elements with numerical energy-normalized scattering functions and of the $b_n(t)$.

The essentials of the SSEA for numerically computed energy-normalized N-electron wavefunctions were published in 1994 by Mercouris et al. [54]. The first application was not only to the multiphoton ionization of H (whose spectrum is known exactly analytically), as a test case, but also to the multiphoton detachment of the four-electron Li$^-$ negative ion, with two free channels, Li $1s^2 2s$ ^{2}S and $1s^2 2p$ ^{2}P^o. Li$^-$ (or Be) is the first system of the Periodic Table for which the proper description of the zero-order electronic structure requires a multiconfigurational Hartree–Fock (MCHF) description. In the context of the review of the SSEA, we also discuss briefly the formulation of the problem in terms of the full atom–EMF interaction, $\mathbf{V}_{ext}(t)$, which is computationally convenient as well as necessary for certain problems involving, say, off-resonance coupling of Rydberg states, for which use of just the electric dipole term is inadequate [55–57].

3. AB INITIO COMPUTATION OF UNUSUAL TIME-DEPENDENT MOLECULAR PROCESSES USING JUDICIOUSLY CHOSEN EXPANSIONS FOR THE $\Psi(t)$

The following examples are drawn from the publications [49–52]. Those results were obtained by solving the TDSE using molecular data that were computed in terms of CI electronic wavefunctions and energies for a large number of values of the internuclear distance R.

3.1. Time-dependent laser-induced molecular formation from repulsive surfaces [49, 52]

The normal experimental or theoretical study of laser-induced time-dependent processes is concerned with transitions that start from a bound state, mostly the ground bound state, and, if the intensity is not very weak, end with some probability inside the continuous spectrum.

Sometime ago [49, 52], we considered a rather novel at that time TDMEP, which involved time-dependent molecular processes in the reverse direction, namely, repulsive-to-bound state molecular radiative transitions. Specifically, the problem that was constructed and the question that we asked were as follows.

There are molecules which, in the Born–Oppenheimer approximation, can be bound only in excited states, such as the "excimer" molecules (HeH)*, (NeH)*, (ArH)*, and (HeF)*. These excited bound states decay to the dissociative continuum of the ground state either via radiative transitions or via radiationless transitions, each having its characteristic probability. Suppose we look at the collision of the (ground repulsive state) free atoms in the

presence of a relatively intense femtosecond laser pulse that can connect the corresponding wavepacket radiatively, on resonance at the right internuclear distance, to, say, the lowest excited bound state in its equilibrium geometry.

The resonance character of the problem might lead one to the conclusion that a first-order theory is sufficient to provide answers. However, since the times for the interaction and for the lifetime of the collision complex in the desired geometry are very short, the pulse intensity has to be relatively high for any significant population transfer to take place. Therefore, it is important to explore the significance of the contribution in higher order of the off-resonance higher lying electronic states. This means that the time-dependent formation and the decay of the first excited state depends not only on the direct interaction between the laser pulse and the colliding atoms but also on the population transfer among the excited states which is induced by the coupling matrix elements among all the states. How can we compute the time-dependent probabilities for these processes and draw useful conclusions?

The construction of such a TDMEP was in harmony with femtosecond experiments of "transition state spectroscopy" that had been done in the late 1980s [58, 59]. It is also relevant to phenomena in current ultracold collision physics that go under the name "photoassociation" [60].

Accordingly, we computed the time-dependent probabilities for the laser-induced molecular formation (LIMF) of $(HeH)^*$, $(NeH)^*$, $(ArH)^*$, and $(HeF)^*$, for laser frequencies around the energy difference between the colliding atoms and the first excited bound state at its equilibrium distance, while taking into account the contribution of higher lying molecular bound states via the nonperturbative solution of the TDSE. The influence of the induced or the spontaneous decays of all the states, i.e., collision time, photoionization, radiative, and radiationless dissociation, was taken into account by using complex energies, where the imaginary part represents the sum of the rates of such decays. The results were obtained for laser pulses of different shapes, duration (in the range of fs), frequency, and intensity.

As exemplars, two of the resonance photoreactions between the repulsive initial state, considered as a narrow wavepacket with a lifetime of a few femtosecond, and the first excited bound state are shown below. The first, (i), is from Ref. [49] and the second, (ii), is from Ref. [52].

(i) $[H(1s) + He(1s^2)]$ repulsive $X^2\Sigma^+$ $\xrightarrow[\text{fs}]{\text{laser}}$ $(HeH)^*$ bound $A^2\Sigma^+$ state,

(ii) $[F(2p^5) + He(1s^2)]$ repulsive $^2\Pi$ $\xrightarrow[\text{fs}]{\text{laser}}$ $(HeF)^*$ bound $2^2\Sigma^+$ state.

The TDSE was solved nonperturbatively by starting from the finite expansion over N molecular stationary states:

$$\Psi(r, R, t) = \sum_{n=1}^{N} b_n(R, t) \, |\Phi_n(r, R)\rangle. \tag{9}$$

For (i), the expansion (9) included the initial state plus 10 Rydberg-bound excited states at their equilibrium distance of $R_0 = 1.5$ a.u. Six were of $^2\Sigma^+$ symmetry, three of $^2\Pi$ symmetry, and one of $^2\Delta$ symmetry. All had been previously obtained from extensive CI calculations together with dipole matrix elements and non-adiabatic couplings [61].

For (ii), the initial state, $1^2\Pi$, is the second repulsive state of the HeF system, the first (lowest) state having $1^2\Sigma^+$ symmetry [62]. The excited bound states in the sum of Eq. (9) consisted of two $^2\Sigma^+$ and two $^2\Pi$ states. The dipole coupling was computed at $R_0 = 2.0$ a.u., which is the equilibrium distance for the first three bound excited $^2\Sigma^+$ states, whose energy differences from the $1^2\Sigma^+$ were calculated as [62]: 9.36 eV for $2^2\Sigma^+$, 10.51 eV for $3^2\Sigma^+$, and 11.58 eV for $4^2\Sigma^+$.

Having computed energies and coupling matrix elements, the calculations were based on the following equations: Substitution of Eq. (9) into the TDSE gives the coupled equations,

$$i\frac{d}{dt}b_m(R,t) = \varepsilon_m b_m(R,t) - E(t)\sum_{n=1}^{N} b_n(R,t)D_{mn}(R) \tag{10}$$

where

$$D_{mn}(R) = \langle \Phi_m(r,R)|r|\Phi_n(r,R)\rangle , \tag{11}$$

$$\varepsilon_m = U_m - \frac{i}{2}\Gamma_m, \, m = 1, 2, \ldots, N, \tag{12}$$

$$E(t) = f(t)F_0 \sin(\omega t), \tag{13}$$

U_m is the energy of the mth state and Γ_m is inversely proportional to the lifetime of each state. $f(t)$ is the temporal shape of the linearly polarized pulse, taken to have forms such a Gaussian or a sech function. F_0 is the peak field strength and ω is the monochromatic frequency.

For the repulsive states at slow collisions, the lifetime is of the order of a few femtoseconds. Our conclusion regarding this quantity was that "as expected and confirmed by our computations, it constitutes a very significant parameter for the realization or not of the excitation probability" [52]. For the excited states, the lifetime is caused by spontaneous emission, predissociation (when present), and by possible photoionization by the same pulse. The rates for these processes are computed from first principles. For example, for the (HeF)* $2^2\Sigma^+$ state, its multichannel predissociation rate (partial as well as total widths) to the repulsive $1^2\Sigma^+$ and $1^2\Pi$ states was computed from first principles in Ref. [63], using the theory of the CESE for unstable states that is presented in Ref. [1].

The solution of the coupled equations as a function of time follows a Taylor expansion which is discussed later in the text. Although the coefficients in Eqs. (10) can be obtained by vibrational averaging, computational economy

LIMF of HeF
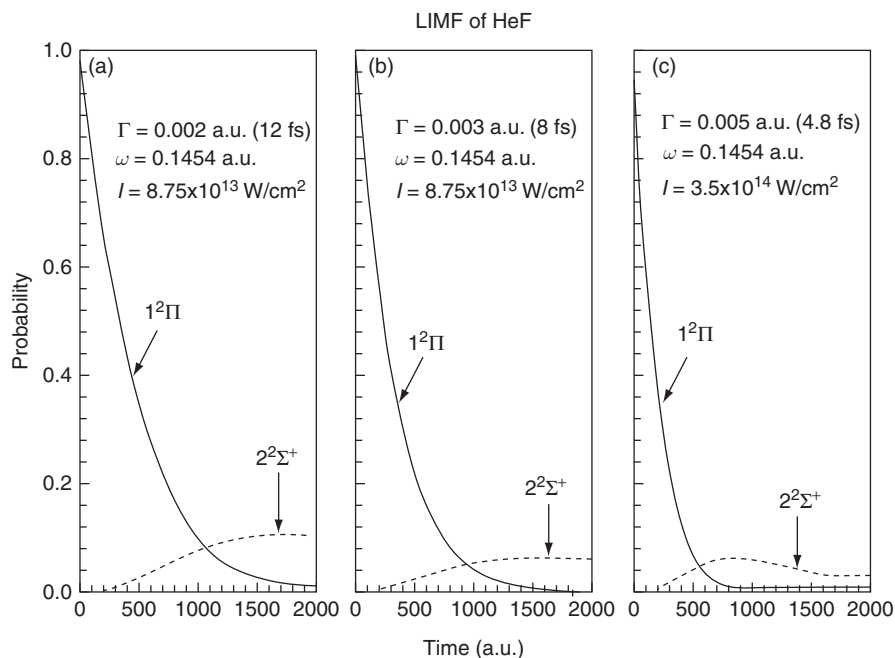
Figure 6.1 Probabilities for transferring population from the $1^2\Pi$ repulsive excited electronic state of HeF to the $2^2\Sigma^+$ bound excited state, for decreasing collision times (a)–(c), and peak intensities from 8.75×10^{13} W/cm^2 to 3.5×10^{14} W / cm^2. (From Ref. [52].)

is secured by choosing only one value of R, the one at the equilibrium of the excited bound state, R_0 [49, 52].

Figure 6.1 shows the results on (HeF)* from Ref. [52], regarding the time-dependent probabilities for transferring population from the $1^2\Pi$ repulsive excited electronic state to the $2^2\Sigma^+$ bound excited state, for different collision times of the two atoms, i.e., for 12 fs, 8 fs, and 4.8 fs, and for peak intensities of 8.75×10^{13} W/cm^2 and 3.5×10^{14} W/cm^2.

3.2. Time-dependent multiphoton dissociation above and below the threshold of diatomic "volcanic" states [50, 51]

In the normal ground states of diatomic molecules, the minimum energy at equilibrium is an absolute minimum. On the other hand, there are a few exceptions where the minimum at which the molecule has its equilibrium geometry is a local minimum, lying above the dissociation threshold, e.g., Refs. [13, 50, 51, 64] and Figure 6.2 below. Because of the special shape of their potential surfaces, we have called such ground states, "volcanic" states. In Refs. [50, 51] the expansion method was applied for the ab initio nonperturbative solution of the TDSE describing the infrared multiphoton
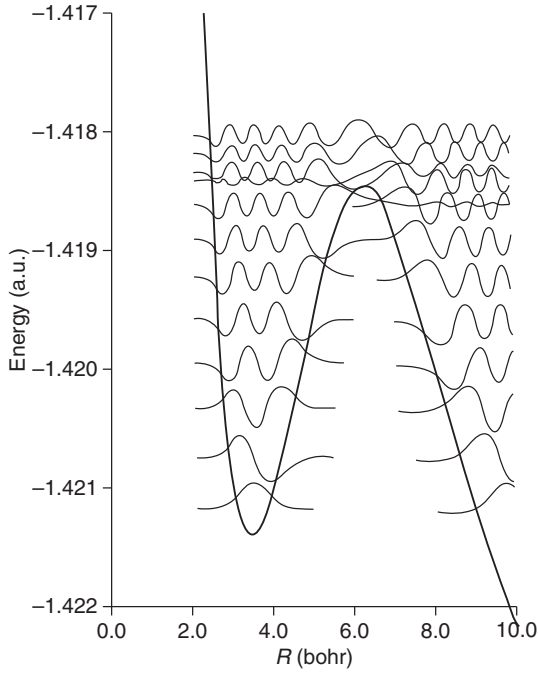
Figure 6.2 The volcano-like potential of the ground state of BeH^{++}. Its minimum is local, since it is above the dissociation limit of $Be^+ + H^+$. The curve was computed by the method of configuration interaction. Also depicted are the corresponding eigenfunctions of the 8 shape resonance states that this potential can support, e.g., Ref. [13]. These, as well as those representing states above the barrier, were obtained from the diagonalization of a basis of 120 box-normalized trigonometric functions. The box length was R_L= 10 a.u. The picture of tunneling is clearly enhanced for the top two shape resonances. (From Ref. [50].)

computation of two such molecules, the BeH^{++} and the NO^{++}. The latter has an excited electronic "volcanic" state, $A^2\Pi$, embedded inside the vibrational spectrum of the ground state, $X^2\Sigma^+$, which is also volcanic.

In Refs. [50, 51] we examined the infrared time-dependent multiphoton dissociation of such molecules. The nonstationary state, $\Psi(t)$, is formally written as a time-dependent sum of the vibrational quasi-bound levels,Φ_n, and of the dissociated states, X_E,

$$\Psi(t) = \sum_{n=1}^{N} a_n(t)\Phi_n + \int_0^\infty b_E(t)X_E dE. \tag{14}$$

For this type of states, the repulsive potential of the fragmentation continuum, e.g., $Be^+ + H^+$, starts asymptotically *below* the local minimum.

Therefore, the energies, ε_n, of the Φ_n are embedded in the energy continuum $[0,\infty)$.

Substitution of Eq. (14) into the TDSE produces coupled equations analogous to those of Eq. 10, only that now there are the additional terms with the coupling matrix elements of bound–free and free–free transitions [50]. The question is how to compute and use conveniently the state functions of the discrete and of the continuous spectrum of the diatomic potentials, and from these, to obtain the coupling matrix elements.

Given that this is a simple and smooth continuum of a one-dimensional potential without structure, we adopted the approach of diagonalizing the unperturbed Hamiltonian, $\mathbf{H}_0 = -\frac{1}{2\mu}\nabla^2 + V(R)$ (no rotation), with a single basis of box-normalized functions, in which case the continuum is discretized. Box normalization of states of the continuum is a decades-old technique of mathematical physics and of QM. In general, for simple problems of essentially one coordinate the approximation is tractable and not demanding computationally. For example, regarding the theme of solving the TDSE for the ionization of an atom by a laser pulse, in the late 1970s Austin [65] produced results of descriptive value using the simple delta function potential and box-normalized scattering stationary states.

When discretizing the continuum by placing the system in a box, a critical element of the approximation is the proper choice of the density of states, since the box-normalized function is proportional to the energy-normalized function, the proportionality coefficient being the square root of the density of the scattering states. For the basis set given below, the Stieltjes derivative approximation [66, 67] indicates that an accurate connection between the energy-normalized X_E and the corresponding discrete X_K of

energy ε_K is $X_E \approx \sqrt{\dfrac{2}{\varepsilon_{K+1} - \varepsilon_{K-1}}} X_K$. [50].

The calculations in Refs. [50, 51] proceeded by first computing from first principles in terms of CI wavefunctions, the potential energy, $V(R)$, and the dipole moment, $D(R)$. Then comes the calculation of the coupling matrix elements, $\langle \Phi_m | D(R) | \Phi_n \rangle$, $\langle \Phi_m | D(R) | X_K \rangle$, and $\langle X_K | D(R) | X_{k'} \rangle$. The stationary states Φ_n and X_K and the corresponding discrete energies, ε_n and ε_K, are obtained from the diagonalization of $\mathbf{H}_0$ on the basis set of the trigono-

metric functions $\dfrac{1}{\sqrt{R_L}}$, $\dfrac{2}{\sqrt{R_L}}\cos\dfrac{2\pi nR}{R_L}$, $\dfrac{2}{\sqrt{R_L}}\sin\dfrac{2\pi nR}{R_L}$, $n = 1,2,\ldots,\text{max}$,

where R_L is the upper integration limit. E.g., for BeH^{++}, a series of convergence tests which included the number of basis functions suggested that a number of only 120 states with $R_L = 10$ a.u. suffices to provide stable results. Of these 120 states, 8 represent the quasi-bound states inside the potential well.

In this framework, the time-dependent dissociation probability is

$$P_D(t) = 1 - \sum_{n=1}^{N} |a_n(t)|^2, \tag{15}$$

while the quantity $|b_K(t)|^2$ gives the probability distribution as a function of ε_K, i.e., it provides the time-dependent photofragment spectrum.

References [50, 51] contain a number of results from these nonperturbative calculations. One of them is the prediction, in a quantitative way, of the process of *below threshold multiphoton dissociation*, which reflects the fact that, for the volcanic molecules, the vibrational states are essentially unstable states (resonances), e.g., Refs. [13, 64], due to tunneling. This means that their energies must be written as complex numbers, $\varepsilon_n - \frac{i}{2}\Gamma_n$, where the tunneling rate Γ_n is obtainable either from semiclassical formulae [64] or from more sophisticated theories [13].

The picture of what is happening with the eigenfunctions as the energy reaches the barrier top can be seen in the spectrum of Figure 6.2 [50]. The number of quasi-bound levels predicted by the calculations is eight. The wavefunctions of the two closest to the barrier top show clearly the mixing of components from the inner and the outer region.

4. THE STATE-SPECIFIC EXPANSION APPROACH (SSEA)

4.1. General

The ab initio computations of time-dependent processes in novel molecular systems that were described in the previous section provided to us evidence, in the early 1990s, of the advantages of implementing the method of expanding $\Psi(t)$ in terms of the stationary states of real, polyelectronic atoms, and small molecules, when attempting the nonperturbative solution of the TDSE. This basic quantum mechanical approach presupposes that, for the problem of interest, the separation of the total $H(t)$ as in Eq. (7) is meaningful. The proviso is the possibility of implementing the expansion method in terms of wavefunctions that represent reliably the stationary states of $\mathbf{H}_{A,M}$ which contribute in a significant way, directly or indirectly, to the phenomenon under investigation. In other words, if the strength of the external EMF is not so high so as to destroy the meaning of the relevant spectra of atoms and molecules, then, conceptually and computationally, the physics of these TDMEPs can still be understood by using as reference point the spectra of $\mathbf{H}_{A,M}$.

The above assumption permeates the theory and methodology described here. It certainly works for many types of problems where the intensity of the field compared to the binding of the affected atomic electrons is

not overwhelming. On the other hand, it is expected that its convergence property will deteriorate rapidly for problems where, together with the pulse that excites the atom (molecule) to the continuous spectrum, an extra intense field of low frequency is applied, thereby causing strong perturbations in the continuous spectrum, which is now essentially "dressed" by the extra field. These types of pump–probe experimental arrangements have been achieved in recent years in terms of the synchronized application of ultrashort excitation pulses and strong IR lasers which probe directly the (multichannel in general) scattering continuum. For treatments of such problems from theoretical and experimental viewpoints, see the articles by Maquet and Taïeb [68] and by Kienberger et al. [69] and especially by Kelkensberg et al. [70] where experimental and theoretical results on the dissociative ionization of H_2 are obtained and compared. In Ref. [70], the wavepacket propagation needed for the problem was achieved in one dimension using the grid method.

Although the case of simultaneously applied two pulses is treatable by the SSEA, e.g., Ref. [71a], the pump–probe scheme of "XUV plus strong IR" pulses presents special difficulties as regards the possibility of proper convergence, since, now, the field-free continuum is perturbed very strongly and may lose its physical and mathematical character. One might argue that a direct numerical multidimensional integration on the space–time lattice is the best approach. However, before we comment on this, it is perhaps interesting to quote Maquet and Taïeb from their paper of 2007 [68, p. 1850]: "In principle, the experimental data could be retrieved by solving the TDSE for the atomic system, in the presence of the two pulses. However, the precise calculation of the response of the rare gas atom presents considerable difficulties. This is because the numerical resolution of the TDSE for a multielectron system remains well beyond the capability of present-day computers and that no satisfactory solutions will be available in the foreseeable future."

The above assessment is appropriate for methods that are based on integrations over space–time lattices. However, the prospects of expansion methods such as the SSEA may turn out to be feasible and practical, especially since they can account for a variety of electronic structures. In such cases, the SSEA which is discussed in this review could be adapted so as to employ a combination of field-free and field-dressed Volkov-type wavefunctions, the latter incorporating the information from the interaction of the IR laser with the scattering electron. It is outside the scope of the present review to report on the progress that we have made within this "field-dressed SSEA."

We return to the normal SSEA, which employs the eigenstates of $H_{A,M}$. As was already mentioned in previous paragraphs, for the monoelectronic H and H_2^+ the notion that the TDSE can be solved using the SSEA is easily acceptable, since one is comfortable with the fact that the exact eigenfunctions are accessible, analytically or numerically, for the discrete and for the continuous spectrum. The same holds for the discrete and for the

energy-normalized continuous levels of the one-dimensional potentials of diatomic molecules. Such calculations have been carried out in, e.g., Refs. [54, 56, 72, 73] for the H atom and in Ref. [53] for the Morse molecule. On the other hand, when it comes to TDMEPs, the nature of the requirements changes drastically, since the exact solutions of the TISE for the spectra of $\mathbf{H}_{A,M}$ are unknown. Therefore, in order for the expansion approach to be practical and tractable, it is desirable to achieve a level of theory and computation capable of satisfying three major requirements:

1. First, the structure and methods of the theoretical approach must be able to compute economically polyelectronic wavefunctions and their energies representing optimally the N-electron, M-nuclei states of both the discrete and the continuous spectrum of $\mathbf{H}_{A,M}$. This means that the theory must be of the many-body type, with separation of the exact wavefunction into a zero-order and a correlation part, the characteristics of which depend on the types of states comprising the expansion. In other words, brute-force methods that simply diagonalize the fixed nuclei $\mathbf{H}_{A,M}$ on approximate wavefunctions that are constructed from a large single set of L^2 functions are not capable of providing accurate N-electron wavefunctions for all the important to the TDMEP states of both the discrete and the continuous spectrum. Of course, special cases of one- or two-electron systems may turn out to be amenable to such computations [74]. In general, however, this approach is very limited and inapplicable when it comes to the reliable treatment of the great variety of TDMEPs requiring the ab initio solution of the TDSE for arbitrary polyelectronic structures.

2. Second, the framework of the approach must allow the practical use and analysis of these wavefunctions. This means that, upon their substitution into the TDSE, the solution of the resulting coupled equations is tractable. "Solution" means that numerically accurate and physically meaningful expansion coefficients, $b_n(t)$ and $b_E(t)$, are obtained.

3. Third, the choice of the form of the atom–field interaction operator must be correct and appropriate for the TDMEPs under investigation. This is crucial not only for the accuracy of the computation of $b_n(t)$ and $b_E(t)$ but also for ensuring that $|b_n(t)|^2$ and $|b_E(t)|^2 dE$ indeed represent the time-dependent occupation probabilities that correspond to the stationary states of interest labeled by Φ_n (discrete states) or by Φ_E (scattering states).

4.2. Choice of the atom–field interaction operator. Formulation in terms of the full multipolar interaction

We start from the last item of the previous section, namely the choice of the form of the interaction operator.

In the general area of atom–field interactions, when these are treated either semiclassically (the field is classical) or in terms of quantum electrodynamics, this subject has given rise to many discussions, expression of different

opinions, and occasional controversy, e.g., Refs. [75–105]. For example, Lamb, Schlicher and Scully [101] introduce their 1987 paper with the following statement: "It is perhaps surprising to note that one of the outstanding problems of modern quantum optics is the choice between the two matter–field interaction Hamiltonians which are commonly used: $-e\vec{E}\cdot\vec{r}$ and $-(e/m)\vec{p}\cdot\vec{A} + (e^2/2m)\vec{A}^2$. These two different interactions correspond to two different gauges of the EMF."

The choices that we made in Ref. [54] [the *electric dipole approximation* (EDA) in the "velocity" form] and in Refs. [55–57] (full interaction in the *multipolar* form [75–77, 106]) were based on this extensive literature and on our analysis as regards the proper nonperturbative solution of the TDSE for specific problems. Elements of this work are presented here and in Section 6. Furthermore, in Ref. [105] we discussed the computation of free–free coupling matrix elements in the EDA, when using, on the one hand energy-normalized scattering functions and on the other hand box-normalized discrete representations of the continuous spectrum.

When solving the TDSE nonperturbatively by the expansion approach where $\mathbf{V}_{\text{ext}}(t)$ is a perturbation, in principle the whole spectrum of states of $\mathbf{H}_{A,M}$ is involved. Of course, the relative importance and contribution of each state depends on the characteristics of the pulse, and this is the most serious feature of the interplay between the probe and the structure and spectrum of the atom (molecule). For example, given a spectrum and a pulse (frequency, intensity, temporal shape), the (few-if any) *on-resonance* states, or the ones that are shifted close to resonance, contribute to the time-evolution of the system much more distinctly than those states which are *off-resonance*. On the other hand, in many cases of large order processes it is the cumulative effect of the numerous off-resonance states in the discrete as well as in the continuous spectrum that determines the overall result. In particular, as intensity increases, the participation of virtual transitions of higher order than the one predicted by the LOPT increases. It is also in this context that the question arises of the choice of the operator that expresses the coupling, $\mathbf{V}_{\text{ext}}(t)$, between the atom (molecule) and the field. The normal choice in the literature of the nonperturbative solution of the TDSE invokes the well-known EDA [2, 106].

In the EDA there is no dependence on the spatial coordinates of the electric field or of the corresponding vector potential. Specifically, suppose we consider the *minimal coupling* Hamiltonian [2, 106] which is obtained by the standard substitution of $\vec{p}$ by $\vec{p} - \frac{e}{c}\vec{A}(\vec{r})$, where $\vec{A}(\vec{r})$ is the vector potential. (Bold letters symbolize operators.) This substitution produces the interaction between the atomic electrons and the EMF as [2, 106]

$$\mathbf{V}_{\text{ext}}^{\text{micoup}}(t) = \frac{e}{mc}\sum_j \vec{A}(\vec{r}_j)\cdot\vec{p}_j + \frac{e^2}{2mc^2}\sum_j \vec{A}^2(\vec{r}_j) \text{ "minimal coupling".} \quad (16)$$

For a pulse of temporal shape $f(t)$ at a single frequency, ω, the corresponding form of the field is chosen as

$$\vec{E}(t) = -\frac{d}{dt}\vec{A}(t) = \vec{E}_o f(t) \sin(\omega t), \tag{17}$$

where $|\vec{E}_o|^2$ is proportional to the radiation intensity.

When the radiation wavelength is much longer than the "atomic dimensions," i.e., when $kr \ll 1$, the "long-wavelength approximation" (LWA) is valid, meaning that (with $\vec{\nabla} \cdot \vec{A} = 0$)

$$\vec{A}(\vec{r}) = \vec{\varepsilon}_{\vec{k},\mu} e^{i\vec{k}\cdot\vec{r}} = \vec{\varepsilon}_{\vec{k},\mu}[1 + \vec{k} \cdot \vec{r} + \ldots], kr \ll 1 \text{ (LWA)}, \tag{18}$$

$\vec{\varepsilon}_{\vec{k},\mu}$ is the polarization vector, μ numbers the two possible transverse polarizations of the field, and $\vec{k}$ is the photon wavevector, with $\vec{k} \cdot \vec{\varepsilon}_{\vec{k},\mu} = 0$. It is the first term that gives the EDA, in which case $\vec{A}(\vec{r})$, (or $\vec{A}(\vec{r},t)$), is independent of the space coordinates. Then, the atomic electron–field interaction causing transitions is reduced to $\vec{A}(0) \cdot \vec{p}$, which is the so-called velocity form.

Loudon [106], in his transparent discussion on the problem of the interaction of atomic electrons with the EMF, comments as follows [106, p. 167]: "This form (Eq. (16) is not convenient for calculations, since it is expressed in terms of the vector potential, which takes different values for different choices of gauge."

In a different gauge, it is possible to construct the *multipolar* Hamiltonian which is obtained by applying a unitary transformation to the minimal coupling Hamiltonian [75–77, 106]. In the *multipolar* Hamiltonian, it is the transverse electric field, $\vec{E}_T(\vec{r})$, and the magnetic field, $\vec{B}(\vec{r})$ (satisfying Maxwell's equation, $\vec{\nabla} \times \vec{E}_T = -\frac{\partial\vec{B}}{\partial t}$), that appear, rather than the vector potential. Now, the interaction is written as

$$\mathbf{V}_{\text{ext}}^{\text{mulpol}}(t) = e\sum_j \int_0^1 \vec{r}_j \cdot \vec{E}_T(\lambda\vec{r}_j)d\lambda - \frac{e}{mc}\sum_j \int_0^1 \lambda\vec{p}_j \cdot \vec{r}_j \times \vec{B}(\lambda\vec{r}_j)d\lambda$$

$$+ \frac{e^2}{2mc^2}\left\{\sum_j \int_0^1 \lambda\vec{r}_j \times \vec{B}(\lambda\vec{r}_j)d\lambda\right\}^2 \text{ "multipolar coupling"}. \tag{19}$$

The λ−integration permits the writing of expressions involving infinite expansions in a compact form.

The three terms of Eq. (19) are the electric, the paramagnetic, and the diamagnetic operators. Now, upon applying the LWA, and the EDA, the corresponding interaction operator is the "length" form, $\vec{E}_T(0) \cdot \vec{r}$, i.e., the operator acting on the electrons is $\vec{r}$. The usual approach to such an analysis

[75–77, 106] involves the Taylor expansion about the origin of the fields, which are described by plane waves, followed by the evaluation of the λ−integrals. The length form is obtained by keeping the first term of the expansion of the electric field.

In what follows, we show how to reduce the first term in Eq. (19) to a workable form for the computation of matrix elements with atomic wavefunctions that are expressed as superpositions of Slater determinants. Note that, concerning orders of magnitude, the second and the third terms are divided by c and by c^2, respectively. In atomic units, $c \approx 137$.

We use the expansion of the plane wave describing the field into partial spherical waves, since the latter waves are convenient and practical for the representation of the angular part of the atomic orbitals. Consequently, the integration over angles is evaluated analytically in terms of the 3−j symbols and the infinite expansion is truncated by the triangular inequalities $|l_i - l_f| \leq l \leq l_i + l_f$, where l_i and l_f are the initial and the final angular momenta, respectively. These inequalities specify which of the 3-j symbols are nonzero. Due to another property, $l + l_i + l_f$ must be even. Consequently, the index l in the expansion of spherical harmonics increases in steps of two and the summation is either a real or a purely imaginary number. For example, in the case of the dipole-allowed transitions $l_f = l_i \pm 1$ and, therefore, $l = 1, 3, \ldots, 2l_i \pm 1$.

In the next step, the λ-integrals are re-expressed as integrals over the radial variable:

$$\int_0^1 j_l (\lambda kr)\lambda^n d\lambda = \frac{1}{r^{n+1}} \int_0^r j_l (kr')r'^n dr',$$ (20)

where the Bessel functions, $j_l(kr)$, result from the partial-wave expansion of the plane waves. For reasons of simplicity, the z-axis is chosen in the direction of the wavevector, $\vec{k}$. For the polarization of $\vec{E}_T$, we choose the x-axis.

The result of these choices (see Ref. [55] for details), is that the operators of the atom–field interaction are put in a computationally convenient form:

$$O_X = X(t) \sum_{l=l_{min}}^{\infty} i^{l+l_{min}}(2l + 1)F_l(r)\Theta_l(\theta,\phi) + c.c..$$ (21)

Specifically, for the electric field operator ($l_{min} = 1$, $X(t) = E_0(t)e^{-i\omega t}$)

$$F_l(r) = \frac{1}{k} \int_0^r \frac{1}{r'}j_l(kr')dr'$$ (22)

and

$$\Theta_l(\theta,\phi) = -\sqrt{\pi}\sqrt{\frac{l(l + 1)}{2l + 1}}(Y_l^1 - Y_l^{-1})$$ (23)

causing transitions with $\Delta m = \pm 1$. For values of $k \to 0$, only the first term survives.

A useful insight is gained by examining the large-r behavior of F_l. We write

$$F_l(r)_{\text{large } r} \sim \frac{1}{k}c_l - \frac{1}{k^2}\int_r^\infty \frac{\sin(kr - l\pi/2)}{r^2}dr, \tag{24}$$

where c_l is the value of the integral (24) from 0 to ∞

$$c_l = \frac{\sqrt{\pi}\,\Gamma\left(^l/_2\right)}{2(l+1)\,\Gamma\left(^l/_2 + {}^1/_2\right)} \tag{25}$$

Thus, for sufficiently large values of r, the operator F_l reaches a constant value. This is in contrast to the LWA, where the values of the length operator increase indefinitely. An elaboration of this result is given in Ref. [55].

4.2.1. Atom–field interaction operators and computations

As already stated, the "velocity" operator ($\vec{p} = -i\hbar\vec{\nabla}$) expresses the EDA to the interaction operator $\mathbf{V}_{\text{ext}}^{\text{micoup}}(t)$ (Eq. 16), while the "length" operator ($\vec{r}$) expresses the EDA to the interaction operator $\mathbf{V}_{\text{ext}}^{\text{mulpol}}(t)$ (Eq. 19). These two operators are directly connected via the Heisenberg equations of motion and so is related a third form, the "acceleration" operator, which, for Coulomb interactions, is $\vec{r}/r^3$. These expressions are expected to give the same answers when exact wavefunctions and an exact treatment in terms of complete sets are carried out. On the other hand, when approximations are made, as is necessary when dealing with real systems with many electrons, the issue arises as to which expression is more appropriate. This holds even for the calculation of the formulae representing the rates for the on-resonance one-photon transitions [107].

In view of the above, the following considerations are relevant:

1. On the one hand, one must account for the fact that the level of accuracy in the computation of off-diagonal matrix elements depends on the degree of the correctness of the matching between the spatial features of the operator and those of the wavefunctions of the two states [107]. Thus, it is easily understood that the length operator, $\vec{r}$, once inside the dipole integral, adds in a smooth way significant contributions from the outer parts of the wavefunctions. Therefore, it is important for the outer part to be numerically accurate, even though its contribution to the total energy of the N-electron state may be very small. For example, this is the case with Rydberg states, for which it is important to compute accurately the wavefunction as its outer orbital reaches the large-r region. Similar

qualitative analysis applies to the velocity and the acceleration operators. For example, the former contains a first derivative, and so the corresponding dipole integrals are more sensitive to wavefunction variations in the middle region than to the smoothly occurring in the asymptotic region spatial decay of the wavefunctions. Finally, as regards the acceleration form, this is the least reliable, since it places great emphasis on the accuracy of this matching very close to the nucleus, a requirement that is not easily satisfied from ordinary calculations and is extremely hard to achieve systematically [107].

The above short comments may serve as a reminder of why constructing different N-electron states of an atomic (molecular) spectrum by diagonalizing the Hamiltonian on a single basis set (irrespective of the required size of such a Hamiltonian matrix) not only is computationally inefficient or impossible but also is unreliable when attempting a quantitative solution of a TDMEP. In other words, suppose that one is interested in the nonperturbative solution of the TDSE at wavelengths and strengths that require the consideration of excited states, in the discrete and the continuous spectrum, of various types. And suppose that the wavefunctions for these states are constructed (when possible, for one- or two-electron atoms) by diagonalizing the electronic, fixed nuclei, $\mathbf{H}_{A,M}$, on a single basis set of discrete functions, such as the Gaussians or B-splines. Regardless of a possible convergence of the calculation in such a model space with respect to the length of the expansion, accuracy is not necessarily obtained. This is because, for a given form of the coupling operator the corresponding level of spatial accuracy of the various excited state wavefunctions that are produced in such a brute-force method need not be uniform. Furthermore, questions about the exact account of the contributions from singularities in the free–free matrix elements arise [105].

2. On the other hand, the treatment of the TDMEP in terms of the expansion method and the nonperturbative solution of the TDSE requires the explicit consideration of a large number of coupling matrix elements of transitions that involve three types of wavefunctions: Bound–bound, bound–free, and free–free. It follows that the optimal choice of the form of the dipole operator may depend on the characteristics of the problem. For example, in phenomena produced during excitation and ionization by short and intense pulses of optical or shorter wavelengths, Rydberg and scattering states may be involved in transitions on- and off-resonance. As a consequence, a serious issue as to the proper choice of the form for the atom–field interaction arises [54–57 and section 6] in contradistinction to the calculation of the rates of one-photon transitions induced by weak fields, in which case the problem is understood in terms of rather simple arguments [107].

4.3. The method

In the case of neutral atoms and of small molecules in the fixed-nuclei Born–Oppenheimer approximation, the electronic spectrum has the characteristics that are shown schematically in Figure 6.3. In the case of negative ions the discrete spectrum consists of only a few states. However, uncovering all of them is experimentally and theoretically hard due to the high total spin that they normally have, e.g., Ref. [108] and references therein.

Figure 6.3 indicates the existence of low-lying and high-lying discrete states, of resonance states in the scattering continuums, and of different scattering channels. Currently existing experimental capabilities suggest that all types of these states can, in principle, be probed in investigations of time-dependent processes, using radiation pulses with photons in the energy range from the microwave to the X-ray region. The SSEA has been developed as a practical and flexible tool for the solution of the TDSE as it applies to TDMEPs that involve single- or multiphoton transitions, mainly in atoms, since it is in atoms where the existing computational methods allow the systematic computation of state-specific wavefunctions for excited discrete and scattering states.

The theory and computation of state-specific wavefunctions for discrete and continuous atomic spectra are discussed in Section 5. These are constructed in terms of numerical as well as of analytic orbitals, each set
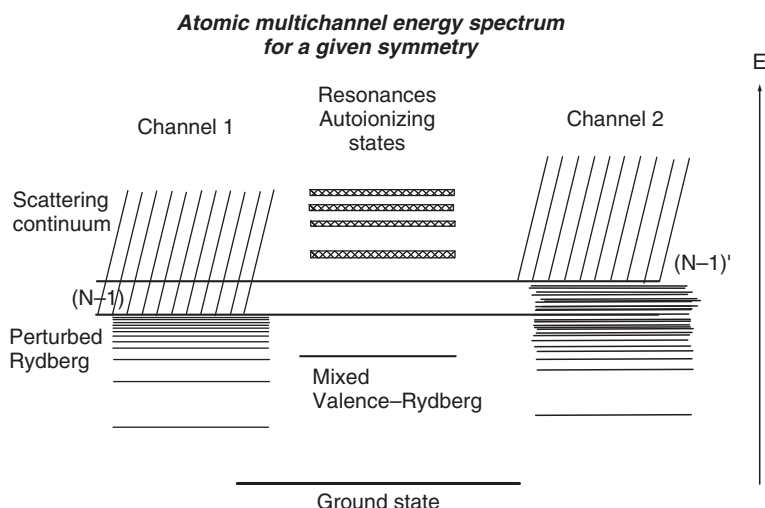
Figure 6.3 A schematically drawn electronic energy spectrum for a given symmetry of a polyelectronic atom or of a molecule for a fixed nuclear geometrical point.

representing different parts of the required zero-order and correlation function space. The same types of approach and computational techniques apply to the calculation of ground or excited electronic states of diatomic molecules [109–111]. For the case of the vibrational continuum in diatomic molecules, numerical as well as analytic orbitals have been used for the generally applicable Morse potential [53]. For the electronic continuum of diatomic molecules, published results [112–114] suggest that the basis set of energy-normalized wavefunctions can be computed in the frozen-core approximation.

Let us assume that the field is polarized linearly and that $\mathbf{V}_{\text{ext}}(t)$ is described in the EDA. There is the question of which form to use. It turns out that only in the length form of the EDA do the expansion coefficients represent directly probability amplitudes, e.g., Refs. [80, 83, 101]. On the other hand, in the velocity form it is easier to handle numerically the singularity that appears in the free–free dipole matrix elements [54, 105]. Therefore, we choose the $\vec{A}(0) \cdot \vec{p}$ form, in which case, once the solution of the TDSE, $\Psi(\vec{r},t)$, is obtained, we must multiply it by the phase factor $e^{-\vec{A}(t)\cdot\vec{r}}$ in order for the new coefficients to acquire their correct meaning as probability amplitudes [83, 101]. Furthermore, in order for the initial state at $t = 0$ to be a state of $\mathbf{H}_{A,M}$, the "preferential" gauge can be chosen in which $\vec{A}(t) = 0$ whenever $\vec{E}(t)$ becomes zero [[81b], [87]].

We now turn to the SSEA method of solving the TDSE. We write

$$|\Psi(\mathbf{r},t)\rangle = \sum_{i,n} \alpha_i(n,t)|\psi_i(n;\mathbf{r})\rangle + \sum_i \int b_i(E,t)|\psi_i(E;\mathbf{r})\rangle dE, \qquad (26)$$

where $\psi_i(n;\mathbf{r})$ are the atomic/molecular bound states plus the multiply excited states (MES) (autoionizing states) and $\psi_i(E;r)$ are the energy-normalized continuum wavefunctions with the index i running over the different channels. Substitution of Eq. (26) into the TDSE results in the system of coupled integro-differential equations:

$$i\frac{d}{dt}\alpha_i(n,t) = \varepsilon_{i,n}\alpha_i(n,t) + iA(t)\sum_{j,m} B_{i,j}(n,m)\alpha_j(m,t) + iA(t)\sum_j \int b_j(E,t)D_{i,j}(n,E)dE$$

$$i\frac{d}{dt}b_i(E,t) = Eb_i(E,t) + iA(t)\sum_{j,m} D_{i,j}(E,m)\alpha_j(m,t) + iA(t)\sum_j \int b_j(E',t)C_{i,j}(E,E')dE',$$

$$(27)$$

$\varepsilon_{i,n}$ are the calculated energies of the bound and of the MES. $B_{i,j}(n,m)$ is the bound–bound dipole matrix element, $D_{i,j}(n,E)$ is the bound–free dipole matrix element, and $C_{i,j}(E,E')$ is the free–free dipole matrix element. The desideratum is to solve Eqs. (27) properly and obtain the expansion coefficients. The degree of convergence for each set of field parameters can be studied as a function of the type and number of the stationary states entering in Eq. (26). The methods for the ab initio state-specific computation of

these wavefunctions are presented in Section 5, with emphasis on the theory of the Rydberg series and the lower part of the continuous spectrum.

4.3.1. The singularity of the free–free dipole integral

The matrix elements $B_{i,j}(n,m)$ and $D_{i,j}(n,E)$ are calculated numerically without difficulty since they contain at least one bound orbital. On the contrary, the free–free dipole matrix elements $C_{i,j}(E,E')$, whose role is crucial in the process of strong field ionization and of ATI, contain an on-shell singularity. Fortunately, this singularity turns out to be integrable, meaning that the integrals containing $C_{i,j}(E,E')$ in Eq. (27) have a finite value. Let us see how.

For hydrogenic atoms, where the scattering wavefunctions are known (these are hypergeometric functions), this singularity can be identified and handled analytically [115, 116]. On the other hand, the SSEA uses numerical scattering orbitals as a basis, computed within a term-dependent, frozen-core HF scheme. This is done so as to be able to handle arbitrary many-electron structures for small as well as for large values of energy. Therefore, a different type of analysis was needed and was implemented in Ref. [54] (See also Ref. [105]). It was shown that the $C_{i,j}(E,E')$ can be written as

$$C_{i,j}(E,E') = C_{i,j}^{\text{nonsingular}}(E,E') + C_{i,j}^{\text{singular}}(E,E') \tag{28a}$$

with

$$C_{i,j}^{\text{singular}}(E,E') = F_1(\varepsilon,\varepsilon')\delta(\varepsilon - \varepsilon') + P\frac{F_2(\varepsilon,\varepsilon')}{(\varepsilon - \varepsilon')}, \tag{28b}$$

where P signifies a principal value integral. The variables ε, ε' are the positive energies of the free electrons above the thresholds of the i,j channels. $F_1(\varepsilon,\varepsilon')$, $F_2(\varepsilon,\varepsilon')$ are well-behaved functions of the energies and of the phase shifts whose numerical calculation is straightforward when the energy-normalized numerical HF scattering orbitals are used.

The integrals in Eqs. (27) are calculated, for each value of t, by performing the δ function and the principal value integration of Eq. (28b). Briefly, we adopt a high-energy cut-off and the energy range is constructed as a mesh of elements $\Delta\varepsilon$. The values of the time-dependent coefficients are to be found at the mesh points. The nonprincipal value integrals of Eqs. (27) are performed by the trapezoidal rule, which is valid when the integrand varies linearly between consecutive energy mesh points. Finally, for the principal value integral it is assumed that the well-behaved part of the integrand $b_j(\varepsilon',t)F_2(\varepsilon,\varepsilon')$ varies linearly with energy between consecutive mesh points and then the integral is calculated exactly. Thus, the system of integro-differential equations (27) is reduced to a system of ordinary differential equations of the following form:

$$i\frac{d}{dt}\vec{x}(t) = [\hat{A} + F(t)\hat{B}]\vec{x}(t), \tag{29}$$

$\vec{x}(t)$ is the vector of the unknown time-dependent coefficients $\alpha_i(n,t)$ and $b_j(E,t)$, $\hat{A}$ is the matrix representation of the field-free Hamiltonian in the N-electron basis set of Eq. (26), $\hat{B}$ is the matrix representation of the dipole operator, and $F(t)$ is the time-dependent part of the interaction in the velocity form.

It should be noted that when the solution is propagated to times t for which the values of $\Delta\varepsilon \times t$ are not very close to zero, the ratio of the oscillating parts $\frac{e^{-i\varepsilon t}}{e^{-i(\varepsilon+\Delta\varepsilon)t}} = e^{i\Delta\varepsilon t}$ of the consecutive time-dependent coefficients $b_j(\varepsilon,t)$ and $b_j(\varepsilon + \Delta\varepsilon,t)$ is not ≈ 1. This fact does not support the assumption that the integrand $b_j(x,t)(D_{i,j}(n,x)$ or $C_{i,j}(x,\varepsilon'))$varies linearly between consecutive energy mesh points. Therefore, instead of applying the trapezoidal rule, one has to perform an analytic integration with respect to x between ε and $\varepsilon + \Delta\varepsilon$ by considering explicitly the oscillating part e^{-ixt} and assuming that the rest of the integrand $e^{ixt}b_j(x,t)(D_{i,j}(n,x)$ or $C_{i,j}(x,\varepsilon'))$ varies linearly in this range. The integration, in cases where the free–free dipole matrix elements do not exhibit on-shell singularity (e.g., in problems of molecular multiphoton dissociation where the dipole operator for large distances may go to zero exponentially), results in a system of differential equations with a numerical type very similar to that of Eq. (29):

$$i\frac{d}{dt}\vec{x}(t) = [\hat{A} + F(t)\hat{B}_1 + F(t)\left(\frac{\sin(0.5\Delta\varepsilon t)}{(0.5\Delta\varepsilon t)}\right)^2 \hat{B}_2]\vec{x}(t) = [\hat{A} + F(t)\hat{B}_1 + \tilde{F}(t)\hat{B}_2]\vec{x}(t),$$

(29a)

where $\hat{B}_1$ contains the bound–bound and free–bound part of $\hat{B}$, while $\hat{B}_2$ contain its bound–free and free–free ones.

The solution of the system of Eqs. (29) is achieved by a method that utilizes the expansion of the vector $\vec{x}(t)$ and of $F(t)$ for $t = t_0 + \Delta t$ around t_0,

$$\vec{x}(t) = \sum_{n=0}^{M} \vec{x}^{(n)}(t_0)\frac{(\Delta t)^n}{n!},$$

(30a)

$$F(t) = \sum_{n=0}^{M} F^{(n)}(t_0)\frac{(\Delta t)^n}{n!},$$

(30b)

where $\vec{x}^{(n)}(t_0)$ is the nth derivative of $\vec{x}(t)$ for $t = t_0$ and $\vec{x}^{(0)}(t_0) = \vec{x}(t_0)$. Then, assuming that it is possible to calculate $\vec{x}^{(n)}(t_0)$, the solution can be obtained by performing the summation of Eq. (30). The details of the integration technique, which follows a Taylor-series expansion method (TSEM), and especially the determination of the number of terms, M, for each t_0, can be found in Ref. [54, appendix B]. The justification for adopting the TSEM is that it is almost five times faster than the standard powerful methods for ordinary differential equations, such as the adaptive Bulirsch-Stöer [117].

As variable parameters for testing convergence are used, the number and the type of the state-specific wavefunctions, the time step Δt, and the overall range in time for the propagation to provide a normalized solution, $\vec{x}(t)$, equal to 1. The criterion of stable normalization is directly related to the overall adequacy of the N-electron basis set.

The following points are relevant to the methodology.

Given that for the velocity form the coefficients are not the correct probability amplitudes, it is convenient to calculate any quantity at those time instants where the vector potential $A(t)$ is equal to zero.

The time step Δt that normally provides convergent results turns out to be of the order of tenths to a few hundredths of the optical cycle $T = 2\pi/\omega$.

By far the greater portion of the number of states entering Eq. (27) comes from the continuous spectrum. In fact, regardless of the number of electrons the system has, the number of the discrete states normally contributing to the sum is relatively small, say a few decades, unless the problem deals explicitly with the Rydberg spectrum. On the other hand, the number of energy-normalized scattering states runs into the many thousands, depending mainly on the pulse characteristics. In fact, thus far, the maximum number of equations that have been processed, is of the order of 10^6 [118], where the necessity came from the presence of double continua.

The solution of Eq. (27) provides the time-dependent coefficients $\alpha_i(n,t)$ and $b_j(E,t)$. Given that these correspond to the true states of the unperturbed system, the quantities of interest can be computed in a direct and transparent way. For example, photoionization probabilities and rates are deduced from Eq. (15) where the summation runs over the discrete states of the system. Also, the total ATI spectrum as well as the partial ATI spectra are obtained from

$$\frac{dP_\varepsilon(t)}{d\varepsilon} = \sum_i \frac{dP_\varepsilon^i(t)}{d\varepsilon} = \sum_i |b_i(E,t)|^2, \tag{31}$$

where $dP_\varepsilon^i(t)$ is the probability that the free electron has energy between ε and $\varepsilon + d\varepsilon$ in the channel i.

Related to the above quantities are the *photoelectron angular distributions* (PAD), which are very sensitive to quantum interference. In order to compute them, the solution $\Psi(\vec{r},t)$ is projected on an energy-dependent state, $\Psi^-(\varepsilon)$, composed of an incoming spherical wave and an outgoing plane wave with phase shift δ_{l_i}. The relevant probability distribution is given by

$$\frac{d^2P_\varepsilon(\hat{k},t)}{d\hat{k}d\varepsilon} = \left|\langle\Psi(r,t)|\Psi^-(\varepsilon)\rangle\right|^2, \tag{32a}$$

where the $\varepsilon = \frac{1}{2}k^2$ is the positive energy of the free electron above threshold and $\hat{k}$ is its direction of propagation. The energy-normalized $\Psi^-(\varepsilon)$ is given by

$$\Psi^-(\varepsilon) = 4\pi\sqrt{\frac{\pi}{2k}}\sum_{l_i}\sum_{m=-l_i}^{l_i} i^{l_i}e^{-i\delta_{l_i}}Y_{l_i,m}^*(\hat{k})Y_{l_i,m}(\hat{r})\mathcal{A}(\psi_{core}^{(i)}(r)\otimes U_{l_i}(\varepsilon;r)), \quad (32b)$$

where $Y_{l_i,m}$ are the spherical harmonics and $U_{l_i}(\varepsilon;r)$ is the energy-normalized radial part of the term-dependent scattering orbital used to construct the N-electron wavefunction in the continuum, $\psi_i(E;r) = \mathcal{A}(\psi_{core}^{(i)}(r)\otimes U_{l_i}(\varepsilon;r))$, $E = E_{core} + \varepsilon$. $U_{l_i}(\varepsilon;r)$, and its phase shift δ_{l_i} are calculated numerically in the fixed-core HF approximation. Combining Eqs. (26, 32a, and 32b), we obtain the probability distribution:

$$\frac{d^2P_\varepsilon(\hat{k},t)}{d\hat{k}d\varepsilon} \propto \left|\sum_{l_i}\sum_{m=-l_i}^{l_i}(-i)^{l_i}e^{i\delta_{l_i}}Y_{l_i,m}(\hat{k})b_i(E,t)\right|^2, \quad (33)$$

which connects the PAD's to the calculated time-dependent coefficients $b_i(E,t)$.

Finally, HHG can be studied by Fourier transforming the induced time-dependent dipole moment, $D(t) = \langle\Psi(\vec{r},t)|\mathbf{D}|\Psi(\vec{r},t)\rangle$, where $\mathbf{D}$ is the dipole operator in the polarization of the EMF [33]. For the one-electron hydrogen atom, our choice of the form of the dipole operator has been the acceleration form since, in this case, the computation of the free–free matrix elements is both efficient and accurate [119]. However, in later work on the multiphoton ionization from the two-electron metastable excited state of He, the 1s2s ^{1}S, we stressed that for many-electron systems, "calculations of harmonic spectra based on the use of the acceleration form of the dipole operator will produce, in general, unreliable results even when some correlations are accounted for" [120].

The first applications of the SSEA to the multiphoton *above-threshold detachment* (ATD) spectra of the negative ion Li$^-$, to the ATI, HHG, and PADs in hydrogen, and in He were published in Refs. [54, 72, 73, 105, 119–123]. Additional types of applications are reviewed briefly in Section 6.

5. THE THEORY AND COMPUTATION OF STATIONARY STATE-SPECIFIC WAVEFUNCTIONS FOR LOW- AND HIGH-LYING STATES

In order to have a SSEA which is applicable to the variety of TDMEPs that may arise depending on the experimental arrangement (real or hypothetical), it is necessary to be able to obtain reliable wavefunctions for each state and

for each class of states of the spectrum of Figure 6.3. In fact, the aim within the state-specific theory is for these wavefunctions to be relatively compact and transparent so as to facilitate the solution of the coupled Eqs. (27) and allow the easy analysis of the nonstationary $\Psi(t)$ for each problem of interest.

The significance of the above statement must be understood in the context of possible problems involving a large variety of electronic structures and/or scattering channels that characterize the states of both the discrete and the continuous spectrum.

Our approach to the quantitative investigation of such problems in prototypical cases has been based on the following assertion: The electronic structures and properties of the states of Figure 6.3 can be explored formalistically and computationally by separating them into two categories. In the first category are states whose wavefunctions are computed from separate, state-specific treatments. For example, such states are the ground state, certain low-lying excited states, relatively isolated MES, and "unperturbed" low-lying Rydberg states. In the second category are states that belong to *channels* and are treated as elements of unperturbed or perturbed symmetry-labeled series in the discrete and the continuous spectrum.

5.1. Methodology for the state-specific computation of N-electron wavefunctions of isolated states

As regards the ground state of a given symmetry, the fundamental theoretical tool is the existence of the energy lower bound. This fact allows Rayleigh–Ritz variational calculations to converge monotonically upon variation of the size of the basis set and/or of linear or nonlinear variational parameters.

As regards the excited states (discrete or resonance states) of a given symmetry that can be treated individually as isolated or as a component of a very small superposition of nearly degenerate states, judicious choices for each system of interest may identify as such a few low-lying discrete states and a number of high-lying multiply excited discrete or resonance states. For low-lying discrete states, say the first three or four in the spectrum of a polyelectronic atom (molecule), it is practical to compute them via the diagonalization of a properly constructed Hamiltonian matrix and optimization of each root separately, based on the property of the separation and of upper boundness of eigenvalues, also known in quantum chemistry as the Hylleraas–Undheim–MacDonald theorem [124, 125]. On the other hand, not only for the low-lying but also for high-lying MES [normally these are doubly excited states (DES)], the state-specific approach bypasses the bottleneck of requiring the presence in a Hamiltonian matrix of vectors representing all the lower states of the same symmetry [1]. By excluding the function space that is expected to represent the channels interacting with the localized component of the MES, it is possible to first optimize the computation

of such states efficiently and reliably and then proceed with the overall mixing of the total wavefunction [1, 126–129]. In this way, it is possible to tackle difficult problems of electron correlation and of CI in the upper part of the discrete spectrum and in the continuous spectrum (see below). As an example of the difficulties that such cases have in store when a state-specific separation of function spaces is not followed and when the corresponding wavefunctions are not optimized in terms of the self-consistent field and of electron correlation, we refer to a paper by Bartschat and Greene [130] on the "$6p^2$" ^1S autoionizing state of Barium. These authors discussed previous discrepancies between R-matrix calculations and attributed them to a lack of proper treatment of relaxation and correlation effects in this state. Such effects are taken into account systematically in the state-specific theory for isolated states, which is outlined below.

The basics of the analysis and computational methodology that we have followed for this category go back to publications from the 1970s [1, 40, 41, 131]. A review of certain important ideas and new results on specific issues were given in Ref. [42]. Below, instead of repeating the arguments concerning the gist of the theory, we quote from the introduction of a 1984 article by Petsalakis et al. [132] on the *sudden polarization effect* in molecules.

"Historical reasons, theoretical constraints and computational convenience have led to the development and application of many-body methods for excited states of atoms and molecules in terms of single orthonormal basis sets corresponding, most often, to an energy optimized one-electron potential of ground states. With such methods, the emphasis is on efficiency in terms of manipulation of the one- and two-electron integrals and on potential generality as regards the types of states that are treatable. Enlargement of the basis set improves the reliability of the computation. However, the $n^4 - n^5$ dependence of the overall calculation (n is the number of one-electron basis functions) quickly puts limitations on the size of the possible many-body calculations, even with today's super computers. Furthermore, certain excited state calculations of energetics or other properties can be very sensitive to the choice of basis sets, regardless of the size of the system. This is mainly due to a lack of suitability of the zeroth-order orbitals, whose induced error is difficult to correct subsequently, even with large-scale electron correlation calculations. This fact can be observed easily in atomic structure calculations where the excited state orbitals corresponding to a particular configuration can be computed accurately by a variety of methods, e.g., hydrogenic, configurational average HF, restricted HF, multiconfigurational HF." [132].

The aforementioned approach to the TIMEP of ground or low-lying excited states that is based on the use of a single basis set characterized for many years the *conventional* quantum chemistry methods. These are the methods which obtain the wavefunctions and real energies either by direct diagonalization of huge Hamiltonian matrices or by incorporating the

electron correlation corrections in a hierarchical way, using zero-order and correlation function spaces constructed from large sets of Gaussian or Slater (or similar) orbitals.

An alternative to the conventional methods of quantum chemistry is the *state-specific* theory, useful especially for excited states [1, 42, 131, 132]. Such a theory is based on the choice and optimization of the function spaces for each excited state of interest, both at the zeroth-order and at the correlation level. This allows the systematic inclusion of relaxation and correlation effects to a very good degree of accuracy and the reliable description of phenomena and calculation of properties with small wavefunctions. Furthermore, physical and chemical concepts become more transparent while aspects of *transferability* of parts of the energy or of the wavefunctions and their distinct effects on spectroscopy, on properties, and on chemical bonding in excited states may be systematized.

The general form of state-specific wavefunctions for discrete and for resonance states is Refs. [1, 42] and references therein,

$$\Psi_n(E) = \Phi_n^{FS} + X_n^{loc} + X_n^{as} \tag{34}$$

where the symbols represent the following:

$\Psi_n(E)$: The energy dependence refers only to the case of resonances, in which case the wavefunction has scattering components corresponding to the open channels. In the SSEA, only the terms $\Phi_n^{FS} + X_n^{loc}$ are used (the *localized* component), since the smooth continuum is represented by a set of numerically obtained, energy-normalized scattering functions, which are then allowed to mix during the solution of the TDSE.

Φ_n^{FS}: This is the zero-order (reference) multiconfigurational description, with configurations consisting of the self-consistently optimized "Fermi-Sea" (FS) orbitals [40–42, 131]. In other words,

$$\Phi_n^{FS} = \sum_k^{finite} c_k \phi_k, \tag{35}$$

where the ϕ_k are symmetry-adapted configurations with self-consistent field orbitals.

A brief discussion on the background and significance of the concept and practical choice of Φ_n^{FS} in the theory and computation of electronic structures and dynamics is given in Ref. [42].

For atoms and diatomics, the Φ_n^{FS} for a state that is treated as isolated (e.g., a multiply excited valence state) can be obtained for the root labeled by the configuration(s) of interest. In cases of strong configurational mixing, the rate of convergence of the overall calculation is sensitive to the radial details of the FS orbitals. This is why in the state-specific theory these are obtained numerically, when possible. When configurations in Φ_n^{FS}

representing different states mix heavily (e.g., cases of valence–Rydberg, covalent–ionic state mixing), the state-specific solution for each root of interest may be very hard if not impossible to achieve correctly via a canonical MCHF calculation, due to the orbital structure of the mixing configurations. An alternative and reliable avenue to the proper Φ_n^{FS} is then to use nonorthonormal configuration-interaction with separately optimized parts of Φ_n^{FS}, for each physically relevant part of the total system, e.g., Refs. [42, 132].

X_n^{loc}: Represents the remaining localized electron correlation for the discrete states or for the localized component of resonances [1, 42]. It is computed variationally by optimizing symmetry-adapted single, pair, triple, etc., correlation functions that are expressed in terms of parameterized Slater- or Gaussian-type orbitals [42, 131]. The combination of state-specific numerical HF or MCHF orbitals (for the zero-order function space), with analytic and variationally optimized orbitals for the correlation function space, is one of the basic features of the methodology which was introduced in the 1970s for efficient computations of ground or excited atomic structures [40–42, 131].

X_n^{as}: It symbolizes the "asymptotic" correlation that is function spaces that represent the energetically open channels and contain the information about the interaction of the free electrons with the core state and about the possible interchannel couplings. It is zero when the state is discrete. For quantities where the open continuum is important, such as the energy-dependent photoabsorption cross-sections, or for the full description of resonance states, the proper computation and consideration of X_n^{as} are essential.

For computations using scattering theory formalism based on real energies, the scattering wavefunctions for each of its open channels are computed from a basis set of a term-dependent, fixed-core HF wavefunctions. The effects of interchannel coupling are computed through a multichannel reaction (K-) matrix approach [126–129] and below. Alternatively, the state-specific approach for resonance states of many-electron atoms and small molecules can be applied in the framework of methods that solve the *complex eigenvalue Schrödinger equation* [1].

Thus far, SSEA computations have been carried out by including in the expansion scattering wavefunctions of real energies and the localized components of resonance states. The basis set of the fixed-core scattering states is computed for a dense energy mesh which is found to secure convergence, each state being energy normalized to a δ function, $\delta(\varepsilon - \varepsilon')$.

5.2. Unified theory and ab initio computation of the wavefunctions and spectra just below and just above the fragmentation threshold, with application to atoms

5.2.1. Introduction

For a given short- or long-range potential with a discrete and a continuous spectrum, the point of energy $\varepsilon = 0$ signifies the necessary change in the

boundary conditions at infinity on the acceptable solutions of the TISE and the consequent fundamental difference in the formalism and computational methods of QM for the rigorous treatment of the respective states and phenomena. In spite of this difference, it is known that, in general, information which is obtained very close, above or below, the fragmentation threshold, $\varepsilon = 0$, can be used to obtain physically meaningful information on the other side of this point. For example, this is the case of "Levinson's theorem" [3], according to which, for a short-range potential, from the variation of the *scattering phase-shift* as $\varepsilon \to 0$ from above, one can obtain the number of bound states that the potential can support for $\varepsilon < 0$.

Based on the fact that significant quantities related to spectroscopy vary with energy near the threshold very slowly, except when resonances are present, formal theories, and notions of smoothness and continuity in this region of the spectrum have been developed in order to deduce useful information from knowledge of only a few data, via extrapolation or, better, as we shall show here, via interpolation.

As regards atoms and molecules and the corresponding long-range Coulomb potential, ever since the early stages of the application of QM to atomic spectra, the point $\varepsilon = 0$, which is the first *ionization threshold* (IT), has created interest in the mathematics, the computation and the physical observation of energy-dependent quantities as the values of energy reach the IT from above (positive values) or from below (negative values). It appears that this issue was first discussed systematically in terms of the use and analysis of hydrogenic Coulomb (and related) wavefunctions of the discrete and the continuous spectrum in 1927 by Sugiura [133] on Hydrogen and in 1929 by Hargreaves [134, 135] on Lithium. For example, the notion of continuity of absorption oscillator strength across the IT for a Coulomb potential was established, with $f_\varepsilon\big|_{\varepsilon=0} = n^3 f_n\big|_{n\to\infty}$, where f_ε involves energy-normalized scattering functions. Furthermore, Hargreaves analyzed aspects of the *quantum defect* in the Rydberg series spectrum, in terms of properties of wavefunctions, such as asymptotic forms and normalization, and of concepts of matching *inner* and *outer* (Coulomb) regions of the "motion" of the outer electron [134, 135].

Starting in the 1950s, the publications of Kuhn and van Vleck [136] and of Ham [137] shone additional theoretical light on the "quantum defect method," mainly by paying attention to the matching conditions at some radius, r_0, for bound solutions. Then, Seaton [138, 139] started a systematic investigation of spectral features of the Coulomb potential, by exploiting mathematical properties of Coulomb functions for both the discrete and the continuous spectrum. His first relevant result related the quantum defect for $n \to \infty$ and electron angular momentum ℓ to the scattering phase shift at $E = 0$ as, $\delta_\ell(0) = \pi \mu_{\infty\ell}$ [138]. Following a significant contribution by Gailitis [140] on near-threshold behavior of cross-sections for Coulomb potentials in terms of multichannel-effective radius theory, a series of papers by Seaton

[141, 142] and references there in, penetrated into and further developed the theory of Coulomb-like spectra, for one or for many channels, close to the IT, based on the mathematical properties of the Coulomb function. The accumulated knowledge led to the standard *Quantum Defect Theory* (QDT) [142]. According to Seaton, "QDT is concerned with the properties of an electron in the field of a positive ion and, in particular, with expressing those properties in terms of analytical functions of the energy. It provides a unified theory of bound states, including series perturbations, autoionization and electron-ion scattering, both elastic and inelastic" (Abstract of [142]).

The notion of unification of the treatment of the highly dense number of states just below and just above the IT was emphasized and pursued from a different, and in some cases more heuristic, point of view by Fano in the 1970s [143–147]—see below.

The development of theory and of a practical methodology for computing usable state-specific N-electron wavefunctions of states across the IT, for the Coulomb potential, or, more generally, of states around the fragmentation threshold for a non-Coulomb potential, via the establishment of analyticity and of continuity across threshold, has been the aim of the work which is briefly reviewed in this section. Its details and prototypical applications can be found in Refs. [126–129]. The fundamentals of the theory were developed and applied by two of us in 1985–1986 [126, 127], soon after the publication of the 1983 comprehensive review article by Seaton [142]. In contradistinction to the standard QDT, D the Komninos-Nicolaides theory and formalism do not utilize explicitly the "base pair" of regular and irregular functions, are not based on the mathematical properties of Coulomb functions, and do not separate the configuration space into an "inner" and an "outer" region.

5.2.2. Background essentials

We start by focusing on Seaton's work [142]. The essence of his approach lies in the construction of a pair of linearly independent solutions for the Coulomb potential, which are analytic in energy (both positive and negative values). The use of such a pair of solutions constitutes the hallmark of the standard QDT.

For the Coulomb potential, the regular solution has the asymptotic form $f_k(r) \sim \sin\left(kr + \frac{z}{k}\log 2kr - l\frac{\pi}{2} + \sigma_l\right)$ and fulfils the condition of analyticity. On the other hand, the irregular solution, whose asymptotic form is $\eta_k(r) \sim \cos\left(kr + \frac{z}{k}\log 2kr - l\frac{\pi}{2} + \sigma_l\right)$, is not analytic in energy. The recipe that Seaton devised in order to establish analyticity across the IT consists of constructing an irregular function in the form of the superposition $g_k(r) = f_k(r) - G(k)\eta_k(r)$, eq. 2.38 of Ref. [142], such that it is an analytic function of the energy. $G(k)$ is expressed in terms of digamma functions, eq. 2.35 of Ref. [142]. Having proven this result, Seaton could derive formulas concerning the upper part of the discrete spectrum from information obtained for the continuous spectrum close to the IT.

A linear combination of the hydrogenic functions mentioned above can be used to describe the asymptotic part of any atomic state where the Coulomb potential dominates beyond a chosen (rather arbitrarily) radius, r_0. Then, by matching this solution with the inner region of the wavefunction, one can obtain, depending on the value of energy, the phase shifts or the quantum defects and from there produce information on spectra. This information is usually produced via the use of QDT parameters which are obtained empirically. In cases where the aim is for the standard QDT to be implemented from first principles, R-matrix-type theories have been employed, e.g., Ref. [130].

Seaton's mathematical analyses and methods can explain, in principle, the perturbed spectra on both sides of the IT of a Coulomb potential. On the other hand, Fano [143, 144] recognized that QDT could be simplified and generalized by imposing conditions of *smoothness* rather than analyticity. As a consequence, he was able to connect aspects of the QDT to a formalism that utilizes a combination of the scattering K-matrix [3] with CI [145–147]. Based on this work, Greene, Fano and Strinati [148] extended the QDT formalism to potentials other than the Coulomb. As they state in the abstract, "Quantum defects are generalized to eigenvalues of a reaction matrix, as in Seaton's work, but this matrix can now be calculated even below threshold energies with the introduction of a 'smooth' Green's function appropriate to QDT applications." In subsequent work, Greene et al. [149] connected QDT to the WKB theory, thereby generalizing the original results of Ham [137].

From the point of view of the state-specific approach, which ultimately employs the method of CI in order to solve the problems with which standard QDT has dealt, two major characteristics of QDT have to be dropped. The first is the use of the base pair of functions and the second is the separation of space into an inner and an outer region. This is because we want to use true wavefunction representations of the eigenstates of both the discrete and the continuous spectrum. This means that, on the one hand, valence state wavefunctions (e.g., for DES or MES) are optimized separately, and on the other hand a complete set of wavefunctions which are regular at the origin have to be used, consisting of square integrable and of delta function energy-normalized scattering orbitals. This method employs off-the-energy-shell multichannel K-matrices which produce the wavefunction over the whole of space, in contrast to on-the-energy-shell K-matrices which produce only the asymptotic part of the wavefunction. In the resulting formulation, the cause of the non-analyticity becomes obvious since it is due to poles corresponding to the energies of the Rydberg series (see section IVa of Ref. [126]).

Having realized the source of non-analyticity of the total wavefunction as a function of energy, Komninos and Nicolaides [126] proposed a mathematical technique that leads to analytic wavefunctions by subtracting the contribution of the poles. Specifically, the wavefunction (i, j are channel

indices):

$$
\tilde{\Psi}_{jE} = U_{jE} + \sum_i \sum_n U_{iE_{in}} \frac{\tau_{in}}{E - E_{in}} \tilde{K}_{iE_{in},jE} + \sum_i P \int dE' U_{iE'} \frac{1}{E - E'} \tilde{K}_{iE',jE}
$$
$$
- \sum_i^{N_{cl}} U_{iE} G_i(E) \tilde{K}_{iE,jE}
\tag{36}
$$

P denotes principal value integration. N_{cl} is the number of channels below the IT, E_i^{th}. We stress that the energy can assume values above E_i^{th} as well.

The K-matrix satisfies a Lippmann–Schwinger type equation:

$$
\tilde{K}_{i\bar{E},jE} = W_{i\bar{E},jE} + \sum_l \sum_n W_{i\bar{E},lE_{ln}} \frac{\tau_{ln}}{E - E_{ln}} \tilde{K}_{iE_{in},jE} + \sum_l P \int dE' \, W_{i\bar{E},lE'} \frac{1}{E - E'} \tilde{K}_{lE',jE}
$$
$$
- \sum_l^{N_{cl}} W_{i\bar{E},lE} G_l(E) \tilde{K}_{lE,jE}
\tag{37}
$$

The quantity

$$
W_{i\bar{E},jE'} \equiv V_{i\bar{E},jE'} - E S_{i\bar{E},jE'}
\tag{38}
$$

is defined in terms of the residual interaction and overlap matrices derived from the matrix elements between zero-order channel functions,

$$
\langle U_{i\bar{E}} | H - E | U_{jE'} \rangle = (\bar{E} - E)\delta_{ij}\delta(E - E') + W_{i\bar{E},jE'},
\tag{39}
$$

Finally, in atomic units,

$$
G_i(E_i^{th} + \varepsilon) = \sum_n \frac{\tau_{in}}{\varepsilon - \varepsilon_{in}} + P \int_0^{1+\varepsilon} d\varepsilon' \frac{1}{\varepsilon - \varepsilon'}
\tag{40}
$$

For each channel, the total energy, E, equals the ionization energy of this channel plus the energy of the Rydberg/free electron orbital. That is, $E = E^{th} + \varepsilon$, where ε can be positive or negative.

For the case of the Coulomb potential,

$$
\varepsilon_{in} = -\frac{Z^2}{2(n - \mu_{i0})^2}, \quad \tau_{in} \equiv \frac{\partial \varepsilon_{in}}{\partial n} = \frac{Z^2}{(n - \mu_{i0})^3}.
\tag{41}
$$

In the wavefunctions entering in the matrix elements of Eq. (38), both the Rydberg and the scattering orbitals are energy normalized. For hydrogenic Rydberg orbitals this is achieved by multiplying the usual volume-normalized orbitals by $n^{3/2}$, e.g., Ref. [150]. Since $\frac{dn}{d\varepsilon} \propto n^3$, this operation results in energy-normalized bound orbitals. This is essential in order that the inner parts of the wavefunctions around the IT have comparable magnitudes.

We emphasize that we employ a fixed-core HF basis set of Rydberg/free orbitals and not hydrogenic ones. This fact implies that they carry a state-dependent zero-order quantum defect or phase shift. Additional important contributions arise from interelectron interactions, such as interchannel couplings and resonances.

The effect of the summation in the G function is to cancel the poles, while the integral simply provides a $-\log \varepsilon$ term which cancels a similar term originating from the sum. Consequently, the wavefunction, thus modified, is now analytic in energy.

For the Coulomb potential, the function G is expressed in terms of digamma functions (see Ref. [126] for details). Indeed, it is analogous to the G function of eq. (2.34) of Ref. [142], which was derived through a totally different approach. Specifically the Seaton G function is defined as a derivative with respect to a variable, λ, whose integer values, ℓ are the quantum numbers of the angular momentum.

We point out that expression (36) for the wavefunction holds in general, regardless of the potential. This fact implies that, given a many-electron system and a particular potential seen by the outer electron, what is important is to be able to compute, at least numerically, a zero-order complete basis set. In cases where valence or inner-hole excited resonances are present, the calculation of their wavefunctions is done separately, as described in Section 5.1.

Furthermore, its has been shown [129] on general grounds, via the use of the Mittag–Leffler theorem for analytic functions, that our G function can be written as

$$G(E) = \begin{cases} J(E), & E > E_{\text{th}} \\ J(E) + \pi \cot \pi \nu, & E < E_{\text{th}} \end{cases}, \tag{42}$$

where ν comes from the functional form of the energy spectrum below the IT, $E \equiv E_\nu$. The explicit form of the function $J(E)$ depends on the potential.

Having obtained the above results, a unitary transformation exists [126, 129] such that the G function in the last term of Eqs. (36 and 37) is replaced by a new function, $G_{\text{transf}}(E)$, which is zero for energies above and $\pi \cot \pi \nu$ for energies below the IT. In other words,

$$G(E) \rightarrow G_{\text{transf}}(E) = \begin{cases} 0, & E > E_{\text{th}} \\ \pi \cot \pi \nu, & E < E_{\text{th}} \end{cases}. \tag{43}$$

The corresponding wavefunction does not have complete analyticity. However, it is smooth across the IT. It is worth noting that this wavefunction is identical to the one derived by Fano via a totally different method, eqs. (17–20) of Ref. [145].

5.2.3. Formal results and outline of the computational methodology

The wavefunctions of Eq. (36) are in a form suitable for computation. However, they do not constitute an orthonormal set. This is rectified by choosing a particular linear combination, the so-called *eigenchannel* wavefunctions, which has the desired property. Specifically, the orthonormal set has the form

$$\Psi_{\lambda E} = \sum_i \Psi_{iE} B_{i\lambda} \cos \eta_\lambda , \qquad (44)$$

where η_λ are the *eigenphase shifts* given by the eigenvalues of the on-the-energy-shell (meaning equal total energies) K-matrix

$$\sum_j K_{iE,jE} B_{j\lambda} = -\frac{1}{\pi} \tan \eta_\lambda B_{i\lambda} \qquad (45)$$

and $B_{i\lambda}$ are real coefficients forming a unitary matrix,

$$\sum_l B_{il} B_{lj}^\dagger = \delta_{ij} \qquad (46)$$

In Eq. (44), multiplication by the cosine of the phase shift ensures normalization.

As defined above, an eigenchannel is a superposition of standing waves in all channels with a common phase shift.

The first use of the eigenchannels was made in the context of the coupled equations approach of scattering theory [3]. However, in such approaches, there are problems of convergence which become progressively serious, if not insoluble for many cases.

In our case, the eigenchannels are used in the context of a K-matrix CI approach whose origins can be found in Fano's work [146, 147].

We now consider wavefunctions that satisfy boundary conditions.

The asymptotic form of the (standing wave) eigenchannels is a simple expression,

$$\Psi_{\lambda E} \rightarrow \sum_i \Psi_i^C \sqrt{\frac{2}{\pi k_i}} \sin (\phi(k_i,r) + \delta_i + \eta_\lambda) B_{i\lambda}, \qquad (47)$$

where Ψ_i^C are the core N-electron wavefunctions and δ_i are the phase shifts for the zero-order basis set. (For example, in the case of the Coulomb potential, this would be a fixed-core HF basis.)

Of special and broad interest is the process of photoionization. In this case, the boundary condition on the real energy axis requires incoming waves in all channels and a single outgoing wave in a particular channel. This is achieved by choosing

$$\Psi_{jE}^{(-)} = \sum_{\lambda} \Psi_{\lambda E} \, e^{-i\eta_{\lambda}} B_{\lambda j}^{\dagger} e^{-i\delta_{j}} \tag{48}$$

as can be confirmed by separating the outgoing- and the incoming-wave components in Eq. (47). The asymptotic form of Eq. (48) is then,

$$\Psi_{jE}^{(-)} \rightarrow \frac{1}{2i} \Psi_{j}^{C} \sqrt{\frac{2}{\pi k_{j}}} e^{i\phi(k_{j},r)} - \frac{1}{2i} \sum_{i} \Psi_{i}^{C} \sqrt{\frac{2}{\pi k_{i}}} e^{-i\phi(k_{i},r)} (e^{-i\delta_{i}} S_{ij}^{\dagger} e^{-i\delta_{j}}), \tag{49}$$

where,

$$S_{ij}^{\dagger} = \sum_{\lambda} B_{i\lambda} e^{-i2\eta_{\lambda}} B_{\lambda j}^{+} \tag{50}$$

is the scattering matrix that incorporates the interchannel interaction.

Combining Eqs. (44 and 48) we express the incoming boundary condition wavefunction in terms of the S-matrix

$$\Psi_{jE}^{(-)} = \sum_{i} \Psi_{iE} \frac{1}{2} (\delta_{ij} + S_{ij}^{\dagger}) e^{-i\delta_{j}}. \tag{51}$$

In order to avoid misunderstandings, we emphasize that the present discussion utilizes real energies and the scattering wavefunctions are defined according to the chosen boundary conditions. We do not use complex energies and corresponding boundary conditions that are appropriate for the energy-dependent definition and computation of resonance states, e.g., Ref. [1].

5.2.4. Presence of MES

As is shown schematically in Figure 6.3, inside both the discrete and the continuous spectrum there are states labeled by doubly or multiply excited valence electron configurations or by inner-hole configurations, whose energy is embedded inside the channels of single-electron excitation of the same symmetry. Their mixing produces perturbation of the discrete Rydberg wavefunctions and spectra or the appearance of resonances in the continuous spectrum.

In order to describe formally and implement computationally the results of such mixings, the theory of the previous paragraphs must be extended. The basis for doing so in the framework of the state-specific methodology is

found in Fano's comprehensive mathematical treatment of the problem of CI in the continuum [146, 147].

Let Φ_q be the bound wavefunctions describing MES. Then, the total wavefunction will be a combination of functions of the type of Eq. (36) and of functions of the form:

$$\Psi_q = \Phi_q + \sum_i P \int dE' U_{iE'} \frac{1}{E - E'} K_{iE',q} \tag{52}$$

where

$$K_{i\bar{E},q} = W_{i\bar{E},q} + \sum_l P \int dE' W_{i\bar{E},lE'} \frac{1}{E - E'} K_{lE',q} \tag{53}$$

and

$$W_{i\bar{E},q} = V_{i\bar{E},q} - E S_{i\bar{E},q} \tag{54}$$

For reasons of simplicity we have not included in Eqs. (44–45) the Rydberg summation and the terms containing the G function, see Eqs. (36 and 37).

Below, we shall illustrate the method for the special case where the interchannel coupling can be neglected, i.e., $W_{ij} \approx 0$, in which case $K_{iE,q} \approx W_{iE,q}$, while only one excited state, say Φ_0, is present. Details about the general case can be found in Ref. [126].

The zero-order channels are coupled indirectly through their interaction with the MES, producing the eigenchannels

$$\Psi_{\lambda E} = \left\{ \sum_i U_{iE} B_{i\lambda} + \left[\Phi_0 + \sum_i P \int d\varepsilon U_{i\varepsilon} \frac{1}{E - \varepsilon} W_{i\varepsilon,0} \right] C_0 \right\} \cos \eta_\lambda. \tag{55}$$

The requirement that the Hamiltonian is diagonal in the space of the $\Psi_{\lambda E}$ functions gives the condition

$$\sum_i W_{0,i\varepsilon} B_{i\lambda} - [E - E_0 - F(E)] C_0 = 0, \tag{56}$$

where E_0 is the zero-order energy of Φ_0 and

$$F(E) = \sum_i P \int dE' W_{0,iE'} \frac{1}{E - E'} W_{iE',0} \tag{57}$$

is an energy shift produced by the second-order interaction. Solving with respect to C_0 and putting,

$$K^r_{iE',j\bar{E}} = W_{iE',0} \frac{1}{E - E_0 - F(E)} W_{0,j\bar{E}} \tag{58}$$

allows us to write the eigenchannels in the form:

$$\Psi_{\lambda E} = \left\{ \sum_i U_{iE} B_{i\lambda} + \sum_{i,j} \int dE' U_{iE'} \frac{1}{E - E'} K^r_{iE',jE} B_{j\lambda} + \Phi_0 C_0 \right\} \cos \eta_\lambda \qquad (59)$$

The eigenphase shifts and the mixing coefficients of the eigenchannel wave-functions are obtained by solving the eigenvalue problem:

$$\sum_j K^r_{iE,jE} B_{j\lambda} = -\frac{1}{\pi} \tan \eta_\lambda B_{i\lambda}. \qquad (60)$$

Because of the special form of the K^r matrix, there is only one nonzero eigenvalue,

$$\tan \eta_0 = -\frac{\pi \sum_j (W_{jE,0})^2}{E - E_0 - F(E)} \qquad (61)$$

corresponding to the eigenvector

$$B_{i0} = \frac{W_{iE,0}}{\sqrt{\sum_j (W_{jE,0})^2}}. \qquad (62)$$

In this case,

$$C_0 = \frac{\sqrt{\sum_j (W_{jE,0})^2}}{E - E_0 - F(E)} \qquad (63)$$

The quantity

$$\Gamma = \pi \sum_j (W_{jE,0})^2 \qquad (64)$$

is equal to the half-life of the excited state.

Thus, the phase shift varies rapidly as E passes through the energy $E_r = E_0 + F(E_r)$. This variation shows up in matrix elements and leads to a resonant behavior. For this reason, $\Psi_{\lambda E}$ represents a resonance state. On the other hand, the eigenvectors corresponding to the zero eigenvalues are solutions of the system

$$\sum_j W_{0,jE} B_{j\lambda} = 0 \qquad (65)$$

and represent continua decoupled from the excited state since in this case $C_0 = 0$. As such, they are of little interest contributing only a smooth back-ground.

A well-studied case of such a resonance state is the one produced by the "2s2p" ^{1}P^o DES of He which is embedded in the 1sεp ^{1}P^o continuum and can be populated through a dipole transition from the 1s^2 ^{1}S ground or the 1s2s ^{1}S metastable state. According to the state-specific methodology, the DES can be represented optimally by a three-term MCHF wavefunction, with configurations 2s2p, 2p3d, and 3s3p, while the scattering basis set is represented by fixed-core 1sεp HF functions. In this way, the computations not only are accurate but are also economic, allowing the transparent solution of the TDSE for novel problems, such as the time-resolved formation of the autoionization profile [151].

Additional applications have been carried out for prototypical (at the time) problems, such as the photoionization of He in the energy region around the second IT [127], or the photoabsorption of the Al ^{2}D relativistic $J = 5/2, 3/2$ spectrum [128, 129]. In the former example, it was possible to compute cross-sections by reaching energies very close to the $n = 2$ threshold [127]. In the latter example, which involves a 13-electron system, the calculation was carried out from first principles and revealed the details of the perturbation at the Breit–Pauli relativistic level of the Al KL3s^{2}n(ε)d ^{2}D channel by the series of correlated excited state wavefunctions labeled by the KL3s3p^2 ^{2}D and KL3s3pnp ^{2}D configurations. Oscillator strengths, quantum defects, and fine structures were obtained and showed, for the first time for such a system, very good agreement with experiment.

6. APPLICATIONS OF THE SSEA

The SSEA has been applied to the solution of a number of prototypical TDMEPs. Here we review briefly the following cases:

1. *The multiphoton electron detachment from Li$^-$ with photon energies of $\hbar\omega = 1.36$ eV [54].*
2. *Time-resolved hyperfast processes of strongly correlated electrons during the coherent excitation and decay of multiply excited and inner-hole excited states [118].*
3. *The significance of electron correlation and of state symmetries in the interaction of strong laser pulses with He   1s^2 ^{1}S [122].*
4. *The computation of the time-dependent excitation of high-lying Rydberg wavepackets by laser pulses interacting with electrons via the full multipolar interaction operator [55–57].*

6.1. The multiphoton electron detachment from Li$^-$ with photon energies of $\hbar\omega = 1.36$ eV [54]

The first application of the SSEA to a many-electron system was to the TDMEP of the multiphoton electron detachment from the ground state of
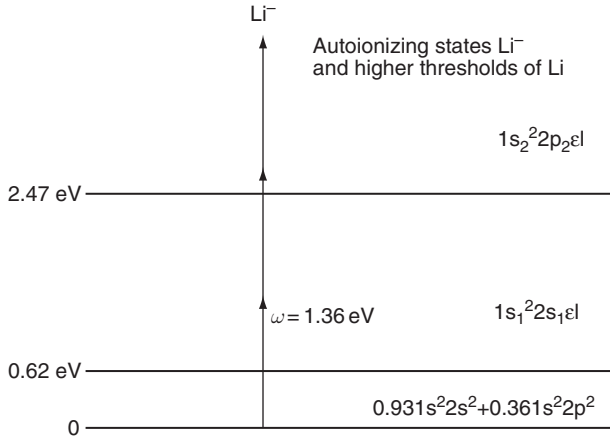
Figure 6.4   The parts of the Li⁻ and Li spectra involved in this study.

the negative ion of Lithium, ^1S [54], with photon energies of $\hbar\omega = 1.36\,eV$ (9116 Å). Figure 6.4 shows the corresponding energy spectrum for the absorption of up to two photons.

The Li⁻ calculation of 1994 [54] constitutes a prototypical demonstration of how the SSEA accounts in a systematic way for the interplay between nonperturbative dynamics (on the one hand) and electronic structure, electron correlation, and interchannel coupling in the continuum (on the other hand). The initial state wavefunction is obtained as a superposition of the most important optimized configurations representing the overwhelming part of electron correlation that is relevant to photoabsorption(Ref. [40] and Section 5). In the case of Li⁻, this correlated wavefunction is dominated by a *multiconfigurational zero-order wavefunction* $[a(1s^22s^2) + b(1s^22p^2)]^1S$, for which the numerical solution of the MCHF equations with $n=2$ and $n=3$ configurations produces $a=0.933$ and $b=0.360$. Thus, instead of a single-electron or a single determinant model (in fact, in order to circumvent the MEP, there are many publications on various topics where negative atomic ions are represented by single-electron parameterized potentials), the ground state was treated as a system of four electrons moving in a multiconfigurational central field while interacting with each other.

Given the energetics shown in Figure 6.4, the absorption of one such photon ejects the electron above the Li $1s^22s$ ^2S threshold, and absorption of two photons ejects it above the Li$1s^22p$ $^2P°$ threshold. Hence, since the singlet excited state discrete spectrum of Li⁻ is empty, this TDMEP involves a correlated initial wavefunction and term-dependent scattering channels corresponding to the two thresholds. Because of the energy range that we chose

to investigate, the higher lying scattering resonances of Li⁻ were not included in the expansion.

In lowest order of transition processes, the scattering open channels are the Li⁻ [1s²2s ²Sεp] ¹Pᵒ and the Li⁻ [1s²2p ²Pᵒ εp] ¹S, ¹P, and ¹D. However, when the solution of the TDSE to all orders is required, additional scattering channels, i.e., states with additional angular momenta, accounting for virtual dipole transitions in the continuum, must be included in the expansion of Eq. (26). Their final number is decided through the study of convergence of the overall calculation of the quantity of interest. The significance of states with angular momenta larger than the ones predicted by LOPT is emphasized in the example (*iii*) concerning He.

In the computations of Ref. [54], the following channels (both parities) were found to produce good convergence:

Threshold 1 (1s²2s ²S): $\Phi_1(L_{(1)};E_1 + \varepsilon) \rightarrow$ 1s²2s ²Sεℓ, $L_{(1)} = {}^1S, {}^1P, {}^1D$

Threshold 2 (1s²2p ²Pᵒ): $\Phi_2(L_{(2)};E_2 + \varepsilon') \rightarrow$ 1s²2p ²Sε'ℓ, $L_{(2)} = {}^1S, {}^1P, {}^1D$

Due to their simple structure, the core wavefunctions 1s²2s ²S and 1s²2p ²Pᵒ were represented by HF wavefunctions. The basis set of bound orbitals and of the energy-normalized scattering orbitals, εℓ and ε'ℓ, were computed numerically from separate calculations via the term-dependent HF scheme.

Details of the calculations and the corresponding results are presented in Ref. [54]. Here we include the results from figure 7 of Ref. [54], as Figure 6.5, which depict the probability $\frac{dP_\varepsilon(t)}{d\varepsilon}$ for ATD, without (i.e., only the HF 1s²2s²   ¹S wavefunction is used) and with electron correlation in the initial state, for peak intensity $I = 1.12 \times 10^{12}$ W/cm², for pulse duration of 7 cycles. The difference in these two spectra was a simple as well as comprehensive demonstration of the dramatic effect that electron correlation may have in such cases of multiphoton ionization.

We give a few details: A series of peaks appear whose separation is different than $\hbar\omega$. This is explained by the fact that the total ATD spectrum consists of two partial ones. The first series of equidistant peaks located at the energy points $n\omega - |E_1 - E_0|$, $n \geq 1$ (the ponderomotive shift is negligible) corresponds to the first threshold, while the second series at $n\omega - |E_2 - E_0|$, $n \geq 2$ corresponds to the second threshold. In addition, the *field-induced interchannel coupling* gives rise to additional peaks in the partial ATD spectra.

When comparing Figures 6.5a and b differences can be seen. For example, the fourth peak located at $2\omega - |E_1 - E_0|$, corresponding to the absorption of two photons above the first threshold, is considerably lower. This means that the angular correlation in the initial state, 1s²2p², is reflected significantly on the final-state probability distribution through the field-induced coupling: 1s²2p² $\overset{\hbar\omega}{\longleftrightarrow}$ 1s²2p₁ε'd $\overset{\hbar\omega}{\longleftrightarrow}$ 1s²2s₁εd. (The initial state MCHF orbitals of Li⁻ are not the same as those of the final-state Li thresholds.) Similarly,
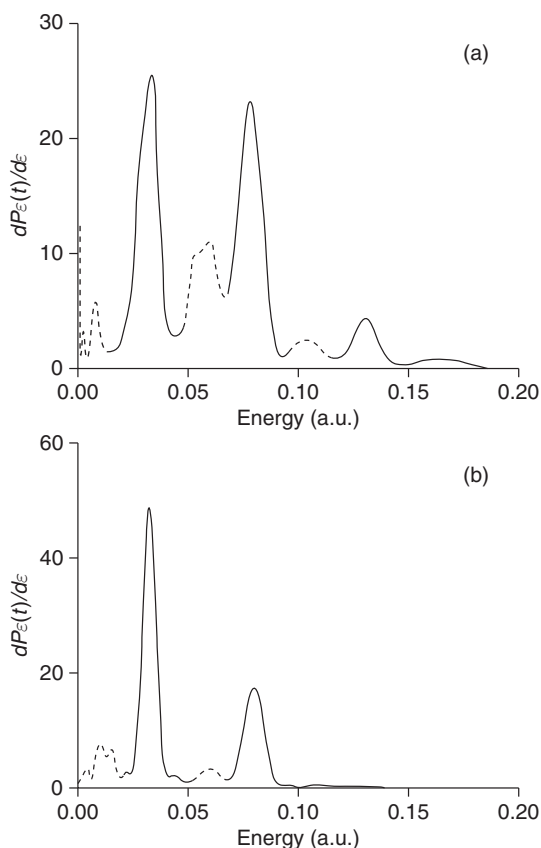
Figure 6.5   Li$^-$1s^{2}2s^2 ATD spectra of Li$^-$ irradiated by a pulse of duration of 7 cycles, with peak intensity I = 1.12 $\times$ 10^{12} W/cm^2 and ω = 1.36 eV. (a) The initial state wavefunction contains the 1s^{2}2p^2 correlation configuration. (b) The initial state wavefunction is represented by the 1s^{2}2s^2 HF function. The solid line corresponds to the peaks of the first threshold, while the dashed line corresponds to the peaks of the second one [54].

the third peak located at $3\omega - |E_2 - E_0|$, corresponding to the absorption of two photons above the second threshold, is larger. Finally, the fifth peak in Figure 6.5a, located at $4\omega - |E_2 - E_0|$, which corresponds to the absorption of three photons above the second detachment threshold, is attributed to initial state correlation.

6.2. Time-resolved hyperfast processes of strongly correlated electrons during the coherent excitation and decay of multiply excited and inner-hole excited states [71a, 118]

Significant advances in the production and use of attosecond pulses have been made during the past few years [152].

As regards the desideratum of electronic spectroscopy in the attosecond regime, in 2002 we published the first ab initio many-electron calculations and analysis with the aim of exploring the degree of relevance of the attosecond scale to the correlated motion of pairs of electrons [71a]. Specifically, our initial work dealt with the computation of the time-dependent coherent excitation and decay of doubly excited resonances which are reached via the interaction of Helium with two high-frequency pulses. The ab initio calculations produced quantitative results about the amplitude of oscillations between the heavily mixing states (electron correlation oscillations) whose frequency is in the attosecond range. Furthermore, the exponential autoionization decay as well as the time-dependent geometrical variations of pairs of electrons due to electron correlation was time-resolved [71a].

A much harder calculation of coherent time-dependent excitation and decay in a polyelectronic, open-shell system was published in 2007 [118]. Specifically, as a prototypical application of the SSEA to a complex system, we chose the problem of the time-resolved coherent excitation and decay of the 2s-hole $1s^2 2s 2p^6 3s^2 3p$ $^{1,3}P^o$ Auger states of Aluminum, where the dominant channels representing one- as well as two-electron continua are taken into account. In the following paragraphs, we explain how these computations were done.

The overall excitation-decay scheme involves the following transitions:

$$
\text{(A) Al } 1s^2 2s^2 2p^6 3s^2 3p \; ^2P^o + h\nu \rightarrow \begin{vmatrix} \text{Al}^+ \; 1s^2 2s 2p^6 3s^2 3p \; ^3P^o + \varepsilon_1 p_1 \\ \text{Al}^+ \; 1s^2 2s 2p^6 3s^2 3p \; ^1P^o + \varepsilon_2 p_2 \end{vmatrix}
$$

$$
\text{(B) Al } 1s^2 2s^2 2p^6 3s^2 3p \; ^2P^o + h\nu \rightarrow \text{Al}^{++}[1s^2 2s^2 2p^5 3s^2 \; ^2P^o \varepsilon \ell \; ^{1,3}P^o]\varepsilon' p \; ^2L
$$

$$
\ell = s, d, \; ^2L = {}^2S, \, ^2P, \, ^2D
$$

$$
\text{(C) Al}^+ \; 1s^2 2s 2p^6 3s^2 3p \; ^{3,1}P^o \xrightarrow{\text{Auger decay}} \text{Al}^{++} \; 1s^2 2s^2 2p^5 3s^2 \; ^2P^o + \hat{\varepsilon}\ell.
$$
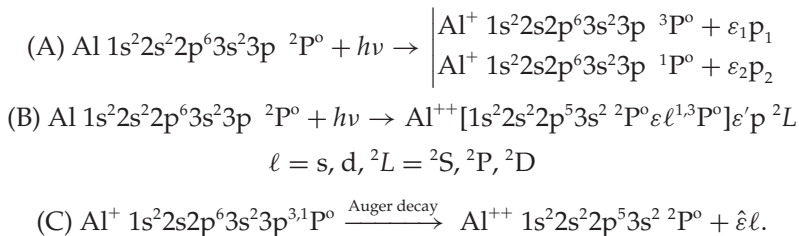
The energy differences in the scheme (A, B, C) are realistic with respect to currently available light-pulse sources. The pulse ejects the 2s electron, creating Auger states in which electron pair rearrangement of the type $(2p,3p) \rightarrow (2s,\hat{\varepsilon}\ell)$, $\ell = s, d$, leads to a symmetry-restricted decay into only two Auger channels, the Al^{++} $1s^2 2s^2 2p^5(^2P^o)(3s^2 \; ^1S)\varepsilon s$, εd $^{1,3}P^o$. Because of constraints of symmetry and electronic structure, this sequence is less complex than other possible ones, such as the ones involving a 2p-hole state or electron pair rearrangements of the type $2p3s \leftrightarrow 2s\varepsilon p$ (rather than the $2p3p \leftrightarrow 2s\varepsilon d$ one). In spite of the fact that open-shell states are involved, the ab initio solution of the TDSE for the above scheme is computationally tractable within the SSEA. In carrying out the relevant calculations the assumption was made that the magnitude of the essential physics is not altered by interchannel coupling, which is therefore left out.

In process (A), the 2s subshell of the ground state is ionized by the electromagnetic pulse. In the EDA, two final LS-coupled core states are reached, each with its own self-consistent field and its own correlation effects. (The approximation which is often made in various types of calculations, namely taking the same orbital and N-electron functions for such multiplet terms, contains errors.) The corresponding energy-normalized scattering orbitals are labeled by $\varepsilon_1 p_1$ and $\varepsilon_2 p_2$ and are computed as term-dependent functions in the fixed HF potential of the core.

In process (B), the same pulse ejects two electrons, one occupying the 3p orbital and one occupying the 2p orbital. The pairs of uncorrelated orbitals representing the two free electrons are labeled by $(\varepsilon d, \varepsilon' p)$. Other combinations of orbital angular momenta for scattering orbitals are left out, for reasons of computational economy. The resulting two-electron continuum is degenerate with the one created by (A) and the subsequent Auger process (C).

In process (C), the Auger electron orbital is labeled by $\hat{\varepsilon}\ell = \hat{\varepsilon}s, \hat{\varepsilon}d$.

For the problem of interest here, the evolution is driven by the coherent time-dependent superposition of the amplitudes for (A), (B), and (C). The structure of the SSEA is such that it allows the control of the type and the size of the computation for each problem of interest. In Ref. [118], in order to render the overall calculation attractive from the point of view of computational effort, we had to reduce its overall magnitude while keeping the parts that produce the important information for this problem.

For example, each physically significant wavefunction entering in the expansion was represented by a state-specific HF function, thereby omitting terms representing the localized electron correlation of each state. Of course, due to the Hamiltonian interaction matrix elements, a variety of CI effects are automatically accounted for, while solving the TDSE via the SSEA, including those causing the autoionization, $(2p,3p) \to (2s,\hat{\varepsilon}d)$. Also, no account for electron correlation in the two-electron continuum produced by direct ionization was taken. This type of possible interaction cannot change the essence of the herein calculated phenomena. In addition, one Auger channel was excluded. Specifically, the Al^+ 2s-hole state decays into the continua $1s^2 2s^2 2p^5 3s^2 \varepsilon\ell$ $^{1,3}P^o$, $\ell = s$ or d, during and after the interaction with the laser pulse, and the matrix elements $< \Phi_0^{ion}(^{1,3}P^o)\varepsilon p\ ^2L | H_{Atom} | \Phi_0^{ion}(^2P^o)\varepsilon\ell)\ ^{1,3}P^o\varepsilon'p\ ^2L >$ account for autoionization. In the spirit of the SSEA, the terms representing the $2p3p \leftrightarrow 2s\varepsilon s$ rearrangement were not included in the final calculations since, for the $^1P^o$ channel which is the most important (see Figures 6.6a and b), the corresponding matrix elements are one order of magnitude smaller than the $2p3p \leftrightarrow 2s\varepsilon d$ ones.

(a)

(b)
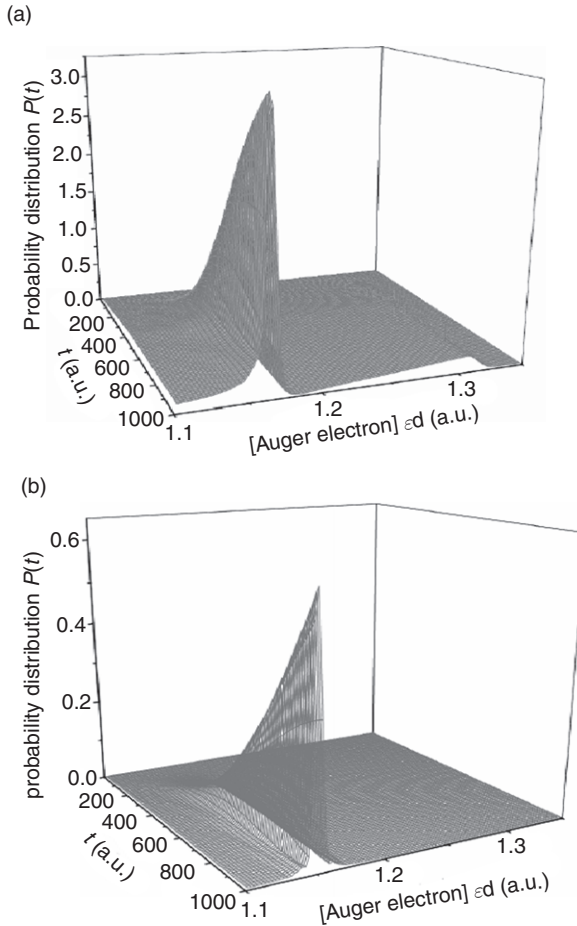
Figure 6.6   (a). Integrated, over the energy ε' of the ε'p scattering orbital, probability distribution of the Al $(1s^2 2s^2 2p^5 3s^2 \varepsilon d)^1 P^o$ ε' p continuum states as a function of energy ε and of time t. The Al ground state $^2P^o$ interacts with a trapezoidal laser pulse of duration 450 a.u. (10.9 fs) with $T_{rise} = T_{off} = 94$ as, frequency $\omega = 4.851$ a.u. (132 eV) and intensity 8.75×10^{11} W/cm^2. For this frequency, the atom is excited to 4.1 eV above the 2s-hole state $(1s^2 2s2p^6 3s^2 3p)^1 P^o$. The percentage of the initial state population that ionizes is very small, only 0.02%. The Auger energy distribution exhibits a Fano-type asymmetry with peak value at 31.7 eV. (b). As in (a), but for the Al $(1s^2 2s^2 2p^5 3s^2 \varepsilon d)^3 P^o$ ε' p continuum states. The Auger energy distribution is essentially symmetric [118].

The explicit form of the time-dependent wavefunction, $\Psi_{\text{SSEA}}(t)$, was,

$$
\begin{aligned}
\Psi_{\text{SSEA}}(t) = {} & a(t)\Phi_0(^2\text{P}^\text{o}) + \int_0^\infty d\varepsilon \sum_L C_3^L(\varepsilon,t)[\Phi_0^{\text{ion}}(^3\text{P}^\text{o})\varepsilon\text{p}\ ^2L] \\[6pt]
& + \int_0^\infty d\varepsilon \sum_L C_1^L(\varepsilon,t)[\Phi_0^{\text{ion}}(^1\text{P}^\text{o})\varepsilon\text{p}\ ^2L] \\[6pt]
& + \iint_0^\infty d\varepsilon d\varepsilon' \sum_L D_3^L(\varepsilon,\varepsilon',t)[(\Phi_0^{\text{ion}}(^2\text{P}^\text{o})\varepsilon\text{d})\ ^3\text{P}^\text{o}\varepsilon'\text{p}\ ^2L] \\[6pt]
& + \iint_0^\infty d\varepsilon d\varepsilon' \sum_L D_1^L(\varepsilon,\varepsilon',t)[(\Phi_0^{\text{ion}}(^2\text{P}^\text{o})\varepsilon\text{d})\ ^1\text{P}^\text{o}\varepsilon'\text{p}\ ^2L]
\end{aligned}
\tag{66}
$$

where, $\Phi_0(^2\text{P}^\text{o})$, $\Phi_0^{\text{ion}}(^3\text{P}^\text{o})$, $\Phi_0^{\text{ion}}(^1\text{P}^\text{o})$, and $\Phi_0^{\text{ion}}(^2\text{P}^\text{o})$ are numerical HF functions for the Al $KL3s^23p$ $^2\text{P}^\text{o}$, Al^+ $1s^22s2p^63s^23p$ $^3\text{P}^\text{o}$, Al^+ $1s^22s2p^63s^23p$ $^1\text{P}^\text{o}$, and Al^{++} $1s^22s^22p^53s^2$ $^2\text{P}^\text{o}$ configurations, respectively. The corresponding energy differences from the ground state, $\Phi_0(^2\text{P}^\text{o})$, are, 4.686 a.u., 4.701 a.u., and 3.457 a.u.. The label L stands for S, P, and D symmetries. The energy-normalized scattering orbitals are obtained numerically in the frozen-core HF approximation. The orbitals ε'p and εd were obtained from two independent computations, the first in the field of $\Phi_0^{\text{ion}}(^{1,3}\text{P}^\text{o})$ and the second in the field of $\Phi_0^{\text{ion}}(^2\text{P}^\text{o})$.

The interaction Hamiltonian (EDA in the length form) had a trapezoidal temporal shape. The values of the field strength, F, were in the range from the weak-field limit, where perturbation theory holds, to higher values. In the nonperturbative regime, one may see a time-dependent large population transfer that takes place from the Al ground state. Furthermore, the time-dependent decay of the Auger states exhibits the expected exponential law. For example, for the Al^+ 2s-hole Auger state $(1s^22s2p^63s^23p)$ $^1\text{P}^\text{o}$, which interacts mainly with the continuum states $(1s^22s^22p^53s^2)^2\text{P}^\text{o}\varepsilon\text{d}$, the autoionization lifetime which is associated with the exponential decay is 5.7 fs.

As another exemplar of the results of these computations [118], we chose to reproduce figure 3 of Ref. [118]. This is shown here as Figure 6.6. It represents the first ab initio theoretical-computational demonstration of the time-resolved formation of the interference-induced asymmetric profile during the creation of an inner-hole Auger state [118, 151, 153].

6.3. The significance of electron correlation and of state symmetries in the interaction of strong laser pulses with He $1s^2$ ^{1}S [122]

For problems where an atom in its ground state interacts with a strong laser pulse, say of intensities higher than 5×10^{13} W / cm^2, the issue arises as to which extent electron correlations determine the time evolution of the system

so as to produce observable characteristics that would be absent if it were not for the participation of electron correlation. The concept has already been discussed in Section (1) with the analysis of the effects of electron correlation in the negative ion of Lithium.

Some time ago, Moiseyev and Weinhold [154] examined the problem of the quantitative understanding of the production of HHG in Helium for photon energies of 5 eV. They adopted a model where the participating in the computations correlated wavefunctions had only ^{1}S and ^{1}P^o symmetries. Based on the corresponding results, they argued that HHG is largely due to what they called dynamic correlations, rather than to one-electron excitation. Specifically, they concluded that "Harmonic generation spectra in He can be treated as a single Floquet mode phenomenon" [154, p. 2103]. Regardless of the level of complexity of the calculations of Ref. [154], we considered that the choice of just the two state symmetries, ^{1}S and ^{1}P^o, which are the ones dictated by LOPT, needed further exploration before reliable conclusions could be drawn [122]. To this purpose we employed the SSEA in order to compute and analyze the time-dependent response of He ^{1}S to a laser pulse of $\lambda = 248$ nm, whose strength is sufficiently high to saturate ionization [122]. The temporal shape of the pulse had the $\sin^2\left(\frac{\pi t}{\tau}\right)$ form, lasting for 20 cycles. We obtained results for

(α) Multiphoton ionization rates for peak intensities $4 \times 10^{14} - 1.3 \times 10^{16}$ W / cm^2.
(β) Spectra of ATI and characteristic PADs.
(γ) The HHG spectrum.

For (β) and (γ), three intensities were used, 6×10^{14}, 8×10^{14}, and 3.46×10^{15} W / cm^2.

Three types of calculation were carried out, with and without electron correlation, since the aim was to study the effect of electron correlation, of DES and of states of symmetry higher than ^{1}P^o, as a function of intensity. Our complete and final results were obtained by including in the expansion the following state-specific wavefunctions, which correspond to the basic features of the energy spectrum:

1. Initial state, He 1s^2 ^{1}S: A ten-term MCHF wavefunction, consisting of the configurations $1s^2, 2s^2, 2p^2, \ldots, 4f^2$. The dominant coefficients are $0.996(1s^2)$, $-0.061(2s^2)$, $0.062(2p^2)$. The orbitals are in numerical form.
2. The discrete spectrum consisted of state-specific wavefunctions representing the Rydberg states $1sn\ell$, up to $n = 20$ and $\ell = 12$. The wavefunction for each of these states, except the first seven of ^{1}S symmetry (see below), was computed numerically by solving the corresponding HF equations.
3. The first seven excited Rydberg states of ^{1}S symmetry were represented by $\alpha_m(1sms) + b_m(1s^2)$ MCHF numerical solutions, $m = 2,3,\ldots$. The solution of the HF equations for the (1sms) ^{1}S states must be done in the

presence of the $1s^2$ ^1S configuration so as to avoid inaccuracies due to convergence errors.

4. The state-specific, correlated, localized wavefunctions of the $n = 2$ DES, $2s^2$, $2p^2$ ^1S, $2s2p$ $^1P^o$ and $2p^2$ ^1D were included. The theory and justification of the computation of the localized component of resonance states is discussed in Ref. [1]. Since it takes 12 photons of $\lambda = 248$ nm to reach these DES, which lie around 60 eV above the ground state, and since the expansion included the scattering states for the one-electron continuum up to 110 eV, it is unnecessary to consider the infinity of DES between 60 and 79 eV (which is the two-electron IT).

5. The energy-normalized scattering wavefunctions, $1s\varepsilon l$, were computed numerically by the fixed-core HF method, for energies up to 4.03 a.u. in steps of 0.004 a.u. and for angular momenta $l = 0, 1, \ldots, 15$.

Using the above wavefunctions, the number of the resulting coupled differential equations, whose solution produces the time-dependent coefficients, is of the order of 16 000.

Here we stress that, regardless of the number of electrons in the atom (molecule), the overwhelming number of terms in the SSEA comes from the continuous spectrum. In general, the number of discrete states with any significant participation is relatively small. Of course, their computation must be done accurately.

The complete list of computations and results can be found in the original work [122]. Here we recall that the SSEA results revealed in a transparent and systematic way the relative role of all types of states in the spectrum. Furthermore, and most important as regards the original motivation of this work, it was demonstrated that, for this nonperturbative problem, in order to describe the phenomena of ATI, of PADs, and of HHG, conclusions based on the consideration of just the two symmetries ^1S and $^1P^o$ are unreliable. Instead, for Helium interacting with the $\lambda = 248$ nm (5 eV) pulse, when the intensity reaches about 10^{15} W / cm^2, in order for reasonably converged results to be obtained, well-represented states with symmetries up to at least ^1S, $^1P^o$, ^1D, and $^1F^0$ must be included. We note that in the SSEA calculations of Ref. [122] we studied convergence quantitatively with symmetries up to $L = 15$.

6.4. The computation of the time-dependent excitation of high-lying Rydberg wavepackets by laser pulses interacting with electrons via the full interaction Hamiltonian [55–57]

In Section 4, we referred to the issue of the proper choice of the form of the EMF–atom interaction. In the example of this section, this issue is discussed in the context of the problem of processes of excitation and ionization involving directly high-lying Rydberg states and wavepackets.

Let us turn to the EDA of Eq. (18). Although the notion of a single r for a transition matrix element may be ambiguous, practically it refers to the less extended wavefunction of the two. One obvious case where the EDA breaks down in normal problems of photoabsorption is when the wavelength becomes very small, i.e., toward the X-ray region. For example, if the initial state is the 1s of hydrogen, then the quantity kr becomes unity when the ionizing radiation has a wavelength of $\lambda \approx 6.6$ Å.

A different source of possible breakdown of condition (18) appears in situations where, even for not too short wavelengths—say, from 8000 Å to 800 Å—the wavefunctions that become involved in the coupling matrix elements are very extended. For example, in hydrogen, for the $n = 50$ Rydberg state, the outer classical point, $r_t = 2n^2$, is at 5000 Å. This means that the quantity kr_t is unity for $\lambda \approx 16600$ Å.

The consequences of such a case were investigated, formally and computationally, in Refs. [55–57]. Specifically, the application involved the ab initio calculation and analysis of angular Rydberg wavepackets in highly excited hydrogen, a theme that was first discussed within the EDA by Corless and Stroud [155]. Among other things, our work showed that, when solving the TDSE to all orders, because of off-resonance couplings the EDA loses its validity completely. This was achieved by comparing the EDA results with those that were obtained, for the first time, from SSEA calculations that employed the full atom–field interaction that was expressed in a suitable form [55–57] based on the *multipolar* interaction (Eq. 19).

The problem can be stated as follows:

Suppose high-lying Rydberg states and wavepackets have been excited and are allowed to interact with an EMF, either the same as the one that caused their excitation or a different one. Such interactions can, in principle, cause a number of phenomena, depending on the features of the field and of the particular spectrum. Given that the degeneracy of a nonrelativistic hydrogenic state is n^2, the number of levels involved at a particular n and its surroundings becomes rapidly huge. Depending on the wavelength and on the intensity of the field, the interaction can couple either closely lying Rydberg states or Rydberg with scattering states, or both. The question that was asked is the following: What is the physically meaningful form of this coupling and how does it affect the time-dependent dynamics? Even if calculations became possible, is it valid to draw conclusions about a number of aspects of the physics of Rydberg states and wavepackets based on the EDA?

6.4.1. On- and off-resonance excitation of Rydberg states and the theme of angular momentum wavepackets

We consider the case discussed by Corless and Stroud [155]. The 1s state of Hydrogen interacts with a weak field of wavelength suitable for exciting Rydberg levels. Because of the small extent of the initial state, the EDA is valid for the weak-field excitation process. Therefore, considering

on-resonance transitions, a narrow laser pulse of central frequency $\omega = [1-1/n^2]/2$ ought to excite only np levels, individually or as radial wavepackets. On the other hand, for the length form of the EDA the magnitude of the intrashell Rydberg–Rydberg interaction matrix elements, which is given by $\frac{3}{2}n\sqrt{n^2-\ell^2}$, increases rapidly as n increases. It is then natural that as n increases, the contribution of the intrashell matrix elements in a non-perturbative solution of the TDSE should affect significantly the dynamics, including the degree of excitation of angular wavepackets.

In view of questions such the degree of validity of the EDA, the form of the operator and the degree of participation of the degenerate and nearly degenerate Rydberg levels, we implemented the SSEA by adopting a model which we named the *multimanifold intrashell approximation* [55–57]. In this approximation, the coupling between states of different principal quantum number were neglected. In other words, only the intrashell coupling matrix elements for each hydrogenic manifold was included in the expansion of the SSEA.

A series of calculations were carried out, without and with the incorporation of the effects of the intrashell matrix elements belonging to a relatively large number of hydrogenic manifolds surrounding the one which is connected to the central frequency of the laser pulse. The intensity is weak, so as to render the effects of multiphoton ionization negligible, while the duration of the pulse was in the picosecond range. Two forms of the atom–EMF interaction operator were used. The first is the EDA in the length form. The second is the interaction to *all* multipole orders, expressed in terms of the first term of the multipolar interaction, Eq. (19). The temporal shape was chosen as a Gaussian, with a FWHM of 10 ps. Such a pulse was found by Parker and Stroud [156] to drive optimally this hydrogenic system toward the formation of coherent wavepackets.

6.4.2. Angular wavepackets excited by the length operator, $\vec{r}$, of the EDA

The calculations were done for long laser pulses (duration of the order of 50 ps), and for weak fields, with peak intensity around 10^8 W/cm^2. Because of the weakness of the fields that were used, scattering functions were excluded from the expansion. A series of results were obtained, of which, for reasons of economy, only a few important ones are presented here. For example, we computed quantities such as the time-dependent probability of hydrogen remaining in the 1s state while interacting with the laser pulse, $P_{1S}(t)$, the distribution of probability over angular momentum states and the constructive and destructive movement of the wavepackets after the end of the pulse.

The resonance excitation was taken systematically up to the $n = 85$ manifold, for which our results are shown in Figures 6.7 and 6.8. For manifolds excited resonantly from the 1s state with $n_{res} < 50$, these weak-field calculations indicate that $P_{1S}(t)$ is essentially insensitive to whether or not the intrashell matrix elements are included. Although we do not show the relevant results here, we report that, when these matrix elements are ignored,
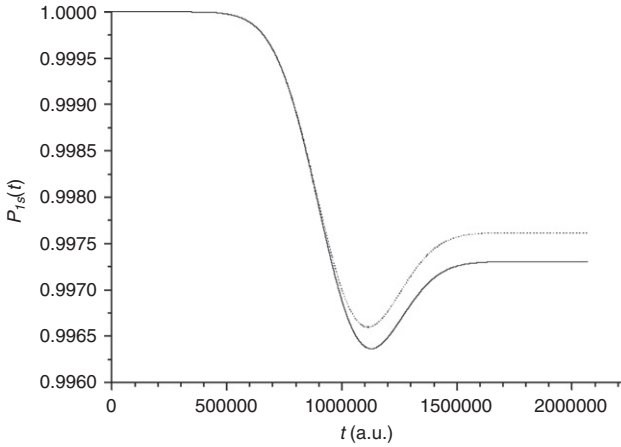
Figure 6.7 Time-dependent survival probability, $P_{1s}(t)$, calculated without (solid line) and with (dotted line) the intrashell interaction matrix elements, within the EDA. The initial hydrogen state, 1s, interacts with a laser pulse of $\omega = (1 - 1/n_{res}^2)/2$, $n_{res} = 85$, of $F = 5 \times 10^{-5}$ a.u. and of duration 50 ps (FWHM = 10 ps).
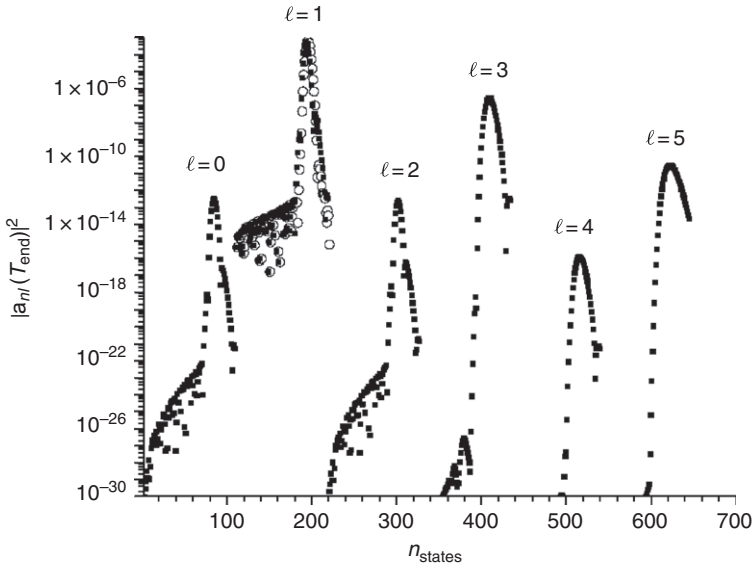
Figure 6.8 The occupation probabilities, $|\alpha_{n\ell}(T_{end})|^2$, at the end of the hydrogen—laser pulse interaction (see the caption of figure (6.7)), for the states with $n \geq 2$. The numbering of the states that are involved in the calculation is given with n_{states}, which counts first the states with $\ell = 0$, then the states with $\ell = 1$, etc. The probabilities obtained without and with the intrashell interaction matrix elements are shown with open circles and solid squares, respectively. The peaks correspond to the various angular momentum quantum numbers ℓ, as shown in the figure.

a coherent wavepacket consisting of np states is generated at the end of the pulse, which oscillates around the nucleus, in agreement with the pioneering findings of Parker and Stroud [156]. Also significant is the fact that the results of our multimanifold intrashell approximation are in essential agreement with those of Nilsen and Hansen [157] where both the intrashell and the intershell matrix elements are included in the overall calculation. Nilsen and Hansen [157] computed the dynamics of wavepacket formation, within the EDA, when the laser pulse excites resonantly the $n_{res} = 10$ and $n_{res} = 11$ levels. Their computations showed that dynamical angular and radial wavepackets containing a large fraction of high angular momentum states could be generated.

Our results [56] concern the resonant excitation of the $n = 85$ manifold, by a laser pulse of F = 5×10^{-5} a.u., of frequency

$$\omega = \left(1 - {}^1\!/n_{res}^2\right)\!\big/2,$$

$n_{res} = 85$ and of Gaussian temporal shape with FWHM = 10 ps. The final size of the hydrogenic basis set (after the usual convergence tests) consisted of hydrogen bound functions with $n = 1, 2,\ldots,110$ and $\ell = 0, 1,\ldots, 10$.

The probability $P_{1S}(t)$ for $n_{res} = 85$ was calculated within the multimanifold approximation, without and with the incorporation of the intrashell matrix elements of each manifold of states included in the expansion. The results are depicted in Figure 6.7. Contrary to the case of lower manifolds, the effect of the intrashell matrix elements is now clearly visible.

Figure 6.8 shows the occupation probabilities, at the end of the pulse, for the states with $n \geq 2$ for various angular momenta ℓ, when only intrashell couplings are included in the computation. The coherent wavepacket which is generated consists, mainly, of both np and nf ($\ell = 3$) states. Although the occupation probabilities for the states with $\ell \neq 1$ are much smaller than the ones with $\ell = 1$, their effect on them is clearly visible. The "partial" wavepackets that consist of purely $\ell = 3$ or $\ell = 5$ states are coherent, having an uncertainty product $\Delta r \Delta p_r$ that is minimum ~ 0.5, with similar behavior to the one with $\ell = 1$, albeit with much smaller amplitudes. We found that this behavior becomes more distinct as the peak intensity increases. Specifically, the wavepacket which is now generated is less coherent and consists of states with $\ell = 1, 3, 5, \ldots$ which are of comparable amplitudes. It appears that as the field becomes more intense, the wavepacket starts breaking up into smaller parts—in this case two—which are oscillating around the nucleus producing destructive and constructive interferences.

On the other hand, when the intrashell couplings are not included in the calculation, the intense field radial wavepacket is qualitatively identical with the ones obtained with weak fields. In this case, the wavepackets for weak as well as for strong fields oscillate in the same way.

6.4.3. Angular wavepackets excited by the full multipolar interaction, $\mathbf{V}_{\text{ext}}^{\text{mulpol}}(t)$

Three categories of calculations were carried out, characterized by the manner in which we accounted for the contribution of the intrashell matrix elements. In all cases, the same basis set was used with peak field strength $F = 5 \times 10^{-5}$ a.u. (intensity of 8.75×10^7 W/cm^2).

The computations of the first category used the EDA with complete neglect of the intrashell matrix elements. The computations of the second category used the EDA and included the intrashell matrix elements. The computations of the third category employed the electric field part of $\mathbf{V}_{\text{ext}}^{\text{mulpol}}(t)$ of Eq. (19) and the intrashell matrix elements of all the manifold states that were included in the expansion. In all cases, given the smallness of the size of the 1s wavefunction compared to the radiation wavelength, the excitation matrix element from the 1s state to the high-lying states is treated within the EDA.

As with the EDA calculations, for reasons of computational feasibility we did not include any scattering states in the basis set, since the field was weak, 8.75×10^7 W/cm^2. On the other hand, for peak intensities many orders of magnitude larger than the one used in this application, the effect of the continuum states on the formation of coherent wavepackets and on the various multiphoton processes cannot be ignored. However, in that case, the solution of the TDSE with the full electric operator would be a formidable task both theoretically and computationally.

The basis set that we used, for each n_{res} from 7 to 50, contained the states $n = n_{\text{res}} - 5, \ldots, n_{\text{res}}, \ldots, n_{\text{res}} + 5$, $\ell = 0, 1, \ldots, n_{\text{res}} - 1$, $m = -\ell, \ldots, \ell$. In spite of the absence of scattering states, as n_{res} increases, the number of the states mixing according to the above algorithm, increases enormously.

For $n_{\text{res}} < 10$, all three categories of calculation produce $P_{1s}(t)$ that are equal. Within the EDA, $P_{1s}(t)$ remains essentially the same whether the intrashell matrix elements are taken into account or not, for $n_{\text{res}} < 50$ and $F = 5 \times 10^{-5}$ a.u.

For $n_{\text{res}} = 10$, the results from the use of the full electric operator start deviating from those for which the EDA was used. As n_{res} increases, this deviation becomes significant both quantitatively and qualitatively [56].

Figure 6.9 shows the three $P_{1s}(t)$ for $n_{\text{res}} = 50$. In this case, the absolute difference of the two EDA $P_{1s}(t)$ is larger than the ones for $n_{\text{res}} < 50$ and its presence is now visible. The most important conclusion is that when a complete calculation is carried out properly, using the intrashell Rydberg–Rydberg interactions in conjunction with the full electric operator, the results indicate clearly that for such or similar problems the EDA is inadequate.
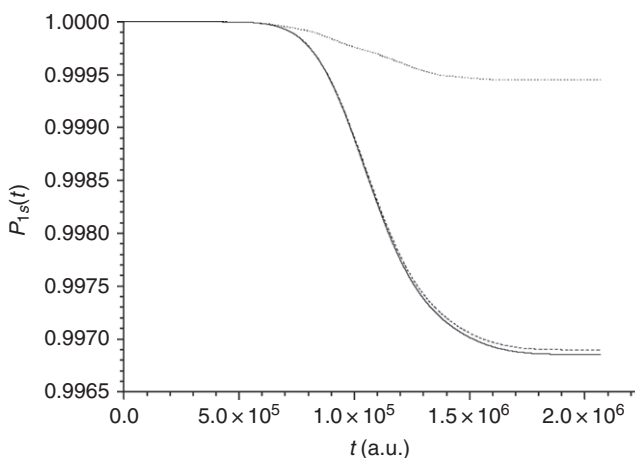
Figure 6.9 The survival probability $P_{1s}(t)$, obtained from three categories of calculation. Solid line: EDA and multimanifold approximation without intrashell matrix elements. Dashed line: EDA and multimanifold approximation with intrashell matrix elements. Dotted line: Full electric operator interaction, in the multimanifold intrashell approximation. The laser pulse characteristics are frequency $\omega = (1 - 1/n_{res}^2)/2$, $n_{res} = 50$, peak field strength $F = 5 \times 10^{-5}$ a.u. (8.75×10^7 W/cm^2), and duration $= 50$ ps (FWHM $= 10$ ps).

7. CONCLUSION

In a series of papers since 1993–1994, we have demonstrated that it is possible to solve quantitatively a variety of TDMEPs in atoms and small molecules, by expanding the nonstationary $\Psi(t)$ in terms of the state-specific wavefunctions for the discrete and the continuous energy spectrum of the unperturbed system. This SSEA to the solution of the TDSE bypasses the serious, and at present insurmountable, difficulties that the extensively used "grid" methods have, when it comes to solving problems with arbitrary polyelectronic, ground or excited states. Furthermore, it allows, in a transparent and systematic way, the monitoring and control of the dependence of the final results on the type and number of the stationary states that enter into the expansion that defines the wavepacket $\Psi(t)$.

The SSEA capitalizes on decades-old theory and experience of computing self-consistent orbitals and correlated wavefunctions for ground and excited states, as well as energy-normalized scattering functions and inner-hole or MES, both with nonrelativistic and with relativistic Hamiltonians. In this context, a unified theory and computational methodology for the computation of wavefunctions of channels for energies just below and just above the fragmentation threshold has been described in Section 5.

Finally, as regards the issue of the operator describing matter–EMF interactions, we have implemented the SSEA at two levels of accuracy, depending on the problems under investigation: The normal case employs the EDA. In exceptional cases, we have demonstrated how to implement the full interaction, using the "multipolar" Hamiltonian.

Obviously, there is much room for further development of the basic concepts of the SSEA and for improvement of its methodology, as well as for additional applications to new and challenging TDMEPs. In all cases, the fundamental issue is how to identify and construct the wavefunctions that are considered relevant to each problem. For example, the possibility of treating correctly the contribution from two-electron continua is an open question. Even if two-electron products of energy-normalized scattering states are used as basis sets, the computational requirements of this (multichannel in general) problem are huge, and so its solution would require dedicated effort and powerful computers.

REFERENCES

[1] C.A. Nicolaides, Theory and state-specific methods for the analysis and computation of field-free and field-induced unstable states in atoms and molecules, in: Advances in Quantum Chemistry Vol. 60, (2010) Chapter 4.

[2] W. Heitler, The Quantum Theory of Radiation, third ed., Clarendon Press, Oxford, 1954.

[3] M.L. Goldberger, K.M. Watson, Collision Theory, J. Wiley, New York, 1964.

[4] D.J. Tannor, Introduction to Quantum Mechanics- A Time-Dependent Perspective, University Science books, Sausalito, 2007.

[5] C. Leforestier, R.H. Bisseling, C. Cerjan, M.D. Feit, R. Friesner, A. Guldberg, et al., A comparison of different propagation schemes for the time dependent Schrödinger equation, J. Comp. Phys. 94 (1991) 59.

[6] N. Balakrishnan, C. Kalyanaraman, N. Sathyamurthy, Time-dependent quantum mechanical approach to reactive scattering and related processes, Phys. Rep. 280 (1997) 79.

[7] M.H. Beck, A. Jäckle, G.A. Worth, H.-D. Meyer, The multiconfiguration time-dependent Hartree (MCTDH) method: A highly efficient algorithm for propagating wavepackets, Phys. Rep. 324 (2000) 1.

[8] G. Nyman, H.-G. Yu, Quantum theory of bimolecular chemical reactions, Rep. Prog. Phys. 63 (2000) 1001.

[9] Y. Komninos, C.A. Nicolaides, Effect of the Rydberg states on the time evolution of nonstationary states below or just above the ionization threshold, Phys. Rev. A 72 (2005) 032716.

[10] C.A. Nicolaides, D.R. Beck, Time dependence, complex scaling and the calculation of resonances in many-electron systems, Int. J. Quantum Chem. 14 (1978) 457.

[11] C.A. Nicolaides, Physical constraints on nonstationary states and nonexponential decay, Phys. Rev. A 66 (2002) 022118.

[12] M. Schönberg, On the general theory of damping in quantum mechanics, Nuovo Cim. 8 (1951) 817.

[13] C.A. Nicolaides, Th.G. Douvropoulos, Shape resonances as poles of the semiclassical Green's function obtained from path-integral theory: Application to the autodissociation of the He_2^{++} $^1\Sigma_g^+$ state, J. Chem. Phys. 123 (2005) 024309.

[14] C.A. Nicolaides, Th. Mercouris, On the violation of the exponential decay law in atomics physics: Ab initio calculation of the time-dependence of the He$^-$ 1s2p^2 ^{4}P nonstationary state, J. Phys. B 29 (1996) 1151.

[15] Th. Mercouris, C.A. Nicolaides, Time dependence and properties of nonstationary states in the continuous spectrum of atoms, J. Phys. B 30 (1997) 811.

[16] Th. Mercouris, C.A. Nicolaides, Stationarity coefficients and short-time deviations from exponential decay in atomic resonance states, Phys. Rev. A 65 (2002) 012112.

[17] M. Drescher, M. Hentschel, R. Kienberger, M. Uiberacker, V. Yakovlev, A. Scrinzi, et al., Time-resolved atomic inner-shell spectroscopy, Nature 419 (2002) 803.

[18] C.A. Nicolaides, Th. Mercouris, Multiphoton ionization of negative ions in the presence of a dc-field. Application to Li$^-$, Chem. Phys. Lett. 159 (1989) 45.

[19] Th. Mercouris, S.I. Themelis, C.A. Nicolaides, Nonperturbative theory and computation of the nonlinear response of He to dc- and ac-fields, Phys. Rev. A 61 (2000) 013407.

[20] S.I. Themelis, Th. Mercouris, C.A. Nicolaides, Quantum mechanical versus semiclassical calculations of dc-field tunnelling rates for He, for field strengths in the range 0.067–1.0 a.u., Phys. Rev. A 61 (2000) 024101.

[21] M. Bylicki, S.I. Themelis, C.A. Nicolaides, State-specific theory and computation of a polyelectronic atomic state in a magnetic field. Application to doubly excited states of H$^-$, J. Phys. B 27 (1994) 2741.

[22] S.I. Themelis, C.A. Nicolaides, Complex energies and the polyelectronic Stark problem: II. The Li n = 4 levels for weak and strong fields, J. Phys. B 34 (2001) 2905.

[23] A. Scrinzi, Ionization of multielectron atoms by strong static electric fields, Phys. Rev. A 61 (2000) 041402(R).

[24] J.S. Parker, G.S.J. Armstrong, M. Boca, K.T. Taylor, From the UV to the static-field limit: Rates and scaling laws of intense-field ionization of helium, J. Phys. B 42 (2009) 134011.

[25] S. Geltman, Short-time dynamics of static field excitation and ionization, J. Phys. B 33 (2000) 4769.

[26] Ph. Durand, I. Paidarová, Ionization of the hydrogen atom: From weak to strong static electric fields, Eur. Phys. J. D 26 (2003) 253.

[27] Y. Komninos, Th. Mercouris, C.A. Nicolaides, Ab initio calculation of time-dependent control dynamics in polyelectronic systems involving bound and resonance states: Application to a quartet spectrum of He$^-$, Phys. Rev. A 77 (2008) 013412.

[28] C.A. Nicolaides, Th. Mercouris, Y. Komninos, The time-dependent formation of the profile of resonance atomic states and its dependence on the duration of ultra-short pulses from free-electron lasers, Phys. Rev. A 80 (2009) 055402.

[29] F.J. Dyson, The radiation theories of Tomonaga, Schwinger and Feynman, Phys. Rev. 75 (1949) 486.

[30] F.H.M. Faisal, Theory of Multiphoton Processes, Plenum Press, New York, 1987.

[31] C.A. Nicolaides, C.W. Clark and M.H. Nayfeh (Eds.), Atoms in Strong Fields, Plenum Press, New York, 1990.

[32] M. Gavrila (Ed.), Atoms in Intense Laser Fields, Academic Press, New York, 1992.

[33] K.C. Kulander, K.J. Schafer, J.L. Krause, Time-dependent studies of multiphoton processes, in ref. [31], p. 247.

[34] K.C. Kulander, Multiphoton ionization of hydrogen: A time-dependent theory, Phys. Rev. A 35 (1987) 445.

[35] K.C. Kulander, Time-dependent Hartree-Fock theory of multiphoton ionization: Helium, Phys. Rev. A 36 (1987) 2726.

[36] K.C. Kulander, Time-dependent theory of multiphoton ionization of Xenon, Phys. Rev. A 38 (1988) 778.

[37] K.C. Kulander, B.W. Shore, Calculations of multiple-harmonic conversion of 1064-nm radiation in *Xe* Phys. Rev. Lett. 62 (1989) 524.

[38] K.C. Kulander, K.J. Schafer, J.L. Krause, Dynamic stabilization of hydrogen in an intense, high-frequency, pulsed laser field, Calculation of photoemission from atoms subject to intense laser fields, Phys. Rev. Lett. 66 (1991) 2601; Phys. Rev. A 45 (1992) 4998.

[39] A. Goldberg, B.W. Shore, Modelling laser ionization, J. Phys. B 11 (1978) 3339.

[40] C.A. Nicolaides, D.R. Beck, Approach to the calculation of the important many-body effects of photoabsorption oscillator strengths, Chem. Phys. Letts. 36 (1975) 79.

[41] C.A. Nicolaides, D.R. Beck, Many-body theory of photoabsorption in atoms and molecules, in: C.A. Nicolaides and D.R. Beck (Eds.), Excited States in Quantum Chemistry, Reidel, Dordrecht, 1979, p. 143.

[42] C.A. Nicolaides, On calculations of correlated wavefunctions with heavy configurational mixing, Int. J. Quantum Chem. 102 (2005) 250.

[43] I. Kawata, H. Kono, Dual transformation for wave packet dynamics: Application to Coulomb systems, J. Chem. Phys. 111 (1999) 9498.

[44] K. Harumiya, I. Kawata, H. Kono, Y. Fujimura, Exact two-electron wave packet dynamics of H_2 in an intense laser field: Formation of localized ionic states H^+H^-, J. Chem. Phys. 113 (2000) 8953.

[45] E.S. Smyth, J.S. Parker, K.T. Taylor, Numerical integration of the time-dependent Schrödinger equation for laser-driven helium, Comp. Phys. Comm. 114 (1998) 1.

[46] T. Kato, H. Kono, Time-dependent multiconfiguration theory for electronic dynamics of molecules in an intense laser field, Chem. Phys. Lett. 392 (2004) 533.

[47] O. Koch, W. Kreuzer, A. Scrinzi, Approximation of the time-dependent electronic Schrödinger equation by MCTDHF, Ap. Math. Comp. 173 (2006) 960.

[48] M. Nest, F. Remacle, R.D. Levine, Pump and probe ultrafast electron dynamics in LiH: A computational study, New J. Phys. 10 (2008) 025019.

[49] Th. Mercouris, I.D. Petsalakis, C.A. Nicolaides, Time-dependent laser-induced molecular formation from repulsive surfaces, Chem. Phys. Lett. 208 (1993) 197.

[50] C.A. Nicolaides, Th. Mercouris, I.D. Petsalakis, Above and below threshold multiphoton dissociation of volcanic ground states. Application to BeH^{++}, Chem. Phys. Letts. 212 (1993) 685.

[51] Th. Mercouris, I.D. Petsalakis, P. Valtazanos, C.A. Nicolaides, Time-dependent multiphoton absorption by NO^{++}. Above and below threshold dissociation and the effect of the first excited surface, J. Phys. B 27 (1994) L519.

[52] I.D. Petsalakis, Th. Mercouris, C.A. Nicolaides, Computation of time-dependent transition probabilities in excimer molecules induced by femtosecond laser pulses, Chem. Phys. 189 (1994) 615.

[53] K.I. Dimitriou, V. Constantoudis, Th. Mercouris, Y. Komninos, C.A. Nicolaides, Quantum and classical dynamics of a diatomic molecule in laser fields with frequency in the region producing maximum dissociation, Phys. Rev. A 76 (2007) 033406.

[54] Th. Mercouris, Y. Komninos, S. Dionissopoulou, C.A. Nicolaides, Computation of strong-field multiphoton processes in polyelectronic atoms: State-specific method and applications to H and Li^- Phys. Rev. A 50 (1994) 4109.

[55] Y. Komninos, Th. Mercouris, C.A. Nicolaides, Theory and computation of the matrix elements of the full interaction of the electromagnetic field with an atomic state. Application to the Rydberg and the continuous spectrum, Phys. Rev. A 65 (2002) 043412.

[56] Th. Mercouris, Y. Komninos, C.A. Nicolaides, Electric dipole versus full interaction in the dynamics of laser excitation of Rydberg wavepackets, J. Phys. B 35 (2002) 1439.

[57] Y. Komninos, Th. Mercouris, C.A. Nicolaides, Long-wavelength approximation in on- and off-resonance transitions, Phys. Rev. A 71 (2005) 023410.

[58] M. Dantus, M.J. Roberts, A.H. Zewail, Real-time femtosecond probing of 'transition states' in chemical reactions, J. Chem. Phys. 87 (1987) 2395.

[59] M. Gruebele, I.R. Sims, E.D. Potter, A.H. Zewail, Femtosecond probing of bimolecular reactions: The collision complex, J. Chem. Phys. 95 (1991) 7763.

[60] K.M. Jones, E. Tiesinga, P.D. Lett, P.S. Julienne, Ultracold photoassociation spectroscopy: Long-range molecules and atomic scattering, Rev. Mod. Phys. 78 (2006) 483.

[61] I.D. Petsalakis, G. Theodorakopoulos, C.A. Nicolaides, R.J. Buenker, Theoretical dipole transition moments for transitions between bound electronic states and non-adiabatic coupling matrix elements between $^2\Sigma^+$ states of HeH, J. Phys. B 20 (1987) 5959.

[62] I.D. Petsalakis, Electronic structure and lifetime of an excimer state of *HeF*, J. Chem. Phys 94 (1991) 290.

[63] I.D. Petsalakis, Th. Mercouris, G. Theodorakopoulos, C.A. Nicolaides, Theory and ab initio calculation of partial widths and interchannel coupling in predissociating diatomic states: Application to *HeF*, Chem. Phys. Lett. 182 (1991) 561.

[64] C.A. Nicolaides, Energy generation from volcanic ground states. Application to cold He_2^{++}, Chem. Phys. Lett. 161 (1989) 45.

[65] E.J. Austin, , Ionisation of model atoms by intense electromagnetic fields, J. Phys. B 12 (1979) 4045.

[66] P.W. Langhoff, C.T. Corcoran, Stieltjes imaging of photoabsorption and dispersion profiles, J. Chem. Phys. 61 (1974) 146.

[67] A.U. Hazi, A purely L^2 method for calculating resonance widths, J. Phys. B 11 (1978) L259.

[68] A. Maquet, R. Taïeb, Two-colour IR + XUV spectroscopies: The 'soft-photon approximation', J. Mod. Opt. 54 (2007) 1847.

[69] R. Kienberger, M. Uiberacker, M.F. Kling, F. Krausz, Attosecond physics comes of age: From tracing to steering electrons at sub-atomic scales, J. Mod. Opt. 54 (2007) 1985.

[70] F. Kelkensberg, C.Lefebvre, W. Siu, O. Ghafur, T. T. Nguyen-Dang, O. Atabek, et al., Molecular dissociative ionization and wave-packet dynamics studied using two-color XUV and IR pump-probe spectroscopy, Phys. Rev. Lett. 103 (2009) 123005.

[71a] C.A. Nicolaides, Th. Mercouris, Y. Komninos, Attosecond dynamics of electron correlation in doubly excited states, J. Phys. B 35 (2002) L271.

[71b] Th. Mercouris, Y. Komninos, C.A. Nicolaides, Theory and computation of the attosecond dynamics of pairs of electrons excited by high-frequency short light pulses, Phys. Rev. A 69 (2004) 032502.

[72] S. Dionissopoulou, Th. Mercouris, C.A. Nicolaides, Ionization rates and harmonic generation for H interacting with laser pulses of λ = 1064 nm and peak intensities in the range $2x10^13$ W/cm^2 − $2x10^14$ W/cm^2, J. Phys. B 29 (1996) 4787.

[73] S. Dionissopoulou, Th. Mercouris, A. Lyras, C.A. Nicolaides, Strong laser-field effects in hydrogen: High-order above-threshold ionization and photoelectron angular distribution, Phys. Rev. A 55 (1997) 4397.

[74] X. Tang, H. Rudolph, P. Lambropoulos, Nonperturbative time-dependent theory of helium in a strong laser field, Phys. Rev. A 44 (1991) R6994.

[75] E.A. Power, S. Zienau, Coulomb gauge in non-relativistic quantum electro-dynamics and the shape of spectral lines, Phil. Trans. R. Soc. 251 (1959) 427.

[76] R.G. Wooley, The electrodynamics of atoms and molecules, Adv. Chem. Phys. 33 (1975) 153.

[77] E.A. Power, T. Thirunamachandran, The multipolar Hamiltonian in radiation theory, Proc. R. Soc. London A 372 (1980) 265.

[78] W.E. Lamb Jr., Fine structure of the Hydrogen atom, Phys. Rev. 85 (1952) 259.

[79] Z. Fried, Vector potential versus field intensity, Phys. Rev. A 8 (1973) 2835.

[80] K.-H. Yang, Gauge transformations and quantum mechanics I. Gauge invariant interpretation of quantum mechanics, Ann. Phys. (N.Y.) 101 (1976) 62.

[81a] J.J. Forney, A. Quattropani, F. Bassani, Choice of gauge in optical transitions, Nuove Cimento B 37 (1977) 78.

[81b] J.J. Forney, A. Quattropani, F. Bassani, Choice of gauge in two-photon transitions: $1s - 2s$ transition in atomic hydrogen, Phys. Rev. Lett. 39 (1977) 1070.

[82] D.H. Kobe, Question of gauge: Nonresonant two-photon absorption, Phys. Rev. Lett. 40 (1978) 538.

[83] D.H. Kobe, A. Smirl, Gauge invariant formulation of the interaction of electromagnetic radiation and matter, Am. J. Phys. 46 (1978) 624.

[84] D.H. Kobe, Gauge-invariant resolution of the controversy over length versus velocity forms of the interaction with electric dipole radiation, Phys. Rev. A 19 (1979) 205.

[85] L. Mandel, Electric dipole interaction in quantum optics, Phys. Rev. A 20 (1979) 1590.

[86] G. Grynberg, E. Giacobino, Choice of gauge and multiphoton transitions, J. Phys. B 12 (1979) L93.

[87] C. Leubner, P. Zoller, Gauge invariant interpretation of multiphoton transition probabilities, J. Phys. B 13 (1980) 3613.

[88] Y. Aharonov, C.K. Au, The question of gauge dependence of transition probabilities in quantum mechanics: Facts, myths and misunderstandings, Phys. Lett. 86A (1981) 269.

[89] K.-H. Yang, Gauge transformations, Foldy-Wouthuysen transformations and conservation of energy, J. Phys. A 15 (1982) 437.

[90] D.H. Kobe, Gauge transformations and the electric dipole approximation, Am. J. Phys. 50 (1982) 128.

[91] G.W. Robinson, Question of gauge for the description of two-photon transitions or light scattering when using incomplete sets, Phys. Rev. A 26 (1982) 1482.

[92] W.P. Healy, Comment on "Maxwell's equations in the multipolar representation", Phys. Rev. A 26 (1982) 1798.

[93] Y. Aharonov, C.K. Au, A reply to "Gauge invariance and experimental processes" Phys. Lett. 95A (1983) 412.

[94] J. Bergou, Gauge invariance and gauge independence in optical transitions, J. Phys. B 16 (1983) L647.

[95] J.R. Ackerhalt, P.W. Milonni, Interaction Hamiltonian of quantum optics, J. Opt. Soc. Am. B 1 (1984) 116.

[96] T.E. Feuchtwang, E. Kazes, P.H. Cutler, H. Grotch, The physical significance of gauge independence and gauge covariance in quantum mechanics, J. Phys. A 17 (1984) 151.

[97] D.H. Kobe, Gauge invariance and the space-translation method, J. Phys. A 17 (1984) 141.

[98] D.H. Kobe, Conventional and gauge-invariant probability amplitudes when electromagnetic potentials are turned on and off, Eur. J. Phys. 5 (1984) 172.

[99] D.H. Kobe, K.-H. Yang, Gauge transformation of the time-evolution operator, Phys. Rev. A 32 (1985) 952.

[100] T.E. Feuchtwang, E. Kazes, Comment on K-H Yang's energy operator and gauge independent transition amplitudes, J. Phys. A 18 (1985) 2859.

[101] W.E. Lamb Jr., R.R. Schlicher, M.O. Scully, Matter-field interaction in atomic physics and quantum optics, Phys. Rev. A 36 (1987) 2763.

[102] P.W. Milonni, J.R. Ackerhalt, Keldysh approximation, $\vec{A}^2$, and strong-field ionization, Phys. Rev. A 39 (1989) 1139.

[103] P.W. Milonni, R.J. Cook, J.R. Ackerhalt, Natural line shape, Phys. Rev. A 40 (1989) 3764.

[104] Y. Gontier, M. Trahin, Multiphoton processes in the velocity gauge, Phys. Rev. A 50 (1994) 2459.

[105] Th. Mercouris, Y. Komninos, S. Dionissopoulou, C.A. Nicolaides, The electric dipole approximation and the calculation of free-free transition matrix elements in multiphoton processes, J. Phys. B 30 (1997) 2133; Effects on observables of the singularity in the multiphoton free-free dipole matrix elements, J. Phys. B 29 (1996) L13.

[106] R. Loudon, The Quantum Theory of Light, second ed., University Press, Oxford, 1983.

[107] C.A. Nicolaides, D.R. Beck, On the length, velocity and acceleration expressions for the calculation of accurate oscillator strengths in many-electron systems, Chem. Phys. Lett. 35 (1975) 202.

[108] N.A. Piangos, C.A. Nicolaides, Very highly excited bound states of atomic negative ions having all their electrons with unpaired spins, J. Phys. B 31 (1998) L147.

[109] E.A. McCullough Jr., Numerical solution of the restricted and multiconfiguration Hartree-Fock equations for diatomic molecules, J. Phys. Chem. 86 (1982) 2178.

[110] N.C. Bacalis, Y. Komninos, C.A. Nicolaides, State-specific theory and method for the computation of diatomic molecules: Application to He_2^{++} $^1\Sigma_g^+$. Phys. Rev. A 45 (1992) 2701.

[111] C.A. Nicolaides, N.C. Bacalis, Y. Komninos, Theory for the direct construction of diabatic states and application to the He_2^{++} $^1\Sigma_g^+$ spectrum, Chem. Phys. Lett. 192 (1992) 486.

[112] L.I. Ponomarev, L.N. Somov, The wavefunctions of continuum for the two-center problem in quantum mechanics, J. Comp. Phys. 20 (1976) 183.

[113] M. Hiyama, H. Nakamura, Two-center Coulomb functions, Comp. Phys. Comm. 103 (1997) 209.

[114] V.V. Serov, B.B. Joulakian, D.V. Pavlov, I.V. Puzynin, S.I. Vinitsky, (e,2e) ionization of H_2^+ by electron impact: Application of the exact nonrelativistic two-center continuum wave Phys. Rev. A 65 (2002) 062708.

[115] J.L. Madajczyk, M. Trippenbach, Singular part of the hydrogen dipole matrix element, J. Phys. A 22 (1989) 2369.

[116] V. Veniard, B. Piraux, Continuum-continuum dipole transitions in femtosecond-laser-pulse excitation of atomic hydrogen, Phys. Rev. A 41 (1990) 4019.

[117] W.H. Press, B.P. Flannery, S.A. Teukolsky, W.T. Vetterling, Numerical Recipes, Cambridge University Press, Cambridge, England, 1986 (chap. 15.).

[118] Th. Mercouris, Y. Komninos, C.A. Nicolaides, Time-resolved hyperfast processes of strongly correlated electrons during the coherent excitation and decay of multiply excited and inner-hole excited states, Phys. Rev. A 76 (2007) 033417.

[119] S. Dionissopoulou, Th. Mercouris, A. Lyras, Y. Komninos, C.A. Nicolaides, High-order harmonic generation and above-threshold ionization in H: Calculations using expansions over field-free state-specific wave functions, Phys. Rev. A 51 (1995) 3104.

[120] C.A. Nicolaides, S. Dionissopoulou, Th. Mercouris, Time-dependent multiphoton ionization from the He 1s2s ^{1}S metastable state, J. Phys. B 29 (1996) 231.

[121] Th. Mercouris, S. Dionissopoulou, C.A. Nicolaides, Multiphoton response of He to short laser pulses of wavelength 248 nm and intensities in the range $10^{14} - 10^{16} W/cm^2$, J. Phys. B 30 (1997) 4751.

[122] C.A. Nicolaides, S. Dionissopoulou, Th. Mercouris, The significance of electron correlation and of state symmetries in the interaction of strong laser pulses of 5 eV with He, J. Phys. B 31 (1998) L1.

[123] S. Dionissopoulou, Th. Mercouris, C.A. Nicolaides, Variation of harmonic generation from He interacting with short laser pulses of 5 eV as a function of pulse rise time and intensity, Phys. Rev. A 61 (2000) 063402; Erratum 62 (2000) 039901.

[124] E.A. Hylleraas, B. Undheim, Numerische Berechnung der 2 S-treme von Ortho-und Par-Helium, Zeits. f. Physik 65 (1930) 759.

[125] J.K.L. MacDonald, Successive approximations by the Rayleigh-Ritz variation method, Phys. Rev. 43 (1933) 830.

[126] Y. Komninos, C.A. Nicolaides, Multi-channel reaction matrix theory and configuration-interaction in the discrete and in the continuous spectrum. Inclusion of closed channels and derivation of quantum defect theory, Z. Phys. D 4 (1987) 301.

[127] Y. Komninos, C.A. Nicolaides, Many-electron approach to atomic photoionization: Rydberg series of resonances and partial photoionization cross sections in Helium, around the n=2 threshold, Phys. Rev. A 34 (1986) 1995.

[128] Y. Komninos, G. Aspromallis, C.A. Nicolaides, Theory and computation of perturbed spectra. Application to the Al ^{2}D relativistic J = 5/2, 3/2 spectrum, J. Phys. B 28 (1995) 2049.

[129] Y. Komninos, C.A. Nicolaides, Quantum defect theory for Coulomb and other potentials in the framework of configuration interaction, and implementation to the calculation of ^{2}D and ^{2}F^o perturbed spectra of Al, J. Phys. B 37 (2004) 1817.

[130] K. Bartschat, C.H. Greene, Short-range correlation and relaxation effects on the $(6p^2)^1S$ autoionizing state of atomic barium J. Phys. B 26 (1993) L109.

[131] D.R. Beck, C.A. Nicolaides, Theory of the electronic structure of excited states in small systems with numerical applications to atomic states, in: C.A. Nicolaides and D.R. Beck (Eds.), Excited States in Quantum Chemistry, Reidel, Dordecht, 1979, p. 105.

[132] I.D. Petsalakis, G. Theodorakopoulos, C.A. Nicolaides, R.J. Buenker, Non-orthonormal CI for molecular excited states I: The sudden polarization effect in 90° twisted ethylene, J. Chem. Phys. 81 (1984) 3161.

[133] V. Sugiura, Sur le nombre des électrons de dispersion pour les spectres continus et pour les spectres de séries de l'hydrogène, J. Phys. Radium 8 (1927) 113.

[134] J. Hargreaves, The dispersion electrons of Lithium, Math. Proc. Cambridge Phil. Soc. 25 (1929) 75.

[135] J. Hargreaves, Some calculations relevant to the quantum defect in the extended Ritz formula, Proc. Cambridge Phil. Soc. 25 (1929) 315.

[136] T.S. Kuhn, J.H. van Vleck, A simplified method of computing the cohesive energies of monovalent metals, Phys. Rev. 79 (1950) 382.

[137] F.S. Ham, The quantum defect method, Solid State Phys. 1 (1955) 127.

[138] M.J. Seaton, The use of extrapolated quantum defects as a check on calculated phases for scattering of electrons by positive ions, Proc. Phys. Soc. A 70 (1957) 620.

[139] M.J. Seaton, The quantum defect method, Mon. Not. R. Astron. Soc. 118 (1958) 504.

[140] M. Gailitis, Behavior of cross sections near threshold of a new reaction in the case of a Coulomb attraction field, Sov. Phys.-JETP 17 (1963) 1328.

[141] M.J. Seaton, Quantum defect theory VII. Analysis of resonance structures, J. Phys. B 2 (1969) 5.

[142] M.J. Seaton, Quantum defect theory, Rep. Prog. Phys. 46 (1983) 167.

[143] U. Fano, Quantum defect theory of ℓ uncoupling in H_2 as an example of channel-interaction treatment Phys. Rev. A 2 (1970) 353.

[144] U. Fano, Unified treatment of perturbed series, continuous spectra and collisions, J. Opt. Soc. Am. 65 (1975) 979.

[145] U. Fano, Connection between configuration-mixing and quantum-defect treatments, Phys. Rev. A 17 (1978) 93.

[146] U. Fano, Effects of configuration interaction on intensities and phase shifts, Phys. Rev. 124 (1961) 1866.

[147] U. Fano, F. Prats, On the connection between the theories of collision and of atomic spectra, J. Natl. Acad. Sci. (India) Pt. IV 33 (1963) 553.

[148] C. Greene, U. Fano, G. Strinati, General form of the quantum-defect theory, Phys. Rev. A 19 (1979) 1485.

[149] C.H. Greene, A.R.P. Rau, U. Fano, General form of the quantum-defect theory. II, Phys. Rev. A 26 (1982) 2441.

[150] H.A. Bethe, E.E. Salpeter, Quantum Mechanics of One- and two-Electron Atoms, Springer-Verlag, Berlin, 1957.

[151] Th. Mercouris, Y. Komninos, C.A. Nicolaides, Time-dependent formation of the profile of the He $2s2p^1P^o$ state excited by a short laser pulse, Phys. Rev. A 75 (2007) 013407.

[152] F. Krausz, M. Ivanov, Attosecond physics, Rev. Mod. Phys. 81 (2009) 163.

[153] M. Wickenhauser, J. Burgdörfer, F. Krausz, M. Drescher, Time resolved Fano resonances, Phys. Rev. Lett. 94 (2005) 023002.

[154] N. Moiseyev, F. Weinhold, High harmonic generation spectra of neutral by the complex-scaled (t,t') method: Role of dynamical electron correlation, Phys. Rev. Lett. 78 (1997) 2100.

[155] J.D. Corless, C.R. Stroud, Optical mixing of Rydberg angular momenta, Phys. Rev. Lett. 79 (1997) 637.

[156] J. Parker, C.R. Stroud, Coherence and decay of Rydberg wave packets, Phys. Rev. Lett. 56 (1986) 716.

[157] H.M. Nilsen, J.P. Hansen, Generation of an angular and radial Rydberg wave packet in a single laser pulse, Phys. Rev. A 63 (2001) 011405 (R).

Theory of Resonant States: An Exact Analytical Approach for Open Quantum Systems

Gastón García-Calderón[a]

Contents

Abstract   The theory of resonant states provides an exact analytical approach for the description of open quantum systems. Resonant states are defined by impos- ing purely outgoing boundary conditions to the solutions to the Schrödinger

[a] Instituto de Física, Universidad Nacional Autónoma de México, Apartado Postal 20 364, 01000 México, D.F., México

E-mail address: gaston@fisica.unam.mx (G. García-Calderón)

equation. This leads to complex energy eigenvalues and hence to a non-Hermitian quantum-mechanical formulation. This paper discusses some rigorous analytical results of this formalism for potentials of finite range with applications to scattering and the time evolution of decay.

1. INTRODUCTION

Resonant states were introduced by Gamow, in 1928, in the early times of quantum mechanics, to describe the process of α decay which refers to a situation where an α particle, initially confined inside a radioactive nucleus, goes out of it by tunneling [1, 2]. This constituted one of the first theoretical treatments of an open quantum system. In order to describe the above process, Gamow considered solutions to the Schrödinger equation which at large distances consist only of purely outgoing waves. This is physically appealing because it yields an outward flux for the decaying particle outside the interaction region. Gamow realized, however, that the absence of incoming waves in the solution at large distances leads to complex energy eigenvalues. This was satisfactory because it led to the interpretation of the imaginary part of the energy as the inverse of the lifetime τ in the exponential decay law $\exp(-t/\tau)$, and thus it provided a theoretical framework for the understanding of the exponential decay law in quantum mechanics. However, since the amplitude of resonant states increases exponentially with distance, the usual rules of normalization, orthogonality, and completeness do not apply. Nonetheless, the approach developed by Gamow was very successful in describing α decay [1, 2] and in fact it constituted also one of the first successful descriptions of tunneling phenomena in quantum mechanics.

The vanishing of the incoming wave in the solution for distances beyond the range of the interaction requires that the corresponding coefficient be zero. For scattering in the energy domain, this corresponds to a complex pole of the S-matrix to the problem. Already in 1939, this was noticed by Siegert who used purely outgoing boundary conditions to derive a dispersion formula for elastic scattering by a potential of finite range [3]. Although Siegert does not refer to Gamow's paper, he mentions that his states correspond to the "radioactive states" of the system [3], which suggests that Siegert was aware of Gamow's work. Years later, in 1961, resonant states were employed by Humblet and Rosenfeld to formulate a theory of nuclear reactions based on Mittag-Leffler resonance expansions of the S-matrix for finite range potentials [4]. This theory was further developed by these authors, Jeukenne and Mahaux [5–12]. It is worth noticing that for scattering, the resonant state requires to be evaluated only at a single spatial point, usually at the radius of the potential, and hence the problem of the exponential grow of the resonant state with distance does not arise in these treatments.

Later developments on the properties of resonant states at the end of the 1960s and along the 1970s involved consideration of the analytical properties of the outgoing Green's function [13–18]. This provided a suitable theoretical framework to address the issues of normalization and eigenfunction expansions involving resonant states.

Regarding the normalization issue, one finds in the literature several procedures. One of them is the regularization method of Zel'dovich [19] that was adopted by Berggren [13]. Another procedure refers to a technique known as complex scaling or complex rotation, which was developed in atomic and molecular physics where one usually deals with long-range interactions [20, 21]. Here we consider a normalization of resonant states that follows from the residues at the complex poles of the outgoing Green function of the problem [17, 18]. This normalization condition is similar to that obtained from the residues at the complex poles of the S-matrix [22]. It may be shown, however, that for finite range interactions both Zel'dovich's regularization method and complex scaling are identical to the expression obtained from the residue at the complex pole of the outgoing Green's function [23].

In general, expansions involving resonant states may be divided in two broad classes: a first class that involves bound, resonant, and continuum states, where usually resonant states are considered in the interval $(0, \infty)$ [13, 17, 21, 24], and a second class that refers to expansions defined in the interval $(0, a)$, where a stands for the radius of the finite range potential, that involves the full set of bound, antibound (virtual), and resonant states. Here, the expansions are purely discrete and follow using Cauchy's integral theorem [15, 16, 18, 25]. Some of these expansions are discussed in Ref. [26].

Since resonances are genuine intrinsic properties of quantum systems, the treatments involving resonant states have been extended from nuclear physics to other realms of physics to describe open quantum systems. Moreover, it has continued to have a vigorous development in that field, mainly using the first class of resonant expansions mentioned above, presumably because they adapt better to the many-body features of nuclei [27, 28]. Resonant states are also known in the literature by a variety of names: Gamow states [29], Siegert states [30, 31], as a combination of both [32] or as quasinormal-modes, as in work originated in the 1990s on leaky optical cavities [33], and more recently on photonic band structures [34].

This work discusses some rigorous analytical results for resonant states. It will be mainly concerned with full discrete resonant expansions, i.e., the second class of expansions mentioned above. We shall restrict the discussion to coherent (elastic) processes in one (1D) and three (3D) dimensions. It is worth mentioning, however, that there is work extending the formalism of resonant states to two dimensions (2D) [35, 36] and also describing incoherent processes [35, 37].

A point we would like to stress is that purely outgoing boundary conditions imply that the corresponding quantum system is open. This fact has not been sufficiently emphasized in the past. As we shall see, the non-Hermitian nature of the Hamiltonian does not prevent that resonant states are able to provide exact analytical descriptions of physical processes. We shall refer to exactly solvable examples of tunneling and decay to exhibit that the results of calculations using the resonant formalism are in fact indistinguishable from numerical integration of the Schrödinger equation using continuum wave solutions. However, the analytical expressions for scattering and decay involving resonant states and complex energy eigenvalues provide a deeper insight into the underlying physics of these processes and also much faster computational algorithms.

We would like to contribute to modify a traditional view that considers the non-Hermitian formulation involving resonant states and complex energy eigenvalues as an approximate, phenomenological, and nonfundamental description of physical processes as scattering and decay.

We would like to point out that the approach presented here, that may be traced as sketched above to a line of developments occurring over the years, has evolved independently of the so-called Rigged-Hilbert space formulation of quantum mechanics [38]. It is not clear at all that the Rigged-Hilbert space formulation is consistent with the formalism discussed here, which is mainly concerned with the second class of resonant expansions defined above, involving purely discrete expansions. One should notice, however, that the integral term contribution in Ref. [17], which belongs to the first class of expansions, may be expanded along the internal interaction region in terms of the full discrete set of bound, antibound, and resonant states [25], thus establishing in this case a link between both classes of expansions.

The non-Hermitian formulation discussed in the present work is also different from a recent formulation involving non-Hermitian Hamiltonians where the mathematical axiom of Hermiticity is replaced by the condition of space–time reflection symmetry [39].

The chapter is organized as follows: Section 2 summarizes first a number of properties of resonant states and then deals with resonant expansions for the outgoing Green's function to the problem and for the retarded time-dependent Green's function. Section 4 discusses scattering and tunneling and provides some examples for multibarrier tunneling to demonstrate that the resonant formalism provides an exact description. Section 5.1 deals with the time evolution of decay and shows that the formalism of resonant states provides an exact description of the dynamics. Section 6 presents some final comments. The Appendix provides the derivation of the residue at a complex pole of the outgoing Green's function and considers some properties of Moshinsky functions.

2. PROPERTIES OF RESONANT STATES IN 3D (THE HALF-LINE IN 1D)

In what follows we shall refer to real spherically symmetric potentials $U(r)$ that are of finite range, i.e., $U(r) = 0$ for $r > a$ for angular momentum $\ell = 0$ in 3D. In this form, in addition to the simplicity in the presentation, the results also hold for the half-line in 1D.

The Hamiltonian H to the system is given by

$$H = -\frac{\hbar^2}{2m}\frac{d^2}{dr^2} + U(r), \tag{1}$$

with m the mass of the particle.

In what follows we shall demonstrate that for real energy E, or wave number k, is impossible to obtain a purely outgoing solution. For the Hamiltonian given in Eq. (1), the radial Schrödinger equation for a continuum wave solution $\psi^{(+)}(k, r)$ may be written as

$$\frac{d^2}{dr^2}\psi^{(+)}(k, r) + [k^2 - V(r)]\psi^{(+)}(k, r) = 0, \tag{2}$$

where $V(r) = 2mU(r)/\hbar^2$ and $k^2 = 2mE/\hbar^2$. For $r \geq a$, the solution to Eq. (2) may be written as

$$\psi^{(+)}(k, r) = A(k)e^{ikr} + B(k)e^{-ikr}. \tag{3}$$

From time reversal invariance, one has

$$\psi^{(+)*}(k, r) = A^*(k)e^{-ikr} + B^*(k)e^{ikr}. \tag{4}$$

Absence of incoming waves in Eq. (3) requires $B(k) = 0$, and similarly, in Eq. (4) requires $A^*(k) = 0$, which clearly leads to the vanishing of the wave function. Hence, it is not possible to have a purely outgoing solution for real values of k.

Resonant states are defined as the solutions to the radial Schrödinger equation,

$$\frac{d^2}{dr^2}u_n(r) + \left[\kappa_n^2 - V(r)\right]u_n(r) = 0, \tag{5}$$

obeying the boundary condition at the origin

$$u_n(r = 0) = 0, \tag{6}$$

and for $r > a$, the purely outgoing boundary condition

$$u_n(r) = A_n e^{i\kappa_n r}, \tag{7}$$

which implies

$$\left[\frac{d}{dr}u_n(r)\right]_{r=a_-} = i\kappa_n\,u_n(a). \tag{8}$$

In Eq. (5)

$$\kappa_n^2 = 2mE_n/\hbar^2 \tag{9}$$

Writing κ_n as

$$\kappa_n = \alpha_n - i\beta_n \tag{10}$$

gives

$$\mathcal{E}_n = \hbar^2\left(\alpha_n^2 - \beta_n^2\right)/2m; \qquad \Gamma_n = 2\hbar^2\alpha_n\beta_n/m. \tag{11}$$

Notice that the time reversed state $u_{-n}(r) = u_n^*(r)$ satisfies the conjugate of Eq. (5) with complex eigenvalue $\kappa_{-n}^2 = \left(\kappa_n^2\right)^*$ and the outgoing boundary condition with wavenumber

$$\kappa_{-n} = -\kappa_n^* = -\alpha_n - i\beta_n. \tag{12}$$

An interesting relationship follows by using Green's theorem between Eq. (5) and its complex conjugate to obtain

$$\left[u_n^*(r)\frac{d}{dr}u_n(r) - u_n(r)\frac{d}{dr}u_n^*(r)\right]_0^a + \left(\kappa_n^2 - \left(\kappa_n^2\right)^*\right)\int_0^a |u_n(r)|^2 dr = 0. \tag{13}$$

Then using the corresponding boundary conditions one readily obtains, provided $\alpha_n \neq 0$, that

$$\beta_n = \frac{1}{2}\frac{|u_n(a)|^2}{\int_0^a |u_n(r)|^2 dr}. \tag{14}$$

The above equation proves that β_n is identical to β_{-n} and cannot be negative. On the other hand, it follows from Eqs. (10, 12, and 14) that the complex solutions are seated on the lower half of the k plane distributed symmetrically with respect to the imaginary k-axis. For $\alpha = 0$ one may have solutions along positive and negative values on the imaginary k-axis.

For complex κ_n, it follows immediately by substitution of Eq. (10) into Eq. (7) that along the external region, the amplitude of a resonant state increases exponentially with distance, namely,

$$u_n(r) = A_n e^{i\alpha_n}e^{\beta_n r}. \tag{15}$$

The time dependence of a resonant state is given by

$$u_n(r,t) = u_n(r)e^{-i\mathcal{E}_n t/\hbar}e^{-\Gamma_n t/2\hbar}, \tag{16}$$

which shows that the amplitude of a resonant state decreases exponentially with time. The decaying width is related to the lifetime τ_n of the state through the relation $\tau_n = \hbar/\Gamma_n$. Since the potential vanishes after a distance, for $r \geq a$, Eq. (16) becomes, using Eqs. (15) and (11),

$$u_n(r,t) = A_n e^{i(\alpha_n r - \mathcal{E}_n t/\hbar)} e^{\beta_n(r - v_n t)}, \tag{17}$$

where the velocity of the decaying particle is $v_n = \hbar\alpha_n/m$. Equation (17) represents a propagating outgoing wave times a factor that depends on both the distance from the interaction region and the time. The increase with distance of the factor $\exp(\beta_n r)$ may be interpreted, following Gamow and Critchfield [2], as due to the fact that at a distance r one finds those particles that left the decaying region at a time $(t - r/v_n)$ when the amplitude there was larger by the factor $\exp(\beta_n r)$. This can be immediately corroborated by comparing $|u_n(r,t)|^2$ and $|u_n(r, t - r/v_n)|^2$, namely,

$$\frac{|u_n(r, t - r/v_n)|^2}{|u_n(r,t)|^2} = \frac{e^{\beta_n[r - v_n(t - r/v_n)]}}{e^{\beta_n[r - v_n t]}} = e^{\beta_n r}. \tag{18}$$

Since the absolute modulus square of the resonance function varies with time, it is of interest to see the result of applying the continuity equation, or more precisely of the continuity equation integrated along the internal region of the interaction,

$$\frac{\partial}{\partial t} \int_0^a |u_n(r,t)|^2 \, dr = -\frac{\hbar}{m} \mathrm{Im} \left[u_n^*(r,t) \frac{\partial}{\partial r} u_n(r,t) \right]_0^a. \tag{19}$$

Now, using Eq. (16) and the boundary conditions given by Eqs. (6 and 8), one obtains

$$\Gamma_n = \hbar \left(\frac{\hbar \alpha_n}{m} \right) \frac{|u_n(a)|^2}{\int_0^a |u_n(r)|^2 \, dr}, \tag{20}$$

which says that the decay width is proportional to the velocity of the decaying particle times the probability to find the particle at the surface divided by the probability to find it inside the interaction region. Notice from the definition of Γ_n given by Eq. (11) that Eq. (20) becomes Eq. (14).

In spite of the above considerations, it is a fact that the function $u_n(r,t)$ for $r > a$ and a fixed value of the time t, diverges with distance, i.e., from Eq. (17) it follows that

$$|u_n(r)|^2 \sim e^{2\beta_n r}. \tag{21}$$

The above is known as the "exponential catastrophe of a resonant state."

2.1. Normalization

One sees from the above results that the usual rules of normalization and eigenfunction expansions do not apply for resonant states. A convenient way to consider these issues for resonant states is via the properties of the outgoing Green's function of the problem [17]. In fact, already in 1954, Peierls called the attention to the relationship between the complex poles of the propagator and resonant states [40].

It is well known that the outgoing Green's function may be written as [41]

$$G^+(r, r'; k) = -\frac{\phi(k, r_<)f_+(k, r_>)}{J_+(k)}, \tag{22}$$

where $r_<$ denotes the smaller of r and r' and $r_>$, the larger. The function $\phi(k, r)$ stands for the regular solution to the Schrödinger equation of the problem, satisfying the boundary conditions at the origin

$$\phi(k, 0) = 0, \qquad \phi'(k, 0) = 1, \tag{23}$$

the prime indicating differentiation with respect to r. The function $f_+(k, r)$ is a solution to the Schrödinger equation of the problem which is irregular at the origin, and it is defined by the condition that for $r > a$ (since the potential is of finite range), it behaves as an outgoing wave, namely,

$$f_+(k, r) = e^{ikr}, \qquad r > a. \tag{24}$$

Finally, the function $J_+(k)$ is given by the Wronskian $J_+(k) = \left[f_+\phi' - f_+'\phi \right]$.

It is well known that for interactions of finite range, the outgoing Green's function can be extended analytically to the whole complex k-plane where it possesses an infinite number of poles, i.e. the zeros of $J_+(k)$ [41]. These poles are in general simple and it is assumed that this is the case here, since poles of second or higher order occur only in special cases [42]. Their distribution in the complex k plane is exactly the same as that discussed above for the set of eigenvalues $\{\kappa_n\}$ obtained from the solution to the resonant eigenvalue equation given by Eq. (5).

Studying the behavior of the outgoing Green's function near one of its complex poles allows to obtain its residue. In general, near a complex pole κ_n one may write

$$G^+(r, r'; k) \approx \frac{\rho_n(r, r')}{k - \kappa_n} + \chi(r, r'; k), \tag{25}$$

where $\chi(r, r'; k)$ is a regular function.

Appendix A provides a detailed derivation for $\rho_n(r, r')$. Following Eq. (A.15), it may be written as

$$\rho_n(r, r') = \left(\frac{2m}{\hbar^2}\right) \frac{u_n(r)u_n(r')}{2\kappa_n}, \tag{26}$$

provided the resonant states $u_n(r)$ are normalized according to the condition

$$\int_0^a u_n^2(r)dr + i\frac{u_n^2(a)}{2\kappa_n} = 1. \tag{27}$$

One sees from Eq. (26) that the residue is proportional to the resonant functions $u_n(r)$ and $u_n(r')$. The factors $2m/\hbar^2$ and $2\kappa_n$, that appear respectively, in the numerator and denominator, are there because the derivation was made in the k plane. As shown by Eq. (A.16) these factors are absent if the derivation performed in the complex energy plane.

The normalization condition given by Eq. (27) is formed by a volume term along the internal interaction region and a surface term. Notice that it is independent of the radius a in the sense that if one chooses a different finite value of a, say B such that $B > a$, the expression remains equal to unity. Notice also that for a bound state, where the complex pole is a purely imaginary positive quantity, i.e., $\kappa_n = i\gamma_n$, the normalization condition given by Eq. (27) corresponds exactly the usual normalization condition for bound states since the surface term may be written as an integral that goes from $r = a$ to $r = \infty$.

An interesting expression follows by considering Green's theorem between Eq. (5) for $u_n(r)$ and a similar equation for $u_m(r)$. Integrating the resulting expression along the internal interaction region yields

$$\left[u_m(r)\frac{d}{dr}u_n(r) - u_n(r)\frac{d}{dr}u_m(r)\right]_0^a + \left(\kappa_n^2 - \kappa_m^2\right)\int_0^a u_n(r)u_m(r)dr = 0. \tag{28}$$

Then using the boundary conditions for $u_n(r)$, given by Eqs. (6) and (8), and analogous expressions for $u_m(r)$ allows to write Eq. (28) as

$$\int_0^a u_n(r)u_m(r)dr + i\frac{u_n(a)u_m(a)}{\kappa_n + \kappa_m} = 0, \tag{29}$$

which, using Eq. (27), yields

$$\int_0^a u_n(r)u_m(r)dr + i\frac{u_n(a)u_m(a)}{\kappa_n + \kappa_m} = \delta_{nm} \tag{30}$$

that provides an orthonormality condition for resonant states, where in addition to a volume term there appears a surface term.

One finds approaches in the literature where the residue is evaluated directly from the expression for $G^+(r, r'; k)$ given by Eq. (22) [14]. One may write the regular solution $\phi(k, r)$ as [41]

$$\phi(k,r) = \frac{1}{2ik} \left[J_+ f_-(k,r) - J_- f_+(k,r) \right], \tag{31}$$

where $f_-(k,r)$ is defined by the condition of purely ingoing wave, $f_-(k,r) = e^{-ikr}$, $r > a$, and $J_-(k)$ by the Wronskian $J_-(k) = [f_-\phi' - f'_-\phi]$. Using Eq. (31) into Eq. (22) allows to write the residue $r_n(r,r') = \lim_{k \to \kappa_n} (k - \kappa_n) G^+(r,r';k)$ at a complex pole κ_n as

$$r_n(r,r') = -\left(\frac{2m}{\hbar^2}\right) \frac{1}{2i\kappa_n} \frac{J_-(\kappa_n)}{\dot{J}_+(\kappa_n)} f_+(\kappa_n,r) f_+(\kappa_n,r'), \tag{32}$$

where the dot indicates differentiation with respect to k, and the Taylor's expansion of $J_+(k)$ around κ_n has been used, i.e., $J_+(k) = (k - \kappa_n)\dot{J}_+(\kappa_n) + \cdots$. Using Eq. (31), one sees that at κ_n, $f_+(\kappa_n,r)$ and $\phi(\kappa_n,r)$ are proportional to each other, namely,

$$f_+(\kappa_n,r) = \frac{2i\kappa_n}{J_-(\kappa_n)} \phi(\kappa_n,r), \tag{33}$$

and hence it follows that the residue $r_n(r,r')$ may also be written in terms of the ϕ's. Moreover, it may be shown [43] that the factor

$$\frac{\dot{J}_+(\kappa_n)}{iJ_-(\kappa_n)} = \int_0^a f_+^2(\kappa_n,r)dr + \frac{i}{2\kappa_n} f_+^2(\kappa_n,a), \tag{34}$$

and hence $r_n(r,r') = \rho_n(r,r')$ provided the u_n's in Eq. (A.15) are replaced by the f_+'s. In other words, the functions $u_n(r)$ are proportional to the f_+'s and similarly to the ϕ's.

2.2. Expansion of the outgoing Green's function

This section discusses a full discrete expansion of the outgoing Green's function in terms of all its poles in the complex k plane. The analysis is simpler here because the outgoing Green's function is a singled value function of k.

In what follows, in order to emphasize the relationship of resonant states with the continuous spectra, the discussion will be restricted to potentials where bound and antibound states are absent. This also simplify the mathematical content. It is important to stress, however, that the approach is complete general.

Let us therefore, following García-Calderón [18, 25], denote by J, the integral

$$J = \frac{i}{2\pi} \int_C \frac{G^+(r,r';k')}{k' - k} dk', \tag{35}$$
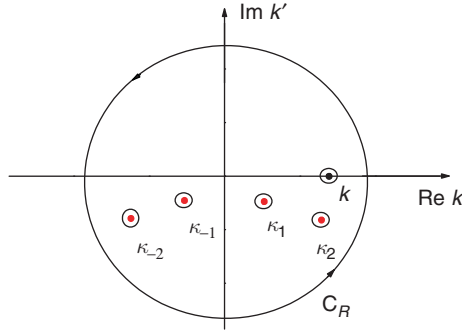
Figure 7.1 Integration contour $C = C_R + c_k + \sum_n c_n$ used to obtain the resonant expansion of $G^+(r, r'; k')$ in terms of the full set of complex poles. See text.

where C, as illustrated in Figure 7.1, represents a large closed contour of radius L in the k *plane* about the origin in the *clockwise* direction which excludes all the poles, κ_n and the value at $k' = k$. Since the integrand is analytic inside this contour, it follows using Cauchy's theorem that $J = 0$ and hence one may write

$$2\pi i J = - \int_{C_R} \frac{G^+(k')}{k' - k} dk' + \sum_n \int_{c_n} \frac{G^+(k')}{k' - k} dk' + \int_{c_k} \frac{G^+(k')}{k' - k} dk' = 0, \qquad (36)$$

where for simplicity $G^+(r, r'; k)$ is denoted by $G^+(k')$. As shown in Figure 7.1, the contour C is formed by a large circle centered at the origin, C_R, the contours c_n that encircle the poles κ_n and c_k encircling the real value $k' = k$. All these contours are in the *counterclockwise* direction. Applying the theorem of residues to the previous expression gives, using Eq. (26),

$$G^+(r, r'; k) = \left(\frac{2m}{\hbar^2} \right) \sum_{n=-N}^{N} \frac{u_n(r) u_n(r')}{2\kappa_n(k - \kappa_n)} + \frac{1}{2\pi i} \int_{C_R} \frac{G^+(r, r'; k)}{k' - k} dk', \qquad (37)$$

which is defined for all $r, r' \geq 0$. Note that by increasing the radius L of the circle C_R, more and more complex poles can be included in the sum term of Eq. (37). However, in the limit $L \to \infty$, $G(r, r'; k)$ diverges unless $r < a$ and $r' < a$. In that case $G^+(r, r'; k)$ goes to zero along all directions in the complex k plane [44, 45], namely,

$$G^+(r, r'; k) \to 0 \qquad \text{as} \qquad |k| \to \infty \qquad (38)$$

and therefore by extending the radius L up to infinity the integral term along C_R in Eq. (37) vanishes exactly. The above holds also if any of r or r' is evaluated at the boundary radius a, but not both of them [18, 44]. The above

conditions are denoted by $(r, r')^\dagger \leq a$. Hence we may write $G^+(r, r';k)$ as an infinite sum over the full set of resonant terms, namely,

$$G^+(r, r';k) = \left(\frac{2m}{\hbar^2}\right) \sum_{n=-\infty}^{\infty} \frac{u_n(r)u(r'_n)}{2\kappa_n(k-\kappa_n)}; \qquad (r, r')^\dagger \leq a. \tag{39}$$

The above expansion has been obtained by a number of authors [15, 16, 18, 46, 47], though authors in Refs. [15, 16] established the expansion only along $(r, r') < a$.

Let us now discuss some properties of Eq. (39). Substitution of Eq. (39) into Eq. (A.1), the equation for $G^+(r, r';k)$, followed by the addition and subtraction of the quantity $\kappa_n^2 u_n(r)$, using Eq. (5), yields

$$\sum_{n=-\infty}^{\infty} \frac{k+\kappa_n}{2\kappa_n} u_n(r)u_n(r') = \delta(r-r'); \qquad (r, r')^\dagger \leq a, \tag{40}$$

Equation (40) holds provided that the following relationships are fulfilled [46, 47],

$$\frac{1}{2} \sum_{n=-\infty}^{\infty} u_n(r)u_n(r') = \delta(r-r'); \qquad (r, r')^\dagger \leq a \tag{41}$$

and

$$\sum_{n=-\infty}^{\infty} \frac{u_n(r)u_n(r')}{\kappa_n} = 0; \qquad (r, r')^\dagger \leq a. \tag{42}$$

Applying the Hamiltonian (1) on the left of Eq. (42) and using Eq. (2), i.e.,

$$Hu_n(r) = \kappa_n^2 u_n(r)$$

one readily obtains

$$\sum_{n=-\infty}^{\infty} \kappa_n u_n(r)u_n(r') = 0; \qquad (r, r')^\dagger \leq a. \tag{43}$$

Equation (41) represents a closure relationship for resonant states and Eqs. (42) and (43) represent, respectively, sum rules obeyed by resonant states.

Now, since

$$\frac{1}{2\kappa_n(k-\kappa_n)} = \frac{1}{2k}\left[\frac{1}{k-\kappa_n} + \frac{1}{\kappa_n}\right] \tag{44}$$

one may substitute Eq. (44) into Eq. (39), using the sum rule given by Eq. (42), to write

$$G^+(r, r';k) = \left(\frac{2m}{\hbar^2}\right)\frac{1}{2k} \sum_{n=-\infty}^{\infty} \frac{u_n(r)u_n(r')}{k-\kappa_n}; \qquad (r, r')^\dagger \leq a \tag{45}$$

that runs over the full set of resonant poles of the system. The above expression, of course also holds if one includes into the expansion bound and antibound states. Equation (45) plays a relevant in the treatment of transient effects in time-dependent tunneling [48] and in the time evolution of decay, as discussed in the Section 2.3.

2.3. Expansion of the time-dependent retarded Green's Function

The solution $\Psi(r,t)$ to the time-dependent Schrödinger

$$\left[i\hbar\frac{\partial}{\partial t} - H\right]\Psi(r,t) = 0, \tag{46}$$

with H given by Eq. (1), as an initial value problem may be written in terms of the retarded Green's function of the problem $g(r,r';t)$ as

$$\Psi(r,t) = \int_0^a g(r,r';t)\Psi(r',0)\,dr', \tag{47}$$

where $\Psi(r,0)$ stands for an arbitrary initial state inside the finite range interaction region, i.e., $V(r) = 0, r > a$.

The time-dependent retarded Green's function $g(r,r';t)$ may be written, using Laplace transform techniques as [17]

$$g(r,r';t) = \frac{1}{2\pi i}\left(\frac{\hbar^2}{2m}\right)\int_{c_0} G^+(r,r';k)e^{-i\hbar k^2 t/2m}\,2k\,dk \tag{48}$$

where $G^+(r,r';k)$ corresponds to the outgoing Green's function of the problem and the integration contour $c_\circ$ along the k plane is shown in Figure 7.2.
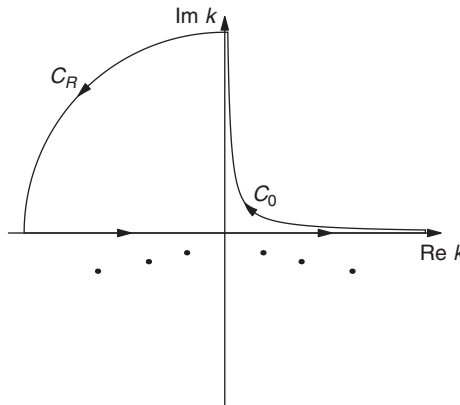
Figure 7.2   Deformation of the contour in the k plane to go from Eq. (48) to Eq. (49).

There are a number of suitable ways to close the integration contour along the k plane. Here we evaluate the integral in Eq. (48) by closing the integration contour as shown in Figure 7.2. As $k \to \infty$ along the upper left quadrant one sees that the integrand to Eq. (48) goes to zero and hence the contour C_R gives zero contribution. Consequently one may write the time-dependent Green's function as

$$g(r,r';t) = \frac{i}{2\pi} \left(\frac{\hbar^2}{2m} \right) \int_{-\infty}^{\infty} G^+(r,r';k) e^{-i\hbar k^2 t/2m} \, 2k dk. \tag{49}$$

2.3.1. Internal region

First, we shall study the case where $r \leq a$. This provides the time evolution of $\Psi(r,t)$ along the internal region of the interaction including also the boundary value at $r = a$. Noticing that in Eq. (47), r' runs along the internal region, one may substitute the expansion for $G^+(r,r';k)$ given by Eq. (45) into Eq. (49). The resulting expression may be written as [25]

$$g(r,r';t) = \sum_{-\infty}^{\infty} u_n(r)u_n(r')M(\kappa_n,t), \qquad (r,r')^\dagger \leq a, \tag{50}$$

where $M(\kappa_n,t) \equiv M(0,\kappa_n,t)$ is the Moshinsky function [49] with $r = 0$. From the general definition given in Appendix B, it follows using Eqs. (B.1) and (B.2), with $z = r$ and $q = \kappa_n$, that

$$M(0,\kappa_n,t) = M(y_n) = \frac{i}{2\pi} \int_{-\infty}^{\infty} \frac{e^{-i\hbar k^2 t/2m}}{k - \kappa_n} dk = \frac{1}{2} w(iy_n), \tag{51}$$

where $w(iy_n)$ is the Faddeyeva function [50], and we denote by y_n^0 the argument y_n with $r = 0$, namely,

$$y_n^0 = -e^{-i\pi/4} \left(\frac{m}{2\hbar t} \right)^{1/2} \left[\frac{\hbar \kappa_n}{m} t \right]. \tag{52}$$

Using the symmetry relations $\kappa_{-n} = -\kappa_n^*$ and $u_{-n}(r) = u_n^*(r)$ allows to write Eq. (50) as

$$g(r,r';t) = \sum_{n=1}^{\infty} \left[u_n(r)u_n(r')M(\kappa_n,t) + u_n^*(r)u_n^*(r')M\left(-\kappa_n^*,t\right) \right], \quad (r,r')^\dagger \leq a. \tag{53}$$

One may then use a property of the functions $M(\kappa_n,t)$ that establishes that [25, 49, 51]

$$M(\kappa_n,t) = e^{-i\hbar \kappa_n^2 t/2m} - M(-\kappa_n,t) \tag{54}$$

provided, using Eq. (52), that the argument $\arg y_n^0$ satisfies $\pi/2 < \arg y_n^0 < 3\pi/2$. It follows by inspection of y_n^0, that proper resonant poles, i.e., poles

$\kappa_n = \alpha_n - i\beta_n$ having $\alpha_n > \beta_n$, fulfill the above condition. Assuming that this is the case, one sees, respectively, that both for $M(-\kappa_n, t)$ and $M(-\kappa_n^*, t)$, $-\pi/2 < \arg y_n^0 < \pi/2$ and hence these quantities do not exhibit an exponential behavior.

It is of interest to exhibit the exponential contribution explicitly. Hence using Eq. (54) one may write Eq. (50) as

$$g(r, r'; t) = \sum_{n=1}^{\infty} u_n(r)u_n(r')e^{-i\hbar \kappa_n^2 t/2m} - I(r, r', t), \qquad (r, r')^{\dagger} \le a, \qquad (55)$$

where

$$I(r, r', t) = \sum_{n=1}^{\infty} \left[u_n(r)u_n(r')M(-\kappa_n, t) - u_n^*(r)u_n^*(r')M(-\kappa_n^*, t) \right] \qquad (56)$$

stands for the nonexponential contributions.

2.3.2. External region
Let us now consider the case $r \ge a$ that allows to obtain the time evolution of $\Psi(r, t)$ along the external region of the interaction [52].

Using Eq. (24) to write $f_+(k, a) = \exp(ika)$ allows to rewrite Eq. (22), for $r' < a$ and $r \ge a$ as,

$$G^+(r, r'; k) = G^+(a, r'; k)e^{ik(r-a)}. \qquad (57)$$

Substitution of Eq. (57) into Eq. (49) yields

$$g(r, r'; t) = \frac{i}{2\pi} \left(\frac{\hbar^2}{2m} \right) \int_{-\infty}^{+\infty} G^+(a, r'; k)e^{ik(r-a)}e^{-ik^2 t} \, 2k \, dk. \qquad (58)$$

Using Eq. (45), we substitute the resonant expansion of $G^+(a, r'; k)$ into Eq. (58) to obtain

$$g(r, r'; t) = \sum_{-\infty}^{\infty} u_n(a)u_n(r')M(r - a, \kappa_n, t), \quad r' < a, \quad r \ge a, \qquad (59)$$

where the function $M(r - a, \kappa_n, t)$ follows from Eq. (B.1) with z replaced by $(r - a)$ and q by κ_n, namely,

$$M(y_n) \equiv M(r - a, q, t) = \frac{i}{2\pi} \int_{-\infty}^{\infty} \frac{e^{ik(r-a)}e^{-i\hbar k^2 t/2m}}{k - \kappa_n} dk \qquad (60)$$

and consequently y_n, given by Eq. (B.2), becomes

$$y_n = e^{-i\pi/4} \left(\frac{m}{2\hbar t} \right)^{1/2} \left[(r - a) - \frac{\hbar \kappa_n}{m} t \right]. \qquad (61)$$

Using the symmetry relations $\kappa_{-n} = -\kappa_n^*$ and $u_{-n}(r) = u_n^*(r)$ allows to write Eq. (59) as

$$g(r,r';t) = \sum_{n=1}^{\infty} \left[u_n(a)u_n(r')M(r-a,\kappa_n,t) + u_n^*(a)u_n^*(r')M\left(r-a,-\kappa_n^*,t\right) \right], \quad (62)$$

where $r' < a$ and $r \geq a$. The functions $M(r-a,\kappa_n,t)$ appearing in Eq. (62) may be written as

$$M(r-a,\kappa_n,t) = e^{i\kappa_n(r-a)}e^{-i\hbar\kappa_n^2 t/2m} - M(a-r,-\kappa_n,t) \qquad (63)$$

provided $\pi/2 < \arg y_n < 3\pi/2$. This requires, as for the case of the internal region, that the resonant poles are proper, i.e., $\alpha_n > \beta_n$, and in addition that in Eq. (61), $(r-a) < \hbar\kappa_n t/m$. When $(r-a) > \hbar\kappa_n t/m$ the behavior of $M(r-a,\kappa_n,t)$ is nonexponential as occurs also for $M(a-r,-\kappa_n,t)$ and $M\left(r-a,-k_n^*,t\right)$. In all these cases $-\pi/2 < \arg y_n < \pi/2$.

It follows then, provided that $(r-a) < \hbar\kappa_n t/m$, that Eq. (62) may be written as

$$g(r,r';t) = \sum_{n=1}^{\infty} u_n(a)u_n(r')e^{i\kappa_n(r-a)}e^{-i\hbar\kappa_n^2 t/2m} - J(r,r',t), \quad r' < a, r \geq a \qquad (64)$$

where

$$J(r,r',t) = \sum_{n=1}^{\infty} \left[u_n(a)u_n(r')M(a-r,-\kappa_n,t) - u_n^*(a)u_n^*(r')M\left(r-a,-k_n^*,t\right) \right] \quad (65)$$

stands for the nonexponential contributions.

3. EXTENSION TO 1D (THE FULL LINE)

The main difference when one extends or generalizes the results presented in the preceding sections to a full one-dimensional description, where we denote the spatial variable by x, i.e., $-\infty \leq x \leq \infty$, is the fact that one goes from a single channel description into a two channel description. Restricting also the discussion to arbitrary potentials of finite range, the resonant states $u_n(x)$ satisfy the Schrödinger equation [53, 54],

$$\frac{d^2}{dx^2}u_n(x) + \left[\kappa_n^2 - V(x)\right]u_n(x) = 0, \qquad (66)$$

where as before $\kappa_n^2 = 2mE_n/\hbar^2$, with $E_n = \mathcal{E}_n - i\Gamma_n/2$, and now $V(x) = [2mU(x)]^{1/2}/\hbar$, where the arbitrary potential $U(x)$ vanishes beyond the interval $0 \leq x \leq L$. The solutions to the above equation satisfy outgoing boundary conditions at $x = 0$ and $x = L$, given, respectively, by,

$$\left[\frac{d}{dx}u_n\right]_{x=0} = -i\kappa_n u_n(0) \tag{67}$$

and

$$\left[\frac{d}{dx}u_n\right]_{x=L} = i\kappa_n u_n(L). \tag{68}$$

The full one-dimensional description introduces the well-known parity symmetry that permits to classify the resonant eigenfunctions as even or odd under the change x for $-x$.

Similarly, the outgoing Green function to the problem satisfies the equation

$$\frac{\partial^2}{\partial x^2}G^+(x,x';k) + \left[k^2 - V(x)\right]G^+(x,x';k) = \left(\frac{2m}{\hbar^2}\right)\delta(x - x'), \tag{69}$$

where $k^2 = 2mE/\hbar^2$, with E the energy. The solution to Eq. (69) satisfies outgoing boundary conditions at $x = 0$ and $x = L$ given, respectively, by

$$\left[\frac{\partial}{\partial x}G^+(x,x';k)\right]_{x=0} = -ikG^+(x = 0,x';k) \tag{70}$$

and

$$\left[\frac{\partial}{\partial x}G^+(x,x';k)\right]_{x=L} = ikG^+(x = L,x';k). \tag{71}$$

The residue at a pole of the Green's function is obtained, in view of the above boundary conditions, by a procedure similar to that discussed in Appendix A. It may be shown that the residue $\rho_n(x,x')$ of $G^+(x,x';k)$ at a pole κ_n is given by [54]

$$\rho_n(x,x') = \frac{u_n(x)u_n(x')}{2\kappa_n} \tag{72}$$

provided the resonant states are normalized according to the condition

$$\int_0^L u_n^2(x)dx + i\frac{u_n^2(0) + u_n^2(L)}{2\kappa_n} = 1. \tag{73}$$

Notice, in a similar form as in the case of the half-line, that for a bound state, i.e., $\kappa_n = i\gamma_n$, the contribution of the surface terms in Eq. (72), corresponds exactly to two integral terms that allow to express the normalization condition for the bound state in the usual form $\int_{-\infty}^{\infty} u_n^2(x)dx = 1$.

By considering the Green's theorem between Eq. (66) for $u_n(x)$ and a similar equation for $u_m(x)$ and then using the corresponding boundary conditions for $u_n(x)$, i.e., Eqs. (67) and (68), and similarly for $u_m(x)$, to obtain

$$\int_0^L u_n(x)u_m(x)dx + i\frac{u_n(0)u_m(0) + u_n(L)u_m(L)}{\kappa_n + \kappa_m} = 0. \tag{74}$$

In general, one may write the full expression for the resonant eigenfunction as

$$u_n(x,t) = u_n(x)e^{-i\mathcal{E}_n t/\hbar}e^{-\Gamma_n t/2\hbar}. \tag{75}$$

We consider the continuity equation integrated along the internal interaction region using Eq. (75) to obtain the one-dimensional analogue of Eq. (19),

$$\frac{\partial}{\partial t}\int_0^L |u_n(x,t)|^2\, dx = -\frac{\hbar}{m}\mathrm{Im}\left[u_n^*(x,t)\frac{\partial}{\partial x}u_n(x,t)\right]_0^L. \tag{76}$$

Then by using the boundary conditions given by Eqs. (67 and 68) we may write the width Γ_n as

$$\Gamma_n = \Gamma_n^0 + \Gamma_n^L, \tag{77}$$

where Γ_n^0 and Γ_n^L define the partial widths for decay, respectively, through $x = 0$ and $x = L$,

$$\Gamma_n^0 = \hbar\left(\frac{\hbar\alpha_n}{m}\right)\frac{|u_n(0)|^2}{\int_0^L |u_n(x)|^2\, dx} \tag{78}$$

and

$$\Gamma_n^L = \hbar\left(\frac{\hbar\alpha_n}{m}\right)\frac{|u_n(L)|^2}{\int_0^L |u_n(x)|^2\, dx}. \tag{79}$$

In the above, we recall that α_n stands for the real part of κ_n, i.e., $\kappa_n = \alpha_n - i\beta_n$.

The above results provide the essential modifications needed to extend the formalism of resonant states to a full one-dimensional description. The analytical properties of the outgoing Green's function on the complex k plane remain the same as for the half-line, so we may write

$$G^+(x,x';k) = \left(\frac{2m}{\hbar^2}\right)\sum_{n=-\infty}^{\infty}\frac{u_n(x)u(x_n')}{2\kappa_n(k - \kappa_n)}; \qquad 0 \le (x,x')^\ddagger \le L, \tag{80}$$

where in 1D, the notation $(x,x')^\ddagger$ means that the expansion does not hold at the points $x = x' = 0 = L$. The closure relation and the sum rules, given, respectively, in the half-line by Eqs. (41)–(43), hold also in the full line. Hence we have

$$\frac{1}{2}\sum_{n=-\infty}^{\infty}u_n(x)u_n(x') = \delta(x - x'), \qquad 0 \le (x,x')^\ddagger \le L, \tag{81}$$

$$\sum_{n=-\infty}^{\infty}\frac{u_n(x)u_n(x')}{\kappa_n} = 0, \qquad 0 \le (x,x')^\ddagger \le L, \tag{82}$$

and

$$\sum_{n=-\infty}^{\infty} \kappa_n u_n(x)u_n(x') = 0 \qquad 0 \le (x,x')^{\ddagger} \le L. \tag{83}$$

In a similar form as considered for the half-line, the expansion of the outgoing Green's function given by Eq. (45) may now be written as

$$G^+(x,x';k) = \left(\frac{2m}{\hbar^2}\right)\frac{1}{2k}\sum_{n=-\infty}^{\infty}\frac{u_n(x)u_n(x')}{k-\kappa_n}, \qquad 0 \le (x,x')^{\ddagger} \le L. \tag{84}$$

One may also derive, using also Cauchy's theorem, an expansion of the outgoing Green's function in the energy or k^2 planes in terms of resonant states [17, 55]. Such an expansion may be written as

$$G^+(x,x';k) = \left(\frac{2m}{\hbar^2}\right)\sum_{n=1}^{N}\frac{u_n(x)u_n(x')}{k^2-\kappa_n^2} + B(E), \qquad 0 \le (x,x')^{\ddagger} \le L, \tag{85}$$

where $B(E)$ stands for a background term which presumably varies slowly with energy and may be neglected provided that the value of N includes the relevant set of resonances.

The time-dependent considerations discussed in Section 2.3 are also valid in 1D [56–58]. One may replace the variable r by the variable x in the corresponding equations of that section taking care of the range of validity of the values of x and x' in these expressions. Thus, for example, along the internal interaction region Eq. (50) becomes

$$g(x,x';t) = \sum_{-\infty}^{\infty} u_n(x)u_n(x')M(\kappa_n,t), \qquad 0 \le (x,x')^{\dagger} \le L, \tag{86}$$

and similarly along the external region $x \ge L$, Eq. (59) becomes

$$g(x,x';t) = \sum_{-\infty}^{\infty} u_n(L)u_n(x')M(x-L,\kappa_n,t), \quad 0 \le x' < L, \quad x \ge L. \tag{87}$$

Notice that there is now the additional expression along the external region for negative values of x,

$$g(x,x';t) = \sum_{-\infty}^{\infty} u_n(0)u_n(x')M(x,\kappa_n,t), \quad 0 < x' \le L, \quad x \le 0. \tag{88}$$

In the sections that follow, we shall switch from 1D (the full line) to 3D (with angular momentum $\ell = 0$, the half-line), or vice versa as the discussion demands it.

4. SCATTERING AND TUNNELING IN THE ENERGY DOMAIN

It is well known since the early days of resonant expansions in 3D, the impossibility of a purely discrete expansion of the S-matrix of the problem [3, 4]. Mittag-Leffler expansions of the S-matrix include always an unknown entire function, which presumably varies slowly with energy and is small. However, this is not in general the case. Subsequent developments that took advantage of a relationship between the S-matrix and the outgoing Green's function of the problem evaluated at the boundary value, showed that it is indeed not possible to get rid of the entire contribution [18, 59]. However, using the outgoing Green's function it may be shown that along the internal region one may have a purely discrete resonant expansion of the continuum wave function [14, 18, 59].

In this section we refer to fully one-dimensional problems to show that along the internal region of the interaction and for tunneling transmission, purely resonant expansions provide an exact description of the corresponding continuum wave solutions to the Schrödinger equation.

Let us therefore consider the relationship between the outgoing Green's function and the continuum wave function of the problem. The continuum wave function satisfies the Schrödinger equation

$$\frac{d^2}{dx^2}\psi(k,x) + [k^2 - V(x)]\psi(k,x) = 0. \tag{89}$$

For a particle approaching the potential from the left $(x < 0)$, the solutions to the above equation read, respectively, for $x < 0$ and $x > L$,

$$\psi(k,x) = e^{ikx} + \mathbf{r}(k)e^{-ikx}, \tag{90}$$

and

$$\psi(k,x) = \mathbf{t}(k)e^{ikx}, \tag{91}$$

where $\mathbf{r}(k)$ and $\mathbf{t}(k)$ are, respectively, the reflection and transmission amplitudes of the problem. Obviously, one may also consider the solutions for scattering from the right $(x > L)$. Applying Green's theorem between Eqs. (89) and (69), followed by integration along the internal region, and then using the boundary conditions (70) and (71), allows to write

$$\psi(k,x') = \left(\frac{\hbar^2}{2m}\right)[ik\psi(k,L) - \psi'(k,L)]G^+(L,x';k)$$

$$+ \left(\frac{\hbar^2}{2m}\right)[ik\psi(k,0) + \psi'(k,0)]G^+(0,x';k), \tag{92}$$

where the prime indicates differentiation with respect to x evaluated at the point indicated in each case. Using Eqs. (90) and (91) into the above equation leads to the expression

$$\psi(k,x) = \left(\frac{\hbar^2}{2m}\right) 2ikG^+(0,x;k), \qquad 0 < x \le L. \tag{93}$$

By considering the solution of the wave function at $x = L$, given by Eq. (91), into the above expression yields for the transmission amplitude

$$\mathbf{t}(k) = \left(\frac{\hbar^2}{2m}\right) 2ikG^+(0,L;k)e^{-ikL}, \tag{94}$$

and similarly, using Eq. (90), yields for the reflection amplitude

$$\mathbf{r}(k) = \left(\frac{\hbar^2}{2m}\right) 2ikG^+(0,0;k) - 1. \tag{95}$$

Since at $x = x' = 0$, the expansion of the outgoing Green's function is divergent, it is not possible to obtain a purely discrete expansion of $r(k)$. As discussed in Ref. [18] for the half-line, the expansion for the reflection amplitude requires at least of two subtraction terms and will not be pursued here. Substitution of Eq. (80) into Eqs. (93) and (94) leads, respectively, to resonance expansions for the continuum wave function along the internal region and the transmission amplitude, namely,

$$\psi(k,x) = ik \sum_{n=-\infty}^{\infty} \frac{u_n(0)u_n(x)}{\kappa_n(k-\kappa_n)}, \qquad 0 < x \le L \tag{96}$$

and

$$\mathbf{t}(k) = ik \sum_{n=-\infty}^{\infty} \frac{u_n(0)u_n(L)}{\kappa_n(k-\kappa_n)} e^{-ikL}. \tag{97}$$

Using Eq. (85) one may also expand the transmission amplitude in the E plane as

$$\mathbf{t}(E) = 2ik\left(\frac{\hbar^2}{2m}\right) \sum_{n=1}^{N} \frac{u_n(0)u_n(L)}{(E - \mathcal{E}_n + i\Gamma_n/2)} e^{-ikL} + Z(E), \tag{98}$$

where $Z(E)$ is a background term.

It turns out that one may also obtain another resonant expansions for $\psi(k,x)$ and $\mathbf{t}$. For scattering from the left this follows by noting that the function $G^+(0,x;k')\exp(-ik'x)$, with $x \le L$, converges along all directions of the k plane as $k \to \infty$, and hence, in an analogous way as discussed in Section 2.2,

by replacing $G^+(r, r'; k')$ in the integrand to Eq. (36) by $G^+(0, x; k') \exp(-ik'x)$ leads to the expansion [60]

$$G^+(0, x; k) = \left(\frac{2m}{\hbar^2}\right) \sum_{n=-\infty}^{\infty} \frac{u_n(0)u_n(x)e^{-i\kappa_n x}}{2\kappa_n(k-\kappa_n)} e^{ikx}, \qquad 0 \le (x, x')^{\ddagger} \le L. \tag{99}$$

Substitution of Eq. (99), respectively, into Eqs. (93) and (94), yields

$$\psi(k, x) = ik \sum_{n=-\infty}^{\infty} \frac{u_n(0)u_n(x)e^{-i\kappa_n x}}{\kappa_n(k-\kappa_n)} e^{ikx}, \qquad 0 < x \le L \tag{100}$$

and

$$\mathbf{t}(k) = ik \sum_{n=-\infty}^{\infty} \frac{u_n(0)u_n(L)e^{-i\kappa_n L}}{\kappa_n(k-\kappa_n)}. \tag{101}$$

4.1. Examples

4.1.1. Model

In order to exemplify the above results we calculate the transmission coefficient *vs* energy in multibarrier resonant tunneling structures which may be modeled by a one-dimensional system formed by alternating $N+1$ rectangular barriers with N rectangular wells. We assume that the electrons possess the same effective mass through the system and that the tunneling process is coherent i.e., elastic [61].

The transmission coefficient $T = |\mathbf{t}|^2$ may be written, using Eq. (98), as [55]

$$T = \sum_{n=1}^{N} T_n + \sum_{n<m}^{N} T_{nm} + D(E), \tag{102}$$

where T_n stands for the n*th* single resonance, T_{nm} represents the interference term between the n*th* and m*th* resonance terms, and $D(E)$ represents the background contribution [55]. The expressions for $T_n(E)$ and $T_{nm}(E)$ are given by

$$T_n(E) = \frac{k^2}{\alpha_n^2} I_n^2 \frac{\Gamma_n^0 \Gamma_n^L}{(E - \mathcal{E}_n)^2 + (\Gamma_n/2)^2} \tag{103}$$

and

$$T_{nm}(E) = 2\mathcal{C}_{nm} \left(\Gamma_n^0 \Gamma_n^L \Gamma_m^0 \Gamma_m^L\right)^{1/2} \times$$

$$\text{Re}\left[\frac{\exp(i\phi_{nm})}{(E - \mathcal{E}_n + i\Gamma_n/2)(E - \mathcal{E}_m - i\Gamma_m/2)}\right], \tag{104}$$

where using $u_s(x) = |u_s(x)| \exp(i\phi_s)$, with $s = n,m$, we have $I_s = \int_0^L |u_s(x)|^2 dx$, the widths Γ_s, Γ_s^0, Γ_s^L, given, respectively, by Eqs. (77)–(79); $C_{nm} = k^2 I_n I_m /(\alpha_n \alpha_m)$ and $\phi_{nm} = [\phi_n(0) + \phi_n(L) - \phi_m(0) - \phi_m(L)]$.

The above representation of the transmission coefficient is appropriate for the description of overlapping resonances situated below the barrier heights of multibarrier tunneling structures [55, 62, 63]. It is worth stressing that there are not free parameters here. All the quantities above depend on the values of the complex poles and these are determined by the potential parameters.

It is well known that for a system with $N + 1$ barriers the resonance levels form groups having each N resonance levels. These minibands are usually sufficiently isolated from each other and hence one may expect that Eq. (102) is an appropriate approximation to calculate the transmission coefficient around a miniband.

We consider a quadruple barrier system with parameters: barrier heights, $U_0 = 0.23\,eV$; width of the two central barriers, $b_2 = b_3 = 5.0\,nm$; width of the two external barriers, $b_1 = b_4 = 3.0\,nm$; and well widths $a_1 = a_2 = a_3 = 3.0\,nm$. The complex poles may be calculated by using the Newton–Raphson method [64] and the set of corresponding resonant states by a modification of the well-known transfer matrix method. The resonance energies and widths of the complex energy poles belonging to the first miniband are, respectively: $\mathcal{E}_1 = 0.1199\,eV$ and $\Gamma_1 = 4.62\,meV$; $\mathcal{E}_2 = 0.1308\,eV$ and $\Gamma_2 = 11.96\,meV$; $\mathcal{E}_3 = 0.1499\,eV$ and $\Gamma_3 = 8.44\,meV$. Notice that all of them possess resonance energies below the height of the barriers.

Figure 7.3 shows the distribution of the first 15 complex poles in the fourth quadrant of the k plane. One sees clearly that the first three-resonance poles are very close together.
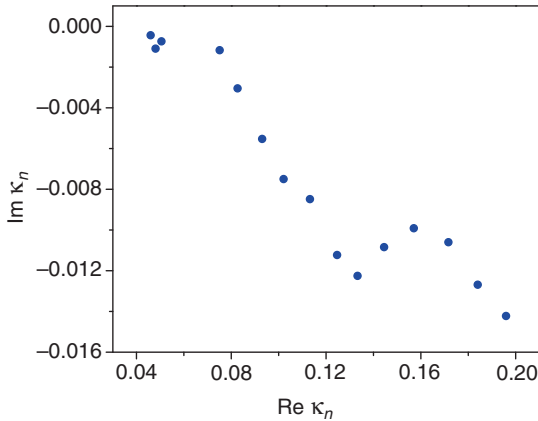
Figure 7.3   Distribution of the first 15 complex poles in the fourth quadrant of the k plane of the quadruple barrier resonant tunneling system with parameters given in the text.
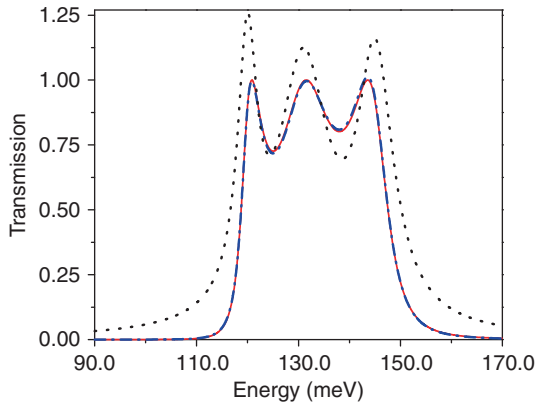
Figure 7.4   Plot of the transmission coefficient *T(E) vs E* for a quadruple barrier system with parameters as discussed in the text, around the first three-resonance miniband. The exact numerical calculation (full line) is indistinguishable from the resonance expansion using the three resonant poles (dashed line). The dotted line represents the calculation without the interference resonant terms.

Figure 7.4 provides the result of the comparison of the exact numerical calculation (full line) using the transfer matrix method and the three resonant approximation, $N = 3$, using Eq. (102), which involves three direct resonance terms T_n, and three interference terms T_{nm} (dashed line). One sees that both calculations are almost identical in the relevant energy range, which implies that the contribution of the background term $D(E)$, which includes the rest of resonance terms, is indeed negligible. Figure 7.4 also shows the result of just adding the three direct resonance terms T_n (dotted line). This shows that the interference terms T_{nm} are crucial to reproduce the exact result.

In order to reproduce the transmission coefficient over a larger energy interval, one needs to include more resonance terms, particularly in the region where the resonance poles overlap strongly, i.e., $|a_{n\pm1} - a_n| \sim \beta_n$, as occurs at energies above the barrier heights. Figure 7.5 yields an example of this for the same system discussed above. The calculation is performed with Eq. (101), which possesses a much better convergence properties than the other expansions. One sees in Figure 7.5 that as the number of poles increases the resonant expansion gets closer to the numerical calculation of the transmission coefficient obtained using the transfer matrix method (full line).

Another example of the application of the resonant formalism to multibarrier systems is to consider the effect on resonant states when some of the values of the potential parameters characterizing the system are generated randomly. We refer to a specific realization of such a disordered system.
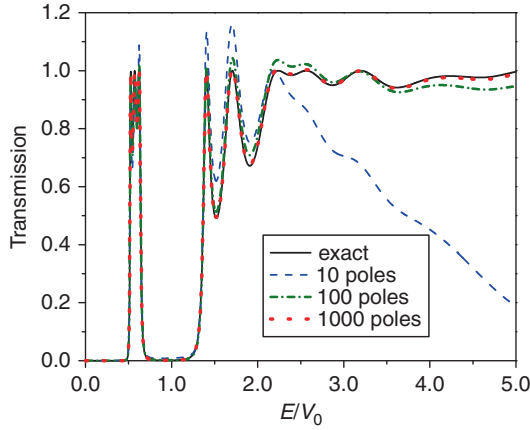
Figure 7.5 Plot of the transmission coefficient *T(E)* vs *E* for the quadruple barrier system with parameters as discussed in the text as a function of different number of poles as indicated in the inset. The considered energy range, using Eq. (101), extends up to five times the height of the barriers. The region of many overlapping resonances requires of much more poles to reproduce the exact numerical calculation.

Here we briefly discuss the example of a multibarrier system involving 20 barriers [63]. The parameters of the potential are as follows; barrier heights $V_0 = 0.3\,\text{eV}$, barrier widths $b = 5.0\,\text{nm}$, and well widths $w = 5.0\,\text{nm}$. The mass $m = 0.067\,m_e$, m_e being the electron mass. The above system corresponds to a symmetric periodic system. We now introduce disorder in the potential profiles by letting the well widths to assume random values W_k within an interval centered at w of width $2\Delta W$, with ΔW the strength of the disorder. That is, each W_k is generated randomly between the interval $(w - \Delta W)$ and $(w - \Delta W)$. Here we consider one of such specific random configurations for the potential profile of the system. Figure 7.6 exhibits a plot of the distribution of the complex energy poles $E_n = \mathcal{E}_n - i\Gamma_n/2$ of the first miniband for this periodic system involving 19 poles. These poles distribute themselves along the E plane forming a "necklace" shape (full circles). The distribution of poles along the E plane for the specific disordered configuration (open circles) reveals that most of these poles are very close to the real energy axis, which implies that their corresponding lifetimes, i.e., $\tau_n = \hbar/\Gamma_n$, become very large. Notice, however, that in this case two of the poles moved away from the real energy axis. The continuous lines show the trajectories that poles of the symmetric case followed to reach the disordered case. Clearly these trajectories are not unique [63].

Figure 7.7 shows the plots of $|u_n(x)|^2$ vs x for the resonant state with $n = 17$ of the above multibarrier system. Figure 7.7a refers to the symmetric
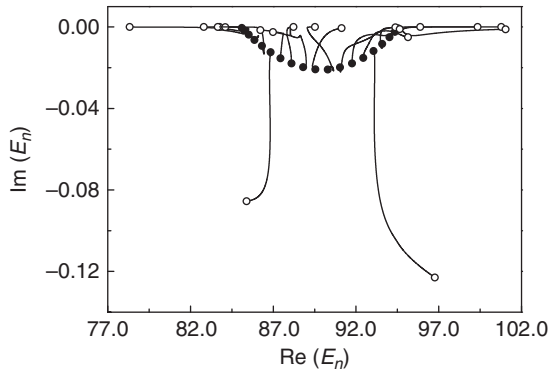
Figure 7.6 Position of the complex poles on the energy plane of the first miniband of the multibarrier system with 20 barriers discussed in the text. Full circles represent the periodic case, whereas open circles refer to the position reached by each pole in the disordered system. The continuous lines indicate the trajectories followed by each pole of the periodic system to its final position in the disordered system. See text.
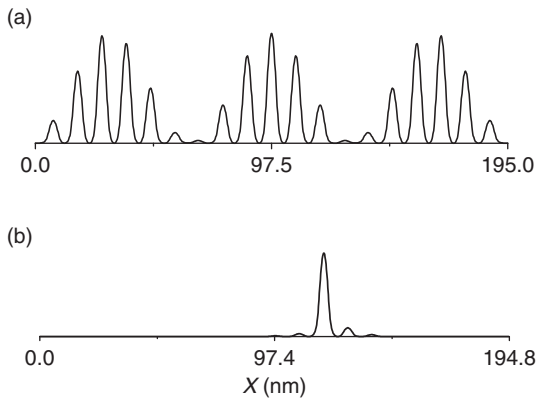
Figure 7.7 Plot of $|u_n(x)|^2$ in arbitrary units, for $n = 17$, along the internal interaction region of the multibarrier system considered in Figure 7.6. Figure (a) refers to the periodic case, whereas Figure (b) corresponds to the disordered system, exhibiting quasi-localization of the resonant state. See text.

case and one sees that the resonant eigenfunction extends through the whole system, whereas Figure 7.7b displays the corresponding resonant state for the disordered case. This state is confined in a short region in the midsection of the system. It may be shown that it remains unaffected by a perturbation on the boundaries of the system that corresponds to Thouless criterion [65] for localized states. Since resonant states eventually decay, we refer to this type of states as quasi-localized resonant states [63].

5. TRANSIENT PHENOMENA

Quantum transients are temporary features that appear in the time evolution of matter waves before they reach a stationary regime. They usually arise as a result of a sudden switch interaction that modifies the confinement of particles in a spatial region or after the preparation of a decaying state [48]. The archetypical quantum transient phenomena is *diffraction in time* which consists of the sudden opening of a shutter to release a semi-infinite beam producing temporal and spatial oscillations of the time evolving wave [49]. A common feature in the mathematical description of quantum transient phenomena is the Moshinsky function, which as we have seen is closely related to the Faddeyeva function. Since in a recent review [48] there appears a discussion on transient phenomena for the dynamics of tunneling based on the present resonant state formalism [54, 66–76], here we restrict the discussion to the time evolution of quantum decay.

5.1. Decay

The time evolution of quantum decay is a subject as old as quantum mechanics. At the end of the 1920s of the last century, the problem of α decay in radioactive atomic nuclei led to a theoretical derivation of the exponential decay law [1, 77]. In the 1950s, Khalfin [78] pointed out the approximate validity of the exponential decay law. It was argued that deviations from this law should occur both at very short and at very long times compared with the lifetime of the decaying system. These theoretical predictions have been confirmed experimentally in recent years in both the short [79] and the long time [80] regimes.

Most theoretical treatments of decay consider the time evolution of an initial state tunneling out of single well [81–85]. However, the present-day possibility of designing the potential parameters of artificial quantum systems [61, 86], opens the way to study the issue of decay in more complex potential profiles as exemplified by semiconductor multibarrier systems of finite length which are formed by a succession of alternating barriers and wells [57] and other artificial multibarrier structures as ultracold atomic gases in optical lattices [86].

5.2. Time-dependent wave function

This section presents a full discrete expansion of the time-dependent wave function in terms of resonant states by using the results in 3D (the half-line) of Section 2.3. We first discuss the solution of the wave function along the internal interaction region and then the propagating solution along the external region out of the range of the interaction. As pointed out at the end of Section 3, the extension to 1D (the full line) follows immediately by replacing

in the expressions below the variable r by the variable x and the corresponding ranges of validity from 3D (the half-line) to 1D (the full line), of course taking into account the properties of resonant states in 1D discussed in Section 3.

5.2.1. Internal region

Substitution of Eq. (50) into Eq. (47) gives the time evolution of the wave function along the internal interaction region in the full time interval,

$$\Psi(r,t) = \sum_{-\infty}^{\infty} C_n u_n(r) M(0,\kappa_n, t), \qquad r \le a, \tag{105}$$

where C_n stands for the expansion coefficient

$$C_n = \int_0^a \psi(r,0) u_n(r) dr, \tag{106}$$

and the Moshinsky function $M(0,\kappa_n, t)$ is given by Eq. (51). It is of interest to address the limits of Eq. (105) as the time $t \to 0$. It follows from Eq. (B.5) that for $t = 0$, the functions $M(0,\kappa_n, t = 0) = 1/2$. This amounts to expand the initial arbitrary function $\psi(r,0)$ as

$$\Psi(r,0) = \frac{1}{2} \sum_{-\infty}^{\infty} C_n u_n(r), \qquad r \le a. \tag{107}$$

If $\psi(r,0)$ is normalized to unity along the internal interaction region, then multiplying Eq. (107) by $\psi^*(r,t)$ followed by integration along the internal region yields

$$\frac{1}{2} \sum_{-\infty}^{\infty} C_n \bar{C}_n = 1, \tag{108}$$

where $\bar{C}_n$ is defined as

$$\bar{C}_n = \int_0^a \Psi^*(r,0) u_n(r) dr. \tag{109}$$

By using the symmetry relation $u_{-n}(r) = u_n^*(r)$ we may write Eq. (108) in the more appealing form

$$\mathrm{Re}\left\{ \sum_{n=1}^{\infty} C_n \bar{C}_n \right\} = 1, \tag{110}$$

which indicates that although $\mathrm{Re}\, C_n \bar{C}_n$ cannot be interpreted as a probability since in general it is not a positive definite quantity, it may be interpreted as

the fraction of $\Psi(r,0)$ in the state $u_n(r)$. This is particularly useful when the above sum adds up almost to unity with only a few resonant terms because it means that one can disregard the rest of them. Clearly, Eqs. (107) and (110) may be obtained also using the closure relation given by Eq. (41). Using the sum rules (42) and (43), one obtains

$$\sum_{n=1}^{\infty} \mathrm{Im} \left\{ \frac{C_n u_n(r)}{\kappa_n} \right\} = 0, \qquad r \leq a \qquad (111)$$

and

$$\sum_{n=1}^{\infty} \mathrm{Im} \left\{ C_n u_n(r) \kappa_n \right\} = 0, \qquad r \leq a. \qquad (112)$$

In order to study the long-time behavior it is more convenient to exhibit explicitly the exponential contributions to Eq. (105), so we substitute Eqs. (55) and (56) into Eq. (47) to obtain

$$\Psi(r,t) = \sum_{n=1}^{\infty} C_n u_n(r) e^{-i\hbar \kappa_n^2 t / 2m}$$

$$- \sum_{n=1}^{\infty} \left[C_n u_n(r) M(-\kappa_n, t) - \bar{C}_n^* u_n^*(r) M\left(-\kappa_n^*, t\right) \right], \qquad r \leq a. \quad (113)$$

The long-time asymptotic expansion for $M(-\kappa_n, t)$ and $M\left(-k_n^*, t\right)$ is given by Eq. (B.7) in Appendix B, so we may write

$$\Psi(r,t) \approx \sum_{n=1}^{\infty} C_n u_n(r) e^{-i\hbar \kappa_n^2 t / 2m}$$

$$- a \sum_{n=1}^{\infty} \left[\frac{C_n u_n(r)}{\kappa_n} - \left(\frac{C_n u_n(r)}{\kappa_n} \right)^* \right] \frac{1}{t^{1/2}}$$

$$- b \sum_{n=1}^{\infty} \left[\frac{C_n u_n(r)}{\kappa_n^3} - \left(\frac{C_n u_n(r)}{\kappa_n^3} \right)^* \right] \frac{1}{t^{3/2}} + \cdots, \qquad (114)$$

where $a = (2m/\hbar)^{1/2} \left(i/2\sqrt{\pi i} \right)$ and $b = (2m/\hbar)^{3/2} \left(1/4\sqrt{\pi i} \right)$. Notice that the term proportional to $1/t^{1/2}$, in view of Eq. (111) cancels out exactly and therefore

$$\Psi(r,t) \approx \sum_{n=1}^{\infty} C_n u_n(r) e^{-i\hbar\kappa_n^2 t/2m} - b \sum_{n=1}^{\infty} \left[\frac{C_n u_n(r)}{\kappa_n^3} - \left(\frac{C_n u_n(r)}{\kappa_n^3} \right)^* \right] \frac{1}{t^{3/2}} + \dots \quad (115)$$

The above equation exhibits the crossover from exponential to an inverse power law behavior, and therefore at asymptotically long times,

$$\Psi(r,t) \approx -b \sum_{n=1}^{\infty} \left[\frac{C_n u_n(r)}{\kappa_n^3} - \left(\frac{C_n u_n(r)}{\kappa_n^3} \right)^* \right] \frac{1}{t^{3/2}} + \dots . \quad (116)$$

The above result may also be obtained by the method of steepest descents [85].

5.2.2. External region

Substitution of Eq. (59) into Eq. (47) gives the time evolution of the wave function along the external region of the potential.

$$\Psi(r,t) = \sum_{-\infty}^{\infty} C_n u_n(a) M(r-a,\kappa_n,t), \qquad r \geq a, \quad (117)$$

where C_n is given by Eq. (106) and the Moshinsky function by Eq. (60). An expression resembling Eq. (117) has been reported in Ref. [87]. These authors consider an approach that does not refer to resonant states. However, it is not difficult to convince oneself that in their expansion the residues at the complex poles κ_n are indeed proportional to the resonant states of the problem.

Similarly to the previous section, it is of interest to analyze, for a fixed value of r, the limits of $\Psi(r,t)$ both as the time t goes to zero and as it becomes very large. It turns out that in both limits the argument y_n, given by Eq. (60), becomes very large. Indeed, it follows from Eq. (61) that at very short time, y_n becomes very large, i.e.,

$$y_n \approx e^{-i\pi/4} \left(\frac{m}{2\hbar t} \right)^{1/2} (r-a), \quad (118)$$

which is independent of the value of κ_n. Consequently, using Eq. (B.7) of Appendix B,

$$M(r-a,\kappa_n,t) \approx e^{i\pi/4} \left(\frac{2\hbar}{m(r-a)^2} \right)^{1/2} t^{1/2} \quad (119)$$

and hence $M(r-a,\kappa_n,t)$ vanishes as $t \to 0$. Therefore, $\Psi(r,t=0)$ vanishes as expected from the initial condition.

Regarding the limit of very long times, it is first convenient to write Eq. (117) as

$$\Psi(r,t) = \sum_{n=1}^{\infty} \left[C_n u_n(a) M(r-a, \kappa_n, t) + C_n^* u_n^*(a) M\left(r-a, -\kappa_n^*, t\right) \right], \quad r \geq a, \quad (120)$$

and proceed as discussed in Section 2.3.2. Hence, provided that the resonant poles $\kappa_n = \alpha_n - i\beta_n$ are proper, i.e., $\alpha_n > \beta_n$ and $(r-a) < \hbar\kappa_n t/m$, we may substitute Eq. (63) into Eq. (120) to obtain

$$\Psi(r,t) = \sum_{n=1}^{\infty} C_n u_n(a) e^{i\kappa_n(r-a)} e^{-i\hbar\kappa_n^2 t/2m}$$

$$- \sum_{n=1}^{\infty} \left[C_n u_n(a) M(a-r, -\kappa_n, t) - \bar{C}_n^* u_n^*(a) M\left(r-a, -\kappa_n^*, t\right) \right], r \geq a. \quad (121)$$

Now, by inspection of the arguments of $M(a-r, -\kappa_n, t)$ and $M\left(r-a, -k_n^*, t\right)$, using Eq. (61), one sees that for a fixed value of r and very long times, in both cases the term proportional to r becomes negligible compared with $\hbar\kappa_n t/m$ and hence y_n behaves essentially as y_n^0, the argument along the internal region given by Eq. (52). Therefore, at asymptotically long times the wave solution for $r > a$ behaves also as $1/t^{3/2}$, namely,

$$\Psi(r,t) \approx -b \sum_{n=1}^{\infty} \left[\frac{C_n u_n(a)}{\kappa_n^3} - \left(\frac{C_n u_n(a)}{\kappa_n^3} \right)^* \right] \frac{1}{t^{3/2}} + \cdots . \quad (122)$$

On the other hand, it is worth noticing, as discussed in Section 2.3.2, that for a fixed value of time t and a value of r, such that $(r-a) > \hbar\kappa_n t/m$, the behavior of both $M(r-a, \kappa_n, t)$ and $M\left(r-a, -\kappa_n^*, t\right)$ is nonexponential and hence (121) does not hold in that situation.

5.3. Comment on the exponential catastrophe

It is of interest to mention that the decaying solution considered by Gamow would consist of just one exponential decaying term, say $n = m$, in Eq. (121), that is,

$$\Psi(r,t)_{Gamow} \approx e^{i\kappa_m(r-a)} e^{-i\hbar\kappa_m^2 t/2m}, \quad r > a, \quad (123)$$

where $\kappa_m = \alpha_m - i\beta_m$, and that for fixed t diverges exponentially with distance. The above is in contrast with the exact solution given by Eq. (117), which, as discussed above is free of any exponential catastrophe.

5.4. Comment on completeness

Completeness of the set of resonant states along the internal region $\mathcal{R} = [0,a]$ relates to two issues. The first, is that an arbitrary function may be expanded in terms of resonant states and the second, that resonant states describe the dynamics exactly.

Equation (107) gives the expansion of an arbitrary function in terms of resonant states and equation (105), or equivalently (113), provides the exact dynamical behavior at all times $t > 0$ and all r along the internal region $\mathcal{R}$. Notice that the sum rule (111) is crucial to obtain the correct asymptotic post-exponential behavior as the inverse power of time $t^{-3/2}$.

5.5. Examples

5.5.1. The δ-potential model

A convenient model to study the time evolution of quantum decay is the δ-potential. This model was considered many years ago by Winter [81] and since then by many authors. In spite of its mathematical simplicity it describes correctly the main physical features of the time evolution of decay along the exponential and nonexponential long-time regimes. Here we discuss it by using the formalism of resonant states and make a comparison with the solution to the problem in terms of continuum states.

We consider a δ-potential of radius a and intensity λ, namely,

$$V(r) = \lambda \delta(r - a), \tag{124}$$

where we choose units in which $\hbar = 2m = 1$.

As the initial decaying state we consider the simple analytical expression provided by the infinite box state

$$\Psi(r, 0) = \left(\frac{2}{a}\right)^{1/2} \sin\left(\frac{p\pi r}{a}\right), \tag{125}$$

where $p = 1, 2, \ldots,$.

5.5.1.1. Complex poles and resonant states The resonant states of the problem obey the Schrödinger equation given by Eq. (5) with boundary conditions given by Eqs. (6 and 7). They read

$$u_n(r) = \begin{cases} N_n \sin(\kappa_n r), & r \leq a \\ \\ A_n e^{i\kappa_n r}, & r \geq a. \end{cases} \tag{126}$$

From the continuity of the above solutions and the discontinuity of its derivatives with respect to r (due to the δ-function interaction) at the boundary value $r = a$, it follows that the κ_n's satisfy the equation

$$F(\kappa_n) \equiv [2i\kappa_n + \lambda(e^{2i\kappa_n a} - 1)] = 0. \tag{127}$$

For $\lambda > 1$ one may write the approximate analytical solutions to Eq. (127) as [25]

$$\kappa_n \approx \frac{p\pi}{a} \left(1 - \frac{1}{\lambda a}\right) - i\frac{1}{a}\left(\frac{p\pi}{\lambda a}\right)^2. \tag{128}$$

Using the above expression for κ_n as the initial value in the Newton–Raphson iteration procedure [64], i.e.,

$$\kappa_n^{r+1} = \kappa_n^r - F\left(\kappa_n^r\right)/\dot{F}\left(\kappa_n^r\right), \tag{129}$$

where $\dot{F} = [dF/dk]_{k=\kappa_n}$, yields κ_n with the desired degree of approximation.

The normalization coefficient of resonant states may be evaluated by substitution of Eq. (126), for $r \le a$, into Eq. (27), to obtain the analytical expression

$$N_n = \left[\frac{2\lambda}{\lambda a + e^{-2i\kappa_n a}}\right]^{1/2}. \tag{130}$$

Similarly, using Eqs. (126, 130, and 125) into Eq. (106) allows to write the expansion coefficient C_n as the expression

$$C_n = \left[\frac{\lambda a}{\lambda a + e^{-2i\kappa_n a}}\right]^{1/2} \left[\frac{2p\pi \sin{(\kappa_n a)}\,(-1)^p}{\kappa_n^2 a^2 - p^2\pi^2}\right]. \tag{131}$$

For a given finite value of the intensity λ and the radius a of the δ-potential one may then evaluate the set of complex poles $\{\kappa_n\}$ and the expansion coefficients $\{C_n\}$ (note that in this case $C_n = \bar{C}_n$), which are the required input to calculate the different quantities of interest for the time evolution of decay.

It is worth noticing that as the intensity of the potential $\lambda \to \infty$, the complex poles $\kappa_n = \alpha_n - i\beta_n$ tend to the real infinite box eigenvalues $n\pi/a$, and similarly, the resonant eigenfunctions $u_n(r)$ tend to the infinite box model eigenfunctions $\phi_n(r) = \sqrt{2/a}\sin{(n\pi r/a)}$. Similarly, the complex poles $\kappa_{-n} = -\kappa_n^*$ go into the real eigenvalues $-n\pi/a$ and the functions $u_{-n}(r) = u_n^*(r)$ into the real functions $\phi_{-n}(r) = -\phi_n(r) = -\sqrt{2/a}\sin{(n\pi r/a)}$. This leads to a basis of states $\phi_n(r)$ and $\phi_{-n}(r)$ that seems larger than the usual basis involving only the states $\phi_n(r)$. However, the closure relationship given by Eq. (41) goes, in the above limit of an infinite value of λ, into the usual closure relationship obeyed by the infinite box states, namely, $\sum_{n=1}^{\infty} \phi_n(r)\phi_n(r') = \delta(r - r')$ with $(r, r') < a$. The above provides an interesting example of the relationship between exactly solvable open and closed systems.

5.5.1.2. **Expansions in terms of continuum wave functions** As is well known, the time evolution of the decaying wave solution given by Eq. (47) may also be calculated by expanding the retarded Green function in terms of the complete set of continuum wave functions of the problem, the so-called *physical wave solutions* $\psi^+(k,r)$ to obtain

$$\Psi(r,t) = \int_0^\infty C(k)\psi^+(k,r)e^{-ik^2t}\,dk, \tag{132}$$

where

$$C(k) = \int_0^a \Psi^*(r,0)\psi^+(r,k)\,dr, \tag{133}$$

and

$$\psi^+(k,r) = \sqrt{\frac{2}{\pi}} \begin{cases} \sin(kr)/J_+(k), & r \le a \\ (i/2)\left[e^{-ikr} - S(k)e^{ikr}\right], & r \ge a, \end{cases} \tag{134}$$

where the S-matrix $S(k) = J_-(k)/J_+(k)$, with $J_-(k) = J_+^*(k)$, the Jost functions [41]. For the δ-potential model $J_+(k)$ is given by

$$J_+(k) = 1 + \frac{\lambda}{k}\sin(ka)e^{ika}. \tag{135}$$

Notice, by extending the above expression to complex values of k that the poles of $S(k)$ and hence the zeros of $J_+(k)$ correspond exactly to the solutions given by Eq. (127). One may evaluate analytically Eq. (133) using Eqs. (125) and (134).

5.5.1.3. **Results** The parameters of the δ-potential in the calculations are $\lambda = 6$ and $a = 1$ and the initial state $\Psi(r,0)$ corresponds to the lowest infinite box state, namely, $p = 1$.

Figure 7.8 shows a plot of the natural logarithm of $|\Psi(r,t)|^2$ as a function of time using, respectively, the resonant expansion given by Eq. (121) (solid line) and the numerical integration of Eq. (132) (dashed line), for $r/a = 1$. Notice that both calculations are indistinguishable from each other. The figure also shows the $1/t^3$ long-time asymptotic contribution using Eq. (122) (dotted line). It is worth mentioning that the time evolution of the system is dominated by the exponential decay law. Closer inspection shows that the decay rate is that of the first resonance state, the reason being that there is a large overlap between the corresponding resonant state $u_1(r)$ and the initial state, i.e., $\operatorname{Re} C_1 \approx 1$ [85]. The long-time nonexponential contribution is very small and one observes a transient behavior in the transition from exponential to the postexponential inverse power law behavior.
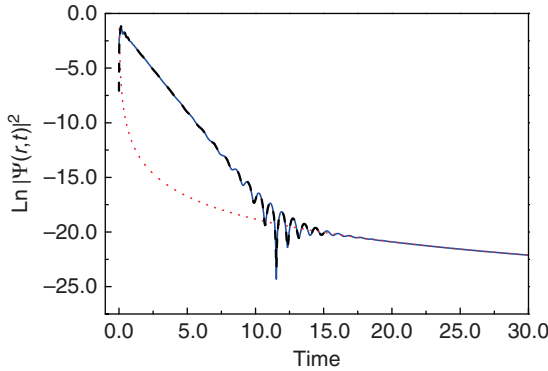
Figure 7.8   Plot of Ln $|\Psi(r,t)|^2$ as a function of time for the δ-potential with parameters $\lambda = 6$ and $r/a = 1$. The resonant expansion (solid line) and numerical integration calculations (dashed line) are indistinguishable. It is also shown the $1/t^3$ long-time asymptotic contribution (dotted line). See text.
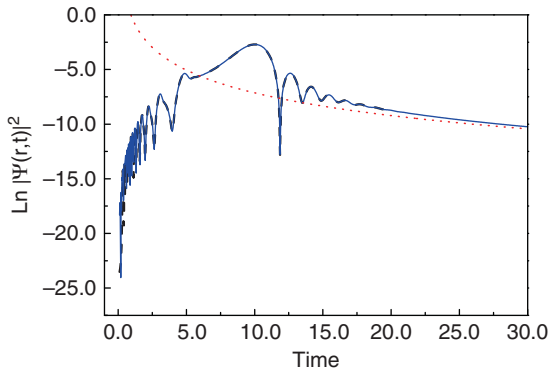
Figure 7.9   Plot of Ln $|\Psi(r,t)|^2$ as a function of time for the δ-potential with parameters $\lambda = 6$ and $r/a = 50$. The resonant expansion (solid line) and numerical integration (dashed line) calculations are indistinguishable. It is also shown the $1/t^3$ asymptotic long-time contribution (dotted line). See text.

Figure 7.9 shows also a plot of the natural logarithm of $|\Psi(r,t)|^2$ as a function of time using, respectively, the resonant expansion given by Eq. (121) (solid line) and the numerical integration of Eq. (132) (dashed line), for $r/a = 50$. The figure also shows the $1/t^3$ long-time asymptotic contribution using Eq. (122) (dotted line). It is worth noticing that both calculations are indistinguishable from each other. One may identify the oscillating structures to the left of the main peak as contributions from higher energy resonant states, which, however, possess very small strength C_n, where we recall Eq. (110). The striking feature of this figures is, however, that there

seems to be a dependence of the decaying behavior with distance. This is related to the small value of the intensity of the δ-potential which implies large decay widths.

5.6. Double-barrier resonant system

As another example, we consider a double-barrier resonant tunneling system in 1D. These artificial quantum systems, formed of semiconductor materials, have been fabricated and studied since the 1970s of last century [61]. Sakaki and co-workers verified experimentally that electrons in sufficiently thin symmetric double-barrier resonant structures exhibit exponential decay [88]. Recent work has examined the conditions for full nonexponential decay in double-barrier resonant systems [56]. Here we want to exemplify the time evolution of the probability density in these systems along the external region using the resonant expansion given by Eq. (121) [89].

We consider a double-barrier resonant system formed by two barriers of equal height U_0 and width b situated at each side of a well of width w with typical parameters of semiconductor GaAlAs − GaAs − GaAlAs structures [61]: $U_0 = 0.23\,\text{eV}$ and $b = w = 5\,\text{nm}$. Hence, the length of the system is $L = 15\,\text{nm}$. Also, the effective mass of the electron is $m = 0.067m_e$, with m_e the electron mass. The above parameters determine the set of poles $\{k_n\}$ and resonant functions $\{u_n\}$ which are required to evaluate in 1D the decaying solution given by Eq. (121) . These parameters may be obtained by techniques similar to those discussed for the δ-potential, as discussed, for example, in appendix B of Ref. [60]. The parameters of the lowest resonance level of the system are $\mathcal{E}_1 = 0.080054\,\text{eV}$ and $\Gamma_1 = 0.001028\,\text{eV}$. The lifetime of the system $\tau = \hbar / \Gamma_1$ is $\tau = 0.64\,\text{ps}$. The initial state is chosen as the lowest energy infinite box state occupying at $t = 0$ the well of the double-barrier system. The overlap coefficient between the initial state and the lowest resonant state u_1 gives, using Eq. (106), $C_1 = 0.877$. Since the initial state is real, $C_1 \bar{C}_1 = C_1^2 = 0.769$, that implies in view of Eq. (110) that most of the strength of the initial state is taken by u_1.

Figure 7.10 exhibits a plot of $|\Psi(x,t)|^2$ as a function of time in units of the lifetime τ (solid line) for the double-barrier resonant system at a fixed distance $x = 10^3 L$. Here the exponential decaying regime lasts for a period of many lifetimes. One observes also, before the onset of the exponentially decaying regime, the contribution that arises from higher energy resonant states and then, at long times, the transition to the nonexponential behavior. By the sake of comparison the t^{-3} contribution is also plotted (dotted line).

Figure 7.11 provides a plot of $|\Psi(x,t)|^2$ as a function of the distance in units of the length L at a fixed time $t = 10\tau$, for the double-barrier resonant system described above (solid line). Notice that the probability density exhibits a propagating wavefront. For comparison, Figure 7.11 shows also the solution for the probability density using the Gamow's
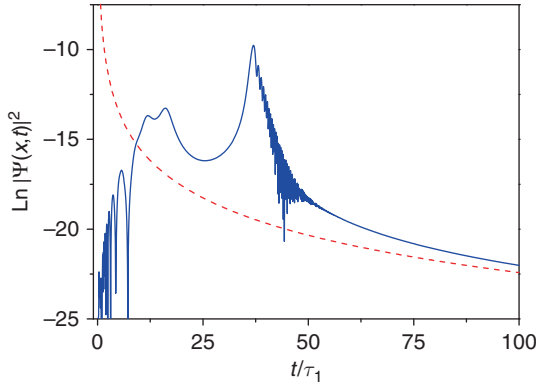
Figure 7.10   Plot of Ln $|\Psi(x,t)|^2$ as a function of time in units of the lifetime $\tau = 0.64$ ps (solid line) at a fixed distance $x = 10^3 L$, for the double-barrier resonant system with parameters as discussed in the text. Also shown is the $1/t^3$ asymptotic long-time contribution (dashed line). See text.
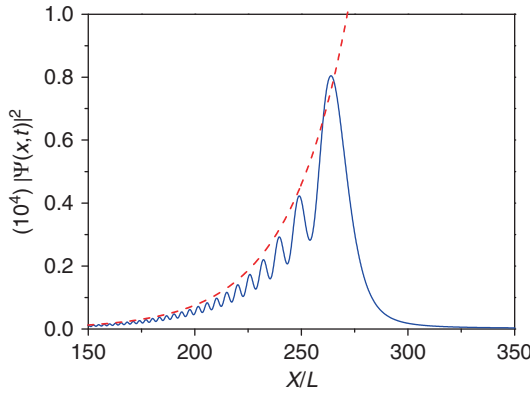
Figure 7.11   Plot of Ln $|\Psi(x,t)|^2$ as a function of the distance in units of the potential radius x/L (solid line) for the double-barrier resonant potential with the same parameters as in the previous figure, at time $t = 10\tau$. Also shown is the purely growing exponential Gamow's solution (dashed line). See text.

solution $\Psi(x,t)_{\text{Gamow}} = \exp[ik_1(x - L)]\exp[-i(\hbar k_1^2 t/2m)]$, which increases exponentially with distance producing an "exponential catastrophe." It is worth emphasizing that the exact decaying solution in terms of resonant states given by Eq. (121) yields a propagating wavefront. There is no exponential catastrophe.

5.7. Survival probability

The survival amplitude yields the probability amplitude that at time t a particle remains in its initial state. The survival amplitude is defined as

$$A(t) = \int_0^L \Psi^*(x,0)\Psi(x,t)\,dx, \tag{136}$$

and the survival probability by

$$S(t) = |A(t)|^2. \tag{137}$$

It follows from the results presented in the Section 5.2 that the survival amplitude may be expanded in terms of resonant states as

$$A(t) = \sum_{-\infty}^{\infty} C_n \bar{C}_n M(0,\kappa_n,t), \tag{138}$$

where C_n and $\bar{C}_n$ are given, respectively, by Eqs. (106 and 109). At long times one may write the survival amplitude, using Eq. (115) into Eq. (136), as

$$A(t) \approx \sum_{n=1}^{\infty} C_n \bar{C}_n e^{-i\hbar^2 k_n^2 t/2m} - b \sum_{n=1}^{\infty} \left[\frac{C_n \bar{C}_n}{\kappa_n^3} - \left(\frac{C_n \bar{C}_n}{\kappa_n^3} \right)^* \right] \frac{1}{t^{3/2}} + \cdots . \tag{139}$$

In general, at asymptotically long times, the behavior of the survival amplitude may depend on many resonance terms. However, in view of Eq. (110), it may happen that a single coefficient dominates over the others, i.e., $C_m \bar{C}_m \approx 1$, which means that the overlap of the initial state with that that resonant state is large. In that case it is justified to make use of a single resonant term for the long-time behavior. This has been a usual assumption in the literature [78, 90–93].

Another quantity of interest for the time evolution of decay is the nonescape probability, defined as,

$$P(t) = \int_0^L |\Psi(x,t)|^2\,dx. \tag{140}$$

Some years ago there was a controversy regarding the long-time behavior of $P(t)$. In Ref. [84] it was argued that it should go as t^{-1}. However, some authors questioned that result and there was finally agreement in that it goes as t^{-3} as recap in Ref. [85].

An interesting application of the formalism of resonant states is in the description of decay in multibarrier resonant tunneling systems [57, 58]. The main result in Ref. [57] is the modification in multibarrier systems of the exponential decay law into a nonexponential oscillating behavior due to the contribution of decaying *Rabi* oscillations. The decaying Rabi oscillations arise from the exponential–exponential interference of closely lying resonances in multibarrier systems. We stress that this contribution differs from

the nonexponential behavior of the survival probability at very short times, which depends on the very high components of the energy spectra of the system. From our analysis we may conclude that decaying *Rabi* oscillations are a distinctive feature of decay in multibarrier systems. We have also shown that by varying appropriately the distinct parameters of the multibarrier system one may design systems with specific values for the *Rabi* frequency and/or the exponential–nonexponential transition. The main expression to describe the above behavior is [58]

$$S(t) = \sum_{n=1}^{M} \left| C_n \bar{C}_n \right|^2 e^{-\Gamma_n t/\hbar} + 2 \sum_{m>n,n}^{M} |D|_{mn} e^{-\bar{\Gamma}_{mn}t/\hbar} \cos\left(\Omega_{mn} t + \xi_{mn}\right), \qquad (141)$$

where $D_{mn} = |D_{mn}| \exp\left(i\xi_{mn}\right)$, $|D_{mn}| = |C_m \bar{C}_m C_n \bar{C}_n|$, ξ_{mn} corresponds to the phase difference between that of $C_m \bar{C}_m$ and $C_n \bar{C}_n$, $\Omega_{mn} = (\mathcal{E}_m - \mathcal{E}_n)/\hbar$ is the *Rabi* frequency and $\bar{\Gamma}_{mn} = (\Gamma_m + \Gamma_n)/2$.

Figure 7.12 shows a plot of the behavior of the survival probability for a quadruple characterized by parameters typical of semiconductor heterostructures [61]: barrier heights $V_0 = 200$ meV, barrier widths, $b_0 = 4.0$ nm, well widths, $w_0 = 5.0$ nm. The effective mass is $m^* = 0.067 m_e$, with m_e the electron mass. Here the first triplet of complex poles $\{\kappa_n\}$ and resonant states $\{u_n(x)\}$ of the problem suffice to describe the behavior of the survival probability, namely Eq. (141) with $M = 3$. The initial state $\psi(x,0)$ is taken by simplicity as a square infinite box state. One sees clearly the oscillating nonexponential behavior of the survival probability in this system.
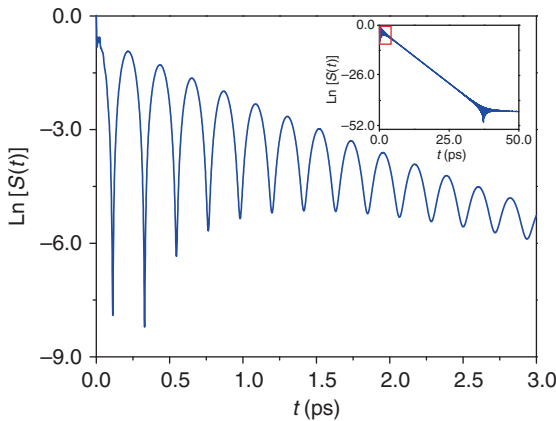
Figure 7.12   Plot of the survival probability $S(t)$ as a function of time for the quadruple tunneling barrier system discussed in the text that exhibits decaying nonexponential *Rabi* oscillations. The inset shows $S(t)$ in a wider time interval that includes the exponential–postexponential transition at long times.
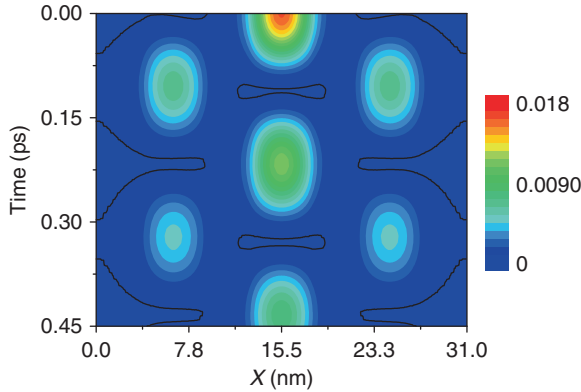
Figure 7.13 Plot of *Breathing* mode of the probability density $|\Psi(x,t)|^2$, along the internal region of the quadruple barrier system when the initial state is placed on the central well. One sees that the internal dynamics consists of a quasi-periodical processes involving spatial oscillations leading to the reconstruction of the initial state. At each oscillation there is a leakage through the ends of the open system.

As discussed in Ref. [58], the resonant states $u_n(x)$ play a crucial role to understand the dynamical behavior along the internal region, especially their mutual interference, which elucidates the underlying mechanism of the observed oscillations of the spatial and time-dependent probability density $|\Psi(x,t)|^2$, plotted in Figure 7.13.

We end this presentation by pointing out that regarding experiment it is necessary to extend to multibarrier systems the techniques used to verify the exponential decay law in double-barrier resonant structures [94]. However, it might be that to test the oscillatory decaying behavior discussed here may require of a new type of experimental setup. Regarding the dynamics of the probability density along the internal region of the multibarrier structure, an interesting possibility is to create the initial wavepacket by an ultrafast laser source and make use of specific spectroscopies to observe the oscillatory motion of the wavepacket [95].

Our results are of a general validity in quantum mechanics and hence one may consider other artificial multibarrier structures as, for example, ultra-cold atomic gases in optical lattices [86] and in optical tests of quantum mechanics [96].

6. CONCLUSIONS

We have shown that demanding purely outgoing boundary conditions on the solutions to the Schrödinger equation for an arbitrary potential of finite range, i.e. $V(r) = 0$, $r > a$ defines the resonant states of the system and leads

to complex energy eigenvalues. The residues at the complex poles of the outgoing Green's function to the problem provide a normalization condition for resonant states that involves an integral term along the internal region of the system plus a surface term at $r = a$. The formalism of resonant states provides a unified description for tunneling in the energy domain, and also in time domain in connection with tunneling transients [48], and the time evolution of decay.

The purely outgoing boundary conditions considered above define a class of open quantum systems. The coupling with the exterior is achieved through the boundary conditions. The time evolution of decay constitutes a sort of dissipative process where matter goes out of the system by tunneling. Notice, however, that the equation of continuity is fulfilled, i.e., see Eq. (20). It might be interesting to place the formalism presented here in the general context of dissipative systems [97, 98].

The relationship of the Rigged-Hilbert space formulation of quantum mechanics with the formalism of resonant states discussed here requires to be clarified. For example, it is not clear that the complex poles κ_{-n} seated on the third quadrant of the complex k plane and their corresponding resonant states u_{-n} play a role in that formalism for times $t > 0$. As we have shown, these poles are essential to obtain the long time $1/t^3$ behavior of decay. In fact the time evolution of decay in terms of the resonant state formalism coincides exactly with the numerical solution to the time-dependent Schrödinger equation of the problem. At a more fundamental level, the above issue is related to the understanding of irreversibility at the quantum level, where the formation and decay of transient states play a fundamental role [93, 99]. Further work is required on this issue.

I have restricted the discussion to the simple problem of a single particle interacting with a potential of finite range. Although the formalism remains valid for a more general class of potentials and may be generalized to deal with effects concerning incoherent processes [35, 37], our main purpose here has been to show that the non-Hermitian formalism of resonant states provides an exact analytical description of tunneling and decay processes in quantum mechanics which is in fact indistinguishable form numerical calculations using continumm wave functions.

ACKNOWLEDGMENTS

APPENDICES

A. DETERMINATION OF THE RESIDUE AT A POLE OF THE OUTGOING GREEN'S FUNCTION

We present here the determination of the residue of the outgoing Green's function of the problem at a complex pole on the complex k plane for a spherical symmetric potential of finite range in the case of zero angular momentum or equivalently a finite range potential in the half-line. The resulting expression for the residue differs slightly from that obtained on the energy plane derived in Ref. [17].

The outgoing Green's function associated to the Hamiltonian given by Eq. (5) satisfies the equation

$$\frac{\partial^2}{\partial r^2} G^+(r,r';k) + \left[k^2 - V(r)\right] G^+(r,r';k) = \left(\frac{2m}{\hbar^2}\right) \delta(r - r'), \qquad (A.1)$$

with the boundary conditions at $r = 0$ and $r = a$ given, respectively, by

$$G^+(0,r';k) = 0 \qquad (A.2)$$

and

$$\left[\frac{\partial}{\partial r} G^+(r,r';k)\right]_{r=a} = ikG^+(a,r';k). \qquad (A.3)$$

Near a complex pole κ_n one then may in general write

$$G^+(r,r';k) \approx \frac{\rho_n(r,r')}{k - \kappa_n} + \chi(r,r';k) \qquad (A.4)$$

where $\rho_n(r,r';k)$ is the residue at the complex pole κ_n and $\chi(r,r';k)$ is a regular function. Substitution of Eq. (A.4) into Eq. (A.1) leads after some simple algebra to the result

$$\frac{1}{k - \kappa_n} \left\{ \frac{\partial^2 \rho_n(r,r')}{\partial r^2} + \left[k^2 - V(r)\right] \rho_n(r,r') \right\} + \left\{ \frac{\partial^2 \chi(r,r';k)}{\partial r^2} + \left[k^2 - V(r)\right] \chi(r,r';k) \right\}$$

$$- \left(\frac{2m}{\hbar^2}\right) \delta(r - r') = 0 \qquad (A.5)$$

Addition and subtraction of $\kappa_n^2 \rho_n(r, r')/(k - \kappa_n)$ to the previous equation and taking the limit $k \to \kappa_n$ leads to the expressions

$$\frac{\partial^2 \rho_n(r, r')}{\partial r^2} + \left[\kappa_n^2 - V(r)\right] \rho_n(r, r') = 0 \tag{A.6}$$

and

$$\frac{\partial^2 \chi(r, r'; \kappa_n)}{\partial r^2} + \left[\kappa_n^2 - V(r)\right] \chi(r, r'; \kappa_n) + 2\kappa_n \rho_n(r, r') = \left(\frac{2m}{\hbar^2}\right) \delta(r - r'). \tag{A.7}$$

Now, substitution of Eq. (A.4) into the boundary conditions given by Eqs. (A.2) and (A.3) adding and subtracting $i\kappa_n \rho_n(r, r')/(k - \kappa_n)$ and taking the limit $k \to \kappa_n$, yields

$$\rho_n(0, r') = 0 \tag{A.8}$$

$$\chi(0, r'; \kappa_n) = 0 \tag{A.9}$$

and also

$$\left[\frac{\partial}{\partial r} \rho_n(r, r')\right]_{r=a} = i\kappa_n \rho_n(a, r') \tag{A.10}$$

$$\left[\frac{\partial}{\partial r} \chi(r, r'; \kappa_n)\right]_{r=a} = i\kappa_n \chi(a, r'; \kappa_n) + i\rho_n(a, r'). \tag{A.11}$$

One sees that Eq. (A.6) for $\rho_n(r, r')$ and its boundary conditions, given by Eqs. (A.8) and (A.10), are identical with Eq. (5) for $u_n(r)$ and its corresponding boundary conditions, Eqs. (6) and (8). Consequently $\rho_n(r, r')$ is proportional to $u_n(r)$, namely,

$$\rho_n(r, r') = u_n(r)P(r'). \tag{A.12}$$

An explicit expression for $P(r')$ may be obtained as follows. Multiply Eq. (5) by $\chi(r, r'; \kappa_n)$ and Eq. (A.7) by $u_n(r)$, subtract one from the other and integrate from $r = 0$ to $r = a$. The result may be written, using Eq. (A.12), as

$$\left[u_n(r)\frac{\partial}{\partial r}\chi(r, r'; \kappa_n) - \chi(r, r'; \kappa_n)\frac{d}{dr}u_n(r)\right]_0^a +$$

$$\int_0^a u_n^2(r)P(r')dr = \left(\frac{2m}{\hbar^2}\right)\int_0^a u_n(r)\delta(r - r')dr. \tag{A.13}$$

It then follows, using Eqs. (6), (8), (A.9), (A.11), and (A.12) that

$$P(r') = \left(\frac{2m}{\hbar^2}\right)\frac{u_n(r')}{2\kappa_n\left\{\int_0^a u_n^2(r)dr + iu_n^2(a)/2\kappa_n\right\}}. \tag{A.14}$$

Substitution of Eq. (A.14) into Eq. (A.12) yields

$$\rho_n(r, r') = \left(\frac{2m}{\hbar^2}\right) \frac{u_n(r)u_n(r')}{2\kappa_n \left\{\int_0^a u_n^2(r)dr + iu_n^2(a)/2\kappa_n\right\}}, \qquad \text{(A.15)}$$

which leads to Eq. (26) with the normalization condition given by Eq. (27), i.e., the expression within the brackets in the denominator to Eq. (A.15) equal to unity.

In the complex energy plane, the residue at a proper resonant pole, i.e. $\mathcal{E}_n > \Gamma_n$, reads [17]

$$\rho_n(r, r') = \frac{u_n(r)u_n(r')}{\left\{\int_0^a u_n^2(r)dr + iu_n^2(a)/2\kappa_n\right\}}, \qquad \text{(A.16)}$$

which, of course, yields the same normalization condition that in the k plane.

B. ASYMPTOTIC PROPERTIES OF THE MOSHINSKY FUNCTION

The Moshinsky function is defined as [49]

$$M(y_n) \equiv M(z, q, t) = \frac{i}{2\pi} \int_{-\infty}^{\infty} \frac{e^{ikz} e^{-i\hbar k^2 t/2m}}{k - q} k dk = \frac{1}{2} e^{(imz^2/2\hbar t)} e^{y_n^2} \text{erfc}(y_n), \qquad \text{(B.1)}$$

where the argument y_n is

$$y_n = e^{-i\pi/4} \left(\frac{m}{2\hbar t}\right)^{1/2} \left[z - \frac{\hbar q}{m} t\right]. \qquad \text{(B.2)}$$

In the above expressions q stands for k, κ_n, or $k_{-n} = -k_n^*$ and z stands for r or x.

In this appendix we shall be interested in evaluating the limits of $M(y_n)$ as $t \to 0$ and as $t \to \infty$.

The properties of the Moshinsky function may be obtained from the properties of the function $\exp\left(y_n^2\right) \text{erfc}(y_n)$. It turns out that this last product corresponds to the Faddeyeva function $w(v) = \exp\left(-v^2\right)\text{erfc}(-iv)$ as defined by Abramowitz and Stegun [51] and Faddeyeva and Terentev [50]. Hence making $v = iy$ one may write the Moshinsky function as

$$M(y_n) = \frac{1}{2}e^{imz^2/2\hbar t}w(iy_n). \tag{B.3}$$

The above expression may be adequate for calculations since very efficient methods to evaluate numerically the function w are available [100].

For small values of the argument y_n it is convenient to consider the series expansion [50, 51]

$$M(y_n) = \frac{1}{2}e^{imz^2/2\hbar t}w(iy_n) = \frac{1}{2}e^{imz^2/2\hbar t}\sum_{s=0}^{\infty}\frac{(-y_n)^s}{\Gamma(s/2+1)}. \tag{B.4}$$

Hence for $|y_n| \ll 1$

$$M(y_n) \approx \frac{1}{2}e^{imz^2/2\hbar t}\left[1 - \frac{1}{2}\pi^{1/2}y_n + \cdots\right]. \tag{B.5}$$

For very large values of the argument y_n, provided it obeys $-\pi/2 < \arg y_n < \pi/2$, one may write the series expansion

$$w(iy_n) \approx \frac{1}{\pi^{1/2}y_n} - \frac{1}{2\pi^{1/2}y_n^3} + \cdots, \tag{B.6}$$

and therefore using Eq. (B.3) one may write $M(y_n)$ as

$$M(y_n) \approx \frac{1}{2}e^{imz^2/2\hbar t}\left[\frac{1}{\pi^{1/2}y_n} - \frac{1}{2\pi^{1/2}y_n^3} + \cdots\right]. \tag{B.7}$$

When the argument y_n lies within the limits $\pi/2 < \arg y_n < 3\pi/2$ one may use the symmetry relation

$$w(iy_n) = 2e^{y_n^2} - w(-iy_n), \tag{B.8}$$

to write the asymptotic expansion

$$w(iy_n) \approx 2e^{y_n^2} + \frac{1}{\pi^{1/2}y_n} - \frac{1}{2\pi^{1/2}y_n^3} - \cdots, \tag{B.9}$$

and consequently, using Eq. (B.3) one may write $M(y_n)$ as

$$M(y_n) \approx \frac{1}{2}e^{imz^2/2\hbar t}\left[2e^{y_n^2} + \frac{1}{\pi^{1/2}y_n} - \frac{1}{2\pi^{1/2}y_n^3} + \cdots\right]. \tag{B.10}$$

REFERENCES

[1] G. Gamow, Zur quantentheorie des atomkernes, Z. Phys. 51 (1928) 204.

[2] G. Gamow, C. L. Critchfield, Theory of Atomic Nucleus and Nuclear Energy-Sources, Clarendon Press, Oxford, 1949, p. 156.

[3] A.F.J. Siegert, On the derivation of the dispersion formula for nuclear reactions, Phys. Rev. 56 (1939) 750.

[4] J. Humblet, L. Rosenfeld, Theory of nuclear reactions I. Resonant states and collision matrix, Nucl. Phys. 26 (1961) 529.

[5] L. Rosenfeld, Theory of nuclear reactions II. The foundations of the optical model, Nucl. Phys. 26 (1961) 594.

[6] J. Humblet, Theory of nuclear reactions III. Physical quantities and channel radii, Nucl. Phys. 31 (1962) 544.

[7] J. Humblet, Theory of nuclear reactions IV. Coulomb interactions in the channels and penetration factors, Nucl. Phys. 50 (1964) 1.

[8] J.P. Jeukenne, Theory of nuclear reactions V. Penetration factors for charged particles in low energy nuclear reactions, Nucl. Phys. 58 (1964) 1.

[9] J. Humblet, Theory of nuclear reactions VI. Unitarity, open and closed channels, Nucl. Phys. 57 (1964) 386.

[10] C. Mahaux, Theory of nuclear reactions VII. Photon channels, Nucl. Phys. 68 (1965) 481.

[11] L. Rosenfeld, Theory of nuclear reactions VIII. Time evolution of scattering process, Nucl. Phys. 70 (1965) 1.

[12] C. Mahaux, Theory of nuclear reactions IX. Few-level approximations, Nucl. Phys. 71 (1965) 241.

[13] T. Berggren, On the use of resonant states and eigenfunction expansions of scattering and reaction amplitudes, Nucl. Phys. A 109 (1968) 265.

[14] W.J. Romo, Inner product for resonant states and shell-model applications, Nucl. Phys. A 116 (1968) 617.

[15] R.M. More, Theory of decaying states, Phys. Rev. 4 (1971) 1782.

[16] R.M. More, E. Gerjuoy, Properties of resonance wave functions, Phys. Rev. 7 (1973) 1288.

[17] G. García-Calderón, R. Peierls, Resonant states and their uses, Nucl.Phys. A 265 (1976) 443.

[18] G. García-Calderón, An expansion of continuum wave functions in terms of resonant states, Nucl. Phys. A 261 (1976) 130.

[19] Y.B. Zel'dovich, On the theory of unstable states, (Sov. Phys.)—JETP 12 (1961) 542.

[20] N. Moiseyev, Quantum theory of resonances: Calculating energies, widths and cross-sections by complex scaling, Phys. Rep. 302 (1998) 211.

[21] B. G. Giraud, K. Kato, Complex-scaled spectrum completeness for pedestrians, Ann. Phys. (N.Y.) 308 (2003) 115.

[22] J. Humblet, Thesis, University of Liège, 1952; Mém. Soc. Roy. Sc. de Liège (8°) 12 (4) (1952) 36.

[23] A. Mattar, G. García-Calderón, unpublished.

[24] M. Berrondo, G. G. García-Calderón, An eigenfunction expansion involving resonant states, Lett. Nuovo Cimento 20 (1977) 34.

[25] G. García-Calderón, in: A. Frank, K. B. Wolf (Eds.), Symmetries in Physics, Springer-Verlag, Berlin, 1992, p. 252.

[26] R. de la Madrid, G. García-Calderón, J. G. Muga, Resonance expansions in quantum mechanics, Czech. J. Phys. 55 (2005) 1146.

[27] J. Okolowicz, M. Ploszajczak, I. Rotter, Dynamics of quantum systems embedded in a continuum, Phys. Rep. 374 (2003) 271.

[28] N. Michel, W. Nazarewicz, M. Ploszajczak, T. Vertse, Shell model in the complex energy plane, J. Phys. G Nucl. Part. Phys. 36 (2009) 013101.

[29] R. de la Madrid, The resonance amplitude associated with the Gamow states, Nucl. Phys. A 812 (2008) 13.

[30] O.I. Tolstikhin, V.N. Ostrovsky, H. Nakamura, Siegert pseudostate formulation of scattering theory: One-channel case, Phys. Rev. A 58 (1998) 2077.

[31] O.I. Tolstikhin, Siegert-state expansion for nonstationary systems. III. Generalized Born-Fock equations and adiabatic approximation for transitions to the continuum, Phys. Rev. A 77 (2008) 032711.

[32] N. Fernández-García, O. Rosas-Ortiz, Gamow-Siegert functions and Darboux-deformed short range potentials, Ann. Phys. 323 (2008) 1397.

[33] E.S.C. Ching, P.T. Leung, A. Maassen van den Brink, W. Suen, S.S. Tong, K. Young, Quasinormal-mode expansion for waves in open systems, Rev. Mod. Phys. 70 (1998) 1545.

[34] A. Settimi, S. Severini, B.J. Hoenders, Quasi-normal-modes description of transmission properties for photonic bandgap structures, J. Opt. Soc. Am. B 26 (2009) 876.

[35] G. García-Calderón, L. Chaos-Cador, Theory of coherent and incoherent processes in quantum corrals, Phys. Rev. B 73 (2006) 195405.

[36] L. Chaos-Cador, G. García-Calderón, Theory of resonant scattering in two dimensions, J. Phys. A Math. Theor. 43 (2010) 035301.

[37] G. García-Calderón, A. Rubio, Effect of inelastic processes on the elastic width in resonant structures, Phys. Rev. B 46 (1992) 9784.

[38] A. Bohm, P. Bryant, Y. Sato, Quantal time asymmetry: mathematical foundation and physical interpretation, J. Phys. A Math. Theor. 41 (2008) 304019.

[39] C.M. Bender, Making sense of non-Hermitian Hamiltonians, Rep. Prog. Phys. 70 (2007) 947.

[40] R.E. Peierls, in: E.H. Bellamy, R.G. Moorhouse (Eds.), The Proceedings of the 1954 Glasgow Conference on Nuclear and Meson Physics, Pergamon Press, New York, 1955, p. 296.

[41] R.G. Newton, Scattering Theory of Waves and Particles, Second ed., Dover Publications Inc., New York, 2002.

[42] E. Hernandez, A. Jauregui, A. Mondragon, Degeneracy of resonances in a double barrier potential, J. Phys. A Math. Gen. 33 (2000) 4507.

[43] G. García-Calderón, unpublished.

[44] G. García-Calderón, M. Berrondo, Note on the asymptotic energy behaviour of the Green function for a cut-off potential, Lett. Nuovo Cimento 26 (1979) 562.

[45] W.J. Romo, Study of the completeness properties of resonant states, J. Math. Phys. 21 (1980) 2704.

[46] J. Bang, F.A. Gareev, M.H. Gitzzatkulov, S.A. Goncharov, Expansion of continuum functions on resonance wave functions and amplitudes, Nucl. Phys. A 309 (1978) 381.

[47] G. García-Calderón, On the overcompleteness of the set of bound, antibound and resonant states, Lett. Nuovo Cimento 33 (1982) 253.

[48] A. del Campo, G. García-Calderón, J.G. Muga, Quantum transients, Phys. Rep. 476 (2009) 1.

[49] M. Moshinsky, Diffraction in time, Phys. Rev. 88 (1952) 625.

[50] V.N. Faddeyeva, M.N. Terentev, in: Academician V.A. Fock (Editor), Tables of values of the function $\omega(z) = e^{-z^2}\left(1 + \frac{2i}{\sqrt{\pi}}\int_0^z e^{t^2}\,dt\right)$, for complex argument, Pergamon Printing & Art Services Ltd., London, 1961.

[51] M. Abramowitz, I.A. Stegun, Handbook of Mathematical Functions, Dover Publications, New York, 1972, p. 297.

[52] G. García-Calderón, I. Maldonado, J. Villavicencio, unpublished.

[53] G. García-Calderón, The effect of asymmetry on resonant tunneling in one dimension, Solid State Commun. 62 (1987) 441.

[54] G. García-Calderón, A. Rubio, Transient effects and delay time in the dynamics of resonant tunneling, Phys. Rev. A 55 (1997) 3361.

[55] G. García-Calderón, R. Romo, A. Rubio, Description of overlapping resonances in multibarrier tunneling structures, Phys. Rev. B 47 (1993) 9572.

[56] G. García-Calderón, J. Villavicencio, Full time nonexponential decay in double-barrier quantum structures, Phys. Rev. A 73 (2006) 062115.

[57] G. García-Calderón, R. Romo, J. Villavicencio, Survival probability of multibarrier resonance systems: Exact analyical approach, Phys. Rev. B 76 (2007) 035340.

[58] G. García-Calderón, R. Romo, J. Villavicencio, Internal dynamics of multibarrier systems for pulsed quantum decay, Phys. Rev. A 79 (2009) 052121.

[59] G. García-Calderón, A. Rubio, An expansion of continuum wave functions in terms of resonant states (II). Solvable models, Nucl. Phys. A 458 (1986) 560.

[60] S. Cordero, G. García-Calderón, Transient effects and reconstruction of the energy spectra in the time evolution of transmitted wave packets, J. Phys. A Math. Theor. 43 (2010) 185301.

[61] D.K. Ferry, S.M. Goodnick, Transport in Nanostructures, Cambridge University Press, Cambridge, UK, 1997.

[62] R. Romo, G. García-Calderón, Strong overlap and transmission in triple-barrier resonant structures, Phys. Rev. B 49 (1994) 14016.

[63] G. García-Calderón, R. Romo, A. Rubio, Effect of disorder in specific realizations of multibarrier random systems, Phys. Rev. B 56 (1997) 4845.

[64] E. Süli E, D. Mayers, An Introduction to Numerical Analysis, Cambridge University Press, Cambridge, UK, 2003.

[65] D.J. Thouless, Electrons in disordered systems and the theory of localization, Phys. Rep. 13 (1974) 93.

[66] R. Romo, J. Villavicencio, Dynamical description of the buildup process in resonant tunneling: evidence of exponential and non-exponential contributions, Phys. Rev. B 60 (1999) R2142.

[67] G. García-Calderón, J. Villavicencio, Time dependence of the probability density in the transient regime or tunneling, Phys. Rev. A 64 (2001) 012107.

[68] G. García-Calderón, J. Villavicencio, F. Delgado, J.G. Muga, Time scale for forerunners in quantum tunneling, Phys. Rev. A 66 (2002) 042119.

[69] R. Romo, Buildup dynamics of transmission resonances in superlattices, Phys. Rev. B 66 (2002) 245311.

[70] G. García-Calderón, J. Villavicencio, Delay time and tunneling transient phenomena, Phys. Rev. A 66 (2002) 032104.

[71] R. Romo, J. Villavicencio, G. García-Calderón, Transient tunneling effects of resonance doublets in triple barrier systems, Phys. Rev. B 66 (2002) 033108.

[72] A. Hernández, G. García-Calderón, Quantum shutter transient solutions and the delay time for a delta potential, Phy. Rev. A 68 (2003) 014104.

[73] G. García-Calderón, J. Villavicencio, Transient time-domain resonances and the time scale for tunneling, Phys. Rev. A 68 (2003) 052107.

[74] G. García-Calderón, J. Villavicencio, N. Yamada, Equivalence between the real-time Feynman histories and the quantum-shutter approaches for the 'passage time in tunneling, Phys. Rev. A 67 (2003) 052106.

[75] N. Yamada, G. García-Calderón, J. Villavicencio, Quantum-shutter approach to tunneling time scales with wave packets, Phys. Rev. A 72 (2005) 012106.

[76] J. Villavicencio, R. Romo, E. Cruz, Tunneling and delay time of cutoff Gaussian wave packets, Phys. Rev. A 75 (2007) 012111.

[77] R.W. Gurney, E.U. Condon, Quantum mechanics and radioactive desintegration, Phys. Rev. 33 (1929) 127.

[78] L.A. Khalfin, On the theory of the decay of a quasi-stationary state, Sov. Phys., Dokl. 2 (1957) 340; Contribution to the decay theory of a quasi-stationary state, Sov. Phys.—JETP 6 (1958) 1053.

[79] S.R. Wilkinson, C.F. Bharucha, M.C. Fischer, K.W. Madison, P.K. Morrow, Q. Niu, et al., Experimental evidence for non-exponential decay in quantum tunnelling, Nature 387 (1997) 575.

[80] C. Rothe, S.I. Hintschich, A.P. Monkman, Violation of the exponential-decay law at long times, Phys. Rev. Lett. 96 (2006) 163601.

[81] R.G. Winter, Evolution of a quasistationary state, Phys. Rev. 123 (1961) 1503.

[82] T. Jittoh, S. Matsumoto, J. Sato, Y. Sato, K. Takeda, Nonexponential decay of an unstable quantum system: Small-Q-value s-wave decay, Phys. Rev. A 71 (2005) 012109.

[83] P. Exner, M. Fraas, The decay law can have an irregular character, J. Phys. A 40 (2007) 1333.

[84] G. García-Calderón, J.L. Mateos, M. Moshinsky, Resonant spectra and the time evolution of the survival and nonescape probabilities, Phy. Rev. Lett. 74 (1995) 33

[85] G. García-Calderón, I. Maldonado, J. Villavicencio, Resonant-state expansions and the long-time behavior of quantum decay, Phys. Rev. A 76 (2007) 012103.

[86] M. Lewenstein, A. Sanpera, V. Ahufinger, D. Bogdan, A. Sen, U. Sen, Ultracold atomic gases in optical lattices: mimicking condensed matter physics and beyond, Adv. Phys. 56, (2007) 243.

[87] W. van Dijk, Y. Nogami, Novel expression for the wave function of a decaying quantum system, Phys. Rev. Lett. 83 (1999) 2867.

[88] M. Tsuchiya, T. Matsusue, H. Sakaki, Tunneling escape rate of electrons from quantum well in double-barrier heterostructures, Phys. Rev. lett. 59 (1987) 2356.

[89] S. Cordero, G. García-Calderón, unpublished.

[90] M.L. Goldberger, K.W. Watson, Collision Theory, Wiley, New York, 1964, p. 450.

[91] C.A. Nicolaides, D.R. Beck, Possibility of observing nonexponential decay in autoinizing states, Phys. Rev. Lett. 38 (1977) 683 .

[92] G. García-Calderón, V. Riquer, R. Romo, Survival probability of a single resonance, J. Phys. A:Mat. Theor. 34 (2001) 4155.

[93] T.G. Douvropoulos, C.A. Nicolaides, Nonexponential decay propagator and its differential equation for real and complex energy distributions of unstable states, Phys. Rev. A 69 (2004) 032105.

[94] M. Tsuchiya, T. Matsusue, H. Sakaki, Tunneling escape rate of electrons from quantum-well in double-barrier heterostructures, Phys. Rev. Lett. 59 (1987) 2356.

[95] K. Leo, J. Shah, E. O. Göbel, T. C. Damen, S. Schmitt-Rink, W. Schäfer, et al. Coherent oscillations of a wave packet in a semiconductor double-quantum-well structure, Phys. Rev. Lett. 66 (1991) 201.

[96] S. Longhi, Nonexponential decay via tunneling in tight-binding lattices and the optical Zeno effect, Phys. Rev. Lett. 97 (2006) 110402.

[97] R.P. Feynman, F.L. Vernon, The theory of a general quantum system interacting with a linear dissipative system, Ann. Phys. (N.Y.) 24 (1963) 118.

[98] A.O. Caldeira, A. J. Leggett, Influence of dissipation on quantum tunneling in macroscopic systems, Phys. Rev. Lett. 46 (1981) 211.

[99] C.A. Nicolaides, Physical constraints on nonstationary states and nonexponential decay, Phys. Rev. A 66 (2002) 022118.

[100] G.P.M Poppe, C.M.J Wijers, More efficient computation of the complex error function, ACM Trans. Math. Softw. 16 (1990) 38.

CHAPTER **8**

Quantum Electrodynamics of One-Photon Wave Packets

M. Stobińska[a], **G. Alber**[b] and **G. Leuchs**[a]

Contents

Abstract Rapid advances in quantum technology have made possible the control of quantum states of elementary material quantum systems, such as atoms or molecules, and of the electromagnetic radiation field resulting from spontaneous photon emission of their unstable excited states to such a level of precision that subtle quantum electrodynamical phenomena have become observable experimentally. Recent developments in the area of quantum information processing demonstrate that characteristic quantum electrodynamical effects can even be exploited for practical purposes provided the relevant electromagnetic field modes are controlled by appropriate cavities. A central problem in this context is the realization of an ideal transfer of quantum information between a state of a material quantum system and a quantum

[a] Max Planck Institute for the Science of Light - Günther-Scharowsky-Str.1, Bau 24, 91058 Erlangen, Germany

[b] Institut für Angewandte Physik, Technische Universität Darmstadt, Hochschulstraß e 4a, 64289 Darmstadt, Germany

E-mail addresses: magda.stobinska@mpl.mpg.de (M. Stobińska), gernot.alber@physik.tu-darmstadt.de (G. Alber), leuchs@physik.uni-erlangen.de (G. Leuchs)

state of the electromagnetic radiation field which contains a small number or even a single photon only. Despite much recent work in cavity quantum electrodynamics, which has explored this problem successfully in cases in which the number of accessible electromagnetic field modes is strongly restricted by a cavity, currently still much less is known about ideal quantum state transfer between matter and few-photon quantum states of the electromagnetic field in the extreme opposite case of free space. In this contribution we review recent work which explores characteristic quantum electrodynamical phenomena governing the interaction of a material quantum system with the electromagnetic field in extreme many-mode cases which are close to cavity-free situations. For this purpose the simplest possible quantum electrodynamical situation, namely the interaction of a single material two-level system with the wave packet of a single optical photon, is investigated in free space and in situations in which a large cavity modifies the mode structure of the electromagnetic field modes. It is demonstrated that perfect excitation of an atom by a properly shaped single-photon wave packet is possible even in free space. In particular, it is demonstrated that perfect excitation of an atom can be achieved by a single optical photon which is prepared initially in an appropriate superposition of plane-wave modes, provided this photon is focused subsequently onto the absorbing atom by a parabolic cavity.

1. INTRODUCTION

Excited bound states of atoms are one of the simplest examples of unstable quantum states which decay radiatively into the continuum of possible one-photon states of the electromagnetic field in free space. The search for a satisfactory theoretical explanation of the line frequencies and intensities of photon emission spectra at the beginning of the last century eventually culminated in Heisenberg's "magical paper" from July 1925 [1, 2] and in the development of modern quantum mechanics [3–6]. Although basic aspects of this spontaneous decay process have already been described theoretically in an adequate way in the early days of modern quantum mechanics [7, 8], interestingly, some of its time-dependent dynamical aspects are still of topical current interest.

To a large part the current interest in this elementary photon emission process is due to recent advances in quantum technology. They have enabled one to prepare quantum states of matter and of the electromagnetic field to such a high level of precision that not only subtle quantum electrodynamical phenomena can be tested experimentally but that these phenomena can also be exploited practically for purposes of quantum information processing [9]. On the one hand it is possible to engineer quantum states of individual atoms or even of multiparticle systems with the help of sophisticated particle traps. In this context electromagnetic fields play a predominant role for achieving the required trapping and they also allow to control the material

quantum states involved with an unprecedented level of accuracy [10, 11]. On the other hand it is also possible to engineer quantum states of the electromagnetic field. Not only classical electromagnetic fields with large photon numbers can be generated by sophisticated pulse shaping techniques [12] but also particular few-photon quantum states of the electromagnetic field can be prepared in a controlled way [13]. Numerous current developments in the area of quantum electrodynamics, for example, have emanated from an early insight of E.A. Purcell [14] that a modified density of field modes of the electromagnetic field influences spontaneous decay rates. This stimulated numerous experiments demonstrating the suppression of spontaneous decay in cavities [15, 16]. More recently it has even been demonstrated that extreme selection of electromagnetic field modes by cavities in combination with trapping of single atoms enables one to control the interaction between single atoms and the electromagnetic field [13]. Thus, it is possible to prepare single-photon single-mode quantum states of the electromagnetic field [17], for example, or to excite a single atom by a single-photon quantum state perfectly with the help of vacuum Rabi oscillations [18]. Despite these significant advances of quantum electrodynamics similar efficient techniques for preparing many-mode few-photon quantum states of the electromagnetic field or for controlling the resulting atom–field dynamics are significantly less well developed. Advances in this direction would be particularly interesting for purposes of quantum information processing. They would significantly enhance the flexibility of exchanging quantum information between the electromagnetic field, which is particularly useful for the transport of quantum information, and matter, which is well suited for the storage of quantum information.

In this contribution we investigate quantum electrodynamical many-mode aspects by exploring the simplest possible situation in this context, namely the interaction of a single atom, modeled by a simple two-level system, with many-mode one-photon quantum states of the electromagnetic field [19]. In particular, we concentrate on the question of how the engineering of electromagnetic field modes influences the atom–field interaction. An interesting problem in this context is the engineering of ideal one-photon multimode quantum states which may excite a single atom perfectly [20]. For purposes of quantum information processing such one-photon multimode states are particularly well suited for transmitting quantum information and for storing it in a material memory again.

This chapter is organized as follows: In Section 2 characteristic aspects of two extreme cases of the interaction of a simple two-state quantum system with the radiation field are discussed, namely the single-mode Jaynes–Cummings–Paul model [21, 22] and spontaneous photon emission in free space [7, 8]. In Section 3 we explore dynamical modifications originating from modifications of the electromagnetic field modes involved. For this purpose the interaction of a single photon with a two-level system in

a closed spherical cavity of arbitrary size [23] and in a half-open parabolic cavity [24, 25] is explored.

2. QUANTUM ELECTRODYNAMICS OF A MATERIAL TWO-LEVEL SYSTEM—BASIC ASPECTS

In this section basic results concerning the interaction of matter with the quantized radiation field are discussed. For this purpose an elementary two-level model of matter is considered which involves two nondegenerate relevant energy eigenstates coupled almost resonantly to the electromagnetic field. Characteristic quantum electrodynamical properties of this model system are particularly apparent in cases in which the quantum states of the electromagnetic field contain only a small number of photons. The resulting dynamics depends significantly on whether only one mode of the radiation field or an infinite number of them participate in the interaction.

2.1. The Jaynes–Cummings–Paul model

One of the simplest models which describes characteristic quantum features of the almost resonant interaction of matter with the radiation field is the Jaynes–Cummings–Paul model [21, 22]. In this model a material two-level system interacts with a single mode of the radiation field. In the Schrödinger picture its dynamics is described by the Hamiltonian

$$\hat{H} = E_{\mathrm{g}}|g\rangle\langle g| + E_{\mathrm{e}}|e\rangle\langle e| + \hbar\omega\hat{a}^{\dagger}\hat{a} + \hbar g\hat{a}|e\rangle\langle g| + \hbar g^{*}\hat{a}^{\dagger}|g\rangle\langle e|. \tag{1}$$

The energies of the material two-level system are denoted by E_{g} and $E_{\mathrm{e}} > E_{\mathrm{g}}$ and $\hat{a}$ ($\hat{a}^{\dagger}$) is the destruction (creation) operator of the almost resonantly coupled electromagnetic field mode of frequency ω, i.e., $E_{\mathrm{e}} - E_{\mathrm{g}} \approx \hbar\omega$. The coupling constant g characterizes the strength of the interaction of the material two-level system with the single mode of the radiation field. In the dipole approximation, for example, which applies in typical quantum optical situations and in which it is assumed that the wavelength of the almost resonantly coupled electromagnetic field mode is significantly larger than the extension of the material charge distribution of the two-level system, this coupling constant is given by

$$\hbar g\hat{a} = -\langle e|\hat{\mathbf{d}}|g\rangle \cdot \hat{\mathbf{E}}_{+}(\mathbf{x}_{0}). \tag{2}$$

Thereby, $\hat{\mathbf{d}}$ is the material dipole operator. The positive frequency component of the electric field operator is denoted by

$$\hat{\mathbf{E}}_{+}(\mathbf{x}) = i\sqrt{\frac{\hbar\omega}{2\epsilon_{0}}}\mathbf{u}(\mathbf{x})\hat{a}, \tag{3}$$

and it has to fulfill the transversality condition $\nabla \cdot \hat{\mathbf{E}}_+(\mathbf{x}) = 0$. ($\epsilon_0$ is the permittivity of the vacuum.) The normalized mode function $\mathbf{u}(\mathbf{x})$ is a solution of the Helmholtz equation

$$\left(\nabla^2 + \omega^2/c^2\right)\mathbf{u}(\mathbf{x}) = 0 \tag{4}$$

and fulfills the boundary conditions of the mode-selecting cavity involved. It is normalized according to the relation $\int_{\mathbb{R}^3} d^3x\, |\mathbf{u}(\mathbf{x})|^2 = 1$. The position of the center of mass of the material charge distribution is denoted by $\mathbf{x}_0$.

Within this model the dynamics of the almost resonantly coupled matter–field system can be described in a straightforward way by expanding the quantum state $|\psi\rangle_t$ at time t in the basis of energy eigenstates of the uncoupled quantum system, i.e.,

$$|\psi\rangle_t = \sum_{n=0}^{\infty}\{a_{e,n}(t)e^{-i(E_e+n\hbar\omega)t/\hbar}|e\rangle \otimes |n\rangle + a_{g,n}(t)e^{-i(E_g+n\hbar\omega)t/\hbar}|g\rangle \otimes |n\rangle\}. \tag{5}$$

The time-dependent Schrödinger equation $i\hbar d|\psi\rangle_t/dt = \hat{H}|\psi\rangle_t$ yields the system of pairs of coupled equations

$$\dot{a}_{e,n}(t) = -ig\sqrt{n+1}e^{i\Delta t}a_{g,n+1}(t),$$
$$\dot{a}_{g,n+1}(t) = -ig^*\sqrt{n+1}e^{-i\Delta t}a_{e,n}(t) \text{ (for } n \geq -1), \tag{6}$$

with $\Delta = (E_e - \hbar\omega - E_g)/\hbar$ denoting the detuning from resonance.

If initially, at $t = 0$, the two-level system is prepared in its excited state $|e\rangle$, i.e., $a_{g,n}(0) = 0$ for $n \geq 0$, Eqs. (6) yield the solution

$$a_{e,n}(t) = a_{e,n}(0)\left(\cos\left(\frac{\Omega_n t}{2}\right) - \frac{i\Delta}{\Omega_n}\sin\left(\frac{\Omega_n t}{2}\right)\right)e^{i\Delta t/2},$$

$$a_{g,n+1}(t) = -a_{e,n}(0)\frac{2ig^*\sqrt{n+1}}{\Omega_n}\sin\left(\frac{\Omega_n t}{2}\right)e^{-i\Delta t/2}. \tag{7}$$

The time evolution of the probability amplitudes $a_{e,n}(t)$ and $a_{g,n}(t)$ exhibits a characteristic periodic energy transfer between the two-level system and the electromagnetic field mode which is characterized by the n-photon Rabi frequency $\Omega_n = \sqrt{\Delta^2 + 4|g|^2(n+1)}$. As the period of this energy exchange depends on the photon number the resulting time evolution exhibits interesting collapse and revival phenomena.

Let us consider a special case in more detail in which initially the two-level system is excited and the single-mode radiation field is in a coherent state $|\alpha\rangle$ with $\hat{a}|\alpha\rangle = \alpha|\alpha\rangle$ and $\alpha \in \mathbb{C}$ [18]. The resulting time evolution of the inversion of the two-level system is given by

$$w(t) := \sum_{n=0}^{\infty} \{|a_{\mathrm{e},n}(t)|^2 - |a_{\mathrm{g},n}(t)|^2\} = \sum_{n=0}^{\infty} |a_{\mathrm{e},n}(0)|^2 \left(\frac{\Delta^2}{\Omega_n^2} + \frac{4|g|^2(n+1)}{\Omega_n^2} \cos(\Omega_n t) \right),$$

(8)

with $a_{\mathrm{e},n}(0) = \exp(-|\alpha|^2/2)\alpha^n/\sqrt{n!}$. In Figure (8.1) the time evolution of this inversion is depicted for resonant coupling, i.e., $\Delta = 0$, and various values of the mean photon number $< n >= \langle \alpha | \hat{a}^{\dagger} \hat{a} | \alpha \rangle = |\alpha|^2$ of a coherent state $|\alpha\rangle$. It is apparent that the initially prepared inversion collapses after a characteristic collapse time of the order of $T_{\mathrm{c}} = 2\pi/|g|$. Furthermore, at multiples of times of the order of $T_{\mathrm{r}} = 2\pi\sqrt{<n>+1}/|g|$ the probability amplitudes interfere constructively again thus causing revivals of the initial
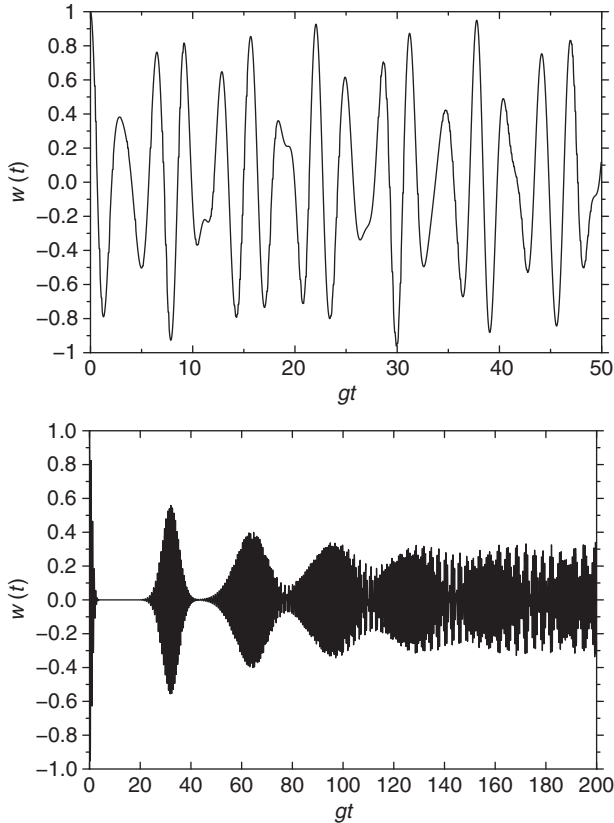
Figure 8.1 Time dependence of the inversion $w(t)$ of Eq. (8) of the two-level system describing its excitation by a coherent single-mode state $|\alpha\rangle$: $< n >= 0.5$ (upper curve), $< n >= 25$ (lower curve).

excitation [26, 27]. Finally, it should also be mentioned that according to Eq. (8) the appearance of collapse and revival phenomena does not necessarily require an initially prepared pure quantum state of the electromagnetic field.

If one considers the extreme case that the two-level system is excited initially but the electromagnetic field is in its ground (vacuum) state one obtains the result

$$w(t) = \frac{\Delta^2}{\Omega_0^2} + \frac{4|g|^2}{\Omega_0^2} \cos(\Omega_0 t) \tag{9}$$

for the inversion of the two-level system. In this case the inversion oscillates periodically between its extreme values and these oscillations are governed by the vacuum Rabi frequency $\Omega_0 = 2|g|$. In particular, this result demonstrates that in the case of the coupling of a two-level system to a single mode of the radiation field the decay of the excited state of the two-level system is not described by an exponential decay law but exhibits a periodic energy exchange which reflects the periodic exchange of a photon between the two-level system and the radiation field.

2.2. Spontaneous emission of a photon in free space

If a material two-level system interacts with the quantized radiation field in free space its dynamics differs significantly from the single-mode case described previously. In order to exemplify these significant differences let us assume that initially the two-level system is prepared in its excited state $|e\rangle$ and that the electromagnetic field is in its ground (vacuum) state $|0\rangle$. In the absence of any mode-selecting cavity all modes of the electromagnetic radiation field couple to this initially excited two-level system. In the Schrödinger picture the field operators of the electric and magnetic field strengths are given by [28]

$$\hat{\mathbf{E}}(\mathbf{x}) = \sum_{\mathbf{k},i} \sqrt{\frac{\hbar\omega_{\mathbf{k}}}{2\epsilon_0}} \left\{ i\mathbf{u}_{\mathbf{k},i}(\mathbf{x})\hat{a}_{\mathbf{k},i} - i\mathbf{u}_{\mathbf{k},i}^*(\mathbf{x})\hat{a}_{\mathbf{k},i}^\dagger \right\} = \hat{\mathbf{E}}_+(\mathbf{x}) + \hat{\mathbf{E}}_-(\mathbf{x}), \tag{10}$$

$$\hat{\mathbf{B}}(\mathbf{x}) = \sum_{\mathbf{k},i} \sqrt{\frac{\hbar}{2\epsilon_0\omega_{\mathbf{k}}}} \left\{ (\nabla \wedge \mathbf{u}_{\mathbf{k},i})(\mathbf{x})\hat{a}_{\mathbf{k},i} + \left(\nabla \wedge \mathbf{u}_{\mathbf{k},i}^*\right)(\mathbf{x})\hat{a}_{\mathbf{k},i}^\dagger \right\} = \hat{\mathbf{B}}_+(\mathbf{x}) + \hat{\mathbf{B}}_-(\mathbf{x}),$$

with their corresponding "positive-" and "negative-frequency" parts $\hat{\mathbf{E}}_+(\mathbf{x})$ and $\hat{\mathbf{E}}_-(\mathbf{x})$ ($\hat{\mathbf{B}}_+(\mathbf{x})$ and $\hat{\mathbf{B}}_-(\mathbf{x})$). If we consider an electromagnetic field in a cubic quantization volume of length L and volume $V = L^3$ and impose periodic boundary conditions a complete set of orthonormal mode functions can be chosen in the form

$$\mathbf{u}_{\mathbf{k},i}(\mathbf{x}) = \mathbf{e}_i(\mathbf{k})\frac{e^{i\mathbf{k}\cdot\mathbf{x}}}{\sqrt{V}}, \, i = 1, 2, \tag{11}$$

with the wave vectors $\mathbf{k} = 2\pi\mathbf{n}/L$ ($\mathbf{n} \in \mathbb{Z}^3$) and with the corresponding real-valued unit-polarization vectors $\mathbf{e}_i(\mathbf{k})$ ($\mathbf{e}_1(\mathbf{k}) \cdot \mathbf{e}_2(\mathbf{k}) = 0$, $\mathbf{e}_1(\mathbf{k}) \wedge \mathbf{e}_2(\mathbf{k}) = \mathbf{k}/|\mathbf{k}|$) fulfilling the transversality condition $\mathbf{e}_i(\mathbf{k}) \cdot \mathbf{k} = 0$ for $i = 1, 2$. Within a perturbative treatment of the spontaneous photon emission process according to Fermi's golden rule the resulting decay of the two-level system is governed by the rate [28]

$$\Gamma = \sum_{\mathbf{k},i} \frac{2\pi}{\hbar} |\langle e|\hat{\mathbf{d}}|g\rangle \cdot \sqrt{\frac{\hbar\omega_{\mathbf{k}}}{2\epsilon_o}} \mathbf{u}_{\mathbf{k},i}(\mathbf{x}_0)|^2 \, \delta(E_g + \hbar\omega_{eg} - E_e) = \frac{\omega_{eg}^3 |\langle e|\hat{\mathbf{d}}|g\rangle|^2}{3\pi\epsilon_0\hbar c^3},$$

$$\tag{12}$$

with the transition frequency $\omega_{eg} = (E_e - E_g)/\hbar'$. Within the framework of the dipole approximation $\mathbf{x}_0$ denotes the position of the center of mass of the two-level system. It is apparent from Eq. (12) that the spontaneous decay rate depends on the number of field modes per unit energy which couple resonantly, i.e., with $\omega_{\mathbf{k}} = (E_e - E_g)/\hbar$, to the spontaneously decaying two-level system. Thus, altering the mode structure of these relevant field modes by a cavity, for example, modifies the spontaneous decay rate. This effect was confirmed in experiments with Rydberg atoms of sodium [29] excited in a niobium superconducting cavity. Rydberg atoms are especially suitable for the experimental verification of modifications of spontaneous decay rates since they possess large dipole matrix elements on microwave transitions. Therefore, the spontaneous emission rate for the atomic transition 23S→22P was investigated which was in resonance with the niobium superconducting cavity at 340 GHz. Thus, the free-space value of $\Gamma = 150\,\text{s}^{-1}$ could be increased to a value of $\Gamma_{\text{cavity}} = 8 \cdot 10^4\,\text{s}^{-1}$.

A nonperturbative treatment of the exponential decay of an excited two-level system has already been given by Weisskopf and Wigner [7, 8] in their seminal work. If the initially prepared quantum state of the matter–field system is of the form $|e\rangle \otimes |0\rangle$ the time evolution of the resulting quantum state can be decomposed according to

$$|\psi\rangle_t = \sum_{\mathbf{k},i} a_{g\mathbf{k}i}(t)e^{-i(E_g+\hbar\omega_{\mathbf{k}})t/\hbar} |g\rangle \otimes \hat{a}_{\mathbf{k},i}^\dagger|0\rangle + a_e(t)e^{-iE_e t/\hbar}|e\rangle \otimes |0\rangle. \tag{13}$$

The resulting dynamics is described by the time-dependent Schrödinger equation with Hamiltonian

$$\hat{H} = E_{\mathrm{g}}|g\rangle\langle g| + E_{\mathrm{e}}|e\rangle\langle e| + \sum_{\mathbf{k}\in I, i} \hbar\omega_{\mathbf{k}}\hat{a}^{\dagger}_{\mathbf{k},i}\hat{a}_{\mathbf{k},i}$$

$$- |e\rangle\langle g| \,\langle e|\hat{\mathbf{d}}|g\rangle \cdot \hat{\mathbf{E}}_{+}(\mathbf{x}_0) - |g\rangle\langle e| \,\langle e|\hat{\mathbf{d}}|g\rangle^{*} \cdot \hat{\mathbf{E}}_{-}(\mathbf{x}_0) \qquad (14)$$

in the dipole- and rotating wave approximation [28]. The rotating wave approximation takes into account the interaction of the two-level system with the almost resonant field modes ($\mathbf{k} \in I$) within a frequency interval of width $\omega_{eg} \gg \Delta\omega \gg \Gamma$ centered around the transition frequency ω_{eg} in a nonperturbative way. The influence of all other (nonresonant) field modes can be taken into account perturbatively. In particular, in second-order perturbation theory these nonresonant modes give rise to a Lamb shift [30, 31]. It should be mentioned that, contrary to the almost resonant modes, for a consistent treatment of this energy shift the coupling of the nonresonant modes of the radiation field to the two-level atom cannot be treated in the dipole approximation because also high-frequency field modes have to be taken into account. Furthermore, mass renormalization has to be included. This way a well-defined and finite expression for the Lamb shift can even be obtained within a nonrelativistic quantum electrodynamical description [31].

The time-dependent Schrödinger equation is equivalent to the differential equations

$$\dot{a}_{\mathrm{e}}(t) = -\frac{\langle e|\hat{\mathbf{d}}|g\rangle}{\hbar} \sum_{\mathbf{k}\in I, i} \sqrt{\frac{\hbar\omega_{\mathbf{k}}}{2\epsilon_0}} \mathbf{u}_{\mathbf{k},i}(\mathbf{x}_0) a_{\mathrm{g}\mathbf{k}i}(t) e^{i(E_{\mathrm{e}}-E_{\mathrm{g}}-\hbar\omega_{\mathbf{k}})t/\hbar},$$

$$\dot{a}_{\mathrm{g}\mathbf{k}i}(t) = \frac{\langle e|\hat{\mathbf{d}}|g\rangle^{*}}{\hbar} \sqrt{\frac{\hbar\omega_{\mathbf{k}}}{2\epsilon_0}} \mathbf{u}^{*}_{\mathbf{k},i}(\mathbf{x}_0) a_{\mathrm{e}}(t) e^{-i(E_{\mathrm{e}}-E_{\mathrm{g}}-\hbar\omega_{\mathbf{k}})t/\hbar} \qquad (15)$$

for the probability amplitudes which yield the integro-differential equation

$$\dot{a}_{\mathrm{e}}(t) = -\sum_{\mathbf{k}\in I, i} \frac{\hbar\omega_{\mathbf{k}}|\langle e|\hat{\mathbf{d}}|g\rangle \cdot \mathbf{u}_{\mathbf{k},i}(\mathbf{x}_0)|^2}{2\hbar^2\epsilon_0} \int_0^t dt' \, a_{\mathrm{e}}(t') e^{i(E_{\mathrm{e}}-E_{\mathrm{g}}-\hbar\omega_{\mathbf{k}})(t-t')/\hbar} \qquad (16)$$

for the probability amplitude $a_{\mathrm{e}}(t)$ of observing the two-level system in its excited state $|e\rangle$ at time $t > 0$. In the continuum limit of a large quantization volume V the summation over the modes of the electromagnetic field can be approximated by

$$\sum_{\mathbf{k}\in I, i} \longrightarrow \sum_i \frac{V}{(2\pi)^3} \int_{\mathbf{k}\in I} d^3\mathbf{k} = \sum_i \int_{\omega\in I} d\omega\rho(\omega), \qquad (17)$$

with $\rho(\omega) = 4\pi V\omega^2/(8\pi^3 c^3)$ enumerating the number of field modes per frequency and per polarization. As long as the spontaneous decay rate Γ of

Eq. (12) is much smaller than the resonance frequency ω_{eg} and the frequency range over which the integrand of Eq. (16) varies significantly, the "pole approximation" [7, 8, 32] may by applied so that Eq. (16) reduces to

$$\dot{a}_e(t) = -\int_0^t dt' \, \Gamma a_e(t')\delta(t - t') = -\frac{\Gamma}{2}a_e(t). \tag{18}$$

Within this approximation the initially excited two-level atom decays exponentially with rate (12) so that for $t > 0$ the quantum state is given by

$$|\psi\rangle_t = \sum_{\mathbf{k}\in I, i}(-i)\langle e|\hat{\mathbf{d}}|g\rangle^* \cdot \mathbf{u}_{\mathbf{k},i}^*(\mathbf{x}_0)\sqrt{\frac{\hbar\omega_\mathbf{k}}{2\epsilon_0}}\frac{e^{-i(E_g+\hbar\omega_\mathbf{k})t/\hbar} - e^{-i(E_e-i\hbar\Gamma/2)t/\hbar}}{E_e - E_g - \hbar\omega_\mathbf{k} - i\hbar\Gamma/2}\hat{a}_{\mathbf{k},i}^\dagger|0\rangle \otimes |g\rangle$$
$$+ e^{-i(E_e-i\hbar\Gamma/2)t/\hbar}|e\rangle \otimes |0\rangle. \tag{19}$$

Thus, at the end of the spontaneous decay process the two-level system approaches a separable pure quantum state with the two-level system in its lower energy eigenstate $|g\rangle$. In this quantum state the mean electric and magnetic field strengths vanish so that the (normally ordered) energy density of the electromagnetic field provides a local measure for the statistical uncertainty of these electromagnetic field strengths.

According to Eq. (19) after the completion of the photon emission process both the two-level system and the electromagnetic field are in pure states. In view of this asymptotic separation it is of interest to ask whether a one-photon state of the electromagnetic field exists which is capable of exciting a material system, such as an atom, perfectly in free space from an initially prepared ground state $|g\rangle$ to an excited state $|e\rangle$ by photon absorption. Within our quantum electrodynamical model this question can be answered in the affirmative in a straightforward way. For this purpose one has to solve Eqs. (15) subject to the final state condition that at a particular time, say $t = 0$, the two-level system is in its excited state and the radiation field in its vacuum state. It is straightforward to show that for $t \leq 0$ this advanced solution of Eqs. (15) is given by the quantum state

$$|\psi\rangle_t = \sum_{\mathbf{k}\in I, i}(-i)\langle e|\hat{\mathbf{d}}|g\rangle^* \cdot \mathbf{u}_{\mathbf{k},i}^*(\mathbf{x}_0)\sqrt{\frac{\hbar\omega_\mathbf{k}}{2\epsilon_0}}\frac{e^{-i(E_g+\hbar\omega_\mathbf{k})t/\hbar} - e^{-i(E_e+i\hbar\Gamma/2)t/\hbar}}{E_e - E_g - \hbar\omega_\mathbf{k} + i\hbar\Gamma/2}\hat{a}_{\mathbf{k},i}^\dagger|0\rangle \otimes |g\rangle$$
$$+ e^{-i(E_e+i\hbar\Gamma/2)t/\hbar}|e\rangle \otimes |0\rangle. \tag{20}$$

Indeed, for $t \to -\infty$ this quantum state is separable. It describes the two-level system initially prepared in state $|g\rangle$ with the radiation field prepared in the particular pure one-photon state which finally excites the two-level system to its excited state $|e\rangle$ perfectly by absorption of a single photon.

For times $t > 0$ the continuation of this time evolution is described by the quantum state of Eq. (19).

3. QUANTUM ELECTRODYNAMICS WITH CONTROLLED MODE SELECTION

In this section characteristic quantum phenomena originating from the exchange of energy between a two-level system and a single-photon radiation field inside a cavity are discussed. First, we consider a possibly large but closed spherical cavity which may contain many almost resonant field modes coupling to a material two-level system positioned in the center of the cavity. By varying the size of this cavity it is possible to describe in a uniform way the transition between the extreme cases of coupling to a single mode of the radiation field and of the free-space limit [23, 33]. Second, we discuss the dynamics of spontaneous photon emission by a two-level system in a half-open parabolic cavity.

3.1. Photon exchange in a closed spherical cavity

The dynamics of a material two-level system positioned at the center $\mathbf{x}_0$ of a spherical cavity, which supports almost resonant field modes, can be described within the theoretical framework discussed in Section 2.2. In the dipole- and rotating wave approximation again the dynamics of this quantum system can be described by the Hamiltonian of Eq. (14) in the Schrödinger picture. However, now the electric field operator of Eq. (10) has to be constructed with the help of mode functions $\mathbf{u}_l(\mathbf{x})$ which are appropriate for a spherical cavity. For this purpose we solve the Helmholtz equation (4) with the boundary condition of an ideal metallic spherical cavity. Thus, the tangential component of $\mathbf{u}_l(\mathbf{x})$ and the normal component of $(\nabla \wedge \mathbf{u}_l)(\mathbf{x})$ have to vanish at the boundary of the spherical cavity. The corresponding solutions of the Helmholtz equation determine the relevant set of possible discrete eigenfrequencies ω_l inside this cavity. For a spherical cavity of radius R the possible mode functions are of the form [33]

$$\mathbf{U}_{nLM}(\mathbf{x}) = N_{nL} j_L(\omega_{nL} r/c) \mathbf{X}_{LM}((\mathbf{x} - \mathbf{x}_0)/|\mathbf{x} - \mathbf{x}_0|),$$

$$\mathbf{V}_{nLM}(\mathbf{x}) = N_{nL} \frac{ic}{\omega_{nL}} (\nabla \wedge j_L)(\omega_{nL} r/c) \mathbf{X}_{LM}((\mathbf{x} - \mathbf{x}_0)/|\mathbf{x} - \mathbf{x}_0|), \qquad (21)$$

with the mode index $l \equiv (nLM)$, the vector spherical harmonics [34]

$$\mathbf{X}_{LM}(\mathbf{y}/|\mathbf{y}|) = -\frac{i}{\sqrt{L(L+1)}} \mathbf{y} \wedge \left(\nabla Y_L^M\right)(\mathbf{y}/|\mathbf{y}|), \qquad (22)$$

and with the spherical harmonics $Y_L^M(\mathbf{y}/|\mathbf{y}|)$ ($L \in \mathbb{N}_0, -L \leq M \in \mathbb{Z} \leq L$) [35]. The dependence of these mode functions on the radial coordinate $r = |\mathbf{x} - \mathbf{x}_0|$ is determined by the regular spherical Bessel functions [35] whose asymptotic behavior is given by

$$\frac{x^L}{(2L+1)!!} \xleftarrow{x \ll 1} j_L(x) \xrightarrow{x \gg 1} \frac{\sin(x - L\pi/2)}{x}, \tag{23}$$

with $(2L+1)!! = (2L+1)(2L-1)(2L-3)\cdots 3 \cdot 1$. The normalization constants N_{nL} are given by

$$N_{nL} = \left(\int_0^R dr r^2 j_L^2(\omega_{nL} r/c) \right)^{-1/2} \xrightarrow{n \gg 1} \frac{\omega_{nL}}{c} \sqrt{\frac{2}{R}}. \tag{24}$$

The eigenvalues ω_{nL} of the electromagnetic field modes are determined by the metallic boundary conditions, i.e.,

$$j_L(\omega_{nL} R/c) = 0, \quad \frac{d(xj_L(x))}{dx} \Big|_{x=\omega_{nL}R/c} = 0. \tag{25}$$

Thus, highly excited field modes with $\omega_{nL} R/c \gg 1$ are characterized by the eigenvalues

$$\omega_{nL} R/c \xrightarrow{\omega_{nL}R/c \gg 1} \pi n + (L+1)\pi/2. \tag{26}$$

Note that the energy density of highly excited field modes is given by $dn/d(\hbar\omega_{nL}) = R/(\pi\hbar c)$ and is thus frequency independent. It should also be mentioned that at the center of the spherical cavity, i.e., at $\mathbf{x}_0$, only the mode functions $\mathbf{V}_{nL=1M=0}(\mathbf{x})$ are nonvanishing. Therefore, in the dipole approximation the two-level system positioned at the center of the spherical cavity can only couple to these field modes.

Inserting the relevant mode functions into the electric field operator of Eq. (10) and solving the time-dependent Schrödinger equation with Hamiltonian (14) yields the time evolution of the quantum state $|\psi\rangle_t$ [23]. As a result, under the condition $|\psi\rangle_{t=0} = |e\rangle \otimes |0\rangle$ in the limit of an infinitely large cavity again the results of Eqs. (19 and 20) are obtained. In particular, with the help of the relevant mode functions $\mathbf{V}_{nL=1M=0}(\mathbf{x})$ the energy distribution of the resulting one-photon state can be determined in a straightforward way. In the radiation zone of the two-level system, i.e., at distances $|\mathbf{x} - \mathbf{x}_0| = r \gg c/\omega_{\text{eg}}$, one can use the asymptotic form of the relevant spherical Bessel functions. Thus, for the quantum state of Eqs. (19 and 20) in this region of space the energy density of the radiation field is well approximated by

$$_t\langle\psi|:\frac{\epsilon_0}{2}\left(\hat{\mathbf{E}}^2(\mathbf{x})+c^2\hat{\mathbf{B}}(\mathbf{x})\right):|\psi\rangle_t = \frac{3\Gamma\hbar\omega_{eg}}{8\pi c}\frac{\sin^2\theta}{r^2}e^{-\Gamma(|t|-r/c)}\Theta(|t|-r/c). \quad (27)$$

Thereby, :: denotes the normal ordering [28] of the field operators, θ is the angle between the dipole moment $\langle e|\hat{\mathbf{d}}|g\rangle$ and the direction of observation $(\mathbf{x}-\mathbf{x}_0)$, and $\Theta(x)$ denotes the Heaviside unit-step function with $\Theta(x)=1$ for $x \geq 0$ and zero elsewhere. The electromagnetic energy density of Eq. (27) is a local measure for the uncertainties of the electric and magnetic field strengths. It is apparent that this energy density has an exponential shape with a spatial extension of the order of c/Γ and with a sudden decrease at distance $|\mathbf{x}-\mathbf{x}_0|=r=c|t|$ from the two-level system. Due to energy conservation the total field energy contained in this one-photon wave packet equals $\hbar\omega_{eg}(1-e^{-\Gamma|t|})$. The mean field energy density can also be decomposed into its electric and magnetic contributions (which are equal) and into its various polarization components. Thus, along direction $\mathbf{e}$ the polarization component of the mean electric energy density, for example, can be represented in the form

$$_t\langle\psi|:\frac{\epsilon_0}{2}(\mathbf{e}\cdot\hat{\mathbf{E}}(\mathbf{x}))^2:|\psi\rangle_t = |\mathbf{e}\cdot\mathcal{E}(\mathbf{x},t)|^2, \quad (28)$$

with the complex-valued electric one-photon energy-density amplitude

$$\mathcal{E}(\mathbf{x},t) = -i\sqrt{\frac{3\Gamma\hbar\omega_{eg}}{16\pi c}}\Theta(|t|-r/c)e^{i\mathrm{sgn}(t)\omega_{eg}(|t|-r/c)}e^{-\Gamma(|t|-r/c)/2}\frac{\sin\theta}{r}\mathbf{e}_\theta \quad (29)$$

and with $\mathrm{sgn}(t)$ denoting the sign of t. Equation (29) is valid in the radiation zone, i.e., for $\omega_{eg}r/c \gg 1$, as long as $\omega_{eg} \gg \Gamma/2$ (compare with Eq. (18) and the validity of the pole approximation). It demonstrates that in the radiation zone the electromagnetic field energy is concentrated completely in the polarization direction $\mathbf{e}_\theta$. Integrating Eq. (28) over all space (thereby neglecting contributions outside the radiation zone) the electric field energy at time t is given by

$$\int_{\mathbb{R}^3} d^3\mathbf{x}\,|\mathcal{E}(\mathbf{x},t)|^2 = \frac{\hbar\omega_{eg}}{2}(1-e^{-\Gamma|t|}). \quad (30)$$

The analogous expression for the magnetic one-photon energy-density amplitude can be obtained from Eq. (29) by the replacement $\mathbf{e}_\theta \longrightarrow \mathbf{e}_\varphi$. Thus, the magnetic energy density is concentrated completely in the direction $\mathbf{e}_\varphi$ and its integrated field energy contribution is also given by Eq. (30).

For finite values of the radius of the spherical cavity R the dynamics of the photon exchange with the two-level system changes significantly. In the extreme limit of a small cavity in which only one cavity mode is in resonance with the spontaneously decaying two-level system the dynamics reduces to

the results of the Jaynes–Cummings–Paul model discussed previously. In cases in which this resonant field mode is highly excited this single-mode limit is realized if $\Gamma dn/d(\omega_{nL=1}) = \Gamma R/(\pi c) \ll 1$ so that the cavity is small in comparison with the extension of a one-photon wave packet which is generated by spontaneous emission in free space and whose spatial extension would be of the order of c/Γ. For larger values of the cavity radius R the two-level system starts to couple to more and more field modes almost resonantly so that eventually in the infinite cavity limit the free-field dynamics is approached. It can be shown that for almost resonant coupling of the two-level system to highly excited modes of the spherical cavity, i.e., $\omega_{eg}R/c \gg 1$, for $t \geq 0$ the time evolution of the excited-state probability amplitude for an initially excited two-level system is given by

$$\langle e| \otimes \langle 0|\psi\rangle_t = e^{-i(E_e - i\hbar\Gamma/2)t/\hbar} + \sum_{M=1}^{\infty} \Theta(t - 2MR/c)e^{-i(E_e - i\hbar\Gamma/2)(t-2MR/c)/\hbar}$$

$$\times \left\{ \sum_{r=0}^{M-1} \binom{M-1}{r} \frac{[-\Gamma(t - 2MR/c)]^{1+r}}{(1+r)!} \right\}. \tag{31}$$

In Figure 8.2 this time evolution is depicted for various sizes of the spherical cavity. For small cavities the characteristic almost periodic energy exchange between the two-level system and the radiation field is apparent. For larger cavity sizes this dynamics is modified. For large cavities with $\Gamma dn/d(\omega_{nL=1}) = \Gamma R/(\pi c) \gg 1$ the initially excited two-level system decays approximately exponentially with rate Γ and is excited again at later times by the spontaneously generated one-photon wave packet whenever it returns again to the center of the cavity where the two-level system is located.

3.2. Spontaneous photon emission in a half-open parabolic cavity

Efficient atom–light interaction in free space [20, 36–38] may provide us with less technologically demanding solutions for quantum communication over large distances than typical cavity quantum electrodynamical solutions [13]. Thus, it has gained a lot of interest recently. An intermediate case between the small-cavity limit and the free-space limit can be realized by a large closed cavity [23] in which an atom couples to a large number of modes and which has been discussed in the previous section. A half-cavity, i.e., a cavity with one mirror, constitutes another example of such a case. The structure of standing light waves in front of a mirror was already analyzed in the pioneering work of K. Drexhage [39]. Later on, it has been verified experimentally that under such circumstances one can witness a change of the density of states of the electromagnetic field modes near the atom by measuring its spontaneous emission rate [40]. A simplified one-dimensional scalar model of a laser-driven atom in a half-cavity has been discussed in Ref. [41], for example.
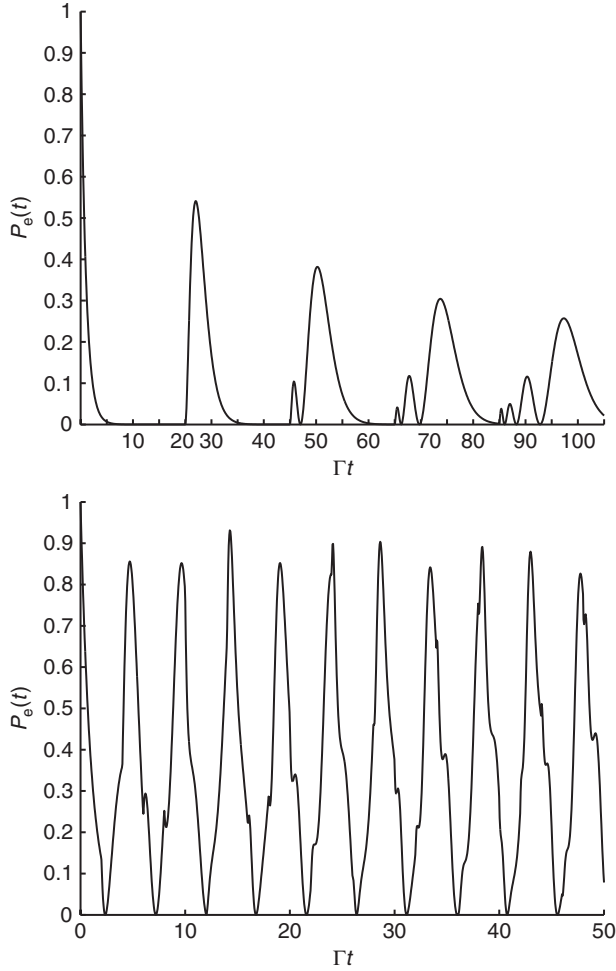
Figure 8.2 Time dependence of the probability $P_e(t)$ of observing the spontaneously decaying two-level system in its excited state at the center of a closed spherical cavity: The number of resonantly interacting field modes is of the order of $\Gamma R/\pi c$ and depends on the size of the cavity R. For $\Gamma R/c = 10$ (upper figure) a spatially localized photon wave packet is generated by spontaneous emission and can be reabsorbed again by the two-level system at the center of the cavity at later times. For $\Gamma R/c = 1$ (lower figure) only a small number of cavity modes interact resonantly and the two-level system performs approximate Rabi oscillations governed by the vacuum Rabi frequency.

As a second example for modifications of the quantum electrodynamical interaction between matter and the radiation field originating from controlled mode engineering in the following we discuss the spontaneous decay of a two-level system, such as an ion [24], in a half-open cavity with a
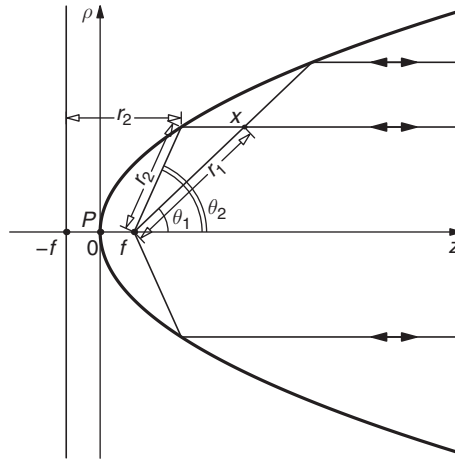
Figure 8.3 Spontaneous photon emission in a parabolic cavity: The two-level system is positioned in the focus *F* of a metallic parabola with focal length *f*. All light rays emanating from *F* which are reflected at the parabolic boundary leave the cavity by propagating parallel to the symmetry axis. They all accumulate the same phase (eikonal) of magnitude $\omega_{eg}(z + f)/c$ which is the same as if these light rays had started in phase from the plane $z = -f$. There are always two possible trajectories to any point **x** inside the cavity. In the semiclassical limit, i.e., $f \gg c/\omega_{eg}$, these two classes of trajectories give rise to the spherical-wave and the plane-wave contributions to the complex-valued energy-density amplitude of Eq. (32).

parabolic shape. The two-level system is assumed to be positioned in the focus *F* of an axially symmetric parabola whose boundary is formed by an ideal metal and is described by the equation $z = \rho^2/(4f)$ (compare with Figure 8.3). The coordinate *z* measures distances from point *P* along the symmetry axis and ρ denotes distances perpendicular to the symmetry axis. The focal point *F* of the parabola has coordinates $(z = f, \rho = 0)$ with $f > 0$ denoting the focal length. A defining property of any parabola is the fact that the distance between any point on its surface and the focal point *F* equals the distance to the plane perpendicular to the symmetry axis located at $z = -f$.

We are particularly interested in possible changes of the spontaneous photon emission process of a two-level system resulting from the presence of the parabolic boundary conditions. The parabolic shape of the mirror ensures that, if a light beam is sent parallel to the symmetry axis of the parabola toward the two-level system, this two-level system interacts with the light coming from the whole 4π solid angle. Similarly, the whole light resulting from spontaneous decay of the two-level system is redirected into a beam propagating parallel to the symmetry axis. Thinking in terms of a semiclassical ray picture only light rays which are emitted from the two-level system along the (negative part of the) symmetry axis return again to the two-level system. Contrary to the closed spherical cavity discussed in the previous

section all other emitted light rays leave the cavity without any reexcitation of the two-level system. Thus, if the dipole moment of the two-level system is oriented along the symmetry axis photon emission along the symmetry axis is suppressed and we do not expect any significant modification of the spontaneous decay process of the two-level system due to the presence of the cavity in cases in which the focal length f is large in comparison with the wavelength of a spontaneously emitted photon [42]. Nevertheless, in analogy to a small cavity or to spontaneous emission in front of a planar mirror [43] significant changes of the spontaneous decay rate are expected if f becomes comparable to the wavelength of a spontaneously emitted photon.

3.2.1. Time evolution of a photon wave packet

First of all, let us consider the dynamics of an almost resonant photon and its resonant energy exchange with a two-level system positioned in the focal point F in the semiclassical limit in which the focal length of the parabola is large in comparison with the photon's wavelength, i.e., $f \gg c/\omega_{eg}$. Furthermore let us concentrate on cases in which the two-level system's dipole moment $\langle e|\hat{\mathbf{d}}|g \rangle$ is oriented parallel to the symmetry axis of the parabola. In particular, we want to investigate solutions of the time-dependent Schrödinger equation $|\psi\rangle_t$ for which at a certain instant of time, say $t = 0$, the two-level system is excited and the electromagnetic radiation field is in its vacuum state, i.e., $|\psi\rangle_{t=0} = |e\rangle \otimes |0\rangle$. Thus, this case describes spontaneous emission of a photon for $t > 0$ and perfect excitation of the two-level system by a one-photon field for $t < 0$. As $f \gg c/\omega_{eg}$, in the radiation zone, i.e., for $\omega_{eg}|\mathbf{x} - \mathbf{x}_0|/c \gg 1$, the distribution of the energy density of the electromagnetic field can be determined with the help of semiclassical methods. This is due to the fact that the one-photon energy-density amplitudes of the electric and magnetic field energies (compare with Eq. (29)) are rapidly oscillating functions of the radial variable $r = |\mathbf{x} - \mathbf{x}_0|$ with a slowly varying envelope which decays on the length scale c/Γ. Stated differently, the condition $\omega_{eg} \gg \Gamma/2$ implies that the phase (eikonal) of these amplitudes exhibits many oscillations within the region of support of these amplitudes.

In the radiation zone the one-photon energy-density amplitudes are solutions of the wave equation whose semiclassical solutions [44] can be constructed with the help of the classical light rays inside the parabolic cavity. Thus, the general form of the energy-density amplitudes of the electric and magnetic field can be constructed semiclassically in two steps. First, one determines their form inside a sphere of radius R_0 around the focal point $F \equiv \mathbf{x}_0$ so that the condition $c/\omega_{eg} \ll R_0 \ll f$ is fulfilled. For the electric field this amplitude is given by Eq. (29) and for the magnetic field it can be obtained from Eq. (29) by the replacement $\mathbf{e}_\theta \longrightarrow \mathbf{e}_\varphi$. Semiclassically,

with this form of these amplitudes one can associate a Lagrangian mani-
fold [44, 45] of radially outgoing straight-line trajectories which start at the
position of the two-level system F and which propagate with the speed of
light. The relevant polarization direction remains constant during transport
along these radial trajectories. In a second step one determines the most gen-
eral semiclassical solution of the wave equation within the parabolic cavity
but outside this sphere of radius R_0. For this purpose one has to construct
the light rays outside this sphere thereby taking into account that they are
reflected at the boundary of the cavity according to the classical reflection
law (equal incoming and outgoing angles). Apart from the reflection process
where one has to take into account the boundary conditions of an ideal metal
the polarization directions remain constant during the propagation along
any of these classical trajectories. The geometry of the parabola implies that
after reflection at the metallic boundary the classical trajectories propagate
parallel to the symmetry axis. Matching the solutions inside the sphere of
radius R_0 and outside the sphere in a smooth way one obtains the one-photon
energy-density amplitude of the electric field at any point $\mathbf{x} \equiv (z,\rho)$ inside the
parabolic cavity. Whereas for times $|t| < f/c$ this energy-density amplitude
is given by Eq. (29), for times $t > f/c$ it is modified due to reflections of light
rays at the boundary of the parabolic cavity and assumes the form

$$
\begin{aligned}
\mathcal{E}(\mathbf{x},t) = \\
-i\sqrt{\frac{3\Gamma\hbar\omega_{eg}}{16\pi c}}\Theta(|t| - r_1(z,\rho)/c)e^{i\mathrm{sgn}(t)\omega_{eg}(|t|-r_1(z,\rho)/c)}e^{-\Gamma(|t|-r_1(z,\rho)/c)/2}\frac{\sin(\theta_1(z,\rho))}{r_1(z,\rho)}\mathbf{e}_{\theta_1} \\
-i\sqrt{\frac{3\Gamma\hbar\omega_{eg}}{16\pi c}}\Theta\left(|t| - \frac{z+f}{c}\right)e^{i\mathrm{sgn}(t)\omega_{eg}(|t|-(z+f)/c)}e^{-\Gamma(|t|-(z+f)/c)/2}\frac{\sin(\theta_2(\rho))}{r_2(\rho)}\mathbf{e}_{\rho},
\end{aligned}
$$

$$(32)$$

with

$$
\sin(\theta_1(z,\rho)) = \frac{\rho}{r_1(z,\rho)}, r_1(z,\rho) = \sqrt{(z-f)^2 + \rho^2}
$$

$$
\sin(\theta_2(\rho)) = \frac{\rho}{r_2(\rho)}, r_2(\rho) = f\left(1 + \frac{\rho^2}{4f^2}\right).
$$

Therefore, at a fixed time t the contribution at position $\mathbf{x} \equiv (z,\rho)$ results from
the interference of contributions originating from radially propagating direct
light rays (first term on the r.h.s. of Eq. (32)) with the contributions from
light rays reflected at the boundary of the cavity (second term on the r.h.s. of
Eq. (32)). Whereas the first type of contributions gives rise to a slowly mod-
ulated spherical wave front emanating from the position of the two-level
system at $F \equiv \mathbf{x}_0$, the reflected trajectories give rise to a (rapidly varying)

plane wave propagating in the z-direction with a slowly varying amplitude. This plane wave is a consequence of the parabolic geometry of the cavity and the fact that for any point on the boundary of the cavity its distances from the focal point F and from the plane $z = -f$ are equal. Therefore, all light rays emitted at any angle θ_2 at F and reflected at the boundary of the parabolic cavity accumulate the same phase (eikonal). This phase is the same as the one originating from a fictitious set of trajectories starting from the plane $z = -f$ and propagating along the z-axis with the speed of light. For large focal lengths in the sense that $2f \gg c/\Gamma$ the two contributions to the energy-density amplitude are well separated in space apart from small regions around the boundary of the parabolic cavity. As a consequence interferences between contributions of these two different types of classical trajectories disappear. Furthermore, for a fixed value of ρ the spherical-wave contribution to Eq. (32) becomes vanishingly small in comparison with the plane-wave contribution in the limit of large values of z. It is apparent from Eq. (32) that the polarization properties of the spherical-wave contribution are not changed by the cavity and are the same as in free space. However, the polarization features of the plane-wave contribution are significantly different. At any point $\mathbf{x}$ its polarization is directed in the $\mathbf{e}_\rho$ direction so that the vector field $\mathcal{E}(\mathbf{x},t)$ represents a vortex field with respect to its polarization properties. The singularity at the symmetry axis is suppressed by the fact that there is no coupling between the radiation field and the two-level system along this axis because the dipole moment of the two-level system is oriented in this direction. Finally, it should be mentioned that the (primitive) semiclassical expression of Eq. (32) breaks down at points close to the boundary of the parabolic cavity where transitional or uniform semiclassical approximations [44, 46] have to be employed.

3.2.2. Modifications of the spontaneous decay rate

In this section it will be demonstrated that depending on the characteristic parameters, namely the focal length f, the resonant wavelength $\lambda = (2\pi)c/\omega_{eg}$, and the orientation of the two-level system's dipole moment $d = \langle e|\hat{\mathbf{d}}|g \rangle$, the spontaneous decay rate of the two-level system may differ significantly from its free-space value as given by Eq. (12).

Since the two-level system is located in a half-open space we start by expanding the electric field operator (10) in mode functions suitable for the parabolic symmetry of the problem. Following the results of Ref. [47] we use mode functions of the form

$$\mathbf{E}^\sigma_{k,\ell,\mu}(\mathbf{r}) = \frac{k}{(2\pi)^{3/2}} \int_{S^2} d\mathbf{n}\, e^{ik\mathbf{n}\cdot\mathbf{r}}\, h_{\ell,\mu}(\mathbf{n})\mathbf{e}^\sigma(\mathbf{n}). \tag{33}$$

Thereby, $\mathbf{k} = k\mathbf{n}$ denotes the wavevector, $\sigma = 1,2$ enumerates the polarization states, and parameters $\ell = 0, \pm 1, \pm 2, \ldots$ and $\mu \in (-\infty, +\infty)$ are additional mode indices. The unit vector $\mathbf{n}$ and the polarization vectors

$\mathbf{e}^1(\mathbf{n})$, $\mathbf{e}^2(\mathbf{n})$ constitute the orthonormal basis which ensures the transversality condition $\nabla \cdot \mathbf{E} = 0$. In particular, we choose these directions in the following form:

$$\mathbf{n} = (\sin\theta\cos\varphi, \sin\theta\sin\varphi, \cos\theta), \tag{34}$$

$$\mathbf{e}^1(\mathbf{n}) = (\sin\varphi, -\cos\varphi, 0), \tag{35}$$

$$\mathbf{e}^2(\mathbf{n}) = (\cos\theta\cos\varphi, \cos\theta\sin\varphi, -\sin\theta). \tag{36}$$

The functions $h_{\ell,\mu}(\mathbf{n})$ are explicitly given by [47]

$$h_{\ell,\mu}(\theta,\varphi) = \chi_\mu(\theta)\frac{e^{i\ell\varphi}}{\sqrt{2\pi}}, \tag{37}$$

with

$$\chi_\mu(\theta) = \frac{\exp\left(-i\mu\ln\left[\tan\theta/2\right]\right)}{\sqrt{2\pi}\sin\theta}. \tag{38}$$

One can easily check the orthogonality and completeness conditions:

$$\int_0^{2\pi}d\varphi\int_0^\pi d\theta\sin\theta\,h^*_{\ell,\mu}(\theta,\varphi)h_{\ell',\mu'}(\theta,\varphi) = \delta_{\ell\ell'}\delta(\mu-\mu'), \tag{39}$$

$$\sum_{\ell=-\infty}^{+\infty}\int_{-\infty}^{+\infty}d\mu\,h^*_{\ell,\mu}(\theta,\varphi)h_{\ell,\mu}(\theta',\varphi') = \delta(\varphi-\varphi')\frac{\delta(\theta-\theta')}{\sin\theta}. \tag{40}$$

Combining Eq. (33) with Eq. (39) one obtains the orthogonality of the mode functions, i.e.,

$$\int d\mathbf{r}\,\mathbf{E}^{*\sigma}_{k,\ell,\mu}(\mathbf{r})\cdot\mathbf{E}^{\sigma'}_{k',\ell',\mu'}(\mathbf{r}) = \delta(k-k')\delta(\mu-\mu')\delta_{\ell\ell'}\delta_{\sigma\sigma'}. \tag{41}$$

If a two-level atom is positioned at $\mathbf{x}$ in free space with the transition dipole parallel to the z-axis, in the dipole approximation the resulting spontaneous decay rate is given by

$$\Gamma(\mathbf{x}) = \frac{1}{(2\pi)^2}\frac{d^2k^3}{2\hbar\epsilon_0}\sum_{\sigma,\ell}\int_{-\infty}^{+\infty}d\mu\int d\mathbf{n}\int d\mathbf{n}'f_k(\mathbf{n},\mathbf{r})f_k^*(\mathbf{n}',\mathbf{r})\cdot e_z^\sigma(\mathbf{n})e_z^\sigma(\mathbf{n}')\,h^*_{\ell,\mu}(\mathbf{n},k)h_{\ell,\mu}(\mathbf{n}',k), \tag{42}$$

with $k = \omega_{eg}/c$. Furthermore, we defined $f_k(\mathbf{n},\mathbf{r}) = \exp(ik\mathbf{n}\cdot\mathbf{r})$, $e_z^\sigma(\mathbf{n}) = \mathbf{e}^\sigma(\mathbf{n})\cdot\mathbf{e}_z$ and used the fact that the summation over ℓ produces $\delta(\varphi-\varphi')$ (see Eq. (40)).

Therefore, the relevant directions $\mathbf{n}$, $\mathbf{n}'$ and the z-axis belong to the same plane which leads to the relation

$$\sum_\sigma e_z^\sigma(\mathbf{n})e_z^\sigma(\mathbf{n}') = e_z^2(\mathbf{n})e_z^2(\mathbf{n}') = \sin\theta\sin\theta'. \tag{43}$$

Taking into account that the integration over μ yields another Dirac delta distribution $\delta(\theta - \theta')$ we finally obtain

$$\Gamma(x,y,z) = \frac{1}{(2\pi)^2}\frac{d^2k^3}{2\hbar\epsilon_0}\int_0^{2\pi}d\varphi\int_0^\pi d\theta\,\sin^3\theta\,|f_k(x,y,z;\varphi,\theta)|^2, \tag{44}$$

with $\mathbf{x} \equiv (x,y,z)$ and $f_k(\mathbf{n},\mathbf{r}) \equiv f_k(x,y,z;\varphi,\theta)$. The relation $|f_k(x,y,z;\varphi,\theta)| = 1$ implies that we recover again the free-space result of Eq. (12).

In the presence of a conducting parabolic mirror the mode functions of Eq. (33) should fulfill the appropriate boundary conditions of an ideal metal. However, it is very challenging to solve the Helmholtz equation under these boundary conditions and the transversality condition simultaneously. Contrary to Ref. [48], a simplified approximation may be obtained by keeping the transversality condition but relaxing the precise conditions on the mode functions on the surface of the parabolic mirror. The transversality condition relates the electric field to the geometry of the system and therefore contributes to some geometrical factor present in the decay rate formula. The boundary condition ensures a possible discreteness of the normal modes. As our physical system is large it is expected that slightly changing the boundary conditions of the parabolic cavity will not influence the decay rate significantly.

We start our approximate treatment by introducing parabolic coordinates (ξ,η,φ) which are related to Cartesian coordinates by

$$x = 2\sqrt{\xi\eta}\cos\varphi, \tag{45}$$

$$y = 2\sqrt{\xi\eta}\sin\varphi, \tag{46}$$

$$z = \xi - \eta. \tag{47}$$

The boundary of the parabolic mirror is described by the equation $\eta = f$. It can be shown [47] that the important η-dependent part of the mode functions possesses the following asymptotic behavior:

$$F_{\ell,\mu}(k;\eta) \sim \frac{\cos\left\{\mu\ln 2k\eta + k\eta - \alpha_{\ell,\mu}\right\}}{\sqrt{\eta}}, \tag{48}$$

with a phase $\alpha_{\ell,\mu}$ whose explicit form is not important for our subsequent discussion. Imposing the parabolic boundary condition on Eq. (48) at the

value $\eta = f$ results in a discrete set of values for μ_m. A simple choice for these discrete values is

$$kf - \alpha_{\ell,\mu} = 0 \, , \, \mu_m \ln 2kf = m\pi \, , m = 1, 2, 3, \ldots \tag{49}$$

This particular choice is consistent with the replacement of the continuous set of modes of Eq. (38) by the discrete set

$$\tilde{\chi}_m(\theta) = \frac{\sin\left(\frac{m\pi \ln[\tan\theta/2]}{\ln 2kf}\right)}{\sqrt{2\pi \ln 2kf} \sin\theta} \quad \text{for } \theta \in [\theta_0, \pi - \theta_0] \tag{50}$$

$$= 0 \text{ otherwise}$$

such that

$$\tan\frac{\theta_0}{2} = \frac{1}{2kf} = \frac{1}{4\pi}\frac{\lambda}{f}. \tag{51}$$

The limitation on the angle θ results from the quantization condition (49) and from the fact that at the boundary the normal modes have to vanish, i.e., $\tilde{\chi}_m(\theta_0) = 0$. This ansatz modifies the formula for the decay rate because the completeness condition is changed according to

$$\sum_m \tilde{\chi}_m(\theta)\tilde{\chi}_m(\theta') = I_{[\theta_0, \pi - \theta_0]}(\theta)\frac{\delta(\theta - \theta')}{\sin\theta}, \tag{52}$$

with I_A denoting the indicator function of the set A. Therefore, the integration over the angle θ involved in Eq. (42) should be performed over the interval $[\theta_0, \pi - \theta_0]$. This leads to a correction of the order of $(kf)^{-4}$ which, however, is not relevant for present-day experiments. In currently planned experiments [24] typical focal lengths and wavelengths are of the order of $f = 2\,\text{mm}$ and $\lambda = 250\,\text{nm}$ which amounts to a value of $kf \simeq 10^4$ [20] so that θ_0 is small. Therefore, we can replace $\sin\theta$ by θ. It is rather obvious that the same is true for any reasonable choice of the boundary conditions because the smallness of this correction is entirely due to the large value of kf.

Hence the only relevant modification of the spontaneous emission rate due to the presence of the parabolic mirror is the replacement of the plane traveling waves $f_k(\mathbf{n}, \mathbf{r}) = e^{i k \mathbf{n} \cdot \mathbf{r}}$ by the standing waves

$$f_k(\mathbf{n}, \mathbf{r}) = \sqrt{2}\sin\left(k\mathbf{n} \cdot (\mathbf{r} - \mathbf{f})\right), \tag{53}$$

where the factor $\sqrt{2}$ ensures the completeness condition. Equation (53) implies that the electric field for any mode of the form of Eq. (33) vanishes at the point P of the parabola. It leads to the following approximate expression

for the spontaneous emission rate in the presence of a conducting parabolic mirror:

$$\tilde{\Gamma}(x, y, z) = \frac{1}{2\pi^2} \frac{d^2 k^3}{2\hbar\epsilon_0} \int_0^{2\pi} d\varphi \int_0^{\pi} d\theta \, \sin^3\theta \, \sin^2\{k[(x\cos\varphi + y\sin\varphi)\sin\theta$$

$$+ (z+f)\cos\theta]\}. \tag{54}$$

If the two-level system is placed at a distance from the point P which is much larger than $\lambda = (2\pi)c/\omega_{eg}$, the interference factor $\sin^2(\ldots)$ is averaged to $1/2$ and the standard free-space result of Eq. (12) is recovered.

If the two-level system is located at the symmetry axis of the parabola, i.e., $x = y = 0$, the integral in Eq. (54) simplifies to

$$\tilde{\Gamma}(z) = \eta\Gamma, \tag{55}$$

with the correction η to the free-space decay rate Γ being given by

$$\eta = \left(1 + 3\frac{\cos\left(2k(z+f)\right)}{4k^2(z+f)^2} - 3\frac{\sin\left(2k(z+f)\right)}{8k^3(z+f)^3}\right). \tag{56}$$

For a focal length $f = 2\,\mathrm{mm}$ this correction factor η is depicted in Figure 8.4. Its value at the focal point F becomes significant for small values of the wave vector $k = \omega_{eg}/c$. This corresponds to cases in which the two-level system is close to the mirror surface, i.e., $|z+f| < \lambda$. However, for larger values of k the variations of η are shifted toward the mirror surface. Far away from the mirror η tends to unity so that the decay rate reduces to its free-space value. According to these results modifications of the spontaneous decay rate could be observable on a scale of 100 nm but only within a distance of the order of the wavelength from the mirror surface.
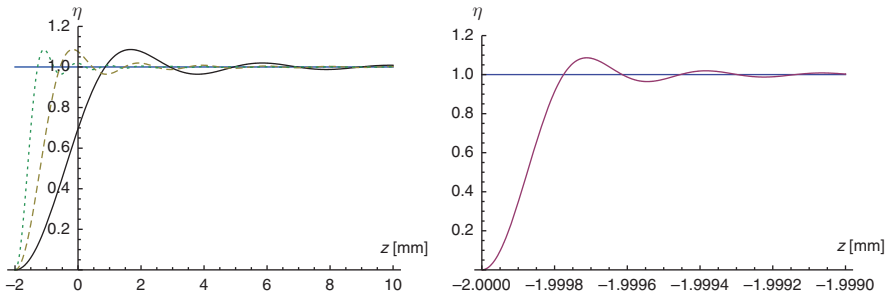
Figure 8.4 Modifications of the spontaneous decay rate according to Eqs. (55 and 56): small values of $k = \omega_{eg}/c$ (left figure): $k = 0.25\pi\,\mathrm{mm}^{-1}$ – solid line, $k = 0.5\pi\,\mathrm{mm}^{-1}$ – dashed line, $k = \pi\,\mathrm{mm}^{-1}$ – dotted line; large value of $k = 10^4\,\mathrm{mm}^{-1}$ (right figure).

4. CONCLUSIONS AND OUTLOOK

Despite significant recent advances in the area of cavity quantum electrody-
namics concerning the control of photonic quantum states and their interac-
tion with matter in cavities, the interaction of few-photon multimode quan-
tum states with matter in free space is still largely unexplored. A detailed
understanding of this interaction and the resulting exchange of quantum
information between radiation field and matter is not only of general phys-
ical interest but also necessary for promising future quantum technological
applications, such as the realization of quantum repeaters.

Here, we have discussed the simplest problem in this respect, namely the
free-space interaction of a single-photon quantum state with an individual
two-level matter system which can be realized by a trapped atom or ion. In
this elementary example it can be demonstrated explicitly that the process
of spontaneous emission of a photon is perfectly reversible provided that
one is able to control the modes and quantum states of the radiation field
in free space. For this purpose the dynamics resulting from the mode struc-
ture of a parabolic mirror has been discussed. It has been shown that using
parabola it is possible to perfectly convert the excitation of an appropriately
prepared asymptotically incoming plane-wave one-photon quantum state
to an atom positioned in the focus of the parabola. The resulting dynamics
depends strongly on the magnitudes of the dominantly excited wavelengths
of the one-photon state. If these wavelengths are short in comparison with
the focal length of the parabola the propagation of the one-photon state can
be described by semiclassical methods and is dominated by the light rays of
the photon inside the parabola. In the opposite limit of long wavelengths
diffraction effects become important and semiclassical treatments become
inappropriate.

Further experimental testing of the discussed theoretical results is
planned. In our future experiment [24, 25] we will use a $^{174}\text{Yb}^{2+}$ ion as a
two-level system with $^1S_0$ and $^3P_1^0$ electronic levels as the ground and the
excited states, respectively, and no hyperfine structure. The atomic transition
frequency of 251.8 nm is in the ultraviolet regime. The ion will be trapped at
the focus of a metallic parabolic mirror with focal length $f = 2.1$ mm which
forms one electrode of a Paul trap. The rf needle-shaped electrode will come
from the back of the mirror through a small hole. This trap design will ensure
almost full 4π-angle ion–light interaction in the strong focusing regime.
The aberration corrections will be done using a diffractive element located
in front of the mirror. The ion has only one decay channel and its dipole
moment will be parallel to the mirror axis. There are several methods which
allow for single-photon pulse generation with the desired spatiotemporal
shape and spectral distribution. The first relies on electrooptic modulation of
a single-photon wave packet [49]. Another experimentally more accessible
method applies a strongly attenuated laser pulse containing $\bar{n} \ll 1$ photons

on average. This technique is widely used in quantum key distribution [50]. We can shape the pulsed temporal mode structure electronically with modulators starting from a continuous-wave laser. Next we will turn it into a radially polarized spatial doughnut mode. After reflection from the mirror surface its polarization at the focal point will only contribute to polarization parallel to the symmetry axis of the mirror and therefore will excite a linear dipole oscillating parallel to this axis. Using this simpler method perfect coupling is achieved if the probability of excitation matches the probability of finding a single photon in the pulse. In addition, as a third option one can generate the properly shaped single-photon Fock state wave function conditionally using photon pairs from parametric downconversion. This method is similar to ghost imaging in the time domain.

Of course, none of these methods will produce an infinitely extended pulse. This is not an obstacle for our experiment however, because one can truncate somewhat the exponential tail of the one-photon wave packet. For example, truncating the pulse to a duration of five lifetimes the excitation probability can be as high as 0.99. For quantum storage applications it is straightforward to expand this scheme to a lambda transition between two long-lived states [51]. Furthermore, efficient coupling in free space opens the possibility for nonlinear optics at the single-photon level.

The investigations discussed here present first steps toward the future goal of obtaining a detailed understanding of the interaction of individual photons with individual atoms in free space. For future applications in quantum information technology the exploration of the limits of perfect exchange of quantum information between the radiation field and these material systems is of particular interest.

REFERENCES

[1] W. Heisenberg, Über quantentheoretische Umdeutung kinematischer und mechanischer Beziehungen, Z. Phys. 33 (1925) 879.
[2] I.J.R. Aitchison, D.A. MacManus, Th.M.Snyder, Understanding Heisenberg's 'Magical' Paper of July 1925: A New Look at the Calculational Details, arXiv:quant-ph/0404009.
[3] M. Born, P. Jordan, Z. Phys. 34 (1925) 858.
[4] E. Schrödinger, Quantisierung als Eigenwertproblem, Ann. Phys. 79 (1926) 361, 489.
[5] E. Schrödinger, Über das Verhältnis der Heisenberg-Born-Jordanschen Quantenmechanik zu der meinen, Ann. der Phys. 79 (1926) 734.
[6] P.A.M. Dirac, The fundamental equations of quantum mechanics, Proc. R. Soc. A 109 (1926) 642.
[7] V. Weisskopf, E. Wigner, Berechnung der natürlichen Linienbreite aufgrund der Diracschen Lichttheorie, Z. Phys. 63 (1930) 54.
[8] V. Weisskopf, E. Wigner, Über die natürliche Linienbreite in der Strahlung des harmonischen Oszillators, Z. Phys. 65 (1930) 18.
[9] Th. Beth, G. Leuchs (Eds.), Quantum Information Processing, Wiley-VCH, Weinheim, 2005.
[10] D. Leibfried, R. Blatt, C. Monroe, D. Wineland, Quantum dynamics of single trapped ions, Rev. Mod. Phys. 75 (2003) 281.

[11] J. Fortagh, C. Zimmermann, Magnetic microtraps for ultracold atoms, Rev. Mod. Phys. 79 (2007) 235.

[12] C. Winterfeldt, Ch. Spielmann, G. Gerber, Colloquium: Optimal control of high-harmonic generation, Rev. Mod. Phys. 80 (2008) 117.

[13] H. Walther, B.T.H. Varcoe, B.G. Englert, T. Becker, Cavity quantum electrodynamics, Rep. Prog. Phys. 69 (2006) 1325.

[14] E.A. Purcell, Spontaneous emission probabilities at radio frequencies, Phys. Rev. 69 (1946) 681 (Note B10).

[15] D. Kleppner, Inhibited spontaneous emission, Phys. Rev. Lett. 47 (1981) 233.

[16] W. Jhe, A. Anderson, E.A. Hinds, D. Meschede, L. Moi, S. Haroche, Suppression of spontaneous decay at optical frequencies: Test of vacuum-field anisotropy in confined space, Phys. Rev. Lett. 58 (1987) 666.

[17] B.T.H. Varcoe, S. Brattke, M. Weidinger, H. Walther, Preparing pure number states of the radiation field, Nature 403 (2000) 743.

[18] W.P. Schleich, Quantum Optics in Phase Space, Wiley-VCH, Weinheim, 2001.

[19] S. Quabis, R. Dorn, M. Eberler, O. Glöckl, G. Leuchs, Focusing light to a tighter spot, Opt. Commun. 179 (2000) 1.

[20] M. Stobińska, G. Alber, G. Leuchs, Perfect excitation of a matter qubit by a single photon in free space, EPL 86 (2009) 14007.

[21] E.T. Jaynes, F.W. Cummings, Comparison of quantum and semiclassical radiation theories with application to the beam maser, Proc. IEEE 51 (1963) 89.

[22] H. Paul, Induzierte Emission bei starker Einstrahlung, Ann. Phys. 11 (1963) 411.

[23] G. Alber, Photon wave packets and spontaneous decay in a cavity, Phys. Rev. A 46 (1992) R5338.

[24] M. Sondermann, R. Maiwald, H. Konermann, N. Lindlein, U. Peschel, G. Leuchs, Design of a mode converter for efficient light-atom coupling in free space, Appl. Phys. B, 89 (2007) 489.

[25] R. Maiwald, D. Leibfried, J. Britton, J.C. Bergquist, G. Leuchs, D.J. Wineland, Stylus ion trap for enhanced access and sensing, Nat. Phys. 5 (2009) 551.

[26] J.H. Eberly, N.B. Narozhny, J.J. Sanchez-Mondragon, Periodic spontaneous collapse and revival in a simple quantum model, Phys. Rev. Lett. 44 (1980) 1323.

[27] I.Sh. Averbukh, N.F. Perel'man, Fractional revivals: Universality in the long-term evolution of quantum wave packets beyond the correspondence principle dynamics, Phys. Lett. A 139 (1989) 449.

[28] L. Mandel, E. Wolf, Optical Coherence and Quantum Optics, Cambridge University Press, Cambridge, 1995.

[29] P. Goy, J.M. Raimond, M. Gross, S. Haroche, Observation of cavity-enhanced single-atom spontaneous emission, Phys. Rev. Lett. 50 (1983) 1903.

[30] H.A. Bethe, The electromagnetic shift of energy levels, Phys. Rev. 72 (1947) 339.

[31] J. Seke, Complete lamb-shift calculation to order α^5 by applying the methods of nonrelativistic quantum electrodynamics, Nuovo Cimento D 18 (1996) 533.

[32] J. Seke, Spontaneous decay of an unstable atomic state: new method for a unified nonrelativistic-relativistic complete treatment, Phys. Lett. A 244 (1998) 111.

[33] G. Alber, G.M. Nikolopoulos, Quantum electrodynamics of a qubit, in: D. Bruss, G. Leuchs, (Eds.), Lectures on Quantum Information, Wiley-VCH, Weinheim, 2007 p. 555ff.

[34] J.D. Jackson, Classical Electrodynamics, Wiley, New York, 1975.

[35] M. Abramowitz, I. Stegun (Eds.), Handbook of Mathematical Functions, National Bureau of Standards Applied Mathematics Series No. 55, US. GPO, Washington, DC, 1964.

[36] I. Gerhardt, G. Wrigge, P. Bushev, G. Zumofen, M. Agio, R. Pfab, et al., Strong extinction of a laser beam by a single molecule, Phys. Rev. Lett. **98**, (2007) 033601.

[37] G. Zumofen, N.M. Mojarad, V. Sandoghdar, M. Agio, Perfect reflection of light by an oscillating dipole, Phys. Rev. Lett. **101**, (2008) 180404.

[38] M.K. Tey, Z. Chen, S.A. Aljunid, B. Chng, F. Huber, G. Maslennikov, et al., Strong interaction between light and a single trapped atom without the need for a cavity, Nat. Phys. 4 (2008) 924.

[39] K.H. Drexhage, Monomolecular layers and light, Sci. Am. 222 (1970) 108.

[40] J. Eschner, Ch. Raab, R. Blatt, Light interference from single atoms and their mirror images, Nature 413 (2001) 495.

[41] U. Dorner, P. Zoller, Laser-driven atoms in half-cavities, Phys. Rev. A **66**, (2002) 023816.

[42] M. Stobińska, R. Alicki, Single-photon single-ion interaction in free space configuration in front of a parabolic mirror, arXiv:quant-ph/0905.4014.

[43] H. Morawitz, Self-coupling of a two-level system by a mirror, Phys. Rev. 187 (1969) 1792.

[44] V.P. Maslov, M.V. Fedoriuk, Semi-Classical Approximation in Quantum Mechanics, Reidel, Dordrecht, 1981.

[45] V.I. Arnold, Mathematical Methods of Classical Mechanics, Springer, Berlin, 1978.

[46] M.V. Berry, K.E. Mount, Semiclassical approximations in wave mechanics, Rep. Prog. Phys. 35 (1972) 315.

[47] C.P. Boyer, E.G. Kalnins, W. Miller, Symmetry and separation of variables for the helmholtz and laplace equations, Nagoya Math. J. 60 (1976) 35.

[48] J.U. Nockel, G. Bourdon, E. Le Ru, R. Adams, I. Robert, J.-M. Moison, et al., Mode structure and ray dynamics of a parabolic dome microcavity, Phys. Rev. E 62 (2000) 8677.

[49] P. Kolchin, C. Belthangady, S. Du, G. Y. Yin, S.E. Harris, Electro-optic modulation of single photons, Phys. Rev. Lett. 101 (2008) 103601.

[50] N. Gisin, G. Ribordy, W. Tittel, H. Zbinden, Quantum cryptography, Rev. Mod. Phys. 74 (2002) 145.

[51] D. Pinotsi, A. Imamoglu, Single photon absorption by a single quantum emitter, Phys. Rev. Lett. 100 (2008) 093603.

Quantum Decay at Long Times

E. Torrontegui[a], J.G. Muga[a], J. Martorell[b],
and **D.W.L. Sprung[c]**

Contents

[a] Departamento de Química Física, Universidad del País Vasco - Euskal Herriko Unibertsitatea, Apdo. 644, 48080 Bilbao, Spain

[b] Departament d'Estructura i Constituents de la Materia, Universitat de Barcelona, 08028 Barcelona, Spain

[c] Department of Physics and Astronomy, McMaster University, Hamilton, Ontario L8S 4M1, Canada

E-mail addresses: jg.muga@ehu.es (J.G. Muga), martorell@ecm.ub.es (J. Martorell), dwsprung@mcmaster.ca (D.W.L. Sprung)

Abstract   We review the post-exponential decay regime in quantum mechanics, with special attention to potential scattering. The mathematical and physical reasons for this regime are discussed using several techniques. In particular, the possible effects of measurement or interaction with the environment are analyzed. Both general and particular results are provided, along with a history of the attempts to observe post-exponential decay. The chapter ends with an outlook for future research.

1. INTRODUCTION

Exponential decay is ubiquitous in the natural sciences. It occurs when a quantity N decreases with time at a rate proportional to its value,

$$\frac{\mathrm{d}N}{\mathrm{d}t} = -\frac{1}{\tau}N, \qquad N = N_0 e^{-t/\tau}. \tag{1}$$

In the quantum world, however, the exponential law is not an obvious consequence of the Schrödinger equation, and its derivation from first principles has been the subject of much scrutiny and debate.

In nuclear physics the decay of natural radioactive nuclei has been studied for more than a century [1]. Gamow [2] developed the first quantal theory for alpha-decay. He explained semi-quantitatively the vast range of alpha-decay lifetimes as a tunneling phenomenon, by imposing "outgoing-wave boundary conditions" on the wave function at the outer edge of the confining barrier. Such an outgoing condition can be satisfied, in general, only for a discrete set of complex energies. The corresponding "Gamow" or "resonant states" are associated with "resonances," a concept that almost always arises in discussions of exponential decay. Gamow states decay exponentially in time and are not square integrable, because the wave function grows exponentially outside the interaction region in coordinate space, but can be used successfully for performing "resonant state" or "pole" expansions of the physical wave function [3, 4].

Weisskopf and Wigner, in another influential paper [5], worked out a more elaborate theory for spontaneous emission from an excited atom interacting

with a quantized radiation field, as introduced by Dirac [6]. This approximate theory also predicts exponential decay and sets a standard paradigm for treating general decay problems in which an initial discrete bound state (or more generally a set of them) is coupled to ("embedded into") a perturbing continuum of states that destabilize the discrete state, making it a decaying resonance.

Exponential decay is a standard topic in quantum mechanics textbooks where it is derived in first-order time-dependent perturbation theory using Fermi's golden rule. What is less well known, at least at textbook level, is that at both short and long times, quantum mechanics predicts deviations from the exponential law. The quantum Zeno effect [7] is associated with the short-time deviation, while deviations at long times are less often discussed. They constitute the central topic of this chapter. This is an interesting regime, where the classical prediction of Eq. (1) differs from the quantal prediction. On the experimental side, access to the post-exponential regime has proven to be difficult. There have been many attempts to provide convincing experimental evidence of post-exponential decay, with scant success [8–12]. Consequently, various ideas have been put forth to explain the lack of success. It has been argued that repetitive measurements on the same system, and the ensuing repeated reduction of the wave packet, or simply the interaction with the environment, would lead to persistence of the exponential regime to times well beyond those expected in an isolated system [13–15]. A recent measurement of post-exponential decay in organic molecules in solution [16] has thus come as a surprise, triggering renewed interest in the subject.

Aside from the challenge of explaining and extending these experimental results, the motives for studying post-exponential decay are manifold. Winter, for example, argued that hidden-variable theories could produce observable effects in samples that have decayed for many lifetimes [17]. More recently Krauss and Dent have suggested important cosmological implications of late-time behavior [18]. At a fundamental level, the detailed form of long-time deviations may help to distinguish between standard, Hermitian quantum mechanics, and non-Hermitian modifications proposed to incorporate a microscopic arrow of time [19–23]. (Details on this later approach may be found in another chapter of the present volume.) Norman pointed out that post-exponential decay could set a limit to the validity of radioactive dating schemes [11]. We have also argued that the deviation could be a diagnostic tool for characteristics of certain cold atom traps [24]. Indeed, due to technological advances in lasers, semiconductors, nanoscience, and cold atoms, microscopic interactions are now relatively easy to manipulate, making decay controllable, and post-exponential decay more accessible to experimental scrutiny and/or applications [25]. For example, under appropriate conditions it could become the dominant regime and be used to implement an Anti-Zeno effect, speeding up decay [26].

Finally, let us also mention that recent experiments on propagation of electric fields in periodic waveguide arrays provide a classical analog of a simple quantum system showing exponential decay [27, 28]. These experiments may allow one to reach the post-exponential regime in a particularly direct way, as we will discuss later.

This review will focus on systems whose decay is exponential over several lifetimes, i.e., systems where an isolated resonance is dominant, or whose decay is characteristic of a post-exponential regime, as for resonances very close to threshold [29, 30]. There are many phenomena where decay is not at all exponential: a trivial example is the survival probability of a freely moving quantum particle represented, say, by a Gaussian wave function. For other examples see Refs. [31–44]. Interesting as they are, these cases and systems are beyond the scope of this review.

There are a number of monographs and review articles on the decay process in quantum mechanics, including post-exponential decay. Among the textbooks, Sakurai [45] summarizes the basic theory. The review of Fonda et al. [13] includes a section on the interpretation of repetitive experimental measurements. The monograph of Goldberger and Watson [46] uses the resolvent method to relate the asymptotic decay law to the threshold behavior of the energy density. Cohen-Tannoudji et al. [47] considered decay in the context of an initial discrete state coupled to a continuum of final states. In the same context Nakazato et al. [48] and Facchi et al. [49, 50] include a discussion of Laplace transforms to extract asymptotic contributions to the survival probability. See also Longhi [51] for a recent extension to the more complex problem of coupling to a cavity with intrinsic gains and losses.

We shall avoid unnecessary repetition of thoroughly reviewed material, although some well-known topics will be briefly outlined for completeness. We shall rather concentrate on some recent results and potential scattering. Decay of a single particle from a trap will be the main physical system discussed in Sections 2, devoted to simple models, and 3, on decay laws depending on the long-range potential tail. Section 4 reviews different physical interpretations given to post-exponential phenomena, Section 5 the difficult route toward experimental observation, and Section 6 a way to enhance post-exponential decay. In the remainder of this section we introduce the seminal work of Khalfin, with a brief account of what preceded it.

1.1. Early results

Two decades after the exponential decay theories of Gamow, and Weisskopf and Wigner, Hellund [52] showed that decay could not be exactly exponential and that it should be slower at long times. Later on, Höhler, going beyond the simplifications of the Weisskopf–Wigner model, obtained a power law for long times [53]; see also Ref. [54].

Khalfin discovered a very general result [55]: that the long-time decay for Hamiltonians with spectra bounded from below is slower than exponential. The argument is this: consider a system described by a time-independent Hamiltonian, H, initially in a normalized nonstationary state $|\Psi_0\rangle$. The survival amplitude of that state is defined as the overlap of the initial state with the state at time t,

$$A(t) = \langle\Psi_0|\exp(-iHt/\hbar)|\Psi_0\rangle. \tag{2}$$

The corresponding survival probability, sometimes called the "nondecay probability" [13], is[1]

$$P(t) = |A(t)|^2. \tag{3}$$

The stationary states, $H|\Phi_{E,\lambda}\rangle = E|\Phi_{E,\lambda}\rangle$ (λ includes any other quantum numbers comprising a complete set of commuting observables), determine a basis. We assume that the Hamiltonian has a continuous spectrum only, or at least that the discrete states of H are orthogonal to Ψ_0. Moreover, we assume that the spectrum is bounded from below: $E_m < E < \infty$. The completeness relation

$$\sum_\lambda \int_{E_m}^\infty dE\ |\Phi_{E,\lambda}\rangle\langle\Phi_{E,\lambda}| = \mathbf{1} \tag{4}$$

then gives

$$A(t) = \int_{E_m}^\infty dE\ \tilde\omega(E)\ e^{-iEt/\hbar}, \qquad \text{where} \qquad \tilde\omega(E) = \sum_\lambda |\langle\Phi_{E,\lambda}|\Psi_0\rangle|^2 \tag{5}$$

is called the "energy density" of the quasi-stationary state. It is then natural to define

$$\omega(E) = \begin{cases} \tilde\omega(E), & E \geq E_m \\ 0, & E < E_m \end{cases} \tag{6}$$

and express the survival amplitude as the Fourier transform of the energy density [56],

$$A(t) = \int_{-\infty}^\infty dE\ \omega(E)\ e^{-iEt/\hbar}. \tag{7}$$

---

[1] Since the survival probability may be difficult to measure, some decay analyses discuss other quantities, such as the nonescape probability from a region of space [57, 58], the probability density at chosen points of space [25, 59, 60], the flux [61–63], and the arrival time [64]. For initially localized wave packets, there is no major discrepancy between survival probability and the nonescape probability [3, 57, 59, 65–67]. Examination of densities, fluxes, or arrival time distributions may be interesting since a new variable is introduced (we shall see later some applications), but at the price of losing the simplicity and directness of the survival probability.

Khalfin showed that when $\omega(E)$ is so bounded from below, the Paley–Wiener theorem [68] requires that

$$\int_{-\infty}^{\infty} dt\, \frac{\ln |A(t)|}{1 + t^2} < \infty. \tag{8}$$

Since the numerator must grow no faster than $\propto t^{2-a}$ with $a > 1$ for this integral to converge as $t \to \infty$, exponential decay is ruled out at sufficiently long times. Assuming that it is bound,

$$P(t) \geq \mathcal{A} e^{-\beta |t|^q}, \tag{9}$$

with $\mathcal{A} > 0$, $\beta > 0$, and $q < 1$. An alternative proof, avoiding the Paley–Wiener theorem, has been given by Nicolaides and Beck [20, 69].

1.1.1. Long-time decay through energy integrals

If the energy density is known, analytic approximations to the post-exponential contribution to $P(t)$ may be found by replacing the integration path in Eq. (5) by a contour integral in the complex plane [13, 20, 70, 71]. We set the origin of energy at threshold, $E_m = 0$, and choose a closed contour consisting of the positive real energy axis, a quarter circle of infinite radius running clockwise from the positive real axis to the negative imaginary axis, and continuing to the origin. Under very general conditions, integration along the circular arc gives a vanishing contribution. Then,

$$A(t) = \int_0^{\infty} dE\, \omega(E)\, e^{-iEt/\hbar}$$

$$= \oint dE\, \omega(E)\, e^{-iEt/\hbar} + \int_0^{-i\infty} dE\, \omega(E)\, e^{-iEt/\hbar} \equiv A_p(t) + A_v(t), \tag{10}$$

where we have analytically continued $\omega(E)$ into the lower half of the complex plane. Depending on the analytic structure of $\omega(E)$, this may or may not be a simple task. The contour integral $A_p(t)$ is $2\pi i$ times the sum of residues of poles in the fourth quadrant, they are exponentially decaying terms.

The integral along the imaginary axis, $A_v(t)$, gives the dominant contribution to the decay at long times. We write the variable of integration as $\tilde{E} = iE$ to obtain

$$A_v(t) = i \int_0^{\infty} d\tilde{E}\, e^{-\tilde{E}t/\hbar}\, \omega(-i\tilde{E}). \tag{11}$$

After many lifetimes, say when $t \gg \tau = \hbar/\Gamma$, with Γ the width of the lowest lying resonance in $\omega(E)$, $A_p(t)$ becomes negligible. At such times t, the exponential factor in Eq. (11) restricts the range of significant contributions to the integral to energies close to threshold, $\tilde{E} \ll \Gamma$.

A simple example showing this is a pure Lorentzian energy density,

$$\omega_L(E) = \frac{\Gamma/(2\pi)}{(E - E_R)^2 + \Gamma^2/4}.$$ (12)

In Section 2.2 we show how this appears approximately for a discrete state coupled to a continuum. (See also Ref. [13] for a similar but more elaborate model.) This energy density has a pole at $E = E_R - i\Gamma/2$, giving the exponential decay contribution

$$A_p(t) = e^{-iE_R t/\hbar}\, e^{-\Gamma t/2\hbar}.$$ (13)

Moreover, when $t \to \infty$,

$$A_v(t) = i\frac{\Gamma}{2\pi} \int_0^\infty d\tilde{E}\, \frac{\exp(-\tilde{E}t/\hbar)}{(-i\tilde{E} - E_R)^2 + \Gamma^2/4} \simeq i\frac{\Gamma}{2\pi} \frac{\hbar}{E_R^2 + \Gamma^2/4} \frac{1}{t} + \mathcal{O}\left(\frac{1}{t^2}\right),$$ (14)

where we have set $\tilde{E} = 0$ in the denominator to evaluate the integral. The asymptotic prediction of this model, when the exponential term in Eq. (13) becomes negligible, is $P(t) \simeq |A_v(t)|^2 \propto t^{-2}$.

Due to the phase $-E_R t/\hbar$ in $A_p(t)$, in the range of times where the two contributions are of similar magnitude, interference oscillations may occur. For a complete analysis of the decay for a more realistic truncated Lorentzian, including an exact expression for $A(t)$ and additional terms in the expansion of $A_v(t)$, see, e.g., Ref. [72].

When E_R decreases toward threshold, at $E_m = 0$, the pole moves towards the negative imaginary axis and the value of $A_v(t)$ increases, eventually making it comparable to $A_p(t)$. In the limit $E_R = 0$ the above decomposition is invalid, implying that the decay ceases to be exponential. This is known as small Q-value decay. For a theoretical analysis of this case and some examples, see Refs. [29, 30]. Small Q-value decay becomes noticeable when $Q \equiv E_R - E_m \leq \Gamma/2$.

The above model has become popular in discussions of exponential decay [73], but Eq. (12) is far from being realistic for the energy density, in particular for the asymptotic law, since the Lorentzian form is generally not valid near threshold.

2. EXAMPLES AND SIMPLE MODELS

Before launching into a discussion of post-exponential decay, it is useful to understand why exponential decay should be the norm in a quantum system, even though sometimes it holds over a limited time interval, or only approximately. The Gamow and Weisskopf–Wigner theories provide a clue,

but a fresh look at the survival amplitude, Eq. (2), could raise doubts about the robustness of exponential decay, since a suitably chosen initial state $\Psi(0)$ and energy density can produce virtually any decay law [74]. This puzzle is perhaps easier to understand in discrete–continuum decay models [75] (see below), and it has also been discussed in the context of scattering processes, e.g., in Refs. [13, 46]. If the initial preparation localizes the wave, it will overlap prominently with scattering wave functions in certain regions of the energy spectrum close to resonant poles, since they are more localized in the interaction region than are ordinary, nonresonant waves. Contributions from broad resonances will decay faster, whereas for a narrow resonance the analytical structure of the pole dominates the behavior, rather than the complete state amplitude, leading in practice to an "effective" Lorentzian energy density and to exponential decay.

2.1. Discrete state embedded in a continuum

As a first example we consider a nondegenerate single-channel system with a simplified Hamiltonian in which continuum–continuum interactions have been neglected:

$$\mathcal{H} = E_\phi |\phi\rangle\langle\phi| + \int dE\, E\, |E\rangle\langle E| + \left\{ \int dE\, W(E)\, |\phi\rangle\langle E| + h.c. \right\}. \qquad (15)$$

Other variants are due to Fano [76], Anderson [77], Lee [78], and Friedrichs [79] and have been successfully applied to study, for example, autoionization, photon emission, or cavities coupled to waveguides. The dynamics can be solved in several ways, using coupled differential equations for the time-dependent amplitudes and Laplace transforms or finding the eigenstates with Feshbach's (P,Q) projector formalism [80], which allows separation of the inner (discrete) and outer (continuum) spaces and provides explicit expressions ready for exact calculation or phenomenological approaches. For modern treatments with emphasis on decay, see Refs. [31, 81]. Writing the eigenvector as [31, 76]

$$|\Phi_E\rangle = |\phi\rangle\langle\phi|\Phi_E\rangle + \int dE'\, |E'\rangle\langle E'|\Phi_E\rangle \qquad (16)$$

and using Laplace transform techniques or the projector P,Q formalism, the coefficients for the discrete state are given by

$$|\langle\phi|\Phi_E\rangle|^2 = \frac{|W(E)|^2}{[E - E_\phi - F(E)]^2 + \pi^2|W(E)|^4}, \qquad (17)$$

where $F(E)$ is the principal value integral

$$F(E) = \mathcal{P} \int dE' \frac{|W(E')|^2}{E - E'}. \tag{18}$$

The essence of the Weisskopf–Wigner approximation is to suppose that $W(E) \to W$ is energy independent. Then, if the range of integration is extended from $-\infty$ to ∞, $F(E) \to 0$ and $|\langle \phi | \Phi_E \rangle|^2$ becomes a Lorentzian,

$$|\langle \phi | \Phi_E \rangle|^2 = \frac{\Gamma/2\pi}{(E - E_\phi)^2 + \Gamma^2/4}, \tag{19}$$

with $\Gamma = 2\pi |W|^2$. If the initial state is ϕ, the energy density is a Lorentzian (Breit–Wigner form) and, as shown in Section 1, its survival probability takes the exponential form:

$$P(t) = e^{-\Gamma t/\hbar}. \tag{20}$$

If the coupling of bound state to continuum is weak, the resonance is long-lived and its width small, so that the constant-W approximation is a good one. However the energy threshold limits its validity. If the resonance energy is close to threshold, this effect will be more noticeable, or even dominant, so that the decay may become totally nonexponential [29, 30].

2.2. Models expressed in the momentum representation

In potential scattering models the basic "mathematical" reason for exponential decay is a complex pole in the fourth quadrant of the momentum complex plane (second Riemann sheet of the energy plane), which, through its exponentially decaying residue, dominates the dynamics for some time. A simple analytical example of the deviation from exponentiality follows from the integral expression for the survival amplitude,

$$A(t) = \langle \Psi_0 | e^{-iHt/\hbar} | \Psi_0 \rangle = \frac{i}{2\pi} \int_C dq \, e^{-izt/\hbar} I(q), \tag{21}$$

where

$$I(q) = \frac{q}{m} \left\langle \Psi_0 \left| \frac{1}{z - H} \right| \Psi_0 \right\rangle, \tag{22}$$

$z = q^2/2m$, and C runs from $-\infty$ to ∞, above all singularities in the lower half complex momentum (q) plane. One-dimensional (1D) motion of a particle of mass m is assumed. Consider now a pole expansion of the form $I(q) = \sum a_k/(q - q_k)$ [3, 82]. Each term can be analyzed separately and later combined linearly, so we concentrate on a single pole, $I(q) = a_r/(q - q_r)$, with q_r assumed to lie above the diagonal of the fourth quadrant and below the

real axis. The integral is evaluated by deforming the contour to run diagonally across the second and fourth quadrants and picking up a "keyhole" contribution from an infinitesimal circle surrounding the pole. This gives

$$A(t) = \frac{1}{2}a_r w(-u_r) = a_r \left\{ \exp\left(-u_r^2\right) - \frac{1}{2}\text{sgn}[\Im(u_r)]w[\text{sgn}[\Im(u_r)]u_r] \right\}, \quad (23)$$

where

$$u_r = q_r/f, \quad f = (1-i)(m\hbar/t)^{1/2}, \quad (24)$$

and $w(z) = \exp(-z^2)\text{erfc}(-iz)$.[2] We have used the relation

$$w(-z) = 2e^{-z^2} - w(z). \quad (25)$$

Equation (23) separates exponential decay, explicitly given by the pole, and its deviation, given by the line integral along the diagonal, evaluated as a w-function. This function has an asymptotic expansion [83, 84]

$$w(z) \sim \frac{i}{\sqrt{\pi}z}\left(1 + \frac{1}{2z^2} + \cdots\right), \quad (26)$$

which, for long times, leads to a $1/t^{1/2}$ behavior. However, an $I(q)$ with a single pole is incompatible with time-reversal symmetry, $A(t) = A(-t)^*$, so the minimal model compatible with time reversal must include, in addition to the resonance at q_r, the antiresonance pole at $-q_r^*$,

$$I(q) = \frac{a_r}{q - q_r} + \frac{a_r^*}{q + q_r^*}, \quad (27)$$

with $a_r = 1 + i\Im q_r/\Re q_r$ [85] (for an application see e.g. Ref. [58]). The contour integral along the diagonal of the complex plane does not enclose this antiresonance pole, so it provides not an exponentially decaying term, but an additional contribution (the $w(u_r)$ function) that is significant only at short and long times [85]. In particular, it exactly cancels the asymptotic $t^{-1/2}$ decay from the resonance pole. However, the second terms in Eq. (26) do not cancel, resulting in a leading $t^{-3/2}$ behavior for $A(t)$.

This model so far is not Hamiltonian, but Hamiltonian realizations are possible. The separable potential considered in Refs. [59, 60, 82] leads to three core (state-independent) poles, two of them forming a resonance/antiresonance pair. Even closer to the minimal decay model is the delta-shell potential discussed in the next section, when only the lowest resonance is excited

---

[2] $\int_{-\infty}^{\infty} \frac{e^{-u^2}}{u-z}\,\mathrm{d}u = i\pi\,\text{sgn}[\Im(z)]\,w\{z\,\text{sgn}[\Im(z)]\}$

and higher resonances can be neglected. Then it is exactly described by Eq. (27).

Independent of the assumed pole expansion, a general and useful result follows from noting that if the resolvent matrix element in Eq. (21) admits a series expansion, $c_0 + c_1 q + c_2 q^2 + \cdots$, the leading term in the asymptotic formula, obtained by term-by-term integration, is

$$A(t) \sim \frac{c_1}{m\sqrt{2\pi i}} \left(\frac{m\hbar}{t}\right)^{3/2}. \tag{28}$$

c_0 does not contribute by symmetry. For explicit examples see Ref. [59] and for further details Section 4.2.

2.3. Exponential decay as a boundary condition

A minimal, solvable 1D "source" model has been proposed recently by Torrontegui et al. [25]. It consists of imposing an exponentially decaying amplitude for all times at one point in space, $x = 0$. This provides an economical approach which mimics analytically the wave function due to an exponentially decaying system with a long-lived resonance, while avoiding a detailed description of the interaction region where the decaying system is prepared. Deviations from exponential decay are observed in the probability density at $x > 0$. See Section 6.1 for further details; the connection with Winter's model, see Section 3.1, is given in Section 6.3.

2.4. 1D well-barrier model of confining potential

A simple 1D Hamiltonian model of a decaying particle, including a full description of the dynamics from the preparation region, consists of a flat well surrounded by equal square barriers: in units $\hbar = 2m = 1$, we write $\mathcal{V}(x) = -\mathcal{V}_0$ when $-a < x < a$; $\mathcal{V}(x) = \mathcal{V}_b$ when $a < |x| < d$ and $\mathcal{V}(x) = 0$ when $|x| > d$. The initial state is chosen symmetric: $\Psi_0(x) = 1/\sqrt{a}$ $\cos(\pi x/2a)\,\Theta(a - |x|)$ and, for $k^2 = E$ the asymptotic behavior, when $E \to 0$, is easily found to be $\omega(E) \propto k^{-1}$. Applying Eq. (11) one finds

$$A_v(t) \propto t^{-3/2}\,, \quad P(t) \propto t^{-3}. \tag{29}$$

3. THREE-DIMENSIONAL MODELS OF A PARTICLE ESCAPING FROM A TRAP

3.1. Winter's model

It is possible to obtain the energy densities and asymptotic decay profiles for specific potential forms in three dimensions.

The first *explicit* example of the validity of Khalfin's prediction was given by Winter [63]. He studied the motion on the half-line $x \geq 0$, with a delta barrier at $x = a$ and zero potential elsewhere. He took the initial wave function to be the ground state of an infinite well, $\Psi_0(x, t = 0) = \sqrt{2/a} \sin(\pi x/a) \Theta(a - x)$, and showed, by making a few analytical approximations, that the mean momentum and the current at long times deviated from those of pure exponential decay.

Recently the same problem has been reanalyzed by Dicus et al. [86], and indeed they confirmed that the survival probability deviates from exponential at long times. This model and its variants have been applied to study the effect of a distant detector (by adding an absorptive potential) [87], anomalous decay from a flat initial state [44], resonant state expansions [3], initial state reconstruction (ISR) [58], or the relevance of the non-Hermitian Hamiltonian concept (associated with a projector formalism for internal and external regions of space) in potential scattering [88]. In Ref. [88] the model was extended to a chain of delta functions to study overlapping resonances.

Del Campo et al. [89] have also generalized the model for a Tonks–Girardeau gas of N bosons with strongly repulsive contact interactions as well as spinless fermions with strongly attractive contact interactions and studied the long-time asymptotics and some new effects in the decay of these systems.

3.2. Short-range potentials

In three dimensions, spherically symmetric potentials $V(r)$ conserve angular momentum. The wave function can be separated into partial waves or channels of given angular momentum ℓ. The radial Schrödinger equation for each partial wave is

$$\frac{d^2 w_\ell}{dr^2} - \frac{\ell(\ell + 1)}{r^2} w_\ell + [k^2 - \mathcal{V}(r)] w_\ell = 0, \tag{30}$$

where $\mathcal{V}(r) = (2m/\hbar^2) V(r)$, $k^2 = (2m/\hbar^2) E$, and $w_\ell(k, r)/r$ is the radial wave function in channel ℓ. One can extract the threshold behavior of the energy density $\omega(E)$ from the low-energy behavior of w_ℓ and, from there, the time dependence of the post-exponential survival probability. For well-behaved potentials this is a standard exercise in potential scattering theory [90]. These potentials decrease as $1/r^3$ or faster when $r \to \infty$ and are less singular than $1/r^{3/2}$ when $r \to 0+$. We will now summarize the derivation given in Ref. [24]. We work with solutions normalized as

$$\int_0^\infty dr\, w_\ell(k', r)^* w_\ell(k, r) = \delta(k' - k), \tag{31}$$

obeying the boundary condition $w_\ell(k, 0) = 0$. At large distances they take the form

$$\lim_{r \to \infty} w_\ell(k, r) = (2/\pi)^{1/2} \sin(kr - \pi\ell/2 + \delta_\ell), \tag{32}$$

where δ_ℓ is the phase shift for partial wave ℓ. It is also useful to introduce solutions normalized to energy,

$$w_\ell(E, r) = \sqrt{\frac{m}{\hbar^2 k}} \, w_\ell(k, r). \tag{33}$$

These are related to the regular solutions $\hat{\phi}_\ell$ (defined by their behavior as Riccati–Bessel functions $\hat{j}_\ell$, $\hat{\phi}_\ell(r) \sim \hat{j}_\ell(kr)$ when $r \to 0$) by

$$w_\ell(k, r) = \sqrt{\frac{2}{\pi}} \frac{\hat{\phi}_\ell}{|f_\ell(k)|}, \tag{34}$$

where $f_\ell(k)$ is the Jost function defined as in [90]. From the definition, Eq. (5), and particularizing to a single partial wave ℓ,

$$\omega_\ell(E) = |\langle u_i | w_\ell(E) \rangle|^2 = \frac{2m}{\pi\hbar^2} \frac{1}{k} \frac{|\langle u_i | \hat{\phi}_\ell \rangle|^2}{|f_\ell(k)|^2}, \tag{35}$$

where $u_i(r)$ is the radial wave function of the initial state, normalized to unity, and it is assumed that $u_i(r) = 0$ beyond some fixed distance $r = r_a$. Aside from the exceptional case where there is a bound state at zero energy, the Jost function, $f_\ell(k)$, tends to a nonvanishing constant $f_\ell(0)$ as $k \to 0$, and the threshold dependence of the energy density follows from that of $\hat{\phi}_\ell(k, r)$. It can be shown that [90]

$$|\hat{\phi}_\ell(k, r)| \leq \gamma_\ell \left(\frac{|kr|}{1 + |kr|} \right)^{\ell+1} e^{|\text{Im}kr|} \quad \text{as } k \to 0, \tag{36}$$

where γ_ℓ is some constant. This guarantees the desired analytic properties and allows the use of Eq. (10). Since the limiting behavior at small k is that of the Ricatti–Bessel functions, it is clear that when $k \to 0$

$$|\langle u_i | \hat{\phi}_\ell \rangle|^2 \propto k^{2l+2} \Rightarrow \omega(E) \simeq \zeta \, k^{2l+1}, \tag{37}$$

where ζ is a constant.

To evaluate $A_v(t)$, we continue this function to small energy on the negative imaginary axis, $\omega(-i\tilde{E}) \simeq \zeta(-i)^{l+1/2} \tilde{E}^{l+1/2}$. Inserting this into Eq. (11) one finds

$$A_v(t) \simeq -(-i)^{l+3/2} \zeta \, \Gamma(l + 3/2) \, t^{-(l+3/2)}, \tag{38}$$

which is the well-known result that in a well-behaved potential, and in a channel with angular momentum ℓ, decay follows a power law, $P(t) \propto 1/t^{2l+3}$, with integer exponent.

3.3. Long-range potentials

We are now going to discuss how the decay law is modified when the outer tail of the potential decreases more slowly than $1/r^3$ and find cases where the decay is no longer a power law. For simplicity we will consider only s-waves, $\ell = 0$.

3.3.1. Inverse square potentials

The potentials with nonsingular inner part, and decreasing as $1/r^2$ when $r \to \infty$, are interesting for their simplicity and for the range of behaviors exhibited [24]. Physically, attractive inverse square potentials occur as effective radial potentials between a charged wire and a polarizable neutral atom [91], the strength factor being proportional to the square of the linear charge density of the wire and thus controllable [91–93]. If combined with a repulsive centrifugal term, an arbitrary α/r^2 potential can be implemented. It is also possible to modify the inner region and implement a potential minimum by a time-varying sinusoidal voltage in the high-frequency limit [93] or by replacing the wire by a charged optical fiber with blue detuned light propagating along the fiber with the cladding removed [92]. Decay experiments with cold atoms, showing exponential laws, have been performed [91], and the ability to modify the potential parameters makes the observation and study of the long-time power law in these systems a realistic prospect.[3]

For s-waves, when $E \to 0$,

$$w(E,r) \simeq \sqrt{\frac{2mk}{\pi \hbar^2}} \frac{1}{|f(k)|} \phi_0(r), \tag{39}$$

where we have omitted the subindex $\ell = 0$. We denote by $\phi_0(r)$ the zero energy solution of the Schrödinger equation that satisfies the boundary conditions $\phi(r = 0) = 0$, $(\partial\phi(r)/\partial r)_{r=0} = 1$. It follows that, near threshold,

$$\langle w(E)|u_i\rangle \propto \frac{\sqrt{k}}{|f(k)|}, \qquad \omega(E) \propto \frac{k}{|f(k)|^2}. \tag{40}$$

In subsections 3.2 and 3.3 we used the property that for short-range potentials $f(0) \neq 0$, giving $\omega(E) \propto k$ when $\ell = 0$. For a potential which behaves as

---

[3] Dipole (r^{-2}) potentials occur also as the effective interaction between an electron and an excited hydrogen atom [94] or a polar molecule [95, 96], but control of the interactions is reduced in this case.

$1/r^2$ as $r \to \infty$, this is no longer true, and several cases must be considered. We write the asymptotic ($r \to \infty$) form of the potential as

$$\mathcal{V}(r) \simeq \frac{\alpha}{r^2}. \tag{41}$$

Implying nothing about the inner part and referring only to the tail, we will call potentials with $\alpha > 0$ (resp. $\alpha < 0$) repulsive (attractive). We shall also distinguish between weakly attractive, $-1/4 < \alpha < 0$, and strongly attractive potentials, $\alpha < -1/4$.

Let us now introduce β via $\beta(\beta + 1) = \alpha$. Weakly attractive potentials correspond to $-1/2 < \beta < 0$ and repulsive potentials to $\beta > 0$. In both cases, the solution of the Schrödinger equation at large r can be written as a linear combination of the Ricatti–Bessel functions $\hat{\jmath}_\beta(kr)$ and $\hat{n}_\beta(kr)$, and the order of the corresponding cylinder functions $\nu = \beta + 1/2$ remains positive. Using analytic properties of the Bessel functions as $kr \to 0$, to lowest order in k,

$$|f(k)| \simeq \mathcal{D}\, k^{-\beta} \; ; \qquad \omega(E) \simeq \zeta\, k^{2\beta+1}, \tag{42}$$

where ζ and $\mathcal{D}$ are constants. This is formally similar to Eq. (37) and corresponds to the analogy between the form of $\mathcal{V}(r)$ in Eq. (41) written in terms of β, $\mathcal{V}(r) = \beta(\beta + 1)/r^2$, and the centrifugal term in Eq. (30). We thus find that

$$A_v(t) \simeq -(-i)^{\beta+3/2}\, \zeta\, \Gamma(\beta + 3/2)\, t^{-(\beta+3/2)}, \tag{43}$$

where β may take any real value greater than $-1/2$. The well-behaved potentials considered before always lead to power laws with integer exponents $2\ell + 3$ for the asymptotic survival probability whereas, for repulsive or weakly attractive inverse square tail potentials, the asymptotic decay law is still a power law but with an exponent that can be adjusted by varying the strength β.

In the above discussion we have assumed that there was no intermediate range of times for which the decay was not exponential or mixed, and yet was not fully asymptotic. For attractive potentials this range exists and can be misleading: explicit calculations show a deviation from the exponential decay law that can be well fitted over a sizeable range of times with a power law, but neither the exponent nor the absolute value is well predicted by the above asymptotic expressions. Further details may be found in Ref. [24].

When $\alpha < 1/4$, then ν, the order of the cylinder functions, becomes imaginary, $\nu \to i\nu' = i\sqrt{0.25 - \alpha}$, and the asymptotic form of the Jost function behaves very differently [24, 94, 95]:

$$\frac{|f(k)|^2}{k} \simeq \mathcal{N} \left[\sinh^2(\nu'\pi/2) + \cos^2(\nu' \ln k + \psi) \right]. \tag{44}$$

The expression for ψ is given in Ref. [24]. Obviously, from this expression one cannot derive any simple form of power-law decay for the asymptotic survival probability. Still, using the method of steepest descents, one can write an approximate form for $A_v(t)$ and argue that the decay must be close to $1/t$, as found in explicit numerical calculations.

3.4. Potentials with α/r^p asymptotic decrease, $2 < p < 3$

The threshold dependence of the energy density for these potentials is still given by Eq. (40), so that the small k behavior is again determined by that of the Jost function. Klaus [97] has given the required expressions for the Jost function. He wrote the potential at large $r \to \infty$ as $\mathcal{V}(r) \simeq q_0/r^{2+\epsilon}$, so his q_0 is our α, and $2 + \epsilon$ is our p. He discussed the case $0 < \epsilon \le 1$ and considered two options: (i) $f(0) \ne 0$ and (ii) $f(0) = 0$. The second case is exceptional so we shall only discuss case (i),

$$f(k) = f(0) \left(1 + a_0\, e^{-i\pi\epsilon/2}\, k^\epsilon\right) + \mathcal{O}(k^\epsilon)\,; \qquad a_0 \equiv -\frac{q_0\, 2^\epsilon}{\epsilon(\epsilon+1)}\, \Gamma(1-\epsilon). \quad (45)$$

We have, inserting this into Eq. (40) and keeping only terms up to order k^ϵ,

$$\omega(E) \simeq \Lambda \frac{k}{|f(0)|^2}(1 - \lambda k^\epsilon)\,; \quad \lambda \equiv 2a_0\, \cos\left(\pi\epsilon/2\right), \qquad (46)$$

where Λ is a constant. Now we can determine $A_v(t)$:

$$\begin{aligned}
A_v(t) &= \int_0^{-i\infty} \mathrm{d}E\, \omega(E) e^{-iEt/\hbar} \\
&= i \int_0^\infty \mathrm{d}x\, e^{-xt}\, \Lambda \frac{e^{-i\pi/4}}{|f(0)|^2} x^{1/2} \left(1 - \lambda e^{-i\pi\epsilon/4} x^{\epsilon/2}\right) \\
&= \frac{i\Lambda e^{-i\pi/4}}{|f(0)|^2} \left(\int_0^\infty \mathrm{d}x\, e^{-xt} x^{1/2} - \lambda e^{-i\pi\epsilon/4} \int_0^\infty \mathrm{d}x\, e^{-xt} x^{(1+\epsilon)/2}\right) \\
&= \frac{i\Lambda e^{-i\pi/4}}{|f(0)|^2} \left(\Gamma(3/2)t^{-3/2} - \lambda e^{-i\pi\epsilon/4}\Gamma((3+\epsilon)/2)t^{-3/2-\epsilon/2}\right). \qquad (47)
\end{aligned}$$

We have written $E = -ix$ and therefore $k = e^{-i\pi/4}\sqrt{x}$. $|f(0)|$ plays the role of a normalization factor, so that if we are primarily interested in the "slope" of the post-exponential decay, it is the values of ϵ and q_0 that influence the slope. When t is very large, the second term in Eq. (47) is negligible, and the decay again follows a simple power law with $P(t) \propto 1/t^3$. In contrast, at intermediate times the second term is sizeable and, depending on the value of ϵ, the effective power law will deviate significantly from inverse cubic. When $\epsilon \to 0$, the truncated expansion in Eq. (46) is no longer adequate.

4. PHYSICAL INTERPRETATIONS OF LONG-TIME DECAY

The Paley–Wiener theorem is rigorous and beyond argument, but perhaps not very illuminating from a physical perspective. We have also seen that post-exponential decay can be attributed to the fact that the pole contribution is eventually comparable to or smaller than a line integral, whose value arises predominantly from a saddle point at threshold, associated with slow particles. This is surely more intuitive, yet not fully satisfying for those seeking a more pictorial, rather than a complex-plane, understanding of the phenomenon, e.g., aided by some analogy. In this vein, Hellund proposed an electrostatic analog [52] which relates quantum emission of radiation to the damped oscillation of a charge described in purely classical (stochastic) terms. He interpreted the deviation from exponential decay as a "straggling phenomenon" characteristic of a diffusion process. Since quantum dynamics cannot be generally reduced to a classical diffusion process it would be interesting to explore the general applicability of this concept in other decay models. Other interpretational efforts are reviewed next.

4.1. Initial State Reconstruction: ISR

The so-called ISR [98, 99] provides a powerful, general argument to explain nonexponential decay for the survival probability (although not necessarily for other quantities, see Section 4.3). Let us define, following Feshbach [80], projection operators $P = |\Psi_0\rangle\langle\Psi_0|$ and $Q = 1 - P$. Then

$$
\begin{aligned}
A(t) &= \langle\Psi_0|e^{-iH(t-t')/\hbar}(P+Q)e^{-iHt'/\hbar}|\Psi_0\rangle \\
&= A(t-t')A(t') + \langle\Psi_0|e^{-iH(t-t')/\hbar}\,Q\,e^{-iHt'/\hbar}|\Psi_0\rangle
\end{aligned}
\tag{48}
$$

for any intermediate time t'. When the second term can be neglected, $A(t) = A(t-t')A(t')$, whose solution $A_e(t) = \exp(-\gamma t)$ is the exponential decay law. The neglected term corresponds physically to "ISR": at intermediate times, t', the system is in states orthogonal to $|\Psi_0\rangle$ (in the subspace Q) but at time t it is found again in the "reconstructed" initial state. Since A_e decreases exponentially, we expect that at long enough times, the second term in Eq. (48) cannot in general be neglected, and the exponential regime ceases to be valid. The second term in Eq. (48) is sometimes called the "memory" term, as it implies that quantum mechanics allows one to determine the absolute age of the decaying system [10]. We introduce the following notation:

$$
A_P(t) \equiv A(t-t')A(t') \quad, \quad A_Q(t) \equiv A(t) - A_P(t).
\tag{49}
$$

These amplitudes depend on t and also on t', but we have not written this second dependence explicitly. The survival probability can be decomposed as

$$P(t) = |A_P(t)|^2 + |A_Q(t)|^2 + 2\text{Re}\left[A_P^*(t)A_Q(t)\right], \tag{50}$$

where again each term depends on t'. The third contribution is an interference term. Muga et al. [58] investigated the relative importance of the three terms. If interference is negligible, the reconstruction process is similar to a consistent "classical" history in which we can assign probabilities to alternative paths, and reconstructed states can indeed be located elsewhere at an intermediate time. In simple terms, when the histories are consistent we may say that events have happened in one or the other order with certain probabilities, without the need to invoke virtual paths and complex amplitudes. On the contrary, if interference matters, the reconstruction is not a consistent history [100]. There remains an arbitrariness in the definition of "negligible," since the interference term is often small compared to the others, but rarely zero. In other words, the "consistency" or "classicality" of the histories is not absolute and sharply defined, but a quality that may, nonetheless, be precisely quantified. Calculations done for Winter's model and for the 2-pole model of Section 2 have shown a significant difference between short- and long-time deviations from exponential decay as far as the role of state reconstruction is concerned. It becomes a consistent history for long times but not for short times. Reconstruction, and long-time decay, was hindered by placing an absorber outside the interaction region; more on this later.

4.2. Free motion and post-exponential decay

In a field-theoretical analysis of a scalar particle coupled to two pions, Jacob and Sach [101] found nonexponential terms decaying like $t^{-3/2}$. Their explanation was geometrical: If a particle is produced at point x having velocity between v and $v + dv$, it will appear after a time t within a spherical shell of radius vt centered on x, and the thickness of the shell will be $t\,dv$. The probability that it will be found within a small element of volume within the shell is inversely proportional to the volume $4\pi t^3 v^2 dv$ of the shell. Hence the probability amplitude is proportional to $t^{-3/2}$. This simple picture, unfortunately, cannot be a universal explanation: for example, the decay amplitude in 1D scattering is generically $t^{-3/2}$, see for instance Section 2.4, Eq. (29), whereas the above argument translated to one dimension would give only $t^{-1/2}$. The post-exponential power-law behavior is sometimes interpreted as expressing the dominance of free motion [7, 102], but explicit calculations of the long-time propagator for specific potential scattering models in one dimension show that this is not the case in general. Muga et al. [59] expressed the propagator as an integral in the momentum q-plane,

$$\langle x|e^{-iHt/\hbar}|x'\rangle = \frac{i}{2\pi} \int_c dq\, I(q) \exp\left(-izt/\hbar\right), \qquad (51)$$

$$I(q) = \frac{q}{m} \left\langle x|\frac{1}{z-H}|x'\right\rangle, \qquad (52)$$

where $z = q^2/2m$, and the contour C runs from $-\infty$ to ∞ passing above the singularities of the resolvent. As in Section 2.2, C is then deformed to pass along the diagonal of the second and fourth quadrants so that the long-time dependence is explicitly extracted from the behavior of $I(q)$ at the origin. By decomposing the resolvent according to

$$\frac{1}{z-H} = \frac{1}{z-H_0} + \frac{1}{z-H_0}V\frac{1}{z-H} \qquad (53)$$

(with H_0 the kinetic energy) $I(q)$ separates into "free" and "scattered" parts, $I = I_f + I_s$, which can be calculated for specific models. For 1D motion on the full line, the free motion part gives $I_f = -i/\hbar$, which implies $\langle x|e^{-iH_0t/\hbar}|x'\rangle \sim t^{-1/2}$ at long times, differing from the generic behavior of the propagator (except for the exceptional case of a zero energy pole of the resolvent matrix element). Indeed, one obtains $\langle x|e^{-iHt/\hbar}|x'\rangle \sim t^{-3/2}$ when the interaction is taken into account. This comes about because of a cancellation between free-motion and scattered contributions, i.e., $I_s(0) = -I_f(0) \neq 0$, which can be checked in specific potentials. For motion restricted to the half-line (or three-dimensional (3D) partial waves) both terms vanish, $I_s(0) = I_f(0) = 0$, so both free and scattering components provide generically terms of the same order, $t^{-3/2}$, to the propagator. Exceptions due to zero energy resonances or specially chosen initial states have been considered by Miyamoto [103–105].

4.3. A classical picture of post-exponential decay

Torrontegui et al. have recently resurrected [106] a frequently overlooked observation by R.G. Newton making use of classical mechanics [61, 62]. Newton noted that if a point source emits classical particles with an exponential decay law and with a suitable velocity distribution, the current density away from the source will eventually depend on time according to an inverse power law. Indeed, we have shown that by adjusting the parameters according to the quantum system, the classical model accurately reproduces the onset, power law, and intensity of post-exponential decay of the quantum probability density of a particle escaping from a trap. For simplicity we assume that the particle is restricted to the half-line, $r \geq 0$, as in quantum s-wave scattering. We shall also assume that the initial quantum state is orthogonal to any bound states (or that there are no bound states), so that it must eventually decay (escape) fully from the trap.

4.3.1. Classical and quantum sources and decay

Consider first a source at $r = 0$ which emits classical particles with velocity v from $t_0 = 0$, so that the fraction of particles emitted between t_0 and $t_0 + dt_0$ is

$$P(t_0)dt_0 = \frac{dt_0}{\tau}e^{-t_0/\tau}, \tag{54}$$

where τ is the emission lifetime. The spatial probability density observed at point r, at time t, is

$$P_{c,v}(r,t) = \frac{1}{\tau v}e^{-(t-r/v)/\tau}\theta\left(t - \frac{r}{v}\right), \tag{55}$$

where θ is the step function. For the more general case in which the emitted particles have a velocity distribution $\rho(v)$,

$$P_c(r,t) = \int_{r/t}^{\infty} dv\, \rho(v)\frac{1}{v\tau}e^{-(t-r/v)/\tau}, \tag{56}$$

or, using $r = (t - t_0)v$,

$$P_c(r,t) = \int_0^t dt_0 \frac{1}{(t-t_0)\tau}\rho\left(\frac{r}{t-t_0}\right)e^{-t_0/\tau}. \tag{57}$$

The behavior for $t >>> \tau$ can be expressed as an asymptotic series,

$$P_c(r,t) \sim \sum_{n=0}^{m} \tau^n[g^{(n)}(0) - g^{(n)}(t)e^{-t/\tau}], \tag{58}$$

where

$$g(t_0) \equiv \frac{1}{t-t_0}\rho\left(\frac{r}{t-t_0}\right), \tag{59}$$

and $g^{(n)}$ is its nth derivative with respect to t_0. The leading term is

$$P_c(r,t) \sim g(0) = \frac{1}{t}\rho\left(\frac{r}{t}\right), \tag{60}$$

which is equivalent to Newton's result [61, 62] (we use the probability density rather than the current density). To advance from here, consider the decay from a quantum trap of a system prepared in a normalized nonstationary state $|\Psi_0\rangle$. The wave function of this state at a point r and time t' is

$$\Psi(r,t) = \langle r|e^{-iHt/\hbar}|\Psi_0\rangle, \tag{61}$$

with corresponding probability density $P_q(r,t) = |\Psi(r,t)|^2$. Using stationary states normalized in energy $u_E(r)$ (such that $\langle u_{E'}|u_E\rangle = \delta(E-E')$), and inserting the completeness relation,

$$\Psi(r,t) = \int_0^\infty dE\, \langle r|u_E\rangle\langle u_E|\Psi_0\rangle e^{-iEt/\hbar}. \tag{62}$$

The u_E are solutions of the s-wave, radial Schrödinger equation,

$$\left[\frac{d^2}{dr^2} - v(r) + k^2\right] u_E(r) = 0, \tag{63}$$

where $v(r) = (2m/\hbar^2)V(r)$ and $k^2 = (2m/\hbar^2)E$. As in Ref. [24] or Section 3.2, it is convenient to define new solutions $w_k(r) = \hbar\sqrt{\frac{k}{m}}u_E(r)$ normalized as $\langle w_{k'}|w_k\rangle = \delta(k-k')$, which obey the boundary condition

$$\lim_{r\to\infty} w_k(r) = \sqrt{\frac{2}{\pi}}\sin[kr + \delta(k)], \tag{64}$$

$\delta(k)$ being the phase shift of the s-partial wave. These solutions are related to the regular solutions $\hat{\phi}_k(r)$ (which behave like the Riccati–Bessel function $\hat{j}_0(kr)$ as $r \to 0$),

$$w_k(r) = \sqrt{\frac{2}{\pi}}\frac{\hat{\phi}_k(r)}{|f(k)|}, \tag{65}$$

where $f(k) = |f(k)|\exp(-i\delta)$ is the Jost function. The partial-wave S-matrix element is $S(k) = f(-k)/f(k)$. Zeroes of $f(k)$ in the upper half complex momentum plane correspond to bound states, while those in the lower half plane are associated with scattering resonances.

For an initially localized nonstationary state

$$\langle r|\Psi_0\rangle = 0 \quad \text{for} \quad r > r_a, \tag{66}$$

the wave function can be written as

$$\Psi(r,t) = \frac{2m}{\pi\hbar^2}\int_0^\infty dE\, \frac{1}{k}\hat{\phi}_k(r)\frac{\langle\hat{\phi}_k|\Psi_0\rangle}{|f(k)|^2}e^{-iEt/\hbar}, \tag{67}$$

which has a form similar to the survival amplitude obtained in Section 3.2 [24]. They have generically the same asymptotic behavior at long times, which corresponds to an energy distribution $\rho(E) = |\langle u_E|\Psi_0\rangle|^2 \sim E^{1/2}$, as $E \to 0$. This long-time asymptotic behavior is governed by the properties when $k \to 0$ of the integrand of Eq. (67). For "well-behaved" potentials, the

$\ell = 0$ Jost function tends to a constant when $k \to 0$. (In the exceptional case that a zero energy resonance occurs $f(k = 0) = 0$.) The $\hat{\phi}_k$ behave near the origin as Ricatti–Bessel functions, $\hat{j}_0(kr)$, and are therefore linear in k. The behavior of the integrand near threshold is thus $\sim E^{1/2}$, and the position probability density behaves like $P_q(r,t) \sim t^{-3}$ at long times.

The energy distribution corresponds asymptotically to a velocity distribution since all particles are eventually released. The two distributions are related by

$$\varrho(E)\mathrm{d}E = \rho(v)\mathrm{d}v. \tag{68}$$

Setting $E = \frac{1}{2}mv^2$, m being the mass of the emitted particles, makes $\varrho(E) \sim E^{1/2} \Rightarrow \rho(v) \sim v^2$. Going back to Eq. (60) and considering the long-time regime $t \ggg \tau$, the classical particle velocity can be approximated by $v = r/t$, so $\rho(r/t) = \rho(v)$, which implies, as expected, that at large t the main contribution to the position probability density is from slow particles. If we consider the same dependence as in the quantum case, $\rho(v) \sim v^2$, Eq. (60) implies an asymptotic behavior $P_c(r,t) \sim t^{-3}$, i.e., the classical model leads to the same power-law dependence as the quantum one. Moreover, in the following we shall see that it can be adjusted to provide the correct amplitude factor as well.

Let us return to Eq. (67) and write the bra-ket factor as

$$\langle \hat{\phi}_k | \Psi_0 \rangle = \sqrt{\frac{\pi}{2}} |f(k)| \langle w_k | \Psi_0 \rangle. \tag{69}$$

Using Eq. (65) and the asymptotic behavior given by Eq. (64), the wave function for $r \to \infty$ may be written as

$$\Psi(r,t) \sim \sqrt{\frac{2}{\pi}\frac{m}{\hbar^2}} \int_0^\infty \mathrm{d}E \, \frac{1}{k} \, \langle w_k | \Psi_0 \rangle \, \sin[kr + \delta(k)] e^{-iEt/\hbar}. \tag{70}$$

At low energy, the phase shift $\delta(k)$ is well described by the effective range expansion

$$k \cot \delta(k) = -\frac{1}{a_0} + \frac{1}{2}r_0 k^2 + \cdots, \tag{71}$$

where a_0 is the scattering length, and r_0 is called the effective range of the potential function. The asymptotic form of the resulting integral can be obtained from the Riemann–Lebesgue lemma [107]. Only the main term which depends on the $k \to 0$ behavior of the integrand is kept. This gives a probability density of the form

$$P_q(r,t) \sim \beta \, [r - a_0]^2 \frac{1}{t^3}, \tag{72}$$

where β is now the strength factor for the asymptotic dependence of the velocity distribution, $\rho(v) \sim \beta v^2$, which will depend on the particular state and potential. It has units of $[\beta] \sim v^{-3}$. In the approximation $v = r/t$ we can write

$$\rho(v) \sim \beta \frac{r^2}{t^2}. \tag{73}$$

Introducing this into Eq. (60) we obtain for the classical probability density at long times

$$P_c(r,t) \sim \beta \frac{r^2}{t^3}. \tag{74}$$

We now compare Eqs. (72 and 74) and to avoid confusion, rewrite $r \to r_q$ for the quantum case and $r \to r_c$ for the classical one. We see that if the classical coordinate is shifted by a_0, $r_c = r_q - a_0$, the classical model will reproduce the quantum probability density. Equivalently, $P_c(r) = P_q(r)$ at long times if the classical source is not at the origin but displaced by the scattering length a_0.

In the exceptional case of a potential with a zero energy resonance $a_0 \to \infty$, and therefore the first term on the r.h.s. of Eq. (71) is absent. This causes the Jost function to have a simple zero at $k = 0$, see Ref. [90], and therefore $|\langle w_{k=0}|\Psi_0\rangle|^2$ is nonvanishing. We then find, instead of Eq. (72), that

$$P_q(r,t) \sim |\langle w_{k=0}|\Psi_0\rangle|^2 m/(\hbar t), \tag{75}$$

which is again in agreement with the classical expression (60) taking $\rho(v = 0) = |\langle w_{k=0}|\Psi_0\rangle|^2 m/\hbar$.

4.3.2. Model calculation

Now we check the above general results with Winter's delta-barrier model [63], see Figure 9.1. The initial state is an eigenstate of the infinite square well potential,

$$\langle r|\Psi_0\rangle = \begin{cases} \sqrt{\frac{2}{L}} \sin\left(\frac{n\pi r}{L}\right) & r \leq L \\ 0 & r \geq L \end{cases}, \tag{76}$$

and the k-normalized basis functions are

$$\langle r|w_k\rangle = e^{-i\delta(k)} \sqrt{\frac{2}{\pi}} \begin{cases} \sin(kr)/f(k) & r \leq L \\ (i/2)[e^{-ikr} - S(k)e^{ikr}] & r \geq L \end{cases}, \tag{77}$$

where $S(k) = f(k)^*/f(k)$, and the Jost function for this model is

$$f(k) = 1 + \frac{\alpha}{2ik}(e^{2ikL} - 1), \tag{78}$$
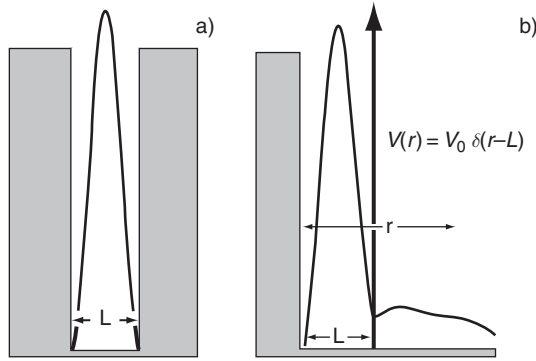
Figure 9.1   Sketch of the Winter model. (a) The initial state is the ground state of an infinite square well. (b) One of the walls is replaced by a delta barrier $V = V_0\delta(r - L)$.

with $\alpha = 2mV_0/\hbar^2$. $\rho(v) = |\langle w_k|\Psi_0\rangle|^2 m/\hbar$ can be calculated exactly and takes the form

$$\rho(v) = \frac{mL}{\pi\hbar}\frac{k^2}{k^2 + \alpha k\sin(2kL) + \alpha^2\sin^2(kL)}\left[\frac{2n\pi\,\sin(kL)}{k^2L^2 - n^2\pi^2}\right]^2. \tag{79}$$

From here the exact classical probability density is calculated numerically using Eq. (57), whereas the quantum density is given by the square modulus of Eq. (62). In the large-t region the probability density has analytical expressions in both quantum and classical cases given by Eqs. (72 and 74), respectively. The coefficient β is easy to find from Eq. (79) in the limit $v \to 0$,

$$\beta = \frac{4m^3L^3}{(1 + \alpha L)^2 n^2\pi^3\hbar^3}. \tag{80}$$

Also, Eq. (77) and $S(k) = e^{2i\delta(k)}$ give for the Winter model the explicit source shift

$$a_0 = \frac{\alpha L^2}{1 + \alpha L}, \tag{81}$$

which, for $\alpha \geq 0$, lies between 0 (for $\alpha L \to 0$, no barrier) and L (for large αL, strong confinement).

Finally, the quantum and classical probability densities both take (shifting the classical point source by a_0) the post-exponential form

$$P_{q,c}(r,t) \sim \frac{4}{n^2(1 + \alpha L)^2}\left(\frac{Lm}{\pi\hbar}\right)^3\left(r - \frac{\alpha L^2}{1 + \alpha L}\right)^2\frac{1}{t^3}. \tag{82}$$
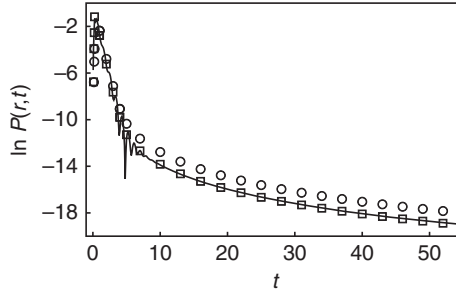
Figure 9.2 The exact probability density obtained numerically versus t: quantum result (solid line); classical solution including the source shift, Eq. (81) (squares); classical solution without applying the source shift (circles). Parameter values: $\hbar = 1$, $m = 1/2$, $L = 1$, $\alpha = 4$, $n = 1$, $r = 2$, $\tau = 0.4$.

The agreement is illustrated in Figure 9.2, where the exact decay curves (numerically integrated) are plotted. The classical density (squares) indeed reproduces the quantum behavior (solid line) if the source shift is taken into account. For comparison we also show a curve in which the shift is not applied, so that the classical source remains at $r = 0$ (circles). Taking the same value for τ, we see that the classical model also agrees with the quantum one in the pre-exponential and exponential zones ($0 < t < 5$ in the drawing). The classical model differs only in the absence of oscillations which occur at the onset of post-exponential behavior, due to quantum interference. The asymptotic behavior is indistinguishable on the scale of the figure from the analytical expression Eq. (82).

The exceptional case of a zero energy resonance corresponds to an attractive delta with $\alpha = -1/L$. In this case from Eqs. (60 and 75) we get

$$P_{q,c}(x,t) \sim \frac{4Lm}{\hbar n^2 \pi^3 t} \tag{83}$$

for both the classical and quantum cases: see Figure 9.3. If α is close to the critical value, say $\alpha = -1/L + \epsilon$, the decay follows a t^{-1} decay law for some substantial period of time until the t^{-3} decay eventually dominates, see Figure 9.4. The smaller is ϵ, the longer does the t^{-1} behavior persist.

The above results, developing the classical model suggested by Newton so as to achieve an accurate match between classical and quantum decays, provide an intuitive physical picture and quantitative description of post-exponential decay of the probability density at points distant from the source. Note that quantum mechanics is required to provide the emission characteristics, but ISR plays no role in the classical, purely outgoing dynamics. We have checked with the methodology of [58] that ISR
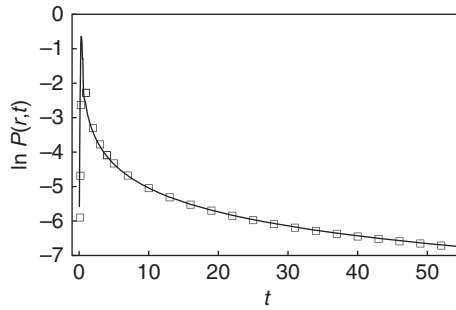
Figure 9.3 Logarithm of the probability density versus t for an attractive delta potential having a zero energy resonance: exact quantum numerical solution (solid line); classical model solution (squares). The long-time behavior is indistinguishable from Eq. (83). $\alpha = -1, \tau = 0.2$, and other parameters as in Figure 9.2.
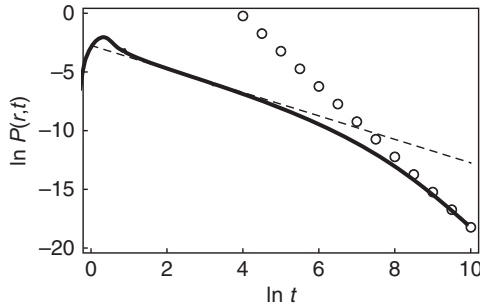
Figure 9.4 Logarithm of the probability density versus t for a delta potential slightly less attractive than required to produce a zero energy resonance: exact quantum numerical solution (solid line) and approximate power-law decays proportional to t^{-1} (Eq. (83), dashed line) and t^{-3} (Eq. (82), circles). $\alpha = -0.98, r = 9, \tau = 0.2$, and other parameters as in Figure 9.2.

terms are negligible in the post-exponential range of times, in the quantum calculation of Figure 9.2. This contrasts with their relevance to the survival probability [58] and indicates different mechanisms for the transition to post-exponential decay inside and outside the source. Indeed, the survival probability $|\langle\Psi(0)|\Psi(t)\rangle|^2$ (as well as $|\langle r|\Psi(t)\rangle|^2$ with $r < L$) is still in its exponential regime when the transition shown in Figure 9.2 (at $r = 2$) takes place, i.e., the purely exponential decay hypothesis (54) for the classical source is justified, and the onset of the post-exponential regime of survival within the trap cannot causally affect the transition observed in the density outside the source.

5. THE PROBLEMATIC EXPERIMENTAL OBSERVATION

As early as 1911, Rutherford looked for experimental deviations from the exponential law in the alpha-decay of ^{222}Ra, but found no deviations up to 27 half-lives. Similar searches have been made over the years, in experiments on the decay of radioactive nuclei and unstable particles, never finding any clear evidence. The experiment of Norman et al. [8] in 1988 is particularly interesting for its accuracy. They observed the decay of a sample of ^{56}Mn, with a half-life of 2.5 h, for a total of 45 half-lives. That corresponds to a reduction of the initial activity by a factor of $\simeq 3 \times 10^{14}$, but no significant deviation from the exponential law was found. (This paper includes a list of prior measurements and their corresponding number of half-lives.) Avignone [108] pointed out, however, that an estimate by Winter implies that deviations from the exponential law would be expected to occur only at times of the order of 200 lifetimes in that experiment, clearly well beyond feasibility. Reference [85] provides simple expressions to estimate the number of lifetimes required for the onset of the nonexponential behavior that are applied to systems discussed by Norman et al. [8].

Other possible reasons for the persistence of exponential decay were summarized by Greenland [10]. As explained earlier, any process suppressing ISR will extend exponential decay to longer times than in an isolated system. In the case of radioactive decay, any fragments leaving the nucleus might interact with the surrounding electrons or with other atoms, suppressing irreversibly the reconstruction of the undecayed state. For the ^{56}Mn experiment it means that the decaying nucleus must not interact with its surroundings for the duration of the experiment.

Long-time deviations from exponential decay have also been sought in particle physics. For a review of experiments up to 1968, see Nikolaev [9]. More recent attempts have similarly failed to detect any deviation. Tomono et al. [109] made precise measurements of the muon lifetime. Their experiment stopped at $17\,\mu$s, around 8 muon lifetimes, whereas theoretical models predict deviations to occur only at times beyond $200\,\mu$s. Novkovic et al. [110] have measured the decay of ^{198}Au up to 25 lifetimes, also finding no evidence for nonexponential decay.

In the field of atomic physics, Robiscoe [111] calculated the long-time correction for the $2P \rightarrow 1S$ transition in a nonrelativistic two-level hydrogenic atom, finding that it would dominate over the exponential term only after 125 lifetimes ($Z = 1$). His calculated modifications to the Lorentzian line shape were also tiny. Assuming a small Γ/E_R ratio, and an atom-field coupling linear in energy (which holds generally for all spontaneous electric dipole processes), he concluded that the deviations are undetectably small for all of the most prominent spontaneous atomic transitions. A more optimistic conclusion was reached by Nicolaides and Mercouris [112] in their study of the decay of an autoionizing state close to threshold, the

He$^-1s2p^2$ ^{4}P core-excited shape resonance, with time-dependent methods. The post-exponential decay occurs in that case after 12 lifetimes.

5.1. Measurement and/or environment effects

5.1.1. Collapse models

Random collapsing interactions have been used to model the effect of the environment (understood in a broad sense that could include the measurement apparatus) on the decaying particle [13, 113]. For example, it is argued that as an unstable elementary particle decays in a bubble chamber, each bubble is a measurement indicating that the particle has not yet decayed (has survived), so that a reduction takes place, resetting the system into the initial undecayed state. The decay law that should be observed in experiment will be therefore an environment-affected $F(t)$ rather than $P(t)$. The probability that the system is not subjected to any measurement in a time interval δt is taken to be $\exp(-\lambda\delta t)$. The survival probability $F(t)$ resulting from these measurements satisfies [13]

$$F(t) = e^{-\lambda t}P(t) + \lambda \int_0^t dt' \, e^{-\lambda t'} P(t')F(t - t'), \tag{84}$$

where $P(t)$ is the survival probability without measurements. The integral is a convolution, and using Laplace transforms one easily finds that $f(s) = \mathcal{L}[F(t)]$ is given by

$$f(s) = \frac{p(s + \lambda)}{1 - \lambda p(s + \lambda)}, \tag{85}$$

where $p(s) = \mathcal{L}[P(t)]$. For the particularly simple case $P(t) = \exp(-\gamma t)$, $F(t) = P(t)$. In general a zero of the denominator of Eq. (85) on the negative real axis gives a contribution to $F(t)$ of exponential form. This term will dominate if the parameter λ is sufficiently large and the corrections to the original lifetime are small. Moreover, the post-exponential regime will be suppressed.

A similar conclusion was reached by Benatti and Floreani [114] with a density operator model for elementary particle decays, taking into account incoherent interactions with the environment.

5.1.2. Unitary model for system–environment coupling

Lawrence [14, 15] studied the effect of interactions with the environment, using a unitary 3D $\ell = 0$ model of a particle confined by a delta-shell potential at $r = a$. Once outside the barrier, the particle interacts with N continuous spins. The interaction Hamiltonian is $H = \eta\Theta(r - a)\sum_{i=1}^{N} S_i$, where the S_i are operators that correspond to projections on a chosen axis of the ith spin and have a continuous spectrum, $S_i|\mu_i\rangle = \mu_i|\mu_i\rangle$, with $\mu_i \in [-1,1]$. This

leads to very simple expressions for the resulting energy density and analytic results for the asymptotic survival probability. Whereas in the absence of environmental coupling the latter shows a t^{-3} dependence, the coupling to N spins leads to $P(t) \sim t^{-2N-3}$, and the exponential regime is extended by a time that increases faster than linearly with N. Although the model is very simple, it provides a convincing demonstration of the relevance of the environment effects and the substantial modifications to the survival probability they entail. It is interesting also that for weak coupling, the dramatic effect at late times is accompanied by a negligible effect at early and intermediate times.

5.1.3. Effects of adiabatic switching and of fluctuations of the interaction

Using the model of Eq. (15) for photoionization, Greenland and Lane [115] studied the effect of laser fluctuations (i.e., fluctuations in discrete to continuum matrix elements). They obtained for the decay rate the usual result, $2\pi W^2$, averaged over the bandwidth and also argued, based on arguments similar to those in Ref. [13], that laser fluctuations eliminate the post-exponential region unless the transition is fast on the timescale of the fluctuations.

The effect of an adiabatic switching-on of the discrete–continuum coupling was examined by Mittelman and Tip [116] and Robinson [117]. The treatment of Robinson is more general and shows, in agreement with Mittelman and Tip, that adiabatic switching can attenuate the correction to exponential decay at long times. However, it differs from Ref. [116] in that the reduction depends on the rise time of the coupling potential instead of the observation time. It thus leaves open the possibility of observing post-exponential decay, in particular for photoionization near threshold. Martorell et al. [118] have recently revisited memory effects due to finite-time switching conditions for the release of the initial state with the analytically solvable model of Section 5.3.

5.1.4. Complex potentials as detector models

The detector model proposed in Refs. [58, 87] is formally Winter's model complemented by an imaginary absorbing potential,

$$H = -\frac{\partial^2}{\partial x^2} + \eta\delta(x-1) - iV_c\Theta(x-X_c)\,, \qquad x \geq 0, \tag{86}$$

and the initial state is as usual the ground state of an infinite well between 0 and 1. This is an "optical model" where the absorbing potential represents the effect of detection of the escaping atom by laser excitation and photon emission in the outer region [119].

This Hamiltonian may hold N_{loc} discrete, localized eigenstates of complex energy with purely exponential decay. The detector is placed at the barrier

edge at $X_c = 1$, or further out. The survival amplitude may be written in terms of eigenstates forming a biorthogonal basis [120],

$$A(t) = \sum_{l=1}^{N_{loc}} C_l \hat{C}_l \, e^{-iE_l t} + \int_0^\infty f(q) \, e^{-i(q^2 - iV_c)t} \, dq, \tag{87}$$

where $C_l = \langle \psi_0 | u_l \rangle$, $\hat{C}_l = \langle \hat{u}_l | \psi_0 \rangle$, $f(q) = \langle \psi_0 | \phi_q \rangle \langle \hat{\phi}_q | \psi_0 \rangle$, and $|u_l\rangle$ and $|\hat{u}_l\rangle$ are, respectively, right and left localized eigenstates. The continuum eigenstates appearing above, $|\phi_q\rangle$ and $|\hat{\phi}_q\rangle$, satisfy

$$H|\phi_q\rangle = E_q|\phi_q\rangle = (q^2 - iV_c)|\phi_q\rangle, \tag{88}$$

$$\langle \hat{\phi}_q | H = E_q \langle \hat{\phi}_q | = (q^2 - iV_c)\langle \hat{\phi}_q |, \tag{89}$$

$$\langle \phi_q | \hat{\phi}_{q'} \rangle = \delta(q - q'). \tag{90}$$

$|\phi_q\rangle$ and its corresponding biorthogonal partner are not the usual scattering states, because the exterior region is not free from interaction ($V(x) \neq 0$ when $x \to \infty$), but the potential is constant there so we can write the solution in the external region in terms of an $\mathcal{S}$-matrix:

$$\phi_q(x) = \frac{1}{(2\pi)^{1/2}} \begin{cases} C_1 \sin kx, & 0 \leq x \leq 1 \\ Ae^{ikx} + Be^{-ikx}, & 1 \leq x \leq X_c \\ e^{-iqx} - \mathcal{S}(q)e^{iqx}, & x \geq X_c \end{cases} \tag{91}$$

where $k = (q^2 - iV_c)^{1/2}$ is the wave number inside, q the wave number outside, and C_1, A,B, and $\mathcal{S}$ are obtained from the matching conditions at $x = 1$ and $x = X_c$. For scattering-like solutions, q is positive. There are two branch points of k in the complex q-plane; we take the branch cut to connect these points. Similarly, the root in $q = (k^2 + iV_c)^{1/2}$ is defined with a branch cut joining the two branch points in the k-plane. In contrast to scattering-like states of the continuum, localized states are characterized by a complex q with positive imaginary part.

At weak intensities, the main effect of increasing V_c is the progressive suppression of long-time deviations, as illustrated in Figure 9.5. Beyond some threshold strength, even the exponential decay is affected. A quantitative approximation to the survival probability helps to understand these effects: Let q_r be the resonance with the longest lifetime and let us assume that it is narrow and isolated. For weak enough absorption, i.e., $N_{loc} = 0$, if all other resonances have already decayed, the integral of Eq. (87) can be approximated, using contour deformation in the complex q-plane, by the residue corresponding to the first resonance plus a saddle contribution,
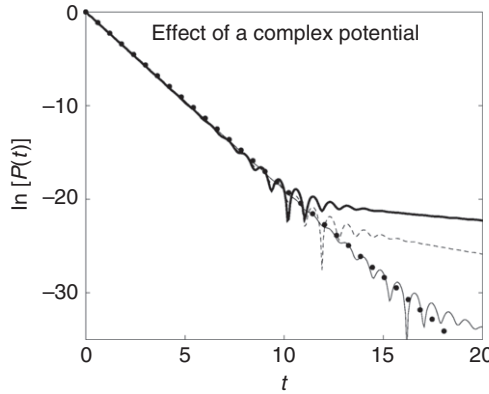
Figure 9.5   ln [P(t)] for different absorptive step potentials, see Eq. (86). $V_c = 0$ (thick solid line), 0.1 (dashed line), 0.3 (thin solid line), and 0.5 (dots). $X_c = 1$ and $\eta = 5$

$$A(t) \approx -2\pi i \operatorname{Res}\left[f(q)\right]_{q=q_r} e^{-i\mathcal{E}_r t} e^{-\Gamma_r t/2} - \frac{\sqrt{\pi i}}{8} \ddot{f}(0) e^{-V_c t} \frac{1}{t^{3/2}}, \qquad (92)$$

where $\mathcal{E}_r$ represents the energy of the decaying particle, Γ_r the corresponding decaying width, and $\ddot{f}(0) = [d^2 f(q)/dq^2]_{q=0}$. The second term is responsible for the deviation from the exponential decay. The novelty with respect to the nonabsorption case, $V_c = 0$, is that the deviation is not given by a purely algebraic term: the usual algebraic dependence is multiplied by the exponentially decaying factor $\exp(-V_c t)$. By increasing V_c, the deviation term decays more and more rapidly until, at threshold, i.e., $\Gamma_r = V_c^{\text{th}}$, the deviation decays faster than the residue term. This threshold value corresponds exactly to the passage from a resonance to a localized, normalizable state with purely exponential decay. While for $V_c < V_c^{\text{th}}$, the dominant term at long times is the saddle contribution (proportional to $\exp(-V_c t) t^{-3/2}$), in the opposite case, $V_c > V_c^{\text{th}}$, the decay is purely exponential, and the dominant contribution comes from the discrete part of the spectrum.

5.1.5. Effect of a distant detector on the survival probability
How is the decay affected by the distance between detector and system in indirect measurements? This is still a controversial and rather crucial question [121–130]. Home and Whitaker [123], in their conceptual analysis of the Zeno effect [123] stated that the only real paradox is that the system is predicted to have its decay affected by a detector at a macroscopic distance. Indeed, a commonsense expectation is that a greater separation of the detector from the initial location of the system ought to reduce the perturbing effects of measurement, but theories confirming this expectation have been

disputed [121, 122, 127]. The need for more work to arrive at a definite conclusion is clear [126]. In Ref. [87], with the Hamiltonian model of Eq. (86), it was shown that the disturbance of the measurement (represented by a complex absorbing potential) on the survival amplitude disappears with increasing distance X_c between the initial state and the detector, as well as by improving its efficiency.

5.1.6. Experimental observation of power laws in organic molecules, quantum dots, or nanocrystals

In view of the arguments favoring persistence of exponential decay at long times, and of perturbing environmental effects on the power-law decay, it came as a surprise that the experiments of Rothe et al. [16] showed a clean power-law decrease after the crossover from the exponential regime. The luminescence decays of several species of dissolved organic molecules were measured, most with lifetimes of the order of nanoseconds, but some up to a tenth of a millisecond. Power-law decays with algebraic exponents between $\simeq 2$ and $\simeq 4$ were deduced. The strategy followed was to look for resonant decays with large Γ and not too small E_R. As shown in Eq. (14), larger Γ increases the asymptotic component and not too small E_R avoids small Q nonexponential decay. Having the molecules in solution increases the widths, and for large molecules, intramolecular structure also favors increased broadening. In this case, environmental effects increase rather than decrease the asymptotic terms.

The theoretical description of luminescence decay in such organic molecules is unfortunately difficult [131–133], and a detailed comparison with theory is missing. The possibility of other origins for the observed power-law decrease in fluorescence has been ruled out by Rothe et al. [16]. Still, very recently Sher et al. [134] have also measured power-law decay in the fluorescence blinking of various semiconductor nanocrystals. They reproduced those with Monte Carlo simulations on a three-level model. These authors claim that their approach can be also useful in the analysis of nonexponential fluorescence decays of molecular systems. In fact colloidal semiconductor quantum dots, nanorods, nanowires, and some organic dyes exhibit power-law distributions of on- and off-times of emission intermittency [135]. They can be explained with models in which an electron jumps into one of the multiple traps and returns, but not all facets of the experiment are well understood. In condensed molecular solids composed of conjugated polymers [37], the power-law luminescence found experimentally is attributed to electron–hole pair recombination and explained using inhomogeneous, statistical theories. Therefore, the field is still open, both theoretically and experimentally, and more conclusive work on these systems would be highly desirable.

5.2. Indirect measurement

Kelkar et al. [136] proposed to extract the long-time survival probability from the low-energy $\ell = 0$ phase shift of α–α scattering, where it is affected by a 2^+ resonant state (virtual formation of ^{8}Be). By fitting the experimental phase shift to a parameterized form, they extracted a power-law behavior $1/t^{6.36}$ for $P(t)$. The explanation for this value is murky, since the long-range part of the α–α potential is dominated by Coulomb repulsion, and the post-exponential decay law should be modified by that long-range potential tail. Applying the recipe for well-behaved potential tails with $\ell = 2$, the exponent would be 7. The result is nevertheless interesting, as it is a different way to approach the problem, which may have application to other systems. Their result corresponds to an estimated changeover time of 30 lifetimes, which makes a direct observation unfeasible.

5.3. Optical analogy of quantum decay

Recently Longhi [27, 137] proposed to use a system of identical parallel waveguides as an analog of a decaying quantum system. A laser beam injected in the first guide leaks amplitude to the second as it travels down the guide. The second guide similarly leaks to the first and third, and so on. Distance along the guide plays the role of time. Let $c_n(t)$ be the amplitude in the guide labeled n at distance t from the point of injection. The system is equivalent to a particle in a tight-binding model with a discrete Hamiltonian

$$H_{TB} = \Delta[|1><2| + |2><1|] + \sum_{n=2}^{\infty} [|n><n+1| + |n+1><n|] \quad (93)$$

in units of g, the coupling parameter between adjacent sites. The site energy ε_0 has been set to zero. Site one is special; its coupling parameter is $g\Delta$, with $0 \leq \Delta \leq 1$. For example, if the first waveguide is placed farther apart from its neighbor, then we expect $\Delta < 1$, and if its profile is different, its site energy ε_1 could differ from ε_0.

The exact time-dependent solution for site 1 is

$$c_1(t) = \sum_{s=0}^{\infty} \alpha^{2s} \frac{2s+1}{t} J_{2s+1}(2t), \quad (94)$$

which plays the role of the survival amplitude. Here, $\alpha^2 \equiv 1 - \Delta^2$ is the "decoupling" parameter. If $\Delta = 0$ (by placing the first guide far from the rest of the system), a well-known sum rule satisfied by the Bessel functions gives $c_1(t) = 1$ at all times. At the other extreme, for $\Delta \sim 1$, small α^2 makes the series converge rapidly.

For sites $n > 1$, the solution is

$$c_n(t) = i^{n-1} \Delta \sum_{s=0} \alpha^{2s} \frac{2s+n}{t} J_{2s+n}(2t) \,. \tag{95}$$

Because $J_N(2t) \sim t^N/N!$ at small t, it is clear that the initial conditions at $t = 0$ have been satisfied.

Longhi showed that there are three distinct regions of t-dependence. At small t, from the properties of $J_1(2t)$,

$$c_1(t) \approx 1 - t^2/2. \tag{96}$$

Next there is an intermediate time region where exponential decay holds, with

$$c_1(t) \approx \frac{1+\alpha^2}{2\alpha^2} \exp\left[-\gamma_0 t/2\right], \quad \text{where} \quad \gamma_0 = \Delta^2/\alpha \tag{97}$$

is the decay constant of the Gamow state. Weak coupling gives very slow decay, and strong coupling $\Delta \sim 1$ very rapid decay. At still longer t, the exponential has fallen so far that it is smaller than the asymptotic value of the sum of Bessel functions. In this limit we use the asymptotic form of each term and perform the sum to obtain an asymptotic value for $c_n(t)$.

Use of the asymptotic approximation

$$J_{n+2s}(2t) \to \frac{(-)^s}{\sqrt{\pi t}} \left[\cos \Phi_n - \frac{4(n+2s)^2 - 1}{16t} \sin \Phi_n\right] ;$$

$$\Phi_{n+2s} \equiv 2t - \left(n + \frac{1}{2}\right)\frac{\pi}{2} - s\pi \tag{98}$$

leads, in lowest order, to

$$c_n(t) \to \Delta \frac{i^{n-1}}{\sqrt{\pi t^3}} \frac{n + (n-2)\alpha^2}{(1+\alpha^2)^2} \cos\left(2t - (2n+1)\frac{\pi}{4}\right) ;$$

$$c_1(t) \to \frac{1}{\sqrt{\pi t^3}} \frac{1 - \alpha^2}{(1+\alpha^2)^2} \cos(2t - 3\pi/4). \tag{99}$$

These expressions are improved by adding the next-to-leading order term from Eq. (98), but it is already evident that the post-exponential survival probability is a power law with exponent -3.[4]

---

[4] The long-time regime has been studied also for finite-time switching in Ref. [118] and to examine its observability as a function of distance in Ref. [25].

It turns out to be an excellent approximation to write $c_1(t)$ as the sum of the exponential term plus the asymptotic approximation, for all but the very shortest times t. The survival amplitude then becomes

$$c_1(t) \approx \frac{1 + \alpha^2}{2\alpha^2} \, e^{-\gamma_0 t/2} + \frac{S_1}{t} J_1 \left(2t - \frac{a_1}{t}\right) \tag{100}$$

for $t \gg a_1$, where the amplitude S_1 and phase a_1 are

$$S_1 = \frac{1 - \alpha^2}{(1 + \alpha^2)^2}, \qquad a_1 = \frac{6\alpha^2}{(1 + \alpha^2)^2} + \frac{3}{16}. \tag{101}$$

The quality of the approximation is illustrated in Figure 9.6 for the case $\alpha^2 = 0.5$. In the crossover region the interference oscillations are nicely reproduced, showing that their phases are correct. The next-to-leading order asymptotic correction makes a clear improvement in the description (upper curves). When $\alpha^2 = 0.1$, there is almost no exponential region, while for large $\alpha^2 = 0.9$, the exponential region would extend to $t \sim 200$ in dimensionless units.

We have recently investigated initial switching effects in this model. It was assumed that the coupling between the first and second sites $\Delta \rightarrow \Delta(t)$ was ramped up from zero to its final value over a time interval T, rather
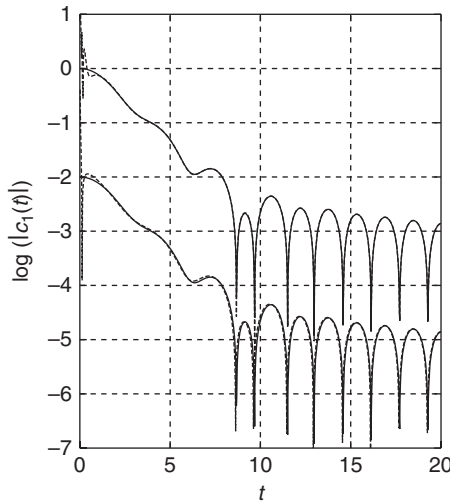
Figure 9.6 Log modulus of survival amplitude for $\alpha^2 = 0.5$ versus t in dimensionless units, in Longhi's discrete model. Solid lines: exact analytical solution; dashed line: approximation of Eq. (100) (upper curve) and Eq. (99) (lower curve, offset by two decades).

than instantaneously at time zero [118] as usually assumed. The result is an additional phase shift T added to a_1 in Eq. (101), and S_1 is multiplied by $\sin T/T$. Together these changes alter the interference between exponential and asymptotic decay contributions in a way which ought to be observable [118].

The group in Milan have carried out two experiments which verify Longhi's theory. In the first [28], they arranged $\Delta = 1$ ($\alpha = 0$), and the amplitude in guide n followed the expected form of the Bessel function $c_n(t) \sim J_n(2t)/t$ [138]. In the second [139], they verified the optical analog of the Zeno effect. To do this, the waveguides were broken into longitudinal segments of length $t = L$. The beam in guide $n = 1$ entering a new segment effectively resets the initial condition (albeit with a reduced amplitude less than unity). The segment length L was chosen to be short, to correspond to the short-time behavior Eq. (96). What they found was that the decay of $c_1(t)$ in each short segment was reset to the quadratic behavior, so that it never reached the exponential decay regime. On the contrary, without segmentation they did see a switch-over to Eq. (97). It will be interesting to see if their experiment can be taken to longer length scales to demonstrate the changeover to post-exponential decay described in Eq. (100).

6. ENHANCING POST-EXPONENTIAL DECAY VIA DISTANT DETECTORS

Most of the proposals to enhance post-exponential decay, making it more visible by advancing its onset time, are based on the idea of observing the survival probability for a resonance close to threshold ("small Q-value decay") [16, 26, 29, 30, 140, 141] or, more precisely, with energy release comparable to resonance width. This is a rare configuration in naturally decaying systems, such as radioactive isotopes [16], or it leads to difficult measurements [115, 136, 141], and realizing it in artificial structures, although possible in principle, is still a pending task [29, 30]. The only realization so far may be the experiment on organic molecules in solution, mentioned in Ref. [16], but this is a rather complex system and its analysis from first principles has not yet been done, so the true mechanism behind the observed data remains to be confirmed, see the discussion in 5.1.6. Another idea is to use the escape of interacting cold atoms from a trap, in the strongly interacting Tonks–Girardeau regime, to enhance the signal [89]. Again, the corresponding experiment has yet to be performed.

In the present section we discuss a quite different strategy with the important advantage of simple implementation. We show, using solvable decay models, that by increasing the distance of the observation point from the source, the transition from exponential to post-exponential decay occurs at higher probability densities and thus becomes more easily observable. Finally, note that when the distance is too large the exponential decay regime

disappears, and with it the transition, so that only nonexponential decay should be observed [61].

6.1. Exponentially decaying source model

In these "source models," unlike the usual initial value problem, the wave function is specified for all times at one point of coordinate space. A simple, solvable 1D case corresponds to switching-on the source suddenly at $T = 0$, with a well-defined "carrier frequency" $\Omega_0 > 0$,

$$\Psi(0, T) = \Theta(T)e^{-i\Omega_0 T}, \tag{102}$$

zero external potential, $V = 0$, and a vanishing wave everywhere (for all X) before the source is switched on, i.e., for $T < 0$. Here we work through a case that was examined recently [106] namely a complex carrier frequency $\Omega_0 = \Omega_{0R} + i\Omega_{0I}$.

We assume a negative imaginary part, $\Omega_{0I} < 0$, so that the density at the source point decreases exponentially,

$$|\Psi(0, T)|^2 = e^{-2|\Omega_{0I}|T}. \tag{103}$$

The real part Ω_{0R} is chosen to be positive so as to generate outgoing waves and thus mimic the behavior of resonance decay above threshold, in the outer region. This provides a simple solvable model for an exponentially decaying system with a long-lived resonance, while avoiding a detailed description of the interaction region in which the decaying system is prepared.

The dynamics of a particle in free space, $V = 0$, is given by the Schrödinger equation

$$i\hbar \frac{\partial \Psi}{\partial T} = -\frac{\hbar^2}{2m} \frac{\partial^2 \Psi}{\partial X^2}. \tag{104}$$

Introducing dimensionless quantities for position, time, and wave function, in terms of some characteristic length L, the number of variables is reduced,

$$x = X/L, \tag{105}$$

$$t = \frac{T\hbar}{2mL^2}, \tag{106}$$

$$\psi(x, t) = L^{1/2}\Psi(X, T). \tag{107}$$

L may be chosen for convenience and we take it as K_{0R}^{-1}, where $K_0 = (2m\Omega_0/\hbar)^{1/2} = K_{0R} + iK_{0I}$ is the dimensioned complex wave number and K_{0R} its real part. The branch cut is drawn just below the negative real axis so that for $\Omega_{0I} < 0$ the imaginary part of K_0 is negative, $K_{0I} := \text{Im}(K_0) < 0$. Defining dimensionless wave number and carrier frequency as $k_0 = K_0 L$ and

$\omega_0 = \Omega_0 2mL^2/\hbar = k_0^2$, this election fixes the real part of the dimensionless wave number to be unity, $k_{0R} = 1$, and the dimensionless dispersion equation becomes

$$\omega_0 = k_0^2 = (1 + ik_{0I})^2, \tag{108}$$

where k_{0I} is the imaginary part, $-1 < k_{0I} < 0$. In terms of these new variables, the Schrödinger equation (104) is now

$$i\frac{\partial \psi(x,t)}{\partial t} = -\frac{\partial^2 \psi(x,t)}{\partial x^2}, \tag{109}$$

and the dimensionless continuity equation is

$$\frac{\partial \rho(x,t)}{\partial t} + \frac{\partial J(x,t)}{\partial x} = 0, \tag{110}$$

where

$$\rho(x,t) = |\psi(x,t)|^2, \tag{111}$$

$$J(x,t) = 2\,\mathrm{Im}\left[\psi^*(x,t)\frac{\partial \psi(x,t)}{\partial x}\right] \tag{112}$$

are the dimensionless probability and current densities. We are interested in waves that decay exponentially in time so the Schrödinger equation must satisfy boundary conditions at the origin

$$\psi(0,t) = e^{-i\omega_0 t}\theta(t), \quad \omega_{0R} > 0, \omega_{0I} < 0, \tag{113}$$

and at infinity, where the wave remains bounded as $x \to \infty$, which guarantees that the wave function does not diverge at $x = \infty$.

To find the solution for $x > 0$ we make the ansatz

$$\psi(x,t) = \int_{-\infty}^{\infty} d\omega\, A(\omega)\, e^{i\sqrt{\omega}x}\, e^{-i\omega t} \tag{114}$$

and determine the function $A(\omega)$ from the boundary condition (113),

$$\psi(0,t) = e^{-i\omega_0 t}\theta(t) = \int_{-\infty}^{\infty} d\omega\, A(\omega)e^{-i\omega t}. \tag{115}$$

Inverting the Fourier transform we obtain

$$A(\omega) = \frac{i}{2\pi(\omega - \omega_0)}. \tag{116}$$

The resulting integral for $\psi(x,t)$ is done most easily in the complex k-plane,

$$k = \sqrt{\omega}. \tag{117}$$

Inserting Eq. (117) into Eq. (114), deforming the contour in the complex k-plane, and using Cauchy's theorem to evaluate the above integral leads finally to

$$\psi(x,t) = \frac{1}{2}e^{ik_s^2 t}\left[w\left(-u_0^{(+)}\right) + w\left(-u_0^{(-)}\right)\right], \tag{118}$$

where $w(z) := e^{-z^2}\text{erfc}(-iz)$ is the Faddeeva (or w) function [83, 84],

$$u_0^{(+)} = u(k_0) = (1+i)\sqrt{\frac{t}{2}}k_0(1-\tau/t), \tag{119}$$

$$u_0^{(-)} = u(-k_0) = -(1+i)\sqrt{\frac{t}{2}}k_0(1+\tau/t), \tag{120}$$

and the modulus of the complex time

$$\tau = \frac{x}{2k_0} \tag{121}$$

generalizes the Büttiker–Landauer traversal time, at least formally, in the present context [142]. Finally as the parameter k_0 will be varied, for a fair comparison of this parameter the number of the emitted particles must be fixed, so the wave function must be normalized. The normalization constant is obtained integrating the continuity equation, Eq. (110),

$$N_+(t=\infty) = \int_0^\infty dt\, J(0,t), \tag{122}$$

where

$$N_+(t) = \int_0^\infty dx\, \rho(x,t) \tag{123}$$

is the norm, counting particles emitted to $x \geq 0$.

As we assume that one particle is emitted as $t \to \infty$, the normalized wave function, denoted by a tilde, is

$$\tilde{\psi}(x,t) = \frac{1}{\sqrt{\int_0^\infty dt\, J(0,t)}}\psi(x,t). \tag{124}$$

Now to have a more transparent physical interpretation we apply some approximations to the exact solution Eq. (118) and separate each w-function into the contribution of the saddle at $k = k_s = x/(2t)$ and the one due to the pole. The dominant contribution of the saddle is obtained from Eq. (114) by

setting $k = k_s$ in $A(\omega)$ and integrating along the steepest descent path given by the straight line $k_I = [k_R - x/(2t)]$,

$$\psi_s(x,t) = \frac{e^{ik_s^2 t}}{2i\sqrt{\pi}} \left(\frac{1}{u_0^{(+)}} + \frac{1}{u_0^{(-)}} \right)$$

$$= \sqrt{\frac{2t}{\pi}} \frac{\tau e^{ik_s^2 t}}{(i-1)k_0(t^2 - \tau^2)}. \tag{125}$$

After the steepest descent path crosses the pole k_0 when $\mathrm{Im}\, u_0^{(+)} = 0$, its residue $\psi_0(x,t)$ must be added to the saddle wave function,

$$\psi_0 = e^{ik_s^2 t} e^{-u_0^{(+)2}} = e^{-i\omega_0 t} e^{ik_0 x}. \tag{126}$$

It follows that the total wave function can be approximated by

$$\psi(x,t) = \psi_s(x,t) + \psi_0(x,t)\Theta\left[\mathrm{Im}\left(u_0^{(+)}\right)\right]. \tag{127}$$

To see the conditions for validity of this expression note that the first and the exponential terms in the asymptotic series expansion for

$$w(z) \sim \frac{i}{\sqrt{\pi} z}\left[1 + \sum_{m=1}^{\infty} \frac{1 \times 3 \times \cdots \times (2m-1)}{(2z^2)^m}\right] + \Theta[-\mathrm{Im}(z)]2e^{-z^2}. \tag{128}$$

reproduce Eq. (127). In our case, large z means large $u_0^{(\pm)}$. Their moduli can be written as

$$\left|u_0^{(\pm)}\right| = \sqrt{x|k_0|}\sqrt{\frac{t}{2|\tau|} \pm \frac{1}{|k_0|} + \frac{|\tau|}{2t}}, \tag{129}$$

which take large values in certain conditions, in particular at times short and long compared to $|\tau|$.

6.2. Transition from exponential to post-exponential decay

The criterion which sets the timescale of the transition is that the moduli of pole and saddle contributions to the total density are equal, or their ratio $R(x,t)$ is one,

$$|\psi_0|^2 = e^{2\mathrm{Im}(\omega_0 t - k_0 x)}, \tag{130}$$

$$|\psi_s|^2 = \frac{t|\tau|^2}{\pi |k_0|^2[t^4 + |\tau|^4 - 2t^2\mathrm{Re}(\tau^2)]}, \tag{131}$$

$$R(x,t) = \frac{|\psi_0|}{|\psi_s|} = \frac{2\sqrt{\pi}|k_0|^2 t^{3/2}}{x} e^{\mathrm{Im}(\omega_0 t - k_0 x)} \times \sqrt{1 + \frac{|\tau|^4}{t^4} - 2\mathrm{Re}\left(\frac{\tau^2}{t^2}\right)}. \tag{132}$$

In addition, the condition $\text{Im}\left(u_0^{(+)}\right) > 0$ (the pole has been crossed by the steepest descent path) must be verified.

Solving $R(x, t) = 1$ with the assumption $t >> |\tau|$, we obtain an expression for the transition time t_p for fixed x,

$$t_p^{3/2} = \frac{xe^{-\text{Im}(\omega_0 t_p - k_0 x)}}{2\sqrt{\pi}|k_0|^2}. \tag{133}$$

First we fix k_0 and observe the density as a function of t for different x values. Figure 9.7 shows the density at the transition versus t_p. The curve depends parametrically on x, which increases from the bottom right corner upward. From this figure we can infer that the probability density at the transition point increases, as the observation point is moved away from the source, improving the possibility of observing the transition. A basic reason for this is the asymptotic growth of $|\psi_s|$ with x^2, whereas the pole term is basically shifted by $\delta x/2k_{0R}$ for a shift δx in the observation coordinate; in other words, the exponential behavior is delayed by increasing x.

Note also the behavior of the transition time t_p as x increases. Initially t_p occurs earlier as x increases, but there is an x value, $x = 1/|k_{0I}|$, beyond which the tendency changes, and t_p then increases with x until the transition is no longer observable.

Another conclusion inferred from Figure 9.7 is that there is a largest value of x for which the transition may be defined by the $R = 1$ criterion, such that $\text{Im}\left(u_0^{(+)}\right) > 0$. This maximum x increases with the resonance lifetime
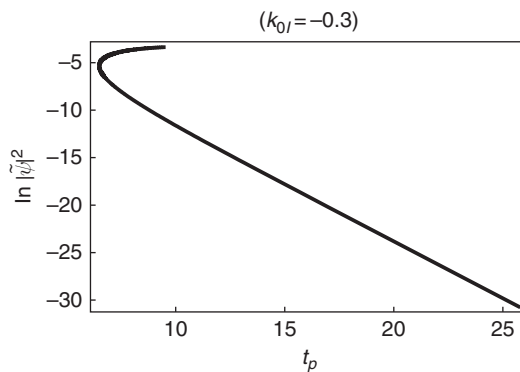
Figure 9.7   Probability density versus $t_p(x)$ at the transition point for fixed $k_0 = 1 - 0.3i$. The drawing covers x running from 0.0001 to 13.
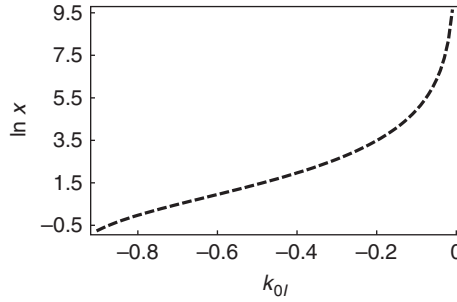
Figure 9.8 Largest *x* value at which an exponential to post-exponential transition is seen, satisfying the conditions $R = 1$ and $\mathrm{Im}\,u_0^{(+)} > 0$ versus k_{0I} (normalized waves). The quantities plotted are defined in Eqs. (105–108).
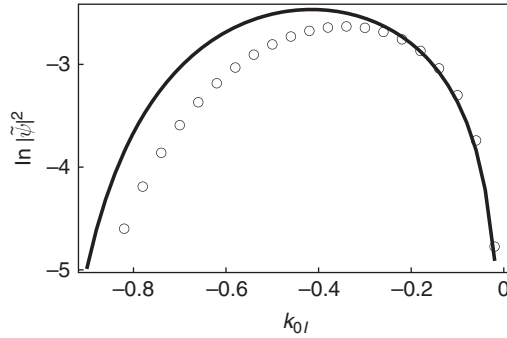
Figure 9.9 Density of normalized waves, at the largest *x* value where the transition is defined, as function of k_{0I}. Circles: density of the approximate solution; solid line: value from the exact wave function.

$\tau_0 = 1/|4k_{0I}|$, and it is plotted versus $|k_{0I}|$ in Figure 9.8. The normalized density at that critical point is shown in Figure 9.9. There is a maximum of the transition point density slightly to the right of $k_{0I} \sim -0.5$. This is consistent with the condition described by Jittoh [29] for purely nonexponential decay,

$$\Gamma/\epsilon = 1/\left[k_{0R}^2 \tau_0\right] = 4|k_{0I}| \geq 2, \tag{134}$$

where Γ and ϵ are the (dimensionless) decay rate and real energy of the resonance, respectively, and we have used the fact that the real part $k_{0R} = 1$ in our units.

6.3. Connection with Winter's model

The source model may be related to Winter's delta model [63] for strong potentials in the $t >> |\tau|$ regime. Here we follow Winter's conventions,

$$V(X) = \begin{cases} \infty, & X < -a, \\ U\delta(X), & X \geq -a. \end{cases} \tag{135}$$

The ground state of the infinite square well is taken as the initial wave function,

$$\Psi(X,0) = \begin{cases} (2/a)^{1/2}\sin(\pi X/a), & -a \leq X \leq 0, \\ 0, & X < -a \quad \text{or} \quad 0 < X. \end{cases} \tag{136}$$

The following dimensionless variables are introduced:

$$q \equiv [a(2mE)^{1/2}]/\hbar, \tag{137}$$

$$t_w \equiv \hbar T/2ma^2, \tag{138}$$

$$x_w \equiv X/a, \tag{139}$$

$$G \equiv 2maU/\hbar^2, \tag{140}$$

$$\psi^w(x_w, t_w) \equiv \Psi(X, T), \tag{141}$$

where

$$E = \frac{\hbar^2 K_{0R}^2}{2m}, \tag{142}$$

and $K_{0R} = \pi/a$ is the wave number of the particle in the initial state, Eq. (136). For $G >> 1$ the total wave function for any T and X outside the barrier can be split into two terms, one due to the pole contribution and the other due to the saddle [63]. These are, respectively,

$$\psi_0^w = \sqrt{\frac{2}{a}}\left(\frac{n\pi}{G}\right)e^{-i\epsilon_w t_w - t_w/2\tau_w}[\cos(n\pi x_w) + i\sin(n\pi x_w)] \tag{143}$$

$$\psi_s^w = \frac{(1+i)(Gx_w+1)}{2n\pi G^2\sqrt{\pi a}t_w^{3/2}}\left[1 - \frac{3i}{2t_w}\left(\frac{1}{n^2\pi^2} - \frac{x_w^2}{6} - \frac{x_w^2(Gx_w+1)}{3}\right) + \cdots\right], \tag{144}$$

where the dimensionless energy ϵ_w and the mean lifetime τ_w are

$$\epsilon_w = n^2\pi^2(1 - 2/G), \tag{145}$$

$$1/\tau_w = \frac{4\pi^3 n^3}{G^2}\left(1 - \frac{4}{G}\right). \tag{146}$$

Now we show that the source model described above can reproduce Winter's model, that is, we show that Eqs. (125 and 126) give the same probabilities as Eqs. (144 and 143). First, from Eqs. (105 and 139) and from Eqs. (106 and 138) we formulate the connection between the spatial and temporal coordinates,

$$x = \pi x_w, \quad t = \pi^2 t_w. \tag{147}$$

Using the dimensioned wave function $\Psi_0(X,T)$ at the pole, we obtain the links between the remaining variables. For the source model we use the normalized one given by Eq. (124) and the fact that the dimensionless wave function is connected to the dimensioned one through Eq. (107), where $L^{-1} = K_{0R}$ and, for the infinite square well of width a, $K_{0R} = \pi/a$. Then the dimensioned pole wave function can be written as

$$\Psi_0(X,T) = \sqrt{\frac{\pi}{aN}}\psi_0(x,t) = \psi_0^w(x_w,t_w), \tag{148}$$

where the normalization constant $N = N_+(t = \infty)$ for the source model is given by Eq. (122). So from Eq. (148) and using Eqs. (126 and 143), we obtain at first order in G,

$$N_+(t = \infty) = \frac{G^2}{2\pi}, \quad k_{0I} = -\frac{\pi}{G^2}. \tag{149}$$

Starting from Eq. (125) and using Eqs. (147 and 149) we may also check that the probability obtained from the saddle wave function in the source model reproduces that of Winter's model for strong potentials $G \gg 1$ in the $t \gg |\tau|$ regime,

$$|\Psi_s(X,T)|^2 = \frac{\pi}{aN}|\psi_s(x,t)|^2 = |\psi_w(x_w,t_w)|^2 \tag{150}$$

to order t_w^{-3}.

In conclusion, observing the density of decay products at an optimal distance from the source significantly improves the observability of the elusive transition to post-exponential decay. The observability of the transition may additionally be enhanced by amplifying the signal with a macroscopic Bose–Einstein condensate wave function. As an example, let us consider an ^{87}Rb quasi-1D Bose–Einstein condensate sample of 10^6 atoms, released to a quasi-1D waveguide from a controllable trap that will determine the resonance energy and lifetime [143]. Then a commercial charge-coupled device camera with $\sim 3\,\mu$m spatial resolution and shot-noise limited detection with at least ~ 10 atoms/pixel may be used to measure the atomic density at the waveguide by resonant absorption imaging [144]. According to the model presented here a sample of 10^6 atoms with lifetime $\sim 400\,\mu$s and release velocity $\sim 1\,$cm/s would provide 9200 atoms/pixel transition density at $t_p \sim 10\,$ms and at a distance of $\sim 100\,\mu$m. These numbers make

the observation of the transition very plausible. Note that even 10^3 initial atoms would be close to the shot-noise observation limit at that space–time point.

7. FINAL COMMENTS

Post-exponential decay is a subtle phenomenon. Since it involves low energies, it is easily perturbed and difficult to detect. However, recent progress in artificial mesoscopic semiconductor structures, or trap design and detection of ultracold atoms, may offer access to this regime for simple quantum systems. We have provided an overview of quantum post-exponential decay, from the early work to the most recent analyses and experiments. Several simple models have been discussed; they help to understand fundamental properties of long-time deviation from exponential decay, provide clues for its control, and suggest new experiments, which is indeed one of major challenges. Further challenges are to gain a full understanding of post-exponential decay in complex systems, such as organic molecules in solution, as well as a more intuitive physical interpretation of the effect at the level of the survival probability.

ACKNOWLEDGMENTS

REFERENCES

[1] M. Razavy, Quantum Theory of Tunnelling, World Scientific, Singapore, 2003, p. 18.
[2] G. Gamow, Zur Quantentheorie des Atomkernes, Z. Phys. 51 (1928) 204.
[3] G. García-Calderón, I. Maldonado, J. Villavicencio, Resonant-state expansions and the long-time behavior of quantum decay, Phys. Rev. A 76 (2007) 012103; G. García-Calderón, A. Rubio, Transient effects and delay time in dynamics of resonant tunnelling, Phys. Rev. A 55 (1997) 3361.
[4] R.M. Cavalcanti, C.A.A. de Carvalho, On the effectiveness of Gamow's method for calculating decay rates, Rev. Bras. Ens. Fis. 21 (1999) 464.
[5] V.F. Weisskopf, E. Wigner, Berechnung der natürlichen Linienbreite auf Grund der Diracschen Lichttheorie, Z. Phys. 63 (1930) 54; Über die Natürliche Linienbreite in der Strahlung des harmonischen Oszillators, 65 (1930) 18.
[6] P.A.M. Dirac, The quantum theory of the emission and absorption of radiation, Proc. R. Soc. Lond. (A) 114 (1927) 243; The quantum theory of dispersion, 710.

[7] C.B. Chiu, E.C.G. Sudarshan, B. Misra, Time evolution of unstable quantum states and a resolution of Zeno's paradox, Phys. Rev. D 17 (1977) 520.

[8] E.B. Norman, S.B. Gazes, S.G. Crane, D.A. Bennett, Tests of the exponential decay law at short and long times, Phys. Rev. Lett. 60 (1988) 2246.

[9] N.N. Nikolaev, Verification of the exponential decay law, Sov. Phys. Usp. 11 (1968) 522.

[10] P.T. Greenland, Seeking non-exponential decay, Nature 335 (1988) 298.

[11] E.B. Norman, B. Sur, K.T. Lesko, R.M. Larimer, D.J. DePaolo, T.L. Owens, An improved test of the exponential decay law, Phys. Lett. B 357 (1995) 521.

[12] T.D. Nghiep, V.T. Hahn, N.N. Son, Non-exponential deviations in decay of unstable systems, Nucl. Phys. B (Proc. Suppl.) 66 (1998) 533.

[13] L. Fonda, G.C. Ghirardi A. Rimini, Decay theory of unstable quantum systems, Rep. Prog. Phys. 41 (1978) 587.

[14] J. Lawrence, Non-exponential decay at late times and a different Zeno paradox, J. Opt. B: Quant. Semicl. Opt. 4 (2002) S446.

[15] R.E. Parrott, J. Lawrence, Persistence of exponential decay for metastable quantum states at long times Europhys. Lett. 57 (2002) 632.

[16] C. Rothe, S.I. Hintschich, A.P. Monkman, Violation of the exponential-decay law at long times, Phys. Rev. Lett. 96 (2006) 163601.

[17] R.G. Winter, Large-time exponential decay and "hidden variables", Phys. Rev. 126 (1962) 1152.

[18] L.M. Krauss, J. Dent, Late time behavior of false vacuum decay: Possible implications for cosmology and metastable inflating states Phys. Rev. Lett. 100 (2008) 171301.

[19] C.A. Nicolaides, D.R. Beck, Possibility of observing nonexponential decays in autoionizing states, Phys. Rev. Lett. 38 (1977) 683, 1037(E).

[20] C.A. Nicolaides, D.R. Beck, Time dependence, complex scaling and the calculation of resonances in many-electron systems, Int. J. Quantum Chem. 14 (1978) 457.

[21] S.D. Druger, M.A. Samuel, Non-exponential decay in auto-ionization near threshold, Phys. Rev. A 30 (1984) 640.

[22] C.A. Nicolaides, Physical constraints on nonstationary states and nonexponential decay, Phys. Rev. A 66 (2002) 022118.

[23] T.G. Douvropoulos, C.A. Nicolaides, Time-dependent tunnelling via path integrals. Connection to results of the quantum mechanics of decaying states, J. Phys. B (At. Mol. Opt.) 35 (2002) 4453.

[24] J. Martorell, J.G. Muga, D.W.L. Sprung, Long-time deviations from exponential decay for inverse-square potentials, Phys. Rev. A 77 (2008) 042719.

[25] E. Torrontegui, J.G. Muga, J. Martorell, D.W.L. Sprung, Enhanced observability of quantum post-exponenetial decay using distant detectors, Phys. Rev. A 80 (2009) 012703.

[26] M. Lewenstein, K. Rzazewski, Quantum anti-Zeno effect, Phys. Rev. A 61 (2000) 022105.

[27] S. Longhi, Non-exponential decay via tunneling in tight-binding lattices and the optical Zeno effect, Phys. Rev. Lett. 97 (2006) 110402.

[28] G. Della Valle, S. Longhi, P. Laporta, P. Biagioni,L. Dou, M. Finazzi, Discrete diffraction in waveguide arrays: Quantitative analysis by STOM, Appl. Phys. Lett. 90 (2007) 261118.

[29] T. Jittoh, S. Matsumoto, J. Sato, Y. Sato, K. Takeda, Non-exponential decay of an unstable quantum system: Small-Q-value s-wave decay, Phys. Rev. A 71 (2005) 012109.

[30] G. García-Calderón, J. Villavicencio, Full-time nonexponential decay in double-barrier quantum structures, Phys. Rev. A 73 (2006) 062115.

[31] F.M. Dittes, The decay of quantum systems with a small number of open channels, Phys. Rep. 339 (2000) 215.

[32] P.M. Radmore, P.L. Knight, Two-photon ionisation: Interference and population trapping, Phys. Lett. A 102 (1984) 180.

[33] E.S. Medvedev, Nonexponential fluorescence decay of polyatomic molecules, Sov. Phys. Usp. 34 (1991) 16.

[34] M. Dworzak, T. Bartel, M. Strassburg, I.L. Krestinov, A. Hoffmann, R. Seguin et al., Optical properties of InGaN quantum dots, Superlatt. Microstruct. 36 (2004) 763.

[35] R.A. Valleé, K. Baert, B. Kolaric, M. Van der Auweraer, K. Clays, Nonexponential decay of spontaneous emission from an ensemble of molecules in photonic crystals, Phys. Rev. B 76 (2007) 045113.

[36] I.S. Nikolaev, P. Lodahl, A.F. Van Driel, A.F. Koenderink, W.L. Vos, Strongly nonexponential time-resolved fluorescence of quantum-dot ensembles in three-dimensional photonic crystals, Phys. Rev. B 75 (2007) 115302.

[37] V.R. Nikitenko, D. Hertel, H. Bässler, Dispersive germinate recombination in a conjugated polymer, Chem. Phys. Lett. 348 (2001) 89.

[38] C.M. Cuppoletti, L.J. Rothberg, Persistent photoluminescence in conjugated polymers, Synth. Met. 139 (2003) 867.

[39] L.S. Schulman, C.R. Doering, B. Gaveau, Linear decay in multilevel quantum systems, J. Phys. A 91 (1991) 2053.

[40] L.S. Schulman, D. Tolkunov, E. Mihokova, Stability of quantum breathers, Phys. Rev. Lett. 96 (2006) 065501.

[41] S. Longhi, Bound states in the continuum in a single-level Fano-Anderson model, Eur. Phys. J. B 57 (2007) 45.

[42] E.J. Robinson, Non-exponential decay due to population trapping in an infinite sequence of discrete states and continua, J. Phys. B (At. Mol. Opt.) 27 (1994) L305.

[43] L.S. Schulman, B. Gaveau, Limited quantum decay, J. Phys. A 28 (1995) 7359.

[44] P. Exner, Unstable system dynamics: do we understand it fully? Rep. Math. Phys. 59 (2007) 351.

[45] J.J. Sakurai, Modern Quantum Mechanics, revised ed., Addison-Wesley, NY, 1994; Supplement II, pp. 481–486.

[46] M.L. Goldberger, K.M. Watson, Collision Theory, John Wiley and Sons, New York, 1964, Ch. 8, pp. 448–450.

[47] C. Cohen-Tannoudji, J. Dupont-Roc, G. Grynberg, Atom-Photon Interactions: Basic Processes and Applications, Wiley, New York, 1992, pp. 220–221.

[48] H. Nakazato, M. Namiki, S. Pascazio, Temporal behaviour of quantum mechanical systems, Int. J. Mod. Phys. B 10 (1996) 247.

[49] P. Facchi, S. Pascazio, La Regola d'oro di Fermi, Bibliopolis, Napoli, 1999.

[50] P. Facchi, S. Pascazio, Quantum Zeno dynamics: Mathematical and physical aspects, J. Phys. A (Math. Gen.) 41 (2008) 493001.

[51] S. Longhi, Non-markovian decay and lasing condition in an optical microcavity coupled to a structured reservoir, Phys. Rev. A 74 (2006) 063826.

[52] E.J. Hellund, The decay of resonance radiation by spontaneous emission, Phys. Rev. 89 (1953) 919.

[53] G. Höhler, Über die Exponentialnäherung beim Teilchenzerfall (On the exponential approximation in particle decay), Z. Phys. 152 (1958) 546.

[54] J. Petzold, Wie gut gilt das Exponentialgesetz beim α-Zerfall? Z. Phys. 155 (1959) 422.

[55] L.A. Khalfin, Contribution to the decay theory of a quasistationary state, Sov. Phys. JETP 6 (1958) 1053.

[56] N.S. Krylov, V.A. Fock, On the two fundamental interpretations of the uncertainty principle for energy and time, Zhurnal Eksper. Teor. Fiz. (USSR.) 17 (1947) 93.

[57] G. García-Calderón, J.L. Mateos, M. Moshinsky, Resonant spectra and the time evolution of the survival and nonescape probabilities, Phys. Rev. Lett. 74 (1995) 337.

[58] J.G. Muga, F. Delgado, A. del Campo, G. García-Calderón, Role of initial state reconstruction in short- and long-time deviations from exponential decay, Phys. Rev. A 73 (2006) 052112.

[59] J.G. Muga, V. Delgado, R.F. Snider, Dwell time and asymptotic behaviour of the probability density, Phys. Rev. B 52 (1995) 16381.

[60] J.G. Muga J.P. Palao, Solvable model for quantum wavepacket scattering in one dimension, J. Phys. A (Math. Gen.) 31 (1998) 9519.

[61] R.G. Newton, The exponential decay law of unstable systems, Ann. Phys. (NY) 14 (1961) 333.

[62] R.G. Newton, Scattering Theory of Waves and Particles, second ed. Dover, Mineola, NY, 2002 (Chapter 19.).

[63] R.G. Winter, Evolution of a quasi-stationary state, Phys. Rev. 123 (1961) 1503.

[64] C. Anastopoulos, Time-of-arrival probabilities and quantum measurements, III: Decay of unstable states, J. Math. Phys. 49 (2008) 022103.

[65] R.M. Cavalcanti, Comment on "Resonant spectra and the time evolution of the survival and nonescape probabilities", Phys. Rev. Lett. 80 (1998) 4353.

[66] W. van Dijk, Y. Nogami, Analytical approach to the wave function of a decaying quantum system, Phys. Rev. C 65 (2002) 024608.

[67] W. van Dijk, Y. Nogami, Comment on "Resonant spectra and the time-evolution of survival and non-escape probabilities", Phys. Rev. Lett. 90 (2003) 028901.

[68] R.E. Paley, N. Wiener, FourierTransforms in the Complex Domain, American Mathematical Society Colloquium Publication, New York, (1934), Vol. 19.

[69] C.A. Nicolaides, D.R. Beck, On the possibility of observing nonexponential decay in autoionizing states, In: Beam-Foil Spectroscopy, I. Sellin, D. Pegg, (Eds.), Plenum Press, New York, 1976, p. 77.

[70] P.L. Knight, Interaction Hamiltonians, spectral lineshapes and deviations from exponential decay law at long times, Phys. Lett. A 61 (1977) 25.

[71] D.S. Onley, A. Kumar, Time dependence in quantum mechanics: study of a simple decaying system, Am. J. Phys. 60 (1992) 432.

[72] K.M. Sluis, E.A. Gislason, Decay of a quantum-mechanical state described by a truncated Lorentzian energy distribution, Phys. Rev. A 43 (1991) 4581.

[73] H. Jakobovits, Y. Rotshchild, J. Levitan, An approximation to the exponential decay law, Am. J. Phys. 63 (1995) 439.

[74] M.L. Goldberger, K.M. Watson, Lifetime and decay of unstable particles in S-matrix theory, Phys. Rev. 136 (1964) B1472.

[75] A. Peres, Non-exponential decay law, Ann. Phys. (NY) 129 (1980) 33.

[76] U. Fano, Effects of configuration interaction on intensities and phase shifts, Phys. Rev. 124 (1961) 1866.

[77] P.W. Anderson, Localized magnetic states in metals, Phys. Rev. 124 (1961) 41.

[78] T.D. Lee, Some special examples in renormalizable field theory, Phys. Rev. 95 (1954) 1329.

[79] K.O. Friedrichs, On the perturbation of continuous spectra, Commun. Pure Appl. Math. 1 (1948) 361.

[80] H. Feshbach, A unified theory of nuclear reactions, Ann. Phys. (NY) 5 (1958) 357; Unified theory of nuclear reactions. II, 19 (1962) 287.

[81] J. Okolowicz, M. Ploszajczak, I. Rotter, Dynamics of quantum systems embedded in a continuum, Phys. Rep. 374, 271-383 (2003)

[82] J.G. Muga, G.W. Wei, R.F. Snider, Survival probability for the yamaguchi potential, Ann. Phys. (NY) 252 (1996) 336.

[83] V.N. Faddeyeva, N.M. Terentev, Mathematical Tables: Tables of the Values of the Function $w(z)$ for Complex Argument, Pergamon, New York, 1961.

[84] A. Abramowitz, I.A. Stegun, Handbook of Mathematical Functions, Dover, New York, 1965.

[85] G. García-Calderón, V. Riquer, R. Romo, J. Survival probability of a single resonance, J. Phys. A 34 (2001) 4155.

[86] D.A. Dicus, W.W. Repko, R.F. Schwitters, T.M. Tinsley, Time development of a quasistationary state, Phys. Rev. A 65 (2002) 032116.

[87] F. Delgado, J.G. Muga, G. García-Calderón, Suppression of Zeno effect for distant detectors, Phys. Rev. A 74 (2006) 062102.

[88] D.V. Savin, V.V. Sokolov, H.J. Sommers, Is the concept of the non-Hermitian effective Hamiltonian relevant in the case of potential scattering? Phys. Rev. E 67 (2003) 026215.

[89] A. del Campo, F. Delgado, G. García-Calderón, J.G. Muga, Decay by tunneling of bosonic and fermionic Tonks-Girardeau gases, Phys. Rev. A 74 (2006) 013605.

[90] J. R. Taylor, Scattering Theory, J. Wiley, New York, 1972.

[91] J. Denschlag, O. Umshaus, J. Schmiedmayer, Probing a singular potential with cold atoms: an atom and a charged wire, Phys. Rev. Lett. 81 (1998) 737.

[92] J. Denschlag, D. Cassettari, A. Chenet, S. Schneider, J. Schmiedmayer, An atom and a wire: towards mesoscopic atom optics, Appl. Phys. B 69 (1999) 291.

[93] L.V. Hau, M.M. Burns, J.A. Golovchenko, Bound states of guided matter waves: An atom and a charged wire, Phys. Rev. A 45 (1992) 6468.

[94] T.F. O'Malley, Effect of long-range final-state forces on the negative-ion photodetachment cross section near threshold, Phys. Rev. 137 (1965) A1668.

[95] W. Domcke, L.S. Cederbaum, On the interpretation of low-energy electron-HCl scattering phenomena, J. Phys. B (At. Mol.) 14 (1980) 149.

[96] H. Estrada, W. Domcke, Analytic properties of the S matrix for a simple model of fixed-nuclei electron-polar-molecule scattering, J. Phys. B (At. Mol.) 17 (1984) 279.

[97] M. Klaus, Exact behavior of Jost functions at low energy, J. Math. Phys. 29 (1988) 148.

[98] L. Ersak, The number of wave functions of an unstable particle, Yad. Fiz. 9 (1969) 458; English translation: Sov. J. Nucl. Phys. 9 (1969) 263.

[99] L. Fonda, G.C. Ghirardi, Remarks on the origin of deviations from the exponential decay law of an unstable particle, Il Nuovo Cimento 7A (1972) 180.

[100] R.B. Griffiths, Consistent histories and the interpretation of quantum mechanics, J. Stat. Phys. 36 (1984) 219; R. Omnès, The Interpretation of Quantum Mechanics, Princeton University Press, Princeton, 1994; M. Gell-Mann, J.B. Hartle, Classical equations for quantum systems, Phys. Rev. D 47 (1993) 3345.

[101] R. Jacob R.G. Sachs, Mass and lifetime of unstable particles, Phys. Rev. 121 (1961) 350.

[102] H.M. Nussenzveig, Causality and Dispersion Relations, Academic Press, New York, 1972.

[103] M. Miyamoto, Free initial wave packets and the long-time behavior of the survival and non-escape probabilities, Phys. Rev. 68 (2003) 022702.

[104] M. Miyamoto, Initial wave packets and the various power-law decreases of scattered wave packets at long times, Phys. Rev. A 69 (2004) 042704.

[105] M. Miyamoto, Long time behaviour of unstable multilevel systems in presence of a zero energy resonance, Open Sys. Inform. Dyn. 13 (2006) 291.

[106] E. Torrontegui, J.G. Muga, J. Martorell, D.W.L. Sprung, Classical picture of post-exponential decay, Phys. Rev. A, 81 (2010) 042714.

[107] E.T. Whittaker, G.N. Watson, A Course of Modern Analysis, fourth ed., Cambridge University Press, Cambridge, 1927, p. 172.

[108] F.T. Avignone, Comment on "Tests of the exponential decay law at short and long times", Phys. Rev. Lett. 62 (1988) 2664.

[109] D. Tomono, S.N. Nakamura, Y. Matsuda, M. Iwasaki, G. Mason, K. Ishida et al., Precise muon lifetime measurement at RIKEN-RAL and prospects at a high intensity muon source, Nucl. Inst. Meth. A 503 (2003) 283.

[110] D. Novkovic, L. Nadderd, A. Kandic, I. Vukanac, M. Durasevic, D. Jordanov, Testing the exponential decay law of ^{198}Au, Nucl. Inst. Meth. A 566, (2006) 477.

[111] R.T. Robiscoe, Corrections to the exponential decay law for the 2P→1S transition in hidrogen-like atoms, Phys. Lett. A 100 (1984) 407.

[112] C.A. Nicolaides, T. Mercouris, On the violation of the exponential decay law in atomic physics: ab initio calculation of the time-dependence of the He- 1s2p^2 ^{4}P non-stationary state, J. Phys. B 29 (1996) 1151.

[113] H. Ekstein, A.J.F. Siegert, On a re-interpretation of decay experiments, Ann. Phys. (NY) 68 (1971) 509.

[114] F. Benatti, R. Floreanini, On the decay law for unstable open systems, Phys. Lett. B 428 (1998) 149.

[115] P.T. Greenland, A. M. Lane, Exposure of decay at non-constant rate by rapid fluctuations, Phys. Lett. A 117 (1986) 181.

[116] M.H. Mittelman, A. Tip, Decay of an adiabatically prepared state, J. Phys. B (At. Mol.) 17 (1984) 571.

[117] E.J. Robinson, Adiabatic switching and lon-time corrections to the exponential decay law, Phys. Rev. A 33 (1986) 1461.

[118] J. Martorell, D.W.L. Sprung, W. van Dijk, J.G. Muga, Memory effects induced by initial switching conditions in a Fano-Anderson model, Phys. Rev. A 79 (2009) 062104.

[119] J.G. Muga, A. Ruschhaupt, A. del Campo (eds.), Time in Quantum Mechanics, Vol. 2, Lecture Notes in Physics 789, Springer, 2010.

[120] J.G. Muga, J.P. Palao, B. Navarro, I.L. Egusquiza, Complex absorbing potentials, Phys. Rep. 395 (2004) 357.

[121] B. Crosignani, P. di Porto, Spontaneous emission and partial detection of the emitted photon: A possible quantum-mechanical non-local effect, Nuovo Cimento B 109 (1994) 555.

[122] B. Crosignani, P. di Porto, Can spontaneous emission be influenced by the presence of a distant detector, Europhys. Lett. 35 (1996) 165; "reply to [130]", 39 (1997) 233.

[123] D. Home, M.A.B. Whitaker, A Conceptual analysis of quantum zeno; paradox, measurement, and experiment, Ann. Phys. (NY) 258 (1997) 237.

[124] M. Hotta, M. Morikawa, Impossibility of distant indirect measurement of the quantum Zeno effect, Phys. Rev. A 69 (2004) 052114.

[125] M.G. Makris, P. Lambropoulos, Quantum Zeno effect by indirect measurement: The effect of the detector, Phys. Rev. A 70 (2004) 044101.

[126] K. Koshino, A. Shimizu, Quantum Zeno effect by general measurements, Phys. Rep. 412 (2005) 191.

[127] S. Wallentowitz, P.E. Toschek, Comment on "Impossibility of distant indirect measurement of the quantum Zeno effect", Phys. Rev. A 72 (2005) 046101.

[128] S. Wallentowitz, P.E. Toschek, Comment on: "Defense of impossibility of distant indirect measurement of the quantum Zeno effect" [Phys. Lett. A 356 (2006) 411], Phys. Lett. A 367 (2007) 420.

[129] M. Ozawa, Defense of "Impossibility of distant indirect measurement of the quantum Zeno effect", Phys. Lett. A 356 (2006) 411.

[130] L.C. Ryff, The presence of a distant detector does not seem to influence spontaneous emission, Europhys. Lett. 39, (1997) 231.

[131] W. Barford, R.J. Bursill, R.W. Smith, Theoretical and computational studies of excitons in conjugated polymers, Phys. Rev. B 66 (2002) 115205.

[132] W. Barford, Excitons in the strong coupling limit of the one-dimensional extended Hubbard model, Phys. Rev. B 65 (2002) 205118.

[133] W. Barford, Theory of singlet exciton yield in light-emitting polymers, Phys. Rev. B 70 (2004) 205204.

[134] P.H. Sher, J.M. Smith, P.A. Dalgarno, R.J. Warburton, X. Chen, P.J. Dobson, et al., Power law carrier dynamics in semiconductor nanocrystals at nanosecond timescales, Appl. Phys. Lett. 92 (2008) 101111.

[135] P. Frantsuzov, M. Kuno, B. Janko, R.A. Marcus, Universal emission intermittency in quantum dots, nanorods and nanowires, Nat. Phys. 4 (2008) 519.

[136] N.G. Kelkar, M. Nowakowski, P. Khemchandani, Hidden evidence of non-exponential nuclear decay, Phys. Rev. C 70 (2004) 024601.

[137] S. Longhi, Tunneling escape in optical waveguide arrays with a boundary defect, Phys. Rev. E 74 (2006) 026602.

[138] M. Razavy, Quantum mechanical irreversible motion of an infinite chain, Can. J. Phys. 57 (1979) 1731.

[139] P. Biagoni, G. Della Valle, M. Ornigotti, M. Finazzi, L. Duò, P. Laporta, et al., Experimental demonstration of the optical Zeno effect by scanning tunneling optical microscopy, Optics Express 16 (2008) 3762.

[140] K. Rzazewski, M. Lewenstein, J.H. Eberly, Threshold effects in strong field photodetachment, J. Phys. B (At. Mol.) 15 (1982) L661.

[141] J. Zakrzewski, K. Rzazewski, M. Lewenstein, Threshold effects in strong-field photodetachment monitored by spontaneous photo-relaxation, J. Phys. B (At. Mol.) 17 (1984) 729.

[142] J.G. Muga, M. Büttiker, Time dependence of evanescent quantum waves, Phys. Rev. A 62 (2000) 023808.

[143] F. Delgado, J.G. Muga, A. Ruschhaupt, Preparation of ultralow atomic velocities by transforming bound states into tunneling resonances, Phys. Rev. A 74 (2006) 063618.

[144] P. Krüger, S. Wildermuth, S. Hofferberth, L.M. Andersson, S. Groth, I. Bar-Joseph, et al., Cold atoms close to surfaces: Measuring magnetic field roughness and disorder potentials, J. Phys. Conf. Ser. 19 (2005) 56.

INDEX

Note: The letters 'f' and 't' following locators denote figures and tables respectively